Loughborough University

This item is held in Loughborough University's Institutional Repository (https://dspace.lboro.ac.uk/) and was harvested from the British Library's EThOS service (http://www.ethos.bl.uk/). It is made available under the following Creative Commons Licence conditions.

creative commons

COMMONS DEED

Attribution-NonCommercial-NoDerivs 2.5

You are free:

- to copy, distribute, display, and perform the work

Under the following conditions:

Attribution. You must attribute the work in the manner specified by the author or licensor.

Noncommercial. You may not use this work for commercial purposes.

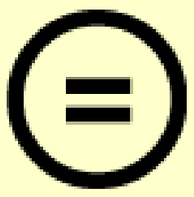

No Derivative Works. You may not alter, transform, or build upon this work.

- For any reuse or distribution, you must make clear to others the license terms of this work.
- Any of these conditions can be waived if you get permission from the copyright holder.

Your fair use and other rights are in no way affected by the above.

This is a human-readable summary of the Legal Code (the full license).

Disclaimer

For the full text of this licence, please go to:
http://creativecommons.org/licenses/by-nc-nd/2.5/

OSCILLATIONS OF CYLINDERS IN WAVES AND CURRENTS

by

R. L. P. VERLEY

A Doctoral Thesis

Submitted in partial fulfilment of the requirements
for the award of

DOCTOR OF PHILOSOPHY of the Loughborough University of Technology
May 1980

© by R. L. P. Verley, 1980

SUMMARY

This thesis contains the results of two research investigations conducted by the author, the first an exploratory investigation into wave induced vibrations, conducted at the British Hydrodynamics Research Association (BHRA), and the second a comprehensive investigation into the forces on cylinders oscillated in still water and in line with various currents, conducted at the River and Harbour Laboratory (VHL), Trondheim, Norway. Questions posed by the results of the first investigation were used in the formulation of the second, and results from the second led to a better understanding of the first.

First investigation: Vibrations of isolated cylinders in regular waves

In this investigation two cylinders were mounted vertically side by side in a wave flume (but a sufficient distance apart so that no interactions occurred). One of these cylinders was effectively rigid, and the other mounted as an inverted pendulum, its natural frequency controlled by springs attached to its upper end, and the motion restricted to either the direction parallel to the wave advance, or perpendicular to this direction.

Reactions were measured at the top of the two cylinders and compared. Under some circumstances vibration of the flexibly mounted cylinder occurred. The major results are summarized as follows:

i) Vibrations were due to the response to vortex shedding and could occur even if the natural frequency of the flexible cylinder was many times higher than the wave frequency.

ii) Parameters controlling the onset of vibration and quantifying the magnitude of vibration have been isolated.

iii) The overall amplitude of the reaction of the rigid cylinder was predicted well by applying Morison's formula and by using coefficient values obtained in oscillatory flow distributed over the cylinder according to the local

values of Keulegan-Carpenter number. The smaller variations in the reaction were not predicted by this model.

iv) The following mathematical models were used to try to predict the experimentally obtained flexible cylinder vibration data for vibrations parallel to the direction of wave advance.

a) The experimental reaction measured on the rigid cylinder was used as input to a dynamic mathematical model of the flexible cylinder, which used still water values of added mass and damping.

b) The experimental rigid cylinder reaction was used as input to a model which included additional 'hydrodynamic' damping due to relative velocity effects.

c) Morison's formula was used to predict the rigid cylinder input reaction to a model using still water added mass and damping.

d) The modified Morison's formula was used to predict both the input reaction to a model and to give additional hydrodynamic damping.

v) Models c) and d) do not include any vortex shedding forces. Model a) adequately predicted the experimental vibrations parallel to the direction of wave advance and also vibrations in the direction perpendicular to wave advance. Models b), c) and particularly d) underpredicted the vibrations.

The results of the models imply that fluid forces were unaltered by the cylinder vibrations, that hydroelastic vibration did not occur, and that a full knowledge of the forcing on a rigid cylinder would be sufficient to predict the response of flexible cylinders.

Furthermore, the results suggested that the use of the modified Morison's formula in the dynamic analysis of offshore platforms may not correctly predict vibrations.

vi) A quasi-steady model of vortex shedding in oscillatory and wave flows has been studied where the instantaneous shedding frequency is considered to be proportional to the instantaneous velocity, and the instantaneous force

amplitude proportional to the square of the instantaneous velocity. The model gave a good qualitative prediction of lift traces found in wave and oscillatory flow experiments, and of the variation in the spectral content of the lift forces with varying Keulegan-Carpenter number.

Second investigation: Oscillations of cylinders in still water and in-line with currents

The experimental apparatus consisted of a horizontal cylinder which was attached horizontally below a massive pendulum. Various cylinders were thus caused to oscillate in still water and in-line with various currents and the forces on the cylinders, as well as the logarithmic decrement of the pendulum motion, were recorded. Due to the nature of the rig there was no extraneous vibration and only a very small decrease in amplitude per cycle. Extremely good accuracy in the measurement of forces and the subsequent calculation of coefficients was obtained. Large ranges of all the parameters of importance were covered, except for Reynolds number which was always subcritical. The major results in still water may be summarized as follows:

i) For oscillations of a cylinder in still water, the drag and inertia coefficients have been accurately determined as functions of x_o/D and $\beta = nD^2/\nu$, where x_o = amplitude of oscillation, D = cylinder diameter, n = frequency of oscillation and ν = kinematic viscosity. It has been found advisable, particularly at low amplitudes, to separate the viscous drag contribution, given approximately by Stokes' unseparated viscous flow equations, from the total drag coefficient.

ii) For very small amplitudes of vibration, the forces on the cylinders were accurately given by the application of Stokes' equations, and an expression has been found for the amplitude up to which the forces may be reasonably approximated by these equations.

The major results in currents may be summarized as follows:

i) It has been found that the force on a cylinder oscillating in line with a steady current is best described by a relative velocity type equation

$$f(t) = .5\rho D\, C_D(t)\, (V-\dot{x})|(V-\dot{x})| - .25\rho\pi\, D^2 C_a(t)\ddot{x} \qquad -(1)$$

where V = steady current velocity, $\dot{x}$, $\ddot{x}$ = instantaneous cylinder velocity and acceleration, $C_D(t)$ and $C_a(t)$ = time dependent drag and added mass coefficients and ρ = fluid density. By taking averages of this equation over a cycle, three time-averaged coefficients are obtained for the steady component of drag, the oscillatory component of drag, and the added mass. The variations of these coefficients with respect to various parameters are presented.

ii) For values of a parameter $V/nD \gtrsim 17$, the flow becomes quasi-steady, and the steady and oscillatory drag coefficients are equal for all amplitudes of oscillation. For $V/nD \gtrsim 30$ the value is equal to the steady drag coefficient on a stationary cylinder.

At lower values of V/nD values of the time averaged steady and oscillatory drag coefficients differ.

iii) The time-averaged oscillatory drag coefficient varies smoothly, other than for $x_o/D \lesssim .2$ when $V/nD \approx 2.0$ or 3.0, from its value in still water at low V/nD, where it is dependent upon x_o/D and β, to the stationary cylinder steady drag coefficient at high V/nD.

iv) The variations in the time-averaged steady drag coefficient are complex, however the three most important observations are:

a) A minimum occurs at $x_o/D \approx 1.0$, which, for $V/nD \lesssim 1.6$, is negative.

b) A maximum, with value 1.0, occurs at $x_o/D \approx 2.3$.

c) A maximum occurs for $V/nD \gtrsim 3$ for $V/\dot{x}_o$ somewhere between 1 and 2, where $\dot{x}_o$ is the velocity amplitude of oscillations. This maximum may take a value up to twice the stationary cylinder steady drag coefficient value.

v) The time-averaged added mass coefficient varies considerably and is closely, but in an inverse way, related to the time-averaged steady drag coefficient.

Flow visualisation experiments have been conducted and the variations in the coefficients have been explained in terms of vortex shedding and wake characteristics.

The sometimes dramatic changes observed in the vortex shedding patterns and in the wake have been fully explained by considering the inherent instability of wake geometries other than the von Kármán type alternating wake, the symmetric vortices which develop after flow reversal occurs, and the distance travelled by the cylinder relative to the fluid in the time between one flow reversal and the next.

These second experiments gave an explanation of the results obtained in waves in the first experiments.

The results obtained in this work provide a step forward in the understanding of two problems in the offshore industry.

i) The fluid-induced damping of cylindrical structures or members vibrating in a flowing fluid.

ii) The forces on a rigid cylindrical member due to a combination of waves and currents.

In addition the results provide an advancement in the understanding of the fluid dynamics of time dependent flows.

ACKNOWLEDGEMENTS

A number of institutions and individuals have provided the author with financial or technical support in the course of the work described in this thesis.

The Department of Energy, through the Offshore Fluid Loading Advisory Group, financed the contract with the British Hydromechanics Research Association (BHRA), under which a large amount of the work of Part II was conducted. BHRA provided finance from general funds for some of the work of Part II and contributed to the author's higher degree fees.

Initial finance for the work of Part III was provided from internal funds by the River and Harbour Laboratory (VHL) and, via Professor G. Moe, from the Norwegian Institute of Technology's fund. The major part of the work of Part III was financed by the Royal Norwegian Council for Scientific and Industrial Research.

The Norwegian Institute of Technology awarded the author a 5 month scholarship which was invaluable for the writing up of the thesis.

VHL contributed to the costs of writing up the thesis and contributed to the author's higher degree fees.

In addition, thanks are owed to the large number of the author's colleagues and to other individuals who have rendered him help.

The author's senior supervisor, Professor D. J. Johns of Loughborough University, gave the author stimulation and encouragement and showed considerable patience with the author throughout the course of the work.

Mr. Michael Prosser, the author's local supervisor at BHRA, was always willing to advise and to discuss problems with the author. The author is indebted to Professor Geir Moe, the author's supervisor at VHL, without whom the experiments of Part III would never have been begun, and who rendered invaluable help in obtaining funding.

The author is particularly grateful to Mr. George Young, without whose efforts the author would not have been able to go to Norway, and to Dr. Alf Tørum, the author's department head at VHL, who gave his continual support to the work.

The various experimental rigs used were built by John Sheehan,

Svein Refseth and Johan Rechsteiner. Ivar Dybvik designed and built some of the specialized instrumentation. Bjørg Reite provided the author with programming advice and Solveig Hasselvold helped with the preparation and routine running of the programs developed. The flow visualization photographs were carefully prepared by Birger Larsen.

Finally, the author is indebted to Elin Falck, who, with the greatest care and patience, typed this thesis - a foreign subject in a foreign language.

CONTENTS

CONTENTS cont.

CONTENTS cont.

CONTENTS cont.

CONTENTS cont.

CONTENTS cont.

CONTENTS cont.

CONTENTS cont.

CONTENTS cont.

CONTENTS cont.

NOMENCLATURE

The main nomenclature is defined below. Some additional nomenclature is used in certain short sections and is fully defined therein.

All the various force coefficients are defined first, followed by the remaining nomenclature.

Force coefficients

C_a = Time dependent 'added mass' coefficients

CA = Time averaged 'added mass' coefficient

CA_{cyl} = Time averaged mass coefficient due to the mass and buoyancy of the cylinder

CA_o = Time averaged mass coefficient for the pendulum rig with no cylinder attached

CA_t = Total time averaged mass coefficient for the pendulum rig with a cylinder attached

C_D = General drag coefficient

C'_D = Unsteady drag coefficient due to vortex shedding forces

$\tilde{C}_D$ = Fourier-averaged oscillatory drag coefficient given by equation (9). Equivalent to CDIND' and CDIND

$\tilde{C}'_D$ = Fourier-averaged oscillatory drag coefficient based on equation (11). Equivalent to CDDEP

$\bar{C}_D$ = Fourier-averaged steady drag coefficient given by equation (8). Equivalent to STCDIND

$\bar{C}'_D$ = Fourier-averaged steady drag coefficient based on equation (11). Equivalent to STCDDEP

C_{D1} = Time dependent steady drag coefficient given in equation (22)

C_{D2} = Time dependent oscillatory drag coefficient given in equation (22)

C_{D3} = Time dependent drag coefficient given in equation (21)

C_{DCRIT} = Critical drag coefficient

CDDEP = Equivalent damping time averaged oscillatory drag coefficient based on equation (21)

CDIND = Equivalent damping time averaged oscillatory drag coefficient based on equation (22)

$CDIND_o$ = Value of CDIND obtained for pendulum rig with no cylinder attached

$CDIND_t$ = Total value of CDIND obtained for pendulum rig with a cylinder attached

$CDIND_{visc}$ = Value of CDIND obtained for Stokes' viscous force

CDIND' = Fourier-averaged oscillatory drag coefficient based on equation (22)

$CDIND'_o$ = Value of CDIND' obtained for pendulum rig with no cylinder attached

$CDIND'_t$ = Total value of CDIND' obtained for pendulum rig with a cylinder attached

C_L = General lift coefficient

C_L^o = Lift coefficient on a stationary cylinder

C_M = General inertia coefficient

CM = Fourier-averaged inertia coefficient = (1+CA)

CMAXOSC = Maximum combined oscillatory drag and inertia coefficient given by equation (44)

C_{P180} = Base pressure coefficient

CRATIO = Ratio between total force compared to that calculated using equation (23), given by equation (45)

STCDDEP = Time averaged steady component of drag coefficient based on equation (21)

STCDIND = Time averaged steady component of drag coefficient based on equation (22)

a = Velocity ratio ($V/\dot{x}_o$). Also length of cylinder over which vortex shedding occurs (Part II)

b = Linear spring constant

B = Buoyancy mass. Also coefficient defined in equation (9') of Appendix 2.1

c = General linear damping coefficient. Also plate length

c_{crit} = Critical linear damping coefficient

$\bar{c}_{cyl}$ = Averaged linear damping coefficient per unit length due to the cylinder. (Pendulum rig)

$\bar{c}_{press}$ = Averaged linear damping coefficient per unit length, Stokes' viscous damping subtracted. (Pendulum rig)

$\bar{c}_{visc}$ = Averaged linear damping coefficient per unit length due to Stokes' viscous damping. (Pendulum rig)

C = General rotational damping factor

C_{cyl} = Cylinder part of rotational damping coefficient

C_o = Residual part of rotational damping coefficient. (Pendulum rig)

C_{sw} = Rotational damping coefficient in still water (Part II)

C_t = Total rotational damping coefficient. (Pendulum rig)

C_{visc} = Rotational damping coefficient due to Stokes' viscous damping

d = Water depth

D = Cylinder diameter

D.M.F. = Dynamic magnification factor

e = Roughness height

E = Coefficient defined in equation (13') of Appendix 2.2

f = General force per unit length

f_{cyl} = Cylinder part of force per unit length measured. (Pendulum rig)

f_o = Residual part of force per unit length measured. (Pendulum rig)

f_t = Total force per unit length measured. (Pendulum rig)

f_r = Frequency ratio between lift frequency and oscillatory or wave frequency

F = General total force

$F_{cyl}^{(1)}$, $F_{cyl}^{(2)}$, $F_{cyl}^{(3)}$ = Force due to cylinder oscillating in various ways (Part III, chapter 7)

F_o = Amplitude of sinusoidal force input

$\bar{F}_{cyl}$ = Cylinder part of steady component of force. (Pendulum rig)

$\bar{F}_o$ = Residual part of steady component of force. (Pendulum rig)

$\bar{F}_t$ = Total steady component of force. (Pendulum rig)

h = Distance from centre of rotation to cylinder centre. (Pendulum rig)

H = Wave height

i = Incremental integer

I_{cyl} = Moment of inertia due to cylinder

I_a = Moment of inertia due to added mass of water

I_o = Moment of inertia of pendulum rig with no cylinder attached

I_t = Moment of inertia of pendulum rig with cylinder attached

k = $2\pi/\lambda$. Also a constant

k_D = $.5\rho D(CDDEP)$

k_L = $.5\rho D\ C_L$

k_s = Stability parameter = $\frac{2m\delta}{\rho D^2}$

k'_s = Modified stability parameter = $\frac{2m\delta}{\rho D^2\ C_L^o}$

K = Keulegan-Carpenter number = UmT/D

K_D = $.5\rho D(STCDDEP)$

L = Cylinder length

m = Mass per unit length of cylinder

m_a = Added mass per unit length

M = Total cylinder mass

M_R = Rotational stiffness of pendulum rig

n = Cylinder natural frequency. Frequency of oscillation of pendulum rig with cylinder attached

n_{lift} = Frequency of lift forces

n_o = Frequency of oscillation of pendulum rig with no cylinder attached

n_v = Vortex shedding frequency

n_w = Wave frequency

p_i = i'th coefficient of amplitude of sinusoidal force input to cylinder in waves (Part II, chapter 5.6)

P = Complex force input to cylinder in waves (Part II, chapter 5.6)

r = Integer - fully defined in Part II, chapter 2.1

R = Reynolds number, VD/ν

R_x = RMS value of difference reaction in-line with direction of wave propagation (Part II)

R_y = RMS value of difference reaction perpendicular to direction of wave propagation (Part II)

S = Strouhal number, $n_v D/V$

t = General time, incremental time step

t_1 = Instant in cycle when $\dot{x} = V$

T = Wave or oscillatory period

T_v = Vortex shedding period $(1/n_v)$

U = General time varying flow velocity

U_{inst} = Instantaneous velocity in wave flow over stationary cylinder

U_m = Velocity amplitude in wave or oscillatory flow

U_o = Free stream velocity, value dependent on longtitudinal position

U_{rel} = Instantaneous relative velocity $(U-\dot{x})$

$\dot{U}$ = Instantaneous flow acceleration

V = Steady flow velocity

V_{inst} = Instantaneous relative velocity (Part III)

x = Distance in longtitudinal direction. Instantaneous deflection of cylinder in pendulum rig

x_o = Amplitude of cylinder oscillation in flow direction

x_{rms} = RMS value of in-line vibrations in waves

$\dot{x}$ = Instantaneous velocity of cylinder in pendulum rig

$\dot{x}_o$ = Velocity amplitude of cylinder in pendulum rig

$\ddot{x}$ = Instantaneous acceleration of cylinder in pendulum rig

y = Instantaneous deflection of cylinder in cross-flow direction (perpendicular to flow direction)

y_o = Ampltiude of cylinder oscillation in cross-flow direction

y_{rms} = RMS value of cross-flow vibrations in waves

$\dot{y}$ = Instantaneous cylinder velocity in cross-flow direction

$\ddot{y}$ = Instantaneous cylinder acceleration in cross-flow direction

z = Distance along a cylinder

Z = Coefficient (see Part III, chapter 7)

α = Separation angle, measured from front stagnation point. Also phase angle

β = Viscous parameter, $nD^2/\nu = R/K$

γ = Defined in Part II, chapter 3.1

δ = General damping logarithmic decrement

δ_o = Logarithmic damping of pendulum rig with no cylinder attached

δ_{st} = Structural logarithmic damping (Part II)

δ_{sw} = Logarithmic damping of cylinder in still water (Part II) $(= \delta_{st} + \delta_{visc})$

δ_t = Logarithmic damping of pendulum rig with cylinder attached

δ_{visc} = Logarithmic damping due ot Stokes' viscous forces on a cylinder

Δ = Boundary layer thickness

η = Dynamic viscosity

θ = Instantaneous angular deflection. Phase angle

$\dot{\theta}$ = Instantaneous angular velocity

$\ddot{\theta}$ = Instantaneous acceleration

λ = Wave length

ν = Kinematic viscosity

ρ = Fluid density

ϕ = Phase angle

ω = General frequency, Rads/s

ω_i = Input frequency, Rads/s

ω_n = Natural frequency, Rads/s

INTRODUCTION

The past thirty years has seen an immense development in the offshore oil industry. The first major area of offshore oil activity was the Gulf of Mexico, where the conditions may be characterized as relatively shallow water and calm seas interspersed with hurricanes. The present area of most major advancement is undoubtedly the North Sea, where the placement of platforms is extending the limits of depth and, particularly, of severity of environmental conditions. The combination of rapid expansion, advancement into increasing depths, severity of environment, and more stringent design and safety regulations has led to a massive research effort into the design, and the assessment of the short and long term reliability, of platforms. With respect to design and safety regulations it is interesting to note that of 200 mobile drilling rigs constructed in 1950-1970, over 10% collapsed and a further 20% suffered severe fatigue failure of structural members (King (1974)). There are three major steps in the design of platforms, involving firstly, the long term prediction of environmental conditions, secondly, the estimation of the forces associated with these environmental conditions and thirdly, the determination of the effects of these forces on an intended structure and its ability to survive the expected extreme environment.

Design has in the past been in terms of determining the worst conditions likely to occur in a given long time period, typically 100 years, estimating the forces due to these conditions and ensuring that the structure can stand up to these. This analysis was generally sufficient for the Gulf of Mexico, however the combined effects of deepening water and lengthening vertical members, causing structural natural frequencies to approach wave loading frequencies, and the more severe conditions of the North Sea, which last over long periods of time, has led to the necessity of conducting sophisticated dynamic and long term fatigue analyses. In this respect it is interesting to note that the collapse in 1961 of the Texas Towers platform occurred in waves only one third of the maximum that the structure had been designed to withstand, and was due to the lowering of the platform fundamental frequency due to the failure of some members. (Wiegel (1972).)

The task of designing for environmental loadings is thus one of the most important and exacting in the offshore field today.

As has been briefly mentioned, of particular importance are vibration and fatigue problems. These apply both in terms of the movement of the platform as a whole at its fundamental frequency, and in terms of vibrations of individual slender members at their natural frequencies.

Direct excitation of the platform fundamental frequency by high frequency waves or by higher harmonics of the wave forces introduced by non-linear effects may occur. It is then necessary to determine the damping of the system in order to evaluate the response. There are three major damping effects, due to internal damping, damping in the foundations and surroundings and damping due to the structure's movement in the fluid surrounding it. This last is considered to be the most important for structures in deeper water, (Penzien (1975)), and at the same time is that which has been least investigated.

Excitation of slender circular members by vortex shedding in currents or waves may occur. Collapse due to vortex excited vibrations in currents is known to have occurred, for example at the Immingham oil terminal, (Wootton, et al. (1972)), and considerable research effort has been directed towards determining the causes of current induced vibrations and the conditions under which they may occur. In waves, on the other hand, little research effort has yet been directed to the problem of possible vortex induced vibrations even though fatigue failure of members is known to have occurred. For example, an experimental pile investigated by Wiegel et al. (1957) collapsed due to structural fatigue failure which the authors attributed to periodic vortex shedding forces. Risers on jacket type platforms are particularly suspectible to oscillation, although collapse has not, as far as the author is aware, been reported.

It is interesting to note the views of a major oil company involved in the North Sea, who consider (Vugts and Hayes (1979)) that the estimation of damping of platform vibrations is one of the most important, and at the same time one of the least known, factors in offshore platform design.

Another important unknown in platform design is the effect of

simultaneously applied waves and currents. The fluid kinematical side of the problem has been investigated to a considerable extent and the structural response calculations are now standard, however there has so far been virtually no research into the magnitude of the forces acting on structures due to this complex flow.

The first investigation of this thesis is concerned directly with the problem of vibrations of slender cylindrical members in waves. The second investigation involves a more fundamental investigation into the forces on cylinders oscillated in line with a current, the results of which may be applied to problems of the damping of vibrations in waves or currents, or forces due to combined waves and currents.

PART I - LITERATURE SURVEY AND INTRODUCTORY DISCUSSION OF WORK APPERTAINING TO THE THESIS

INTRODUCTORY COMMENTS

In this Part is presented a literature survey and general introductory description and discussion of topics relevant to the experimental work undertaken and described in Parts II and III. In this description the phenomena associated with flow around a cylinder are discussed for flows of various complexity from steady flow around a stationary cylinder to wave flow around an oscillating cylinder. The author has chosen to cover rather an extensive range of topics, firstly, in the belief that a thorough knowledge and understanding of previous investigations is a prerequisite to sucessful research, and secondly, because a large range of topics seems, to the author, to be relevant to the work.

The literature survey naturally emphasizes the work which has been of particular interest or importance to the author, and reflects the author's personal preferences and approaches, and is not an attempt to present the literature from a detached, historical perspective.

1. STEADY FLOW AROUND A CYLINDER

1.1. Brief history of the origin

It is extremely difficult to determine where or when the particular field of fluid dynamics that may be called steady flow about an object started. Indeed it is difficult to define exactly what one means by 'started' - from the earliest times one must have been aware that there are forces associated with a flow around a body, however an understanding of the problem and a mathematical formulation were not available until the 19th century. The parameters which are most intimately associated with fluid flow around a body are the Reynolds number and Strouhal number, and it is perhaps useful to trace the origins of these parameters.

The equations of motion of a viscous fluid were developed by Navier (1827), Poisson (1831), Saint-Venant (1843) and Stokes (1845). Stokes (1851) appears to have been the first to have recognized that Reynolds number is the parameter that determines the flow field within given boundaries. Strouhal (1878) noted that the frequency of Aeolian tones from a wire was dependent upon the flow velocity and not the wire's physical properties, and Rayleigh (1879) pointed out that the Strouhal number, describing the relationship between the tones, the flow and the wire diameter, should be a function of the Reynolds number (which was not at the time yet named). Reynolds (1883) conducted experiments on the onset of turbulence in flow through tubes, and his name has been given to the major parameter of dependence found. From that time onwards there were gradually more and more contributions to the field, but probably the greatest single contributions were the introduction of the concept of the boundary layer by Prandtl (1904), and the theory of the vortex street, Kármán (1911). An interesting history of boundary layer theory is given by Tani (1977).

1.2. The relationship between flow and Reynolds number

The Reynolds number, $R = VD/\nu$, where V = flow velocity, D = diameter and ν = kinematic viscosity, is the most important parameter describing the flow around a cylinder, and may be regarded as describing the relative magnitudes of inertia and viscous forces. In Fig. 1 flow patterns for various ranges of R are sketched.

1.2.1. Low Reynolds numbers

At values of $R \ll 1$ the dominant process is the diffusion of vorticity away from the body. Stokes (1851) solved the Navier-Stokes equation, neglecting inertia forces, and obtained the well known relationship $C_D = 24/R$ for a sphere. Experimental results, Castleman (1925), showed that Stokes' equation gives the drag accurately up to $R \approx 1$. Oseen (1910) modified the equations by taking into account inertia forces, and his value of drag coefficient is found to agree with experimental results up to slightly higher values of R. Stokes' equations lead to a purely symmetric flow around the body, whereas Oseen's lead to a parabolic area of vorticity behind the cylinder. The flow for $R \lesssim 1$ is sketched in Fig. 1a.

As Reynolds number is increased above 1 a number of phenomena occur which have been investigated both experimentally and numerically. At low R (< 45), Thom (1933), Kawaguti (1953), Apelt (1961) and Keller and Takami (1966) used finite difference numerical solutions to the complete Navier-Stokes equations. Very good agreement between the results and experiments (for example those of Tritton (1959)) was obtained, however the method is limited to $R \lesssim 100$ by computer storage and processing time.

For R = 10 ~ 40 a pair of recirculating vortices occur behind the cylinder, their length increasing with increasing R (Fig. 1b). Beyond the vortices the wake is straight and narrow. Taneda (1956) has measured the length of the vortices which increases linearly with R. The vortices first appear at $R \approx 6$. More recently, Coutanceau and Bouard (1977) have investigated this area numerically for a

steady flow and also for an impulsively started flow. At R = 30 ~ 50 the flow becomes unstable for small disturbances which first affect the wake downstream (Fig. 1c). By R ≈ 50 the oscillations have moved to the cylinder and affect the two standing vortices (Homann (1936a)).

The form of the wake oscillations in the area R = 50 ~ 150 is the classical von Kármán wake consisting of two rows of laminar vortices of opposite sign, as in Fig. 1d, the first photographs of which were produced by Ahlborn (1902). Von Kármán (1911) produced a theory of the vortex street for this range of R, and Roshko (1955) refers to this range as the 'stable' region. The vortices are viscous and diffuse by viscous diffusion, velocity spectra in the wake showing the characteristic wake frequency and a gradual loss of energy moving down the wake with no transfer to other frequencies. In this range Kovasznay (1949), and Roshko (1955) have accurately measured the Strouhal number, $S = n_v D/V$, where n_v = frequency of shedding of pairs of vortices which Roshko gives as $S = .212 (1-21.2/R)$.

In the region R = 150 ~ 300 there is a transition region to what Roshko terms the 'irregular range', but which is more normally referred to as the subcritical regime. This regime lasts up to the beginning of the critical regime, somewhat above $R \approx 10^5$, and is sketched in Fig. 1,e, and is described more fully in the following section.

1.2.2. High Reynolds numbers

It might be expected that for R >> 1 the fluid could be treated as inviscid and visous terms dropped from the equations of motion. This is not, however, the case because a real fluid, of even very small viscosity, behaves very differently to a hypothetical non-viscous fluid at a boundary, obeying the no-slip condition. This fact can alter the whole flow radically. The no-slip condition causes a thin layer of fluid near the solid boundary, known as the boundary layer, to be formed, the fluid velocity varying from zero at the solid boundary to the external stream value through this thin boundary layer, the thickness of which $\to 0$ as $R \to \alpha$. In this layer viscous

effects are significant, but outside it the viscous effects are negligible.

The most important single phenomenon associated with the boundary layer is its separation which occurs whenever there is an appreciable fall in the velocity of the external stream. On a cylinder, separation occurs from the sides and the pressure on the rear face of the cylinder is approximately equal to that just outside the boundary layer at separation, which is low due to the higher velocity here compared to the free stream. Near the front of the cylinder the pressure is higher, being nearly stagnation pressure, and thus there is a net force on the cylinder which is of the order of $.5\rho D\ V^2$, per unit length, leading to a steady drag coefficient defined by

$$C_D = \frac{\text{Drag force/unit length}}{.5\rho D\ V^2}$$

There are a large number of experimental results for C_D, as well as other quantities, for $R = 300 \simeq 10^7$. Representative curves for C_D, the pressure drag coefficient, C_{DP}, the base pressure coefficient, C_{P180}, the separation angle, α, and the Strouhal number, S, as functions of R are shown in Fig. 2. These curves are evidently very strongly interrelated and may be characterized by four distinct ranges or 'regimes', known as the subcritical regime where C_D is nearly constant, the critical regime where C_D suddenly drops to a very low value, the supercritical regime where C_D rises again, and finally the transcritical regime where C_D is once again nearly constant. In Fig. 3 characteristic pressure distributions for the regimes are shown, and in Figs. 1e, f, g and h are sketched flow patterns representing each regime.

Reviews of the characteristics of the flow in these regimes are given by Morkovin (1964), Batchelor (1970), Goldstein (1957) and Berger and Wille (1972).

Amongst the first to achieve Reynolds numbers up to critical were Relf (1914) and Prandtl (1914) and amongst other notable contributions to values of C_D are those of Wieselberger (1921, R up to 9×10^5), at Gottingen (1923, R up to 8×10^5), by Delaney and Sorensen (1953, R up to 5×10^6), Roshko (1961, R up to 10^7), Schmidt (1966, R up to 5×10^6), Achenbach (1968, R up to 5×10^6), and Jones (1969,

R up to $2x10^7$).

Pressure distributions, the base pressure coefficient and the pressure drag coefficient have been provided by, amongst others, Hiemenz (1911), at Gottingen (1923, R up to $8x10^5$), by Flachsbart (1932, R up to $9x10^5$), Dryden and Hill (1930, R up to $4x10^6$), Fage and Falkner (1931, R up to 10^6), Roshko (1961, R up to 10^7) and Jones (1961, R up to $2x10^7$).

Strouhal numbers have been measured by Relf and Simmons (1924, R up to $8x10^5$), Kovasznay (1949, R up to 10^4), Delaney and Sorensen (1953, R up to $2x10^6$), Roshko (1961, R up to 10^7), and Jones (1969, R up to $2x10^7$).

Separation angles can be obtained from experiments where pressure distributions are given.

Skin friction drag coefficients can be obtained from the difference between C_D and C_{DP}, in addition, direct measurements have been conducted by Schiller and Linke (1933, R up to $4x10^4$), Fage and Falkner (1931, R up to 10^6), and Achenbach (1968, R up to $5x10^6$).

It should be mentioned that the understanding of the various regimes owes much to the work of Roshko (1955, 1961, 1969).

The characteristics of the various regimes are discussed below.

Subcritical Regime

The subcritical regime lasts from $R \approx 300$ to $R \approx 2x10^5$, and is characterized by laminar separation, a transition to turbulence a fairly small distance downstream from the separation point and tubulent vortices. C_D, C_{DP}, S, and α are virtually constant throughout this regime. Schiller and Linke (1933) showed that the transition to turbulence occurs progressively nearer the cylinder as R is increased, occuring 1.5 diameters downstream at R = 3500 and 0.7 diameters at R = 8500. Roshko (1955) showed that the wake was entirely turbulent by 40~50 diameters downstream and that the Strouhal number could be expressed as $S = .212(1-12.7/R)$ for $R = 300 \sim 10^5$.

Thom (1929) estimated that the skin friction coefficient was $4R^{-1/2}$ throughout the subcritical regime, this being confirmed by Schiller and Linke (1933) for R up to $4x10^4$.

Critical Regime

As R is increased through the subcritical regime the transition from laminar to turbulent flow in the shear layers emanating from the separation points moves towards the cylinder. Eventually the transition occurs so soon after separation that the boundary layer, which is now turbulent and can withstand a higher pressure gradient, reattaches to the cylinder, and a second, turbulent, separation occurs further round the cylinder. The regime is thus characterized by so called 'separation bubbles', between the first separation and the reattachment, by a large separation angle (up to 140^{o}), a narrow wake, a low value of critical drag coefficient, C_{DCRIT}, and a high value of S.

The separation bubbles were first noted by Bursnall and Loftin (1951). The low value of C_{DCRIT}, (and the other characteristics of the regime), are wholly dependent on the formation of the separation bubbles, which are fairly unstable and can easily be disturbed by any free stream turbulence, roughness on the cylinder, etc. (as will be discussed in subsequent sections). The exact value of R at which the critical regime is found, and the exact value of C_{DCRIT} are similarly dependent on these small effects. Bearman (1969) showed that with very careful experimentation the regime could be delayed, the drop in C_D occuring more abruptly and the minimum value, C_{DCRIT}, being particularly low.

The critical regime is thus not, as Prandtl (1914) suggested, caused by the transition from laminar to turbulent flow in the boundary layer before separation.

Supercritical Regime

As R is further increased, to about $6x10^5$ on a smooth cylinder, turbulence begins to occur so early that the separation bubbles are not formed. This first occurs at individual points along the cylinder, particularly where there are any minute surface defects, and so called 'turbulent wedges' are formed. Gross three dimensionality is produced, well correlated periodic vortex shedding ceases and

there is just a vague, highly turbulent wake. Again the disturbance to the bubbles is very dependent upon surface conditions, free-stream turbulence, vibrations, etc., which can instigate the turbulent streaming. As the bubbles are no longer formed the separation angle decreases and C_D increases again.

Transcritical Regime

By about R = $3x10^6$ the process of destruction of the separation bubbles is complete, transition to turbulence occurs in the boundary layer before separation, and one returns to a situation rather like the subcritical, but with turbulent separation. Regular vortex shedding occurs, separation occurs later and C_D is less (compared to the subcritical), - all as foreseen by Prandtl (1914). In the transcritical regime C_D, α, C_{DP}, C_{P180}, S, etc., reach nearly constant values.

In this regime the frictional drag coefficient is higher, Achenbach (1968), as the boundary layer is turbulent, however it is still no more than 1% of the total drag coefficient and can normally be ignored.

Numerical work at high Reynolds numbers

The finite difference numerical solution of the full Navier-Stokes equations is too complicated and time consuming to be applied to values of R much above 100. This solution includes viscosity over the whole flow field, whereas this is unnecessary outside the boundary layer. In any case, for R $\gtrsim$ 300 turbulence appears in the wake downstream of the cylinder, and so the solution could not be applied for higher values of R without introducing models of turbulence. For high R, therefore, potential flow models based on the vorticity equation are used, which has the advantage that viscosity is not involved. Vorticity is most often modelled by point vortices, and this method was first used by Rosenhead (1931) to predict the rolling up of a vortex sheet. The method was also used by Abernathy and Kronauer (1962) to investigate the interactions between two parallel

lines of vortices. Similarly Gerrard (1967), Sarpkaya (1968), Laird (1971) and others have investigated the flow behind a cylinder, Gerrard was particularly interested in lift forces, and Sarpkaya in an impulsively started flow.

Clements (1973) used the method for the flow behind a rectangular cylinder (where the separation points are fixed), and Chaplin (1973) extended Laird's work, where the boundary layer was also modelled by discrete vortices, obtaining fairly good values of C_D and C_L. More recently Stansby (1977, 1978) has used the method for a variety of flows. Laird (1971) conducted a particularly simple and, in this author's opinion, explanatory investigation into vortex shedding from a cylinder. He showed that a vortex forming on one side of the cylinder will reduce the circulation at some point on the shear layer emanating from the other side, a shear layer with a weak point will tend to break there, and the free end of a shear layer tends to roll up into a vortex.

One major problem with the method is to decide where to introduce vorticity into the flow, which is related to the separation point (the boundary layer connot be modelled precisely because of its dependence on viscosity and the non-inclusion of viscosity in the method). In earlier work some rather doubtful assumptions were made (e.g. fixing separation at 90°), but more recently numerical work has tried to mate an investigation of the boundary layer equation to separation with the discrete vortex model. Sarpkaya (1979) outlines such a numerical method which is detailed in Sarpkaya and Schoaff (1979a). With this model Sarpkaya has managed to reproduce experimental results for all the characteristics of the flow (C_D, C_L, S, separation angles, vortex street configuration, etc.) for an impulsively started flow continued to very large times. He also gives a qualitative description (based on the model) of how the interaction of the shear layers, base pressure and diffusion and dissipation processes lead to alternate vortex shedding. The model has also been applied to a cylinder oscillating in a steady current, Sarpkaya and Schoaff (1979b), to be discussed in a later chapter.

Unsteady lift and drag

The alternate shedding of vortices from a cylinder in a flow produces unsteady forces on the cylinder at the vortex shedding frequency in the lift direction (perpendicular to the flow), and at twice this frequency in the in-line direction (parallel to the flow), (McGregor (1957)). A number of investigations have been directed towards determining the magnitudes of the coefficients associated with these forces. There is considerable spread in the results, partly due to the fact that the forces are very dependent on the correlation length of vortex shedding, which is again dependent upon end-effects, cylinder length, free-stream turbulence, any shear in the flow, etc.

The coefficients are non-dimensionalized in the same way as the drag force and are termed C_L and C_D' for the unsteady lift and drag, respectively. In Fig. 4 are shown various results for C_D' and C_L as functions of R.

McGregor (1957) and Gerrard (1961) showed that for $R = 10^4 \sim 10^5$ C_L is an order of magnitude greater than C_D'.

Amongst other investigations are those by Fung (1960, R up to 2×10^5, rms values of C_D' and C_L), Humphreys (1960, R up to 5×10^5, C_L only), Glenny (1966, R up to 2×10^6, C_L only) and Jones (1969, R up to 2×10^7, C_L only).

In very carefully conducted experiments, Bishop and Hassan (1964a, R up to 10^4) showed the strong inter-relationships between C_D, C_D' and C_L. They found that these coefficients all varied in a related way with time even for a constant stream velocity.

Effects of roughness

In Fig. 5 are shown representative curves of C_D versus R for various roughnesses. It has already been seen that roughness disturbs the separation bubbles characteristic of the critical regime. The first major investigation of roughness effects was by Fage and Warsap (1929) who showed that roughness promotes the transition from laminar to turbulent flow and causes the critical regime to occur

earlier and C_{DCRIT} not to be so low. They also investigated the effects of small diameter wires placed at various angles to the front stagnation point, and found that even a wire of diameter as little as 3% of the boundary layer thickness, placed at 65° to the front stagnation point, greatly affected the flow and C_D. Achenbach (1971) found that, for large enough roughnesses, transition from laminar to turbulent flow occurred in the boundary layer before separation, and no separation bubbles were obtained (as Prandtl (1914) suggested), and Roshko (1970) tentatively explained the increasing values of transcritical C_D with increasing roughness as being due to thickening of the boundary layer.

Szechenyi (1975), in tests with R up to $6x10^6$, showed that for R above the critical value, C_D was dependent on the roughness Reynolds number, where the roughness height, e, replaces diameter in the Reynolds number. He showed that a smooth cylinder behaved as if it had a roughness of $e/D = 3.5x10^{-5}$, and obtained the Strouhal number as a function of the roughness Reynolds number. More recently Miller (1977) has investigated roughness effects for R up to $6x10^6$ and included very rough cylinders. His results are in good agreement with, and extend, Szechenyi's.

Effects of free stream turbulence

A number of investigations have been conducted into the effects of free stream turbulence, however none, to the author's knowledge, in the transcritical regime. Fage and Warsap (1929) showed that increased turbulence causes the critical regime to occur at lower R and to extend over a rather larger range of R, but hardly affects the values of C_D. Taylor (1936) showed that both turbulence intensity and scale should alter the value of R at which the critical regime occurs. Schubauer (1937) showed that increased turbulence intensity causes earlier transition from laminar to turbulent flow in the boundary layer. Ko and Graf (1972) investigated experimentally the effects of turbulence scale and intensity for R up to $8x10^3$ and found that both, but particularly intensity, had an effect. An intensity of 21% of the free stream velocity raised the drag coefficient by 25% compared to the turbulence free value.

Surry (1969) has investigated the effects of turbulence on the unsteady coefficients C_D' and C_L.

Correlation lengths of vortex shedding

The shedding from a cylinder and the unsteady lift and drag forces are not correlated over the whole length of the cylinder, but rather the shedding occurs in cells, the length of which varies with R, cylinder roughness, turbulence, cylinder vibration, etc. In general the correlation length decreases with increasing R, and, according to Gerlach and Dodge (1970), is 15~20 diameters at R = 150 ~ 10^5 and .5 diameter for R $\gtrsim$ 10^5. Humphreys (1960), however, gives the correlation length as 1.56 diameters at R = $2x10^5$. These tests did not, however, go up to transcritical values of R where there is some belief that the correlation length might increase. Small vibrations of a cylinder may dramatically increase the correlation length, particularly if the vibration is of the same frequency as forces from vortex shedding.

End effects

All the previous discussions have been concerned with a nominally two dimensional flow. If a cylinder is relatively short, then the low base pressure will be raised due to flow around the ends of the cylinder and C_D is then reduced and S increased. At Gottingen (1923) the effects on C_D of lengths of cylinder to diameter ratios L/D from 1.0 to 40 were investigated for R = $8.8x10^4$. Benard (1907) suggested that for L/D $\gtrsim$ 27, and Gowda (1975) for L/D $\gtrsim$ 45 one would obtain freedom from end effects. End plates can also be used on shorter cylinders to produce two dimensional flow. Gowda (1975) found that for a cylinder with L/D = 18 it was necessary to have plates with a diameter of at least 10 cylinder diameters to avoid end effects on the vortex shedding frequency. Stansby (1974) found that end plates of about 5 cylinder diameters would give essentially two dimensional base pressure measurements.

2. SIMPLE TIME-DEPENDENT FLOWS

The foregoing sections have emphasized the relationship between the form of the wake, which is dependent on the separation and vortex shedding processes, and the values of C_D, S, etc., in a steady flow over a stationary cylinder. This thesis is basically concerned with unsteady flows, particularly those where flow reversal occurs. As a first step towards these flows this section will consider simple time dependent flows, where flow reversal does not occur.

Blasius (1908) first analysed the problems of impulsively started flow and steady accelerated flow around a cylinder, and determined that separation would first occur at the rear stagnation point and after the cylinder had travelled a distance of .176 diameters for an impulsively started flow, and .26 diameters for a steady accelerated flow.

Rubach (1914) and Prandtl (1927) have conducted photographic studies of the flow about impulsively started and steady accelerated cylinders. In Fig. 6 sketches of the flow at progressive time instants in a steady accelerated flow from rest are shown, from Schlichting (1979). In the initial instants of the flow the pattern is shown in Fig. 6,a. Separation occurs at the rear stagnation point when the cylinder has travelled about .26 diameters, and the separation points then move progressively forward and a pair of vortices builds up symmetrically behind the cylinder, as in Fig. 6,b,c,d and e. Eventually, if $R \gtrsim 50$, one of the vortices grows more than the other and is subsequently shed, followed by the other vortex, as in Fig. 6,f. Thereafter vortices grow and shed from alternate sides of the cylinder.

Experiments have shown that for impulsively started flow the first vortex is shed after the cylinder has travelled about 3 diameters (Sarpkaya (1968)), whereas for steady accelerated flow the value is 4.8 diameters (Sarpkaya (1963a, 1963b)). These first vortices are considerably larger and contain more circulation than subsequent vortices. Furthermore, the drag coefficient at about this time is larger then the appropriate steady flow value, by about 30% for an impulsively started flow.

Asher and Dosanjh (1968) have investigated impulsively started flows for values of R up to 2×10^5.

In other experiments by, for example, Iversen and Balent (1951) and Laird (1956), the total force on a cylinder in steady accelerated flow is determined as a function of a single parameter, known as the Iversen modulus, $\frac{\dot{U}D}{U^2}$, where U and $\dot{U}$ are fluid velocity and acceleration.

Pressure distributions around a cylinder at various instants after an impulsive start were measured by Schwabe (1935), who also found that the maximum value of C_D was about twice the steady value.

Honji and Taneda (1969) considered cylinders accelerated from one velocity to another, and Tatsuno and Taneda (1971) considered cylinders decelerated from one velocity to another. However, in both these cases the Reynolds number was always less than 50.

It is here interesting to quote Sears, as reported by Rott (1964), who also considered an impulsive change from one steady velocity to another steady velocity. He showed that

"the initial motion following any impulsive change of the boundary conditions consists of the superposition of the velocity pattern existing just before the change and the inviscid flow velocity pattern due to the impulsive boundary values (together with the corresponding infinitely thin wall vortex sheets)".

Sarpkaya (1976a) adds:

"In other words, at the initial instants of the impulsive change C_D is equal to its steady state value and $C_M = 2$. As time progresses neither C_D nor C_M remains the same, and changes with the changes in the flow, ever dominated by the past history and ever affected by the gross features of the current state".

The most important conclusion of this section is that in the flows considered Reynolds number is not sufficient to determine the flow patterns or the drag coefficient (even when neglecting effects due to roughness, free flow turbulence, etc.). In experiments under steady accelaration, Sarpkaya (1963b), the Reynolds number when separation first occurred was 1.24×10^4, and below this value no separation had occurred in evident contrast with predictions from steady flow. The reason for the difference is the effects of limited distance travelled (or time), i.e. the cylinder must travel a sufficient distance for a wake to develop, and unless the cylinder has travelled a long distance at a particular Reynolds number (has been at the Reynolds number for a long time compared to the vortex shedding period) then Reynolds number will not be the most important factor determining the flow patterns and force coefficients.

3. OSCILLATORY AND WAVE FLOWS ABOUT A CYLINDER

A large number of investigations have been conducted into the forces due to pure oscillatory flow or waves, but as yet, in this author's opinion, there have been only three major milestones: the suggestion of an empirical formula to analyse wave forces by Morison et al. (1950) (a milestone because of the extent of its subsequent use); the first correlation of experimental data in oscillatory flow using a new parameter, by Keulegan and Carpenter (1958), and the thorough investigation of the coefficients in oscillatory flow for smooth and rough cylinders and up to very high values of Reynolds number, by Sarpkaya (1976a, 1976b).

The discussion of wave forces will be limited to those on vertical cylinders. The essential difference between wave flows and oscillatory flows is that particle motions in wave flows are elliptical and the motion decays with depth, i.e. the problem becomes three dimensional whereas for an oscillatory flow the particle motion is rectilinear and the flow two-dimensional. Experimental investigations in waves are complicated due to the extra parameters involved and the difficulty in varying parameters independently and over sufficiently large ranges. The major advances in our understanding have been through experiments in oscillating currents, nevertheless eventually the additional problems in waves need to be tackled.

A good introduction to the early work on wave forces on cylinders is given by Wiegel (1964).

Lamb (1945) showed that in the absence of separation the force per unit length of a stationary cylinder in an accelerating fluid can be expressed as

$$f = .25\rho\pi D^2 (1+C_a) \dot{U} \qquad -(1)$$

and that the 'added mass' coefficient C_a takes a value 1.0. In waves it is usual to write $(1+C_a) = C_M$ called the 'inertia coefficient'.

In a steady separated flow of velocity V it has already been shown that the force per unit length of a cylinder is given by

$$f = .5\rho D C_D V^2 \qquad -(2)$$

Morison et al. (1950) suggested that for the wave case, where there is both acceleration and flow separation, the total force could be written as the sum of equations (1) and (2), but that the coefficients C_M and C_D would not have the values associated with an unseparated flow and a steady current velocity, respectively. They thus suggested that the following empirical formula, now known as 'Morison's formula', could be used

$$f = .25\rho\pi D^2 C_M \dot{U} + .5\rho D C_D|U|U \quad \text{per unit length} \qquad -(3)$$

This formula has been used in virtually all investigations since.

It should be noted that the inertia term in equation (3) is basically the sum of two parts which are both proportional to $.25\ \rho\ \pi\ D^2\dot{U}$. The first part, with a coefficient value of 1.0, is the Froude-Krylov force which is the force on the body due to the pressure gradient in the fluid. The second part, with a coefficient value of C_a, represents the forces due to the extra accelerations due to the fluid having to move round the body, Hogben (1974).

Some of the first experimental investigations into wave forces are those by Morison (1951) and Morison et al. (1954). Wiegel et al. (1957) measured forces on a test pile in real waves, their values of C_D and C_M exhibiting order of magnitude scatter. (Amongst other factors due to inability to estimate velocities accurately, wave irregularities, effects of currents, the use of R only in plotting and the fact that their test pile was surrounded by the piles supporting the test platform. Their work provides a good example of undertaking large scale tests, with the associated proliferation of unknown parameters, at a too early stage in the understanding of the problem.) The method used in these three investigations was to determine C_D and C_M at the points in the cycle when the acceleration and velocity were zero, respectively.

3.1. The Keulegan-Carpenter number

In oscillatory or wave like flow, the distance that the horizontal component of fluid travels in one direction before flow reversal occurs is limited. In each half cycle the motion may be thought of as starting from rest, accelerating to a maximum velocity and then decelerating to rest again, the flow then reversing direction and a new flow starting from rest. In a similar way to the impulsive and constant accelerated flows already considered, it is to be expected that the amplitude of fluid motion is an important parameter in determining the form of the wake. (However, vortices or turbulence in the upstream flow remaining from the previous half cycle complicate matters.) Keulegan and Carpenter (1958) realized this and correlated their results for C_D and C_M in an oscillatory flow with respect to a parameter taking this into account. The parameter is now called the 'Keulegan-Carpenter number', K,

$$K = U_m T/D = 2 \pi A/D$$

where U_m = maximum velocity in a cycle, T = period of flow oscillations, and A = amplitude of motion.

Keulegan and Carpenter used a Fourier averaging technique to obtain average values of C_D and C_M over a cycle.

3.2. Dimensional Analysis

Sarpkaya (1976a, 1976b) has defined a lift coefficient, C_L, where

$$C_L = (\text{Maximum lift force})/.5\rho D\ U_m^2$$

and shown that this and the coefficients C_D and C_M in equation (3) are, for a smooth cylinder, dependent upon the following parameters:

$$C_D,\ C_M,\ C_L = f(K,\ \beta,\ t/T)$$

where $\beta = D^2/T\nu$, and t = time.

The parameter $\beta = R/K$, where R is defined with respect to U_m, is the viscous parameter used here.

Usually some sort of time average values of C_D and C_M are used (by the use of Fourier averages or a least squares method), and the last group is dropped.

For a rough cylinder a further group is introduced, e/D, where e is the roughness height.

Isaacson and Maull (1976) showed that for wave motion two additional parameters are needed, kd and kH, where $k = 2\pi/\lambda$, d = water depth, H = wave height and λ = wave length. If diffraction effects and wave non-linearities can be ignored then kH can be dropped.

3.3. Interpretation of the Keulegan-Carpenter number

The parameter K can be considered to represent the ratio of the distance travelled by the fluid to the cylinder diameter. K can alternatively be considered to be proportional to an estimate of the number of vortices shed per flow cycle, or to the ratio of the frequency of vortex shedding to the frequency of flow oscillations. ($K = U_m T/D$. In a current, the frequency of vortex shedding is proportional to V/D, and it is expected that this can loosely be applied to waves also, with V replaced by U_m.)

At low values of K the flow travels only a small distance in one direction, insufficient for separation to occur, before the flow reverses direction. One would expect C_D to be low (neglecting viscous frictional forces) and C_M to take its unseparated flow value, i.e. 2. This is found to be the case, Keulegan and Carpenter (1958).

Similarly, from the work of the previous chapter one would expect that at slightly larger K the flow would travel a sufficient distance before reversal that separation could occur and two symmetric vortices develop. For still larger K there may be a sufficient distance travelled for one vortex to grow asymmetrically and to be shed. At very large K, when the flow travels many diameters before reversal, one could expect many vortices to be shed, alternately, each half

cycle. Thus the flow is rather like the starting flows considered in the preceeding chapter, with K indicating the distance travelled by the cylinder with respect to its diameter before flow reversal destroys the flow and a new, starting type flow starts in the opposite direction. The flow patterns are in fact rather more complicated, particularly for K less than about 30, due to the interaction between vortices developing in one cycle and those from the previous cycle. A fuller description will be given in a later section.

One might expect that, for large values of K, the parameter K would become less important, and the Reynolds number more important in determining the flow. The flow becomes quasi-steady as the period over which the flow velocity changes becomes very large compared to the vortex shedding period, which may be taken to represent the time taken for the flow to adjust to the imposed changes. The boundary layer can also be shown to become quasi-steady for large K.

In chapter 4 it will be shown that a boundary layer behaves quasi-steadily (i.e. behaves at all instants like a <u>steady</u> flow at the instantaneous flow velocity) if

$$\frac{\Delta^2 \dot{U}}{\nu U} \ll 1$$

where Δ = boundary layer thickness, $\dot{U}$ = flow acceleration and U = flow velocity. For a steady boundary layer the thickness is of the order

$$(\frac{\Delta}{D})^2 = \frac{1}{R}$$

from which it can be deduced that the boundary layer is quasi-steady for $D/x_o \ll 1$, i.e. for large K.

3.4. Lift forces in oscillatory and wave flows

Various authors have obtained Fourier components for the lift in terms of the first few multiples of the wave or oscillatory frequency, or have noted the dominant lift frequency which is always an integral multiple of the wave or oscillatory flow frequency.

Sawaragi et al. (1976) obtained K up to 20 in waves and determined the first three Fourier components of lift. Their results are in very good agreement with those of Chakrabarti et al. (1976) who obtained the first five Fourier components of lift in waves for K up to 16. Isaacson and Maull (1976) obtained five coefficients in waves for K up to 22, and Maull and Milliner (1978) obtained six coefficients in an oscillatory flow for K up to about 30. In addition Bidde (1971) and Chang (1964) have given dominant lift forces over various ranges of K in waves, and Sarpkaya (1976a) in an oscillating flow has given the ratio of the dominant lift frequency to the flow frequency, f_r (always an integer), and has calculated $S = f_r/K$, for R up to 10^6 and K up to 200. The results of Isaacson and Maull and Maull and Milliner are reproduced in Fig. 7 and those of Sarpkaya in Fig. 8.

In all the above cases $f_r = 2$ for $6 \lesssim K \lesssim 16$ and $f_r = 3$ for $16 \lesssim K \lesssim 20$. The only results for higher K are those of Sarpkaya (1976a) and these show that f_r increases in steps as K increases in such a way that $S \approx .2$ at low R and $S \approx .3$ at high (transcritical) R. There is no definite value of K where f_r steps from one integer value to the next. For example Sarpkaya (1976a) recorded $f_r = 2$ for values of K up to 18, and $f_r = 3$ for K as low as 14. For a continuous run at, say, K = 16, then some cycles will have $f_r = 2$ and some $f_r = 3$. Sarpkaya has plotted the highest values of K at which a particular value of f_r occurred as a function of R and K for smooth cylinders, and this is reproduced in Fig. 8, and points have also been added for cases where $f_r = 4$ was dominant.

The spectra all show the same trends except that those of Sawaragi et al. (1976) and Chakrabarti et al. (1976) show a dominant lift force with $f_r = 1$ for $1 \lesssim K \lesssim 6$, whereas those of Isaacson and Maull (1976) and Maull and Milliner (1978) show no power at any frequency for $K \lesssim 5$. Bidde (1971) and Chakrabarti (1978) have noted

force traces where $f_r = 1$ for $K \lesssim 5$.

Although particular multiples of the wave frequency are dominant in the lift force over particular ranges of K, it must be emphasized that there are always several frequencies present and that there appears to be a gradual move from one dominant multiple to the next (higher) as K is increased, (see Fig. 7). Further development of this idea will be undertaken in Part II, where a quasi-steady model of the shedding in oscillatory flow will be presented.

3.5. Vortex patterns in oscillatory and wave flows

The agreement between various authors for the dominant frequency of lift forces is not extended to their interpretation of flow visualization experiments conducted to trace vortex movements, even though it is vortex shedding which causes the lift forces. Bidde (1971) claimed to see a von Kármán type vortex street of many vortices at K = 3 ~ 4. It is likely that his visualization technique caused him to confuse general turbulence with vortices shed from the cylinder.

Isaacson (1974) has conducted flow visualization tests by oscillating a cylinder in still water and has shown that, at least for $K \lesssim 25$, the number of vortices shed in a half cycle is generally equal to (f_r-1). This is because the last vortex shed in one half cycle is, at the beginning of the next half cycle, swept over the cylinder and, due to its circulation, increases the velocities and promotes vortex shedding from that same side of the cylinder. Thus for K in the range 6 ~ 15 one vortex is shed in each half cycle, and is shed from the same side in both half cycles. Sarpkaya (1976a) also noted such a phenomenon. Similarly Isaacson showed that for K = 16, two vortices are shed in each half cycle, the last in one half cycle and the first in the next being shed from the same side, such that $f_r = 3$.

Using a discrete vortex model, Stansby (1977) was able to reproduce this effect, though for higher values of K the rule that (f_r-1) = the number of vortices shed per half cycle broke down.

Zdravkovich and Namork (1977), working in waves, showed that

when a vortex is swept back over the cylinder it promotes shedding from the same side, and that the two vortices, of opposite rotation, then move away from the cylinder as a pair. This is illustrated in Fig. 9, taken from their paper. There is no indication in Isaacson's work whether he noted this effect or not. Zdravkovich and Namork noted that at K = 5.4 (shown in Fig. 9), and also for K up to 7.8, the vortex pair formed in the trough half cycle was stronger than that formed in the crest half cycle and considered that the circulation in vortices as the trough is approached is increased due to contraction of vortex lengths. Chakrabarti (1978), in a discussion of this paper, suggested that this leads to a lift force with a frequency equal to the wave frequency, (f_r = 1), as found by Chakrabarti et al. (1976), Sawaragi et al. (1976), and Bidde (1971). f_r = 1 has not been found, to the author's knowledge, in oscillatory flow experiments and Isaacson (1974) does not appear to have observed it in waves.

For K = 9.3 Zdravkovich and Namork (1977) found that one vortex pair moved away from the cylinder in each half cycle, originating from opposite sides of the cylinder in successive half cycles. Chakrabarti (1978) interpreted the pattern to give f_r = 2. From Isaacson and Maull (1976) one would expect one vortex to be shed in each half cycle, always from the same side, and f_r = 2.

Both Sawaragi et al. (1976) and Iwagaki et al. (1976) have indicated that for certain ranges of K the last vortex shed in a half cycle is swept over to the opposite side of the cylinder (to that where it was formed) and back over the cylinder together with the last but one vortex shed (see Fig. 10, taken from Sawaragi et al.) This occurs for K = 8 ~ 13 and K = 20 ~ 26 according to Sawaragi et al. corresponding to f_r = 2 and 3, respectively. From Isaacson (1974) one would expect to see 1 and 2 vortices shed, respectively, per half cycle for these two cases, whereas Sawaragi et al.'s sketches (Fig. 10) show 2 and 3 vortices, respectively. It is to be suspected that the definition of shedding is so vague that there is great difficulty in determining if a vortex was 'shed' or merely began to form. If one compares Isaacson and Maull's sketches for K = 8 (Fig. 11, sketches (IV) and (V)), with Sawaragi et al.'s (Fig. 10, sketch III) one may imagine that they saw similar patterns, but that Isaacson interpreted the second vortex as being only partially

formed and swept back onto the cylinder, whereas Sawaragi et al. interpreted this as the vortex moving across to the other side. Similar observations apply to Isaacson and Maull's sketches for K = 16 (Fig. 11) and Sawaragi et al.'s for K = 20 ~ 26 (Fig. 10, sketch V).

The observations of Iwagaki et al. are similar to those of Sawaragi et al. except that their pattern corresponding to Fig. 10, sketch III occurs at K ≈ 16, rather than K = 8 ~ 13. However Sawaragi et al. defined K as an average value over the length of the cylinder. Furthermore Iwagaki et al. observed a pattern, between those illustrated by Fig. 10, sketches II and III, where the two vortices in one half cycle are formed asymmetrically, but are swept back over the cylinder on their respective sides (K = 6 ~ 12).

Sketches of the flow by Maull and Milliner (1978) for K = 7.7 and K = 21.1 show the same trends as Isaacson and Maull (1976), but with some 'pairing' similar to that of Zdravkovich and Namork (1977).

Bearman et al. (1978) indicate that for K ≈ 15 various effects may occur which might be covered by the varying descriptions above. He states that for K ≈ 15 "only two main vortices are formed per 1/2 cycle and one tends to grow more rapidly than the other, ... At flow reversal the large vortex passes rapidly over one side of the body where it is now of opposite sign to the vorticity being generated there. The induced flow of the reversal vortex helps to give quickly a second large vortex of opposite sign. Where the 2 vortices are of roughly the same strength the pair transport themselves smartly away from the cylinder. At low K vortices sometimes appear to circle the body or, in some cases, nearly all the vortex activity is restricted to either the upper or lower half of the cylinder".

It appears evident that there are some discrepancies in the various flow visualization results, possibly due to different interpretations of patterns, and possibly partly due to differences between wave flows and pure oscillatory flows. No authors have, as yet, directly related flow patterns to lift forces measured.

3.6. Determination of the values of the coefficients C_D, C_M and C_L

Some experiments aimed at determining values of the coefficients have already been mentioned. Rance (1969), using an oscillating water tunnel, determined C_D and C_L on smooth cylinders for R up to 10^6. He assumed $C_M = 2.0$ and calculated C_D at the instant of maximum force. He also indicated that the Strouhal number was constant at 0.2.

Thirriot et al. (1971) determined C_D and C_M as functions of K by oscillating a cylinder in water. They noted that at very low K the value of C_D increased again. Sarpkaya (1976a) refers to this as a second 'peak', however this may be misleading as the value merely rises as K is reduced. The reason for this will become evident from the results of the experiments described in Part III, chapter 9 of this thesis. Sarpkaya and Tuter (1974) and Sarpkaya (1975), using a small U-tube type water tunnel, measured C_D, C_M and C_L at low Reynolds numbers and in a similar tube Maull and Milliner (1978) have measured drag and lift forces. Sarpkaya (1976a, 1976b) has conducted a large number of experiments up to very high values of R (2×10^6) and for K up to 200. He obtained results for C_D, C_M and C_L for smooth and rough cylinders.

Similar high Reynolds number results have been obtained by oscillating cylinders in water by Yamamoto and Nath (1976), for C_D, C_M and C_L and by Garrison et al. (1977) for C_D and C_M, and Løken et al. (1979) have obtained C_D and C_M in an oscillating water tunnel.

Matten (1977) reports tests in large laboratory waves where he compared in-line and lift forces on smooth and rough cylinders. Sarpkaya, in a discussion after the presentation of Matten's paper at the OTC conference, maintained that Matten's results of forces could be accurately predicted using Sarpkaya's (1976b) pure oscillatory flow coefficients distributed over the cylinder according to the local values of K and R. Chakrabarti et al. (1976) conducted tests in waves and measured forces on small unit lengths of a cylinder as well as total forces on the cylinder. Application of the locally obtained coefficients predicted the total forces within 10%. Values of C_D, C_M and C_L for the first five harmonics were pre-

sented as functions of K.

Example results of C_D, C_M and C_L, from Sarpkaya (1976b), are shown in Figs. 12 and 13. It is seen that transition in oscillatory flow starts at a lower Reynolds number and spans a larger range than in steady flow, and the value of C_{DCRIT} is not as low as in steady flow. The turbulence present is probably responsible for the early transition, and the other effects are due partly to the fact that in any one cycle the velocity may vary such that the instantaneous flow is subcritical, critical, supercritical or transcritical at various instants, and partly due to the averaging inherent in the analysis method. From Fig. 13 it is seen that for smooth cylinders the lift coefficient exhibits a maximum at K = 10 ~ 15, and that for very high R, C_L tends to a value 0.2.

3.7. Movement of the separation points in oscillatory flow

Iwagaki et al. (1976) have compared measured flow separation points on a cylinder in waves with a theory based on the velocity distribution in the boundary layer obtained by Iwagaki and Ishida (1974). Iwagaki et al. (1976) also measured pressure distributions around the cylinder and showed the effects of vortex shedding on the pressure distribution.

Grass and Kemp (1978) have conducted experiments oscillating smooth and rough cylinders in water at K = 38 and, using flow visualization techniques, have noted the movement of the separation points through a cycle. They found that separation starts at the rear of the cylinder just after flow reversal and moves progressively forwards, first rapidly and then less rapidly, passing through a point of inflection at the maximum velocity point. As the flow decelerates again it imposes an additional velocity gradient causing the flow separation angle to increase again. By extrapolation they determined that separation first started when the cylinder had travelled .16D (as opposed to theoretical results of .17D for impulse flow and .26D for steady acceleration). Their work has shown that it is useful to look at each half cycle as a separate event, starting at rest, accelerating to maximum velocity and then decelerating to rest again.

3.8. Analysis based on the Blasius equation

Maull and Milliner (1978) have analysed in-line and lift forces on a cylinder in an oscillating flow. Rather than using Morison's formula they non-dimensionalized force/unit length with respect to $\rho D^3/2T^2$. They also suggested that instead of using Morison's formula one might consider the forces on a cylinder to be divided into an inertia term with $C_M = 2$ (as in unseparated flow), and a term dependent upon the vortex circulation, position and movement (i.e. the Blasius equation). Maull and Milliner's method has the advantage that forces due to circulation, movement of vortices, etc., only affect one term of their equation rather than both, as is the case with Morison's formula.

3.9. Roughness effects in oscillatory flow

The only extensive tests on rough cylinders at high Reynolds' numbers that the author is aware of are those of Sarpkaya (1976a, 1976b). Example curves of C_D and C_M versus R for K = 60 and various roughness are shown in Fig. 14.

It is seen that the effects of roughness in oscillatory flow are similar to those in a steady current, the critical regime occurs earlier, and values of C_D are increased. It is also seen that there is an inverse relationship between C_D and C_M, when C_D is high C_M is low, and vice versa. The lift coefficient, C_L, is found to be virtually independent of roughness and β and is approximately equal to the maximum value for a smooth cylinder.

3.10. The approach of oscillatory flow force coefficients to the steady flow values

It has already been seen that the Keulegan-Carpenter number, K, is important in defining the wake, and thus the values of the

coefficients. It might be expected that K be of decisive importance at low values of K, but that at high values of K the parameter R would be most important as the flow becomes quasi-steady.

Various values of K have been suggested where the flow can be considered to be quasi-steady and steady current values of coefficients used, and values as low as 50 or 100 have been suggested.

It is interesting to compare data for values of Reynolds number of critical and above for various values of K, and roughness. Data from Fage and Warsap (1929), Szechenyi (1975) and Miller (1977) in steady flows, and Sarpkaya (1976b) in oscillatory flows were compared by Verley (1977a). In Fig. 15 the transcritical values of C_D and C_M are compared, in Fig. 16 the critical values, and in Figs. 17 and 18 are plotted the values of R where C_{DCRIT} occurs, and where C_D is 95% of its transcritical value, respectively, all for various roughnesses, e/D. The steady current data has been plotted at K = 1000, and it is suggested that it is at about this value that steady current values of the coefficients will apply. On a smooth cylinder, however, the transcritical value of C_D is nearly independent of K. In Fig. 19 is shown an example plot of C_D versus R for a roughness e/D = 1/50, and for various values of K, and the approach of the curves to the steady current curve as K is increased is clearly seen.

3.11. Errors in the time averaged values

Keulegan and Carpenter (1958) compared a predicted time history obtained by using their time averaged values of C_D and C_M with the actual time history used in obtaining C_D and C_M. They found that for small and large K the agreement was good, but that in the area K = 5 ~ 30 there were some differences and the peak force was underestimated by up to 20%. Sarpkaya (1976a) has evaluated the error in two ways, firstly by comparing the maximum measured force with the maximum predicted, and secondly as a percent error over the cycle. He found that it is only in the area of K = 10 ~ 20 that there is any significant error. Sarpkaya showed that a major reason for the error in this region was the vortex induced forces in the in-line direction (their forces having a component in the lift direction,

quantified by the lift coefficient in magnitude and by f_r in frequency, and a component in the drag direction at twice this frequency). When accounting for these vortex induced forces the agreement was considerably improved.

Bearman et al. (1978) showed that analysis of nominally identical force cycles in oscillating flow led to various, inversely related, values of C_D and C_M, i.e. if in a cycle the calculated value of C_D was high, then the value of C_M was low, and vice versa. Ramberg and Niedzwecki (1979) show that one can obtain different pairs of C_D and C_M values which fit the force measurements equally well. They also show that an error of only 5% in estimating the phase between the wave and the force could lead to errors of 10% in the calculated values of both C_D and C_M.

3.12. Comparison of forces in oscillatory and wave flows

There are very few investigations in waves where force coefficients have been obtained which can be compared with those obtained from pure oscillatory flow. Miller and Matten (1976) found C_D values in the range K = 10~25 which were slightly greater than those from oscillatory flow tests. Susbielles et al. (1971) indicated that the use of C_D and C_M values from pure oscillatory flow gives a good representation of local forces in waves. Chakrabarti et al. (1976) have determined C_D and C_M on pile sections in waves and the agreement with pure oscillatory flow results is fair, except that they obtained a large value of C_M at low K. As has already been mentioned, Sarpkaya, at the OTC conference in 1977, claimed that the application of his values of C_D and C_M gave a good prediction of the forces measured by Matten (1977) in waves.

3.13. Forces at very small Keulegan-Carpenter numbers

The forces on a cylindrical body at very low K are of more than academic interest, for example the damping of vibrations of a struc-

ture in still water is directly proportional to the oscillating drag coefficient and this damping is required when estimating so called hydroelastic vibrations, (see King (1977) for a survey of this subject).

Stokes (1851) calculated the velocity field around an oscillating cylinder, from which the forces on the cylinder can be derived. The solution applies for large β, becoming increasingly accurate as β is increased. Batchelor (1970) gives a simpler derivation. Stokes (1901) analysed the forces on an oscillating pendulum and showed that the force could be expressed as two terms proportional to the cylinder velocity and acceleration, respectively.

The damping force is given by the velocity term from which it can be derived that the damping force per unit length of cylinder is

$$f = 2\rho\pi^2 D^2 n \left\{ \sqrt{\frac{1}{\pi\beta}} + \frac{1}{\pi\beta} \right\} \dot{x} \qquad -(4)$$

(According to Tani (1977) Stokes, in deriving his equations in 1851, hovered between the choice of the boundary condition at the body as the 'no-slip' condition or zero friction. He chose the first, thus using one of the most important ideas of boundary layer theory which did not appear until 1905.)

The parameter β is proportional to $(D/\Delta)^2$, where Δ is the boundary layer thickness, and boundary layer theory applies if $\Delta \ll D$, i.e. for large β. The application of equation (4) has been shown for values of β from 40 to 5×10^5 (Stuart and Woodgate (1955) and Bramley (1970)).

Williams and Hussey (1972), reanalysing Stokes' work, determined that a further condition for the application of the equations is that $x_o/D \ll 1$, where x_o is the amplitude of the vibrations (i.e. $K \ll 1$). Stuart and Woodgate (1955) found that the equation applied at $\beta \approx 40$ for $x_o/D \lesssim 0.1$, and for larger amplitudes the damping became approximately proportional to velocity squared. Bramley (1970) found that for $\beta \approx 3600$, the damping was given correctly for $x_o/D \lesssim 0.2$, and Wootton (1969) found that for $\beta \approx 5\times10^4$ the damping was correct for $x_o/D \lesssim .12$.

Skop et al. (1976) noted the damping of vibrations of cylinders in water, and the damping was given correctly by Stokes' equations for $x_o/D < .3 \sim .4$. They equated the damping to the oscillatory drag coefficient C_D and for larger amplitudes found good agreement with the results of Keulegan and Carpenter (1958), Sarpkaya and Tuter (1974), etc. Similar results were also found by Petrauskas (1976).

This topic will be returned to in Part III as the author has conducted similar tests, Verley (1978a).

4. THEORETICAL WORK ON TIME-DEPENDENT BOUNDARY LAYERS

A considerable amount of work has been conducted, mostly theoretical, on the time-dependent boundary layer in a combined steady and oscillatory current. Most of this work has been for flat plates, though some other shapes have been considered. The flow is, however, always considered to be unseparated.

Little theoretical or experimental work has been conducted on cylinders apart from for the rather special case of in-line hydroelastic vibrations, and this will be considered in the next chapter.

A number of researchers have turned their attention to investigating time dependent boundary layers. Nearly all have investigated Falkner-Skan time dependent boundary layers, i.e. layers where the velocity outside the boundary layer of a flat plate can be described as

$U(x) = kx^i$ where k is a constant and x is the distance along the plate

When i = 0, flat plate flow results and when i = 1, stagnation point flow results. Time dependent oscillations of this velocity are investigated, usually limited to small amplitudes of oscillation.

A boundary layer may be considered quasi-steady if the period of unsteadiness is long compared to the time required for a sudden change to spread through the boundary layer by molecular diffusion, or, in the case of a turbulent boundary layer, by turbulent diffusion.

The earliest studies of time dependent boundary layers were by Blasius (1908) who considered impulsively started and steady accelerated flows, and which have already been discussed.

Moore (1951, 1957a), who was considering aircraft and missile flight simulated as a flat plate with changing velocity, found that the flow is quasi-steady if $\Delta^2\dot{U}/\nu U \ll 1$. If, on the contrary, this parameter is very large, then a shear solution applies, i.e. there is an inner, thin boundary layer which reacts as if the fluid outside it were at rest. Moore found that there were two solutions of the boundary layer equation, for respectively high and low values of $\Delta^2\dot{U}/\nu U$.

Moore (1957a, 1957b) also discussed at length the meaning of separation in a time dependent boundary layer and considered that the onset of flow reversal was not a sufficient criterion, as flow reversal can occur without separation within the boundary layer if the separation point is moving along the body against the stream direction. Instead he considered that a separation bubble first appears at the position on the wall above which, at some point in the boundary layer, the shear and the velocity simultaneously vanish, and the separation point is very near to this point.

Stewartson (1951) has considered an impulsive change from one velocity to another, and found that the initial motion after the impulsive change was of the shear wave type, while later stages were of a quasi-steady type. Watson (1958) considered cases of 1) impulse change from one velocity to another, 2) a steady acceleration, and 3) a decaying, oscillating velocity superimposed on a steady velocity. He found that, immediately after an impulse change, a second, very thin boundary layer, whose thickness grew as $\sqrt{\nu t}$, where t is time, develops, and the rest of the boundary layer behaves as if it were inviscid as far as the impulse is concerned. Gradually the inner boundary layer grows thicker and distorts the flow until the steady state is reached. In the initial moments there is a high skin friction due to the thinness and corresponding high shear in the inner layer. For the oscillating case he found that the skin friction leads the velocity by $\pi/4$ at high frequencies.

Lighthill (1954) considered a steady flow with small amplitude sinusoidal fluctuations superimposed, for either the Blasius boundary layer (flat plate, no pressure gradient) or in flows on a plate with a pressure gradient. Lighthill expanded his expression for the velocity outside the boundary layer using a momentum integral method and using one term. He performed two expansions, for high and low values of $\omega x/V$, where ω is frequency and x is the distance along the plate. He found that at low values of this parameter the boundary layer behaves in a quasi-steady way. For a plate he found that if $\omega c/V \lesssim .6$, where c is the length of the plate, the boundary layer will behave quasi-steadily. For high frequencies, however, the oscillations are contained within a thin boundary layer (Stokes' layer) of thickness $\sim(\nu/\omega)^{1/2}$, this layer acting as if the flow outside it was stationary. The skin friction then leads the velocity

fluctuations by $\pi/4$. Lighthill suggested that, near separation, the shear-wave (high frequency) solution would apply, and that this would lead to large oscillations in the position of separation.

Lin (1956) considered only the high frequency solution and was able to use a higher order solution, not limiting the amplitude of the velocity oscillations. He found that flow reversal may occur within the boundary layer, even though it does not occur in the free stream. This is because the oscillating velocity penetrates deep into the usual boundary layer with undiminished amplitude, whereas the steady velocity component is slowed down.

Hori (1961) used a power series expansion for the low frequency case. He expressed the potential velocity distribution over a cylinder as the first two terms of a Taylor series, and used vanishing skin friction as a criterion of separation. In this way he tried to see the effects of flow oscillation on the movement of the separation point, which he found moved $\pi/2$ ahead of the velocity fluctuations, but with extremely small amplitude. In later papers he looked at the effect of oscillating circulation, (Hori (1962a)), rotational oscillations of a cylinder, (Hori (1962b)), and an arbitrarily shaped body (Hori (1962c)).

Rott and Rosenzweig (1960) have considered high and low frequency solutions of the general Falkner-Skan family, and Lam and Rott (1960) have considered an expansion of 15 terms of the frequency parameter, all these being for small amplitude oscillations.

Gersten (1965) considered low and high frequency solutions to the second order of amplitude.

Pedley (1972), who was particularly interested in the thermal boundary layer (for the design of a hot film anemometer for use in blood vessels), used asymptotic expansions for the high and low frequency solutions and did not limit the oscillating velocity amplitude other than that it had to be greater than the steady velocity component, and considered Falkner-Skan type boundary layers, $U = xi$, with $i = 0$, $1/3$, and 1.

A problem common to all of these solutions is that of which solution to apply for frequencies which are neither very low nor very high. Various criteria calculated using the two methods are compared (e.g. phase, or amplitude of shear stress, etc.) to see if they overlap at some intermediate frequency. Pedley (1972) found

that for the skin friction there was generally a reasonable overlap (at different frequencies for different pressure gradients), but that for the thermal boundary layers there was no overlap.

Hill and Stenning (1960) have conducted experimental measurements on the boundary layer on a flat plate in a steady flow with an oscillating component whose amplitude was about 1/10 of the steady flow's. They used either no pressure gradient in the x direction or a small adverse gradient, and varied $x\omega/V$ between .1 and 10, where V was the steady component of velocity. They found that the low frequency solution of Lighthill (1954) for the Blasius layer (no pressure change with x) predicted the results accurately for values of $x\omega/V$ from .1 to .6, and over a somewhat smaller range with a pressure gradient. They concluded that Lighthill's high frequency solution should predict both phase and amplitude of the boundary layer fluctuating profile correctly for $x\omega/V \gtrsim 10$, and the amplitude for $x\omega/V \gtrsim 3$. The phase was given considerably better in the range $3 \lesssim x\omega/V \lesssim 10$ for a shear wave type solution taking into account first order convective effects.

None of the methods discussed can be applied near separation. The use of potential flow velocity distributions by Hori (1961, etc.) is unreasonable, even in a steady flow this leads to a prediction of separation at 108° from the front stagnation point (rather than the correct figure of about 80°).

Experimental work on cylinders oscillating in-line with a current will be considered in the next section.

5. OSCILLATIONS OF A CYLINDER IN A CURRENT

In the previous chapter it was seen that there has been a considerable amount of theoretical work on the boundary layer in a flow comprising of a steady and an oscillatory component. Some experimental work has been conducted on cylinders oscillating in line with a current, a situation which is dynamically equivalent to that of a combined steady and oscillatory current acting on a stationary cylinder apart from an additional inertia force, the Froude-Krylov force, being the mass of fluid displaced times acceleration. The equivalence can perhaps most easily be seen by considering axes fixed to the cylinder, in which case the boundary conditions are identical in the two cases, and the only additional force is one compensating for the acceleration of the frame of reference, i.e. the above mentioned Froude-Krylov force, (see also Batchelor (1970), p 139).

From the point of view of this thesis one is interested in the oscillations of a cylinder in-line with a current, and most such experiments have been conducted in order to illuminate the problem of hydroelastic vibrations, and the experiments conducted only over the ranges of parameters where hydroelastic vibrations occur, a notable exception being the work of Mercier (1973). The problem of hydroelastic vibrations is very similar for the cross-flow and in-line directions, and most research has been conducted into the cross-flow direction (vibrations perpendicular to the flow direction). Review papers of hydroelastic vibration work are given by King (1977), Blevins (1977), and Berger and Wille (1972). In the next section a brief summary of hydroelastic vibration research is given, for both cross-flow and in-line vibrations.

5.1. Hydroelastic vibrations

By 'hydroelastic vibrations' in this thesis is meant the phenomena which occur when vortex shedding forces have a frequency near that of an oscillating cylinder. The problem is most often associated with the vibrations of flexible cylinders which can occur in currents under certain circumstances. The problem is, however, often investi-

gated by physically forcing cylinders in currents.

Although the term 'hydroelastic vibrations' is perhaps a misnomer when the cylinder is externally forced, the term is nevertheless used.

Hydroelastic vibrations may occur if the frequency of oscillation of a cylinder (natural or forced) is near to a multiple of the frequency of vortex shedding. The vortex shedding frequency of a pair of vortices, n_v, is controlled by the Strouhal number, S, such that

$$n_v = SV/D$$

On a rigid cylinder at subcritical Reynolds numbers $S \approx .2$, and for transcritical Reynolds numbers $S \approx .3$.

Associated with each vortex shed is a force on the cylinder with components both in-line and cross-flow, and thus the cylinder experiences forcing at the vortex shedding frequency in the cross-flow direction and at twice this frequency in the in-line direction. One might thus expect, for subcritical values of R, that resonance may occur at values of a parameter V/nD, where n is the cylinder oscillation frequency, of 5 and 2.5 in the cross-flow and in-line directions, respectively. In fact there is a complicated non-linear feedback mechanism such that resonances do not occur at exactly these values of V/nD, and the vortex shedding forces are affected by the oscillations. In addition there is a second type of in-line hydroelastic vibrations, associated with a symmetric form of vortex shedding, which occurs at lower values of V/nD.

This non-linear interaction whereby the vibrations of a cylinder affect and alter the vortex shedding forces (which for an elastic cylinder cause the vibrations) is a fundamental characteristic of the phenomenon. Thus if vibrations occur due to the response of a cylinder to vortex shedding, but the vortex shedding forces are unaltered, i.e. are the same as on a rigid cylinder, then the term 'hydroelastic vibrations' is not used.

The essential features of hydroelastic vibrations may be summarized as follows.

i) If a cylinder is forcibly oscillated at a frequency n, or if a flexible cylinder with natural frequency n has sufficiently low mass and damping, then, when the forcing

frequency from vortex shedding approaches n, so called 'lock-on' occurs. That is to say that the vortex shedding frequency becomes controlled by the cylinder oscillation frequency. For cross-flow vibrations the vortex shedding frequency is thus equal to the oscillating frequency, and for in-line vibrations is equal to one half the oscillating frequency. For the cross-flow direction, lock-on occurs for a range of velocities to either side of that where resonance was expected. Den Hartog (1954) considered this area to be $\pm$ 20% of the value of V/nD where $n_v = n$, and Marris (1962) considered it to be $\pm$ 35%. Wootton (1969) has shown that the range depends on the cylinder roughness, length to diameter ratio, and mass and damping characteristics, as has Koopman (1967).

Koopman (1967), Ramberg and Griffin (1974, 1976) and Novak and Tanaka (1975) show that when $n_v = n$, a rapid increase in the correlation length of vortex shedding occurs with increasing amplitude of oscillation.

ii) When this lock-on occurs, the vortex shedding becomes correlated along the whole length of the cylinder, and the vortex strengths are increased, Davies (1976), leading to increased lift forces, Griffin et al. (1975) and Feng (1968). There is a minimum amplitude of vibration, below which the vortex shedding is not controlled by the cylinder oscillation frequency and increased correlation does not occur. This so called 'threshold amplitude' depends on the value of V/nD, and various results for cross-flow vibrations are shown in Fig. 20,a, and for in-line vibrations in Fig. 20,b. It is seen that the lowest value of the threshold amplitude is when the natural vortex shedding frequency coincides with the cylinder oscillation frequency and the value would appear to be about .06 diameters in both cases. A commonly accepted value for cross-flow vibrations is .1 diameter and King and Every (1976) consider that the value for in-line vibrations is .01 ~ .02 diameters.

iii) A dimensional analysis of the problem (e.g. King et al.

(1973)) indicates that the amplitude of hydroelastic vibrations at resonance is a function of four parameters

$$y_o/D = f(V/nD,\ 2m/\rho D^2,\ \delta,\ C_L)$$

where y_o = amplitude of vibrations, m, δ = mass per unit length and logarithmic damping of the system, and C_L = lift coefficient. For analysis in the in-line direction C_L is replaced by C_D' and y_o is replaced by x_o. For a surface piercing cylinder x_o and y_o are considered to be maximum amplitudes common to the fluid and cylinder, King (1977).

Vickery and Watkins (1962) considered the energy balance between forcing on the cylinder due to vortex shedding and energy dissipated by damping, and determined that the maximum amplitude of response, at resonance, for a general mode shape would be

$$y_o/D = \frac{\rho D^2}{2m\delta}\left(\frac{V}{nD}\right)^2 \frac{C_L}{4\pi} \frac{\int_o^L (y/y_o)dz}{\int_o^L (y/y_o)^2 dz} \qquad -(5)$$

where, here, y is the amplitude of vibration at a particular position, z, along the cylinder and the integral terms account for the mode shape. On the basis of this it was considered that the second two terms in the dimensional analysis could be combined to give a single parameter, the so called 'stability parameter' $k_s = 2m\delta/\rho D^2$.

For a simple analysis one might consider a cylinder of length L, mass per unit length m, spring constant b and damping factor c, and with a uniform mode shape such that the deflection at any instant is the same along the length of the cylinder. The cylinder is considered to be undergoing a sinusoidal forcing given by

$$F(t) = F_o \sin \omega t$$

The equation of motion is

$$M\ddot{y} + c\dot{y} + by = F_o \sin \omega t$$

where M = mL. The solution is

$$y_o = \frac{F_o}{b} \cdot \frac{1}{\sqrt{(1-(\frac{\omega}{\omega_n})^2)^2 + (\frac{2c\omega}{c_{crit}\omega_n})^2}}$$

$$= \frac{F_o}{b} \cdot (D.M.F.)$$

where (D.M.F.) stands for Dynamic Magnification Factor.

At resonance

$$y_o = \frac{F_o c_{crit}}{2\ b\ c} = \frac{F_o \pi}{b\delta}$$

where c_{crit} = critical damping (= $2M\omega_n$) and δ = damping logarithmic decrement.

For the cross-flow direction it is considered that the forcing is sinusoidal (Bishop and Hassan (1964a)) and given by

$$f(t) = .5\ \rho\ D\ V^2\ C_L \sin(2\pi\ n_v\ t) \qquad \text{per unit length}$$

Assuming full correlation, then

$$F_o = .5\rho\ D\ V^2\ C_L\ L$$

from which one can obtain

$$\frac{y_o}{D} = (\frac{V}{nD})^2 (\frac{1}{k_s})\ \frac{C_L}{4\pi^2}\ \delta(D.M.F.) \qquad -(6)$$

or at resonance

$$\frac{y_o}{D} = \left(\frac{V}{nD}\right)^2 \left(\frac{1}{k_s}\right) \frac{C_L}{4\pi} \qquad -(7)$$

which, for this linear mode shape, is the same as equation (5) obtained by Vickery and Watkins (1962).

iv) The maximum cross-flow response occurs at values of V/nD between 5 and 8 (King (1974)), although Meier-Windhorst (1939) found that the value was dependent upon the mass of the cylinder, and Wootton (1969) found that the value was dependent upon k_s. Nevertheless for reasonably constant V/nD one expects the response to be dependent upon k_s and C_L. Furthermore it is considered that C_L for an oscillating cylinder is primarily dependent upon y_o/D. For cross-flow response King (1975), Griffin et al. (1975) and Blevins (1972) found that there was a unique relationship between y_o/D at resonance and k_s, shown in Fig. 21,a. The cross-flow response is thus seen to have a maximum amplitude of about 2 diameters for very low k_s, and the amplitude falls off as k_s increases, there being no noticeable response for $k_s \gtrsim 16$. King (1975) shows a similar curve, shown in Fig. 21,b, for the in-line response (for both asymmetric and symmetric shedding forms). Using equation (5) the relationship between C_L and y_o/D at resonance can be obtained from experiments where k_s and y_o/D are measured. A typical form of the curve is shown in Fig. 22,a from King (1975) where it is seen that as y_o/D is increased the value of C_L first increases to a maximum at $y_o/D \approx .05$, and then decreases gradually again to zero for $y_o/D \approx 2$. King considers that the increase in C_L up to $y_o/D \approx .05$ is due to increasing correlation of the vortex shedding, and that C_L in fact decreases monotonically with y_o/D, and if the value is extrapolated to $y_o/D = 0$ it is approximately that value measured on a stationary rigid cylinder.

v) From Fig. 21,b it is seen that maximum in-line response is only about 0.2 diameters and that a value of k_s of

about 1.2 is sufficient to supress vibrations. The reason for this is evident from equation (5) as in-line response occurs at about 1/2 the value of V/nD of cross-flow response, and the oscillating drag coefficient, C_D', is typically $\sim C_L/6$.

vi) If equation (5) is used to analyse in-line vibrations, (but with C_D' replacing C_L) then a similar shaped curve to that of Fig. 22,a is obtained for x_o/D versus C_D'. King (1975), however, considered that the equation for in-line response should be written with relative velocity terms, as

$$F_{(t)} = .5\rho D\ (C_D + C_D' \sin\omega t)\ (V-\dot{x})^2$$

in which case C_D' is found to increase monotonically with y_o/D (Fig. 22,b and c), due to having to overcome a damping term which is now included (expanding $(V-\dot{x})^2$ for $V >> \dot{x}$ gives $V^2 - 2V\dot{x}$, the second term being a term opposing structural velocity, i.e. a damping term).

vii) Although the two terms, δ, and $2m/\rho D^2$ could be combined at resonance, giving k_s, they cannot be so away from resonance (see equation (6)), and in fact it is seen that for a constant value of k_s one would expect a broader excitation range for lower δ, as in fact found, Koopman (1967).

viii) The terms mass and damping have been rather loosely defined to now. Nearly all researchers have taken still water values for damping, and the mass to include the added mass of water calculated as the displaced mass of water, and Figs. 21,a, b are drawn under this assumption. Sarpkaya (1978) points out that the added mass and the fluid part of the damping are essentially fluid terms and should not be mixed up with structural terms. Furthermore there is no reason to believe that the values are the same at resonance as in still water (in still water the damping and added mass are given by unseparated flow values, at resonance the flow can by no means be considered to be unseparated).

Sarpkaya (1978) oscillated a cylinder transverse to a steady current stream and measured the inertia and damping forces on the cylinder. He found that the added mass coefficient increased from its unseparated value of 1.0 at low V/nD, to 2.0 at V/nD $\approx$ 4.5, and then decreased rapidly to negative values for V/nD $\gtrsim$ 5.3. This thus confirms that still water added mass should not be used and indicates why Wootton (1969), Meier Windhorst (1939) and Glass (1970) found that larger values of k_s and $m/\rho D^2$ led to resonance at higher V/nD.

ix) Various authors have noted that the steady component of drag for cylinders undergoing hydroelastic vibrations increases. Sarpkaya (1978) found that there was a maximum at V/nD = 5.0, and that larger amplitude vibrations led to a higher steady component of drag, for $y_o/D \approx .84$ the value was $C_D = 3.2$. Mercier (1973) noted the same effects, though his increase was not as much (for $y_o/D = 1.0$, he recorded a maximum of $C_D = 1.7$).

x) Equation (5) is evidently oversimplified in that it does not reproduce several effects which occur with hydroelastic vibrations. For example the lock-on effect, whereby the wake frequency is controlled by the cylinder frequency, is not reproduced, nor is the hysteresis whereby amplitudes of vibration against V/nD are different for increasing and decreasing V/nD, as shown by, amongst others, Bishop and Hassan (1964b). Bishop and Hassan seem to have been the first to suggest that the behaviour of the system may best be modelled as a non-linear oscillator, and Hartlen and Currie (1968) developed a model based on a van der Pohl's type non-linear oscillator for the lift force coupled to the body motion by linear dependence on velocity. They found qualitative agreement with results of Ferguson and Parkinson (1967). Various authors have further modified the model, for example Griffin et al. (1975), and Blevins (1972, 1975). However, as Sarpkaya (1979) notes, the further developments of the method to give better predictions resemble "a highly non-linear equation system being conditioned to suit

qualitatively the observations".

As has already been mentioned, a discrete vortex model of cross-flow hydroelastic vibrations in currents has been developed by Sarpkaya and Shoaff (1979b). The model has predicted many of the experimentally observed features of the phenomenon, the amplitude of vibration, the position of the separation points and their oscillation, the lock-on effect, the increase in the steady component of drag, the position of vortices in the wake, etc. Based on his results, Sarpkaya (1979) proposes a mechanism causing the lock-on phenomenon.

xi) Sarpkaya (1979) suggests that the reason for the symmetric form of vortex shedding associated with in-line vibrations for $V/nD = 1.5 \sim 2.5$, is that in this range of V/nD and amplitude of vibration the flow reverses twice per cycle. As the cylinder moves down-stream from its mid position it initially has a velocity greater than the stream velocity. At some point (dependent on the ratio $V/\dot{x}_o$, where $\dot{x}_o$ is the velocity amplitude of the cylinder) as the cylinder decelerates, flow reversal occurs, and two vortices start to grow symmetrically. These vortices continue to grow as the cylinder reverses direction and moves against the stream. The relative distance travelled is insufficient for asymmetry to start (cf. the simple time dependent flows already discussed). The vortices are carried away from the cylinder by the stream symmetrically at first, and then asymmetrically.

Sarpkaya considers the forcing on the cylinder to be due to a drag overshoot occurring as occurs in impulsively started flow.

The experiments in Part III will enable a closer look at this phenomenon discussed by Sarpkaya.

xii) Cross-flow induced vibrations have been observed for Reynolds numbers up to 7×10^6. Frequencies of vortex shedding under such conditions in air (where there are no problems of added mass effects) have been recorded by several authors, and in general it is found that at subcritical Reynolds numbers the Strouhal frequency corresponding to

maximum vibrations is S ≈ .16, the value rising through the critical regime to a value of S ≈ .21 at transcritical Reynolds numbers,(Wootton (1969), Dickey and Woodruff (1956), Pagon (1934) and Jones (1969)). Wootton et al. (1972) in full scale tests found that hydroelastic vibrations occurred in the critical and supercritical ranges of Reynolds number, whereas on a stationary cylinder there is no coherent vortex shedding.

On a stationary cylinder the vortex shedding is very dependent on roughness, free stream turbulence, etc., whereas on an oscillating cylinder these effects seem to become secondary compared to the effects of the oscillations.

xiii) Tests on flexible cylinders which undergo hydroelastic vibration, e.g. those by King (1974), show that the in-line vibrations are divided into two distinct regions, one lasting from V/nD = 1.5 ~ 2.5 and associated with symmetric vortex shedding of two vortices per cycle, and a second region, for V/nD = 2.5 ~ 4.0 and associated with asymmetric vortex shedding of one vortex per cycle. Griffin and Ramberg (1976) forcibly oscillated a cylinder in an air flow at R = 190 and reported to have found both types of vortex shedding througout the entire range of their experiments, V/nD = 2.1 ~ 4.4.

xiv) Measurements conducted on the vortex spacing behind cylinders undergoing cross-flow induced vibration (Koopman (1967), Griffin and Ramberg (1974)) showed that as the amplitude of vibration was increased, within the lock-on range, the lateral vortex spacing decreased, and became zero at about y_o/D = .8 ~ 1.3. For greater amplitudes of vibration it was found that a third vortex was shed per two cycles, i.e. in one cycle there was a single vortex shed, of positive sign, say, and in the next two of negative sign were shed, one being of smaller size than the other, but of increasing size as the amplitude was further increased. Griffin and Ramberg (1976) found similar effects for the in-line oscillations where one vortex is shed per cycle. At an amplitude of y_o/D = .15 ~ .2

the vortex spacing became zero, and at larger amplitudes a third vortex was shed per two cycles.

xv) Griffin and Ramberg (1974) for the cross-flow direction, and Griffin and Ramberg (1976) for the in-line direction where one vortex is shed per cycle, found that the longitudinal spacing of vortices in the lock-on range was inversely proportional to cylinder frequency. For forcing frequencies above n_v and $2n_v$ in the cross-flow and in-line directions, respectively, where n_v is the shedding frequency from a stationary cylinder, the longitudinal spacing was shorter than that associated with a stationary cylinder, whereas for lower frequencies the spacing was greater.

xvi) Several authors have oscillated cylinders cross-wise to a flow at other frequencies than near the Strouhal frequency. Stansby (1976) has found that subharmonic lock-on can occur when the frequency is twice and three times the vortex shedding frequency.

5.2. Oscillations in-line with a current away from hydroelastic vibration effects

As far as the author is aware the only investigations into oscillations of a cylinder in-line with a current which have included oscillations far away from the frequency of forcing caused by vortex shedding are by Tatsuno (1972) and Mercier (1973) whose data has been partially reanalysed by Matten (1976). Mercier's work included the forced oscillation of cylinders cross-flow to a stream as well as in-line with a stream, however only the work in-line with a stream will be discussed here.

Mercier's work may be summarized as follows:

i) The steady component of drag was analysed according to the following equation

$$\bar{C}_D = \frac{\text{Steady component of force}}{.5\rho D\ V^2 L} \qquad -(8)$$

Values of $\bar{C}_D$ versus nD/V for x_o/D = 0.5, 1.0, 1.5, 2.0, 2.5 and 3.0 are shown in Fig. 23. It is seen that there is a peak in $\bar{C}_D$ at values of nD/V around 2.5 (V/nD ≈ 4), though the value is rather dependent upon the amplitude of vibration. No hysteresis effect was found when comparing results for increasing V/nD with those for decreasing V/nD.

ii) The oscillatory component of drag was analysed according to the following equation

$$\tilde{C}_D = \frac{\text{Fundamental component of oscillatory drag}}{.5\rho D\, L\dot{x}_o^2 \cdot (8/3\pi)} \quad -(9)$$

where $\dot{x}_o$ is the velocity amplitude of vibration.

There was considerable scatter in the results, nevertheless Fig. 24,a represents the values obtained for $\tilde{C}_D$ versus V/nD for x_o/D = 0.2, 0.5, 0.75, 1.0, 1.5, 2.0, 2.5 and 3.0, and Fig. 24,b represents $\tilde{C}_D$ versus x_o/D for various V/nD. At values of V/nD = 0 (i.e. in still water), the results agree reasonably with those of other researchers (e.g. Keulegan and Carpenter (1958)).

As V/nD is increased $\tilde{C}_D$ decreases to about 0.7 at V/nD ≈ 2 for all x_o/D, and for higher V/nD the values of $\tilde{C}_D$ increase rapidly, particularly for lower x_o/D. No negative values of $\tilde{C}_D$ were recorded although the lowest value of V/nD tested (apart from V/nD = 0) was 2.4, so that the negative values corresponding to the in-line hydroelastic vibrations already discussed in the range $1.5 \lesssim V/nD \lesssim 4$ would be expected to have been observed.

iii) The oscillatory inertia force was analysed as

$$C_M = \frac{\text{Fundamental component of inertia force}}{.25\rho\pi\, D^2 L\dot{x}_o} \quad -(10)$$

Mercier's data has been replotted in Fig. 25 for C_M versus x_o/D for various V/nD.

iv) It is noted in passing that $\bar{C}_D$, $\tilde{C}_D$ and C_M are based on equations exactly equivalent to equation (22) to be used by this author in Part III, and that $\bar{C}_D$ is equivalent to the author's STCDIND, $\tilde{C}_D$ is equivalent to CDIND and C_M is equivalent to CM.

v) Mercier conducted spectral analysis of the lift force (force perpendicular to the stream direction) for x_o/D = 0.75 and V/nD = 3.36, 4.02, 5.29, 5.95.

For V/nD = 5.95 most of the power was at 1/2 times the oscillating frequency, with progressively smaller components at 3/2 and 5/2 times the oscillating frequency. At V/nD = 5.29 there was approximately equal power at the 1/2 and 3/2 components, and by V/nD = 4.02 most power was at the 3/2 component, with a small contribution at 1/2. For V/nD = 3.36 most power was at the 1 component, with a small amount at 5/2.

From Mercier's Fourier coefficient analysis it is evident that the half-powers of lift occur over a narrow range in a region of V/nD = 3 ~ 5, the exact value depending on x_o/D. The larger the value of x_o/D, the higher the order of the half-power component which is dominant.

Mercier associated these half-power components with vortex shedding which involved the shedding of a single large vortex from one side of the cylinder in one cycle, and from the other side in the next cycle.

Matten (1976) has reanalysed Mercier's results, but instead of using the above equations he considered that the force per unit length of a cylinder oscillating in-line with a current should be described by the so called 'modified Morison's formula', the same as the author's equation (21) to be used in Part III, and written as

$$f(t) = .5\rho D\, C_D(V-\dot{x})|(V-\dot{x})| - .25\rho\pi\, D^2 C_M \ddot{x} \qquad -(11)$$

Matten used Fourier coefficient analysis to derive two time averaged coefficients, one for the steady component of drag and the other

for the oscillating component. These are referred to here as $\bar{C}'_D$ and $\tilde{C}'_D$, respectively. ($\bar{C}'_D$ is equivalent to the author's STCDDEP and $\tilde{C}'_D$ to CDDEP.)

In Fig. 26 Matten's reanalysis of Mercier's data is plotted for $\bar{C}'_D$ versus V/nD for various x_o/D (with the addition of data for $x_o/D = .5$ which Matten did not plot). In Fig. 27 $\tilde{C}'_D$ versus V/nD is plotted for various x_o/D. The very large variations in the coefficients that Mercier found are considerably reduced, suggesting that the relative velocity form of equation (11) may represent the physical situation better. Matten claimed that the relative velocity equation is true if $\bar{C}'_D$ is equal to $\tilde{C}'_D$. There is no reason for these to be the same unless C_D in equation (11) is invarient with time, and the author considers this unlikely. Matten claimed that the values of $\bar{C}'_D$ and $\tilde{C}'_D$ are "of similar magnitude and nature over the range of reduced velocity given". From the figures, however, there appear to be considerable differences.

Petrauskas (1976) has looked at the steady force on, and damping of, cylinders oscillating in-line with various currents. The cylinders were mounted on a flexible mounting, and then 'plucked' and the decay of the motion noted. He found that for values of $V/nD \lesssim .7$ the damping was given by the Stokes' damping (derived from equation (4)). As V/nD was further increased, the damping increased and appeared to approach a damping given by the use of a relative velocity drag with a value of $C_D = .25$. He explained his results at low values of V/nD by interpreting the results of Lighthill (1954) to imply that if V/nD is very low, then the oscillating boundary layer is contained wholly within the boundary layer of the steady flow, and the two flow fields are independent. Lighthill showed this for the boundary layer, however his results cannot be extended directly to cover the area near and after separation on the cylinder.

Tatsuno (1972) has conducted a flow visualization investigation for cylinders oscillated at various amplitudes and frequencies in-line with a steady current, the Reynolds number being 100. Tatsuno's experiments were conducted in the ranges $V/nD = .8 \sim 20$ and $x_o/D = .1 \sim 1$, and he was most interested in the relationship between the frequency of cylinder oscillations and the wake frequency.

Tatsuno found that there were two ranges where the wake frequency was controlled by the cylinder, at $V/nD = 7 \sim 9$ when the wake

and cylinder frequencies were equal, and V/nD = 3 ~ 6 where the frequency of oscillation of the wake was one half the cylinder frequency and in each wake oscillation cycle 4 vortices were shed, two of one sign of circulation followed by two of the other (see Fig. 4 of Tatsuno's paper, also reproduced in Fig. 155,a). In this range of V/nD the separation points moved through large angles, particularly for larger x_o/D, and the wake was very wide. The area where this synchronization occurred moved to higher V/nD as x_o/D was increased, for example it occurred for V/nD = 3.3 ~ 4.4 for x_o/D = .1 and for V/nD = 4.0 ~ 6.5 for x_o/D = .54.

No other ranges of V/nD were found where the cylinder frequency controlled the wake frequency. At low V/nD, however, it was found that a pair of symmetric vortices were shed in each oscillation cycle, but that a certain distance downstream from the cylinder the vortices reformed, some disappearing, and an alternate, von Kármán type street appeared, the frequency of which was unrelated to the cylinder oscillation frequency, though slightly dependent on the amplitude of cylinder oscillations, larger x_o/D giving a lower frequency.

Tatsuno's results will be compared with results obtained by the author in Part III.

6. VIBRATIONS OF CYLINDERS IN WAVES OR OSCILLATORY FLOWS

6.1. Experimental investigations

Amongst the earliest investigations falling into this category is that of Laird (1962), who oscillated flexible cylinders in still water with an amplitude of oscillation of 6 diameters. He found that the maximum drag force could be up to 4.5 times, and the lift forces up to 1 times, the drag in a steady current velocity equal to the maximum oscillating velocity, U_m.

For low structural natural frequencies the frequency of vibration in the cross-flow direction was about n_v, and in the drag direction about $2n_v$, where n_v was defined as

$$n_v = .9U_mS/D \quad , \text{ with } S = .2$$

For higher structural natural frequencies vibrations occurred at, or very near, the cylinder natural frequency in both the in-line and cross-flow directions.

Sawaragi et al. (1977, 1978) conducted laboratory experiments with a flexibly mounted cylinder in waves for values of the root-mean-square of the local instantaneous value of Keulegan-Carpenter number over the length of the cylinder of up to 20, and for values of structural to wave frequency ratio of 0.5 to 7.5. They found that the major response, both in-line and cross-flow, was at the integral multiple of the wave frequency nearest to the natural frequency. They found that the ratio between the r.m.s. value of cross-flow vibrations, and the r.m.s. value of in-line vibrations, y_{rms}/x_{rms}, was greater than 1.0 for $K \gtrsim 6$ and $n/n_w \gtrsim 1.4$, where n_w is the wave frequency, and that this ratio exhibited maxima (i.e. most cross-flow response) when the natural frequency was near to an integer multiple of the wave frequency, and that these maxima were greatest if the value of K was such that the dominant lift force frequency on a stationary cylinder was expected to be at this same integral multiple of the wave frequency. Bullock et al. (1978) agreed in general with these results and presented a more complete picture of the relation-

ship between y_{rms}/x_{rms}, K and n/n_w, for $n/n_w \lesssim 5$. However for $n/n_w = 3$, Sawaragi et al. obtained a value of y_{rms}/x_{rms} of 2.6, whereas Bullock et al.'s value was 1.5.

Using results from Sawaragi et al. (1976) for the components of lift force on a similar but stationary cylinder in waves, Sawaragi et al. (1977, 1978) developed a model to predict the cross-flow response of the flexible cylinders. They included a hydrodynamic damping term, $.5\rho D\ C_D\ \dot{x}$, opposing the cylinder velocity (in the cross-flow direction) because "since the horizontal water particle velocity is negligible in the direction of lift force, the pile must be subjected to a fluid damping force in proportion to the moving velocity of the pile". The choice of C_D in this damping term is not stated.

For the in-line direction Morison's formula, modified for relative velocitites (i.e. with a similar term to the above damping term), was used and the in-line response was well predicted when account was taken of the wave non-linearities.

Bullock et al. developed a similar mathematical model for in-line response and again found reasonable prediction of the experimental response when using values of C_D and C_M obtained from oscillatory flow tests and distributed according to the local values of K, using 2nd order wave theory, accounting for wave non-linearities and using relative velocities in Morison's formula. An exception was for n/n_w near 2.0, and K = 10 ~ 17, when the lift force on a stationary cylinder has a dominant component at twice the wave frequency. They suggested that the underestimation of in-line response by the mathematical model in this area was due to the very large cross-flow response which fed back and caused the vortex shedding to be stronger. Apart from in this range Bullock et al. considered that vibrations in waves do not affect the vortex shedding or the forces on a cylinder in waves (over their ranges of parameters), i.e. that hydroelastic vibrations do not occur. Both Sawaragi et al. (1977, 1978) and Bullock et al. (1978) considered that their in-line responses were caused by higher components of the wave force introduced by wave non-linearities and the velocity squared term in Morison's formula. They did not account for any vortex shedding forces, even though both attributed the cross-flow response to these forces.

Both Chako and Colonell (1973) and Haritos et al. (1978) have looked at responses of cylinders in waves, but in both cases the conditions were inertia dominant (very low K). Haritos et al. predicted the vibrations well, both in-line and cross-flow, and in the in-line case used for their mathematical model forcing given by Morison's formula, not with a relative velocity term. It is, however, to be expected that the inclusion of relative velocities would make a negligible difference, the damping introduced being extremely small.

Sarpkaya and Rajabi (1979) have conducted tests on flexibly mounted cylinders free to oscillate perpendicular to a pure oscillatory flow. The results are for smooth and rough cylinders and, apparently, at high values of Keulegan-Carpenter and Reynolds numbers (no data enabling these to be calculated are given). Their analysis is similar to that given in chapter 5.1 for cross-flow vibrations in a current, except that instead of the cross-flow forcing being proportional to V^2 it is considered to be proportional to $U_m^2/2$, as it is supposed that the rate of energy transfer to the cylinder is proportional to the root-mean-square value of velocity. On a stationary cylinder in an oscillating current it has already been seen that the lift frequency varies through the cycle, however at resonance, which occurred at a value of $U_m/nD = 5.4$, the shedding was perfectly synchronized to the cylinder frequency, in part justifying the use of a sinusoidal forcing function.

Sarpkaya and Rajabi attributed the scatter in the results for cross-flow response in a current to the fact that the value of C_L for a stationary cylinder is not taken into account, and they therefore employed a stability parameter defined as

$$k'_s = \frac{2\pi m\delta}{\rho D^2 C_L^o}$$

where m and δ are in-vacuo values, (as discussed previously), and C_L^o is the lift coefficient on a stationary cylinder. (The factor π has appeared because they conducted the analysis in terms of damping ratio rather than damping logarithmic decrement.)

The analysis of Vickery and Watkins (1962) assumes that the lift coefficient on an oscillating cylinder is a function of y_o/D,

whereas Sarpkaya and Rajabi assume that the ratio of the lift coefficient to that on a stationary cylinder is a function of y_o/D.

Sarpkaya and Rajabi found that there was a unique relationship between maximum amplitude of response, y_o/D, and their stability parameter k_s', for all rough and smooth cylinders, which is reproduced in Fig. 28. They also suggested that this figure could be applied to steady flow induced oscillations and for any after-body shape, providing that y_o/D and C_L^o are replaced by r.m.s. values. It is indeed surprising that the various effects of roughness, K, R and the different manner in which the lift frequency varies through a cycle of oscillatory motion at high and low K can all be incorporated by including C_L^o. The vibrations of the cylinder so alter the vortex shedding, in both frequency and amplitude, that it is surprising that the lift coefficient bears a constant relationship to that on a stationary cylinder.

Sarpkaya found that the maximum lift coefficient on an oscillating cylinder occurred at a value of V/nD slightly below that where perfect synchronisation and maximum response amplitude occurred.

6.2. Dynamic analysis of offshore platforms

It has already been explained that the major reason for undertaking the experiments to be described in this thesis was the desire to investigate the damping of vibrations of jacket-type offshore platforms or structural members. It would therefore seem appropriate here to give a brief description of the present methods used to account for damping in the dynamic analysis of such platforms.

As structures are designed and built for progressively deeper water, damping becomes more important due to the natural frequencies of the structure approaching wave frequencies. Investigators who have been involved in the development of complex computer programs for the dynamic analysis of these platforms have considered damping from three effects.

i) Structural damping - usually very small

ii) Foundation damping - difficult to estimate and very dependent on soil conditions

iii) Hydrodynamic damping - due to the fluid induced damping of motion of the structure.

As structures become larger, the damping attributed to the last of these becomes dominant, Penzien (1975).

The hydrodynamic damping considered to apply in almost all investigations is that which is derived from the modified Morison's formula where relative velocities and accelerations are used. The force f per unit length on a flexible cylindrical member then becomes

$$f = .5\rho D\, C_D(U-\dot{x})\,|(U-\dot{x})| + .25\rho\pi D^2 C_M \dot{U} - .25\rho\pi D^2 (C_M-1)\ddot{x} \qquad -(12)$$

where U = fluid velocity, $\dot{U}$ = fluid acceleration, $\dot{x}$ = structural velocity, $\ddot{x}$ = structural acceleration, and it is considered that the values of C_D and C_M to be used are those that would apply for a stationary cylinder in the same flow conditions.

The inertia term in equation (12) is more complex than a direct substitution of $(\dot{U}-\ddot{x})$ for $\dot{U}$ in equation (3), because, as explained in chapter 3, the inertia term of equation (3) is made up of two parts. One of these, the Froude-Krylov force representing the force on the body due to the pressure gradient in the fluid, is not affected by body movement, provided that the extent of the movement is very small compared to the wave length. (See also Hogben (1976).)

If $U_m \gg \dot{x}_o$, as is usually the case, the drag term may be approximated as

$$.5\rho D\, C_D(U|U| - 2|U|\dot{x})$$

The equation of motion for a cylinder with displacement x everywhere along its length (say part of a member) may in general be written

$$m\ddot{x} + c\dot{x} + bx = f(t) \qquad -(13)$$

where m, c and b are the mass, damping factor and restoring constant per unit length.

Combining equations (12) and (13) under the assumption that

$U_m >> \dot{x}_o$, collecting $\dot{x}$ and $\ddot{x}$ terms on the left hand side and introducing the added mass per unit length, $m_a = .25\rho\pi\ D^2(C_M-1)$, one obtains

$$(m+m_a)\ddot{x} + (c+\rho D\ C_D|U|)\dot{x} + bx = .5\rho D\ C_D\ U|U| + .25\rho\pi\ D^2\ C_M\ \dot{U} \qquad -(14)$$

The right hand (forcing) side of equation (14) is identical to Morison's formula (3) for a stationary cylinder, and thus the effect of introducing relative terms into Morison's formula has been to introduce the added mass and the hydrodynamic damping. The hydrodynamic damping coefficient in this case is $\rho D\ C_D|U|$.

It should be noted that even if the $2|U|\dot{x}$ term is extremely small compared to the $U|U|$ term (i.e. $U_m >> \dot{x}_o$), then it is still of fundamental importance for response near resonance as it is, in effect, a damping term, and at resonance damping provides the sole limitation to the response.

A constant damping coefficient could be obtained by using the average value of $U = 2\ U_m/\pi$.

For the dynamic analysis of platforms in an irregular sea the drag term is usually linearized by equivalent linearization assuming the probability density of U to be Gausian. This leads to a linear damping term

$$.5\rho DC_D(8/\pi)^{1/2}(U_{rel})_{rms}\dot{x}$$

where $(U_{rel})_{rms}$ is the root-mean-square of the relative velocity, $U_{rel} = (U-\dot{x})$. This method was proposed by Borgman (1967) and has been used extensively by, amongst others, Foster (1967), Malhotra and Penzien (1970) and Gerwick (1975).

Some investigators have used equation (9) directly in a time-domain solution where no linearization is necessary.

The use of the above form of equation can lead to high damping values. Gerwick (1975) states that values of hydrodynamic damping of 5-10% of critical are "usually accepted", and Penzien (1975) has found that the damping increases with depth, and for a platform in 1000 ft depth he obtained hydrodynamic damping of 10% of critical.

The relative velocity assumption, at least with the stationary cylinder values of C_D, would appear to contrast sharply with full scale measurements by Earle and Mandery (1972) who obtained values of damping of 3.5% of critical in both calm weather and hurricane conditions on the same platform.

6.3. Initial discussion on the use of the modified Morison's formula

The discussion is confined to the drag term of the modified Morison's formula, although similar comments apply to the inertia term.

The modified Morison's formula is essentially a quasi-steady formula, where 'steady' in this case is understood to mean a wave flow on a stationary cylinder. The equation states that the drag force at any instant where the instantaneous relative velocity is $U_{rel} = (U-\dot{x})$ is identical to that in a 'steady' case with a velocity $U_{inst} = U_{rel}$. It is considered that the basic parameters of the flow, K, R, etc., are essentially the same so that the same values of the coefficients can be used. It is interesting to examine when the situation of vibrations in waves may reasonably be expected to become quasi-steady.

From the work described in chapter 4 on the boundary layer on a cylinder in combined steady and oscillatory flow, it is evident that unseparated flow of a cylinder oscillating in a steady current will be quasi-steady for large V/nD, and this may be expected to apply in the wave situation for large U_m/nD, as U_{inst}/nD is large for most of the cycle. Similarly for low V/nD (and U_m/nD) over the unseparated part of the cylinder the oscillating flow is expected to be the same as for a cylinder oscillating in still water, and the outer flow the same as on a stationary cylinder.

In an oscillatory or wave flow U_m/D is used to characterize the vortex shedding frequency and thus the rapidity of development of the wake. For large values of U_m/nD there are many vortices shed per vibration cycle, at least over most of the wave cycle, and the situation can be reconciled with the idea of quasi-steadiness. For

low values of U_m/nD, however, the oscillations are rapid compared to the vortex shedding, and the wake cannot keep pace with the changing velocity.

It is possible that for low values of U_m/nD and small amplitude oscillations, the oscillations may be the same as for a cylinder in still water over the rear portion of the cylinder also, as the flow velocities in the rear of a cylinder in a steady current are very low. It is only in the area of separation that the situation will be very different to that for a cylinder in still water, and it should be emphasized that the separation points may move over the cylinder during the vibration cycle (Lighthill (1954)).

Thus from an initial discussion it appears that the modified Morison's formula, used with stationary cylinder values of C_D and C_M, is only expected to predict the forces for large values of U_m/nD. It is also possible that the oscillatory forces for small amplitude oscillations at low U_m/nD may be approximately given by those in still water, i.e. as in chapter 3.13.

PART II - EXPERIMENTAL INVESTIGATION INTO VIBRATIONS OF CYLINDERS IN WAVES

INTRODUCTORY COMMENTS

One fundamental difficulty with an investigation into vibrations in waves, as the author sees it, is that the problem being dealt with is extremely complicated, there are a large number of parameters which are difficult to vary, other than over relatively small ranges, and the majority of which cannot be varied independently. The work presented in this Part reflects these difficulties and is by no means complete. The major weakness of the results obtained is that although considerable understanding of the processes involved has been gained, and some major parameters have been indicated, the author has been unable to non-dimensionalize the results satisfactorily.

The work was undertaken by the author at BHRA in the period 1974 to 1976 and during three months of 1978 under a contract with the Department of Energy into the vibrations of cylinders in waves. The work is described, chronologically, in a number of reports, Verley (1975a, 1975b, 1976, 1977b, 1978b) and Verley and Every (1977, 1978). The contracted work has been considerably extended by the author. The work involved investigation into the vibrations of isolated cylinders, pairs of cylinders in close proximity and groups of several cylinders. Only the work on isolated cylinders and some few results from pairs of cylinders will be considered in this thesis (the co-author Every conducted the tests on groups of cylinders).

A chronological description of the tests and the results obtained, including some discussion, will be undertaken in the following chapters, followed by a more extensive discussion in chapter 5.

1. DESCRIPTION OF THE APPARATUS

The aim of the research contract under which this work was undertaken was to gain a better understanding of the vibration problems associated with conductor tube banks on offshore platforms. As a first stage in the investigation it was decided to study a single isolated cylinder with variable dynamic properties in the range of those appertaining to a conductor tube.

Due to the variation in values of coefficients obtained by various researchers on rigid cylinders in waves and the small amount of data available, it was considered advisable to compare directly the forces on a flexible cylinder with those on a rigid cylinder mounted beside it, but with a sufficient distance between the cylinders that no interactions should occur. It was anticipated that the rigid cylinder would provide reference data against which to compare the flexible cylinder, thus isolating the effects due to flexibility and avoiding uncertainties in the estimated forces for rigid cylinders based on uncertain coefficient values and inaccuracies in estimated flow kinematics.

1.1. The flexible cylinder

Because of the difficulty in varying the structural properties of an elastic cylinder, it was decided to use a rigid cylinder flexibly mounted as an inverted pendulum, and such is meant throughout this Part when 'flexible cylinder' is referred to.

The flexible cylinder was pin-jointed to the dummy cylinder at its bottom end and helical springs on long wires were attached to the upper end to give the natural frequencies required (see Fig. 29). The springs were anchored above the water level to stiff cantilevers and forces were measured by strain-gauging one of the cantilevers as a half-bridge. Natural frequencies were easily altered by changing the helical springs. Initially motion was permitted only in the direction parallel to the wave propagation, which is refered to as the 'in-line' direction. Long inextensible wires were employed

to restrain motion in the direction perpendicular to the wave propagation, the 'cross-flow' direction. For later tests, in the cross-flow direction, the sets of restraining wires and helical springs were changed around to permit cross-flow motion and force measurement and to prevent in-line motion.

The decision to restrain one motion whilst looking at the other motion was taken because it simplified the test rig considerably and eased the analysis. King (1974), looking at steady flow induced hydroelastic vibrations, found that restraining motion in one direction had little or no effect on the response in the other direction.

All the tests have been conducted with the above arrangement of an inverted pendulum with the natural frequency provided by helical springs.

It is recognised that the restriction of vibration to one direction of motion at a time is a simplification which may alter the flow field.

1.2. The rigid cylinder

The rigid cylinder was also pin-jointed at its lower end to a dummy cylinder, and forces were measured on it by a half bridge strain-gauged stiff P.V.C. cantilever mounted inside the dummy cylinder at the upper end, as in Fig. 30. This method was employed for the rigid cylinder throughout all tests. The natural frequency of the rigid cylinder was 16.5 Hz in water.

1.3. Wave flume

Only regular waves have been used in the investigation.

The wave flume used for the tests was 20 m long, 1.5 m deep and 1 m wide. A hinged flap type hydraulically driven wave maker was installed at one end, the amplitude and frequency of movement being controlled by a simple oscillator. The test cylinders were placed about halfway down the length of the flume. The beach had a slope of 20^{o} and was covered with a 5 cm thick porous rubber matting. The reflection coefficient was estimated to be between 2 and 5% over the range of the wave frequencies used.

1.4. Test set-up

The tests were conducted with the top of the test cylinders 0.08 m below the water surface in 1.2 m of water. The length of the test sections of the cylinders was 0.76 m. Above and below the test cylinders dummy cylinders were mounted to minimise end effects, there being a gap of approximately 0.5 mm between the test sections and the dummy sections.

The test set-up is sketched in Fig. 29.

1.5. Wave measurements

All wave measurements were taken using a twin wire resistance type wave gauge. The wave gauge was self-compensating for changes in temperature and salinity, and allowed specific calibration factors to be selected at will.

1.6. Outputs recorded

Initially outputs were taken from the strain gauges at the top of the two cylinders and fed through amplifiers into a U.-V. recorder. Preliminary tests in the in-line direction indicated that the output from the flexible cylinder was the same as from the rigid cylinder, but (sometimes) with a higher frequency component superimposed. To look at the higher frequency component the two signals were subtracted electrically and the resultant 'difference reaction' trace displayed on the U.-V. recorder. This difference trace represented the effects due to flexibility, and this was the basic variable quantified. The circuitry is sketched in Fig. 31. This difference trace was not used when testing in the cross-flow direction, in which case the method used to quantify the vibration is described in the next section.

All outputs had variable amplification so that the three traces,

one from the top of each cylinder and one for the difference, could be calibrated to give the same deflection on the U.-V. recorder for the same force input. The outputs were calibrated in terms of force applied at the top of each cylinder, and there was found to be less than 1% deviation in the calibrations from the best linear fits. The calibration was carried out by applying various forces to the top of each cylinder using a pulley system and weights. The measurements in the tests thus represent the reactions measured at the top of the cylinders.

1.7. Tests conducted

Several test series have been conducted for both the in-line and cross-flow directions. The cylinder diameter, D, and still water values of natural frequency, n, and logarithmic damping, δ_{sw}, have been varied over the following ranges.

In-line tests

D	.0190, .0254, .0508 m
n	from 1.7 to 6.7 Hz
δ_{sw}	from .05 to .3

Cross-flow tests

D	.0254 m
n	from 2.2 to 5.4 Hz
δ_{sw}	from .08 to .7

The wave frequency, n_w, was varied in the range .5 to 1.0 Hz, and the wave height between .05 and .25 m.

Various damping factors were obtained by having one of the springs controlling the flexible cylinder natural frequency passing

through a bath of silicone fluid, as in Fig. 32. By using various silicone fluids the damping could be varied over the range $\delta_{sw} = .05 \sim .7$, and was perfectly linear over the range of amplitudes of vibration encountered.

Various methods of quantifying the vibration reaction have been used. In initial tests in the in-line direction, the highest peak-to-peak value of the difference reaction in a 15 second recording period was taken by eye from the U.-V. traces. In later tests, r.m.s. values were taken using a true reading r.m.s. meter set with a time constant of 15 seconds. This r.m.s. value is denoted R_x.

In the cross-flow direction it was not possible to subtract the rigid cylinder reaction from the flexible cylinder reaction. This was because the variation due to lift forces, on top of which was superimposed vibration, was sometimes similar to and sometimes the mirror image of that on the rigid cylinder, depending, presumably, on whether vortex shedding occurred from the same or opposite sides of the two cylinders. (This made no difference in the in-line tests.) Therefore, in order to compare the results with those of the in-line direction, the average amplitude of the vibration component of the flexible cylinder reaction was estimated by eye and converted to r.m.s. using a form factor of 1.11 (as for a sinusoid). The r.m.s. value calculated is denoted R_y. The results are thus inherently less accurate than the in-line results.

1.8. Experimental procedure

For each wave frequency, at which each flexible cylinder natural frequency and damping combination was to be tested, the procedure was as follows:

After the previous test, the water in the wave flume was allowed to settle until there was no visible movement of the surface (about 10 minutes). The oscillator driving the wave generator was set for the appropriate wave frequency and the lowest wave height and the wavemaker was started. Recording of the traces was started after about 10 waves had passed the cylinders, and continued for a period of about 20 seconds. The amplitude of the wavemaker was then in-

creased to the next wave height (without stopping the wavemaker), and results again recorded after about 10 waves at the new height had passed. The four lowest wave heights were tested in this manner, i.e. without stopping between wave heights. For the higher wave heights, however, the water in the flume was allowed to settle between tests at each wave height. Testing was conducted at 7 wave heights at each of 5 wave frequencies.

2. RESULTS

2.1. Initial results in the in-line direction

Initial testing in the in-line direction showed that for low wave heights there was no visible difference between the traces from the rigid and flexible cylinders. For larger wave heights the flexible cylinder trace resembled that from the rigid cylinder, but with a higher frequency component superimposed which was at, or very near, the flexible cylinder natural frequency, as in Fig. 33. The trace obtained by subtracting the rigid cylinder reaction from the flexible cylinder reaction, the difference reaction, thus consisted of a trace at, or very near, the natural frequency and this 'difference trace' quantified the differences between the flexible and rigid cylinders.

From the traces of Fig. 33 and other similar traces it has been noted that the average number of vibration cycles in the difference trace per wave cycle is equal to the integral multiple of the wave frequency nearest to the natural frequency.

The initial results have been quantified in Fig. 34 against U_m/nD, where U_m is the maximum horizontal fluid velocity calculated at the top of the cylinder using linear wave theory. Experimental points are plotted for n = 6 and 1.65 Hz.

From these results it can be seen that vibration of the flexible cylinder first started at a value of $U_m/nD \approx 1.0$, for any cylinder natural frequency and wave frequency within the limits $1.65 < n \lesssim 6$, $.5 < n_w < 1.0$ and for a value of logarithmic damping of $\delta_{sw} = 0.08$. It is of interest to note that vibrations occurred even for the highest ratio of natural to wave frequency, 6/.6 = 10, the criterion $U_m/nD \gtrsim 1.0$ apparently being the only criterion to be satisfied for vibration to occur.

For a given value of U_m/nD more response occurred for higher values of n. For the higher natural frequencies there is little scatter from the curves shown in Fig. 34, however for lower natural frequencies there is, for any particular natural frequency, greater

response for some wave frequencies than for others. Which wave frequency gave greatest response varied depending on the natural frequency, however greater response appeared to occur when the natural frequency was nearer to an integral multiple of the wave frequency.

To illustrate the effects of the natural to wave frequency ratio, a flexible cylinder with a natural frequency of 2.50 Hz was tested in waves of frequency 0.775, 0.792, 0.820, 0.836, 0.845, 0.861 and 0.910 Hz, yielding ratios of $3n_w/n$ of 0.93, 0.95, 0.98, 1.00, 1.02, 1.03, and 1.09, respectively. The traces yielded an average frequency of 3 n_w in all cases. The effect of the ratio n/n_w can clearly be seen in the results, Fig. 35, where there is greater response the nearer the ratio is to 3.000, i.e. the nearer $3n_w/n$ is to 1.00.

Example traces are shown in Fig. 36 where it is seen that for an integral ratio of n/n_w the difference reaction is much more even, and of greater amplitude, than when n/n_w is away from an integral value.

In all further results the natural to wave frequency ratio is expressed as a parameter $|(1-rn_w/n)|$, where r expresses the number of oscillations of the difference trace per wave cycle, i.e. r is an integer such that rn_w/n is as near to 1.0 as possible. Thus the nearer the parameter $|(1-rn_w/n)|$ is to 0.0, the nearer the natural frequency is to an integral multiple of the wave frequency and the greater response expected.

2.2. Further tests

Tests have been conducted for three cylinder diameters in the in-line direction, and one diameter in the cross-flow direction. The natural frequency and damping of the flexible cylinders were varied and r.m.s. values of the difference reaction were measured.

The results are plotted as R_x/nD^3 for the in-line direction and R_y/nD^3 for the cross-flow direction in Fig. 37. Average curves are plotted for the points in various ranges of δ_{sw} and $|(1-rn_w/n)|$. Example curves, with points, are shown in Fig. 38.

The parameters R_x/nD^3 and R_y/nD^3 are not non-dimensional, but are used for convenience as they were found to collapse the results

for all cylinder diameters, natural frequencies and wave frequencies. Non-dimensionalization will be discussed in a subsequent chapter.

From the results it is seen that vibration first starts at $U_m/nD \approx 1.0$ for both the in-line and cross-flow directions. Greater response occurs for lower values of $|(1-rn_w/n)|$, but the parameter has less effect for higher values of δ_{sw}. Increased damping reduces the response, but not by very much. The cross-flow results are similar to the in-line except that the response is about twice as great. Example traces from the cross-flow direction are shown in Fig. 39.

At this stage the question arose as to whether the forcing on the flexible cylinder was similar to, or entirely different from that on the rigid cylinder. Two simple experiments were devised to investigate this and are presented in the next section.

2.3. Comparison of the forcing on the rigid and flexible cylinders

The mode shape of the flexible cylinder (an inverted pendulum) means that in free vibration the reaction at the top of the cylinder is exactly twice as great as that at the bottom of the cylinder (as the centre of inertia is 2/3 of the way up the cylinder from the centre of rotation).

If one considers the response of the flexible cylinder from the point of view of the Duhamel integral, then one can consider the response as the linear superposition of responses to a series of impulses of varying intensity which together make up the input force time history. After each impulse is applied, the cylinder oscillates in free vibration. If one thus took an experimentally measured reaction from the bottom of the flexible cylinder, multiplied it by 2.0 and subtracted it from the reaction from the top of the cylinder, then all the superimposed free vibration components would be removed, and only the impulse forcing would remain. The magnitude of the forcing would not be shown unless it acted purely at the top of the cylinder, and if it acted 1/3 of the way down the cylinder, it would also be removed.

An experiment was conducted where also the cross-flow reactions at the bottom of the flexible cylinder were measured using a strain-

gauged cantilever similar to that shown in Fig. 30, except that it was pin-jointed to the cylinder.

In Fig. 40 example traces from this experiment are shown. It is seen that the trace from the flexible cylinder with free vibration removed is very similar to that recorded from the top of the rigid cylinder. This indicates that the forcing on the flexible cylinder was similar in nature to that on the rigid cylinder. Furthermore the amplitudes of the traces are similar, probably indicating that the forcing is being applied very near the top of the cylinders. (It is possible that the forcing is applied lower, but is of larger magnitude on the flexible than on the rigid cylinder.)

In order to investigate the comparison of the forcing on the rigid and flexible cylinders further, the rigid cylinder trace in the cross-flow direction was used as input to a simple mathematical model of the equation of motion of the flexible cylinder, and the output predicted from the model was compared with that obtained with the actual flexible cylinder in experiments. The equations were modelled using a finite difference solution programmed on a pocket calculator. Still water values of damping were used in the model. In Fig. 41 are shown the traces from the rigid and flexible cylinders in an experiment together with the predicted flexible cylinder trace. It is seen that the predicted response is very similar to the actual response.

This model will be further built on in the following chapter.

2.4. Initial indications of the causes of the vibration

It seems, from the initial brief investigations of the previous section, that the cross-flow forcing on the flexible cylinder is similar to that on the rigid cylinder, and that the flexible cylinder response may be predicted using the rigid cylinder reaction as input to a dynamic model and with damping given by the still water experimental value for the flexible cylinder.

It will be shown in chapter 4.3 that the rigid cylinder reaction traces in the cross-flow direction are very similar to those obtained by other investigators, who considered their traces to be caused

by vortex shedding, and to traces produced by a quasi-steady model of vortex shedding forces to be considered in chapter 4.2. Therefore, it is considered that the cross-flow forces on the rigid and flexible cylinders are due to vortex shedding forces.

The response in the in-line direction is very similar to that in the cross-flow direction, exhibiting the same dependence on the parameters U_m/nD, δ_{sw} and $|(1-rn_w/n)|$. It therefore seems likely that this vibration is also a response to vortex shedding forces.

3. MATHEMATICAL MODELS TO PREDICT VIBRATIONS

It has been seen in the previous chapter that the flexible cylinder's in-line and cross-flow vibrations were probably both caused by response to vortex shedding forces. Furthermore the forces causing the vibration, at least in the cross-flow direction, appeared to be similar to the forces on the rigid cylinder, and the response seemed to be reasonably well predicted when still water values of damping were used. However, insufficient data was analysed, and the pocket calculator solution of chapter 2.3 was too time consuming to be applied to many time series. It was therefore decided to investigate the prediction of the flexible cylinder response using computer collected experimental data and computerized mathematical models.

In Part I, chapter 6.2 it was seen that the modified Morison's formula is usually used for the dynamic analysis of cylindrical structures in waves. This formula does not include any cross-flow forcing terms, and no account is taken of vortex shedding forces (other than their effect on the time averaged drag and inertia coefficients). It is thus interesting to compare the in-line response with that predicted using the modified Morison's formula. It was also seen in Part I, chapter 6.2 that the relative velocity term in the modified Morison's formula leads to an additional damping term, the so called hydrodynamic damping. In Part I, chapter 6.3 it was suggested that the use of the relative velocity formulation may be unreasonable other than for high values of U_m/nD. It is thus of interest to investigate the effects of this damping term in the in-line direction. This was done both by using the complete modified Morison's formula, in which case both the forcing and damping are given (see equation (14)), and also by using the forcing given by the rigid cylinder reaction in conjunction with the hydrodynamic damping given by the modified Morison's formula. The following mathematical models were therefore developed.

Case A The reaction from the rigid cylinder in experiments was used as input to a mathematical model of the flexible cylinder where damping was given by experimental values in still water.

Case B The reaction from the rigid cylinder in experiments was used as input to a mathematical model of the flexible cylinder

where damping was given as structural damping (not still water damping) plus that obtained from the modified Morison's formula with C_D distributed over the cylinder according to local values of K and using data from experiments in oscillating flow.

Case C The Morison's formula was used to predict the reaction of the rigid cylinder which was in turn used as input to the model with damping given by the still water value. This case is the same as Case A except that the input reaction is changed.

Case D The full modified Morison formula was used, giving both the input force and the damping in addition to structural damping. This case is the same as Case B except that the input reaction is changed.

Case D was very similar to those considered by Bullock et al. (1978) and Sawaragi et al. (1978), except that first order wave theory was used and the test section of the cylinder did not penetrate the water surface.

In Cases A and B the experimental reactions of the rigid cylinder are used as input, and thus the inputs to the models include the vortex shedding forces measured on a rigid cylinder, which Cases C and D do not.

For the cross-flow direction only the model of Case A has been used.

Unfortunately only one set of data for isolated cylinders could be collected, and this was only analysed for the model of Case A. Therefore, results from tests where two cylinders were mounted side by side and five diameters apart (centre to centre) were also used. It was found that the results were the same as for isolated cylinders, i.e. there did not appear to be any interactions between the cylinders. (Proximity effects first began to be noticed when the cylinders were 3 diameters apart.) In these tests data was recorded for 20 seconds at each wave height. Some of the results for cases A and B above are given in Verley (1978b).

3.1. Derivation of the mathematical models

The mathematical models were used to give a predicted flexible cylinder reaction trace and an r.m.s. value of the difference reaction by modelling the flexible cylinder as a first degree of rotational freedom system, the equation of motion being solved in the same time domain.

The flexible cylinder was an inverted pendulum, and the system is sketched below.

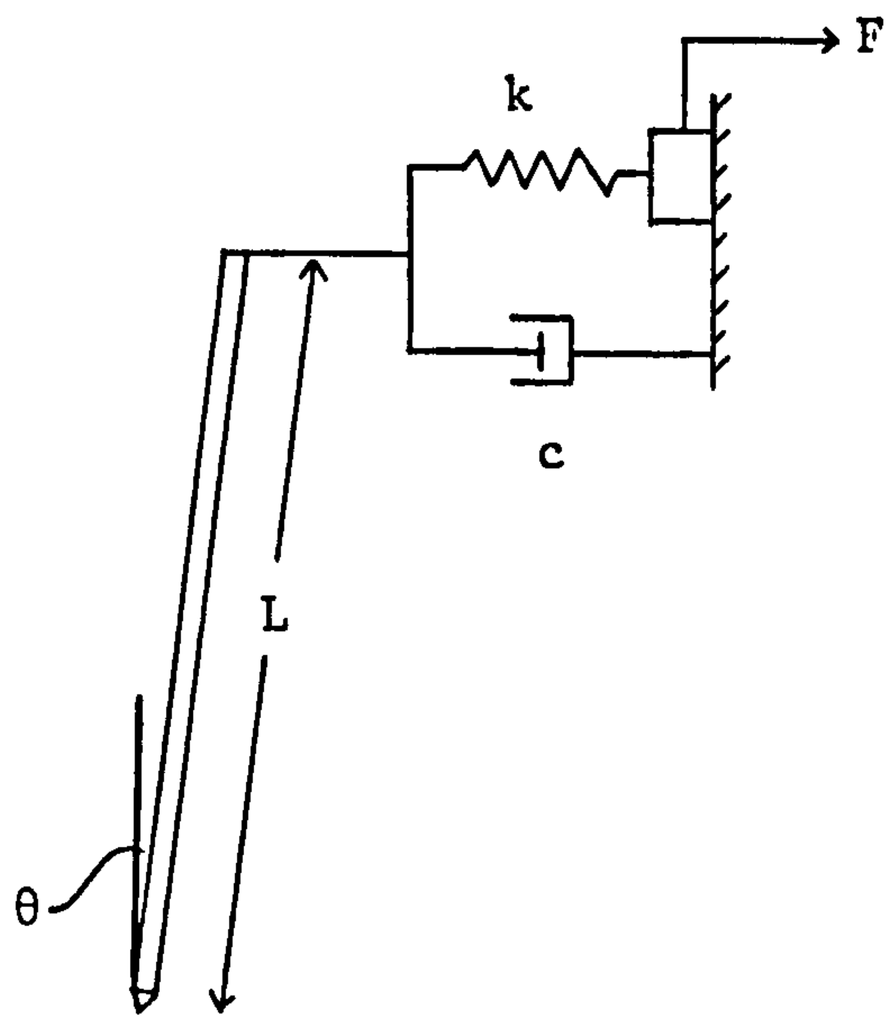

The equation of motion of a first degree of rotational freedom system can in general be written as

$$\left.\begin{aligned} I\ddot{\theta} + C\dot{\theta} + M_R\theta &= Fz \\ \text{Furthermore}\quad \omega_n^2 &= M_R/I \\ C_{crit} &= 2I\omega_n \\ \delta &= 2\pi\ C/C_{crit} \\ C &= cL \\ M_R &= kL^2 + (B-M)gL\theta \end{aligned}\right\} \qquad -(15)$$

where I = moment of inertia, C = rotational damping coefficient M_R = rotational stiffness, Fz = moment and δ = logarithmic damping.

This applies for small θ.

Model for Case A

From the diagram and using the relationships of (15) the equation of motion for the cylinder at a time instant, t, may be written:

$$\ddot{\theta}_t + \frac{C_{sw}\dot{\theta}_t}{(I_{cyl}+I_a)} + 4\pi^2 n^2 \theta_t = \sum_{z=0}^{L} \frac{f_t z dz}{(I_{cyl}+I_a)} = \frac{F_t L}{(I_{cyl}+I_a)} \qquad -(16)$$

where θ_t, $\dot{\theta}_t$ and $\ddot{\theta}_t$ = angular displacement, velocity and acceleration at a time instant, t, I_{cyl} = inertia of the cylinder about the centre of rotation (in air), I_a = inertia of the added mass of water about the centre of rotation, n = natural frequency in water, f = force per unit length at each level z and $F_t L$ is the moment input to the model where F_t is obtained from the rigid cylinder time history in the experiments. The damping used is the damping measured in still water which is made up of a structural damping term, C_{cyl}, and viscous fluid damping, C_{visc}, i.e.

$$C_{sw} = C_{cyl} + C_{visc}$$

The still water damping was obtained from the logarithmic damping of vibrations in still water and was found to be constant within the range of amplitudes of vibration encountered in the experiments. The structural damping was obtained from vibrations in air, and the remaining damping, C_{visc}, agreed within 5% with that calculated using Stokes' equations (Part I, chapter 3.13).The inertia of the added mass, I_a, was calculated using the small amplitude, still water value of added mass, i.e. using the displaced mass of water.

A fourth order Runge-Kutta solution of the equation for θ as a function of time was written by the author, and the time step used was 0.04 sec. The highest natural frequency used was 4.17 Hz.

The mathematical model was tested by choosing values of n and C_{sw} and using impulse and step inputs. The frequency and logarithmic damping of the model output were checked together with the deflection for the case of the step input. The frequency of vibrations was found to be about 1% lower than that input to the model (this

is usual for the numerical technique used), and the damping and deflection produced were within 1% of the theoretical values. It was therefore considered that the model and programming were correct.

The reaction of the rigid cylinder in the experiments was used as input to the model, and from the output, $\theta(t)$, a predicted flexible cylinder reaction was produced (from the knowledge of the cylinder length and spring constant, b). The output time history was stored on the computer together with a difference reaction. The r.m.s. value of the difference reaction was taken over the last 15 seconds, as there were initial transients, associated with the starting of the mathematical model, which were present during the first 5 seconds or so of the response.

Model for Case C

The model for Case C is the same as that for Case A, except that the input reaction, i.e. the right hand side of equation (16), is derived from Morison's formula. i.e. the right hand side of (16) becomes

$$\sum_{z=0}^{L} f_t z\ \Delta z = \sum_{z=0}^{L} \left[.5\rho D\ C_D\ U_t|U_t| + .25\rho\pi\ D^2\ C_M\ \dot{U}_t\right] z\ \Delta z$$

which can be written

$$.5\rho D\ U_M^2 \sum_{z=0}^{L} \left[C_D\ \cos\theta|\cos\theta| - \frac{\pi^2 C_M}{K} \sin\theta\right] z\ \Delta z \qquad -(16a)$$

where the phase $\theta = 2\pi t/T$, T = wave period and $\theta = 0$ at the wave crest C_D, C_M and K are local values at each level, and $\Delta z = .02$ m, i.e. the cylinder length is divided into 38 levels.

It is noted that the inertia of the added mass, I_a, is still calculated using the displaced mass of water.

Models for Cases B and D

The force, Δf, on a small length, Δz, of a moving cylinder in waves is assumed given by the modified Morison's formula:

$$\Delta f = .5\rho D\ C_D(U-\dot{x})\left|(U-\dot{x})\right|\Delta z + .25\rho\pi D^2\ C_M\ \dot{U}\Delta z - m_a\ddot{x}\Delta z \qquad -(17)$$

where U, $\dot{U}$ and $\dot{x}$, $\ddot{x}$ refer to local values of fluid and cylinder velocities and accelerations, respectively, and m_a is the added mass per unit length = $.25\rho\pi\ D^2(C_M-1)$.

The drag term can be written as

$$\gamma\left[.5\rho D\ C_D(U^2-2U\dot{x}+\dot{x}^2)\Delta z\right]$$

where $\gamma = +1$ when $U \geq \dot{x}$

and $\gamma = -1$ when $U < \dot{x}$

The equation of motion for the cylinder at a time instant, t, may be written

$$I_{cyl}\ddot{\theta}_t + C_{cyl}\dot{\theta}_t + M_R\theta_t = \sum_{z=0}^{L}\{\gamma\left[.5\rho D\ C_D(U^2-2U\dot{x}+\dot{x}^2)_t z\ \Delta z\right]$$

$$+ .25\rho\pi D^2\ C_M\dot{U}_t z\ \Delta z - m_a\ddot{x}_t z\ \Delta z$$

where C_{cyl} is the structural rotational damping coefficient calculated by noting the logarithmic decrement of vibrations in air and using (15).

Using the relationship

$$\dot{x} = z\dot{\theta}$$

and collecting terms in θ, $\dot{\theta}$ and $\ddot{\theta}$ on the left hand side, one obtains

$$\ddot{\theta}_t + \frac{1}{I_{cyl}+I_a}\left[C_{cyl} + \sum_{z=0}^{1}\{\gamma(\rho D\ C_D U_t z^2\Delta z - .5\rho D\ C_D z^3\dot{\theta}_{t-1}\Delta z)\}\right]\dot{\theta}_t + 4\pi^2 n^2\theta_t$$

$$= \frac{1}{I_{cyl}+I_a}\sum_{z=0}^{1}\left[\gamma(.5\rho D\ C_D U_t^2 z\Delta z) + .25\rho\pi D^2\ C_M\dot{U}_t z\Delta z\right] \qquad -(18)$$

where I_a is the inertia of the added mass given by

$$I_a = \sum_{z=0}^{L} m_a z^2 \Delta z$$

It was found, as might be expected, that $\dot{x}_o << U_m$, where $\dot{x}_o$ is the velocity amplitude of the cylinder vibrations. Thus

$$\gamma U_t^2 \approx U_t |U_t|$$

and the right hand side of equation (18) becomes the reaction due to the Morison's formula, as in (16a). The left hand side of equation (18) is the same as that of equation (16) except that the hydrodynamic damping is given by the term in curled brackets rather than the viscous damping term.

The value of $\dot{\theta}_{t-1}$ within the curled brackets on the left hand side of equation (18) was given by its value at the previous time step. This was necessary, otherwise the equation would be non-linear due to a $\dot{\theta}^2$ term, and hence extremely difficult to solve.

One simplification to equation (18) was employed, namely that the added inertia, I_a, used was the still water value, i.e. as if $C_M = 2$ in equation (18). This was used irrespective of the values of C_M on the forcing side of the equation. The error is considered to be small as the added inertia was only about 20% of the total inertia.

Equation (18) was used for the model of Case D, and for Case B the right hand side was replaced by the reactions measured on the rigid cylinder, i.e. the same as the right hand side of equation (16).

3.2. Prediction of forces on the rigid cylinder using Morison's formula

In order that the use of the modified Morison's formula can

be justified it must first be shown that the forces on a rigid cylinder are reasonably predicted by Morison's formula, and values of C_D and C_M must be determined.

The forces on the rigid cylinder could in principle have been determined from reactions measured at the upper and lower ends of the cylinder and used to determine C_D and C_M values, using an integrated form of Morison's formula. Average values over the whole length of the cylinder would be determined as no account could be taken of variations in the coefficients with local Keulegan-Carpenter number.

Instead of the above method, an attempt was made to predict the reaction at the top of the rigid cylinder in the in-line direction by using Morison's formula with values of C_D and C_M varying along the cylinder in accordance with the varying local Keulegan-Carpenter number, and choosing the values of C_D and C_M from the results of Part III where cylinders were oscillated in still water. These values are virtually identical to those of Sarpkaya and Tuter (1974). In Part I, chapter 3.12 it was seen that several researchers have shown that coefficients determined in oscillatory flow may be successfully used to predict forces in waves.

Equation (16a) was used to calculate the rigid cylinder in-line reaction.

It was found that the amplitude of the reaction predicted by equation (16a) agreed very well with that measured, except for the highest wave frequencies (.9, 1.0 Hz), particularly for the largest heights, when the amplitude was over predicted. The most probable reason for this is that in the experiments the waves were very 'poor', being near breaking and three-dimensional, at these highest frequencies, particularly for the higher heights. Some representative examples of actual rigid cylinder reactions compared with reactions predicted using Morison's formula for lower frequencies are shown in Fig. 42. It is seen that the amplitude and general shape of the reaction traces are predicted well. However the smaller distortions of the traces are not predicted, as is also the case in oscillatory flow for $10 \lesssim K \lesssim 30$.

On the basis of the above, the mathematical models of Cases A-D were only used to predict vibration for frequencies $\lesssim .9$ Hz.

3.3. Results of the mathematical models

As has been mentioned only one set of tests for isolated cylinders could be used, and only the model of Case A was run on these data. The results are presented in Fig. 43 for both the in-line and cross-flow directions. The experimental results are marked 'EXPERIMENTAL' and those from the model, 'A'.

Representative results from the pairs of cylinders are presented in Figs. 44 to 46 for various values of δ_{sw} and $|(1-rn_w/n)|$. In Fig. 44 δ_{sw} is in the range .05 to .07 and $|(1-rn_w/n)| = .03$. In Fig. 45 the damping is in the same range and $|(1-rn_w/n)|$ is from .03 to .1. In Fig. 46 both δ_{sw} and $|(1-rn_w/n)|$ are high, being in the ranges .16 to .21 and .1 to 1.0, respectively. The experimental results are marked 'EXPERIMENTAL', and those for each model are marked with the relevant letter.

3.4. Discussion of the results

It is immediately evident from the results that the only model which predicts the measured vibration reasonably is that of Case A, i.e. using the rigid cylinder reaction as input and the measured still water damping. This is true for both the in-line and cross-flow directions. All the other models underpredict the vibration, particularly that using the modified Morison's formula.

There is considerable scatter in the results, though it is noted that it is nearly always the response to all wave heights for a particular combination of n and n_w which lie high, say, rather than arbitrary points. (For example the solid diamonds and open squares of Fig. 45.) It is also evident that if a particular data point from the experiments appears to be high, say, then those predicted by the models of Cases A and B are usually also high. This indicates that not all the factors controlling the vibration have been uncovered.

The most important conclusions of these results are that the modified Morison's formula (Case D) underpredicts the vibration con-

siderably, and that this method of calculating the vibration of offshore platforms should be called into question until similar tests to these are conducted at the relevant values of Reynolds and Keulegan-Carpenter numbers. The use of the simple Morison's formula without accounting for relative velocities gives a better, though still low, prediction of the vibration, presumably due to its non-inclusion of vortex shedding forces. In order to estimate the vibration correctly it is necessary to have a rather better estimate of the forces on a rigid cylinder than the present Morison's formula, specifically including vortex shedding forces, at least for the values of K involved here.

Furthermore the vibration does not appear to alter the forces on the cylinder, and the response of a flexible cylinder can be predicted from a full knowledge of the forces on a rigid cylinder, including forces from vortex shedding. i.e. there are no hydroelastic effects for the range of parameters tested.

Alternatively it is possible that the relative velocity form is correct but that the coefficients are altered by the vibration, the net effect being that the response is the same as when calculated without relative velocity effects. A sensitivity analysis to see how different values of C_D would have to be from those on a rigid cylinder for Case B to give the same vibration as Case A.

4. A DESCRIPTION OF VORTEX SHEDDING FORCES IN OSCILLATORY AND WAVE FLOWS

4.1. Traces of cross-flow vortex shedding forces on the rigid cylinder in waves

There is considerable evidence from the results presented that the forcing which the flexible cylinder undergoes is the same as that on the rigid cylinder. Thus a complete description of the forcing which the rigid cylinder is subjected to, including that due to vortex shedding, should be sufficient to determine the response of a flexible cylinder.

Some research has already been conducted into the forces on rigid cylinders in oscillatory flows or waves. In Part I, chapter 3.4 it was seen that various researchers have given the relative magnitudes of the lift components at the first few multiples of the wave frequency for varying K. Unfortunately the present results do not lend themselves to a complete analysis. Only reactions at the top of a rigid cylinder have been measured rather than forces over small lengths of a cylinder and the time series collected are too short to enable an accurate spectral analysis of the frequency content of the forces to be obtained. Nevertheless, the traces of the cross-flow reaction from the rigid cylinder have been examined qualitatively and several general observations may be made.

i) Traces for different wave frequencies but the same value of K exhibit similar trends in terms of number of oscillations per wave cycle and general shape of the traces.

ii) Cross-flow forces first become apparent at values of K between 4 and 5, the cross-flow trace sporadically exhibiting oscillations, one per half wave cycle and usually only in one half of each wave cycle.

iii) By a value of $K \approx 7$ there is a very regular, almost sinusoidal cross-flow forcing at twice the wave frequency, as in Fig. 47,a. As K is further increased the trace becomes more saw-toothed, but still performs two oscillations per wave period. The steep parts of the trace

are always very near the peak and trough of the wave (maximum velocity), and are in the same direction at both the peak and trough. Fig. 47,b is typical of traces for values of K from 8 ~ 11. The traces in this range are still fairly even, though there is some variation from cycle to cycle in amplitude and shape. The oscillation in the wave crest half cycle is often slightly larger than that in the wave trough half cycle.

iv) In the region K = 12 ~ 13, as in Fig. 47,c, the trace is still saw-toothed in form, but changes with time, there often being several cycles of saw-toothed form followed by cycles with small or no amplitude, followed again by several cycles with a saw-toothed trace, the direction of the saw-tooth often having reversed.

v) In the range K = 13 ~ 15 a trace such as that in Fig. 47,d occurs where the trace consists of a dominant component at twice the wave frequency. The amplitude in the wave crest half cycle is rather larger than that in the wave trough half cycle. Again there is considerable variation with time, the trace sometimes almost dying away and sometimes becoming particularly large, and the exact shape of the trace varies slightly from cycle to cycle.

vi) For K above about 16 and to the maximum tested (~22), the traces may be characterized by Fig. 47,e, f, g and h with Fig. 47,e as the most commonly occurring trace. On first examination it may appear that there are considerable differences between these traces, however only small adjustments in the amplitudes and positions of the various oscillations are necessary in order to change one shape to another. Fig. 47,g for example resembles both Fig. 47,e and h fairly closely, and indeed appears to be in between them, although Fig. 47,e and h do not appear at first sight to resemble each other.

All these traces consist mainly of components at two and three times the wave frequency, with Fig. 47,f being mainly at two times and Fig. 47,h mainly at three times the wave frequency. Also in this range of K there was

considerable variation from cycle to cycle and with time. For example Fig. 47,i shows a length of trace where the oscillations first resemble those of Fig. 47,e and then change in shape to resemble those of Fig. 47,h. Once again it is often found that the amplitudes in the wave crest half cycle are larger than those in the wave trough half cycle.

4.2. A simple model of lift forces in oscillatory and wave flows

Before embarking on a discussion of the cross-flow traces obtained from rigid cylinders in waves, it is appropriate to describe a very simple quasi-steady model of lift forces caused by vortex shedding in oscillatory flows. The model, despite its over-simplicity, is nevertheless instructive and gives some insight into the phenomena associated with vortex shedding in waves.

The fundamental assumptions of the model are as follows:

i) If one considers a steady flow of velocity V, then the vortex shedding and the cross-flow forcing frequencies are considered to be sinusoidal and defined by the Strouhal relationship with S = .2.

$$n_v = .2V/D$$

and the period $T_v = 1/n_v$.

The instantaneous value of lift force is given as

$$f(t) = .5\rho D\ C_L\ V^2\ \sin\phi = k_L V^2 \sin\phi \qquad -(19)$$

with $k_L = .5\rho D\ C_L$

where ϕ is the phase of the lift cycle = $2\pi\ t/T_v$.

ii) For vortex shedding in waves it is supposed that (19) may apply quasi-steadily, i.e. using instantaneous values of V and T_v. The instantaneous vortex shedding frequency is thus proportional to the instantaneous velocity, and

the instantaneous value of the lift force is proportional to the instantaneous velocity squared times the sine of the phase of the lift cycle.

iii) A step by step scheme was programmed in Fortran for use on the VHL NORD-10 computer whereby at each increment of time (1/50 wave period) the instantaneous velocity and vortex shedding period were calculated, together with the increase in phase of the vortex shedding assuming that the vortex shedding period was constant over the time increment. The instantaneous force was then calculated as $k_L U_{inst}^2 \sin\phi$, where ϕ is the phase ($\neq 2\pi t/T_v$, the phase must be cumulated from step to step as T_v varies).

iv) It is assumed that at the beginning of each half wave cycle the flow starts from scratch again and the phase is brought to either 0^o or 180^o, which amounts to deciding from which side of the cylinder the first vortex will be shed in the next half cycle. An attempt was made to simulate the reported suggestion, that the first vortex shed in a half cycle is shed from the same side as the last vortex shed in the previous half cycle, by having a test at flow reversal so that ϕ in the new half cycle was set to 0^o if ϕ at the end of the previous was $< 180^o$, otherwise ϕ was set to 180^o. However it is considered that this amounts to too many assumptions about the relationship between when a vortex can be considered to be shed (in the understanding that it then promotes shedding from the same side of the cylinder immediately after flow reversal) and the forces. Suffice it to say that if ϕ is set to 0^o at the beginning of each half wave cycle, then the trace will repeat every half wave cycle, and if ϕ is set to 180^o the trace in each half cycle will be the mirror image of that in the previous and will repeat every wave cycle. These two types of trace lead to power at only even and only odd multiples of n_w, respectively.

The model has been run with both ϕ in a new half cycle being set to 0^o and being set to 180^o. A decision as

to the most appropriate may be judged from a comparison of the time histories produced with those from experiments.

v) It is expected that the model should give best results for higher values of K, when the flow becomes more nearly quasi-steady.

4.2.1. Results of the simple model

In Fig. 48 are shown traces of $k_L U^2_{inst} \sin\phi$, non-dimensionalized by $k_L U^2_m$, for three wave periods at values of K = 5, 10, 12.5, 15, 18.5, 20, 22, 30, 40, and 100.

For K up to 15 the traces most resemble experimental traces when ϕ at flow reversal is set to 0o. For K up to 15 there are two oscillations per wave cycle, and it is in this area that several authors have noted the same and that one vortex is shed from the same side of the cylinder in each half wave cycle. For increasing K in this range the traces become more and more saw-toothed with a steep part near the maximum velocity points.

For values of $K \gtrsim 16$ experimental traces are found which resemble the predicted traces for ϕ at flow reversal set to both 0o and 180o.

Spectral analysis for the traces over exactly 6 wave cycles has been conducted and the results are plotted, for various K, in Fig. 49. For $K \gtrsim 16$ both the spectra for conditions with ϕ at flow reversal set to 0o and 180o are plotted (odd and even powers of the wave frequency, respectively).

As K is increased there is increasingly more power at the higher frequencies.

In Fig. 50 the peak values of the spectra at the various multiples of the wave frequency are plotted against K. This diagram is qualitatively similar to those obtained by Sawaragi et al. (1976), Isaacson and Maull (1976) and Maull and Milliner (1978), see for example Fig. 7.

Further discussion of these results is given in the following section.

4.3. Discussion of vortex shedding from rigid cylinders in oscillatory and wave flows

In general the experimental traces in waves resemble those obtained in oscillatory flows by various researchers, except that there seems to be more variation with time and there is often a difference in amplitude between the oscillations in the wave crest half cycle and those in the wave trough half cycle.

The traces produced by the simple quasi-steady model of the previous section are also quite similar to traces obtained in oscillatory and wave flows except that they are, of course, more even.

The trace from waves for K = 5 ~ 7, Fig. 47,a, is very similar to that produced by the quasi-steady model, Fig. 48, for similar K.

One can compare Fig. 47,b in waves which is typical for values of K = 8 ~ 11 with Mercier (1973)'s Fig. 14,c for K = 9.4, with Sarpkaya and Tuter (1974)'s Fig. 7 for K = 12.4, and with the quasi-steady model in Fig. 48 at K = 12.5. All of these are similar, showing a saw-toothed trace at twice the wave frequency.

Fig. 47,c for K = 12 ~ 13 in waves compares well with Mercier's Fig. 14,d at K = 12.6, both showing considerable variation with time.

There is considerable similarity between Figs. 47,f and g in waves for K = 16 ~ 22 and Mercier's Fig. 14,e and f at K = 15.7 and 19, respectively, and the quasi-steady model of Fig. 48 for K = 16.5 and 20, respectively. Figures similar to Fig. 47,g in waves have also been produced by Sarpkaya and Tuter at K = 16 (their Fig. 5), and by Maull and Milliner at K = 21 (their Fig. 15, when replotted against an axis of time).

A further example recorded in waves is shown in Fig. 47,j recorded at K = 14, and this compares very well with the quasi-steady model for K = 15 shown in Fig. 48. Lastly the model trace for K = 40 shows a remarkable resemblance to Fig. 53 of Sarpkaya (1976a). Sarpkaya does not, however, state the value of K for his figure, but merely that it is at "relatively high Keulegan-Carpenter number".

It is evident, particularly from the quasi-steady model, that although various researchers have noted step increases in the dominant lift force frequency as K is increased, there is nevertheless a gradual increase in the higher order components, and indeed a

gradual introduction of power at new, higher components.

For relatively low values of K the flow, from the point of view of vortex shedding, may be considered to increase rapidly from zero at flow reversal to the maximum velocity and then decrease rapidly again to the next flow reversal. The combined effects of increasing amplitude ($k_L U^2_{inst}$) and frequency of the vortex shedding force leads to a large, rapidly applied force at or very near each maximum velocity point of the wave. For higher values of K the change in flow velocity is more gradual, i.e. the period over which it changes is much longer than a vortex shedding period, and thus there are many vortex shedding cycles per wave half cycle, and the frequency and amplitude increase gradually to the maximum velocity point and then decrease again.

Evidently the peak values of the force trace will, assuming a constant value of lift coefficient, C_L in equation (19), depend on where in the cycle the vortex is shed. If the vortex is shed at such a point that the maximum force is at the maximum velocity point, i.e. that $\sin\phi = 1$ or -1 at a maximum velocity point, then a particularly large force will occur. For example the positive peaks in the first half wave cycle of Fig. 48 for K = 22 have a value of only 0.5 as they occur away from a maximum velocity point, whereas the negative peak occurs at a maximum velocity point and thus has value -1.0. The difference between the various traces found for $K \gtrsim 16$ can be explained by two effects. Firstly, residual circulation from previous half wave cycles and variations in the flow, non-linearities, turbulence, etc. may slightly promote or delay vortex shedding, causing the forces associated with it to occur either nearer or further away from the maximum velocity points, leading, respectively, to increased or decreased peak force values. Secondly, the trace shapes are dependent on whether the first vortex in successive half wave cycles is shed from the same, or from opposite sides of the cylinder, which is again dependent on the test conditions and, particularly, on the manner in which the last vortices shed in a half wave cycle are swept back over the cylinder and influence the initial shedding in the next half wave cycle.

The larger amplitude of the vortex induced forces in the wave peak half cycle compared to those in the wave trough half cycle is probably due to wave non-linearities generating a larger velocity

amplitude in the wave peak half cycle. The difference in forces is most noticeable for high wave heights when the non-linearities are greatest.

The quasi-steady model does not take any account of the fact that in an accelerating flow a vortex is able to build up to a more than quasi-steady circulation and the force associated with it is particularly large (see Sarpkaya 1963b, 1976a). The quasi-steady model is expected to perform best at relatively high values of K, where the flow is more nearly quasi-steady, as seen in Part I chapter 4, and the effects of the vortices from the previous half cycle on the shedding in the next half cycle become less important.

On each plotted spectrum from the quasi-steady model in Fig. 49 is shown the frequency defined by the Strouhal number used in the model, 0.2, and the maximum velocity, i.e. $.2U_m/D$. It is seen that the power from the model is at the few multiples of the wave frequency to either side of this frequency.

Isaacson (1974) considered the number of lift cycles per wave cycle to be equal to the number of vortices shed per half cycle plus 1, and that the first vortex shed in a half cycle is shed from the same side of the cylinder as the last vortex in the previous half cycle. Isaacson found, as have other researchers, that for $K \lesssim 12$ one vortex is shed per half cycle and is shed from the same side of the cylinder in each half cycle. Evidently the rule that $f_r = 1$ +(vortices shed per half cycle) is oversimplified. The definition of 'shed' is very uncertain and, as seen in Part I, chapter 3.4, various researchers consider that they have seen various numbers of vortices shed per half cycle at the same values of K, although their values of f_r have been in agreement. The problem arises from the fact that vortices may start to develop as the flow decelerates, and at flow reversal it is extremely difficult to see if they are shed (defining 'shedding' perhaps as when the feeding shear layers are cut), or even what happens to them. However, according to Isaacson, the range of K covered by the results of this Part in waves covers 1 or 2 vortices 'shed' per half wave cycle.

Any signal which repeats itself with a certain frequency will, when Fourier analysed, be found to contain power only at multiples of that frequency. Short lengths of the experimental traces are found to repeat every half or full wave cycle, with some smaller varia-

tions. The variations in the trace from one cycle to the next, the changing of sides of vortex shedding from the cylinder, and the longer term changes in the traces, for example as in Fig. 47,i, will cause there to be peaks in a spectral analysis of the signal at both even and odd multiples of the wave frequency, but these will be spread out rather than being spikes as would be the case for a perfectly repeating function.

The spectral analysis of the signal from the quasi-steady model for K = 20, shown in Fig. 49, can be compared with a spectral analysis of an experimental trace, Fig. 51, also at K ≈ 20. It is seen that the peaks for the spectral analysis of the experimental trace are more rounded, however there are quite definite peaks at multiples of the wave frequency. It must be pointed out that the results from the spectral analysis of the experimental signal are only qualitative, as the 90% confidence limits of the spectral estimates are .3 times and 2.3 times the plotted estimates. It is evident that the vortex forcing on a rigid cylinder exhibits peaks at multiples of the wave frequency, but that there is some spread in power to frequencies between multiples.

5. GENERAL DISCUSSION OF WAVE INDUCED VIBRATIONS OF CYLINDERS

5.1. Vibration starting at $U_m/nD \approx 1.0$

The most important parameter isolated is U_m/nD. It was found that vibration occurred if $U_m/nD \gtrsim 1.0$ for all values of n, n_w, δ_{sw}, and D. This parameter is expected to express the ratio of vortex shedding frequency to natural frequency.

The parameter K is of lesser importance here as it controls the ratio of the frequency of vortex shedding to the wave frequency.

From the spectral analysis of the quasi-steady model of vortex shedding in waves, Fig. 49, it is evident that as K increases there is increasing power at the higher multiples of the wave frequency. For example the power at $4n_w$ increases from 0.1 units at K = 5 to 0.21 units at K = 17.5 at which stage there are noticeable components at $5n_w$ and $6n_w$. When one considers that variations with time, etc. as previously discussed, will lead to a rounding of the peaks and spreading of power to between multiples of the wave frequency, then it is reasonable to suppose that the highest frequency at which there is significant power, for a given wave frequency, increases gradually (and not stepwise) with K. Thus U_m/nD (= $K\, n_w/n$) may represent the ratio of the highest frequency present in the vortex force trace to the natural frequency. It is only when a forcing frequency approaches the natural frequency that the dynamic magnification factor becomes significantly greater than 1, and there is expected to be a difference between the rigid and flexible cylinder traces. This evidently first occurs at $U_m/nD \approx 1.0$.

5.2. Effect of the wave to natural frequency ratio parameter

This parameter has been expressed as $|(1-rn_w/n)|$ and expresses how near the natural frequency is to an integral multiple of the wave frequency. It has been seen that the vortex forcing on the rigid cylinder leads to power peaks at integral multiples of the wave frequency, and thus more response is expected the nearer the natural frequency is to one of these peaks.

The response of a cylinder subjected to various wave frequencies around a particular value of r, as in Fig. 34 for example, shows well the effect of the parameter, larger response occurring for smaller values of the parameter. However, in tests where wave frequencies between 0.5 and 1.0 Hz were used, there were often anomalies where there was, say, less response for a particular wave frequency than expected. The range of wave frequencies is such that the value of r in the parameter $|(1-rn_w/n)|$ varies, i.e. one is comparing vibration near to one multiple of the wave frequency with that near another. The parameter will only give consistent results if the forcing is similar in magnitude at the two multiples of the wave frequency. The parameter is also rather sensitive to small changes in n_w, which is found to vary a little from wave to wave.

The variation in response for various wave frequencies around the particular value of r = 3 shown in Fig. 34 is considerably less than would be calculated if one assumed all power in the vortex induced force to be at $3n_w$. The table below shows the actual response in arbitrary units at $U_m/nD = 5.5$ for the various values of $3n_w/n$ compared with that calculated assuming all forcing to be at $3n_w$ and giving equal response for $3n_w/n = 1.003$.

$\frac{3n_w}{n}$	Actual response	Calculated response
.930	37	14
.950	43	18
.984	62	46
1.003	70	70
1.014	65	48
1.033	58	26
1.092	31	9.5

The reason that there is less variation in response is because a proportion of the total response, particularly when $3n_w/n \neq 1.000$, is response to other frequencies in the forcing, i.e. caused by the spreading of frequencies previously described due to variations in the regularity of the forcing function.

5.3. Effects of damping

For values of $|(1-rn_w/n)| \gtrsim .03$ there would not be expected to be much dependence on damping. Even if all power in the forcing function was at the frequency rn_w, then for $|(1-rn_w/n)| = .05$ the effect of increasing damping, δ_{sw}, from 0 to 0.4 would only reduce the response by 40%, i.e. one has to accurately hit resonance for damping to be important. Even if $|(1-rn_w/n)| = 0.00$ the response, in terms of r.m.s., would not be so dependent on damping as would be the case if the forcing was purely sinusoidal at the natural frequency, when response would be $\alpha\ 1/\delta_{sw}$. This is due to the response at other frequencies being less dependent on damping. For example for a white noise input the response would be $\alpha\ \sqrt{1/\delta_{sw}}$.

Indeed for small values of $|(1-rn_w/n)|$ there was a larger damping effect, however there are so few results, with considerable scatter, that a comparison of the measured effects of damping with those predicted assuming sinusoidal forcing at rn_w, say, cannot be conducted.

5.4. Causes of the vibrations

In section 2.4 it was indicated that the cause of the vibrations is probably the response to vortex shedding forces. This can now be discussed further.

Both the frequency content and shape of the cross-flow traces from the rigid cylinder in waves were very similar to those obtained by other researchers in waves and oscillatory flows, and also similar to those predicted by the quasi-steady model of vortex shedding

forces. Thus it is reasonable to assume that the cross-flow forcing on the rigid cylinder is due to vortex shedding forces. Furthermore it is evident that these forces are applied close to the top of the cylinder. This is indicated by the fact that the traces from the rigid cylinder were similar to those in a two-dimensional flow at a value of K equal to that at the top of the cylinder, and by the test in chapter 2.3 where the vibration component was removed from the flexible cylinder trace showing a forcing of similar magnitude to that from the rigid cylinder.

The cross-flow vibration was predicted well by a dynamic model of the flexible cylinder which used as input the reaction measured on the rigid cylinder and for damping used the still water experimental values. This indicates that the forcing on the flexible cylinder was very similar to that on the rigid cylinder and that no hydroelastic effects occurred. It is perhaps surprising that the still water, unseparated flow, damping applied, however it should be pointed out that the response was not strongly dependent on damping, so that damping may in fact have changed somewhat. However increased damping as given by the modified Morison's formula evidently did not occur.

In the in-line direction there are several factors other than vortex shedding forces which can lead to vibrations, for example wave non-linearities and the velocity squared term in Morison's formula, which produces power at odd multiples of the wave frequency and will lead to vibrations whenever the natural frequency is near to an odd multiple of the wave frequency. The problem is to try and determine to what extent the vibration in the experiments was caused by response to these non-linear effects and to what extent it was caused by response to vortex shedding.

There are several factors which indicate that the majority of the in-line response was due to response to vortex shedding. Firstly, the in-line response behaved exactly like the cross-flow response, in that it started at $U_m/nD \approx 1.0$, and exhibited the same dependence upon the parameters $|(1-rn_w/n)|$ and δ_{sw}. The response was, however, rather greater in the cross-flow direction. Secondly, the mathematical models considered in chapter 3 which used as input the reaction calculated using Morison's formula, correctly predicted the rigid cylinder reaction, but underpredicted the response of the flexible cyl-

inder. Thirdly, there was no greater response when the flexible cylinder's natural frequency was near an odd multiple of the wave frequency than when it was near an even multiple, nor did the spectra from the rigid cylinder in the in-line direction show relatively more energy at odd multiples of the wave frequency (other than at 1 x the wave frequency).

In the in-line direction, it appears that the response of the flexible cylinder is predicted accurately by a mathematical model using the reaction measured on the rigid cylinder as input and with damping given by the still water value. It seems that it is necessary both to account for vortex shedding forces and also not to include hydrodynamic damping calculated by considering relative velocities. It seems that the relative velocity form of Morison's formula is conceptually incorrect for the low values of U_m/nD of these experiments, and that it is better to consider the forces due to the waves and the vibrations separately, i.e. as if the waves were acting on a stationary cylinder and the cylinder was vibrating in still water. This is supported by the experiment of Petrauskas (1976) in currents described in Part I, chapter 5.2 (though for lower values of V/nD), and, for the unseparated part of the flow around the cylinder, by the work of Lighthill and Moore considered in Part I, chapter 4.

5.5. Comparison with other researchers' results

Both Bullock et al. (1978) and Sawaragi et al. (1978) have conducted similar experiments in waves, but with surface piercing cylinders. Both these investigations indicated that the in-line response of the cylinder, quantified as an r.m.s value of amplitude of response over diameter, could be predicted by the use of the modified Morison's formula, using values of coefficients appropriate to oscillatory flow, using higher order wave theories and accounting for the variation in water height on the cylinder. Neither of these investigations considered an in-line component of vortex shedding to cause vibration, despite the fact that both considered their cross-flow vibration to have been caused by vortex shedding. Both considered, rather, that in-line vibrations were caused by the various

non-linearities introduced in the forcing.

Sarpkaya (1976a, b) showed that there is an in-line component of vortex shedding forces, particularly for $10 \lesssim K \lesssim 30$, which is the range of both the above mentioned investigations and the experiments of this thesis.

Both Bullock et al. and Sawaragi et al. quantified their results in terms of an r.m.s. of the response amplitude, and thus included the basic forcing at the wave frequency, which is the majority of the signal for low values of U_m/nD and is significant even for high values. It is possible that the surface piercing cylinder condition led to further non-linearities which, in turn, led to response which was greater than that caused by vortex shedding.

In the results presented here there is no indication that hydroelastic response occurred, i.e. where the vibration altered the forces causing the vibration. Bullock et al. indicate that hydroelastic response occurs when $n/n_w = 2.00$ and $K = 10 \sim 17$, when the vortex shedding force also has a major component at twice the wave frequency. These conditions were not covered by the tests presented here.

Sarpkaya has found that cross-flow hydroelastic vibrations occur in an oscillating flow for values of $U_m/nD \approx 6$ at high, but unstated, values of K. In this situation hydroelastic effects are much more likely to occur, partly due to the very uniform, two-dimensional flow and partly due to the fact that at high values of K the vortex shedding is more even (see for example Fig.48 for $K = 100$ produced by the quasi-steady vortex shedding model).

5.6. Non-dimensionalizing the results

Results were found to collapse when plotted on axes of R_x/nD^3 or R_y/nD^3, for the in-line and cross-flow directions, respectively, versus U_m/nD. Collapse was achieved for all values of wave frequency, natural frequency, cylinder diameter and damping. However the axes R_x/nD^3 and R_y/nD^3 are not non-dimensional, and have in fact dimensions of velocity. These axes are thus meaningless and can only be used as a convenient aid to plotting the results until some non-dimen-

sional, meaningful parameter is discovered.

A simple analysis of the situation is conducted below:

Consider the vortex forcing of significance to be acting on a length, a, at the top of the cylinder, and that a is small compared to the cylinder length L, which is consistent with the discussion of chapter 5.4. The system may be considered as sketched below.

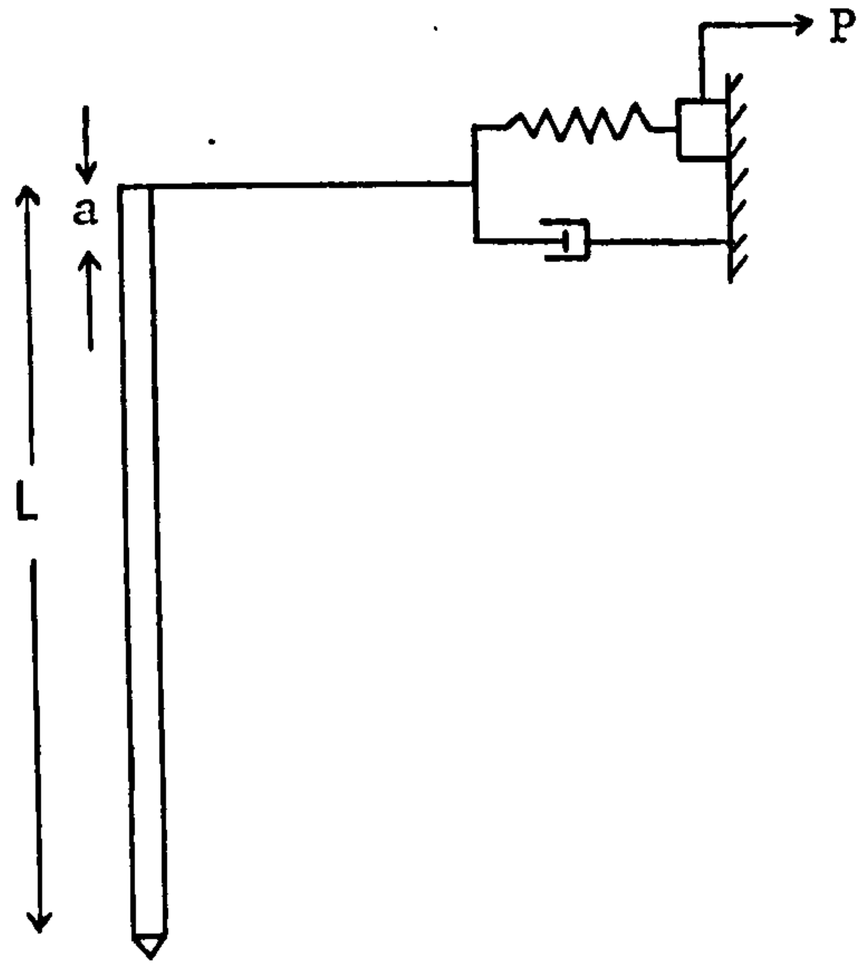

The output signal from the system, P, is equal to the spring force produced by the cylinder deflection.

$$-P = by$$

The moment of inertia about the centre of rotation is $mL^2/3$ and, as $\ddot{y} = \ddot{\theta}L$, the equation of motion may be written

$$(mL/3)\ddot{y} + c\dot{y} + by = aP(t)$$

where y, $\dot{y}$ and $\ddot{y}$ are the deflection, velocity and acceleration of the top of the cylinder.

It is asumed that the input to the system, P(t) can be represented by a series of sinusoidal functions

$$P(t) = \sum_{i=1}^{\infty} \left[P_i \cos (2\pi n_i + \phi_i)\right]$$

where n_i and ϕ_i are the frequency and phase of the i'th function.

Writing the coefficients of the series as dimensionless force coefficients, p_i:

$$P(t) = .5\rho D\, U_m^2 \sum_{i=1}^{\infty} \left[p_i \cos\,(2\pi n_i + \phi_i)\right]$$

Thus the equation of motion can be written as

$$(1/3mL)\ddot{y} + c\dot{y} + by = .5\rho D\, U_m^2\, a \sum_{i=1}^{\infty} \left[p_i \cos(2\pi n_i + \phi_i)\right]$$

For which the steady state solution is

$$y = \frac{.5\rho D\, U_m^2}{b}\; a \sum_{i=1}^{\infty} \left[(D.M.F.)_i\, p_i \cos(2\pi n_i + \phi_i + \theta_i)\right]$$

where $(D.M.F.)_i$ and θ_i are the dynamic magnification factor and phase angle for each input frequency.

Now substituting for b, where

$$b = \frac{(2\pi n)^2 mL}{3}$$

yields

$$\frac{y}{D} = \frac{3}{8\pi^2} \left(\frac{a}{L}\right)\left(\frac{\rho D^2}{m}\right)\left(\frac{U_m}{nD}\right)^2 \sum_{i=1}^{\infty} \left[(D.M.F.)_i\, p_i \cos(2\pi n_i + \phi_i + \theta_i)\right]$$

(which is similar to equation (7) derived in Part I, chapter 5.1 for hydroelastic vibrations in a current). Substituting for y gives

$$F = .5\rho\, n^2 D^3 L \left(\frac{U_m}{nD}\right)^2 \left(\frac{a}{L}\right) \sum_{i=1}^{\infty} \left[(D.M.F.)_i\, p_i \cos(2\pi n_i + \phi_i + \theta_i)\right]$$

For the rigid cylinder the natural frequency is considerably higher than the highest forcing frequency, and thus one can assume $(D.M.F.)_i = 1$ and $\theta_i = 0$ for all i.

Thus the difference reaction, F_{DIFF}, is given by

$$F_{DIFF} = .5\rho\, n^2D^3L \left(\frac{U_m}{nD}\right)^2 \left(\frac{a}{L}\right) \sum_{i=1}^{\infty} (D.M.F.)_i\, p_i \cos(2\pi n_i + \phi_i + \theta_i)$$

$$- p_i \cos(2\pi n_i + \phi_i)$$

Therefore

$$F_{DIFF} = .5\rho\, n^2D^3L \left(\frac{U_m}{nD}\right)^2 \left(\frac{a}{L}\right) \sum_{i=1}^{\infty} (D.M.F.)_i\, p_i \cos(2\pi n_i + \alpha_i)$$

Taking the r.m.s. of this yields

$$R_x \text{ or } R_y = .5\rho\, n^2D^3L \left(\frac{U_m}{nD}\right)^2 \left(\frac{a}{L}\right) \sum_{i=1}^{\infty} ((D.M.F.)_i - 1)\, p_i \frac{1}{2} \qquad -(20)$$

Thus this analysis would suggest plotting of

$$\frac{(R_x \text{ or } R_y)}{.5\rho n^2 D^3 L}$$

as a function of (U_m/nD), (a/L), and a complicated response parameter, which is an integrated effect of the amplitude of input at each input frequency and the dynamic magnification of the system to these frequencies.

This last parameter cannot be evaluated without a complete analysis of the forces on a rigid cylinder, but is, in general, a function of the p_i's n_i/n's, and damping. Some properties of this function have already been seen in the preceeding sections.

The parameter $(R_x \text{ or } R_y)/.5\rho\, n^2D^3L$ differs in effect from the parameter plotted as 1/n (as ρ and L are constant throughout the tests).

This means that plotting of the results on axes of

$$\frac{(R_x \text{ or } R_y)}{.5\rho n^2 D^3 L} \text{ versus } U_m/nD$$

would result in lines of lesser slope for increasing n.

The inability to non-dimensionalize the results is rather unsatisfactory, however it is considered that the most important result obtained is that, for the considered range of parameters, the flexible cylinder response can be predicted from a complete knowledge of the forces on a rigid cylinder. Furthermore, the use of Morison's formula does not give an adequate description of the forces in the in-line direction, and the use of a modified form of the formula to obtain hydrodynamic damping, using relative velocities and stationary cylinder coefficients, grossly underpredicts vibration, whether the forces on the rigid cylinder are used or the forces are considered given by Morison's formula.

PART III - EXPERIMENTAL INVESTIGATION INTO THE FORCES ON CYLINDERS OSCILLATED IN STILL WATER AND STEADY CURRENTS

INTRODUCTORY COMMENTS

In this section, an experimental investigation into the forces on cylinders oscillated in still water and in-line with steady currents is presented and discussed. Before this author moved to Norway, Professor Geir Moe of the Norwegian Institute of Technology, working from the structural point of view, had realized that the use of the relative velocity form of Morison's formula leads to higher calculated damping and reduced estimated vibrations of offshore structures, but that there had been no fundamental investigation into the formula, and that possible overestimation of damping would have far reaching consequences. Discussions with Professor Moe led to the author, in March 1977, putting forward a proposal, Verley (1977c), for a fundamental investigation into the problem.

In the experimental program to be presented here, various cylinders were oscillated from a pendulum in still water and currents, and the damping of the motions and the in-line forces on the cylinders were measured. Flow visualization experiments were also conducted.

Various reports have been prepared in the course of the investigation (Verley (1978a), Moe and Verley (1978), Verley and Moe (1979a)) and the work has been described at various colloquia and conferences (Verley (1977d), Verley and Moe (1978), Verley and Moe (1979b)).

1. DESCRIPTION OF THE APPARATUS

1.1. Principle of the experimental rig

The basic experimental apparatus is drawn in detail in Fig. 52. It consisted of a massive pendulum which spanned a current flume and to which a horizontal cylinder was attached and submerged in either still or flowing water. The pendulum was sufficiently massive that the damping was small, there being at most a 2% decrease in amplitude per cycle. The position of the cylinder was monitored by a linear spring and force transducer, and from this signal the damping of the motion of the pendulum was calculated and this could be related to the oscillatory drag coefficient. In addition, the forces on the cylinder in the horizontal direction were measured, and from these force time histories could be calculated oscillating drag and inertia coefficients and steady component of drag coefficients.

1.2. Current channel used for the experiments

The flume, which was specially built for the experiments, is sketched in Fig. 53. The flume was built of plywood, lined with waterproof plastic and with a see-through plastic panel on one side where the rig was mounted. The water supply to the flume was from tanks in the roof, which were kept at a constant level by pumping water continuously from the sumps in the cellar. The flume was supplied with water via a valve, stilling box and calibrated standard V-weir. The V-weir was mounted about 50 cm above the water level held in the channel, and the water fell from the weir into a stilling chamber which contained chicken-wire baskets filled with aluminium turnings. From this stilling chamber was a contraction to the main part of the flume, the beginning of which was filled with 1 m long, 10 cm diameter plastic pipes. These pipes have been found to be advantageous in obtaining an even flow. The main part of the channel was

10 m long, 0.5 m wide, and 0.7 m deep, with a water depth of .55 m used in the experiments. The water level was held constant for the various flow rates by adjusting an overflow weir at the end of the channel. From here the water was led down to the cellar sump.

The flume was commissioned by Mr. J. E. Horne, a final year student working under the supervision of Professor Moe and the author, and horizontal and vertical flow profiles where the rig was placed are shown in Fig. 54, obtained from Mr. Horne's data.

1.3. Flow velocity calibrations

The calibrations were conducted by the author. A Nova Streamflo 403 propellermeter was used to measure flow velocities, which were measured in the flow, without the cylinder present, at the point where the middle of the cylinder would be. This author feels that this type of propellermeter is not particularly reliable, particularly for low velocities, as hair, small dust particles, etc. can easily become tangled up in the propeller spindles and alter the calibration, often by only small amounts which may not be noticed. Throughout the channel velocity calibrations, the propellermeter was therefore continually recalibrated against the velocities of floating particles timed over known distances. The flume was calibrated by noting the flow rate (using the weir calibration) for eleven velocities covering the range used in the experiments. It was found that the relationship between flow rate and velocity varied by only about 5% between the various velocities, and this variation was not related to velocity, indicating that the velocity profiles were similar for the various velocities and that the 5% variation was almost certainly due to the propellermeter. An average of all the flow rate to velocity relationships was taken, and this was used throughout the experiments to calculate the flow velocity from the known flow rate.

1.4. The pendulum rig

The rig is shown in detail in Fig. 52. The basic pendulum consisted of a main horizontal beam spanning the channel and supported on knife edges. At each end of the beam hung long rods to the bottom of which were attached heavy weights, approximately 23 kg on each side. Hanging down from the centre of the horizontal beam, and rigidly attached and braced to the beam, was a bar to which was attached the force transducer used to measure forces on the cylinder. The cylinder was held between two end plates which were attached to two arms. These arms were braced by a horizontal bar to which the force transducer was also attached, thus forming an H, and the cylinder was held between the lower arms of the H. The upper ends of the arms were pin-jointed to the horizontal beam using 2 mm stainless steel pins running in PTFE low friction bearings. (PTFE has the nearly unique and, in this case, important property that it has a very low starting friction, virtually the same as its sliding friction.) Thus the cylinder and its support arms could swing quite freely and independently of the pendulum if it were not for the force transducer connecting them.

1.4.1. End plates

The end plates were 16 cm in diameter and it was hoped that they would help to ensure 2-dimensionality of the flow. The end plates and the parts of the arms which were under water were made of 2 mm thick aluminium plate and the edges were rounded.

1.4.2. Higher frequency tests

The pendulum rig as described in the foregoing section had a natural frequency of 0.4764 Hz in air with no cylinder attached.

A number of tests were conducted with a modified rig, where

the weights were raised 30 cm and strong, linear springs were attached to the pendulum, see Fig. 52. With this arrangement the natural frequency, again for no cylinder attached and in air, was 1.409 Hz.

1.4.3. Inertia and natural frequency of the rig and cylinders

All the individual parts of the pendulum were weighed and the total mass, inertia and centres of gravity and inertia of the rig calculated, and from these the theoretical natural frequency was calculated. The natural frequency, for small amplitude oscillations in air, was measured to be 0.1% higher than the calculated frequency, which was considered confirmation that the masses and inertias were correctly measured and calculated.

The mass and inertia of the two pendulum systems with no cylinder attached are tabled below.

	Mass kg	Inertia kgm^2
Low frequency (early tests)	52.36	62.726
Low frequency	52.77	62.750
High frequency	11.05	16.621

(The low frequency rig was slightly altered after the first few tests had been conducted by the addition of a strengthening member to the cylinder support arms, hence the two figures above.)

The diameters, masses, inertias and inertias of the added masses of the cylinders (assuming added mass = mass of fluid displaced), together with the natural frequency of the two pendulum systems with various cylinders attached are listed below.

Cylinder Dia	Mass	Cylinder Inertia	Added mass Inertia	Natural frequency low	high
m	kg	kgm^2	kgm^2	Hz	Hz
.01275	0.3535	0.173	0.021	0.4764	1.403
.0202	0.1250	0.061	0.052	0.4762	1.403
.0252	0.1955	0.096	0.081	0.4760	1.401
.0320	0.1050	0.051	0.131	0.4758	1.400
.0350	0.3750	0.184	0.157	0.4757	1.397
.0502	0.3305	0.162	0.323	0.4744	
.0701	0.4800	0.235	0.630	0.4717	
0	0	0	0	0.4764	1.409

The last row represents the rig without any cylinder attached.

It is seen that the maximum variation in the frequency for the low frequency pendulum system is 1.0% for the 7 cm cylinder. This cylinder was only used in tests in still water. The maximum variation otherwise is 0.4%. For the high frequency set up the maximum variation is 0.85%. In all calculations the correct values of frequency for the relevant cylinder were used.

The calculations of inertia used in the analysis for the total system with each particular cylinder attached includes an inertia term due to the added mass and this added mass is calculated as being the displaced mass of water. Now it should in fact be the displaced mass of water times the added mass coefficient which will be found in the results to vary between 1.1 and -.4. The maximum error in the total inertia of the system caused by always using the displaced mass of water is 0.7% for the 5.02 cm cylinder.

2. INSTRUMENTATION

2.1. Measurement of pendulum motion

The motion of the cylinder was measured by attaching a force transducer to the pendulum via a linear spring. The force transducer was a Bofors type $\pm$ 2 kg, and was found to be linear within measureable accuracy. The spring was chosen to give suitable force per unit displacement and was from a standard set of Terry springs. The wire attaching the pendulum to the spring and transducer was 3 m long, and the maximum movement of the pendulum at the point of attachment was $\pm$ 4 cm, and thus the change in angle of the wire and thus of the horizontal component of force, over the extent of the motion, was negligible.

2.2. Measurement of force on the cylinder

The cylinder and mounting arm combination was hinged to the main horizontal beam at the upper end and held to a bar attached to the beam by a ring-type force transducer. The transducer had to satisfy the conflicting demands of high sensitivity, to measure small forces accurately, and high stiffness, so as to obtain as high a natural frequency as possible of vibrations of the cylinder and support arms system.

On the second attempt a transducer was built which was sufficiently sensitive and the system had a natural frequency of 14 Hz with the heaviest cylinder attached and in water. The ring was equipped with four strain gauges wired as a whole bridge circuit. The transducer was found to be linear within the accuracy of measurement.

The force transducer was mounted such that it measured forces perpendicular to the line between the pivot points of the pendulum and the centre of the cylinder. Thus when the pendulum was deflected the force measured was not quite horizontal. The maximum deflection

of the pendulum in the tests was 12°, and thus the error in the horizontal force measurement at maximum deflection was about 2%. For smaller deflections the error was correspondingly less, i.e. for 6° it was 0.6% (corresponding to $x_o/D = 2.9$ for the 2.54 cm cylinder).

2.3. Amplification and recording

The two force transducers, to measure position of and horizontal force on the cylinder, have been described. The instrumentation is sketched below.

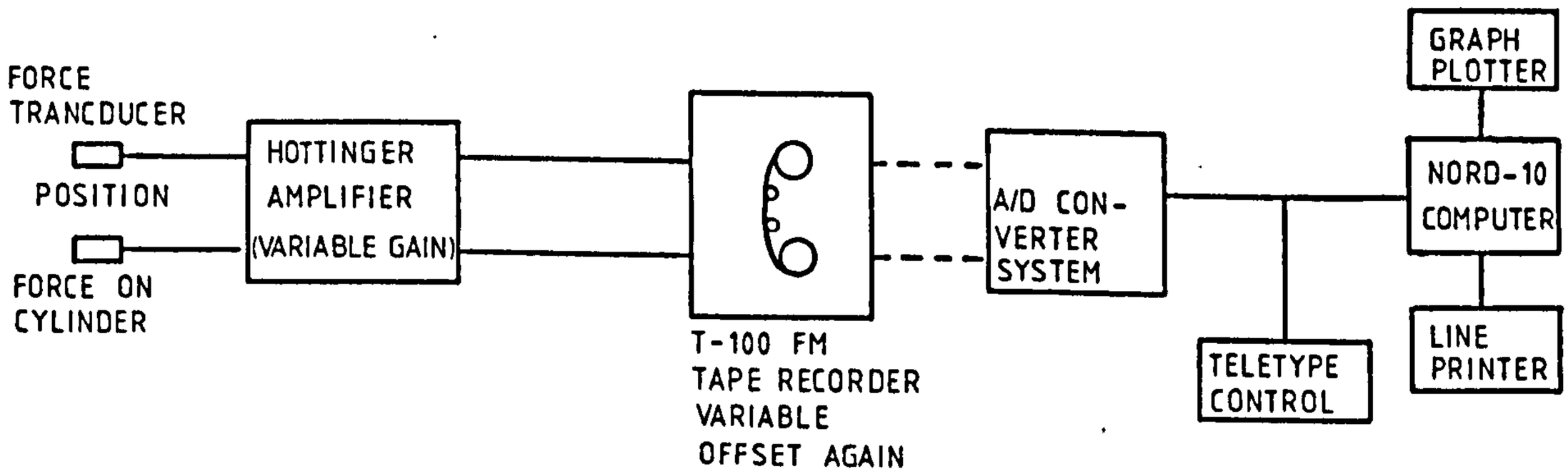

The transducers were coupled to two Hottinger Baldwin variable gain amplifiers (type TVE-0IA), and the outputs from these connected to a Tandberg T-100 FM tape recorder with variable offset and gain. In the experiments the time histories were first recorded on tape and then played back at higher speed (2 or 4 times) to the computer, using a standard data collection program. The signals could also be recorded on a U.-V. recorder during experimentation.

2.4. Calibration of the instrumentation system

Although the force transducers to measure the position of and forces on the cylinder had been calibrated and checked for linearity in the laboratory before the rig was assembled, in-situ calibration tests were also conducted. For both cases voltages at output from the amplifiers were measured using a digital volt meter (D.V.M.).

2.4.1. Position transducer

The position transducer was calibrated by deflecting the pendulum, without the heavy weights attached, and noting the D.V.M. reading. The pendulum deflection was measured using a water level point gauge measuring to 1/10 mm mounted horizontally and used to measure the deflection at the bottom end of the bars which carry the weights. The calibration was conducted in terms of output of the amplifier, set at known sensitivity, for unit horizontal deflection at the cylinder centre. Repeated testing, also after the experiments were conducted, showed that the calibration did not vary by more than 0.4%.

With a constant input to the amplifier the output was measured for the various sensitivities which could be set. The outputs were correct to within 0.1%.

2.4.2. Force transducer

The transducer to measure force was calibrated by applying forces to the cylinder using standard weights and a very low friction pulley. The calibration was repeatable within 0.5% both before and after the experiments were conducted.

Loads were also applied vertically to the cylinder to see if the transducer was sensitive to these. It was found that the sensitivity in this direction was 0.6% of the horizontal sensitivity.

Again the outputs for a constant input and various amplifier sensitivities were correct to within 0.1%.

2.4.3. FM recorder

The FM recorder had a built-in amplifier which could give additional amplification of 1, 2, 5 or 10 times, of which 1, 2 and 10 times were used. The recorded tapes were played back and digitized at either 2 or 4 times the original recording speed, which was 15/16 in/sec. The following test was therefore conducted to check the FM recorder.

A 0.400 v signal was applied to the two inputs and recorded at 15/16 in/sec, firstly with a gain of 1 and then with a gain of 10. The recorded signals were then played back at 15/16, 1 7/8 and 3 3/4 in/sec, and the outputs measured using the D.V.M. The outputs are given in the table below.

CHANNEL 1	Output Playback speed		
Input 0.400 v	15/16	1 7/8	3 3/4
Gain 1x	.402	.399	.399
10x	4.03	4.00	4.00

CHANNEL 2	Output Playback speed		
Input 0.400 v	15/16	1 7/8	3 3/4
Gain 1x	.397	.399	.399
10x	4.01	4.01	4.01

Thus the maximum error in the playback at 1 7/8 or 3 3/4 in/sec was 0.25%.

To minimize flutter the anti-flutter capability of the recorder was used (using a further channel to monitor flutter in tape speed by recording a fixed high frequency). Using this the values of the outputs in the above table did not vary from the figures given over a 20 second period, (without the anti-flutter the variation was ~2%).

2.5. Calibration accuracy of the recorded signals

From the above it is considered that the calibration of the signals at input to the computer's A/D converter are better than 1%. Furthermore it is considered that most of this inaccuracy is in the form of uncertainty of the calibration constants rather than variation in them.

A further possible problem besides calibration inaccuracies is amplifier drift during experiments. This will be considered in a subsequent section.

2.6. Amplifier sensitivity

The Hottinger amplifiers are designed so that the sensitivity, i. e. the calibration constant, can be varied in known steps. The sensitivity ranges are in terms of microstrain input for full deflection, and the selectable ranges are 100, 200, 500, 1000, etc., up to 100000. The calibration constant of the force transducer was 612.7 gm/volt $\pm$ 0.5% on the 5000 range, and thus on the 100 range, with an additional 10 x amplification on the FM tape recorder, a maximum sensitivity of 1.23 gm/volt could be obtained. For the deflection the calibration was 9.083 cm/volt $\pm$ 0.4% on the 2000 range, and thus maximum sensitivity was 0.04 cm/volt.

The range of the (8-bit) A/D converter used for the digitisation was $\pm$ 5 v.

For a particular test run the sensitivities of the amplifiers were set so that the signal recorded on the tape recorder, which could be monitored, was nearly full scale, $\pm$ 5 v (the procedure will be given in more detail shortly). For the position signal this involved only an adjustment of the amplifier sensitivity as the signal had almost equal positive and negative amplitudes. However the force signal, when there was a current present, consisted of a constant voltage, corresponding to the direct component of force, and a superimposed oscillatory voltage, due to the oscillatory force components. For high current velocities, particularly for small amplitudes of motion, the steady force component may be very much larger than the

amplitude of the oscillatory components. In order to obtain as high an accuracy as possible of the oscillatory component the input to the tape recorder was offset (a facility present on the tape recorder), so that the oscillating component oscillated about ~0 v. The offset voltage used was noted so that the direct component of force could be correctly calculated.

The computer program used to digitize the signals was a standard VHL program written for use with the Hottinger amplifiers. Using this program it was only necessary to stipulate the calibration constants for a known sensitivity scale once, and then merely to note the sensitivity range used for each particular test run.

2.7. Amplifier drift

Amplifier drift was under most circumstances immeasureable, in fact no drift was noticed over a period of many hours. Noticeable drift occurred under two circumstances. Drift was apparent during the first hour or so of operation after the amplifiers were switched on, almost certainly due to the warming up of the strain-gauges. The equipment was therefore always switched on at least 5 hours before experiments were conducted.

Drift was otherwise noticeable over, say, 100 cycles when the amplification of the signal was greatest, i.e. with the amplifier set on the 100 range and the amplification of the FM tape recorder at 1, 2 or 10. Calculation of damping and oscillatory coefficients was not affected as these calculations are conducted with reference to the local signal double amplitude. However, the calculation of the mean drag, i.e. the mean offset of the signal, was affected by amplifier drift. For the lowest flow rates the drift could be a significant part of the mean offset. Therefore, in conducting the experiments for the lower flow velocities, the pendulum motion was stopped periodically, the amplifiers set to the most sensitive and the drift checked (this will be covered in more detail in the description of the experimental procedure). Some test runs were discarded due to drift.

3. EXPERIMENTAL METHOD

3.1. Experiments conducted

Altogether a large number of experiments have been conducted in still water using various cylinder diameters, using a similar, but smaller pendulum to that described (and analysing results by hand from U.-V. traces) and with different pendulum inertias. The results, however, are virtually identical for similar values of β and therefore only those results obtained with the described rig will be presented in full here.

Again results in currents for the oscillating component of drag coefficient have been obtained both with the described pendulum and with a previous, smaller version where the results were analysed by hand. (The results presented in Verley (1978a), Moe and Verley (1978), Verley (1977d), and Verley and Moe (1979a) were produced with the initial, smaller rig and covered only results for the oscillatory drag coefficient.) A full description will only be given of the results obtained with the described pendulum rig.

The combination of cylinder diameter and flow rate are given by the 'Test Number' of the test. The last figure in the test number determines the cylinder diameter from the table below.

Last figure	Cylinder diameter
0	0
1	.0202
2	.0252
3	.0320
4	.0350
5	.0502
6	.0701
7	.01275

The velocity of flow, and whether the high or low pendulum frequency was used, are determined from the first figures of the Test Number. The flow velocities tested, in the order in which they were tested, are given below. In some cases the smallest and in other cases the largest cylinders were tested first.

Low pendulum frequency

	Flow Velocity	Test Numbers							
	0	20	21	22	23	24	25	26	
Before extra	.128	30*	31	32		34	35		
stiffening	.288	40	41	42		44	45		
added	.445	50	51	52		54	55		
	.233	60	61	62		64	65		
	0	120	121	122	123	124	125	126	127
	.179	70	71	72		74	75		
After extra	.081	80	81	82		84	85		
stiffening	.048	90	91	92		94	95		
added	.039		101	102		104	105		
	.059		111	112		114	115		
	.028		131	132		134	135		

* Data for test 30 was accidentally destroyed.

High pendulum frequency

Flow Velocity	Test Numbers					
0	700	701	702	703	704	
.039	200	201	202		204	205
.028	210	211	212		214	215
.048	220	221	222		224	225
.059		231	232		234	235
.081	240	241	242		244	245
.128	250	251	252		254	255
.288	260	261	262		264	265
.103	270	271	272		274	275

In addition some tests were conducted in air, both with and without cylinders attached.

After test series 60-65 the pendulum was slightly modified by the addition of an extra stiffening bar to the cylinder support system. This was done because some twisting of the cylinder was observed in the tests at the highest flow velocities. As will be seen the results in still water after the modification (tests 120-126) gave virtually indentical results to those before the modification (tests 20-26).

The maximum amplitude of motion of the cylinders in the experiments was about .15 m for the low pendulum frequency tests, and .08 m for the high frequency tests (due to limitations of the springs which were used to raise the frequency). Data was collected for amplitudes of motion down to about .001 m. From these values the variation in the parameter x_o/D, where x_o = amplitude of motion, for the various cylinders can be calculated.

The ranges of the other major parameters were

V/nD	.6 to 47
$V/\dot{x}_o$	.05 to 50
$\beta = nD^2/\nu$	80 to 3500.

3.2. Experimental procedure

In order to obtain the force coefficients for the various cylinders it is necessary to conduct the experiments with the cylinders and also with no cylinder attached to the pendulum. The data obtained with no cylinder attached gives the damping of the system due to friction, motion through air and motion of the end plates through the water, and forces on the transducer due to fluid forces on the end plates and inertia forces due to the motion of the rig (these will be considered in more detail in later sections). The data obtained from the rig with no cylinder attached is subtracted from that from tests with the various cylinders to yield effects due to the cylinders. The variation in the amplitude of motion for any one test condition is about two orders of magnitude, and forces vary by even more, so it is evident that it is necessary to vary the sensitivity of the amplifiers in the course of the experiments. In order to give some overlapping the following routine was initially employed.

The pendulum motions were worked up to maximum amplitude by hand and the sensitivity of the amplifiers and, if necessary, the offset of the force signal to the tape recorder adjusted so that the signals to the tape recorder varied within the range $\pm$ 5 v (full scale). Having set the amplification the pendulum was oscillated by hand at full amplitude for a few cycles and then released. After about 2 cycles recording was started and continued until the smallest of the two signals was oscillating at about $\pm$ 1.5 v. The sensitivity of the amplifiers was then increased (by a factor of 2 or 2.5) and the motion built up by hand until it was considerably more than $\pm$ 5 v. The motion was allowed to die down until both signals were within the range $\pm$ 5 v, which was usually after at least 10 cycles, and recording started and continued until one signal was down to about $\pm$ 1.5 v. This procedure was repeated down to the smallest amplitudes. (The range of sensitivity of the motion amplifier varied from 1000 for the low and 500 for the high pendulum frequency test to 10.) Over some ranges of the test parameters the force output decreased in amplitude more rapidly than the motion output, and in these cases tests were conducted at 2 force amplifier sensitivities

for each motion sensitivity. In this way the signals were always held in the range $\pm$ 5 to $\pm$ 1.5 volt, and the overlap was such that the whole range of amplitudes was covered twice. For each condition the amplifier sensitivities and the force amplifier offset were noted, together with the tape recorder footage at the beginning and end of the recording.

For the lower flow velocities ($V \lesssim .1$ m/s) where drift of the force amplifier is important, it was decided to stop the pendulum between each sensitivity variation, and to check that no drift had occurred (by turning to the most sensitive range). Also the smallest amplitude condition was tested first, and then progressively larger amplitudes. An example of the noted conditions for one test is shown in Fig. 55.

4. ANALYSIS OF THE DATA

A schematic description of the various computer programs used to analyse the data is given in Appendix 1.

From the time histories of the pendulum motion, the damping coefficient for the rig, as a function of amplitude, could be calculated from the logarithmic decrement of the motion. From the force time histories, the average steady force and, using the method of Fourier averages, the oscillatory drag and inertia coefficients could be calculated, as functions of amplitude.

From the results of damping, steady force and Fourier oscillatory coefficients for the rig with a particular cylinder attached, were subtracted the results for the rig with no cylinder attached, at corresponding amplitudes, yielding damping due to, steady forces on and oscillatory coefficients for the cylinder.

From the damping and from the oscillatory drag coefficient were subtracted the still water viscous drag values, calculated using Stokes' equations (Part I, chapter 3.13, equation (4)). The reason for this will become evident from the results in still water. The remaining damping and oscillatory drag coefficient are those due to separation and pressure effects and represent the effects over and above the purely viscous forces.

From this remaining damping was calculated oscillatory drag coefficients which could also be compared with those obtained from the Fourier analysis of the force time histories. From the steady forces on the cylinder were calculated time-averaged steady drag coefficients.

4.1. Digitization

Digitization of the signals was conducted using an 8-bit, $\pm$ 5 v range A/D converter controlled by a NORD-10 minicomputer using a VHL standard data collection program. Digitization intervals were 0.04 sec and 0.02 sec of experimentation time for the experiments at the low and high pendulum frequencies, respectively. These represent about 53 and 35 samples per oscillation cycle, respectively.

The A/D converter was rather 'coarse', being only 8-bit, giving an accuracy of only + 0.039 volt. However, as will be discussed in a later section on the measurement of damping, considerable improvement of this accuracy was obtained and in fact the coarseness was not found to be a problem.

4.2. Basic equations

The results have been analysed using two equations. In the first the force per unit length of the cylinder is considered to be given by the relative velocities and accelerations (fluid acceleration is zero however), and written

$$f(t) = .5\rho D\ C_{D3}(t)\ (V-\dot{x})|(V-\dot{x})| - .25\rho\pi D^2\ C_a(t)\ddot{x} \qquad -(21)$$

where C_{D3} and C_a are time dependent drag and added mass coefficients. There is in this situation no Froude-Krylov force, and the inertia coefficient which would apply with the fluid oscillating rather than the cylinder would be given by $C_M = C_a + 1$. $\dot{x}$ and $\ddot{x}$ are the structural velocity and acceleration, respectively.

The second equation used assumed that the forces due to the steady current and the cylinder oscillations could be written independently, i.e.

$$f(t) = .5\rho D\ C_{D1}(t)V^2 - .5\rho D\ C_{D2}(t)\dot{x}|\dot{x}| - .25\rho\pi D^2\ C_a(t)\ddot{x} \qquad -(22)$$

Here C_{D1} and C_{D2} are drag coefficients associated with the steady and oscillatory drag forces in (22), respectively.

The drag coefficients in (21) and (22) are given numbered subscripts to avoid confusion. Equation (21) is identical to equation (11) used in Part I. Equation (21) is also the same as (12), used in the dynamic analysis of platforms, when V replaces U and $\dot{U} = 0$.

C_{D3}, C_{D1}, C_{D2} and C_a are in general functions of time. In this thesis time averaged coefficients will be used.

Two methods are commonly used to determine time averaged coefficients in wave or oscillatory flows. In the first the oscillatory

drag and inertia coefficients are related to the first two Fourier coefficients of the time series, that is to say the sine and cosine coefficients at the fundamental, oscillatory frequency. This method was used by Keulegan and Carpenter (1958). The other commonly used method is a least squares fitting of the two coefficients to the force measured in a cycle, as used by Sarpkaya (1976a, etc.).

The following methods are used in this thesis. The oscillatory drag force is determined from the damping measured, and used to calculate time averaged oscillatory drag coefficients from (21) and (22). The steady component of drag force measured is equated to the steady components of equations (21) or (22), to give time averaged steady drag coefficients. Time averaged oscillatory drag and inertia coefficients are determined from the time histories of force on the cylinder using the Fourier analysis method used by Sarpkaya (1976a). A detailed derivation of the coefficients is given in Appendix 2, where it is also shown that all the coefficients are equivalent to those determined by equating to Fourier coefficients, as used, for example, by Matten (1976) in his reanalysis of the data of Mercier (1973).

In equation (21) the steady and oscillatory drag forces are mutually dependent and the time-averaged oscillatory drag and steady drag coefficients determined are denoted CDDEP and STCDDEP, respectively.

In equation (22) the steady and oscillatory drag forces are independent, and the time-averaged coefficients are denoted CDIND and STCDIND, respectively.

The time-averaged added mass coefficient is the same for both equation (21) and (22), and is called CA. The coefficient which will be plotted, however, is the inertia coefficient, CM = CA+1.

CDDEP and STCDDEP are thus the time-averaged oscillatory and steady components of $C_{D3}(t)$ in equation (21) and CDIND and STCDIND are the time-averaged values of $C_{D1}(t)$ and $C_{D2}(t)$ in equation (22), respectively. CDDEP and CDIND represent contributions over and above the viscous contribution calculated from Stokes' equations (and nearly always very much smaller).

Thus, using time averaged coefficients, equation (21) may be rewritten as

$$f(t) = .5\rho D(STCDDEP).(\text{steady component of } (V-\dot{x})|(V-\dot{x})|)$$
$$+.5\rho D(CDDEP).(\text{oscillatory component of } (V-\dot{x})|(V-\dot{x})|)$$
$$-.25\rho\pi D^2(CA)\ddot{x} \qquad -(23)$$

Similarly equation (22) may be rewritten as

$$f(t) = .5\rho D(STCDIND)\ V^2$$
$$+.5\rho D(CDIND)\ \dot{x}|\dot{x}|$$
$$-.25\rho\pi D^2(CA)\ddot{x} \qquad -(24)$$

The above equations apply to the experimental condition of a cylinder oscillating in a steady current. For a condition of a stationary cylinder in a combined steady current, of velocity V, and oscillatory current, of instantaneous velocity U, equations (23) and (24) would still apply, but with CM (= 1+CA) replacing CA, -U replacing $\dot{x}$ and $-\dot{U}$ replacing $\ddot{x}$.

A time-averaged oscillatory drag coefficient from equation (22) was also determined by the method of Fourier averages applied to the force time histories. This coefficient is called CDIND'. Values of CDIND and CDIND' were found to be virtually identical when compared from tests in still water, but there was rather more scatter in the results of CDIND'. Therefore results of CDIND, i.e. obtained from the damping, are presented in this thesis.

4.3. Equations for evaluation of the various coefficients

The derivations of the equations for the evaluation of the various coefficients are detailed in Appendix 2. The equations are, however, reproduced below.

4.3.1. Oscillatory drag coefficients, CDDEP and CDIND

These coefficients are derived from the damping of the rig. The equation of free oscillation of the pendulum rig with a cylinder attached may be written as

$$I_t\ddot{\theta} + C_t\dot{\theta} + M_R\theta = 0$$

where I_t = total inertia (including that due to the cylinder and the added mass of water), C_t = total rotational damping coefficient, M_R = rotational stiffness and θ, $\dot{\theta}$ and $\ddot{\theta}$ = angular displacement, velocity and acceleration, respectively.

The total damping coefficient, C_t, is made up of that due to the cylinder, C_{cyl} and that, C_o, due to other effects such as friction, drag on the end plates, etc.

Thus

$$C_t = C_o + C_{cyl}$$

If L is the length of the cylinder and h the distance from the axis of rotation to the cylinder axis, then

$$C_{cyl} = \bar{c}_{cyl}\, h^2 L$$

where $\bar{c}_{cyl}$ is the linear average damping coefficient per unit length of cylinder.

By definition

$$C_t = 2I_t\, n\delta_t$$

where δ_t is the logarithmic damping with the cylinder attached.

C_o is determined from experiments with no cylinder attached to the pendulum as

$$C_o = 2I_o n_o \delta_o$$

and therefore

$$\bar{c}_{cyl} = \frac{2I_t \dot{n}\delta_t - C_o}{h^2 L}$$

where the subscript $_o$ refers to conditions with no cylinder attached.

The viscous drag damping coefficient (Part I, chapter 3.13) is given by

$$\bar{c}_{visc} = 2\rho\pi^2 D^2 n\left[\sqrt{\frac{1}{\pi\beta}} + \frac{1}{\pi\beta}\right] \qquad -(25)$$

and the damping due to separation effects is thus

$$\bar{c}_{press} = \bar{c}_{cyl} - \bar{c}_{visc} \qquad -(26)$$

The system will be such that the damping will be a minimum, and thus c_{press} represents a least energy form of averaging.

The average damping $\bar{c}_{press}$ can be related to similarly averaged oscillatory drag coefficients for use in equations (23) and (24) by equating work done.

The work done by a force f over a small displacement, dx, is

$$fdx = f\dot{x}\,dt$$

Therefore

$$c_{press} = \frac{\int_o^T f\dot{x}\,dt}{\int_o^T \dot{x}^2\,dt}$$

where f is given by equation (21) and (22) to yield respectively CDDEP and CDIND and integration is over a cycle.

The results of the integrations using f given by (21) and (22) are:

$$CDDEP = \frac{-\bar{c}_{press}\,\dot{x}_o}{.5\rho D\,\dot{x}_o^2 B} \qquad -(27)$$

where B = 2a for $V \geq \dot{x}_o$, where $a = V/\dot{x}_o$

and B is given by equation (9') of Appendix 2.1 for $V < \dot{x}_o$.

$$CDIND = \frac{-3\bar{c}_{press}}{8n\rho D\ x_o} \qquad -(28)$$

4.3.2. Oscillatory drag and inertia coefficients CDIND' and CM

These coefficients are determined through a Fourier coefficient analysis of the force time histories. It is seen from equation (21) that the oscillatory part of the forcing side of the equation is identical to that in a pure oscillatory flow except that C_a replaces C_M due to the effects of the Froude-Krylov force in oscillatory flow. Thus the equations derived by, amongst others, Sarpkaya (1976a) for oscillatory flow can be used to determine CDIND' and CA. (CA is the time averaged value of C_a.) Thus if the velocity is assumed given by

$$U = -U_m \cos(2\pi nt)$$

$$CDIND' = \frac{-3n\pi}{2} \int_o^T \frac{f_{cyl}(t)\ \cos(2\pi nt)dt}{\rho D\ L\ U_m^2} \qquad -(29)$$

and

$$CA = (CM-1) = \frac{4U_m}{\pi^2 D} \int_o^T \frac{f_{cyl}(t)\ \sin(2\pi nt)dt}{\rho D\ L\ U_m^2} \qquad -(30)$$

where $f_{cyl}(t)$ is the force time history on the cylinder through a cycle.

Now the force time history obtained with a cylinder attached to the rig, $f_t(t)$, includes contributions due to the drag and inertia forces on the end plates and the cylinder support arms. One could obtain a cylinder force time history by subtracting that obtained

with no cylinder attached from that obtained with a cylinder attached, at the same amplitude of oscillation, i.e.

$$f_{cyl}(t) = f_t(t) - f_o(t)$$

However it is easier to obtain drag and inertia coefficients with no cylinder attached, as $CDIND'_o$ and CA_o, using $f_o(t)$ for f_{cyl} in the above equations, and then subtracting these at each amplitude from the values obtained with a cylinder attached, $CDIND_t$ and CA_t. This is permissible as

$$\int_o^T (f_t(t)-f_o(t))\cos(\frac{2\pi t}{T})dt = \int_o^T f_t(t)\cos(\frac{2\pi t}{T})dt - \int_o^T f_o(t)\cos(\frac{2\pi t}{T})dt$$

and

$$\int_o^T (f_t(t)-f_o(t))\sin(\frac{2\pi t}{T})dt = \int_o^T f_t(t)\sin(\frac{2\pi t}{T})dt - \int_o^T f_o(t)\sin(\frac{2\pi t}{T})dt$$

In the tests with no cylinder attached a reference value for 'diameter', D of .0252m is used. In subtracting the values of $CDIND'_o$ and CA_o from those obtained with a particular cylinder attached, account must be taken of the reference diameter value used.

Thus, for the oscillatory drag coefficient for a cylinder of diameter D, one obtains

$$CDIND' = CDIND'_t - \frac{.0252\ CDIND'_o}{D}$$

where values of CDIND', $CDIND'_t$ and $CDIND'_o$ are at the same amplitude of oscillation, x_o.

In order to obtain the inertia coefficient for the cylinder, CM, not only the no cylinder value must be subtracted, but also the contribution due to the mass and buoyancy of the cylinder, CA_{cyl}. (The derivation of which is explained in chapter 7.)

Thus

$$CM = 1 + CA_t - CA_o - CA_{cyl}$$

Throughout this thesis values of CM will be plotted, rather than of CA, mainly so as to compare with results obtained by other researchers.

Values of CDIND' and CM were calculated for every oscillation cycle of the force time history. The values obtained were then averaged over a 3% range of amplitude.

4.3.3. Steady drag coefficients STCDDEP and STCDIND

These coefficients are determined by equating the force on the cylinder to the steady components of equations (21) and (22).

The steady force on the cylinder, $\bar{F}_{cyl}$, at a particular amplitude of oscillation, x_o is given as

$$\bar{F}_{cyl} = \bar{F}_t - \bar{F}_o$$

where $\bar{F}_t$ is the average force measured in experiments with a cylinder and $\bar{F}_o$ in experiments without a cylinder.

The force on the cylinder is equated to the steady components of equations (21) and (22), i.e.

$$\bar{F}_{cyl} = \frac{1}{T}\int_o^T f \, dt$$

where f is given by equations (21) and (22). Conducting the integrations, which are fully documented in Appendix 2.2, yields

$$\text{For } V \geq \dot{x}_o \qquad STCDDEP = \frac{\bar{F}_{cyl}}{.5\rho D\, V^2\left(1 + \frac{\dot{x}_o^2}{2V^2}\right)} \qquad -(31)$$

$$V < \dot{x}_o \qquad STCDDEP = \frac{\bar{F}_{cyl}}{.5\rho D\, \dot{x}_o^2 E}$$

where E is a coefficient dependent on the ratio $V/\dot{x}_o$, and is given by equation (13') of Appendix 2.2.

$$\text{STCDIND} = \frac{\bar{F}_{cyl}}{.5\rho D\ V^2} \qquad -(32)$$

5. SOURCES OF INACCURACY

5.1. Inaccuracies in the estimation of damping

The logarithmic decrement of a signal is defined as

$$\delta = \frac{1}{i} \ln\left(\frac{h_o}{h_i}\right)$$

where h_o is the signal amplitude of a particular cycle, and h_i is the amplitude i cycles later.

Errors in the estimation of δ are introduced by errors in the estimation of h_o/h_i.

The various coefficients to be calculated are expected to vary with amplitude of motion and thus δ must be defined at particular amplitudes of motion. The calculation of a single value of δ is necessarily over a range of amplitudes from h_o to h_i and represents some form of average value over the range of amplitudes h_o to h_i. So as not to average out changes with amplitude of δ, and therefore of CDDEP or CDIND, it is desireable to have h_o/h_i as near 1.0 as possible. However the inherent error in the estimation of δ increases rapidly as h_o/h_i decreases. This is especially critical as the digization is conducted with only 8-bits.

For values of $h_o/h_i \lesssim 1.5$, as is always the case in the analysis conducted in this thesis

$$\% \text{ error in } \delta \approx \frac{\% \text{ error in } h_o/h_i}{h_o/h_i - 1} \qquad -(33)$$

i.e. 1% error in h_o/h_i when $h_o/h_i = 1.01$ leads to a 100% error in δ, whereas when $h_o/h_i = 1.1$ the error is 10%, and when $h_o/h_i = 1.5$ the error is 2%. Thus it can be seen that the error in δ increases dramatically as h_o/h_i approaches 1.0, for a given error in h_o/h_i.

Thus the choice of h_o/h_i in the calculation of δ has to try to

satisfy the conflicting demands of desired high accuracy in δ and estimation over as small a range of amplitude as possible.

Estimates of the error in h_o/h_i may be made as follows:

The A/D converter had a resolution of + .039 v, the maximum difference between actual and digitized voltage being + .039. The smallest amplitude that the motion trace was allowed to decrease to in an experimental run was about 1.5 volt, indicating a maximum error in the estimate of h_i of about +2.5%, and rather less for h_o.

Thus the very largest error in estimating h_o/h_i is 2.5%, for the unfortunate combination of small amplitude and maximum error in h_i, i.e. +.039 volts, and zero error in h_o (increasing error in h_o in fact decreases the error in h_o/h_i, for this given + .039 v error in h_i).

The vast majority of results will have a smaller error due to the fact that the amplitude was nearly always greater than 1.5 v (varying between 5 v and 1.5 v), and the low probability of the above mentioned unfortunate combination. One might perhaps estimate a 'reasonable' error of h_o/h_i as, say, 1%.

Now if the damping is sufficiently small that the amplitude of motion decreases by less than .039 volt per oscillation cycle, as was in fact nearly always the case, then the error in h_o/h_i will be less than the above due to the analysis method. This can best be explained with the aid of the diagram below.

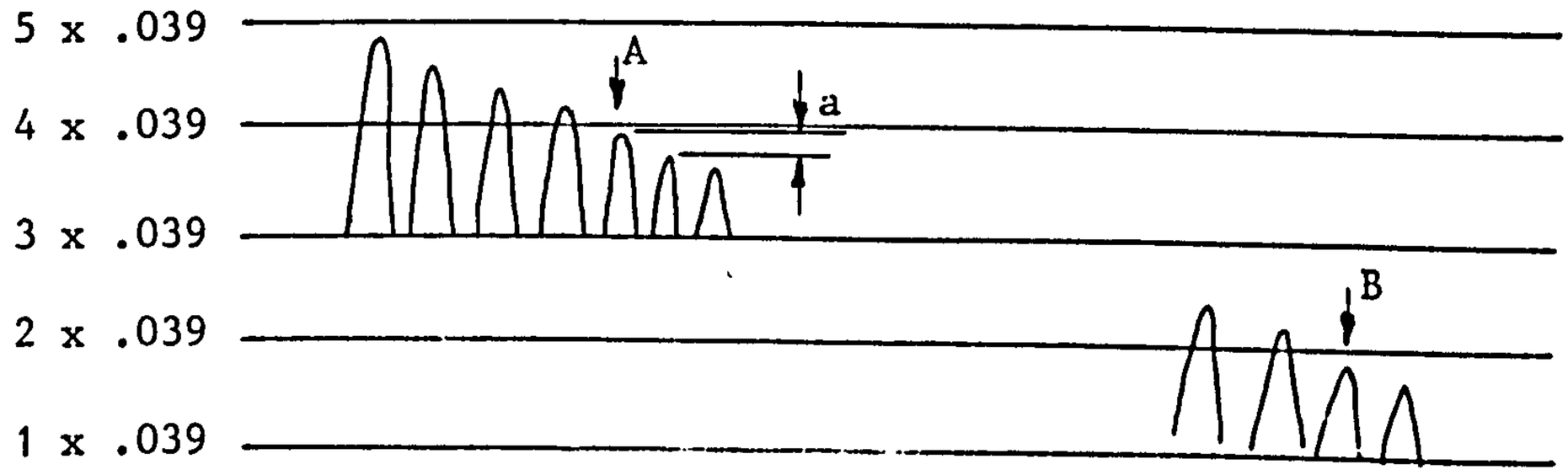

The signal voltage is shown with respect to an axis in steps of .039 volts. The A/D converter gives any voltage between, say, (1 x .039) and (2 x .039) volts the value (1 x .039) volts. The program to calculate δ picked out the first peak in a time series less

than a given step value, e.g. the first peak with a value less than (4 x .039) volts in the figure is that marked A, and this was given the value (4 x .039) volts in the program. Similarly the peak B is given the value (2 x .039) volts.

The maximum difference between the actual value of the peak of A and that assigned in the program is thus -a volts, where a is the difference between one peak and the next, assumed constant over the range of a calculation of δ, (which is reasonable for $h_o/h_i \lesssim 1.5$ and constant damping over this range).

Now the ratio of the amplitudes of succesive peaks is $\exp(\delta)$, and thus

$$\frac{a}{h} = (1 - 1/\exp(\delta))$$

or the <u>percentage</u> error in the estimation of h_o/h_i, assuming the damping to be constant over this range is

$$100(1 - 1/\exp(\delta)) \qquad -(34)$$

Combining (33) and (34) gives an estimate of the percentage error in the calculated value of δ as

$$\frac{100(1 - 1/\exp(\delta))}{(h_o/h_i - 1)} \qquad -(35)$$

with a maximum 'reasonable' value of

$$\frac{1}{(h_o/h_i - 1)} \qquad -(36)$$

or an absolute maximum value of all the error sources combining of

$$\frac{2.5}{(h_o/h_i - 1)}. \qquad -(37)$$

From (33) and (36) it is seen that the error will be less than the 'reasonable' estimate for values of $\delta < .01$.

Least error is therefore given for low δ and high h_o/h_i. The

disadvantage of high values of h_o/h_i has already been mentioned. Low δ is also advantageous in that one desires to have as little change in amplitude of oscillation from cycle to cycle, so that the flow may be considered to be a 'steady' oscillating flow, as opposed to one decreasing rapidly in amplitude. This is probably of importance to the interaction of vortices in one cycle with those from the previous cycle. Low δ is obtained by having high inertia, hence the reason for the massive pendulum design.

5.1.1. Choice of the ratio h_o/h_i

The program written to calculate values of δ used a (nearly) constant value of h_o/h_i. A time series of motion for a .0252 m diameter cylinder in still water was analysed using different values of this ratio. The amplitude assigned to a particular value of δ is that of $h_{i/2}$, i.e. the amplitude of the cycle half way between that with amplitude h_o and that with amplitude h_i.

For very small values, $h_o/h_i \lesssim 1.05$, there was considerable scatter in the results, and for very large ratios, $h_o/h_i \gtrsim 2$ there was a noticeable change in curves drawn through the results. A value of 1.2 was chosen for all subsequent analysis. It should be mentioned that when there was a current the damping varied much less with amplitude, and so the need to limit h_o/h_i to small values, due to the averaging effect over amplitude, became less important. Thus as there was no noticeable evening out of the curves in the still water test using $h_o/h_i = 1.2$ it was considered that this was never an important effect.

For small currents the damping is less at small amplitudes and increases with increasing amplitude. The test rig had greater damping for larger diameter cylinders. In still water, at an amplitude of .25 diameters, the logarithmic decrement of the smallest and largest cylinders tested (.0202 m, .0701 m diameter respectively) were $\delta = .0018$ and $\delta = .0036$ respectively, indicating an accuracy in the estimates of δ, using (26), of .9% and 1.8%, respectively.

The absolute maximum error for a value of $h_o/h_i = 1.2$ is, from (37), 12.5%, and the 'reasonable' value is, from (36), 5%.

It is in the estimation of δ that the majority of the error in the calculation of CDDEP and CDIND lies. A less coarse A/D converter would have considerably improved the errors, for example a 12-bit converter would have had an absolute maximum error of only 0.8% for $h_o/h_i = 1.2$. The 8-bit converter was the only one available, and it will become evident from the results that the accuracy was quite sufficient.

In order to obtain a larger number of points for δ versus amplitude the time history was stepped down in 7% steps of amplitude, and δ calculated between each amplitude and the next but two, i.e. about 20% down. This is illustrated in the figure below.

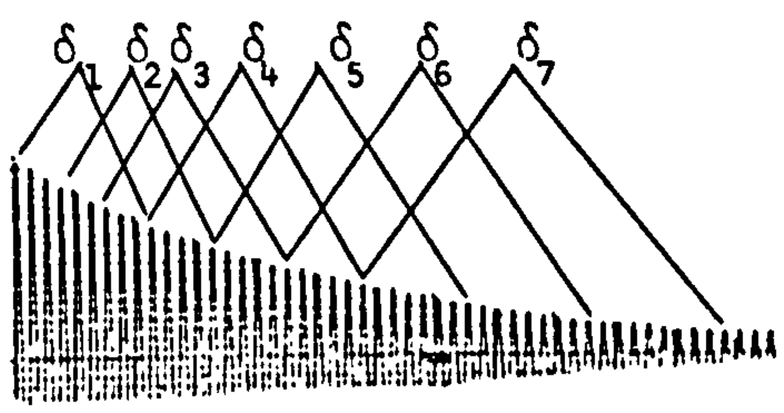

5.2. Inaccuracies in the estimation of the steady drag force

The steady drag force was estimated by calculating the average of the force signal over the same range as each damping estimate was taken, i.e. over about a 20% amplitude range.

5.2.1. Digitization error

A digitization error due to the coarseness of the 8-bit A/D converter is introduced.

The digitized value of any point will be between 0 and .039 volts lower than the actual value. As the average is taken over between several hundred and several thousand points, the actual mean will be very nearly .039/2 = .0195 volts higher than the estimated. This was not accounted for in the programs written, however the lowest force measured was represented by about 0.8 volts, and thus the maximum error due to this effect is about 2.4%.

5.2.2. Damping effect error

If one assumes that there is a damped harmonic oscillation about a zero mean value from an initial value h_o, say, i.e. that the curve may be described as

$$h = h_o \cos(2\pi nt)\exp(-\delta t)$$

then integration of this curve, over an integral number of cycles, will not give a zero mean.

It can be shown that the difference between the true mean (zero in this case) and that calculated by integrating the curve is given by

$$\text{difference} = \frac{-h_o n}{i}\left[\frac{1 - \delta\exp(-\delta i/2)}{4\pi^2 n^2 + \delta^2}\right]$$

where i is the number of cycles over which the integration is conducted. It is evident that the largest difference occurs for large amplitude oscillations with high damping and the integration conducted over few cycles.

In the experiments high damping only occurs when there is a large current velocity, in which case the steady component of force is large and this error still represents only a small percentage error. The error may be significant in small currents where the steady force is small, and with large amplitude vibrations where the oscillatory forces are large and the damping is also larger. The maximum error in the steady component force due to this effect is estimated, using the above equation, to be about 0.15% of the oscillatory amplitude. It is difficult to judge whether this will be significant or not. The smallest ratio of steady to oscillatory velocity, $V/\dot{x}_o$ was about .05, indicating that the steady force may be very much less than the oscillatory, and the error from this effect correspondingly larger. However it appears that in this region the steady drag coefficient, STCDIND, is very high, tending to decrease the error again. The results plotted in this thesis did not account for these errors, however some data, where the effect was expected

to be greatest, was reanalyzed accounting for this effect. The difference in the results was very slight and it is therefore assumed that the effects of the damping on the estimation of the steady force were negligible.

6. SUBTRACTION OF NO-CYLINDER VALUES

It has already been seen that values of force, damping, $CDIND'_o$ and CA_o obtained with no cylinder attached to the rig have to be subtracted from the values obtained with a cylinder attached in order to isolate the effects due to the cylinder. It was found that for low velocities of flow the force data with no cylinder attached were unreliable due to amplifier drift and the inaccuracies in measuring the very small forces involved. For some velocities, tests with no cylinder were not conducted and in one case the data was accidentally destroyed, and thus the no cylinder data for these cases had to be estimated from the data at other velocities. Data for these cases were obtained by multiplying data at other flow velocities by appropriate factors. In order to do this the data was curve-fitted. The curve-fitted results of the data from tests with no cylinder were subtracted from the data obtained with a cylinder attached at each particular value of amplitude x_o. Curve fitting also eliminated errors which would occur if, for example, linear interpolation was used (due to scatter or spurious data points which occurred occasionally, most often caused by voltage 'spikes').

Curve fitting was also necessary in order to extrapolate between experimental points. The values of x_o/D were not identical in all tests, and it was desired to compare data from different conditions at identical values of x_o/D, therefore the final results, after calculation of the various coefficients, were also curve-fitted.

The curve-fitting procedures are detailed below.

6.1. Curve-fitting

The curve-fitting routines consisted of library routines modified by the author, which provided a least squares polynomial fit, of order up to 18, to up to 500 points, with the possibility of weighting any number of the points.

The 'x-axis' in the curve-fitting used in the results was always the amplitude of oscillation, x_o/D.

There are a number of problems with any curve-fitting procedure

which make it difficult to apply the technique generally without considerable forehand knowledge about the points to be fitted. Some of the problems are indicated below.

i) Too low an order of polynomial will even out 'bumps' in a complicated curve.

ii) Too high an order of polynomial can lead to the fitting of a complicated curve through a few points, which are in fact best fitted by a simpler curve.

iii) If there is a gap in the data points, particularly if a high order polynomial is used, then the fitted polynomial may exhibit oscillations in this gap.

iv) The least squares method reacts strongly to a 'spurious' point which may lie away from the rest of the points.

v) Apparently simple curves, as for example those obtained for the oscillatory drag coefficient in still water (Fig. 70), may nevertheless need high order polynomials to fit them. In the case of the oscillatory drag coefficient the peak is otherwise underestimated. Weighting may advantageously be applied in areas where changes in the curve are expected, or where particular accuracy is desired.

vi) If the data cover a wide range of values (for example damping in the experiments could vary over an order of magnitude), then the lower values will have correspondingly less importance attached to them, and the fitted curve will exhibit larger <u>percentage</u> deviation for the low values, as the procedure is to minimize the <u>absolute</u> deviation. If the percentage error is desired to be as little at low values as at high (as in the case of damping here), then it is advisable to change the data values so that they vary less, for example by taking the logarithm first (a variation of 2 orders of magnitude from, say, 10 to 1000 then becomes a variation from 1 to 3). As another example, results of CDIND with no cylinder attached to the rig were approximately proportional to $1/x_o$, and consequently varied greatly with x_o/D. Therefore, by multiplying CDIND by x_o before conducting the curvefitting, the values were virtually con-

stant. Any program which uses curve-fitted coefficients which have been produced from data which has been altered by taking logs, etc., before conducting the curvefitting, must be aware of the alterations so as to apply their inverses after calculating values at desired points, e.g. if curve-fit coefficients are produced for (CDIND . x_o) versus x_o/D, then a program calculating CDIND at a particular value of x_o/D has to first substitute the particular value of x_o/D into the coefficients, evaluating (CDIND . x_o) at this value, and then to divide by x_o. It is therefore necessary to keep very careful track of data alterations used to suit curve-fitting routines.

In many respects, curvefitting 'by-eye' represents an exceedingly advanced form of fitting, the effectiveness of which can rarely be duplicated by a computer routine! (However in our case, fitting by eye does not produce data which can easily be used in further numerical routines, as polynominal coefficients can.)

For the various data considered in this investigation it was necessary under different circumstances to use different orders of polynominal, to take logs, to multiply by x_o, to use weighting, etc., to suit the data of the particular condition. This dependence of the curve-fitting routine on the data to be fitted cannot easily be reconciled with the desire to automise the process as far as possible. The analysis programs took a large amount of computer time, and it was desired to run the programs in batch processing.

Representative results for the various expected data forms were therefore analysed several times using various combinations of polynomial order, etc., to try to find suitable combinations for the majority of the results. The results were then analysed in batch processing. All results were then studied by plotting the actual points and curvefitted curves, and those which were deemed unsatisfactory were reanalysed with other combinations of polynomial order, etc., until satisfactory results were obtained. The process was, however, rather time consuming.

Curve-fitting was <u>not</u> a method used primarily to improve poor results. Representative example curves with actual points plotted on are given in the main results. Also examples of actual points

and those predicted at particular values of x_o/D for various variables are given in chapter 10.1. In figures where actual and curve-fitted points are shown the curve-fitted points are shown with larger symbols.

6.2. No-cylinder values of force

The effects of amplifier drift on the estimation of the steady component of force have already been mentioned. Drift was most significant in tests with very small steady forces, particularly if the test covered a long time span. Drift was found to be a problem in estimating the steady component of force in low velocity currents for the rig with no cylinder attached. Also in this case the voltage deflection was small, even on the most sensitive range, being about .2 volts, again indicating inaccuracy.

In Fig. 56 are shown the measured points for force, $\bar{F}_o$, in Newtons, versus x_o/D for the rig with no cylinder attached in various current velocities, for the low pendulum frequency. There is very little scatter in the results for higher current velocities and more scatter for the lower velocities. There is a small increase in force with increasing amplitudes. Similarly in Fig. 57 two curves are shown for the high pendulum frequency case. The increase in force with amplitude is rather greater (however if the increase is caused by a decreasing $V/\dot{x}_o$ effect, then it is approximately the same for the two cases).

In Fig. 58 are plotted the low amplitude values of the square root of the force measured against velocity, for both the high and low pendulum frequency cases for the data in the above figures and for other cases. An impression of the scatter is shown by the vertical length at each point. It is seen that for velocities greater than about .07 m/s, the points are joined by a straight line. Apparently for lower velocities there is a rather greater force than that suggested by an extrapolation of the straight line. Although this may be due to a more dominant viscous drag term at lower velocities, the effect could have been due to amplifier drift and general inaccuracies at the low flow velocities. The results for forces on

the cylinders were obtained in two ways: by subtracting, from the forces measured in experiments with cylinders, forces given by the straight line, and forces given by the curved line drawn in Fig. 58.

For example for the low pendulum frequency tests, the values to be subtracted for velocities lower than .1 m/s were calculated by multiplying those of test 70, obtained in a .179 m/s current, by an appropriate scaling factor, e.g. for the tests in .028 m/s current, using the straight line curve of Fig. 58, the results were multiplied by .025 at all amplitudes.

For the high pendulum frequency tests, test 260, at a velocity of .288 m/s, was scaled appropriately for all the tests at other velocities.

Fig. 58 is drawn for the small amplitude results, the increase in force due to increasing amplitude of motion was assumed to scale in the same manner. The no-cylinder force is, however, less important for large amplitudes of motion, as at small velocities of flow the drag force on the cylinder increases very rapidly with increasing amplitude, whereas the no-cylinder force increases by only a small amount.

It was found that there was virtually no difference between results obtained when subtracting the no-cylinder forces given by the straight line relationship between $\sqrt{\bar{F}_o}$ and x_o/D, and those given by the curve relationship in Fig. 58, other than for a flow velocity of .028 m/s and to a lesser extent .039 m/s. The force difference between these two approximations represents a value of STCDIND for the .0202 m diameter cylinder of .2 and .08 for the .028 and .039 m/s currents, respectively, and correspondingly less for larger cylinder diameters.

Results obtained using the curved relationship of Fig. 58 for the no-cylinder force seemed to give a better collapse than those using the straight line approximation, when comparing results for the same values of V/nD and x_o/D (the important parameters in this case), but for different cylinder diameters and flow velocities. It was therefore assumed that the curved relationship did approximate the no-cylinder forces better than the straight line relationship. The various coefficient results presented in this thesis have therefore been obtained using the curved relationship.

6.3. No-cylinder values of damping

In Fig. 59 are shown the calculated actual points for the damping factor of the rig in still water with no cylinder attached, C_o, for the low pendulum frequency case. The curve-fitted points at various values of x_o/D are also shown (the larger symbols). In Fig. 60 are shown points for the high pendulum frequency case. It is seen that the damping increases with x_o/D, particularly for low velocities, that higher velocities lead to higher damping, and that there is virtually no scatter in the results. The high frequency pendulum evidently had higher damping. (A value of C_o = .2 represents .053% and .067% of critical for the low and high frequency pendulums, respectively, which indicates how low the damping is.)

In Figs. 61 and 62 the values of C_o for various values of x_o/D are plotted against velocity. It is evident that damping changes smoothly with amplitude and velocity, and values at other velocities can be accurately estimated. For the low frequency pendulum case data did not exist for flow velocities of .128, .059, .039 and .028 m/s. Data for .128 m/s flow was obtained by suitably adjusting the data at .179 m/s, and data for the other velocities were obtained from the data at .081 m/s. As an example the data at .128 m/s is obtained by multiplying that at .179 m/s by 1.1 and subtracting .021. In Fig. 61 the estimated data for these flow velocities are shown.

Similarly for the high frequency pendulum, data for flow velocities of .059 and .028 m/s were obtained from the data at .048 m/s, and the estimated points are shown in Fig. 62.

The damping of the rig with no cylinder attached is only a significant proportion of that with a cylinder attached for zero flow velocity, the smallest cylinder diameters (the .035 m diameter or smaller) and for the very smallest amplitudes of oscillation, say $x_o/D \lesssim .25$. This can be seen from Fig. 63 where the damping measured against x_o/D is shown for the low frequency pendulum rig in still water with no cylinder attached, and with each of the cylinders attached.

6.4. No-cylinder values of oscillatory drag coefficient, $CDIND'_o$

From section 6.3 it is evident that the damping of the rig with no cylinder attached is virtually constant with amplitude. However from equation (28) it is seen that $CDIND_o \propto \delta_o/x_o$. The oscillatory drag coefficient obtained from the Fourier analysis of the force time history, $CDIND'_o$, is therefore expected to be approximately $\propto 1/x_o$. In Fig. 64 is shown $CDIND'_o$ for the low frequency rig with no cylinder attached in still water. The curve-fitted points shown have been obtained in the manner described below.

Before applying the curve-fitting procedures the data for $CDIND'_o$ was multiplied by 50 x_o. The data of Fig. 64 are replotted in Fig. 65 for $CDIND'_o \cdot 50x_o$. It is seen that the scatter is very small except for $x_o/D \lesssim .25$. In Fig. 66 are plotted results for the low pendulum frequency at various flow velocities. The results for a velocity of .081 m/s lie only very slightly higher than those for zero velocity, and there was no difference between those at .048 m/s and zero velocity. For flow rates of .059, .039 and .028 m/s, therefore, the data for .048 m/s was used.

Although results for $CDIND'_o$ for the high pendulum frequency rig were obtained, they will not be presented in this thesis. Suffice it to say that the procedure was similar to that for the low frequency tests.

6.5. No-cylinder values of mass coefficient, CA_o

For velocities of flow of .233 m/s and with the largest cylinders attached, it was found that twisting of the frame holding the test cylinder could occur. This was prevented by adding a stiffening bar. Tests in still water were conducted both before and after fitting, and it was found that there was no difference in the curves of damping, force, or $CDIND'_o$. However the coefficient CA_o was altered. The two curves are shown in Fig. 67, and it is noted that the values are <u>negative</u>. In Fig. 68 are shown curves of CA_o versus x_o/D for the low frequency pendulum rig with no cylinder attached

for various current velocities. It is seen that the values of CA_o are independent of x_o/D and that they are virtually identical to the appropriate still water values, except for the very highest velocity, .445 m/s when the value of CA_o was slightly changed. The values for a current of .048 m/s (Test 90) were used for tests at lower flow velocities.

For the high frequency pendulum rig tests, which were conducted after all the low frequency tests, the rig was in its modified version, i.e. with the stiffening bar. The value of CA_o was the same for all values of velocity (CA_o = 1.68, based on a diameter, D = .0252), and the curves are not reproduced here.

The explanation of the negative values of CA_o will be given in the next chapter, where the mass force due to the mass and buoyancy of each cylinder is considered.

7. INERTIA EFFECTS DUE TO THE MASS AND BUOYANCY OF THE CYLINDERS

The inertia force measured on the rig, with a cylinder attached and in water, is expressed, in terms of the cylinder diameter and the acceleration of the centre of the cylinder, as

$$F = .25\rho\pi\, D^2 L\, CA_t \ddot{x} \qquad -(38)$$

where

$$CA_t = CA + CA_{cyl} + CA_o \qquad -(39)$$

where CA (= CM-1) is the added mass coefficient which it is desired to obtain, CA_{cyl} is the mass coefficient due to the mass and buoyancy of the oscillating cylinder and CA_o is the mass coefficient due to the oscillation of the mass of the measuring system (the frame consisting of cylinder end plates, support arms and strengthening member) and is given by tests in water conducted with no cylinder attached.

The values of CA_o have been discussed in the previous chapter; suffice it to say that the values for the low pendulum frequency tests were negative, and that this is due to the action of gravity, as will become evident in the following.

Consider the value of CA_{cyl}, due to the inertia force of a cylinder of length L, diameter D and mass M oscillating <u>in air</u> with pure oscillatory motion and amplitude x_o. The force at any instant on the cylinder is given by Force = Mass. Acceleration, i.e.

$$F^{(1)}_{cyl} = M \ddot{x}$$

where $\ddot{x}$ is the instantaneous acceleration.

This can also be written in the form

$$F^{(1)}_{cyl} = .25\rho\pi\, D^2 L\, CA^{(1)}_{cyl} \ddot{x}$$

and therefore

$$CA_{cyl}^{(1)} = \frac{M}{.25\rho\pi\ D^2 L} \qquad -(40)$$

where the $^{(1)}$ indicates that this is calculated for pure oscillatory motion in air.

Now consider oscillations in air of the cylinder attached to the pendulum. Because of the arc of the motion there will be a component of the gravitational force perpendicular to the axis through the cylinder centre and centre of rotation of the pendulum, i.e. acting in-line with the force transducer. This force has a magnitude, for a deflection angle θ of the pendulum, given by

$$Mg\ \sin\theta \approx Mg\ \theta = mg\ x/h$$

where x is the instantaneous deflection of the centre of the cylinder, and h is the distance from the centre of the cylinder to the axis of rotation. Therefore in this case

$$F_{cyl}^{(2)} = M\ddot{x} - Mg\ x/h$$

and

$$CA_{cyl}^{(2)} = \frac{1}{.25\rho\pi\ D^2 L\ddot{x}} \cdot M(\ddot{x} - gx/h)$$

and, as $\ddot{x} = 4\pi^2\ n^2\ x$, this can be written

$$CA_{cyl}^{(2)} = CA_{cyl}^{(1)}\ \left(\frac{4\pi^2 n^2 - g/h}{4\pi^2 n^2}\right) \qquad -(41)$$

where $^{(2)}$ indicates that this is calculated for the cylinder attached to the pendulum and oscillating in air.

Experiments were conducted for both the low and high frequency pendulums oscillating in <u>air</u> with no cylinder attached, and with various cylinders attached. The results are given below

D	n	M(kg)	CA_o *	CA_t	Measured CA_{cyl}	Calculated CA_{cyl}
.0252	.4764	.196	-2.65	-3.30	-.65	-.663
.0350	.4764	.375	-1.36	-2.01	-.65	-.659
.0202	1.409	.125	3.54	2.61	.93	.959
.0350	1.409	.375	1.80	.87	.93	.960

* This value is adjusted for the relevant cylinder diameter.

The agreement between the measured and calculated values of CA_{cyl} is satisfactory and also indicates that the computer programs worked correctly.

It is evident that a negative value of CA_{cyl} will occur if $gx/h < \ddot{x}$. Similarly a negative value of CA_o was obtained for the low frequency pendulum system. The cylinder and the cylinder support system in these cases is effectively being 'held back' by the pendulum rather than being forced.

Consider now a cylinder attached to the pendulum and oscillating in water. There will be a buoyancy force as well as the gravitational force, and in this case the force on the cylinder may be written as

$$F_{cyl}^{(3)} = M\ddot{x} - (M-B)gx/h$$

where B is the buoyancy mass and is given by the displaced mass of water.

From this it can be derived that

$$CA_{cyl}^{(3)} = CA_{cyl}^{(1)} Z$$

where

$$Z = \left(\frac{4\pi^2 n^2 M - (M-B)g/h}{4\pi^2 n^2 M}\right) \qquad -(42)$$

In the table below the values of $CA_{cyl}^{(3)}$ for the various cylinders are calculated.

D	n	M	B	$CA_{cyl}^{(1)}$	Z	$CA_{cyl}^{(3)}$
.01275	.4764	.354	.043	8.31	-.374	-3.108
.0202	.4762	.125	.107	1.168	.775	.905
.0252	.4760	.196	.166	1.176	.760	.894
.0320	.4758	.105	.268	.392	3.434	1.346
.0350	.4757	.375	.321	1.169	.774	.905
.0502	.4744	.331	.660	.501	2.568	1.287
.0701	.4717	.480	1.286	.373	3.679	1.372
.0202	1.403	.125	.107	1.168	.974	1.138
.0252	1.401	.196	.166	1.176	.972	1.143
.0320	1.400	.105	.268	.392	1.281	.502
.0350	1.397	.375	.321	1.169	.974	1.139
.0502	1.386	.331	.660	.501	1.184	.593

An indication that this procedure is correct is given by the fact that the value calculated for CM at very small amplitudes of vibration was $2.1 \pm .04$ for all cylinder diameters and both pendulum frequencies, and this value is in good agreement with that obtained by other researchers.

8. PARAMETERS OF IMPORTANCE

For a dimensional analysis it is assumed that the drag force on the cylinder is a function of (V_{inst}, ρ, D, x_o, η, n, t), where η is the dynamic viscosity. This analysis yields

$$\frac{F}{\rho D\ V_{inst}^2} = fn(x_o/D,\ V_{inst}D/\nu,\ V_{inst}/nD,\ V_{inst}t/D)$$

The last group can be replaced by t/T, which is a combination of the two last groups, where T = 1/n. Each of the two middle groups can be expressed as two groups with respectively V and $\dot{x}$, as $V_{inst} = (V-\dot{x})$, i.e.

$$\frac{F}{\rho D\ V_{inst}^2} = fn(x_o/D,\ VD/\nu,\ \dot{x}D/\nu,\ V/nD,\ \dot{x}/nD,\ t/T)$$

combining the third and fifth groups yields $\beta = nD^2/\nu$ instead of the third group, and removing dependent groups gives

$$\frac{F}{\rho D\ V_{inst}^2} = fn(x_o/D,\ \beta,\ V/nD,\ t/T)$$

The final group is discarded as time averages of the coefficients are used. The results have been plotted using V/nD as one parameter and either x_o/D or $V/\dot{x}_o$ (= V/nD divided by $2\pi\, x_o/D$) for various ranges of β.

9. RESULTS IN STILL WATER

Only the results for the tests in still water will be presented in this chapter. Results for the tests in various currents will be presented in the following chapter.

9.1. Oscillatory drag coefficient

For zero flow velocity the oscillatory part of equation (22) reduces to that of equation (21), and CDIND ≡ CDDEP.

The main tests conducted have been listed in section 3.1. It has already been mentioned that the Stokes' viscous damping contribution, $\bar{c}_{visc}$, was subtracted from the cylinder damping (equation (26)), before CDIND was calculated. The reason for this will become evident from the following.

In Fig. 63 are shown calculated points and the curve-fitted results for damping of the rig versus x_o/D with various cylinders and with no cylinder attached.

From these results, and those for other cylinders, results for CDIND, where the viscous contribution has <u>not</u> been subtracted, are shown in Fig. 69, i.e. $\bar{c}_{cyl}$ is used for c_{press} in equation (28). It is seen that for small values of x_o/D the curves for lower values of β lie higher than those for higher values of β, and that as x_o/D approaches zero the curves all go asymptotically to very large values.

It has been shown in Part I, chapter 3.13 that for x_o/D smaller than about 0.1 the damping force on the cylinder is given by Stokes' equations, i.e. by equation (25).

Using equation (28), the drag coefficient due to viscous force can be expressed as

$$CDIND_{visc} = \frac{-3\pi^2}{4} \left(\frac{D}{x_o}\right) \left[\sqrt{\frac{1}{\pi\beta}} + \frac{1}{\pi\beta}\right] \qquad -(43)$$

From which it is seen that the (unseparated) viscous contribu-

tion is $\propto 1/(x_o/D)$ and approximately $\propto\sqrt{1/\beta}$, (as $\sqrt{1/\pi\beta} >> 1/\pi\beta$).

This thus suggests that the effects noticed above in the experimental values of CDIND at low x_o/D are due to viscous contributions.

Therefore in Fig. 70 are plotted values of CDIND with the viscous contribution removed, i.e. using equation (26) for $\bar{c}_{press}$ in (28). For larger x_o/D the results are virtually unchanged, however as x_o/D approaches zero the curves all approach CDIND = 0. These curves thus represent the value of oscillatory drag coefficient over and above that given by Stokes' equations, i.e. by equation (43). The curves may be thought of as representing the oscillatory drag coefficient component due to pressure, i.e. separation induced forces. (See also chapter 12.5.)

In all subsequent plotting, for both still water tests and tests in currents, the Stokes' viscous contribution is subtracted before the oscillatory drag coefficients are calculated. Stokes' viscous damping is only expected to apply for unseparated flow whereas it has been subtracted under all circumstances. However, other than for very low flow velocities and low values of x_o/D, the contribution is small compared to the total oscillatory drag forces. Also, as will be seen, at very low flow velocities the experimental values of CDIND and CDDEP are virtually identical to those for zero flow, indicating that the subtraction of viscous forces is still reasonable.

By fitting a curve to Fig. 70 for values of $x_o/D \lesssim .5$ and comparing the total drag coefficient, given by this curve plus the viscous contribution given by equation (43), to the viscous contribution, it can be calculated up to what value of x_o/D the drag coefficient, and therefore also the damping, is given by Stokes' viscous equations. In Verley (1978) it was shown that the viscous contribution is 90% or more of the total for

$$x_o/D \lesssim .53\ (1/\beta)^{1/6}$$

for which x_o/D varies from .26 for $\beta = 70$ to .14 for $\beta = 3500$, and .05 for $\beta = 10^6$.

The implications of the above equation are probably one reason why various authors have obtained various values of x_o/D up to which they consider Stokes' viscous theory to apply.

9.1.1. Scatter in the results

Figs. 69 and 70 were plotted from curve-fitted results at various x_o/D.

In Fig. 71 the actual experimental data points for some of the values of β are plotted. It is seen that only a very small amount of scatter is found. Further experiments showed that there was more scatter at very low values of x_o/D. Scatter appeared to be about $\pm$ .5 at x_o/D = .05 and $\pm$ .05 at $x_o/D \gtrsim .2$.

Altogether in the course of the experiments a large number of results for CDIND versus x_o/D for various β have been obtained, using various cylinders attached to various pendulum rigs. An idea of the extremely good repeatability of the results can be obtained by comparing the results of Fig. 71 with those of Fig. 72 obtained some months later, and Fig. 73 obtained with a smaller pendulum and calculating values of logarithmic damping by hand from U-V traces of the motion output. The results can also be compared with those of Sarpkaya and Tuter (1974), whose results were obtained in an oscillatory flow and have been reanalysed, subtracting the viscous contribution, and are plotted in Fig. 74. A curve drawn through these results is almost identical to those of the above figures for similar β, but the results show rather more scatter than the author's.

9.1.2. Values of oscillatory drag coefficient from Fourier analysis of forces, CDIND'

In the previous sections, values of the oscillatory drag coefficient CDIND (= CDDEP) obtained from the damping of the pendulum motion have been presented. Values of the oscillatory drag coefficient have also been obtained from a Fourier coefficient analysis of the forces measured on the cylinder, i.e. CDIND' as described in chapter 4.3.2. Some results for CDIND' versus x_o/D are shown in Figs. 75 and 76. (The viscous contribution has again been subtracted.) From these it is seen that the results for $x_o/D \gtrsim 1.0$ are

virtually identical to those for CDIND. For lower values of x_o/D the results of CDIND' lie somewhat higher, and there is also more scatter. For low x_o/D the force trace is predominantly inertia dominated, and there is hence less accuracy in the results of CDIND'.

9.2. Inertia coefficient

Curve-fitted results of CM versus x_o/D for the low and high frequency pendulums are shown in Figs. 77 and 78, respectively, and the actual points for some of the low cylinder frequency results are shown in Fig. 79. Results from Sarpkaya and Tuter (1974) are also shown on Fig. 77. The low frequency pendulum results are similar to those of Sarpkaya and Tuter, however the large amplitude values are rather lower (~20%) than Sarpkaya and Tuter's. There is little scatter in the results for $x_o/D \lesssim 2.0$, with increasing scatter thereafter when the oscillatory forces become drag dominant. Values of CM obtained with the high pendulum frequency lie rather higher, for similar β, than those from the low, at least for $x_o/D \gtrsim 1.0$. There is no apparent explanation for this, however the high pendulum frequency results exhibited considerably more scatter.

It is noted here that CM is plotted rather than CA for comparison purposes. The actual inertia force on the cylinder can be calculated from the results by subtracting 1.0 from the values of CM. CM, as has been explained, represents the force for a case where the flow is oscillating and the cylinder is stationary.

10. RESULTS IN CURRENTS

10.1. Example results

Examples of the raw results for the damping, C_o, the steady force, F_o, and the inertia, CA_o, for tests with no cylinder in various currents have already been presented in chapter 6.

Due to the large amount of data collected, only a few examples of raw results for tests with a cylinder attached are presented. The general variation and scatter in these examples are, however, entirely representative for all the results collected.

In Fig. 80 are shown examples of the damping, C_{cyl}, for various cylinders attached in various currents. It is seen that there is virtually no scatter except for results at the very highest flow velocities, when the scatter is still only about $\pm$ 5%.

In Fig. 81 are shown examples of the steady force, $\bar{F}_t$, for the rig with various cylinders attached in various currents. Again there is very little scatter.

From the damping data the oscillatory drag coefficients CDIND and CDDEP are calculated, and from the steady force data the steady drag coefficients STCDIND and STCDDEP are calculated. From the force time histories the inertia coefficient CM is calculated.

An impression of the scatter in the oscillatory drag coefficients can be obtained from Fig. 82, CDIND$\cdot$ x_o/D versus $V/\dot{x}_o$. The scatter is evidently very small other than for the highest flow velocities at the smallest amplitudes of oscillation, when the scatter is about $\pm$ 10%. It is nevertheless in this area where the method of equating the oscillatory drag force to the measured damping is most advantageous. The oscillatory drag force is extremely small compared to the steady drag force and small compared to the inertia force, and the results for CDIND', calculated from the force time histories, exhibit very much more scatter because of the smallness of this component. The smallness of the oscillatory drag force compared to other forces does not, however, imply that it is unimportant, precisely because of its relationship to damping. (See Part I, chapter 6.2.)

Example results of the steady drag coefficient, STCDDEP, are shown in Figs. 83 and 84. It is seen that there is very little scatter for high values of V/nD, and rather more, though still little, at lower V/nD, mostly because of amplifier drift, as discussed in chapter 2.7. The examples, at low V/nD, in Fig. 84, serve to show the good repeatability of the results. The three curves shown are obtained with different flow velocities and cylinder diameters, nevertheless the curve for the higher values of V/nD are slightly higher than those for lower V/nD, in accordance with the overall results, (see Fig. 96). For V/nD $\lesssim$ 1.5 the scatter was rather more, being about $\pm$ .3 (in STCDDEP), between various tests at similar values of V/nD.

Example results of the inertia coefficient, CM, are shown in Figs. 85 to 87. The scatter is small for low flow velocities, particularly at low x_o/D where the inertia forces dominate, as in Fig. 85. For higher velocities of flow, Fig. 86, there is more scatter, and for very high velocities, Fig. 87, there is extremely large scatter, particularly for low x_o/D. The reason for this scatter at high V/nD is that the inertia force is then extremely small compared to the steady force, particularly at low x_o/D, and is comparable in magnitude with the variations in force due to turbulence, variations in flow velocity and the alternating forces from vortex shedding. It is not very important to quantify the inertia coefficient in this range precisely because of its small magnitude, and the inertia coefficient has not been plotted in the results where it exhibits large scatter.

10.2. Results for oscillatory drag coefficients

The time averaged oscillatory drag coefficient based on equation (21), CDDEP, is plotted against various axes in Figs. 88 to 91, and based on equation (22), CDIND, in Figs. 92 to 94, for β = 200-500. In this range of β the results for the still water oscillatory drag coefficient versus x_o/D are virtually identical for all β, (see Fig. 70) and the values of CDDEP and CDIND in currents are also the same for all β in this range.

Values of CDIND' are not plotted. They were found to be virtually the same as for CDIND, however exhibiting rather more scatter.

10.2.1. CDDEP, for β = 200-500

From Fig. 88, CDDEP versus x_o/D, it is seen that as V/nD is reduced CDDEP seems to approach the still water values, particularly for low and high x_o/D. For x_o/D between about 1 and 2.5, i.e. in the region where in still water there is a particularly large value of CDDEP (= CDIND) due to a very strong vortex developing immediately behind the cylinder, the value of CDDEP at low V/nD is lower. It is probable that the strong vortex which occurs in still water is easily disturbed, even by a small current, and CDDEP does not attain such a high value.

When CDDEP is replotted against V/nD, in Fig. 89, it is seen that, for any particular value of x_o/D, the value of CDDEP is more or less constant below a certain value of V/nD and that this value increases with x_o/D, i.e. for x_o/D = .4 the limit is reached at V/nD $\approx$ .8 whereas for x_o/D = 4 it is at about 5. This suggests that it might be a value of $V/\dot{x}_o$ below which CDDEP becomes reasonably constant and reasonably near its still water value. Indeed when plotted against $V/\dot{x}_o$, in Fig. 90, it appears that the curves for all $x_o/D \gtrsim .3$ become reasonably constant for $V/\dot{x}_o \lesssim .2 \sim .3$. For smaller values of x_o/D there are insufficient results at low values of $V/\dot{x}_o$ to see what happens to the curves at these low values.

Thus one might suggest that for values of $V/\dot{x}_o \lesssim .25$ the flow, as far as the oscillatory component is concerned, will be virtually the same as in still water and the oscillatory drag coefficient CDDEP will be similar, though rather lower in the area $1.0 \lesssim x_o/D \lesssim 2.5$, possibly because in still water the very high value of oscillatory drag coefficient in this region is due to an unusually large vortex developing just behind the cylinder. It is suggested that this vortex may be particularly vulnerable to disturbance by even a very small current. (It will be seen from the flow visualization experiments that the position of the vortex is indeed different with a small current, though the general flow development in a cycle, i.e. in

terms of number of vortices shed, etc. is similar to the still water case.)

Fig. 91, CDDEP versus $V/\dot{x}_o$ for various V/nD, is presented for the sake of completeness.

From Fig. 89 it is seen that for high values of V/nD, CDDEP approaches the value 1.0 for all x_o/D. The value CDDEP = 1.0 is significant. In experiments conducted where the pendulum was rigidly held so that the cylinder was stationary, the drag coefficient measured was $1.0 \pm .05$ over the whole range of the velocities covered by the experiments. Thus, for increasing V/nD, the drag coefficient approaches its quasi-steady value, as expected from the discussions of Part I, chapters 4 and 6.3.

By comparing Figs. 89 and 90 it is evident that it is a value of V/nD, rather than of $V/\dot{x}_o$, above which CDDEP can be considered to be equal to 1.0, and one might consider $V/nD \approx 30$ to be a suitable value.

10.2.2. Negative values of CDDEP

CDDEP exhibits negative values for small amplitudes of motion at values of V/nD around 2.0 and 3.0. These negative values are associated with the phenomenon of hydroelastic vibrations, where the cylinder oscillation interacts with the vortex shedding process leading to a reinforcement of the oscillation, as described in Part I, chapter 5.1. The results will be discussed further in subsequent chapters.

10.2.3. CDDEP for other values of β

Curves for other values of β are not presented. There were far fewer data points for other ranges of β and the curves are very similar in form to those presented in chapter 10.2.1. The differences occur at low values of $V/\dot{x}_o$ and are as follows.

In chapter 10.2.1 it was seen that for high values of V/nD,

CDDEP approached 1.0, the quasi-steady value. For values of $V/\dot{x}_o \lesssim .25$, CDDEP becomes fairly constant and reasonably near to the still water value, for all x_o/D. For higher values of β it was found that for $V/\dot{x}_o \lesssim .25$ CDDEP still approached the still water values, (for any particular x_o/D, CDDEP is lower for higher β, see Fig. 70), and at high values of V/nD, CDDEP still approached 1.0, the quasi-steady value.

10.2.4. CDIND

The time averaged oscillatory drag coefficient based on equation (22), CDIND, is plotted in Figs. 92 to 94 against various parameters.

As $V/\dot{x}_o \to 0$ the oscillatory parts of equations (21) and (22) become identical, and CDIND becomes equal to CDDEP. (At $V/\dot{x}_o = .1$ CDIND is 2% greater than CDDEP, and at $V/\dot{x}_o = .3$ it is 13% greater.) From Fig. 94 it is seen that at low values of $V/\dot{x}_o$ the results for CDIND are similar to those for CDDEP, reflecting this. At larger $V/\dot{x}_o$, CDIND becomes asymptotically very large, either positive or negative, indicating that equation (22), where the steady and oscillatory drag force are written independently of each other, does not provide a satisfactory framework for an empirical description of the physical processes involved. Conversely the well behaved changes in CDDEP against $V/\dot{x}_o$ (and other parameters) indicates that it does represent the physical phenomena better, indicating that the steady stream velocity V does affect the oscillatory component of force.

Graphs of CDIND are presented, however, as it is easier to form a mental picture of the expression CDIND $\dot{x}|\dot{x}|$, and hence to evaluate the effects of current, say, on the oscillatory drag force, than of the oscillatory component of CDDEP $(V-\dot{x})|(V-\dot{x})|$. In the first case the oscillatory drag force is dependent only upon values of CDIND and $\dot{x}$, whereas in the second case the force is dependent upon values of CDDEP, $\dot{x}$ and V.

10.2.5. The effect of steady currents on the oscillatory drag forces

These effects can best be seen by examining curves of CDIND.

The effect of increasing current, characterized as increasing V/nD, on the oscillatory drag force for a particular oscillation amplitude, x_o/D, and frequency, n, can be seen directly from Fig. 93, CDIND versus V/nD.

The effects of current are most pronounced for smaller values of x_o/D. For $x_o/D \lesssim .1$ there are two negative minima at V/nD ≈ 2.2 and 2.9, associated with the hydroelastic interaction effects discussed in Part I, chapter 5.1 and to be further discussed in a later chapter.

For x_o/D = .2 ~ 1.4 the oscillatory drag force increases with V/nD, first gently and then more steeply, particularly for low x_o/D. For higher x_o/D the drag force decreases at first and then increases.

It is seen that for V/nD ≈ 3.3 the oscillatory drag coefficient is equal to about 1.7 and virtually independent of x_o/D for $x_o/D \gtrsim .2$. For V/nD $\gtrsim$ 3.3 the coefficient decreases with increasing x_o/D (the oscillatory drag <u>force</u>, however, which is proportional to CDIND·x_o, still increases with x_o/D, although only gradually).

10.3. Results for the inertia coefficient, CM

Once again it is noted that CM is plotted and not CA, and the actual inertia force on the cylinder in the physical experiments may be calculated by subtracting 1.0 from CM.

10.3.1. CM for β = 200-1200

The inertia coefficient, CM, is plotted against x_o/D for various values of V/nD in Fig. 95, for β in the range 200-1200. Results with the high and low pendulum frequencies were the same where they overlapped. The curves are quite complex, however a number of observa-

tions may be made.

As V/nD is reduced the curves approach the still water curve, particularly for lower values of x_o/D. However, even for the lowest value of V/nD = .8, the curve at larger amplitudes, although nearer to the still water curve than higher V/nD curves are, is still considerably higher than the still water curve.

At very small x_o/D the value of CM in still water is about 2.1. For low V/nD this also applies, and as V/nD is increased CM decreases to a minimum of CM ≈ 1.3 at V/nD = 5. As V/nD is further increased the small x_o/D value of CM increases again, to CM ≈ 1.9 at V/nD = 19. For larger values of V/nD it was not possible to determine CM at low values of x_o/D. (See, for example Fig. 87 for V/nD = 24.)

For $x_o/D \approx 1.5$ there is very little variation in CM with x_o/D.

For V/nD $\lesssim$ 4 there is a maximum in CM at $x_o/D \approx .8$ and a minimum at $x_o/D \approx 2.2$. It will be seen that the steady drag coefficient, STCDDEP, exhibits similar, but opposite trends at these values of x_o/D.

For V/nD = 2 ~ 5 there is a further maximum, at x_o/D varying from about .12 to .3. It will be seen that STCDDEP also exhibits peaks near these values.

10.3.2. CM for other values of β

There were only few points for higher values of β, and these covered only fairly low values of x_o/D. However the results did not appear to be any different from those for β = 200-1200. In still water CM was found to vary much less than CDDEP with β, and this is evidently also true in currents.

10.3.3. The effect of steady currents on the inertia forces

For $x_o/D \lesssim 1.5$ the inertia force first decreases from its still water value as V/nD is increased, to a minimum at V/nD ≈ 5, and then increases again. For $x_o/D \gtrsim 1.5$ there is an increase in the inertia force as V/nD increases.

10.4. Results for steady component of drag coefficients for all β

The time averaged steady component of drag coefficient based on equation (21), STCDDEP, is plotted against various parameters in Figs. 96 to 99, and based on equation (22), STCDIND, in Figs. 100 to 103. All values of β are covered by these results as there was found to be no dependence on β within the range covered by these experiments.

10.4.1. STCDDEP

From Fig. 96, STCDDEP versus x_o/D, a number of interesting observations may be made. For $V/nD \lesssim 4$ STCDDEP exhibits a maximum at $x_o/D \approx 2.3$, and a minimum at $x_o/D \approx 1.0$, which for $V/nD \lesssim 1.5$ is negative. For still lower x_o/D an additional maximum occurs for $V/nD \gtrsim 3$ at increasing values of x_o/D for increasing V/nD. For example for $V/nD = 3.6$ the maximum is at $x_o/D \approx .3$, and for $V/nD = 5.9$ it is at $x_o/D \approx .75$. From Fig. 98, STCDDEP versus $V/\dot{x}_o$, it is seen that this maximum occurs at values of $V/\dot{x}_o \approx 1.5$. There is, however, some variation in the value of $V/\dot{x}_o$ of the peak. For $V/nD = 5.4$ the peak occurs at $V/\dot{x}_o \approx 1.2$ and for $V/nD = 2.9$ it occurs at $V/\dot{x}_o \approx 2.1$. Suffice it to say that this peak (if it occurs) is nearly always in the range $V/\dot{x}_o = 1 \sim 2$.

From Fig. 97, STCDDEP versus V/nD, it is seen that for high values of V/nD the curves for all x_o/D approach STCDDEP = 1.0, the quasi-steady value. As in the case of CDDEP a value of $V/nD \approx 30$ may be taken as the value above which the coefficient may be considered to take the quasi-steady value. Similarly from Figs. 98 and 99, for STCDDEP versus $V/\dot{x}_o$, it is evident that $V/\dot{x}_o$ is not the parameter controlling when the flow becomes quasisteady. (For example for $x_o/D = 6.0$ STCDDEP becomes 1.0 at $V/\dot{x}_o \approx 1.0$, whereas for $x_o/D = .05$ this does not occur until $V/\dot{x}_o \approx 15$.)

As x_o/D approaches zero STCDDEP must approach 1.0, the steady flow stationary cylinder value measured (and here STCDDEP ≡ STCDIND). It is evident from Fig. 96 that STCDDEP does approach 1.0, however

it is surprising how much the value is altered by even very small amplitude oscillations, particularly for small values of V/nD. For example, for V/nD = .8 vibrations of only 5% of a diameter will cause CDDEP to be reduced to ≈ .1. Despite the fact that there was some scatter in the results for STCDDEP at values of V/nD $\lesssim$ 1.5 this scatter was no more than $\pm$ .3 from the curves shown and, as there were some 15 tests at values of V/nD $\lesssim$ 1.5, obtained with various flow rates, cylinder diameters and pendulum frequencies, it is considered extremely unlikely that there could have been any error on all these tests causing the value of STCDDEP to be consistently low.

10.4.2. STCDIND

From Figs. 102 and 103 it is seen that values of STCDIND are only well behaved for large values of $V/\dot{x}_o$, where the values are virtually the same as those for STCDDEP. (As the steady component of equation (22) becomes identical to that of equation (21) as $V/\dot{x}_o \to \infty$.) Once again it appears that equation (22), where the steady and oscillatory drag forces are written independently, does not provide a reasonable description of the physical processes involved.

10.4.3. The effect of oscillations on the steady drag force

The effect of oscillations on the steady drag force can most easily be seen from curves of STCDIND, as this coefficient, for a given force, is dependent only on V and not on $\dot{x}$. Thus the variation in STCDIND with x_o/D for a constant value of V/nD shows the variation in steady drag force with amplitude of motion.

From Fig. 100, STCDIND versus x_o/D, and Fig. 101, STCDIND versus V/nD, a number of comments may be made.

It is for the lowest values of V/nD that the steady force is most affected by the oscillations. For V/nD $\lesssim$ 3 the steady drag force decreases from its stationary cylinder value as x_o/D is increased from zero, and has a minimum at $x_o/D \approx 1$, which, for V/nD $\lesssim$ 1.6, may

be negative. The steady drag force then increases to a maximum at $x_o/D \approx 2.3$.

For higher values of V/nD the steady force increases gradually as x_o/D is increased, though for certain values of V/nD $\lesssim$ 6 there is a small maximum at a fairly low value of x_o/D. For example from Fig. 101, for V/nD $\approx$ 4, there is a small peak at $x_o/D \approx .3$, and for V/nD $\approx$ 5.5 there is a peak at $x_o/D \approx 1.0$. However these peaks are little more than inflections on rising curves.

Even for very large values of V/nD there is some increase in the steady force, for example for V/nD = 24 the steady force is twice its stationary cylinder value for oscillation amplitudes $x_o/D \approx 5$.

At $x_o/D \approx 1.5$ there is little variation in STCDIND with V/nD.

Very large variations in the steady force may occur particularly for low values of V/nD. For example for V/nD = 1.7, the steady force varies from about 0.5 times the stationary cylinder value at $x_o/D \approx 1$ to over 12 times at $x_o/D \approx 2.3$. For V/nD = .8 there is no apparent maximum within the range of the results.

It is, however, difficult to judge if these force variations will be significant in terms of overall forces on the cylinder, as at low V/nD, particularly for larger x_o/D, the oscillatory forces dominate. Therefore total force coefficients have been calculated and are presented in the next section.

10.5. Maximum force coefficients

10.5.1. Total oscillatory force coefficient

In chapter 10.2.5 and 10.3.3 it has been seen that there is a considerable effect of current on the oscillating drag force and a lesser effect on the inertia force. It is difficult to determine the importance of the large variations in oscillatory drag, as it is not easy to see how large this force is in relation to the inertia force.

In order to judge the changes in total oscillatory forces due

to currents, a total oscillatory force coefficient was defined as the maximum oscillatory force, non-dimensionalized by $.5\rho D \dot{x}_o^2$. Unfortunately it was only decided to calculate this coefficient after the other coefficients had been analysed, and lack of time and finance forbade a reanalysis of the time series to extract maximum experimental forces. Therefore the maximum forces were calculated from the values of oscillatory drag and inertia coefficients already obtained. These coefficients are average values over the cycle, and the maximum force calculated from them is not necessarily the same as the experimental maximum force. This will, in general, only necessarily be the case if the coefficients are invarient over a cycle. Nevertheless, the coefficient is expected to give an impression of the way the maximum oscillatory forces change with velocity.

The derivation of the maximum oscillatory force coefficient from the oscillating drag and inertia coefficients is detailed fully in Appendix 3, and the coefficient is expressed as

$$\text{CMAXOSC} = \frac{\text{Calculated maximum oscillatory force}}{.5\rho D \dot{x}_o^2} \qquad -(44)$$

It should here be noted that the maximum oscillatory force coefficient calculated here is the maximum combined effect of the oscillatory drag and an inertia force expressed via CM and not CA. I.e. a Froude-Krylov force has been included and coefficient values apply to a situation of combined steady and oscillatory flow on a stationary cylinder. CM has been chosen rather than CA for consistency with the rest of the results presented.

The coefficient is plotted against x_o/D for various V/nD in Fig. 104. At low x_o/D the coefficient increases rapidly with decreasing x_o/D. This is due to the fact that the inertia force is dominant at low x_o/D and non-dimensionalization is in terms of velocity squared rather than acceleration. (If the oscillatory drag force was zero and CM constant, then CMAXOSC would be $\propto D/x_o$.)

For $V/nD \lesssim 4.0$ there is virtually no effect of V/nD (velocity) on the oscillatory force, and for further increases in V/nD there is a monotonous increase in the maximum oscillatory force. For example for $V/nD = 37$ and $x_o/D = 1.5$ the maximum oscillatory force is about 5 times its still water value.

10.5.2. Total overall force coefficients

In previous sections the effects of current on the oscillatory forces and coefficients, and the effects of oscillations on the steady forces have been discussed, however it remains to see the effects of current and oscillatory amplitude on the total forces.

Total forces, calculated from the time averaged coefficients, were examined in two ways. Firstly, a total force coefficient was defined with respect to the maximum relative velocity and secondly, the calculated maximum force was compared to that predicted using the relative velocity based equation (23) with values of CA = 2.0, CDDEP = 1.0 and STCDDEP = 1.0.

MAXC

The first coefficient is thus defined as

$$MAXC = \frac{\text{Calculated max. force (steady + oscillatory)}}{.5\rho D(V+\dot{x}_o)^2} \qquad -(45)$$

Fig. 105 shows the maximum total force coefficients MAXC plotted against x_o/D for various V/nD.

As x_o/D is reduced from $x_o/D \approx 1.5$ the coefficient MAXC increases rapidly, particularly for low values of V/nD, then, at some smallish value of x_o/D, a maximum is reached and the curve falls rapidly again. This shape is due to the combined effect of the inertia contribution increasing the total oscillatory drag coefficient, CMAXOSC, very rapidly with reducing x_o/D (as in Fig. 104) at the same time that the oscillatory contribution is reducing compared to the steady drag contribution. Eventually, at $x_o/D = 0$, the oscillatory contribution is zero and MAXC takes the value 1.0, the steady drag coefficient. The small and negative values of STCDDEP for low V/nD and $x_o/D \approx 1.0$ do not reduce MAXC as the steady force is evidently small compared to the total oscillatory force at these low values of V/nD.

There is a small maximum for $V/nD \lesssim 5$ at $x_o/D \approx 2.0$ and this

is due to the maximum in the steady drag coefficient in this region. This maximum is only just noticeable for the lowest values of V/nD, despite the fact that there is a very pronounced peak in STCDDEP and STCDIND for small values of V/nD, as the steady force is small compared to the oscillatory. For larger V/nD, say $\gtrsim$ 3, the steady component is larger, however the steady component does not then vary so much with x_o/D. For high values of V/nD, where the steady component is dominant, particularly for larger x_o/D, the steady force varies much less with x_o/D.

Fig. 105 is not particularly useful, from the scientific point of view, as it is a complicated combination of various forces dependent on different factors. It does, however, provide a simple method of estimating maximum forces in combined waves and currents on a stationary cylinder. (Note, not for the test condition of a cylinder oscillating in a current because of the use of CA = 2.0 in equation (23) rather than CA = 1.0.)

FORCE RATIO

The force ratio is defined as

$$\text{CRATIO} = \frac{\text{Calculated max. force from experimentally defined coef.}}{\text{Calculated max. force with CA=2.0, CDDEP=1.0, STCDDEP=1.0}} \quad -(46)$$

This ratio is shown plotted in Fig. 106 against x_o/D, for various V/nD.

For values of V/nD $\lesssim$ 3.0 the ratio decreases from 1.0 at x_o/D = 0 to a minimum of about 0.8 at $x_o/D \approx 1.3$, and then increases again, first rapidly and then less rapidly, reaching a value of about 1.35. When there is a current the ratio is always within the above limits, however for $x_o/D < 1.6 \sim 2$ the ratio is higher than in still water, and for higher x_o/D the ratio is lower than in still water.

For V/nD between 3 and 6 the peaks which occurred in STCDDEP at various, small x_o/D, corresponding to $V/\dot{x}_o = 1 \sim 2$, are reproduced in CRATIO, as are the minima around $x_o/D \approx 1$.

Although for low V/nD STCDDEP can be negative around $x_o/D \approx 1$, CRATIO is only reduced to about .8, indicating that the steady force

is considerably smaller than the oscillatory forces. As V/nD increases steady forces become more important, but there is also less variation in STCDDEP (and also less variation in CDDEP, and, to a lesser extent, CM).

For $x_o/D \approx 2.3$ there is only a noticeable maximum in STCDDEP for $V/nD \lesssim 4$, and here the oscillatory force is evidently much larger and no effect is evident on CRATIO. For larger V/nD, where the steady component becomes more dominant, there is no peak in STCDDEP for $x_o/D \approx 2.3$. In fact for large values of V/nD there is little variation in CRATIO at all, reflecting the evenness of STCDDEP at high V/nD.

10.6. Repeatability of the results

An idea of the repeatability of the results may be obtained from Fig. 89, CDDEP versus V/nD and Fig. 97, STCDDEP versus V/nD. Here all the experimental points for $x_o/D = .6$ and .3, respectively, have been plotted. It is evident that there is very little scatter from the mean curves drawn, even though the points are from various diameter cylinders in various current flows, and using both the low and high frequency pendulums.

11. FLOW VISUALIZATION TESTS

Before a complete discussion of the quantitative results for the force coefficients is undertaken it is necessary to present the results of the flow visualization tests conducted. The values of the coefficients are totally dependent upon the flow past the cylinder, and the visualization of the flow has led to a very much more complete understanding of the reasons for the variations in the values of the various coefficients.

The flow visualization program was fairly brief, being a qualitative rather than a quantitative study of the flow patterns. Nevertheless a large amount of information and understanding of the flow was obtained, and it is evident that a flow visualization study is one of the most powerful tools available for studying complex flows.

11.1. Experimental method

The experiments were conducted with a 3.50 cm diameter plastic cylinder which had two passageways drilled in it, each leading to two, 1 mm diameter holes. The holes were placed each side of the front and rear stagnation points, as shown in Fig. 107.

A solution of potasium permanganate dye was introduced into the boundary layer through the holes. The rate at which the dye was introduced could be controlled and was adjusted, as necessary, to suit the test flow conditions.

Some tests were conducted with a dye source upstream of a smooth cylinder and flow patterns with this configuration compared with those obtained with the configuration described above, in order to check that the introduction of dye into the boundary layer did not disturb it and alter the flow patterns. No differences between the patterns using these two methods were found, and this applies particularly to Figs. 119 and 124 where it had earlier been suspected that the holes in the cylinder were causing 'tripping' of the boundary layer.

11.1.1. Filming rate

A Nikon F2A camera was used for the photography, and was mounted on the pendulum so that it moved with the cylinder. The cylinder position was offset with respect to the vertical axis of the pendulum in these tests in order that the bars carrying the heavy weights were not between the camera and the cylinder axis. The camera was driven by an oscillator at a fixed number of photos per second. The photographic series always started with the pendulum vertical, and thus photographs were always taken at the same instants in each test. The filming rate was intended to be 7 3/4 frames per oscillation cycle, so that after 4 cycles photographs would have been taken at 32 evenly spaced values of phase of oscillation. For the majority of the tests the flow pattern exactly repeated itself either every cycle or every other cycle, and thus the photographs yield respectively 16 and 32 photographs evenly spaced over a representative cycle of oscillation.

11.1.2. Values of t/T for the photograph sequences

The photographs for each test are presented sequentially for just over 4 cycles of oscillation. One cycle is presented on each line of photographs. The leftmost photograph of the first line was taken immediately after the cylinder had reversed direction and was moving from left to right. The photographs on subsequent lines are for subsequent cycles. The values of t/T for each photograph are shown below, where t is the time elapsed in the cycle, and T the period. (The actual filming rate was slightly higher than that intended: 7.77 frames per oscillation, which was the nearest that it was possible to obtain.)

.04, .169, .297, .426, .555, .683, .812, .941
.070, .198, .327, .456, .584, .713, .842, .970
.099, .228, .357, .485, .614, .743, .871, 1.000
.129, .257, .386, .515, .644, .772, .901, 1.030
.158, .287, .416, .544, .673, .801, .930, 1.059

It is immediately obvious from the photographs whether the flow pattern repeats itself every cycle or every other cycle, and the development of the pattern may be studied from the photographs accordingly.

11.1.3. Summary of flow visualization test conditions

For ease of comparison and discussion, all the photograph sequences have been grouped together in Figs. 105 to 147. The conditions are arranged in increasing x_o/D at each, increasing value of V/nD. The table below summarizes the test conditions presented.

FIG.	V/nD	x_o/D	$V/\dot{x}_o$	FIG.	V/nD	x_o/D	$V/\dot{x}_o$
108	0	.19	0	126	3.0	.07	6.82
109	0	.41	0	127	3.0	.19	2.46
110	0	.66	0	128	3.0	.27	1.77
111	0	.74	0	129	3.0	.29	1.65
112	0	1.13	0	130	3.0	1.18	.41
113	0	1.79	0	131	3.0	1.71	.28
114	0	1.96	0	132	3.0	2.29	.21
115	0	2.11	0	133	3.0	3.34	.14
116	0	2.64	0	134	3.8	.09	7.03
117	0	3.70	0	135	3.8	.31	1.95
118	1.0	.12	1.29	136	3.8	.41	1.68
119	1.0	.33	.48	137	3.8	1.24	.49
120	1.0	.90	.18	138	5.0	.06	12.6
121	1.0	1.50	.11	139	5.0	.24	3.32
122	1.0	2.17	.07	140	5.0	.64	1.24
123	2.0	.12	2.65	141	5.0	1.69	.47
124	2.0	.34	.94	142	5.0	3.57	.22
125	2.0	.97	.33	143	12.0	.30	6.37
				144	12.0	1.57	1.22
				145	12.0	3.63	.53
				146	20.0	.41	6.95
				147	20.0	3.51	.54

In those cases where a current is present the flow direction is from the left hand side of the photographs.

11.2. Discussion of flow visualization photographs in still water

The photograph series to be discussed are presented in Figs. 108 to 117, for increasing x_o/D. From these photograph series, sketches have been made of the patterns at various representative values of x_o/D, and these are presented in Fig. 148.

At very small amplitudes of oscillation there is no separation, as seen in the photographs of Fig. 108, for $x_o/D = .19$.

As the amplitude of motion is increased separation occurs, initially at the rear stagnation point, and the separation point then moves forward, and a symmetric pair of vortices is formed. This is seen in the photographs of Fig. 109, for $x_o/D = .41$. The vortices are not shed, and after the flow has reversed direction they are swept back over the cylinder and interact with the new vortices being formed. The pattern over one cycle is also sketched in Fig. 148,a.

In the photographs of Fig. 110, for $x_o/D = .66$, the vortices are seen to develop slightly more in each half cycle and very slight asymmetry is evident. This is sketched in Fig. 148,b.

By a value of $x_o/D = .74$, as photographed in Fig. 111, a definite asymmetry is present, one vortex developing more than the other in each half cycle. This larger vortex is on the same side of the cylinder (the upper side in Fig. 111) in both half cycles. Vortex pairing, as described by Zdravkovich and Namork (1978), also appears to be occurring and a typical cycle of motion is sketched in Fig. 148,c.

As x_o/D is further increased the larger vortex grows even further and is apparently shed, as photographed in Fig. 112 for $x_o/D = 1.13$. This larger shed vortex is developed from the same side of the cylinder in both half cycles (the lower in Fig. 112). (It is here briefly mentioned that the side appeared to be arbitrary. In repeated testing, shedding from the other side was also obtained. However, once shedding was established from one side it remained

from that side.)

Development of the vortex takes a large proportion of the half cycle, i.e. the vortex rolls up fairly slowly. A typical cycle is sketched in Fig. 148,d.

Vortex pairing, as described by Zdravkovich and Namork (1978), is not apparent.

It is recalled that at this value of K(= 7.1) a very even, nearly sinusoidal, lift force trace at twice the wave frequency was observed on a cylinder in waves (Part II, chapter 4).

As x_o/D is further increased the second vortex begins to develop more. The sketches in Fig. 148,e are from photographs for x_o/D = 1.47, however the photographs are of poor quality and are not reproduced here. The first vortex forms and sheds rapidly, near the maximum velocity point of the cycle, and the second vortex develops more gradually and towards the end of each half cycle. This value of K(= 9.2) was in Part II, chapter 4, associated with a saw-toothed lift trace at twice the wave frequency, the steep part of the trace, near the maximum velocity points, presumably being due to the rapid shedding of the first vortex. The second vortex formed develops very close to, and just behind the cylinder, and at flow reversal it often appears to be swept round the cylinder. Isaacson and Maull (1976) sketched this vortex as being swept back onto the cylinder, (see Fig. 11). It is in fact difficult to see what happens to the second vortex, however it appears that sometimes it is swept onto the cylinder, and sometimes around the cylinder. These comments also apply to larger values of x_o/D. Sawaragi et al. (1976) noted that the second vortex was swept around the cylinder for K = 8 ~ 13.

As x_o/D is further increased the second vortex develops more and more, as in the photographs of Figs. 113 and 114 for x_o/D = 1.79 and 1.96, respectively. It also appears that for these values of x_o/D the second vortex is very large and developed in one half cycle, whereas in the other half cycle the first vortex is particularly prominent and the second hardly visible (the reproductions of the figures are of poorer quality than the originals, and the second vortex in the right hand half cycle of Figs. 113 and 114 is not visible at all). The sketches in Fig. 148,f have been produced from the photographs of Fig. 113 at x_o/D = 1.79.

By a value of x_o/D = 2.11, Fig. 115 and sketched in Fig. 148,g,

the second vortex develops to a large size and a third vortex appears to start to be formed. However the second vortex does not seem to be shed, and at flow reversal appears sometimes to be swept onto the cylinder, sometimes around the cylinder and is sometimes swept back over the side of the cylinder from which it was formed. The first vortex is formed from the same side of the cylinder in both half cycles, as is the second vortex, and no change-over was observed over quite long experiments at the same nominal value of x_o/D. Which side of the cylinder the second vortex was swept over at flow reversal did not appear to alter the side from which the first vortex in the next half cycle was developed from. (This can be seen by comparing the last 4 photographs of the top and bottom row of Fig. 115.)

The photographs for $x_o/D = 2.36$ were very similar to the above and are not reproduced here. A typical cycle is sketched in Fig. 148,h.

By a value of $x_o/D = 2.64$, photographed in Fig. 116, the second vortex is shed, at least in one half cycle, and a third vortex is formed. A typical cycle is sketched in Fig. 148,i.

The wake in each half cycle begins to resemble more a von Kármán type alternating wake and the only major effect as x_o/D is further increased is to introduce further vortices in each half cycle. By a value of $x_o/D = 3.7$, photographed in Fig. 117, the third vortex is shed in each half cycle and a fourth is beginning to form at flow reversal.

It is evident that, as x_o/D is increased, there is a gradual development of the vortices and a gradual introduction of further vortices in each half cycle. This is the reason for the gradual change of power from the second to the third component as K is increased from 10 to 20 (see Part II, chapter 4). Nevertheless the flow may be characterized as being made up of a certain number of 'shed' vortices per half cycle over quite a large range of amplitudes, for example 2 vortices for $K = 6 \sim 16$, as according to Isaacson and Maull (1976). Furthermore the difficulties in determining whether a vortex is 'shed' and the difficulty in seeing (at least with the flow visualization method used here) whether the last vortex formed is swept onto, around or back over the cylinder are the probable reasons for the differences in vortex patterns presented by various authors, as discussed in Part I, chapter 3.5.

11.3. Discussion of flow visualization photographs in currents

11.3.1. Basic considerations which help to explain the phenomena observed

There are three fundamental ideas which help to explain the phenomena observed in the flow visualization tests.

i) Downstream of the cylinder the wake tries to form a stable von Kármán type alternating vortex wake. This will occur even if vortices are shed in other configurations, for example in symmetric pairs, in which case at some point downstream the vortices interact and reform and an alternating wake results.

ii) For values of $V/\dot{x}_o \lesssim 1$ flow reversal will occur twice in each oscillation cycle. Each cycle may thus be divided into two 'part cycles' in one of which the cylinder is travelling with the flow and faster than the flow and in the other the cylinder is travelling slower than the flow or against the flow. These two part cycles are hereafter referred to as the 'minor' and 'major' part cycles, respectively, and they are shown in the sketch below.

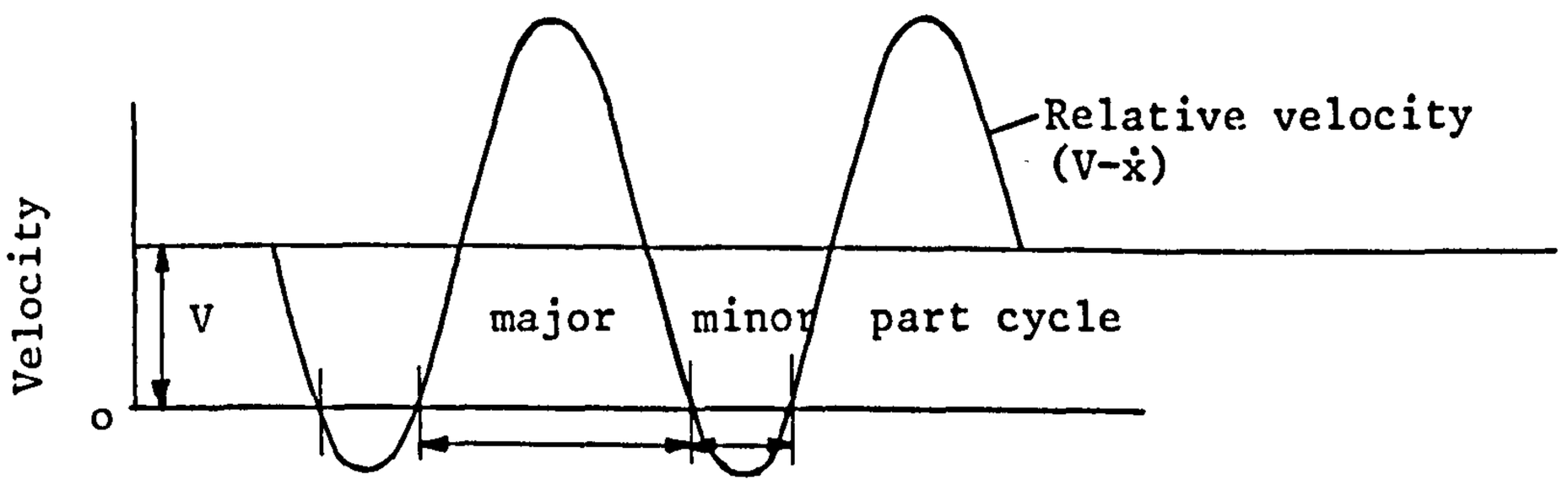

Expressions for the distance the cylinder travels relative to the current in the two part cycles will be derived in a later section. It is, however, mentioned here that the lower $V/\dot{x}_o$ is, the more nearly equal the two part cycles are; the higher the value of V/nD for a given value of $V/\dot{x}_o$, the greater the difference between the

relative distance travelled in the major and minor part cycles, and, for a given V/nD, as x_o/D is decreased ($V/\dot{x}_o$ increased), the relative distance travelled in both part cycles decreases.

iii) After flow reversal has occurred, the flow in a new part cycle begins from rest and a symmetric pair of 'starting' vortices begins to form. If a sufficient relative distance (between the cylinder and current) is travelled before the next flow reversal occurs then these vortices may develop asymmetrically and be shed. i.e. one can consider each part cycle in a similar manner to the starting flows discussed in Part I, chapter 2.

Some discussion is necessary concerning this concept of 'flow reversal'. By flow reversal is not meant the local flow reversal associated with separation which occurs in a steady current, but rather a general flow reversal associated with a more general change in direction of the flow near the cylinder. This flow reversal does not necessarily occur at the same instant as the reversal in the instantaneous relative velocity $(V-\dot{x})$, due to the different extents to which the steady and oscillating flow components are affected by the boundary layer (cf. Part I, chapter 4). In fact it is apparent that the velocity of flow near the cylinder varies with position on the cylinder, and may in certain circumstances be in opposite directions on different parts of the cylinder at the same instant of time. Nevertheless this flow reversal which leads to the initiation of these starting vortices is associated with, but does not necessarily occur at the same instant as, the reversal in the instantaneous relative flow $(V-\dot{x})$. For example, for V/nD = 2.0 symmetric starting vortices associated with flow reversal were observed even when $V/\dot{x}_o = 3.0$ but, for V/nD = 3.0, the highest value at which they were observed was $V/\dot{x}_o = 1.7$.

Evidently paragraph ii) above is subject to this same qualification such that the relative velocity in the above figure should in some way take account of the dif-

ferent extents to which the steady and oscillating components are affected by the boundary layer.

The above three general points explain the majority of the observed flow patterns.

It is also pointed out that

$$V/\dot{x}_o = \left(\frac{V}{nD}\right)\left(\frac{D}{x}\right)\frac{1}{2\pi}$$

i.e. an increase in x_o/D for a fixed value of V/nD represents a decrease in $V/\dot{x}_o$. In the experiments, photograph sequences have been obtained for various values of x_o/D for fixed values of V/nD. Certain of the phenomena to be described are dependent upon the ratio $V/\dot{x}_o$, and others are dependent upon x_o/D, however for phenomena which are basically dependent upon $V/\dot{x}_o$ it is often easier to describe the effects of changing x_o/D for a fixed V/nD, though it must be kept in mind that the fundamental parameter is actually $V/\dot{x}_o$.

11.3.2. General description of the flow patterns and reasons for their occurrence

Several general observations may be made with respect to the flow visualization results, these general observations will be discussed in more detail in subsequent sections.

The flow patterns observed may be divided into three distinct ranges of V/nD and the fundamental differences between the ranges concerns the flow patterns when $V/\dot{x}_o$ is in the region of 1, and are caused by the different extents of relative motion between the flow and the cylinder in the major part cycle in these different ranges of V/nD. The characteristics of the ranges of V/nD are described below.

$V/nD \gtrsim 6.5$

For a given value of V/nD the flow at large x_o/D (i.e. low $V/\dot{x}_o$)

resembles that in still water at an equivalent value of relative distance travelled (this will be discussed in chapter 11.3.4). There are several vortices shed alternately in each part cycle, the actual number shed being dependent on V/nD and x_o/D. As x_o/D is decreased, fewer vortices are shed in each part cycle. When x_o/D is decreased sufficiently that $V/\dot{x}_o$ approaches 1, flow reversal only just occurs and there is virtually no relative movement in the minor part cycle and no vortices are shed in this part cycle. The pattern in the major part cycle still resembles that in still water at an equivalent relative distance travelled, and this relative distance is sufficiently high that 3 or more vortices are shed alternately (more for higher V/nD), see for example Fig. 144. The flow may also be thought of as resembling that in a steady current which is stopping and starting, i.e. alternate shedding occurs in the major part cycle, being most rapid when the relative velocity is highest, and then slowing down and stopping as the flow slows down, reverses and goes through the minor part cycle, the alternate shedding then starting again in the next major part cycle. This resemblance to a steady flow pattern is more evident for higher values of V/nD, where there are more vortices shed in the major part cycle.

As x_o/D is further decreased, i.e. as $V/\dot{x}_o$ becomes larger, the vortex shedding is rapid in the major part cycle, near the maximum velocity point, and less rapid in the minor part cycle, i.e. it appears to conform with the postulation of a quasi-steady flow with a constant Strouhal number so that the vortex shedding frequency is proportional to the instantaneous relative velocity. Nevertheless, as will be seen, the vortex shedding frequency and the flow patterns are affected by the oscillations.

V/nD = 2.8 ~ 6.5

In this range of V/nD the flow is considerably different to that described above for $V/\dot{x}_o$ in the range of about .5 to 4, particularly when $V/\dot{x}_o$ is between about 1 and 2.

For large amplitude oscillations, i.e. for low values of $V/\dot{x}_o$, the flow pattern in each part cycle resembles that in an equivalent still water half cycle, as was the case for V/nD $\gtrsim$ 6.5.

For any particular value of V/nD in this range, as x_o/D is reduced, and therefore $V/\dot{x}_o$ increased, fewer vortices are developed in each part cycle. There becomes a point where in the major part cycle a pair of vortices develops, first symmetrically and then slightly asymmetrically, and at flow reversal these are swept back over the cylinder. Each vortex moving over the cylinder causes a further vortex to be developed, and the two vortices interact and cancel each other or move away as a pair, (this interaction will be discussed more fully in a later section). An example of this may be seen in Fig. 137, for V/nD = 3.8, x_o/D = 1.24 and $V/\dot{x}_o$ = .49, and this is also sketched as the first sketch below.

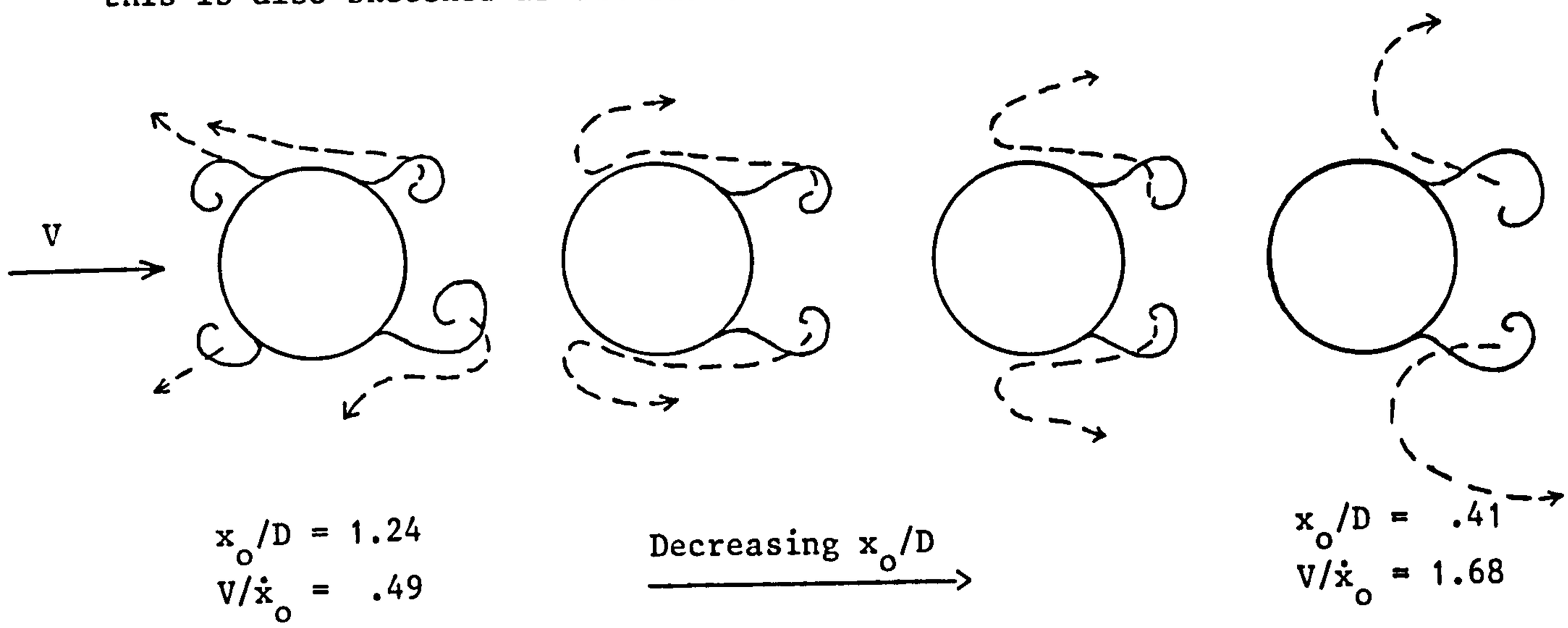

--------> showing movement of vortices in one cycle

As x_o/D is further reduced and $V/\dot{x}_o$ increases, the two symmetric vortices formed in the major part cycle are swept to a lesser extent over the cylinder in the minor part cycle and cause only small vortices to be formed in the minor part cycle, which tend to be absorbed into the first pair. The movements of the vortices formed in the major part cycle are sketched above for decreasing x_o/D. In the last sketch, corresponding to Fig. 137, the vortices remain close to the cylinder throughout most of the cycle, building up to a considerable size and finally being swept downstream as a pair in the next cycle. Associated with these phenomena will be high values of STCDDEP.

In the above, and also in much of the following description of the flow patterns, the flow will be described as if the cylinder were stationary and the flow consisted of steady and oscillatory

parts. The flow patterns are expected to be identical. However, particularly as the photographs are taken with respect to axes fixed to the cylinder, it is easiest to describe patterns with respect to a stationary cylinder. I.e. vortices are not in the experiments 'swept back over the cylinder', but rather the cylinder is driven forward through the vortices.

The near wake is thus comprised of a number of symmetric pairs of vortices which are shed at the rate of one pair per cycle (see, for example, Fig. 136 or 129). At some point downstream the vortices begin to rearrange themselves, some cancelling each other out, and a von Kármán type alternating street results (this cannot be seen on Figs. 136 or 129. However the wake is starting to re-form at the right hand side of Figs. 118 and 123, and, although these are for $V/nD < 2.8$, the process is similar for $V/nD = 2.8 \sim 6.5$).

If x_o/D is allowed to (very slowly) decrease further, then at some point the asymmetry in the wake quite suddenly moves up towards the cylinder and radically affects the shedding process itself which becomes asymmetric and is characterized by strong vortices, a wide wake and large movements of the separation points, all of which cause STCDDEP to be high. This change of the wake occurs at some point when the value of $V/\dot{x}_o$ is between 1 and 2, and will be discussed more fully in chapter 11.3.3. Thus for example for $V/nD = 3.8$ the symmetric shedding of Fig. 136, where $x_o/D = .41$ and $V/\dot{x}_o = 1.68$, changes over to the asymmetric form of Fig. 135, where $x_o/D = .31$ and $V/\dot{x}_o = 1.95$. For $V/nD = 3.0$ the symmetric and asymmetric forms are represented by Fig. 129 ($x_o/D = .29$, $V/\dot{x}_o = 1.65$) and Fig. 128 ($x_o/D = .27$, $V/\dot{x}_o = 1.77$), respectively.

The form of the symmetric vortex shedding immediately before, and the form of the asymmetric shedding immediately after, this fundamental change in the wake will be more fully described in subsequent sections.

As x_o/D is further decreased the oscillations in the wake and the separation points and the size of the vortices gradually reduce until the wake appears similar to that behind a stationary cylinder. The wake is, however, as in the case for $V/nD \gtrsim 6.5$, modified and controlled to a certain extent by the oscillations, as will be discussed later.

V/nD $\lesssim$ 2.8

The effects on the flow of reducing x_o/D are similar to those in the previous range of V/nD to the point at which symmetric vortices are shed, one pair per cycle. For further reduction in x_o/D, however, no change over to asymmetric shedding occurs, but rather the symmetric vortices tend to roll up progressively less, there is progressively less movement in the separation points and the vortices continue to re-form to an alternating wake at some point downstream. See, for example, Fig. 118 for V/nD = 1.0, x_o/D = .12 and $V/\dot{x}_o$ = 1.29. Eventually the vortices are little more than ripples on separation layers leading to the formation region of an alternating wake. Even for $V/\dot{x}_o \approx 15$ there are definite vortices, one pair shed per cycle. These eventually group together to form an alternating wake, but no attempt has been made herein to determine when the wake becomes indistinguishable from that behind a stationary cylinder.

11.3.3. Discussion of the effects associated with the change over from symmetric to asymmetric vortex shedding

Form of symmetric shedding immediately before transition to asymmetric shedding

In Fig. 149 are sketched flow patterns through one cycle of oscillation for various V/nD. In all cases the first sketch is from photographs taken just after the cylinder has reversed direction and is travelling from left to right, and the third sketch is about at the extreme of the cylinder motion to the right hand side (the steady current flow is from left to right), i.e. the sketches are synchronized with respect to the motion of the cylinder. The sketches for V/nD = 3.0 and 3.8 are within the range where wake transition occurs. The sketches at V/nD = 1.0 and 2.0 and 12.0 are for values

of x_o/D where one might expect transition to occur (i.e. $V/\dot{x}_o$ = 1 ~ 2), though transition does not in fact occur for these values of V/nD.

It is seen from Fig. 149 that the wake width is greatest for V/nD = 3.8. Unfortunately there are no photograph sequences for $6.5 \gtrsim V/nD \gtrsim 3.8$, however brief tests conducted at V/nD = 5.0 indicated that the wake width was narrower again. Thus it seems that the wake width is greatest at V/nD ≈ 3.8, which is also where STCDDEP is greatest. It can be seen, particularly by studying the photograph sequence corresponding to the sketches of Fig. 149, that for V/nD ≈ 3.8 the vortices are strongest and close to the cylinder for the greater proportion of the cycle.

For V/nD = 2.8 ~ 6.5 the vortices are 'fed' for a greater length of time than vortices in a steady current on a stationary cylinder and may be expected to be larger. This is expected to be more so for higher values of V/nD. In a steady current on a stationary cylinder the vortex shedding frequency is controlled by the Strouhal number and increases in proportion to V. At a velocity corresponding to V/nD = 5 on an oscillating cylinder two vortices are shed, alternately, in the time taken for a single oscillation of the cylinder, and each vortex is fed for about 1/2 this time. Now, for the symmetric vortex case on an oscillating cylinder, both the vortices appear to be fed for virtually the whole cycle. Thus at V/nD ≈ 2.5 they would be fed for about the same time as in a steady current and at V/nD ≈ 5.0 for about twice as long as in a steady current. Thus, where symmetric shedding occurs, one may expect larger vortices for increasing V/nD. This is indeed the case up to V/nD ≈ 3.8. It seems that for higher values of V/nD the symmetric form is not so stable, there is a tendency for more asymmetry and the vortices are not so close to the cylinder for such a large proportion of the cycle, but are rather swept downstream. Evidently these effects increase with V/nD (due to the larger relative distance travelled) and for $V/nD \gtrsim 6.5$ a third vortex is formed and the symmetric shedding no longer occurs. (V/nD = 12.0 is sketched in Fig. 149 and here 4 or 5 vortices are formed in a cycle.)

It is also seen from Fig. 149 that the longtitudinal spacing of the symmetric vortex pairs increases approximately proportional to V/nD. This is to be expected as the shedding frequency is con-

stant, but the flow velocity increases with V/nD and the drift velocity of the vortices is expected to be fairly constant. Similar effects have been found by researchers looking at vortex spacing in the lock-on ranges of hydroelastic vibration effects, as discussed in Part I, chapter 5.2. (In fact the drift velocity of the vortices in these figures, as a proportion of V, is calculated to be .8 $\pm$ .1, which is in agreement with the results of Griffin and Ramberg (1976) who found values of .8 to .96 for both stationary cylinders and lock-on to oscillating cylinders.)

It is briefly noted that some secondary vortex shedding occurs, as can be seen in the sketches of Fig. 149 for V/nD = 3.0 and 3.8. This secondary vortex shedding will be discussed fully in chapter 11.3.6.

The phenomenon is thus due to the relative distance travelled by the cylinder with respect to the flow in the major part cycle being such that only one pair of vortices can develop symmetrically before flow reversal. The vortices are close to the cylinder throughout the major part cycle and also in the minor part cycle until they are forced out by the cylinder travelling between them. In the next major part cycle the vortices are swept downstream and a new pair begins to form.

Form of asymmetric shedding immediately after transition from symmetric shedding

The form of the asymmetric wake just after the wake transition varies with V/nD. In all cases for V/nD = 2.8 ~ 6.5 vortices are shed at the rate of two per cycle and the flow pattern in one cycle is the mirror image of that in the previous cycle. Furthermore if one asigns the signs + and - to clockwise and anticlockwise rolled vortices, respectively, then the shedding of vortices into the wake is in the order ++--++--, etc. (As opposed to +-+-+-, etc. from a stationary cylinder.)

In Fig. 150 sketches of the flow patterns through one cycle at various values of V/nD are shown. Again the first sketch is at a point when the cylinder starts to move from left to right and the

third sketch is one half cycle later. The sketches at the extreme right hand side show the vortices in the wake from the previous three cycles.

From the right hand sketches of Fig. 150, it is seen that the vortex spacing in the wake increases in proportion to V/nD, the reasons being the same as discussed for the symmetric shedding case. From these figures the drift velocity of the vortices, as a proportion of V, is calculated as $.95 \pm .05$.

From the sketches of Fig. 150, or from the original photograph sequences, it is seen that the shear layers feeding the vortices move through large angles over the cylinder, and there is more movement for higher values of V/nD. For V/nD = 3.0 the movement seems to be through an angle of about 100° and for V/nD = 5.0 through an angle of about 220°. The second vortex of a particular sign of rotation appears to be of similar size and strength for all three values of V/nD. However the first vortex of a particular sign increases in size and circulation with increasing V/nD. Furthermore the first vortex shed of a particular sign, although fed by fluid from one side of the cylinder, is, when shed, on the opposite side of the cylinder centreline, because of the large swing of the separation points and the wake. This can be seen from the sketches of Fig. 150 where the first clockwise vortex (denoted 1) is fed by fluid from the top side of the cylinder, but when shed is seen to be below the centreline of the cylinder. For V/nD = 3.0 this first vortex (1) is considerably smaller than the second (denoted 2). For V/nD = 3.8 the two are of similar size and for V/nD = 5.0 vortex 1 is considerably larger than vortex 2. Thus, in each cycle, two vortices are shed of the same sign and are placed in the wake, one to each side of the centreline. Each of these vortices tends to form a pair in the wake with a vortex of the opposite sign - the first vortex in a cycle pairs with the second vortex in the previous cycle, and the second vortex pairs with the first in the next cycle. As there are only two vortices shed per cycle at both V/nD = 3.0 and 5.0 one expects the total circulation in the vortices to be greater for V/nD = 5.0, as is the case.

The form of the wake further downstream has not been studied in any detail, however it appears that the various pairs of vortices of opposite sign gradually merge and cancel each other out.

The change from symmetric to asymmetric shedding

It seems that this change from symmetric to asymmetric shedding is associated with the inherent instability of a symmetric vortex wake and the corresponding stability of an alternate vortex wake. An alternate vortex wake forms naturally a small distance downstream from a stationary cylinder. It has been seen that from the oscillating cylinder symmetric vortex pairs are shed, remain symmetric a number of diameters downstream (the actual distance being dependent on a number of factors), and then start to rearrange themselves into an alternating wake. This occurs rather further downstream than would occur from a stationary cylinder.

For values of $V/nD \lesssim 2.8$ the distance to where the wake reforms decreases as x_o/D decreases. For example for $V/nD = 2.0$ and $x_o/D = .14$ there are 3 pairs of symmetric vortices clearly visible before the wake starts to re-form, but for $x_o/D = .11$ there are only 1 or 2 pairs (the vortex spacing being unaltered). For $V/nD = 2.8 \sim 6.5$, however, there is little change in the distance, and in fact just before the change from symmetric to asymmetric shedding occurs the wake appears to be made up of particularly strong vortices (e.g. Fig. 129 or 136), and the wake reforms a particularly large distance downstream.

If the amplitude of motion is allowed to decrease very slowly indeed, then, at some point when the value of $V/\dot{x}_o$ is between 1.0 and 2.0, the point at which the wake reforms to an alternating vortex wake moves up towards the cylinder and in the course of some 5 to 10 cycles it has moved sufficiently close to the cylinder that the shedding from the cylinder is radically altered. Quite why the wake is suddenly unable to sustain the symmetric vortex form for a distance downstream is unclear. However the symmetric vortex form is unstable and there is probably less energy in the wake for lower values of x_o/D (as the relative distance travelled is less). One might suggest that at some point the last symmetric vortices before the reformation point of the wake are sufficiently weak that they begin to be 'pulled' out of symmetry by the wake further downstream, and this occurs as a chain reaction up the wake. This explanation is rather speculative, however it is quite evident that the change from a symmetric to an asymmetric wake commences downstream and then

works its way upstream. The process has been filmed and in Fig. 151 are shown prints taken from the film at the same point in 10 successive cycles, and the upstream movement of the asymmetry can clearly be seen. (The prints are of rather poor quality, and negative, as they are printed directly from 16 mm colour film.)

The value of $V/\dot{x}_o$ at which this change over occurs is dependent upon a number of factors, but it seems that for higher V/nD it occurs at slightly lower $V/\dot{x}_o$. The change over can occur at slightly different values for nominally identical tests and seems to be influenced by any stream fluctuations, etc. which can trigger the process. The transition from symmetric to asymmetric shedding with decreasing x_o/D (increasing $V/\dot{x}_o$) occurs at a lower value of x_o/D than the transition from asymmetric to symmetric shedding with increasing x_o/D. For example for V/nD = 3.0 these transitions were at x_o/D = .21 ($V/\dot{x}_o$ = 2.28) and x_o/D = .26 ($V/\dot{x}_o$ = 1.86), respectively.

The value of STCDDEP is expected to be particularly high for $V/\dot{x}_o$ in the range 1 ~ 2 for both the symmetric and asymmetric vortex shedding forms due to the particularly strong vortices, wide wakes and large angles of movement of the separation points. The force measurement tests and the flow visualization tests were conducted separately so that it is impossible to tell where the peak in STCDDEP is with respect to the change over from symmetric to asymmetric shedding. It is, however, evident that the peak is very close to the change over.

Reasons why the change over does not occur for $V/nD \lesssim 2.8$

For values of $V/\dot{x}_o$ smaller than, but fairly close to 1, two symmetric vortices are formed in the major part cycle and are swept back over the cylinder in the minor part cycle. Two vortices of reverse circulation are formed which counter the effects of the first vortices, and high values of STCDDEP do not occur. This can be seen in Fig. 119 for example. For $V/\dot{x}_o$ = 1 ~ 2 only one pair of symmetric vortices are formed per full cycle, however these vortices are not fully developed (i.e. if the relative distance travelled had been greater they could have developed further symmetrically before asymmetry sets in) and so STCDDEP does not reach a high value.

Nor does the change over to an alternating wake occur for the following reason: A von Kàrmàn type alternating wake forms at a reasonably constant distance downstream of a cylinder irrespective of the velocity (at least for the subcritical Reynolds numbers encountered here). As has been seen, the distance between symmetric vortex pairs formed at the oscillatory frequency is proportional to V/nD. For small values of V/nD there is room for one or two pairs of symmetric vortices between the cylinder and the point at which an alternating wake might be expected to form. An alternating wake thus appears able to form at approximately the same point as behind a stationary cylinder without affecting the vortex shedding. (See, for example, Fig. 118 for V/nD = 1.0, x_o/D = .123 and $V/\dot{x}_o$ = 1.29.) In fact for very small amplitudes of vibration at low V/nD there are slight wrinkles, one pair for each cycle, on what otherwise appear to be normal separating shear layers which roll up into alternate vortices exactly as from a stationary cylinder.

In the sketch in Fig. 149 for V/nD = 2.0 (from the photograph sequence of Fig. 123) it can be seen that when the symmetric vortices initially begin to develop there is a certian asymmetry, however with further development the symmetric form recovers. For rather larger values of V/nD the asymmetry increases and for rather smaller values it does not occur at all.

Reasons why the change over does not occur for V/nD $\gtrsim$ 6.5

For values of V/nD $\gtrsim$ 6.5 the symmetric form of vortex shedding does not occur. This is because x_o/D must be so large in order to satisfy the $V/\dot{x}_o$ = 1 ~ 2 criterion that the wake develops beyond that stage, becoming asymmetric and, for large enough V/nD, further vortices form in each cycle. Wake swing becomes considerably less and STCDDEP is reduced correspondingly.

11.3.4. Flow patterns at low values of $V/\dot{x}_o$

At values of $V/\dot{x}_o \lesssim 1$ flow reversal occurs twice in each cycle and the flow may be divided into two parts, each comprising of a start from rest, acceleration to a maximum velocity (of $V+\dot{x}_o$ in one part and $V-\dot{x}_o$ in the other), and a deceleration to rest again. It is interesting to compare the flow pattern in each of these part cycles with that for oscillations in still water with the same relative distance travelled between the cylinder and the flow.

Expressions for the distance travelled by the cylinder relative to the fluid in each part cycle, non-dimensionalized by 2D, are derived in Appendix 4, and are found to be dependent on V/nD and $V/\dot{x}_o$ (or can be expressed in terms of any two of the parameters V/nD, $V/\dot{x}_o$ and x_o/D). These expressions are derived without any account being taken of the discussion in chapter 11.3.1, paragraph iii). On those of Figs. 108 to 147, where $V/\dot{x}_o < 1.0$, the distances travelled by the cylinder relative to the flow in the two half cycles, non-dimensionalized by 2D, are noted. Thus direct comparison with values of x_o/D in still water may be made, and the flow patterns may be compared with those in still water.

In Fig. 152 flow patterns are sketched from the photograph sequences for various values of non-dimensional relative distance travelled. Also indicated are the value of V/nD, x_o/D and either 'A' or 'B', 'A' indicating the major part cycle, and 'B' the minor part cycle.

It is seen that similar flow patterns are produced for widely varying V/nD and x_o/D, but for the same non-dimensional relative distance travelled between the cylinder and the flow in the particular part cycle sketched.

The flow patterns are similar to those in still water at a rather lower value of x_o/D. The reason for this is probably the larger reduction in the steady flow component than in the oscillating component near the cylinder, such that the effective relative distance travelled is less than if a purely oscillatory flow was used. The vortices formed when there is a steady flow appear to be stronger than in the still water cases. Also for oscillations in still water

it was often found that vortices formed in one cycle were formed behind the cylinder and at flow reversal could be swept either onto or around the cylinder. In currents the vortices appear to be formed further out from the cylinder centreline and at flow reversal are always swept back over the same side of the cylinder.

There often appears to be a greater tendency for a vortex travelling back over the cylinder after flow reversal to cause an oppositely signed vortex to be formed and for the two to move off as a pair, as described by Zdravkovich and Namork (1978). In fact Fig. 121, where $x_o/D = 1.5$ and the relative distance travelled in the two part cycles are 1.7 and 1.2 (and $V/\dot{x}_o = .11$), resembles fairly closely Zdravkovich and Namork's figure for $x_o/D \approx 1.5$ with one vortex 'pairing' occurring in each part cycle from one side of the cylinder in one part cycle and from the other in the other part cycle. In still water, on the other hand, one large vortex was developed from the same side of the cylinder in both half cycles. Thus the pattern, when there was a small steady flow component, resembled the pattern in waves more nearly than the pure oscillatory flow case did.

11.3.5. Flow patterns at high values of $V/\dot{x}_o$

For high values of $V/\dot{x}_o$ the flow patterns, in general terms, resemble those on a stationary cylinder in a steady flow. Vortex shedding occurs from alternate sides of the cylinder and an alternating wake is formed. Nevertheless, even for very large values of $V/\dot{x}_o$, there are noticeable effects due to the oscillations.

For Fig. 134, for $V/nD = 3.8$, $x_o/D = .09$, and $V/\dot{x}_o = 7.03$, two vortices form symmetrically in each cycle and then develop unsymmetrically and are shed. It is evident that the process repeats every cycle even though there are small variations from cycle to cycle.

Similarly for Fig. 138, for $V/nD = 5.0$, $x_o/D = .06$, and $V/\dot{x}_o = 12.6$, two vortices are formed and shed in each cycle. The flow is different from a steady flow around a stationary cylinder in that the two vortices start to build up symmetrically. Thus even vibrations of only 6% of a diameter, giving a velocity amplitude only 12%

of the steady flow velocity, have led to radical changes in the flow pattern.

It appears that for V/nD less than at least 5.0 and for V/nD $\gtrsim$ 1 there are always two vortices shed per cycle, and this is true even for very large values of $V/\dot{x}_o$. (There are too few tests to enable a more exact determination of an upper boundary, however for V/nD = 1.0 and $V/\dot{x}_o \approx 15$ and in the above case of V/nD = 5.0, $V/\dot{x}_o$ = 12.6 two vortices were shed per cycle.)

In Fig. 143, for V/nD = 12.0, x_o/D = .30, and $V/\dot{x}_o$ = 6.37, and Fig. 146, for V/nD = 20.0, x_o/D = .41, $V/\dot{x}_o$ = 6.95, the flow resembles more nearly that for a stationary cylinder. A careful study of the figures, however, indicates that there are, respectively, exactly 4 1/2 and 7 vortices shed per cycle giving values of the Strouhal number of .18 and .175, respectively. (For a stationary cylinder the value measured was .21.)

11.3.6. Separation and secondary vortex shedding

For large values of $V/\dot{x}_o$ there is little movement of the separation points. At low values of $V/\dot{x}_o$ the flow patterns resemble those in still water. Grass and Kemp (1978) have shown that in each half cycle in oscillatory flow, separation first starts at the rear stagnation point and then moves rapidly forward. The flow visualization method used in the results presented here does not lend itself to a determination of the separation point in these very early stages of the flow, mainly due to the forced introduction of dye from the cylinder. However, if one neglects the early stages after flow reversal, when the separation possibly moves rapidly back from the rear stagnation points and developing vortices are very small, then for low $V/\dot{x}_o$ the separation points do not move very much in each part cycle, and after each flow reversal new separation points develop from the other half of the cylinder.

For $V/\dot{x}_o$ around 1 and V/nD $\lesssim$ 6, however, there is considerable movement in the separation points, and indeed the separation is in many ways rather different to separation in a steady flow. This is particularly evident for the symmetric shedding case. As an example

one may take Fig. 123, $V/nD = 2.0$, $x_o/D = .12$, $V/\dot{x}_o = 2.65$ where the following sketches represent the development of the pattern through part of a cycle, drawn for the upper side of the cylinder only (the pattern is symmetric).

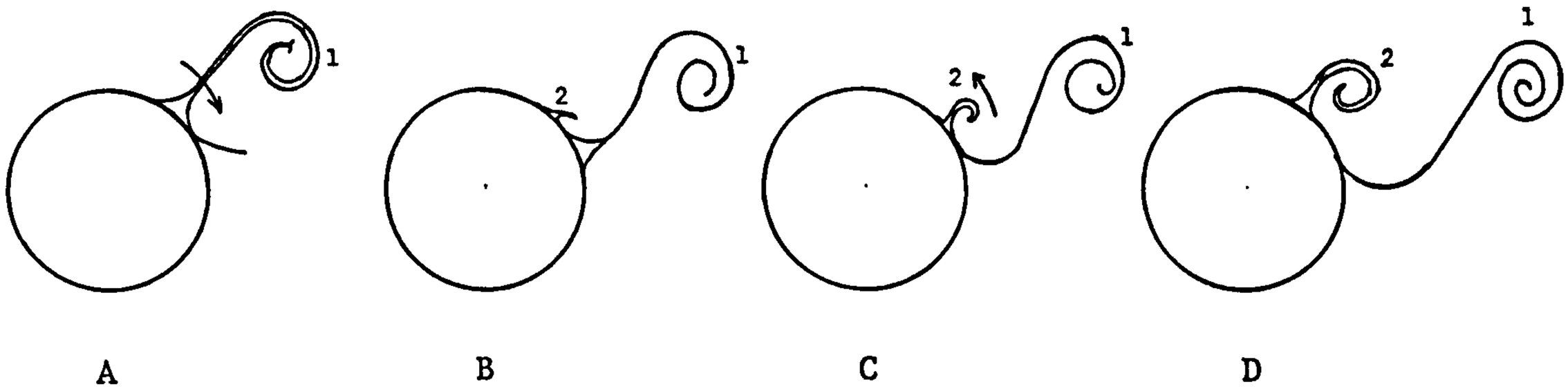

It is seen that separation and the development of a vortex appear to start at some point on the cylinder not at the rear, and at least for sketches C and D the flow is towards the developing vortex from both sides of vortex 2, i.e. the flow on either side of this vortex is in opposite directions. Vortex 2 may thus be characterized as being formed form the shear layers emanating from two separation points, one for the flow in each direction. Indeed it appears that fluid which has earlier left the cylinder and is in the shear layer leading to vortex 1 is, at some stage, partly dragged back onto the cylinder. At the same time the positions of the shear layers from the cylinder are moving over the surface of the cylinder.

Secondary vortices are also formed within the area described by the two shear layers leading to the developing vortex, as has been sketched in Fig. 149. It is found that one of these vortices develops more for larger amplitudes of oscillation, sketched below for $V/nD = 2.0$.

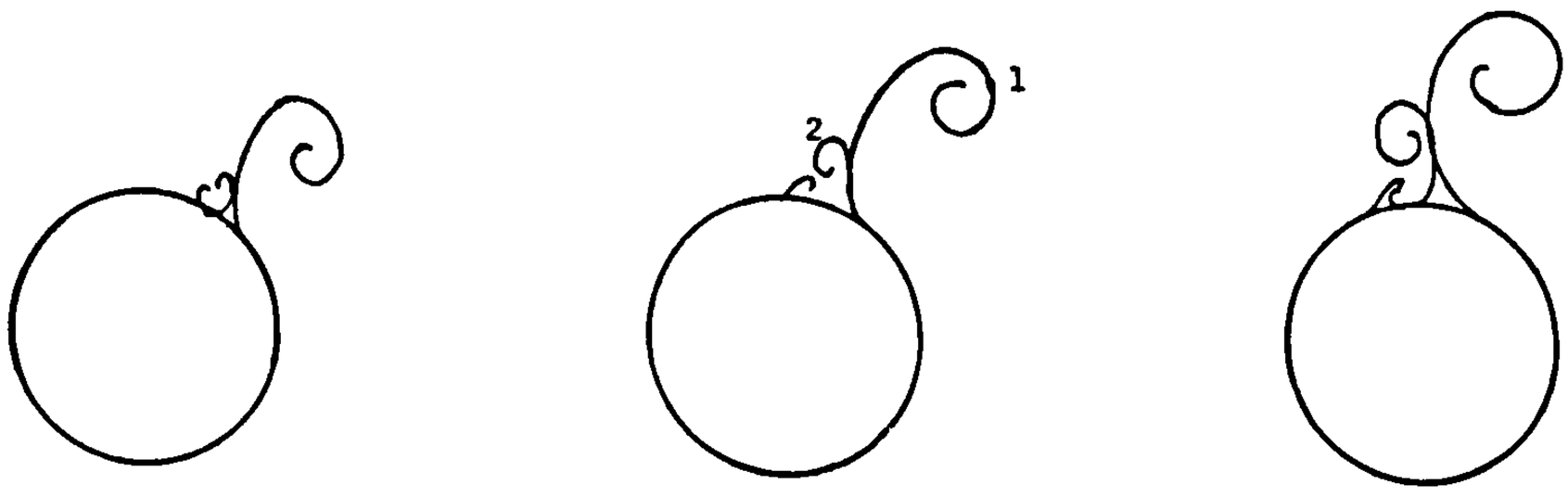

$x_o/D = .15$ $x_o/D = .43$ $x_o/D = .45$

The development of this vortex, marked 2 in the above diagrams, is dependent on the extent to which the main vortex, 1, is swept back over the cylinder in the minor part cycle. (The sketches above show the instant when the main vortex, 1, is at its furthest point to the left, with respect to the cylinder.) This backward movement of vortex 1 can be expected to cause a vortex of reverse rotation to form. (Indeed it is for this reason that, in oscillatory flows, the first vortex shed in a half cycle is generally shed from the same side as the last vortex in the previous half cycle.) Indeed, one expects that the greater the extent to which vortex 1 is swept back, the greater the development of vortex 2, and this appears to be the case. Photograph sequences for increasing amounts to which vortex 1 is swept back over the cylinder can be seen in Figs. 123, 136, 124 and 119, where the first three correspond approximately to the above sketches.

If the oppositely signed vortex, 2, is small compared to the main vortex, 1, then it is absorbed into the main vortex (for example Fig. 123). If, however, it is of similar size then the two move off as a pair and tend to cancel each other out (for example Fig. 124).

Secondary vortices are also developed in the asymmetric shedding form, although in this case the secondary vortices are of similar size and smaller than the main vortex and do not tend to interfere with it, but are rather dragged into the wake behind it. (e.g. see Figs. 127 and 128.)

Evidently the separation and indeed the boundary layer flow are extremely complex on a cylinder in a relative velocity flow and, as suggested by Lighthill (1954), large movements of the separation points occur.

11.3.7. Phase relationship between vortex shedding and cylinder movement

The photograph sequences indicate that there is little difference in the form of the vortex shedding over quite wide ranges of V/nD, although hydroelastic vibrations occur over only a small range. Similar symmetric vortex shedding occurs for V/nD = 1.0 ~ 5.0, as can be seen for example in the sketches of Fig. 149, although the hydroelastic vibrations (i.e. negative values of oscillatory drag) associated with symmetric shedding occur only for V/nD ≈ 2.0. It is, however, evident from the sketches, all of which span one cycle and begin with the cylinder at its full deflection to the left, that the phase relationship between the vortex shedding and the cylinder motion varies with V/nD. For V/nD = 2.0 the vortices are in the earlier stages of growth as the cylinder moves from left to right. Sarpkaya and Schoaff (1979a, b) show, for alternate vortex shedding, that the highest values of lift coefficient are associated with the early stages of vortex development. Thus this may also be expected to give the lowest local pressures on the rear half of the cylinder and hence tend to reinforce the motion of the cylinder.

For V/nD = 3.0 and small x_o/D, where alternate shedding occurs, the phase relationship between the vortex development and the cylinder motion is similar to the above case for V/nD = 2.0.

A more detailed study of the phase relationships has not been conducted in this thesis, however some further observations could be made from the enclosed figures.

11.3.8. Minimum and maximum in STCDDEP at $x_o/D \approx 1.0$ and 2.3, respectively

In Fig. 96 it can be seen that for $V/nD \lesssim 4.0$ there is a minimum value of STCDDEP at $x_o/D \approx 1.0$, and a maximum at $x_o/D \approx 2.3$. The minimum value is lower for lower V/nD, and for $V/nD \lesssim 1.6$ it is negative. It has not been possible to give an adequate explanation as to why these minima and maxima occur, however it is believed that the minimum may be due to vortices formed in the major part cycle being swept back over the cylinder in the minor part cycle causing negative drag effects, similar to those described by Maull and Milliner (1978).

It should perhaps be mentioned that a negative value of STCDDEP, the steady component of drag, does not necessarily mean that the drag coefficient, ($C_{D3}(t)$ in equation (21) or $C_{D1}(t)$ in equation (22)) is at any instant negative. For example a negative value will occur if the average drag coefficient in the major part cycle is sufficiently smaller than that in the minor part cycle (how much smaller is dependent on $V/\dot{x}_o$).

11.3.9. Variations in the oscillatory coefficients CDDEP and CM

The inspection of the flow visualization results with respect to the oscillating components of force is very much more difficult than for the steady component, due to their dependence on phase. It would be necessary to know rather accurately the forces, or pressure distribution on the cylinder, associated with the various forms of vortex and in the various stages of development, and the inspection of the photographs would have to take into account the phase relationship between the cylinder movement and the forces associated with the vortices. Such an analysis is beyond the scope of the present data and would, in any case, be extremely time consuming.

12. GENERAL DISCUSSIONS OF THE RESULTS FOR OSCILLATIONS IN CURRENTS

A considerable amount of discussion, particularly with respect to the effects of the wake on the steady drag coefficient, has been undertaken in the previous chapter. This chapter will be mainly concerned with the quantitative results.

12.1 Relationship between the variations in STCDDEP, CDDEP and CM

It is perhaps surprising that for any particular value of x_o/D the value of CDDEP varies smoothly, other than for small x_o/D when $V/nD \approx 2.0$ and 3.0, from approximately its value in still water at very low V/nD, to 1.0 at high V/nD. (See Figs. 88 and 89.) This is especially surprising when it is seen that CM (Fig. 95) and STCDDEP (Figs. 96 and 97) vary considerably with the various parameters, and CDDEP is just as dependent on vortex shedding and the wake as CM and STCDDEP are.

The variations in CM are remarkably correlated to the variations in STCDDEP (see Figs. 95 and 96). STCDDEP exhibits a maximum at $x_o/D \approx 2.3$, whereas CM exhibits a minimum. At $x_o/D \approx 1.0$ for $V/nD \lesssim 4$ there is a minimum in STCDDEP, whereas there is a maximum in CM at $x_o/D \approx 0.8$. There also appear to be maxima in CM for V/nD = 3 ~ 10, corresponding to the peaks which occur in STCDDEP at $V/\dot{x}_o = 1 \sim 2$ for the same values of V/nD.

When there is no current, i.e. V/nD = 0, there is an inverse relationship between the oscillatory coefficients CDDEP and CM. For example Sarpkaya (1976b) has shown that increasing roughness increases CDDEP and decreases CM. Also there is a maximum in CDDEP and a minimum in CM around $x_o/D \approx 2.2$, associated with the large vortex which is formed behind the cylinder at this value. In general, for V/nD = 0, vortex formation which causes an increase in CDDEP causes a decrease in CM.

There is, in these results, an evident correlation between CDDEP and CM at least for values of $x_o/D \gtrsim 1.0$. For increasing V/nD the values of CDDEP for $x_o/D \gtrsim 1.5$ decrease whereas the values of CM increase. These variations are inversely related in a similar way to

the inverse relationship between CDDEP and CM in still water for increasing β. For $x_o/D \lesssim 1.0$ the curves of CM are rather more complicated than those of CDDEP exhibiting maxima corresponding to the minima in STCDDEP at $x_o/D \approx 1.0$ and the maxima at $V/\dot{x}_o = 1 \sim 2$. Evidently the curves for STCDDEP, CDDEP and CM are interrelated as may be expected.

It is possible that the forces associated with the various phenomena which lead to the minima in STCDDEP and the maxima in CM at $x_o/D \approx 1.0$ vary in phase with, or 180° out of phase with, the motion of the cylinder. This would lead to the observed inversely related variations in STCDDEP and CM with no significant variation in CDDEP.

It is difficult to see what mechanism could lead to the maxima which occur in both STCDDEP and CM at $V/\dot{x}_o = 1 \sim 2$, but which does not affect CDDEP. It is unlikely that this mechanism, or indeed the various mechanisms leading to the various variations, can be fully understood before investigations are conducted into the variations in a cycle of the instantaneous values of $C_{D3}(t)$ and $C_a(t)$ in equation (21).

12.2. Conditions for quasi-steady flow

The values of CDDEP and STCDDEP, i.e. the time-averaged oscillatory and steady drag coefficients based on equation (21), are equal for all amplitudes of motion for $V/nD \gtrsim 17$. For $V/nD \gtrsim 30$ their common value is 1.0, the value obtained for STCDDEP on a stationary cylinder. Thus, for $V/nD \gtrsim 17$ the variation in the instantaneous drag coefficient through a cycle of oscillation is small, and for $V/nD \gtrsim 30$ the motion is quasi-steady. A value of $V/nD = 17$ represents about 7 vortices shed per cycle of oscillation.

For values of $V/nD \lesssim 17$, CDDEP and STCDDEP diverge, indicating that the instantaneous drag coefficient, $C_{D3}(t)$ in equation (21), varies through a cycle of oscillation. No attempt has been made to measure instantaneous values of coefficients, however it is evident from the flow visualization tests that considerable variation occurs (as the flow patterns vary considerably and the force coefficients

are strongly related to the flow patterns).

The divergence in CDDEP and STCDDEP at lower values of V/nD does not imply that equation (21) is incorrect, merely that C_{D3} varies with time through each cycle. It has already been seen that equation (22), where separate parts are written for the steady and oscillatory drag forces, gives unacceptable variations in the coefficients, indicating that that equation is not of the right form.

12.3. Hydroelastic vibrations

It has already been mentioned that the negative values of the oscillatory drag coefficients found for V/nD around 2.0 and 3.0 are due to the phenomenon of hydroelastic vibrations, which has been described in Part I, chapter 5.1.

Results from all the tests recorded for CDIND versus V/nD for $1.0 < V/nD < 3.8$ and for $x_o/D = .05, .075, .1$ and $.2$ are plotted in Fig. 153. There are fewer points for the lower values of x_o/D because not all the tests were continued to so small amplitudes of motion. Each point plotted is the curve fitted point obtained from the data for a particular flow rate and cylinder diameter.

As mentioned in chapter 9.1.1 there is more scatter for the lowest values of x_o/D. For $x_o/D = .05$ the scatter in CDIND is about $\pm .5$.

Despite the few points, curves have been drawn in in Fig. 153. The first peak (i.e. maximum negative value of CDIND) occurs at V/nD = 2.1 ~ 2.3, and is associated with symmetric vortex shedding, one pair being shed per cylinder oscillation. This peak is at the same value of V/nD as that where maximum response was found by King (1974) for lightweight inverted elastic cantilever cylinders caused to vibrate by a current flow. There is a minimum in -CDIND for V/nD = 2.4 ~ 2.5, King typically finding a minimum of response at V/nD between 2.5 and 2.7. There is a second maximum negative value of CDIND at V/nD ≈ 2.9, associated with alternate vortex shedding from the cylinder, one vortex being shed per cylinder oscillation. King found a peak in the response for inverted elastic cantilever cylinders for V/nD somewhere between 3.0 and 3.6, the value depending on vari-

ous parameters. Every (1978), using cylinders mounted as inverted pendulums, found that the peak associated with symmetric vortex shedding occurred at V/nD between 1.9 and 2.3, depending on the value of the stability parameter, k_s, and found that for the asymmetric vortex shedding, values of response near maximum were obtained over a range of V/nD, for example for V/nD = 2.8 ~ 4.3 when k_s = .03, for V/nD = 2.5 ~ 3.8 when k_s = .07, for V/nD = 2.8 ~ 3.6 when k_s = .7 and for V/nD = 2.7 ~ 3.1 when k_s = 1.0. The reason for this is probably in part due to the varying amplitude of vibration over the length of the cylinder.

In the experiments of this thesis it was not found that CDIND decreased continually as x_o/D was decreased. The minimum value of CDIND appeared to occur for x_o/D somewhere between .02 and .05, however there are so few data points that the value, and its possible dependence on V/nD, cannot be determined.

In the plotted results of Fig. 153, β varies from 200 to 3500 and, as for all the results for the oscillatory drag coefficient, the viscous contributions, as determined by equation (43), have been subtracted. If the results are plotted without the viscous contribution subtracted then there is more scatter in the curves.

From the results and using equation (7), results of maximum x_o/D in the two regimes versus k_s may be obtained, and these curves are shown in Fig. 154. It is seen that for k_s = 0, $x_o/D \approx .16$ for both the regimes and x_o/D falls off gradually as k_s is increased, reaching x_o/D = .05 at $k_s \approx 32$ and 107 for the first and second regimes, respectively. The results of King (1975), plotted in Fig. 21, show that $x_o/D \approx .18$ for k_s = 0, but that x_o/D is reduced to about .05 at the very much lower value of $k_s \approx .7$. Every (1978) found that for $k_s \approx 1.0$, x_o/D varied between .03 and .14 (in his tests the same value of k_s could be obtained by using various values of damping, cylinder mass and water depth).

The very great difference between these results and those of King is perhaps surprising, however there are a number of factors which may contribute to this. In the experiments considered in this thesis the cylinder mode shape was a pure translation, the cylinder lengths were quite short (L/D = 7~16) and end plates were fitted, thus it is expected that the situation was suitable for near perfect vortex correlation and maximum negative values of CDIND. In addition

the cylinder motion was always a decay from a larger amplitude to smaller amplitudes, thus a flow regime could be established at a larger amplitude of motion and still exist at smaller amplitudes, whereas this may not have happened for motion of increasing amplitude or for a free elastic cylinder. The tests of King and Every used bottom mounted cantilevers and inverted pendulums, respectively, thus the amplitude of vibration varied over the length of the cylinders, a situation where the vortex correlation may not be so great. The results of Every indicate that, at least under some circumstances, very much larger amplitudes of vibrations may occur than those predicted by King's curve.

For cross-flow vibrations Sarpkaya (1978) showed that free cylinder response, with a linear mode shape, could be predicted by the results obtained by the forced oscillation of a cylinder in a current.

It would be interesting to investigate the regimes where hydroelastic vibrations occur in greater detail, using forced cylinder tests similar to Sarpkaya's. As this thesis was not directly concerned with the hydroelastic vibration problem no further testing has been conducted, and the results are left as they stand; - interesting, but not fully explained.

12.4. Comparison of the results with those of other researchers

The only quantitative data with which the results can be compared are those of Mercier (1973) whose data was also reanalysed by Matten (1976). A qualitative comparison may be made with the flow visualization results of Tatsuno (1972), and Griffin and Ramberg (1976).

12.4.1. Comparison of quantitative results

Values of CDDEP, STCDDEP and CM, calculated using Matten's method from Mercier's results, have already been presented in Part I, and are shown in Figs. 27, 26 and 25, respectively. These can be compared with the present results in Figs. 88, 96 and 95, respectively. It is pointed out that Mercier's results exhibit considerable scatter, there are few points and Mercier noted that extraneous vibration was a problem.

CM

Curves of CM versus x_o/D for various V/nD from Mercier's results are shown in Fig. 25, and may be compared with Fig. 95 from the present results. It is seen that the curves exhibit similar trends, particularly at low values of x_o/D.

The value of CM at low x_o/D in Fig. 25 decreases as V/nD is increased to about 6 and then increases again in a similar manner to the present results. Furthermore for V/nD = 3.4 there is a peak in Mercier's value of CM at $x_o/D \approx .5$, (this value cannot be stated very precisely due to lack of data points). The present results also exhibit such a peak. Mercier obtained a nearly constant value of CM = 1.2 ~ 1.3 independent of x_o/D for $V/nD \approx 7$. In the present results a nearly constant value of 1.5 is obtained at $V/nD \approx 7$.

At larger values of x_o/D there are greater differences between Mercier's results and the present results, and the two sets of results exhibit opposite trends with increasing V/nD, Mercier's value of CM decreasing and apparently approaching the still water values of CM as V/nD is increased.

It is probable that Mercier's results are rather inaccurate for higher V/nD and larger x_o/D, when the inertia force is small compared to the other forces and extraneous vibrations are greatest.

CDDEP

Curves of CDDEP versus V/nD for various x_o/D from Mercier's re-

sults are shown in Fig. 27, and may be compared with Fig. 88 from the present results.

Mercier's results appear to approach the quasi-steady value (1.2 in this case) for large V/nD in a similar manner to the present results. The results are similar to the present results for low x_o/D, however at large x_o/D, and particularly for low V/nD, the results are lower than the present, and there is indeed relatively little effect of x_o/D. Mercier's results, particularly for large x_o/D, do not approach the still water values as V/nD is reduced. For large x_o/D as V/nD is decreased, Mercier's values of CDDEP decrease, whereas the present results increase, approaching the still water values.

It appears that Mercier's results for both CM and CDDEP are similar to the present for low x_o/D, but for larger x_o/D Mercier's results of CM and CDDEP are lower than the present results.

STCDDEP

Curves of STCDDEP versus V/nD for various x_o/D from Mercier's results are shown in Fig. 26, and may be compared with Fig. 96 from the present results.

The two sets of results are fairly similar, for high V/nD the quasi-steady values are approached, and for low x_o/D there is a peak value at a value of V/nD dependent on x_o/D. (The curves shown for Mercier's x_o/D = 1.5, and particularly 1.0 are oversmoothed with respect to the data points and should exhibit more of a peak.) These peaks occur at the same values of V/nD as in the present results, and the peak values are close. In fact, bearing in mind the lack of data points and the scatter in Mercier's results, the results are in good agreement with the present.

12.4.2. Comparison of flow visualization results

Griffin and Ramberg (1976), at a Reynolds number of 190, found two basic types of vortex shedding throughout the range V/nD = 2.1 ~ 4.4, which they described as asymmetric and symmetric, respectively, and considered that the symmetric form was the same as that

observed in in-line hydroelastic vibrations for V/nD ≈ 2. In fact their 'symmetric' shedding looks very unsymmetric and indeed bears a close resemblance to the form of shedding just after the change from symmetric to asymmetric shedding described in section 11.3.3. For example Fig. 5a from Griffin and Ramberg, for V/nD = 3.0, x_o/D = .12, may be compared with Fig. 127, V/nD = 3.0, x_o/D = .19, or the sketches of Fig. 150. It is considered that Griffin and Ramberg did not, in fact, observe symmetric shedding of the type described herein, due to insufficiently large values of x_o/D at the values of V/nD chosen.

Griffin and Ramberg's asymmetric shedding form consisted of one vortex per cycle shed from alternate sides of the cylinder. At V/nD = 2.8 they found that the transverse vortex spacing decreased with increasing x_o/D and that at some stage a third vortex was shed per two cycles. This author has not observed this form of shedding. For instance for V/nD = 3.0 there are two vortices shed per cycle. One of these vortices is much smaller however and perhaps may not exist at all at lower Reynolds numbers or the slightly lower V/nD of Griffin and Ramberg's tests. However, as can be seen from Figs. 126, 127 and 128 the transverse spacing <u>increases</u> with x_o/D.

There is considerably better agreement in the results presented here with those of Tatsuno (1972), obtained at R = 100. Due to the difficulty in obtaining Tatsuno's paper some of his figures are reproduced in Fig. 155. Tatsuno found that for V/nD = 3 ~ 7 there occurred what he termed "1/2-fold lock-on", characterized, at least for some values of x_o/D, by two vortices shed per cycle, in one cycle the wake being deflected to one side and two vortices of, say, positive circulation being shed and in the next cycle the deflection being to the other side and two vortices of negative circulation being shed. This is very similar to the author's results, and the bounds of V/nD are similar. Tatsuno's results for V/nD = 3.82, x_o/D = .267, shown in Fig. 155,a, can be compared with the sketch for V/nD = 3.8, x_o/D = .31 in Fig. 150 where the similarity is evident.

For V/nD $\gtrsim$ 4.2 Tatsuno obtained, for certain amplitudes of motion, the vortex shedding form shown in Fig. 155,b for V/nD = 4.9, x_o/D = .267. In each cycle a symmetric pair of vortices develop, however they appear to amalgamate whilst, or immediately after, forming, and downstream only one vortex is evident for each cycle. This figure

is very similar to the author's Fig. 139, V/nD = 5.0, x_o/D = .24. (For larger x_o/D two vortices are clearly shed in each cycle, as in Fig. 140, with a pattern similar to Fig. 155,a. This author believes that Tatsuno also considered this to be the case, however the author has not succeeded in deciphering his paper sufficiently to be more categoric.)

For V/nD $\lesssim$ 3 Tatsuno found that vortices were shed symmetrically from the cylinder, one pair per cycle, and that a certain distance downstream the vortices combined and re-formed to form a von Kármán type alternating wake. Two examples are shown, in Fig. 155,c,d. These are evidently very similar to the author's results. Tatsuno found that the distance to where the wake reformed increased with x_o/D, as was also observed by this author. However the distances observed by Tatsuno do not agree with the distances observed by this author.

Tatsuno's 1/2-fold lock-on occurred at higher values of V/nD for larger x_o/D, which is in agreement with the author's observations that the phenomenon is fundamentally dependent on the parameter $V/\dot{x}_o$. Tatsuno observed a second lock-on range, termed "1-fold lock-on", characterized by alternate shedding of one vortex per cycle, and observed for V/nD = 7 ~ 9. The author has not conducted any flow visualization tests in this range, and so no comments can be made.

Both Griffin and Ramberg and Tatsuno have determined the boundaries of V/nD and x_o/D where the cylinder oscillation frequency controls the wake frequency, and the results are summarized in Fig. 20. It should be mentioned that in both cases the wake frequency was measured downstream after possible reorganization of the wake had occurred. Indeed Tatsuno mentions that for low V/nD there are two vortices shed from the cylinder per cycle, but that further downstream the wake Strouhal frequency is independent of the oscillation frequency and dependent only on x_o/D.

From the present tests it is evident that the vortex <u>shedding</u> is controlled by the cylinder oscillation frequency up to large values of V/nD. In the present tests, however, the wake has not been studied further downstream after possible wake reorganization.

12.5. Comment on 'pressure induced' damping and the oscillatory drag forces

In the results presented for damping and the oscillatory drag coefficients, the contributions calculated using Stokes' viscous equations have been subtracted, and the remaining parts are referred to as the pressure induced drag or damping. It must be pointed out that the Stokes' damping has both viscous and pressure contributions, which are, in fact, equal for a cylinder. The pressure contribution is due to the effects of the boundary layer modifying the surface pressure (compared to pure inviscid flow). (See Batchelor (1970) p. 353.) Nevertheless this is a rather different, and usually very much smaller, effect than the forces caused by the separation of the flow and the consequent large pressure differences between the fore and the aft of the body. It might therefore be better to refer to the damping and oscillatory drag coefficients calculated after the subtraction of Stokes' damping as being those due to separation effects.

12.6. Effects of the arc of motion of the test cylinder

Due to the method employed the test cylinders oscillated back and forth on an arc of 70 cm radius, rather than performing pure rectilinear motion as might be desired and has been obtained by other experimenters, either by oscillating cylinders in still water or by using U-tube water tunnels.

It is not considered that the curved motion had any noticeable effect for the following reasons.

i) The results for cylinders oscillated in still water were in nearly perfect agreement with those of Sarpkaya and Tuter (1974), indicating that there could be little difference in the flows. Sarpkaya and Tuter used a U-tube water tunnel to oscillate water past stationary cylinders.

ii) Under some circumstances, particularly for cylinder oscillations in still water, flow patterns were set up

where vortex shedding occurred from only one side of the cylinder, or where a vortex shed from one side was different to one shed from the other side. From which side of the cylinder these conditions occurred appeared to vary arbitrarily. For example for $x_o/D \approx 2$ in still water a very definite pattern occurs in each half cycle where one vortex is formed from one side of the cylinder, is shed and moves away from the cylinder. A second vortex is formed from the opposite side and develops immediately behind the cylinder. Each characteristic vortex is shed from the same side of the cylinder in the two half cycles. In Fig. 8, for $x_o/D = 1.96$, the first vortex is shed from the upper side and in Fig. 9, for $x_o/D = 2.11$, from the lower side. When test conditions were repeated the first vortex could be found to be shed from either the top or the bottom of the cylinder, and when the pattern was established it continued indefinitely. Had there been any significant effect of the curved motion one would have expected that the flow pattern would show a preference for the one or the other side of the cylinder. No such preference was noted.

iii) In currents it was often found that a particular vortex pattern occurred in one oscillation cycle and the mirror image occurred in the next. For example in Fig. 127, for $V/nD = 3.0$, $x_o/D = .19$, it is seen that in one cycle the wake is swung over to one side of the cylinder and in the next cycle to the other side. The patterns, however, appear identical in the two cycles, (apart from the reflection), again implying that the flow has not 'noticed' the non-rectilinear motion of the cylinder.

12.7. Reynolds numbers

The Reynolds numbers throughout these tests, other than for very small amplitude oscillations in still water (when the parameter x_o/D is most important), were subcritical. Based on the steady vel-

ocities used (V) the values of R vary between 600 and 2.5×10^4. The maximum value of R, based on the relative velocity, was about 5×10^4.

12.8. Corrections to the drag coefficients

The value of the steady drag coefficient measured on stationary cylinders in the experiments was $1.0 \pm .05$. Over the Reynolds number range of the experiments, 600 ~ 10^4, the value generally accepted varies in the range 1.0 ~ 1.2.

12.8.1. Blockage

No corrections have been applied to the values of drag coefficients in these experiments to account for blockage. Corrections for blockage would not be more than 3%.

12.8.2. Velocity profile

The drag coefficients are based on the free stream velocity at the centre of the channel where the cylinder was placed. Accounting for the effects of the velocity profile the drag coefficients, (or at least the steady component) should be up to 5% higher.

12.8.3. End effects

No account has been taken of possible end effects, though it is emphasized that end plates were attached to the cylinder to minimize these effects.

12.9. Comments on the results of Part II

In Part II it was found that, within the ranges of parameters considered, wave forces on the flexible cylinder were the same as those on the rigid cylinder and the damping and added mass of the flexible cylinder were the same as if it was oscillating in still water. The largest value of U_m/nD (at the top of the cylinder) in the experiments was about 7 and the amplitudes of vibration were, at most, 0.3D. The vibration frequency was always several times the wave frequency.

The wave flow of the experiments of Part II cannot be considered to be quasi-steady, which would only occur for very large values of Keulegan-Carpenter number (Part I, chapter 3.10).

From Fig. 97, for CDIND versus V/nD, it is seen that for any particular x_o/D the value of CDIND, and therefore of the damping, approaches the still water value for low V/nD, particularly for larger amplitudes of oscillation. For $x_o/D \gtrsim .2$ the total damping (inclusive of Stokes' damping) will be close to the still water value for $V/nD \lesssim 3.5$ (the Stokes' damping contribution being a progressively larger proportion for smaller x_o/D). The large variations in the curves for $x_o/D \lesssim .1$, at V/nD = 1.5 ~ 3.5 are due to the effects of hydroelastic vibrations. It is unlikely that these effects could occur in the wave experiments of Part II due to the low values of Keulegan-Carpenter number (non-steadiness), and the rapid variation in the parameters with depth. From the results of Part III one might thus expect the damping to be virtually the same as in still water for V/nD less than at least 3, if hydroelastic vibrations do not occur. In the experiments of Part II the maximum value of U_m/nD was 7. This value was, however, at the top of the cylinder and thus values lower down were correspondingly lower, and also 7 represents the maximum value at maximum velocity, the average value being lower. Thus the cylinder in waves may well be acting as if it had a low value of 'V/nD', supporting the experimental evidence that the damping was always about the same as in still water.

The application of the Part III steady components of drag results to the wave force of the Part II experiments seems to be unreasonable due to the marked non-steadiness of the flow.

Perhaps the most important result of the tests of Part III,

from the point of view of the Part II work, is that the drag coefficient applying to two different flow components may be very different, and the extension of Morison's formula to the modified version (equation (12)), with the use of a time averaged drag coefficient applicable for the stationary cylinder case, is not expected to give the correct damping values.

12.10. Comments on the analysis method used

It is first instructive to look at the methods used for the analysis of data for a cylinder in pure oscillatory motion.

12.10.1. Analysis for a pure oscillatory motion

Keulegan and Carpenter (1958) used a Fourier coefficients method which can be explained as follows. The Morison's formula can be written as

$$f = .5\rho D\, U_m^2 \left[C_D \cos\theta|\cos\theta| - \frac{\pi^2}{K} C_M \sin\theta \right] \qquad -(47)$$

The force time history in an experiment will in general, when Fourier analysed, have sine and cosine components at the fundamental and higher harmonics of the fundamental. Equation (47), when Fourier analysed, has a sine component at the fundamental and cosine components at all odd harmonics of the fundamental, the fundamental being dominant, its amplitude being 5 times the 3rd harmonic and 35 times the 5th. The experimental force cannot, generally, be perfectly described by Morison's formula.

The sine and cosine components of the force time history at the fundamental frequency are equated to the same components of equation (47) yielding averaged values of C_M and C_D, respectively, i.e. the value of C_D is obtained purely by comparing the fundamental component of the measured force in phase with velocity with that of equation (47).

When trying to reproduce the experimental time history or to predict a force time history for similar circumstances (similar values of R and K), then the values of C_D and C_M are used in equation (47). This produces a force with a sine component at the fundamental and cosine components at the fundamental and odd harmonics, and in effect the one value of C_D is considered to apply to all the cosine harmonics and there is not considered to be any higher order sine components. Evidently, in the analysis of an experimental force, one could define a series of drag coefficients each applying to a particular harmonic and not necessarily equal.

The other main method used to analyse force data in a pure oscillatory flow is the method of least squares. In this case the error between the measured force and that predicted by equation (47) is minimized to give values of C_D and C_M. The C_M values obtained with this method are identical to those obtained using a Fourier analysis. The value of C_D, on the other hand, is different as account is taken of the higher order components.

12.10.2. Analysis for a combined steady and oscillatory motion

Only the analysis based on equation (21), a relative velocity form of Morison's formula, will be considered here.

The analysis method used in this thesis is a Fourier coefficients type of analysis. In this case the zero (steady), and fundamental sine and cosine components of the measured force are equated to the same components of equation (21), yielding the averaged coefficients STCDDEP, CM and CDDEP, respectively. For values of $V/nD \lesssim 17$ it was found that the coefficients for the steady and fundamental oscillatory drag components of the measured force were not the same.

It is difficult to see how the results can be used directly in equation (21), which requires a single value of drag coefficient to apply to all components. One could perhaps suggest the use of STCDDEP for the drag coefficient for high values of $V/\dot{x}_o$ when the steady force is dominant. In this case the steady force would be given accurately and fundamental and higher harmonic drag forces would be estimated, though not necessarily accurately. Similarly

for low $V/\dot{x}_o$ the value of CDDEP could be used in (21) yielding an accurate estimate of the dominant fundamental oscillatory drag force. Alternatively equation (23) could be used with appropriate values of STCDDEP, CDDEP and CA. In this case the steady component and the fundamental oscillatory components would be given accurately, but no higher harmonics would be estimated at all.

A least squares method could have been used to give average drag and inertia coefficients for use in equation (21). In this case the drag coefficient would be some sort of average fit to all the harmonics of the drag force. The use of (21) with these least squares method derived coefficients would thus give an estimate of all the harmonics of the drag force (most accurately for the most dominant).

The experiments described in this Part of the thesis were originally undertaken with a view to investigating damping of vibrations. In this case the Fourier method used is best as it gives the fundamental drag component accurately, and this is the only component which affects the damping. In particular this method gives the damping accurately even at very large values of $V/\dot{x}_o$ when the steady component of drag is dominant and a drag coefficient obtained by the least squares method would be weighted in favour of the steady component and could give a very inaccurate estimate of the fundamental component of drag (i.e. of the damping). (The damping of a structure may be of fundamental importance even if this force is very small compared to other forces, as discussed in Part I, chapter 6.2.)

Thus, in cases where the oscillatory drag force is of interest from the point of view of its quantification of damping, the Fourier coefficient method is most advantageous and equation (23) should be used.

In cases where one is interested in overall forces, for example for a stationary cylinder in a combined steady and oscillatory current, then the least squares coefficients for use in equation (21) would probably be better. Equation (21) contains only two coefficients whereas equation (23) contains three and equation (21) also gives estimates of forces at higher harmonics of the fundamental frequency. (At the time of writing the author is reanalysing the data collected in these experiments using the least squares method.)

12.11. Possible extensions to the work

There are a number of continuations to the work which appeal to the author as being of interest.

In the previous section it was mentioned that reanalysis of the data using equation (21) in a least squares analysis has already commenced. The author feels that it is important to compare instantaneous forces throughout the cycle with those predicted using the time-averaged values, and, if possible, to study the instantaneous values of the coefficients $C_{D3}(t)$ and $C_a(t)$ in equation (21) through the cycle and to relate variations in these coefficients to the flow patterns observed. It is already evident from the large differences between STCDDEP and CDDEP, even when $V/\dot{x}_o \approx 1$, that the coefficients $C_{D3}(t)$ and $C_a(t)$ in equation (21) vary considerably in an oscillation cycle.

Lift forces have not been studied at all in these experiments even though very large lift forces may be expected to be associated with the asymmetric vortex shedding form. Any future investigation ought to take these forces into consideration.

The flow visualization tests conducted were fairly brief and it would be desirable to study the wake in more detail, particularly with respect to vortex spacing measurements, the manner in which a symmetric row of vortices reforms to an asymmetric wake, and the downstream interactions between vortices formed from the asymmetric vortex shedding form.

In Part I it was mentioned that oscillations in still water (or oscillatory flow past a stationary cylinder) are in some ways similar to impulsively started and constant acceleration flows except that flow reversal leads to the wake in one half cycle becoming the upstream part of the flow in the next half cycle, resulting in complex vortex interactions. The present rig could be used to study the flow patterns and forces on the cylinder in progressive half cycles after the pendulum was released from rest at an extreme deflection. The first half cycle would represent the forces for a sinusoidal motion through perfectly still water and in subsequent half cycles the effects on the forces of the wake becoming the upstream flow could be studied.

The problem approached in the experiments of Part III, that of oscillations in a steady current, is simpler than the conditions which are often of interest to the offshore industry. As a next step it would be useful to study flows consisting of two superimposed oscillating components (or oscillations of a cylinder in an oscillating flow) where the frequencies are different. This could represent, for example, vibrations of structures in waves or the low frequency oscillations of a tethered platform in waves where the oscillation period of the structure is often 1 ~ 2 minutes. This line of approach might lead to a method to tackle the even more complex situation of many sinusoidal components superimposed (representing a wave spectrum for example).

CONCLUSIONS

The main conclusions of the thesis may be divided up into three sections corresponding to the three Parts of the thesis.

Conclusions for Part I

i) There is in general good agreement between results obtained in regular waves and in oscillatory flows for the flow patterns observed around a stationary cylinder, the force coefficients obtained and the spectral content of the lift force.

ii) An oscillatory or wave flow is expected to become more quasi-steady as the Keulegan-Carpenter number is increased. Nevertheless oscillatory flow coefficients do not become equal to the steady flow values until a value of K of about 1000.

Conclusions for Part II

i) Morison's formula, used with oscillatory flow values of C_D and C_M, gave a good estimate of the overall forces on the rigid cylinders in waves, but not of the vortex shedding forces.

ii) A quasi-steady model of vortex shedding gave a good qualitative description of the frequency content of lift forces on cylinders in waves and currents.

iii) Vibrations of the flexible cylinders were caused by excitation from vortex shedding forces and occurred for $U_m/nD \gtrsim 1.0$ in both the in-line and cross-flow directions, the vibration amplitude being mainly dependent on U_m/nD, δ_{sw} and a frequency parameter $|(1-rn_w/n)|$.

iv) For the experiments considered, the wave induced forces on the flexible cylinder, including those due to vortex shedding, were the same as on the rigid cylinder, and no hydroelastic effects were discerned.

v) The vibrations of flexible cylinders, within the range of parameters considered here, can be predicted from a full knowledge of the forces on a stationary cylinder, including those due to vortex shedding. The use of the modified Morison's formula leads to an underprediction of vibration, partly due to the non-inclusion of vortex shedding forces and partly due to the overestimation of damping.

Conclusions of Part III

The experimental method, using a massive pendulum to produce oscillatory motion, gave accurate and repeatable results and can be recommended, particularly for the investigation of the oscillatory drag forces.

Results in still water

i) For small amplitudes of motion, the damping and oscillatory drag coefficient were given, within measureable accuracy (better than 1%), by the values obtained through application of Stokes' equations for unseparated viscous flow.

ii) For larger amplitudes of oscillation, separation occurs and additional damping and oscillatory drag occurs. The oscillatory drag coefficient, over and above that given by Stokes' equations, and the inertia coefficient have been quantified for $x_o/D \lesssim 6$ and found to be dependent on x_o/D and β.

Results in currents

i) The results have been found to be best quantified using a relative velocity Morison type equation from which three time averaged coefficients have been determined, for the oscillatory com-

ponent of drag (CDDEP), the direct component of drag (STCDDEP) and the inertia (CM). These coefficients have been found to be functions of three parameters, β, x_o/D and V/nD (or $V/\dot{x}_o$).

ii) For any particular value of x_o/D the oscillatory drag coefficient, CDDEP, varies smoothly from its still water value at low values of $V/\dot{x}_o$ to the quasi-steady value at high values of V/nD, other than for values of V/nD around 2.0 to 3.0 when $x_o/D \lesssim .2$, in which case negative values of CDDEP occur due to the phenomenon of hydroelastic vibrations.

iii) The steady component of drag coefficient, STCDDEP, exhibits a number of complex and remarkable variations, but for increasing values of V/nD it approaches the quasi-steady value and for $V/nD \gtrsim 30$ is equal to the quasi-steady value, for all x_o/D. A minimum value of STCDDEP, which is negative for $V/nD \lesssim 1.5$, occurs for $V/nD \lesssim 4$ at $x_o/D \approx 1.0$. For values of $2.8 \lesssim V/nD \lesssim 6.5$ a maximum in STCDDEP occurs, with a value up to twice the quasi-steady value, when the value of $V/\dot{x}_o$ is somewhere between 1.0 and 2.0.

iv) The inertia coefficient CM is found to be close to its still water value, for any particular value of x_o/D, at low values of V/nD. For values of $V/nD \gtrsim 3.5$ and $x_o/D \gtrsim 1.5$, the inertia coefficient has a near constant value of 1.5 ~ 1.6. For $x_o/D \lesssim 1.5$ the variations in CM are complex, the value first decreasing with increasing V/nD to a minimum at $V/nD \approx 5$ and then increasing again. The variations in CM are closely related to the variations in the steady drag coefficient STCDDEP. Maxima occur in CM for $2.8 \lesssim V/nD \lesssim 6.5$ at values of $V/\dot{x}_o = 1 \sim 2$.

v) Despite the large variations in the individual coefficients, the value of the maximum force in a cycle varies only between 80% and 135% of the value calculated using drag and added mass coefficients equal to 1.0.

vi) The quantitative results are in fairly good agreement with those of other researchers, but cover larger ranges of parameters and exhibit considerably less scatter.

Flow visualization experiments

i) The variations in the flow patterns with x_o/D for oscillations in still water have been detailed and, in general, agree with previous researchers' observations.

ii) For cylinders oscillating in a current, the effects of varying x_o/D are similar within broad ranges of V/nD. Three ranges may be defined as $V/nD \lesssim 2.8$, $2.8 \lesssim V/nD \lesssim 6.5$, and $V/nD \gtrsim 6.5$. The flow patterns in each range of V/nD may be divided into three ranges, namely high values of $V/\dot{x}_o$, values of $V/\dot{x}_o$ around 1 and low values of $V/\dot{x}_o$. It is particularly for the middle range of V/nD, with $V/\dot{x}_o$ around 1, where remarkable effects have been noted, including the sudden change over from symmetric to asymmetric vortex shedding. These effects lead to the peaks in STCDDEP.

iii) For values of $V/\dot{x}_o \lesssim 1$, the flow pattern, for all values of V/nD, resembles in each part cycle the pattern observed for oscillations in still water at a similar value of non-dimensional relative distance travelled.

iv) When $V/\dot{x}_o \approx 1$ and $2.8 \lesssim V/nD \lesssim 6.5$ the flow is found to radically change, as the amplitude of motion is slightly reduced, from a symmetric to an asymmetric shedding form. This effect has been explained by considering the combined effects of relative distance travelled by the vortices with respect to the flow, the development of symmetric vortices after flow reversal, and the stability of a von Kármán type wake.

For $V/nD \gtrsim 6.5$, the symmetric shedding form is not found, and for $V/nD \lesssim 2.8$ the shedding form remains symmetric and no change over to asymmetric shedding occurs.

v) For large values of $V/\dot{x}_o$ the patterns resemble those in currents, the shedding frequency varying approximately with the relative velocity.

REFERENCES

ABERNATHY, F. H., and KRONAUER, R. E. (1962): "The formation of vortex sheets". J. Fluid Mech., 13, pp. 1-20.

ACHENBACH, E. (1968): "Distribution of local pressure and skin friction around a circular cylinder in cross-flow up to Re = $5x10^6$". J. Fluid Mech., 34, pp. 625-639.

ACHENBACH, E. (1971): "Influence of surface roughness on the cross-flow around a circular cylinder". J. Fluid Mech., 46, pp. 321-335.

AHLBORN, F. (1902): "On the mechanisms of hydrodynamic resistance". Abh. Geb. Naturwiss Bd, 17. (In German.)

APELT, C. J. (1961): "The steady flow of a viscous fluid past a circular cylinder at Reynolds numbers 40 and 44". ARC, Rep. and Memo, No. 3175.

ASHER, J. A., and DOSANJH, D. S. (1968): "An experimental investigation of the formation and flow characteristics of an impulsively generated vortex street". Trans. ASME, pp. 596-606, Dec. 1968.

BATCHELOR, G. K (1970): "An introduction to fluid dynamics". Cambridge Univ. Press.

BEARMAN, P. W. (1969): "On vortex shedding from a circular cylinder in the critical Reynolds number regime". J. Fluid Mech., 37, pp. 577-585.

BEARMAN, P. W., GRAHAM, J. M. R., and SINGH, S. (1978): "Forces on cylinders in harmonically oscillating flow". Symp. on Mech. of Wave-Induced Forces on Cylinders, Univ. Bristol, England, Sept. 1978. Paper A3.

BENARD, H. (1907): "Formation of the centres of rotation behind a moving object". C. R. Hebd Séane, Acad. Sci., Paris, 147, pp. 839-842. (In French.)

BERGER, E., WILLE, R. (1972): "Periodic flow phenomena". Ann. Rev. Fluid Mech., Vol. 4, pp. 313-340.

BIDDE, D. D. (1971): "Laboratory study of lift forces on circular piles". J. Waterways and Harb., ASCE, 97, WW4, pp. 595-614.

BISHOP, R. E. D., and HASSAN, A. Y. (1964a): "The lift and drag forces on a circular cylinder in a flowing fluid". Proc. Roy. Soc., Lond., A, 277, pp. 32-50.

BISHOP, R. E. D., and HASSAN, A. Y. (1964b): "The lift and drag forces on a circular cylinder oscillating in a flowing fluid". Proc. Roy. Soc., Lond., A, 277, pp. 51-75.

BLASIUS, H. (1908): "Grenzschichten in Flussigkeiten mit kleiner Reibung". Z. Math. u. Phys., 56, pp. 1-37. (NACA TM 1256 - English translation.)

BLEVINS, R. (1972): "Vortex induced vibration of circular cylindrical structures". Paper presented at ASME's Winter Ann. Gen. Meeting, New York, Nov. 26-30, 1972.

BLEVINS, R. (1975): "Fluid forces induced by vortex shedding". ASME, paper 75-FE-10.

BLEVINS, R. D. (1977): "Flow induced vibrations". Van Nostrand Reinhold Co., New York.

BORGMAN, L. E. (1967): "Spectral analysis of ocean wave forces on piling". J. Waterwyas and Harb., ASCE, 93, WW2, pp. 129-156.

BRAMLEY, M. J. (1970): "On the hydrodynamic damping of a circular cylinder". M.Sc. Thesis, Imperial College, London.

BULLOCK, G. N., STANSBY, P. K., and WARREN, J. G. (1978): "Loading and response of cylinders in waves". 16th Coastal Eng. Conf., Hamburg, Paper 145, pp. 2415-2432.

BURSNALL, W. J., and LOFTIN, L. K. (1951): "Experimental investigation of localized regions of laminar boundary layer separation". Nat. Adv. Comm. Aero., Wash., Tech. Note 2338.

CASTLEMAN, R. A. (1925): NACA Tech. Note No. 231.

CHACKO, E. J., and COLONELL, J. M. (1973): "Laboratory experiments to determine the structural response of a vertical pile subjected to wind-generated water waves". Report for US Office of Naval Research, Report no. AD-759 703.

CHAKRABARTI, S. K., WOLBERT, A. L., and TAM, W. A. (1976): "Wave forces on vertical circular cylinder". J. Waterways and Harb., ASCE, 102, WW2, pp. 203-221.

CHAKRABARTI, S. K. (1978): Discussion of paper "Formation and reversal of vortices around circular cylinders subjected to water waves", by ZDRAVKOVICH, M. M., and NAMORK, J. E. J. Waterways and Harb., ASCE, 104, WW2, pp. 259-260.

CHANG, K. S. (1964): "Transverse forces on cylinders due to vortex shedding in waves". M.Sc. Thesis presented to M.I.T., Cambridge, Mass.

CHAPLIN, J. R. (1973): "Computer model of vortex shedding from a cylinder". J. Hydr. Div. ASCE, 99, HY1, pp. 155-165.

CLEMENTS, R. R. (1973): "An inviscid model of two-dimensional vortex shedding". J. Fluid Mech., 57, pp. 321-336.

COUTANCEAU, M., and BOUARD, R. (1977): "Experimental determination of the main features of the viscous flow in the wake of a cylinder in uniform translation. Part 1. Steady flow". J. Fluid Mech., 79, part 2, pp 231-256.

DAVIES, M. E. (1976): "A comparison of the wake structure of a stationary and oscillating bluff body, using a conditional averaging technique". J. Fluid Mech., 75, pp. 209-231.

DELANEY, N. K., and SORENSEN, N. E. (1953): "Low speed drag of cylinders of various shapes". Nat. Adv. Comm. Aero., Wash., Tech. Note 3038.

DEN HARTOG, J. P. (1954): "Recent technical manifestations of Von Kármán's vortex wake". Proc. Nat. Acad. of Sci., pp. 155-157.

DICKEY, W. L., and WOODRUFF, G. B. (1956): "The vibration of steel stacks". Trans. ASCE, 121, pp. 1051-1054.

DRYDEN, H. L., and HILL, G. C. (1930): "Wind pressure on circular cylinders and chimneys". Bur. Stand. J. Res., Wash., 5, pp. 653-693.

EARLE, E. N., and MANDERY, W. L. (1972): "Determination of dynamic characteristics of offshore platforms from random vibrations". Offshore Tech. Conf., Houston, Texas, Paper OTC 1840, pp. 197-204.

EVERY; M. J. (1978): "Hydroelastic modelling of marine piles". BHRA report RR1459.

FAGE, A., and WARSAP, J. H. (1929): "The effects of turbulence and surface roughness on the drag of circular cylinders". A.R.C. Rep. and Memo. No. 1283.

FAGE, A., and FALKNER, V. M. (1931): "The flow around a circular cylinder". A.R.C., Rep. and Memo, No. 1369.

FENG, C. C. (1968): "The measurement of vortex-induced effects in flow past stationary and oscillating circular and D-section cylinders". M.Sc. Thesis, Univ. British Colombia, 1968.

FERGUSON, N., and PARKINSON, G. V. (1967): "Surface and wake flow phenomena of the vortex excited oscillation of a circular cylinder". J. Eng. Ind., Trans. ASME, Series B, 89, pp. 831-838.

FLACHSBART, O. (1932): "Winddruck auf Gasbehälter". Report of the AVA, Gottingen, IVth series, pp. 136-138.

FOSTER, E. T. (1967): "Predicting wave responses of deep ocean towers". Proc. ASCE conf. on Civ. Eng. in the Oceans, San Fransisco, pp. 75-95.

FUNG, Y. C. (1960): "Fluctuating lift and drag acting on a cylinder in a flow at supercritical Reynolds numbers". J. Aerospace Sci., 27, pp. 801-814.

GARRISON, C. J., FIELD, J. B., and MAY, M. D. (1977): "Drag inertia forces on a cylinder in periodic flow". J. Waterways and Harb., ASCE, 103, WW2, pp. 193-204.

GERLACH, C. R., and DODGE, F. T. (1970): "An engineering approach to tube flow-induced vibrations". Proc. Conf. on Flow Induced Vibrations in Reactor System Components, Argonne Nat. Lab., pp. 205-225.

GERRARD, J. H. (1961): "An experimental investigation of the oscillating lift and drag of a cylinder shedding turbulent vortices". J. Fluid Mech., 11, pp. 244-255.

GERRARD, J. H. (1967): "Numerical computations of the magnitude and frequency of the lift on a circular cylinder". Phil. Trans. Roy. Soc., 261, pp. 137-162.

GERSTEN, K. (1965): "Heat transfer in laminar boundary layers with oscillating outer flows". AGARDograph, 97, pp. 423-

GERWICK, B. S. (1975): "Application of concrete and production caissons to seismic areas". Offshore Tech. Conf., Houston, Texas, Paper OTC 2408, pp. 721-730.

GLASS, R. J. (1970): "A study of the hydroelastic vibrations of spring supported cylinders in a steady fluid stream due to vortex shedding". Ohio Univ. Ada, Proj. No. N.00014-69-C-0148.

GLENNY, D. E. (1966): "A review of flow around circular cylinders, stranded cylinders and struts inclined to the flow direction". Austr. Def. Sci. Services Aero. Res. Lab., Mech. Eng. Note 284.

GOLDSTEIN, S. (1957): "Modern developments in fluid dynamics". Oxford Univ. Press.

GOWDA, B. H. L. (1975): "Some measurements of the phenomenon of vortex shedding and induced vibration of circular cylinders". Technische Universitat Berlin, Report DLR-FB 75-01.

GRASS, A. J., and KEMP, P. H. (1978): "Flow visualization studies of oscillatory flow past smooth and rough circular cylinders". Symp. on Mech. of Wave-Induced Forces on Cylinders, Univ. Bristol, England, Sept. 1978, Paper B2.

GRIFFIN, O. M., SKOP, R. A., and KOOPMANN, G. H. (1973): "The vortex-excited resonant vibration of circular cylinders". J.Sound and Vib., 31, pp. 235-249.

GRIFFIN, O. M., and RAMBERG, S. E. (1974): "The vortex-street wakes of vibrating cylinders". J. Fluid Mech., 66, pp. 553-576.

GRIFFIN, O. M., SKOP, R. A., and RAMBERG, S. E (1975): "The resonant, vortex-excited vibrations of structures and cable systems". Offshore Tech. Conf., Houston, Texas, Paper OTC 2319, pp. 731-741.

GRIFFIN, O. M., and RAMBERG, S. E. (1976): "Vortex shedding from a cylinder vibrating in-line with an incident uniform flow". J. Fluid Mech., 75, part 2, pp. 257-271.

GRIFFIN, O. M. (1978): "Vortex-excited unsteady forces on resonantly vibrating, bluff structures". Naval Research Lab., Washington D.C., Memorandum Report 3820.

GÖTTINGEN (1923): (Experiments on the drag of cylinders). Reports of the AVA, Göttingen, 2, pp. 23-

GÖRTLER, H. (1944): "Verdrängungswirkung der Laminaren Grenzeschicht und Drückwiderstand". Ing. Archiv, 14, pp 286-305.

HARITOS, N., SHARP, B. B., and STEVENS, L. K. (1978): "A study of a simple pile structure in an ocean environment". Symp. on Mech. of Wave-Induced Forces on Cylinders, Univ. of Bristol, England, Paper G3.

HARTLEN, R. T., BAINES, W. D., and CURRIE, I. G. (1968): "Vortex-excited oscillations of a circular cylinder". Univ. Toronto, Dept. Mech. Eng., UT Mech. E TP 6809.

HIEMENZ, K. (1911): "Die Grenzschicht an einem in den gleichförmigen Flüssigkeitsstrom eingetauchten geraden Kreiszylinder".- Göttingen dissertation, 1911. (Also Dinglers, J., 326, pp. 321-324.)

HILL, P. G., and STENNING, A. H. (1960): "Laminar boundary layers in oscillatory flow". J. of Basic Eng., ASME, pp. 593-608.

HOGBEN, N. (1974): "Fluid loading on offshore structures, a state of art appraisal: Wave loads". Maritime Tech. Monograph, No. 1, Roy. Inst. of Nav. Arch.

HOMANN, F. (1936): "Einfluss grosser Zähigkeit bei Strömung um Zylinder". Forschg. Ing. - Wes., 7, 1-10.

HORI, E. (1961): "Unsteady boundary layers. (1st Report, Theory of the boundary layer on a symmetrical body in a fluctuating main stream.)". Bull. of JSME, 4, No. 16, pp. 664-671.

HORI, E. (1962a): "Unsteady boundary layers. (2nd Report, Flow around a body with a fluctuating circulation.)". Bull. of JSME, 5, No. 17, pp. 57-64.

HORI, E. (1962b): "Unsteady boundary layers. (3rd Report, Boundary layer on a circular cylinder in rotational oscillation.)" Bull. of JSME, 5, No. 17, pp. 64-72.

HORI, E. (1962c): "Unsteady boundary layers. (4th Report, Calculation of boundary layer around a body with arbitrary shape by use of a series expansion method.)". Bull. of JSME, 5, No. 19, pp. 461-470.

HUMPHREYS, J. S. (1960): "On a circular cylinder in a steady wind at transcritical Reynolds numbers". J. Fluid Mech., 9, pp. 603-612.

ISAACSON, M.de St.Q. (1974): "The forces on circular cylinders in waves". Ph. D. Thesis, Cambridge Univ., England.

ISAACSON, M.de St.Q., and MAULL, D. J. (1976): "Transverse forces on vertical cylinders in waves". J. Waterways and Harb., ASCE, 102, WW1, pp. 49-60.

IVERSEN, H. W., and BALENT, R. (1951): "A correlating modulus for fluid resistance in accelerated motion". J. Appl. Phys., 22, pp. 324-328.

IWAGAKI, Y., and ISHIDA, H. (1974): "Laminar boundary layer around a circular cylinder under oscillatory waves". Proc. 14th Coastal Eng. Conf., pp. 1848-1862.

IWAGAKI, Y., and ISHIDA, H. (1976): "Flow separation, wake vortices and pressure distribution around a circular cylinder under oscillatory waves". 16th Coastal Eng. Conf., pp. 2341-2356.

JONES, G. W. (1969): "Unsteady lift forces generated by vortex shedding about a large, stationary, and oscillating cylinder at high Reynolds numbers". ASME paper 68-FE-36.

KÁRMÁN, Th.v. (1911): "Über den Mechanismus des Widerstandes, den ein bewegter Körper in einer Flüssigkeit erzeugt". Nachr. Ges. Wiss.Göttingen, Math-phys. Kl., pp. 509-517, and 547-556 (1912). Also Coll. Works I, 324-338.

KAWAGUTI, M. (1953): "Discontinuous flow past a circular cylinder". J. Phys. Soc. Japan, 8, pp. 403-406.

KELLER, H. B., and TAKAMI, H. (1966): "Numerical studies of steady viscous flow about cylinders". Proc. Symp. on Num. Solution of Non-linear Differential Equation (Univ. Wisconsin).

KEULEGAN, G. H., and CARPENTER, L. H. (1958): "Forces on cylinders and plates in an oscillating fluid". J. Res., Nat. Bureau Standards, 60, No. 5, pp. 423-440.

KING, R., PROSSER, M. J., and JOHNS, D. J. (1973): "On vortex excitation of model piles in water". J. Sound and Vibration, 29, part 2, pp. 169-188.

KING, R. (1974): "Vortex excited structural oscillations of a circular cylinder in flowing water". Ph.D. Thesis, submitted to Loughborough University, England.

KING, R. (1975): "An investigation of the criteria controlling the sustaining self-excited oscillations of cylinders in flowing water". Paper presented 4th Bienniel Symp. on Turbulence in Liquids, Univ. of Missouri-Rolla, USA. Sept. 1975.

KING, R., and EVERY, M. J. (1976): "Hydroelastic model tests of two tripod structures for an ore terminal". B.H.R.A. Report 1357.

KING, R. (1977): "A review of vortex shedding research and its application". Ocean Eng., 4, pp. 141-171.

KO, S. C., and GRAF, W. H. (1972): "Drag coefficient of cylinders in turbulent flow". J. Hydr. Div., ASCE, 98, HY5, pp. 897-912.

KOOPMANN, G. H. (1967): "The vortex wakes of vibrating cylinders at low Reynolds numbers". J. Fluid Mech., 28, pp. 501-512.

KOVASZNAY, L. S. G. (1949): "Hot wire investigation of the wake behind cylinders at low Reynolds numbers". Proc. Roy. Soc., A, 198, No. 1053, pp. 174-190.

LAIRD, A. D. K., JOHNSON, C. A., and WALKER, R. W. (1959): "Water forces on accelerated cylinders". J. Waterways and Harb., ASCE, 85, WW, pp. 99-119.

LAIRD, A. D. K. (1962): "Water forces on flexible oscillating cylinders". J. Waterways and Harb., ASCE, 88, WW3, pp. 125-135.

LAIRD, A. D. K. (1971): "Eddy formation behind circular cylinders". J. Hydr. Div., ASCE, 97, HY6, pp. 763-775.

LAM, S. H., and ROTT, N. (1960): "Theory of linearized time-dependent boundary layers". Cornell Univ., GSAE Report, AFOSR TN-60-1100.

LAMB, Sir H. (1945): "Hydrodynamics". 6th ed., Dover Publications, New York.

LIGHTHILL, M. J. (1954): "The response of laminar skin friction and heat transfer to fluctuations in the stream velocity". Proc. Roy. Soc., London, A, 224, pp. 1-23.

LIN, C. C. (1956): "Motion in the boundary layer with a rapidly oscillating external flow". 9th Int. Cong. of Appl. Mech., Univ. of Brussels, Sept. 1956.

LØKEN, A. E., TORSET, O. P., MATHIASSEN, S., and ARNESEN, T. (1979): "Aspects of hydrodynamic loading in design of production risers". Offshore Tech. Conf., Houston, Texas, Paper OTC 3538, pp. 1591-1601.

MAIR, W. A., and MAULL, D. J. (1971): "Bluff bodies and vortex shedding - a report on Euromech 17". J. Fluid Mech., 45, pp. 209-224.

MALHOTRA, A. K., and PENZIEN, J. (1970): "Nondeterministic analysis of offshore structures". J. Eng. Mech., ASCE, 96, EM6, pp. 985-

MARRIS, A. W. (1962): "A review of vortex streets, periodic wakes and induced vibration phenomena". ASME, paper 62-WA-106.

MATTEN, R. B. (1976): "Calculation of drag forces on a circular cylinder in a combined plane oscillatory and uniform flow field using Morison's equation". N.M.I., Draft Report, April 1976.

MATTEN, R. B. (1977): "The influence of surface roughness upon the drag of circular cylinders in waves". Offshore Tech. Conf., Houston, Texas. Paper OTC 2902, pp. 185-192.

MAULL, D. J., and MILLINER, M. G. (1978): "Sinusoidal flow past a circular cylinder". Coastal Engineering, 2, pp. 149-168.

McCROSKEY, W. J. (1977): "Some current research in unsteady fluid dynamics". J. Fluid Eng., ASME, 99, pp. 8-39.

McGREGOR, D. M. (1957): "An experimental investigation of the oscillating pressure on a circular cylinder in a fluid stream". Toronto Univ. Inst. Aerophys., Tech. Note No. 14.

MEIER-WINDHORST, A. (1939): "Flutter-vibrations of cylinders in steady flow". Mitt. des Hydr.Inst. des Technischen Hochschule, Munchen, 9. (In German.)

MERCIER, J. A. (1973): "Large amplitude oscillations of a circular cylinder in a low-speed stream". Ph. D. Thesis, Stevens Inst. of Tech., Hoboken, N. J.

MILLER, B. L., and MATTEN, R. B. (1976): "A technique for the analysis of wave loading data obtained from model tests". N.M.I. Report R 136.

MILLER, B. L. (1977): "The hydrodynamic drag of roughened circular cylinders". Reprint of paper presented at the RINA, April 8th, 1976, (with additional comments). N.M.I. Report R 13.

MOE, G., and VERLEY, R. L. P. (1978): "An investigation into the hydrodynamic damping of cylinders oscillated in steady currents of various velocities". River and Harbour Lab. Report STF60 A78049 ISBN. 82-595-1538-5.

MOORE, F. K. (1951): "Unsteady laminar boundary-layer flow". NACA Report TN 2471.

MOORE, F. K. (1957a): "Aerodynamic effects of boundary layer unsteadiness". Paper presented at 6th Anglo-American Aero. Conf.

MOORE, F. K. (1957b): "On the separation of the unsteady boundary layer". Paper presented at IUTAM Symp. on Boundary-layer Research, Freiburg, August 1957.

MORISON, J. R., O'BRIEN, M. P., and SCHAAF, S. A. (1950): "The forces exerted by surface waves on piles". Petroleum Trans., AIME, 189, pp. 149-154.

MORISON, J. R. (1951): "The design of piling". Proc. 1st Conf. Coastal Eng., pp. 254-258.

MORISON, J. R., JOHNSON, J. W., and O'BRIEN; M. P. (1954): "Experimental studies of forces on piles". Proc. 4th Conf. on Coastal Eng., pp. 340-370.

MORKOVIN, M. V. (1964): "Flow around a cylinder - A kaleidoscope of challenging fluid phenomena". ASME, Symp. Fully Separated Flows, Philadelphia, pp. 102-118.

NAVIER, C. L. M. H. (1827): "Mémoire sur les lois du mouvement des fluides". Mém. Acad. R. Sci., Paris, 6, pp. 389-416.

NOVAK, M., and TANAKA, H. (1975): "Pressure correlations on a vibrating cylinder". Proc. 4th Int. Conf. on Wind Effects on Buildings and Structures, ed. EATON, K. J., Cambridge Univ. Press, pp. 227-232 and p. 273.

OSEEN, C. W. (1911): Ark. f. Mat. Astr. og Fys., 7, No. 29.

PAGON, W. W. (1934): "What aerodynamics can teach the civil engineer". Part I. Eng. News Record, p. 348 (Mar. 1934). Part II. Eng. News Record, p. 41 (Jul. 1934).

PEDLEY, T. J. (1972): "Two-dimensional boundary layers in a free stream which oscillates without reversing". J. Fluid Mech., 55, part 2, pp. 359-383.

PENZIEN, J. (1975): "Seismic analysis of platform-structure-foundation systems". Offshore Tech. Conf., Houston, Texas. Paper OTC 2352, pp. 153-166, May 1975.

PETRAUSKAS, C. (1976): "Hydrodynamic damping and "Added Mass" for flexible offshore platforms". US Corps of Eng., Coast. Eng. Res. Center, Tech. Paper 76-18.

POISSON, S. D. (1831): "Mémoir sur les équations générales de l'équilibre et du mouvement des corps solides élastiques et les fluides". J. Ec. Polytech., Paris, 13, pp. 139-186.

PRANDTL, L. (1904): "Über Flüssigkeitsbewegung bei sehr kleiner Reibung". Verh. Int. Math. Kongr., 3rd, Heidelberg, 1904, pp. 484-91. Also Coll. Works, II, 575-584. (Also NACA Memo No. 452, 1928 - in English.)

PRADTL, L. (1914): "Der Luftwiderstand von Kugeln". Nachr. Ges. Wiss. Göttingen, Math.-phys. Kl., pp. 177-190. (Also Coll. Works, II, 597-608 - in English.)

RAMBERG, S. E., and GRIFFIN, O. M. (1974): "Vortex formation in the wake of a vibrating, flexible cable". J. of Fluids Eng., ASME, 96, pp. 317-322.

RAMBERG, S. E., and GRIFFIN, O. M. (1976): "Velocity correlation and vortex spacing in the wake of a vibrating cable". J. of Fluids Eng., ASME, 98, pp. 10-18.

RAMBERG, S. E., and NIEDZWECKI, J. M. (1979): "Some uncertainties and errors in wave force computations". Offshore Tech. Conf., Houston, Texas, Paper OTC 3597, pp. 2091-2102.

RANCE, P. J. (1969): "Wave forces on cylindrical members of structures". Hydr. Res. Station, Wallingford, Ann. Report.

RAYLEIGH, LORD (1879): "The Aeolian harp". Sc. Papers, 1, pp. 413-414.

RELF, E. F., and SIMMONS, L. F. S. (1924): "The frequency of eddies generated by the motion of circular cylinders through a fluid". A.R.C., Rep. and Memo, No. 917.

REYNOLDS, O. (1883): "An experimental investigation of the circumstances which determine whether the motion of water shall be direct or sinuous, and of the law of resistance in parallel channels". Phil. Trans. Roy. Soc., 174, pp. 935-982. (Also Papers on Mech. and Phys. Subjects, 2, 51- .)

ROSENHEAD, L. (1931): "The formation of vortices from a surface of discontinuity". Proc. Roy. Soc., A, 134, pp. 170-

ROSHKO, A. (1955): "On the development of turbulent wakes from vortex streets". NACA Tech. Note TN 1191.

ROSHKO, A. (1961): "Experiments on the flow past a cylinder at very high Reynolds numbers". J. Fluid Mech., 10, pp. 345-351.

ROSHKO, A., and FISZDON, W. (1969): "On the persistence of the transition in the near wake". Prob. of Hydrodyn. and Continuum Mech., Soc. Ind. and Appl. Math., Phil., pp. 606-616.

ROSHKO, A. (1970): "On the aerodynamic drag of cylinders at high Reynolds numbers". Paper at US Japan Research Seminar on Wind Loads on Structures, Univ. of Hawaii.

ROTT, N., and ROSENZWEIG, M. L. (1960): "On the response of the laminar boundary layer to small fluctuations of the free-stream velocity". J. Aerospace Sci., 27, pp. 741-747, 787.

ROTT, N. (1964): "Theory of time-dependent laminar flows". In Theory of Laminar Flows, F. K. Moore (Ed.), Princeton Univ. Press, 1964.

RUBACH, H. (1914): "Über die Entstehung und Fortbewegung des Wirbelpaares bei zylindrischen Körpern". Göttingen dissertation, (Also VDI-Forschungsheft 185 (1916).)

SAINT-VENANT, B. (1843): "Note à joindre un mémoir sur la dynamique des fluides". C. R. Acad. Sci., Paris, Ser. A, 17, pp. 1240-44.

SARPKAYA, T. (1963a): "Lift, drag and added-mass coefficients for a circular cylinder in a time dependent flow". J. Appl. Mech., ASME, Series E, pp. 13-15.

SARPKAYA, T. (1963b): "Vortex formation and resistance in unsteady flow". J. Appl. Mech., ASME, Series E, pp. 16-24.

SARPKAYA, T. (1966): "Separated flow about lifting bodies and impulsive flow about cylinders". AIAA Journal, 4, No. 3, pp. 414-420.

SARPKAYA, T. (1968): "An analytic study of separated flow about circular cylinders". ASME, J. Basic. Eng., 90, pp. 511-520.

SARPKAYA, T., and TUTER, O. (1974): "Periodic flow about bluff bodies, Part I: Forces on cylinders and spheres in a sinusoidally oscillating fluid". Naval Postgrad. School, Monterey, Report NPS-59 SL 74091.

SARPKAYA, T. (1975): "Forces on cylinders and spheres in a sinusoidally oscillating fluid". J. App. Mech., ASME, 42, No. 1, pp. 32-37.

SARPKAYA, T. (1976a): "Vortex shedding and resistance in harmonic flow about smooth and rough circular cylinders at high Reynolds numbers". Naval Postgrad. School, Monterey, Report NPS-59 SL 76021, Feb. 1976.

SARPKAYA, T. (1976b): "In-line and transverse forces on smooth and sand-roughened cylinders in oscillatory flow at high Reynolds numbers". Naval Postgrad. School, Monterey, Report NPS-69 SL 76062, June 1976.

SARPKAYA, T. (1978): "Fluid forces on oscillating cylinders". J. Waterways and Harb., ASCE, 104, WW4, 1978, pp. 275-290.

SARPKAYA, T. (1979): "Vortex induced oscillations - a selective review". J. Appl. Mech., ASME, 46, pp. 241-258.

SARPKAYA, T., and SHOAFF, R. L. (1979a): "An inviscid model of two-dimensional vortex shedding for transient and asymptotically steady separated flow over a cylinder". AIAA 17th Aerospace Sci. Meeting, New Orleans, Paper No. 79-0281, Jan. 15th-17th, 1979.

SARPKAYA, T., and SHOAFF, R. L. (1979b): "A discrete vortex analysis of flow about stationary and transversely oscillating circular cylinders". Naval Postgrad. School, Monterey, Tech. Report No. NPS-69SL79011.

SARPKAYA, T., and RAJABI, F. (1979): "Dynamic response of piles to vortex shedding in oscillating flows". Offshore Tech. Conf., Houston, Texas, Paper OTC 3647, pp. 2523-2528.

SAWARAGI, T., NAKAMURA, T., and KITA, H. (1976): "Characteristics of lift forces on a circular pile in waves". Coastal Eng. in Japan, 19, pp. 59-71.

SAWARAGI, T., TAKAYUKI, N., and MIKI, H. (1977): "Dynamic behaviour of a circular pile due to eddy shedding in waves". Coastal Eng. in Japan, 20, pp. 109-120.

SAWARAGI, I., and NAKAMURA, T. (1978): "Dynamic behaviour of vertical cylinder due to wave force". 16th Coastal Eng. Conf., Hamburg, Paper 143, pp. 2378-2396.

SCHILLER, L., and LINKE, W. (1933): "Druck und Reibungswiderstand des Zylinders bei Reynoldsschen Zahlen 500 bis 40000". Zeitschr. f. Flugtechn. u. Motorluftschiffahrt, 24, pp. 193-198.

SCHLICHTING, H. (1979): "Boundary layer Theory (7th Edition)". McGraw-Hill Book Co.

SCHMIDT, L. V. (1966): "Fluctuating force measurements upon a circular cylinder at Reynolds numbers up to $5x10^6$". Meeting on Ground Wind Load Problems in Relation to Launch Vehicles, NASA Langley Res. Center.

SCHUBAUER, G. (1937): "The effect of turbulence on the transition in the boundary layer of an elliptic cylinder". Proc. 5th Int. Conf. on Fluid Mech.

SCHWABE, M. (1935): "Über Druckermittlung in der instationären ebenen Strömung". Ing.-Arch., 6, pp. 34-50. (Also NACA, Tech. Note No. 1039 (1943), in English.)

SKOP, R. A., and GRIFFIN, O. M. (1973): "A model for the vortex-excited response of bluff cylinders". J. Sound and Vib., 27, pp. 225-233.

SKOP, R. A., and GRIFFIN, O. M. (1974): "On a theory for the vortex-excited oscillations of flexible cylindrical structures". J. Sound and Vib., 41, pp. 263-274.

SKOP, R. A., RAMBERG, S. E., and FERER, K. M. (1976): "Added mass and damping forces on circular cylinders". ASME paper 76-PET-3.

STANSBY, P. K. (1974): "The effects of end plates on the base pressure coefficient of a circular cylinder". Aeronautical Journal, pp. 36-37, Jan. 1974.

STANSBY, P. K. (1976): "Base pressure of oscillating circular cylinders". J. Eng. Mech., ASCE, 102, EM4, pp. 591-600.

STANSBY, P. K. (1977): "An inviscid model of vortex shedding from a circular cylinder in steady and oscillating far flows". Proc. Inst. Civ. Eng., part 2, 63, pp. 865-880.

STANSBY, P. K. (1978): "Fluid loading and the discrete vortex model". Fluid Mech. in Underwater Tech.: The University Contribution. One day Seminar, Soc. Underwater Tech., Jan 1978.

STEWARTSON, K. (1951): "On the impulsive motion of a flat plate in a viscous fluid". Quart. J. of Mech. and Appl. Math., 4, pp. 182-198.

STOKES, G. G. (1845): "On the theories of internal friction of fluid in motion". Trans. Cambridge Philos. Soc., 8, pp. 287-305. (Also Math. and Phys. papers, 1, pp. 75- .)

STOKES, G. G. (1851): "On the effect of the internal friction of fluids on the motion of pendulums". Trans. Cambridge Phil. Soc., 9, (II), pp. 8-106.

STOKES, G. G. (1901): "On the motion of bodies through viscous liquids". Math. and Phys. Papers, Cambridge Univ. Press, 1880-1905. 3, pp. 1-141.

STROUHAL, V. (1878): "About a special type of excitation". Ann. d. Physik und Chemie, 3rd Series, 5, pp. 216-251. (In German.)

STUART, J. T., and WOODGATE, L. (1955): "Experimental study of aerodynamic damping on a vibrating circular cylinder". Phil. Mag., 26, No. 372, pp. 40-46.

SURREY, D. (1969): "The effect of high intensity turbulence on the aerodynamics of a rigid circular cylinder at subcritical Reynolds numbers". UTIAS Report 142.

SUSBIELLES, G. G. (1971): "Wave forces on pile sections due to irregular and regular waves". Offshore Tech. Conf., Houston, Paper OTC 1006.

SZECHENYI, E. (1975): "Supercritical Reynolds number simulation for two dimensional flow over circular cylinders". J. Fluid Mech., 70, pp. 529-542.

TANEDA, S. (1956): "Experimental investigation of the wakes behind cylinders and plates at low Reynolds numbers". J. Phys. Soc. Japan, 11, pp. 302-307.

TANI, I. (1977): "History of boundary layer theory". Ann. Rev. of Fluid Mech., Vol. 9, pp. 87-112.

TATSUNO, M., and TANEDA, S. (1971): "Visualization of the unsteady flow past cylinders and plates decelerated from a steady speed". J. Phys. Soc. Japan, 31, NO. 4, pp. 1266-1274.

TATSUNO, M. (1972): "On the vortex street behind a cylinder vibrating in the flow direction". Bull. Res. Inst. Appl. Mech., Kyushu Univ., 36, pp. 25-37 (In Japanese).

TAYLOR, G. I. (1936): "Statistical theory of turbulence - Part V, Effect of turbulence on boundary layers". Proc. Roy. Soc., London, A, 156, pp. 307-317. (Also Scientific Papers, II, pp. 356-364.)

THIRRIOT, C., LONGREE, W. D., and BARTHET, H. (1971): "Sur la perte de charge due à un obstacle en mouvement periodique". Proc. 14th Congress, IAHR, pp. B2-1-B2-8.

THOM, A. (1929): "The laminar boundary layer of the front part of a cylinder". ARC, Rep. and Mem., No. 1194.

THOM, A. (1933): "Flow past circular cylinders at low speed". Proc. Roy. Soc., A, 141, pp. 651-669.

TOEBES, G. H. (1969): "The unsteady flow and wake near an oscillating cylinder". J. Basic Eng., ASME, 91, pp. 493-502.

TRITTON, D. J. (1959): "Experiments on the flow past a cylinder at low Reynolds numbers". J. Fluid Mech., 6, pp. 547-567.

VERLEY, R. L. P. (1975a): "1st progress report on the investigation into the vibrations of conductor tubes". BHRA draft report, April 1975.

VERLEY, R. L. P. (1975b): "Study of wave forces on conductor tubes. Report on Stage 1 of Contract K/A72B/568/CB/A72B". BHRA draft report, August 1975.

VERLEY, R. L. P. (1976): "Progress report on the second stage of an investigation into the vibration of conductor tubes". BHRA draft report, July 1976.

VERLEY, R. L. P. (1977a): "On the estimation of drag and inertia coefficients for smooth and rough cylinders in steady currents and in waves for values of Keulegan-Carpenter number greater than 10 and Reynolds numbers above critical". VHL Note, 602284/RV/RWF, April 1977.

VERLEY, R. L. P. (1977b): "Proposal for a number of experiments to investigate the phenomenon of hydrodynamic damping". VHL internal note RV/AS, 7th March 1977.

VERLEY, R. L. P. (1977c): "The use of relative velocities in Morison's equation leads to "Hydrodynamic Damping". Is this reasonable?". Talk given at ARAE Meeting on Wave effects on small bodies, Paris, 8th Nov. 1977.

VERLEY, R. L. P., and EVERY, M. J. (1977): "Wave induced vibrations of flexible cylinders". Offshore Tech. Conf., Houston, Texas, Paper OTC 2899, pp. 167-174.

VERLEY, R. L. P. (1978a): "Oscillations of a cylinder in still water".
River and Harbour Lab. Report STF60 A78046 ISBN 82-595-1536-9.

VERLEY, R. L. P. (1978b): "An experimental investigation into hydrodynamic damping in waves".
BHRA report TN 1492, Sept. 1978.

VERLEY, R. L. P., and EVERY, M. J. (1978): "An investigation into the vibration of conductor tubes".
BHRA report RR 1392, April 1978.

VERLEY, R. L. P., and MOE, G. (1978): "The effect of cylinder vibration on the drag force and the resultant hydrodynamic damping".
Paper I5, IAHR Symp. on Mech. of Wave induced Forces on Cylinders, Bristol, Sept. 1978.

VERLEY, R. L. P., and MOE, G. (1979a): "The forces on a cylinder oscillating in a current (Applications: Combined wave and current loading. Hydrodynamic damping of vibration)".
River and Harbour Lab. Report STF60 A79061 ISBN 82-595-1885-6.

VERLEY, R. L. P., and MOE, G. (1979b): "Steady and oscillatory forces on a cylinder oscillating in-line with a steady current".
Paper presented to IAHR Symp. on Vortex shedding from Bluff Bodies in Oscillatory flow. Imperial College, London, July 1979.

VICKERY, B. J., and WATKINS, R. D. (1962): "Flow-induced vibrations of cylindrical structures".
Proc. 1st Australian Conf., Univ. Western Australia.

VUGTS, J. H., and HAYES, D. J. (1979): "Dynamic analysis of fixed offshore structures: A review of some basic aspects of the problem". Eng. Struct., 1, pp. 114-120, April 1979.

WATSON, J. (1958): "A solution of the Navier-Stokes equations illustrating the response of a laminar boundary layer to a given change in the external stream velocity". Quart. J. of Mech. and Appl. Math., 11, Pt. 3, pp. 302-325.

WIEGEL, R. L., BEEBE, K. E., and MOON, J. (1957): "Ocean wave forces on circular cylindrical piles". J. Hydr. Div., ASCE, 83, HY2, April 1957, pp. 1-34.

WIEGEL, R. L. (1964): "Oceanographical Engineering". Prentice-Hall, 1964.

WIEGEL, R. L. (1972): "Ocean wave spectra, eddies, and structural response". IUTAM-IAHR Symp. on Flow-Induced Structural Vibrations, Karlsruhe. Ed. E. Naudascher, pp. 531-573.

WIESELSBERGER, C. (1921): "Neuere Feststellungen über die Gesetze des Flüssigkeits - und Luftwiderstands". Phys. Z, 22, pp. 321-328.

WILLIAMS, R. E., and HUSSEY, R. G. (1972): "Oscillating cylinders and the Stokes' paradox". Phys. of Fluids, 15, No. 12, pp. 2083-2088.

WOOTTON, L. R. (1969): "The flow induced oscillations of piles".
NPL Aero Special Report 025.

WOOTTON, L. R., WARNER, R. M., SAINSBURY, R. M., and COOPER, D. H. (1972): "Oscillations of piles in marine structures".
CIRIA, England, Report 40.

YAMAMOTO, T., and NATH, J. H. (1976): "High Reynolds number oscillating flow by cylinders".
15th Coastal Eng. Conf., Hawaii, July 1976, Chapter 136, pp. 2321-2340.

ZDRAVKOVICH, M. M., and NAMORK, J. E. (1977): "Formation and reversal of vortices around circular cylinders subjected to water waves".
J. Waterways and Harb., ASCE, 103, WW3, pp. 378-383.

APPENDIX 1

SCHEME OF THE VARIOUS COMPUTER PROGRAMS

Program 1 - Digitization

Standard VHL program for digitization of signals. The tape recorded signals from the experiments are calibrated, digitized and stored on disk in a standard format file for later access by other programs.

Program 2 - Calculates the damping and the steady component of force for the rig, with or without a cylinder attached, as a function of x_o/D

i) Start at beginning of data file (largest amplitude, x_o).
Calculate amplitudes of all maxima and minima of motion.

ii) Go back to beginning.
Start at largest amplitude.
Go down progressively ~ 7%, noting exact amplitude and how many cycles between these.

iii) From these calculate damping between one amplitude maximum and the next but two (i.e. ~ 20% down in amp.).
Calculate amplitude of motion ½ way between these.

iv) From forces integrate to find average force between one amplitude maximum and the next but two (i.e. same range as in iii).

v) Find a curve fit equation of order n(from 8-18) for

i) Damping versus x_o/D

ii) Force versus x_o/D

(For no cylinder D is given the value .0252.)

vi) Store and write out to terminal

i) Experimental data (Temperature, D, n, etc.)

ii) Curve fit equation coefficients

iii) Values of Damping and Forces at 24 particular values of x_o/D, calculated from the curve fit coefficients

iv) Actual Damping and Forces versus x_o/D.

Program 3

Calculates the various time-averaged oscillatory and steady drag coefficients. Uses as input 2 files made by Program 2 - one for a test with a cylinder and the other for a test with no cylinder in the same velocity of flow.

i) From data file for no cylinder

Read curve fit equations of damping and forces versus x_o/D.
Correct to give equations for damping and force as a function of amplitude, x_o.

ii) From cylinder data file

For all amplitudes, both curve fitted and actual, calculate the various steady and oscillatory drag coefficients, and the various parameters to be plotted against.

iii) Write out data to the line printer and store for plotting.

Program 4

Calculates CDIND and CM from time histories of force.

i) Open data file.
Ask if test is with cylinder or without.

ii) If with, then

Read from previous analysed no cylinder data file the coefficients of the curve fit equations for CDIND and CM as functions of x_o/D - correct to give them as functions of x_o.

If without, then

Set no cylinder CDIND′ and CM curve fit coefficients to 0.

iii) Start at beginning of data file.
From position time history find zero crossing points.
Integrate over each cycle the forces to give CDIND′ and CM.

iv) Subtract CDIND′ and CM for no cylinder at each amplitude.

v) Take averages of CDIND′ and CM over 2% ranges of amplitude.

vi) Curve fit CDIND′ and CM versus x_o/D and calculate for 24 given values of x_o/D.

vii) Write out to file and print to line printer:
Test data (Temperature, D, n, etc.)
Curve fit equation coefficients.
Curve fitted points of CDIND′ and CM versus x_o/D.
Actual values of CDIND′ and CM versus x_o/D.

Program 5 - Plotting program

i) Choose x-axis wanted (x_o/D, V/nD, $V/\dot{x}_o$).

ii) Choose y-axis wanted (The various steady and oscillatory coefficients).

iii) Choose data file to be plotted.

iv) Plot Any combination of the following

a) Actual points

b) Predicted points

c) Line through predicted points

d) Write test data below

Go back to iii) or stop.

APPENDIX 2

DRAG COEFFICIENTS FROM THE VARIOUS FORMULAE

A2.1. Derivation of the time-averaged oscillatory drag coefficients

The relevant equations for the drag force are:

$$f = .5\rho\ D\ C_{D3}(t)\ (V-\dot{x})|(V-\dot{x})| \qquad (1')$$

$$f = .5\rho\ D\ C_{D1}(t)\ V^2 - .5\rho\ D\ C_{D2}(t)\ \dot{x}|\dot{x}| \qquad (2')$$

The time averaged oscillatory drag coefficient obtained from (1') will be called CDDEP.

The time averaged oscillatory drag coefficient obtained from (2') will be called CDIND.

The method used to obtain the time averaged coefficients is to equate the work done represented by the damping due to separation effects on the cylinder, $\bar{c}_{press}$, to the work done represented by (1') or (2'), i.e.

$$\bar{c}_{press} = \frac{\int_0^T f\dot{x}\ dt}{\int_0^T \dot{x}^2\ dt} \qquad (3')$$

where f is given by equation (1') and (2') to yield respectively CDDEP and CDIND.

The integrations of (3') are conducted below.

From equation (2')

$$\bar{c}_{press} = \frac{\int f\ \dot{x}\ dt}{\int \dot{x}^2\ dt} = - \frac{\cdot 5\rho\ D\ \ CDIND \int \dot{x}^2 |\dot{x}|\ dt}{\int \dot{x}^2\ dt}$$

Now

$$\dot{x}^2|\dot{x}| = \dot{x}^3$$

$$\int \dot{x}^2\ dt = 2\pi^2\ nx_o^2$$

defining $\dot{x} = \dot{x}_o\ \sin(\frac{2\pi t}{T})$

then $\cdot 5\rho\ D(CDIND)\int_o^T \dot{x}^3\ dt = \cdot 5\rho\ D(CDIND)\dot{x}_o^3 \int_o^{T/2} \sin^3(\frac{2\pi t}{T})dt$

$$= \rho\ D(CDIND)\dot{x}_o^3 \int_o^{T/2} [3/4\ \sin(\frac{2\pi t}{T}) - \frac{1}{4}\ \sin(\frac{6\pi t}{T})]dt$$

Evaluating the integral

$$= \frac{2\rho D(CDIND)\dot{x}_o^3}{3n\pi}$$

$$\therefore \bar{c}_{press} = - \frac{\rho D(CDIND)\dot{x}_o^3}{3n^2\pi^3 x_o^2}$$

rearranging yields

$$CDIND = \frac{-3\ \bar{c}_{press}}{8n\rho D x_o} \qquad (4')$$

From equation 1'

Rewriting (1') as

$$f = k_D\ (V-\dot{x})|(V-\dot{x})|$$

where $k_D = \cdot 5\rho D(CDDEP)$, and CDDEP is the time average value of C_D (t) in (1').

Let $\dot{x} = \dot{x}_o \cos 2\pi nt$

Separate integrations must be conducted depending on whether $|V| \geq \dot{x}_o$ or $|V| < \dot{x}_o$. Let us for convenience choose a coordinate system so that V is positive. Then

<u>If $V \geq \dot{x}_o$</u>

$$\int f\dot{x}dt = -2k_D \int_o^{T/2} (V^2 - 2V\dot{x} + \dot{x}^2)\, \dot{x}dt$$

$$= -2k_D \left[\dot{x}_o V^2 \int_o^{T/2} \cos(2\pi nt)dt - 2V\dot{x}_o^2 \int_o^{T/2} \cos^2(2\pi nt)dt + \dot{x}_o^3 \int_o^{T/2} \cos^3(2\pi nt)dt \right]$$

Since the former and the latter integrands are symmetric functions they integrate to zero and all that remains is the middle integral which yields

$$+k_D 2V\dot{x}_o^2 \left[t + \frac{1}{4\pi n} \sin(2\pi nt) \right]_o^{T/2}$$

$$= \frac{-k_D V \dot{x}_o^2}{n}$$

$$\bar{c}_{press} = \frac{-k_D V \dot{x}_o^2}{n} \cdot \frac{1}{2\pi^2 n\, x_o^2} = -2k_D V$$

<u>Rearranging yields</u> $CDDEP = \frac{-\bar{c}_{press}}{\rho V D}$ ———

which can be written as:

$$CDDEP = \frac{-\bar{c}_{press} \dot{x}_o}{.5 \rho D \dot{x}_o^2 B}$$

-(5')

(for $V \geq \dot{x}_o$)

where $B = 2a$

and $a = V/\dot{x}_o$

If $V<\dot{x}_o$

When $V\geq\dot{x}$ $|(V-\dot{x})|$ is $V-\dot{x}$

$V<\dot{x}$ $|(V-\dot{x})|$ is $-(V-\dot{x})$

The integration $\int f\dot{x}dt$ in (3') must be carried out in two parts, according to the above.

For $\dot{x} = \dot{x}_o \cos 2\pi nt$

$$\int f\dot{x}dt = -2k_D\int_o^{t_1}(V^2-2V\dot{x}+\dot{x}^2)\dot{x}dt+2k_D\int_{t_1}^{T/2}(V^2-2V\dot{x}+\dot{x}^2)\dot{x}dt \quad \text{—(6')}$$

t_1 is given by $V = \dot{x}_o \cos 2\pi nt_1$, or

$$t_1 = \frac{1}{2\pi n}\ \text{Arc}\ \cos\left(\frac{V}{\dot{x}_o}\right) \qquad \text{——————} \quad (7')$$

(6') can be rewritten

$$\int f\dot{x}dt = w1 + w2 + w3$$

where

$$w1 = -2k_D\int_o^{t_1} V^2\,\dot{x}dt + 2k_D\int_{t_1}^{T/2} V^2\dot{x}dt$$

$$w2 = 4k_D\int_o^{t_1} V\dot{x}^2dt - 4k_D\int_{t_1}^{T/2} V\dot{x}^2dt$$

$$w3 = -2k_D\int_o^{t_1} \dot{x}^3dt + 2k_D\int_{t_1}^{T/2} \dot{x}^3dt$$

Evaluating w1, w2 and w3.

<u>w1</u>

$$w1 = 2k_D V\dot{x}_o^2\left[-\int_o^{t_1}\cos(2\pi nt)dt + \int_{t_1}^{T/2}\cos(2\pi nt)dt\right]$$

$$= 2k_D V^2 x_o\left[-\left[\sin(2\pi nt)\right]_o^{t_1} + \left[\sin(2\pi nt)\right]_{t_1}^{T/2}\right]$$

$$\therefore w1 = -4k_D V^2 x_o \sin(2\pi n t_1)$$

<u>w2</u>

$$w2 = 4k_D V\dot{x}_o^2\left[\int_o^{t_1}\cos^2(2\pi nt)dt - \int_{t_1}^{T/2}\cos^2(2\pi nt)dt\right]$$

$$= 4k_D V\dot{x}_o^2\left[\int_o^{t_1}\left[\tfrac{1}{2}+\tfrac{1}{2}\cos(4\pi nt)\right]dt - \int_{t_1}^{T/2}\left[\tfrac{1}{2}+\tfrac{1}{2}\cos(4\pi nt)\right]dt\right]$$

$$=4k_D V\dot{x}_o^2\left[\left[t/2+\frac{1}{8\pi n}\sin(4\pi nt)\right]_o^{t_1} - \left[t/2+\frac{1}{8\pi n}\sin(4\pi nt)\right]_{t_1}^{T/2}\right]$$

$$\therefore w2 = 4k_D V\dot{x}_o^2\left[t_1-\frac{1}{4n} + \frac{1}{4\pi n}\sin(4\pi nt_1)\right]$$

<u>w3</u>

$$w3 = -2k_D\dot{x}_o^3\left[\int_o^{t_1}\cos^3(2\pi nt)dt - \int_{t_1}^{T/2}\cos^3(2\pi nt)dt\right]$$

$$= \frac{-2k_D\dot{x}_o^3}{4}\left[\int_o^{t_1}\left[\cos(6\pi nt)+3\cos(2\pi nt)\right]dt - \int_{t_1}^{T/2}\left[\cos(6\pi nt)\ 3\cos(2\pi nt)\right]dt\right]$$

$$= \frac{-k_D\dot{x}_o^3}{2}\left[\left[\frac{1}{6\pi n}\sin(6\pi nt) + \frac{3}{2\pi n}\sin(2\pi nt)\right]_o^{t_1} - \left[\frac{1}{6\pi n}\sin(6\pi nt)\right.\right.$$

$$\left.\left. + \frac{3}{2\pi n}\sin(2\pi nt)\right]_{t_1}^{T/2}\right]$$

$$\therefore w3 = \frac{-k_D \dot{x}_o^3}{2} \left[\frac{1}{3\pi n} \sin(6\pi n t_1) + \frac{3}{\pi n} \sin(2\pi n t_1) \right]$$

$$\therefore \bar{c} = \frac{\int f \dot{x} dt}{\int \dot{x}^2 dt} = \frac{(w1+w2+w3)}{2\pi^2 n x_o^2}$$

$$\bar{c}_{press} = \frac{\rho (CDDEP) n D A}{4\pi^2 x_o}$$

$$\text{or } CDDEP = - \frac{4\pi^2 x_o \bar{c}_{press}}{\rho n D A}$$

where

$$A = \left[- \frac{4V^2}{n^2} \sin(2\pi n t_1) + 16 V x_o \pi^2 t_1 - \frac{4 V x_o \pi^2}{n} + \frac{4\pi}{n} V x_o \sin(4\pi n t_1) \right.$$

$$\left. - \frac{x_o^2 4\pi^2}{3} \sin(6\pi n t_1) - 12 x_o^2 \pi^2 \sin(2\pi n t_1) \right]$$

$$\text{and } t_1 = \frac{1}{2\pi n} \text{Arc cos} \left(\frac{V}{\dot{x}_o} \right)$$

writing $a = V/\dot{x}_o$, A can be rewritten as

$$A = \frac{\dot{x}_o^2}{n^2} \left[- (4a^2+3)\sin(\text{Arc cos } a) - 2\pi a + 4a \text{Arc cos } a \right.$$

$$\left. + 2a \sin(2 \text{Arc cos } a) - \frac{1}{3} \sin(3 \text{Arc cos } a) \right]$$

$$= \frac{\dot{x}_o^2}{n^2} \left[\frac{4}{3}(1-a^2)^{\frac{1}{2}}(2+a^2) + 2a(\pi - 2 \text{ Arc cos } a) \right]$$

(Note that:

$$\sin(\text{Arc cos } x) = \sqrt{1-x^2}$$

$$\sin(2 \text{Arc cos } x) = \sin(\text{Arc cos } (2x-1)) = 2x(1-x^2)^{\frac{1}{2}})$$

$$\therefore \text{CDDEP} = \frac{\dot{x}_o \bar{c}_{press}}{.5\rho D\dot{x}_o^2 B} \qquad -(8')$$

$$\text{Where } B = \left[\frac{4}{3\pi}(1-a^2)^{\frac{1}{2}}(2+a^2)+\frac{2a}{\pi}(\pi-2\text{Arc cos } a)\right] \quad (\text{for } V<\dot{x}_o)$$

Thus (5') and (8') may be written as

$$\text{CDDEP} = \frac{\dot{x}_o \bar{c}_{press}}{.5\rho D\dot{x}_o^2 B} \qquad -(9')$$

with $B = 2a$ for $V \geq \dot{x}_o$

and $B = \left[\frac{4}{3\pi}(1-a^2)^{\frac{1}{2}}(2+a^2)+\frac{2a}{\pi}(\pi-2\text{Arc cos } a)\right]$ for $V<\dot{x}_o$

This is the same as the result that Matten (1976) obtains by a Fourier coefficients analysis with ($\dot{x}_o \bar{c}_{press}$) replacing the amplitude of the fundamental oscillatory component of drag force.

A2.2 Derivation of time-averaged steady component of drag coefficients.

The time averaged steady component of drag coefficient from (1') will be termed STCDDEP, and from (2') STCDIND.

From the force measurements the average force on the cylinder, $\bar{F}_{cyl}$ over several oscillations (the same number as used in the calculation of $\bar{c}_{press}$) was calculated,

$$\bar{F}_{cyl} = \bar{F} - \bar{F}_o$$

where $\bar{F}$ is the force measured in experiments with a cylinder, and $\bar{F}_o$ in experiments without a cylinder.

This can be related to the steady force given by (1') or (2') to yield the steady drag coefficients.

The average force on the cylinder over a cycle is

$$\bar{F}_{cyl} = \frac{1}{T}\int_o^T f\,dt \qquad \text{(10')}$$

f is given by (1') and (2') to yield STCDDEP and STCDIND, respectively. The integrations are conducted below.

From equation (2')

$$\bar{F}_{cyl} = \frac{.5\rho D}{T}\int_o^T C_{D3}V^2\,dt$$

$$\therefore \text{STCDIND} = \frac{\bar{F}_{cyl}}{5\rho DV^2} \qquad \text{(11')}$$

From equation (1')

Again separate equations will be derived for the cases $V \geq \dot{x}_o$ and $V < \dot{x}_o$.

$\underline{V \geq \dot{x}_o}$

$$\bar{F}_{cyl} = \frac{2K_D}{T}\left[\int_o^{T/2} V^2 dt - 2V\int_o^{T/2} \dot{x}dt + \int_o^{T/2} \dot{x}^2 dt\right]$$

$$= \frac{2K_D}{T}\left[\left[t\right]_o^{T/2} - 2Vx_o\left[\sin(2\pi nt)\right]_o^{T/2} + \dot{x}_o^2\left[t/2+\frac{1}{8\pi n}\sin(4\pi nt)\right]_o^{T/2}\right]$$

$$= \frac{2K_D}{T}\left[\frac{T}{2}+\dot{x}_o^2\left(\frac{T}{4}\right)\right] = K_D\left(1+\frac{\dot{x}_o^2}{2}\right)$$

Rearranging yields $STCDDEP = \dfrac{\bar{F}_{cyl}}{\cdot 5\rho DV^2\left(1+\frac{1}{2a^2}\right)}$ -(12')

(for $V \geq \dot{x}_o$)

$\underline{V < \dot{x}_o}$

$$\bar{F}_{cyl} = K_D\,\frac{2}{T}\left[-\int_o^{t_1}(V^2-2V\dot{x}+\dot{x}^2)dt + \int_o^{T/2}(V^2-2V\dot{x}+\dot{x}^2)dt\right]$$

$$\therefore \bar{F}_{cyl} = \frac{2K_D}{T}\left[X1+X2+X3\right]$$

$$X1 = -\int_o^{t_1} V^2 dt + \int_{t_1}^{T/2} V^2 dt$$

$$X2 = 2V\int_o^{t_1} \dot{x}dt - 2V\int_{t_1}^{T/2} \dot{x}dt$$

$$X3 = -\int_o^{t_1} \dot{x}^2 dt + \int_{t_1}^{T/2} \dot{x}^2 dt$$

Evaluating X1, X2, X3:

$$X1 = V^2\left[-\left[t\right]_o^{t1} + \left[t\right]_{t_1}^{T/2}\right] = \cdot V^2\left[-2t_1+T/2\right]$$

X2

$$X2 = 2V\dot{x}_o\left[\int_o^{t_1} \cos(2\pi nt)dt - \int_{t_1}^{T/2} \cos(2\pi nt)dt\right]$$

$$= 2Vx_o\left[\left[\sin(2\pi nt)\right]_o^{t_1} - \left[\sin(2\pi nt)\right]_{t_1}^{T/2}\right]$$

$$\therefore X2 = 4Vx_o \sin(2\pi nt)$$

X3

$$X3 = \dot{x}_o^2\left[-\int_o^{t_1} \cos^2(2\pi nt)dt + \int_{t_1}^{T/2} \cos^2(2\pi nt)dt\right]$$

$$= \dot{x}_o^2\left[-\int_o^{t_1} \tfrac{1}{2}+\tfrac{1}{2}\cos(4\pi nt)dt + \int_{t_1}^{T/2} \tfrac{1}{2}+\tfrac{1}{2}\cos(4\pi nt)dt\right]$$

$$= \dot{x}_o^2\left[-\left[t/2 + \frac{1}{8\pi n}\sin(4\pi nt)\right]_o^{t} + \left[t/2 + \frac{1}{8\pi n}\sin(4\pi nt)\right]_{t_1}^{T/2}\right]$$

$$\therefore X3 = \dot{x}_o^2\left[-t_1 + \frac{1}{4n} - \frac{1}{4\pi n}\sin(4\pi nt_1)\right]$$

Therefore

$$\bar{F}_{cyl} = \frac{2K_D}{T}\left[X1 + X2 + X3\right]$$

$$= \dot{x}_o^2\, K_D\left[a^2 - \frac{2a^2}{\pi}\text{ Arc cos } a + \frac{4a}{\pi}\sin(\text{Arc cos } a)\right.$$

$$\left. + \tfrac{1}{2} - \frac{\text{Arc cos } a}{\pi} - \frac{1}{2\pi}\sin(2\text{Arc cos } a)\right]$$

where $a = V/\dot{x}_o$

This can be written as

$$\bar{F}_{cyl} = \frac{\dot{x}_o^2 K_D}{\pi}\left[3a(1-a^2)^{\frac{1}{2}} + \tfrac{1}{2}\,(1+2a^2)\,(\pi-2\text{Arc cos } a)\right]$$

rearranging yields

$$\text{STCDDEP} = \frac{F_{cyl}}{.5\rho D\dot{x}_o^2 E} \qquad \text{(13')}$$

where

$$E = \frac{1}{\pi}\left[3a(1-a^2)^{\frac{1}{2}} + \tfrac{1}{2}(1+2a^2)(\pi-2\text{Arc cos } a)\right]$$

(13') is identical to the equation obtained by Matten by a Fourier coefficients analysis.

APPENDIX 3

TOTAL OSCILLATORY DRAG COEFFICIENT

Assume $U = U_m \sin(\omega t)$

$\dot{U} = \omega U_m \cos(\omega t)$

and force given by

$$f = .25\rho\pi D^2 C_M \dot{U} + .5\rho D C_D U|U|$$

$$\therefore f = .25\rho\pi D^2 C_M \omega U_m \cos(\omega t) + .5\rho D C_D U_m^2 \sin(\omega t)|\sin(\omega t)|$$

expressing the total (oscillatory) force in terms of the velocity.

$$COSC = \frac{f}{.5\rho D U_m^2} = \frac{.25\pi D^2 C_M \omega}{.5 D U_m} \cos(\omega t) + C_D \sin(\omega t)|\sin(\omega t)|$$

$$COSC = \frac{\pi}{2} C_M \frac{\omega D}{U_m} \cos(\omega t) + C_D \sin(\omega t)|\sin(\omega t)| \quad -(a)$$

Find maximum value

Write $(\omega t) = \gamma$

$$\frac{d\ COSC}{d\gamma} = \frac{-\pi}{2} C_M \frac{\omega D}{U_m} \sin(\gamma) + 2 C_D \sin(\gamma)\cdot\cos(\gamma) = 0$$

$$\therefore \cos(\gamma) = \frac{\pi}{4} \frac{C_M}{C_D} \frac{\omega D}{U_m} = \xi \quad -(b)$$

if $\xi > 1$ then the maximum force is purely inertial and given by substituting $\beta = 0$ into (a).

$$\frac{f_{max}}{.5\rho D\ U_m^2} = CMAXOSC = \frac{\pi^2 C_M}{K}$$

otherwise substitute for β in (a).

$$CMAXOSC = \frac{\pi}{2} C_M \frac{\omega D}{U_m} \cdot \cos(\gamma) + C_D \sin^2(\gamma)$$

$$= \frac{\pi}{2} C_M \left(\frac{\omega D}{U_m}\right)^2 \frac{\pi C_M}{4 C_D} + C_D \left[1 - \left(\frac{\pi}{4} \frac{C_M}{C_D} \frac{\omega D}{U_m}\right)^2\right]$$

$$= C_D + \frac{\pi^2}{16} \frac{C_M^2}{C_D} \left(\frac{\omega D}{U_m}\right)^2$$

$$= C_D + \frac{\pi^4 C_M^2}{4 C_D K^2} \qquad -(c)$$

This is in agreement with the result obtained by Sarpkaya (1976a). Thus the maximum oscillatory force coefficient is given by:-

$$CMAXOSC = \frac{f_{max}}{.5\rho D\ U_m^2} = \frac{\pi^2 C_M}{K} \qquad \text{if } \xi \gtrsim 1$$

and

$$CMAXOSC = \frac{f_{max}}{.5\rho D\ U_m^2} = C_D + \frac{\pi^4 C_M^2}{4 C_D K^2} \qquad \text{if } \xi < 1$$

where $\xi = \frac{\pi}{4} \frac{C_M}{C_D} \frac{\omega D}{U_m}$

For the tests of this thesis the above equations apply with CDIND for C_D and CM for C_M.

APPENDIX 4

NON-DIMENSIONAL DISTANCE TRAVELLED BY A CYLINDER IN OSCILLATORY MOTION RELATIVE TO A STEADY CURRENT

Consider a situation where $V < \dot{x}_o$ such that flow reversal occurs twice every cycle and the cycle can be divided up into two parts with respectively positive and negative relative velocity. This is shown by the diagram below.

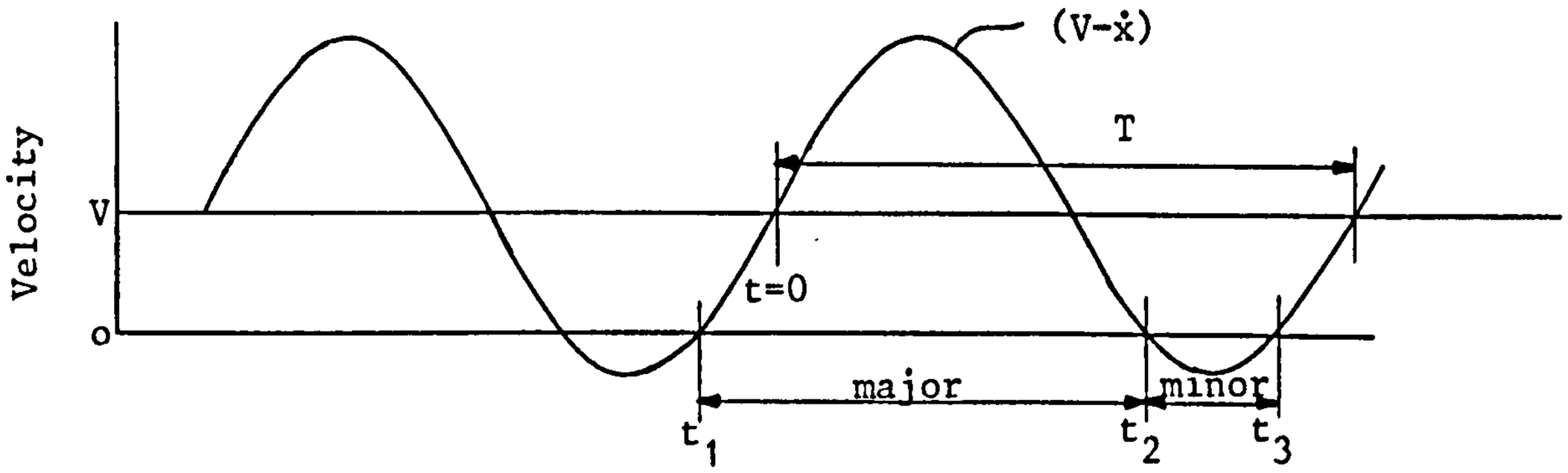

The relative distance travelled in the major part cycle is the distance travelled in the time interval $T' = t_2 - t_1$, and the relative distance in the minor part cycle is that distance travelled in the time $t_3 - t_2$.

Defining

$$-\dot{x} = \dot{x}_o \sin(\frac{2\pi nt}{T})$$

$$\therefore (V-\dot{x}_o) = (V+\dot{x}_o \sin(\frac{2\pi nt}{T}))$$

∴ relative distance travelled in the major part cycle is given by

$$2\int_{t_1}^{T/4}(V+\dot{x}_o \sin(\frac{2\pi t}{T}))dt$$

similarly the relative distance travelled in the minor part cycle is given by

$$2\int_{3T/4}^{t_3}(V+\dot{x}_o \sin(\frac{2\pi t}{T}))dt$$

now $t_1 = \frac{-T}{2\pi}\sin^{-1}(V/\dot{x}_o)$

$t_3 = T+t_1$

$t_2 = T/2-t_1$

Therefore the relative distance travelled in the major part cycle is

$$2\left[Vt - \frac{T\dot{x}_o}{2\pi}\cos\frac{2\pi t}{T}\right]_{t_1}^{T/4}$$

$$= \frac{VT}{2} + \frac{VT}{\pi}\sin^{-1}(V/\dot{x}_o) + 2x_o\cos\left[\sin^{-1}(V/\dot{x}_o)\right]$$

non-dimensionalizing by 2D gives the non-dimensional relative distance travelled in the major part cycle as

$$\frac{V}{2nD}\left\{\frac{1}{2} + \frac{1}{\pi}\sin^{-1}(V/\dot{x}_o) + (\frac{\dot{x}_o}{V})\frac{1}{\pi}\cos\left[\sin^{-1}(V/\dot{x}_o)\right]\right\}$$

This may be written

$$\frac{x_o}{D}\left[\pi a + 2a \sin^{-1} a + 2\sqrt{1-a^2}\right]$$

where $a = V/\dot{x}_o$.

Similarly for the minor part cycle the non-dimensional relative distance travelled is given by

$$\frac{x_o}{D}\left[\pi a - 2a \sin^{-1} a - 2\sqrt{1-a^2}\right]$$

As an alternative method to the direct integration one can calculate the total relative distance travelled in the major part cycle as the distance travelled by the stream in the time $T' = t_2 - t_1$, plus the distance travelled by the cylinder, i.e.

$$VT' + 2x_o \cos \sin^{-1}(V/\dot{x}_o)$$

which gives the same result as the above integration.

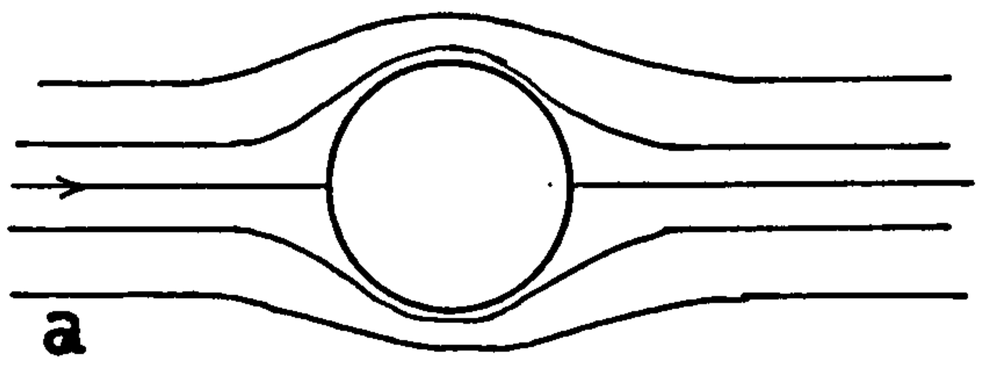

R<1

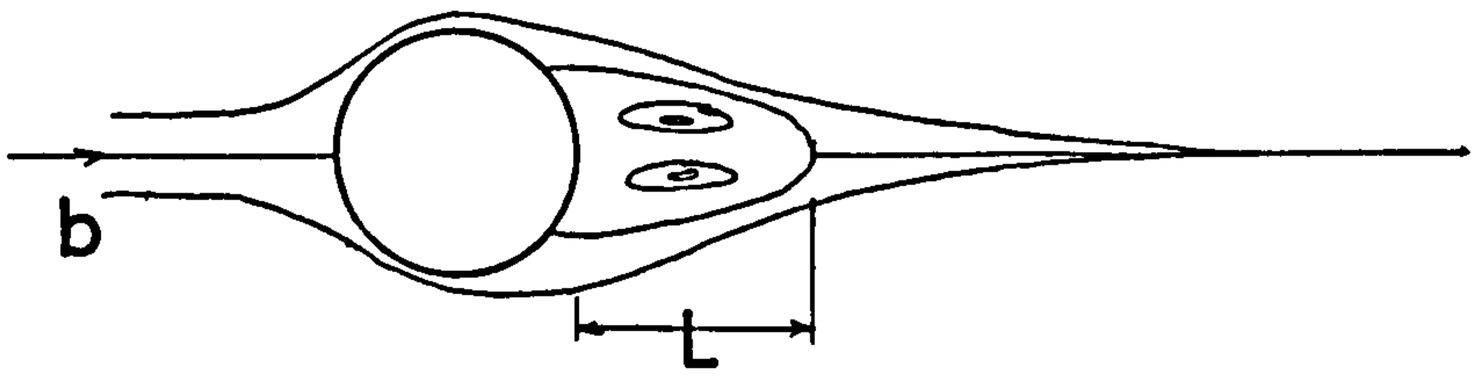

R=10~40

L increases with R

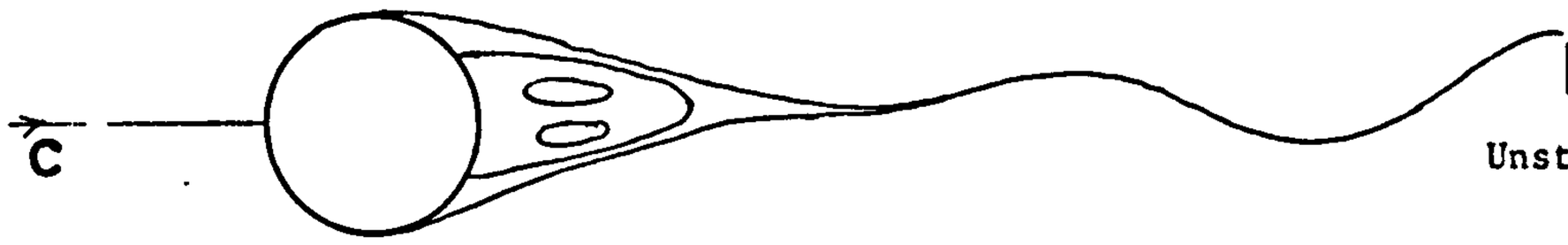

R=30~50

Unstable downstream

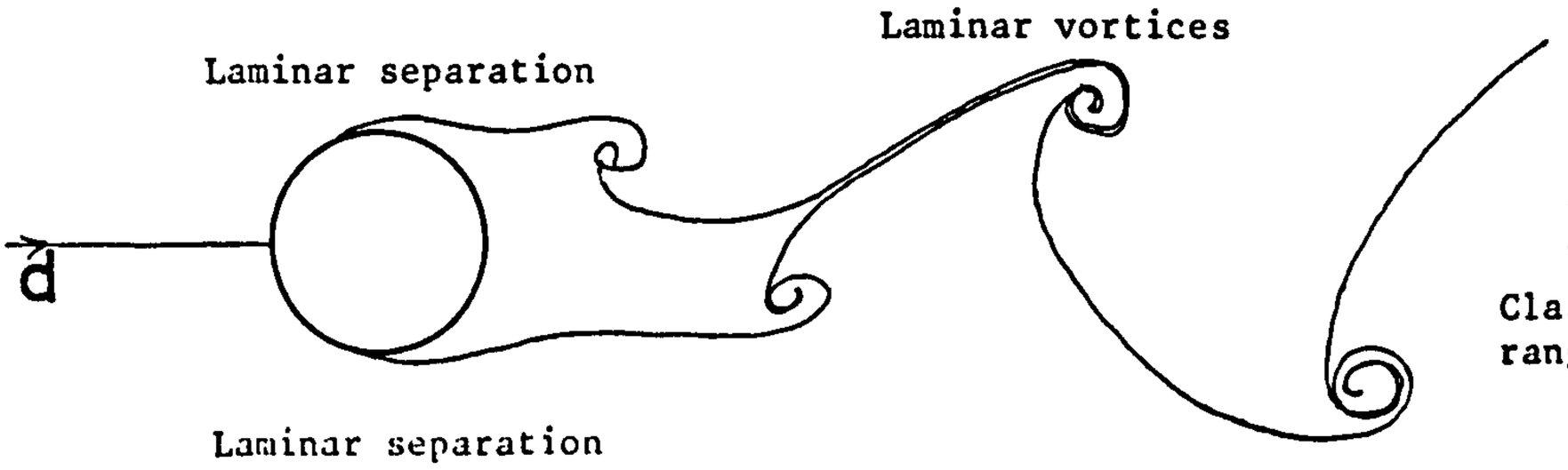

R=50~150

Classical von Kármán range

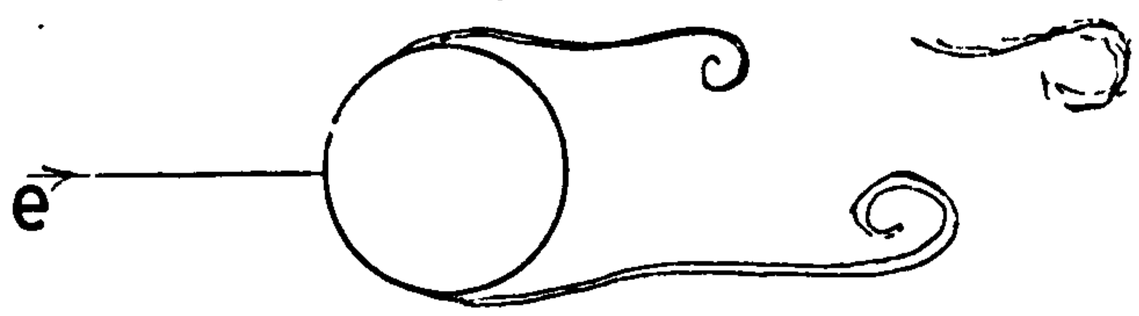

turbulent vortices downstream

R=300~2x10^5

Subcritical regime

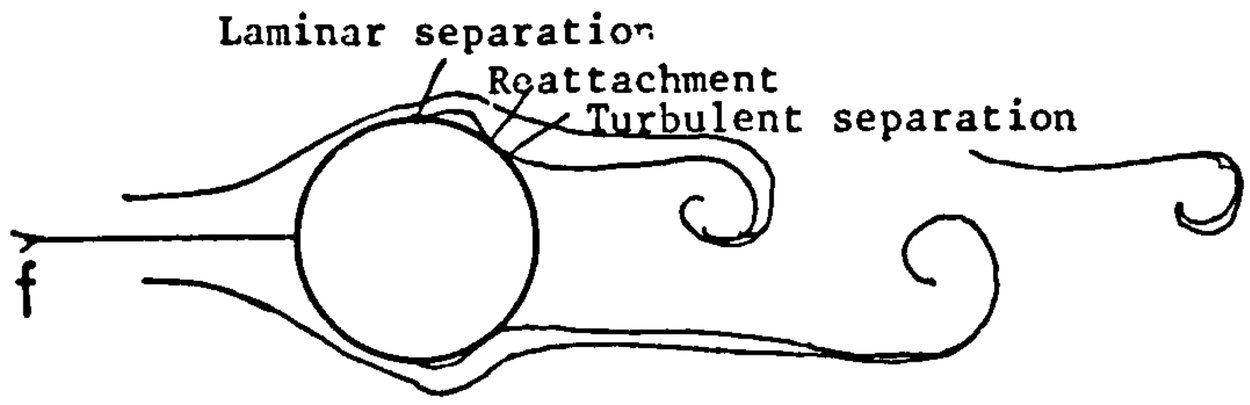

Critical regime

R=2-6x10^5

Gross 3-dimensionality general turbulent wake

Supercritical regime

R=6x10^5-3x10^6

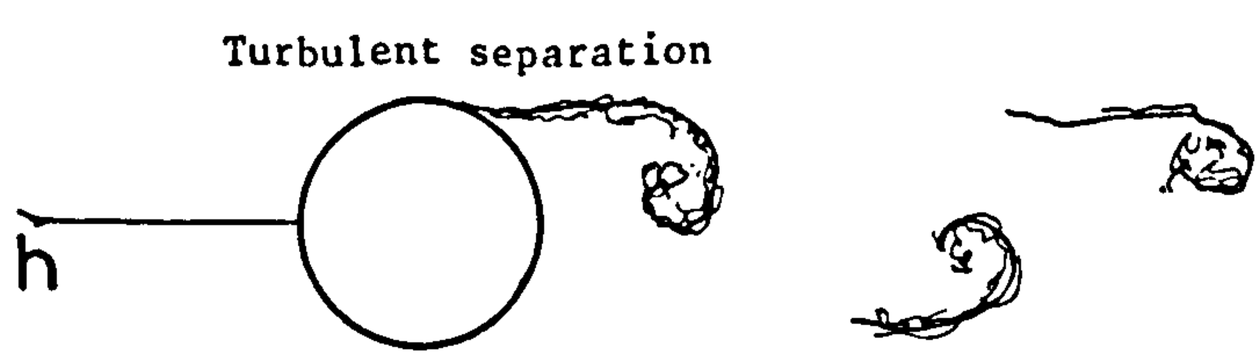

General turbulent wake downstream

Transcritical regime

R≥3x10^6

Fig. 1. Sketches of the flow past a circular cylinder for various ranges of Reynolds number.

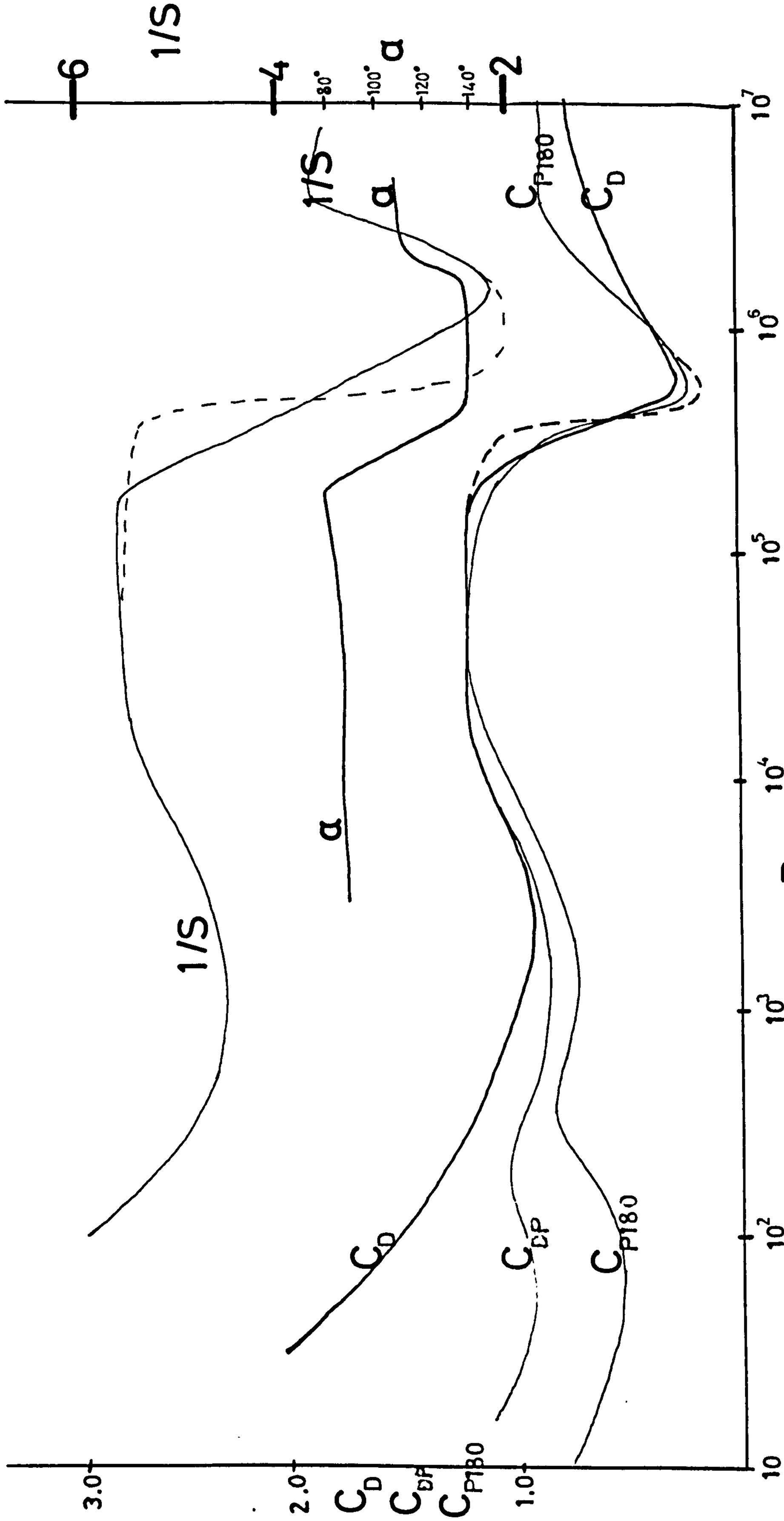

Fig. 2. Typical curves of C_D, C_P, C_{P180}, 1/S and α versus Reynolds number.

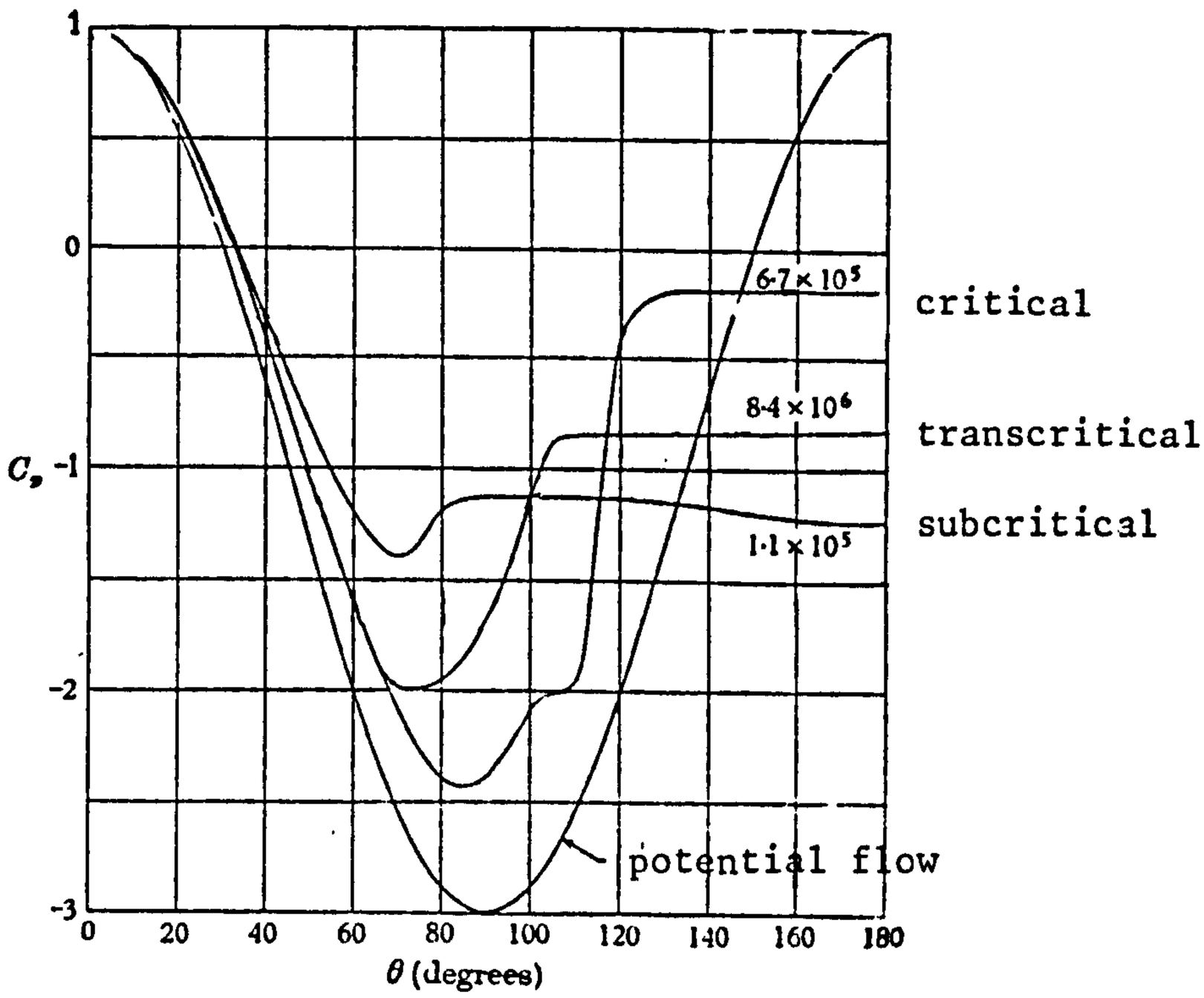

Fig. 3. Representative steady component pressure distributions around a cylinder at subcritical, critical and transcritical Reynolds numbers. From Roshko (1968).

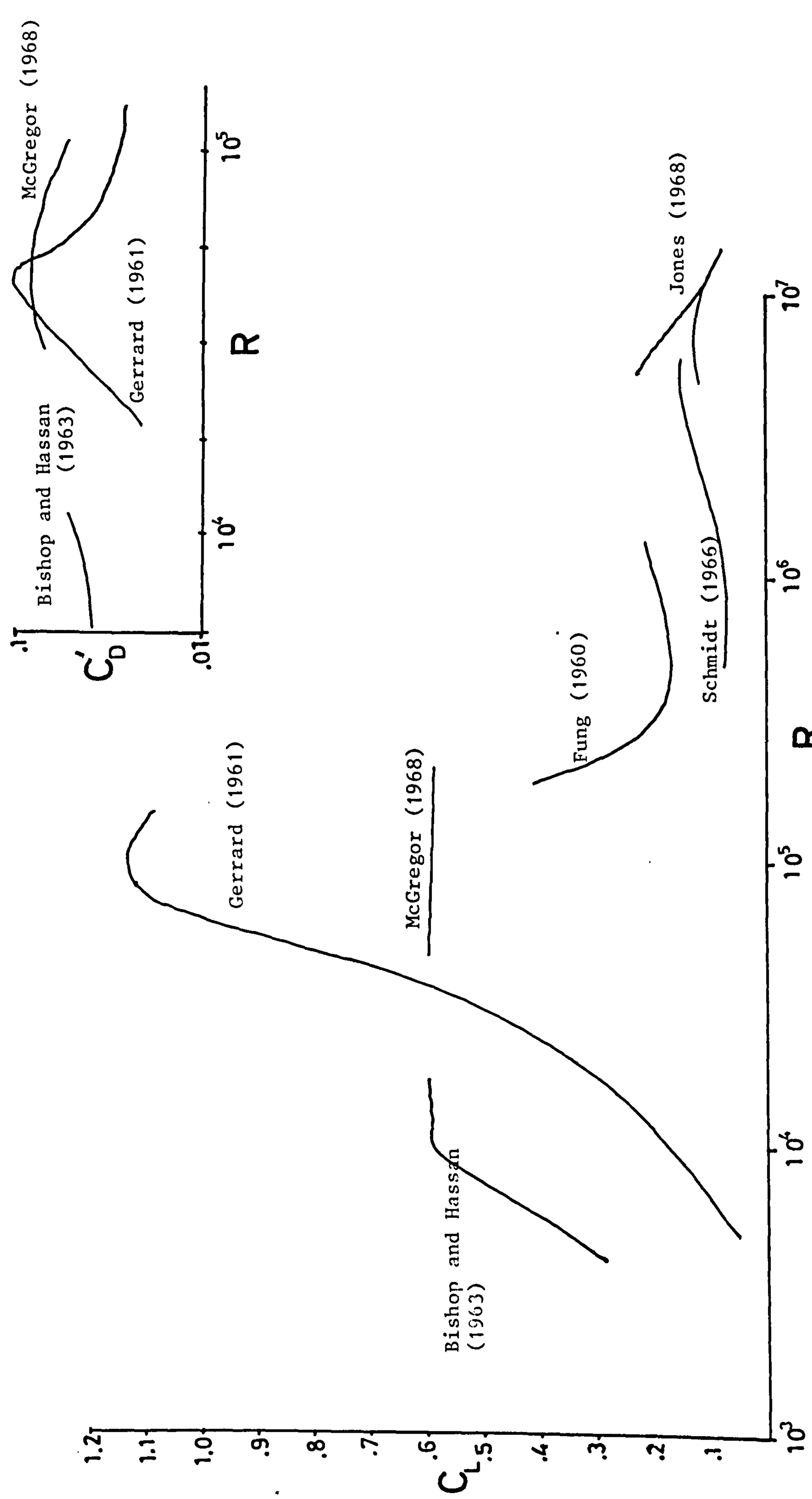

Fig. 4. R.m.s. values of unsteady lift and drag coefficients, C_L and C_D' versus Reynolds number. From various sources.

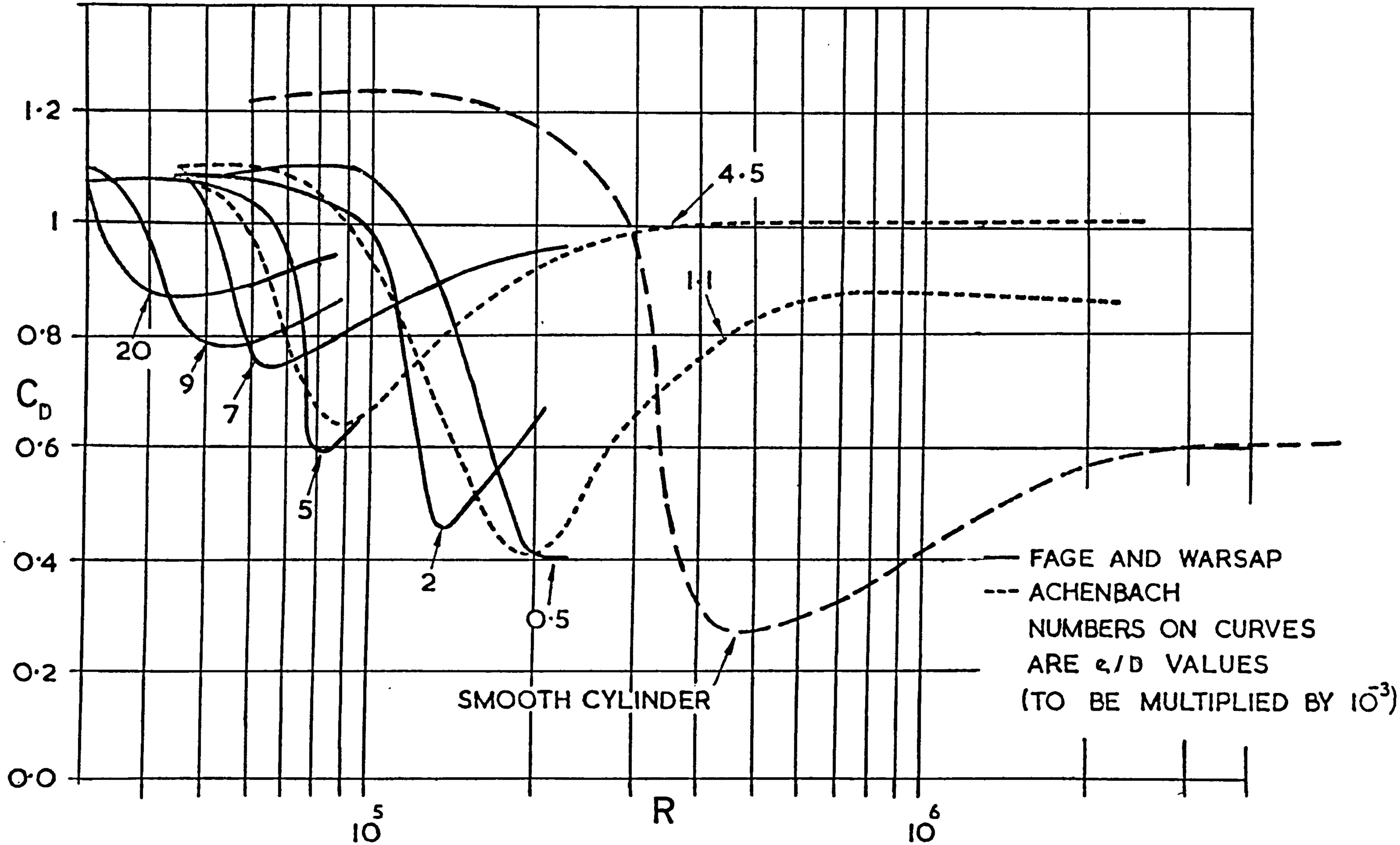

Fig. 5. Example curves showing the effects of roughness on the drag of a cylinder in steady flow. From Miller (1977).

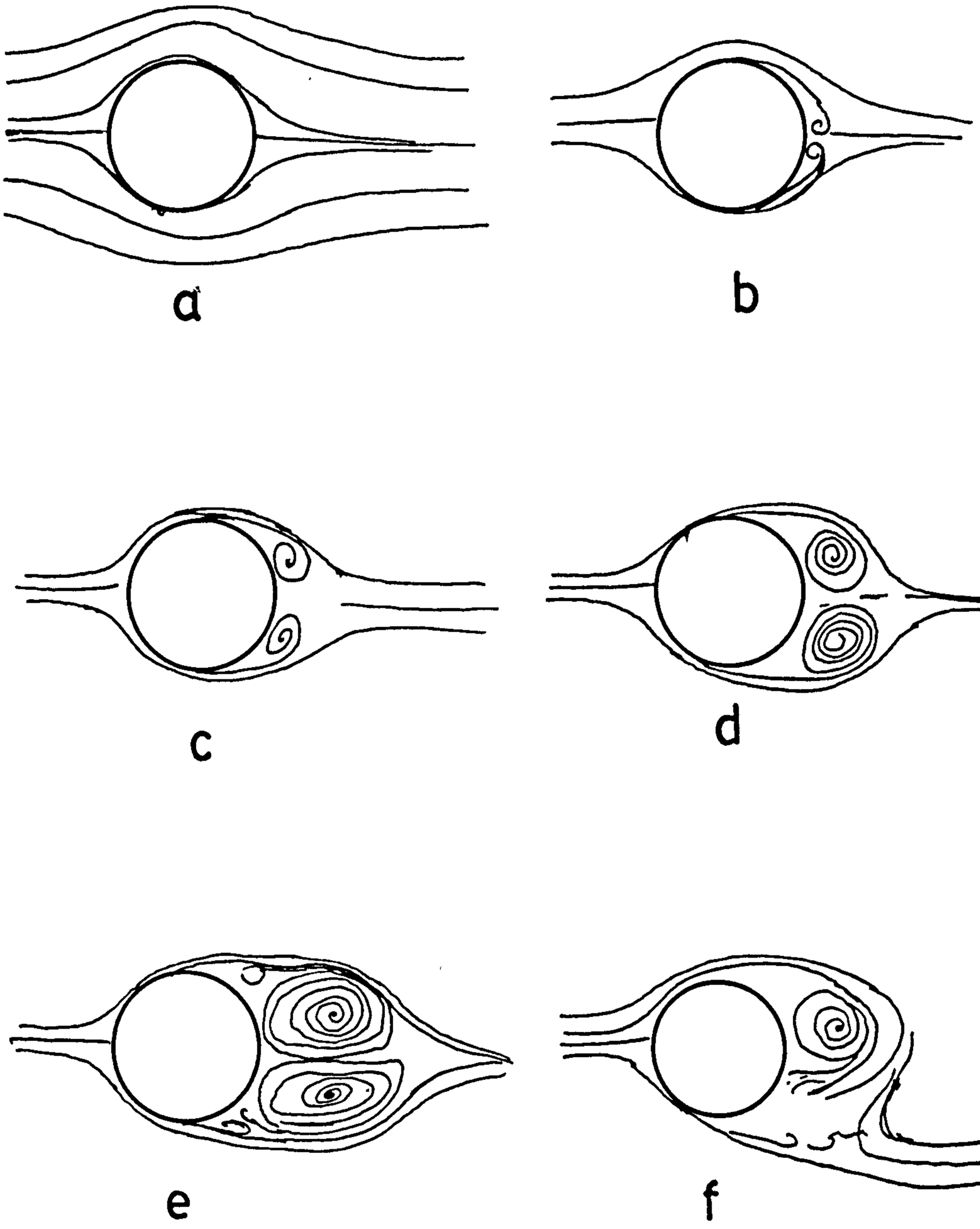

Fig. 6. The flow pattern around a cylinder in a constantly accelerating fluid from rest. Sketched from photographs of Prandtl given in Schlichting (1979).

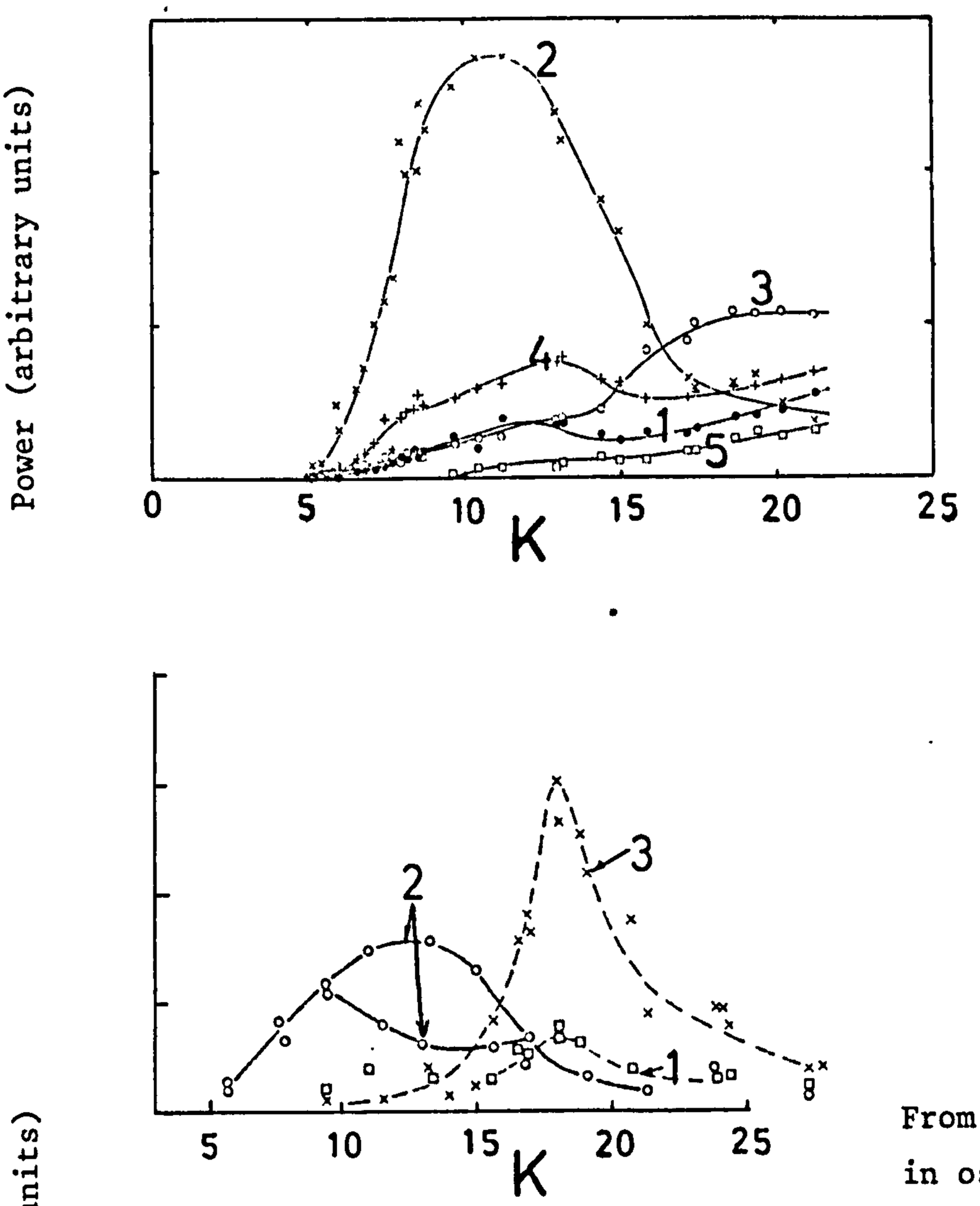

From Isaacson and Maull (1976) in waves

From Maull and Milliner (1978) in oscillatory flow

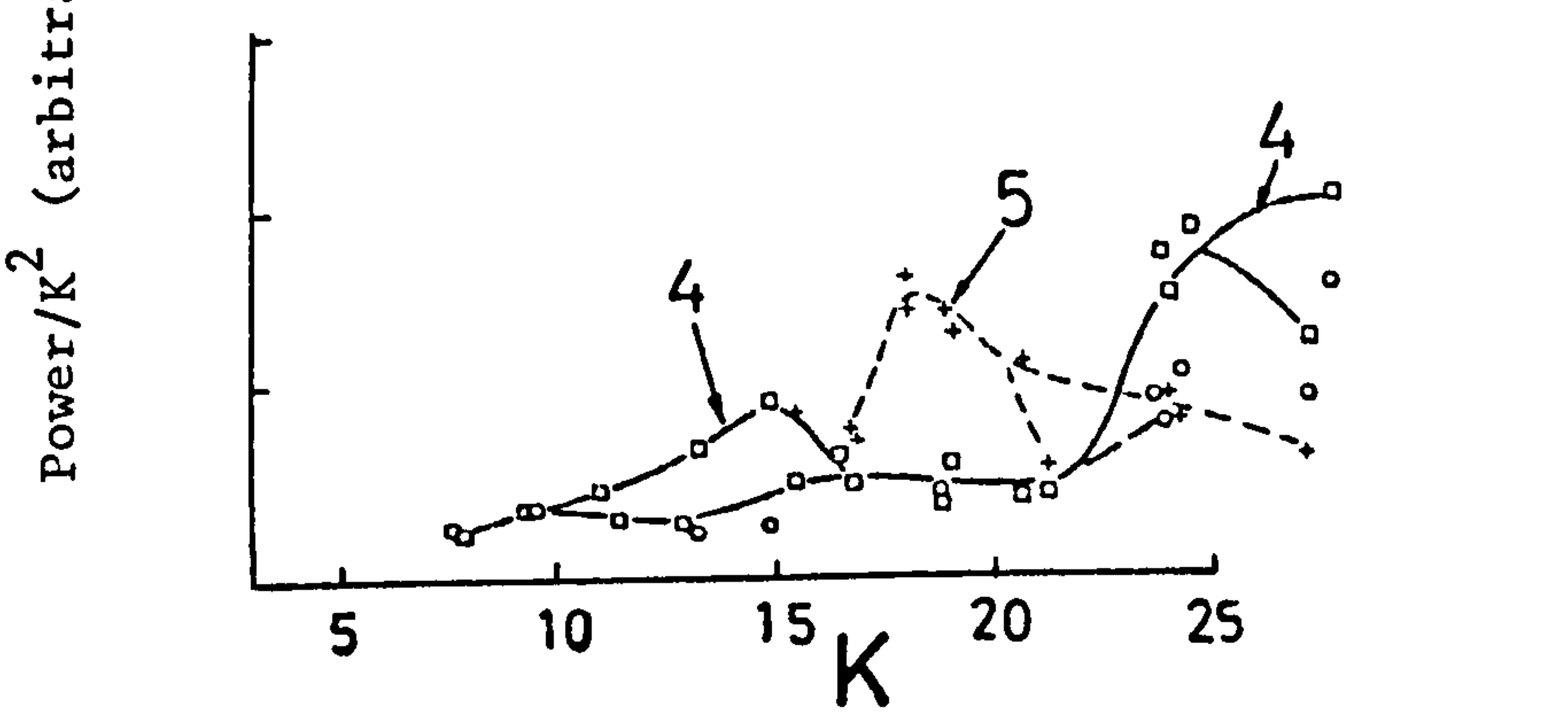

Numbers on the curves represent harmonics of the fundamental frequency.

Fig. 7. Power distribution of the lift at various multiples of the fundamental frequency in waves and oscillatory flows.

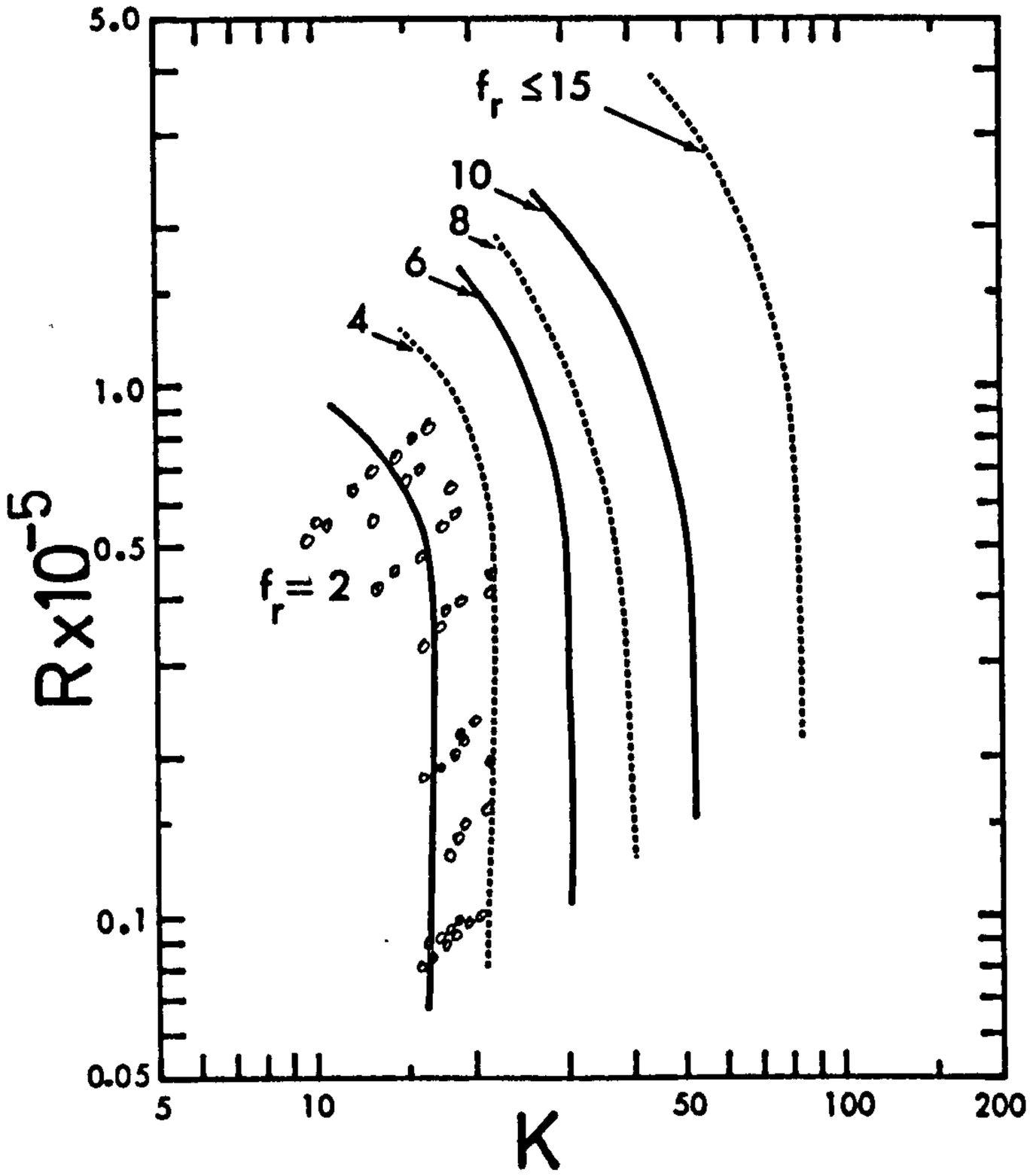

Fig. 8. Highest value of K for particular lift to flow frequency ratios, f_r. From Sarpkaya (1976a). All points for $f_r = 4$ plotted in.

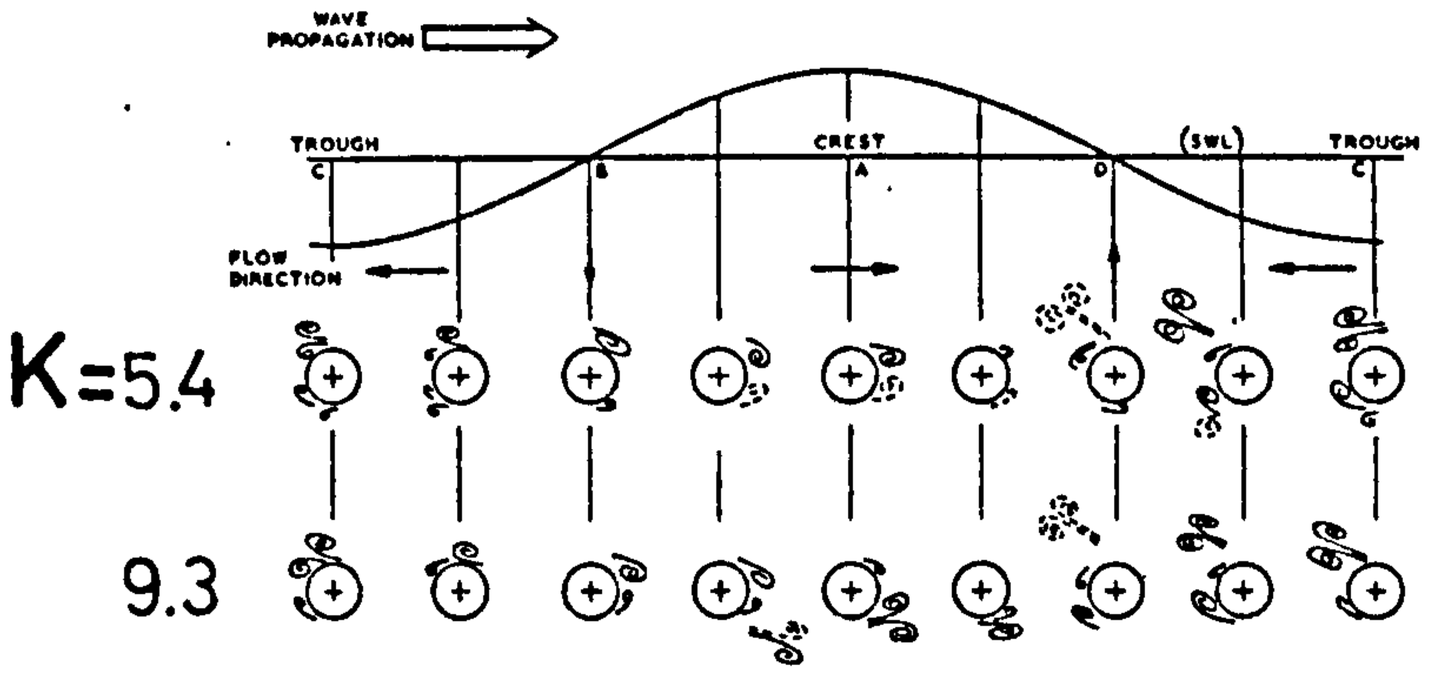

Fig. 9. Flow patterns around a vertical cylinder in waves for K = 5.4 and 9.3. From Zdravkovich and Namork (1978).

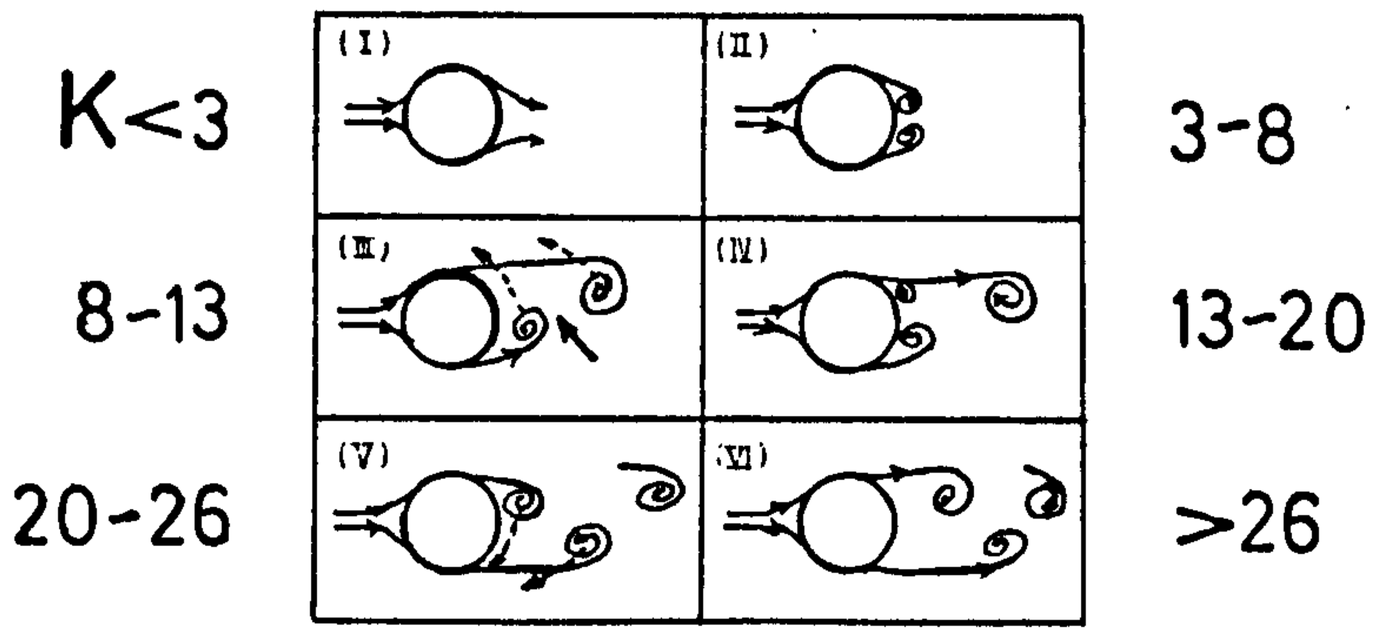

Fig. 10. Flow patterns around a vertical cylinder in waves for various K. From Sawaragi et al. (1976).

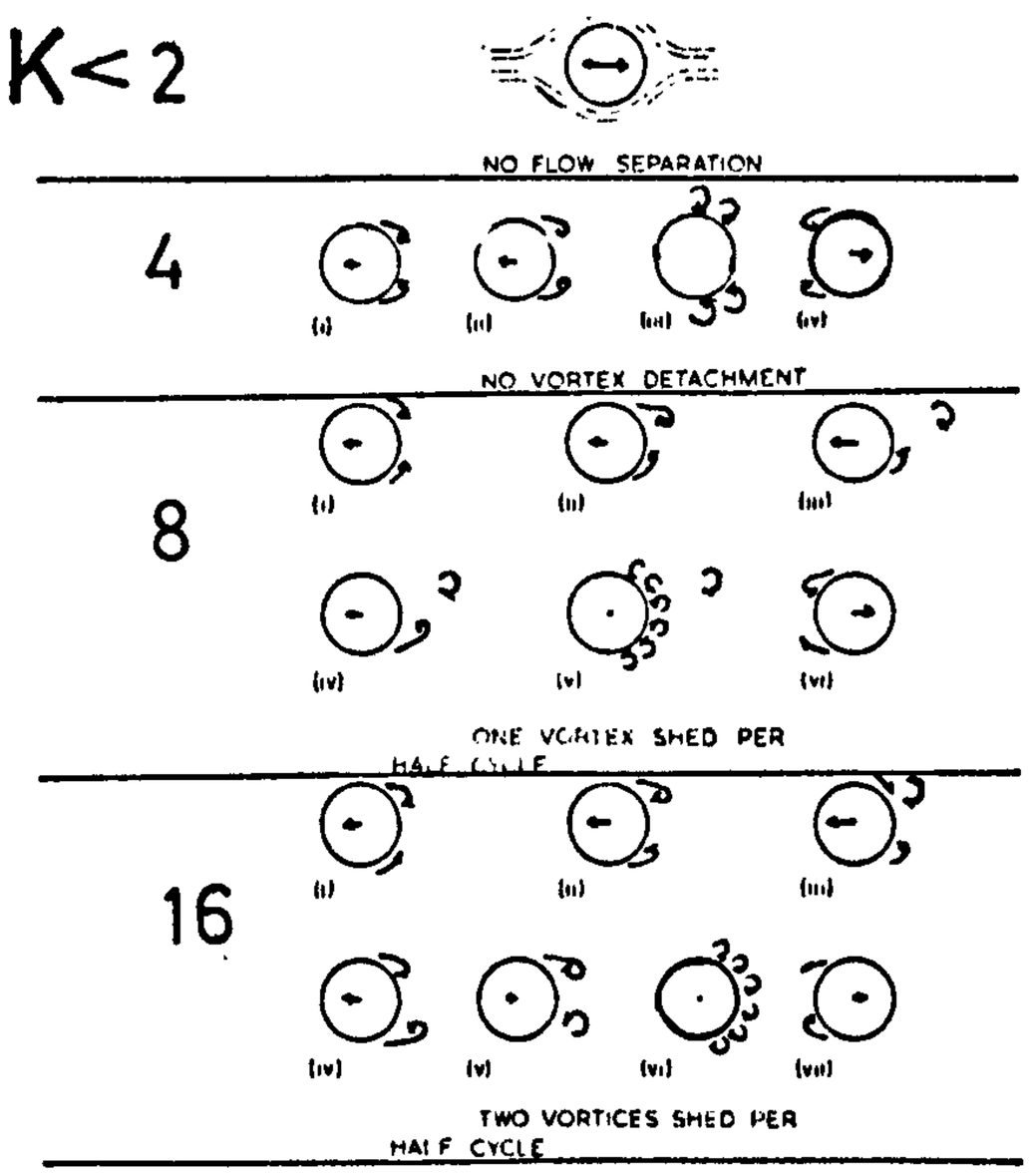

Fig. 11. Flow patterns around a vertical cylinder in oscillatory flow for K < 2 and K = 4, 8, 16. From Isaacson and Maull (1976).

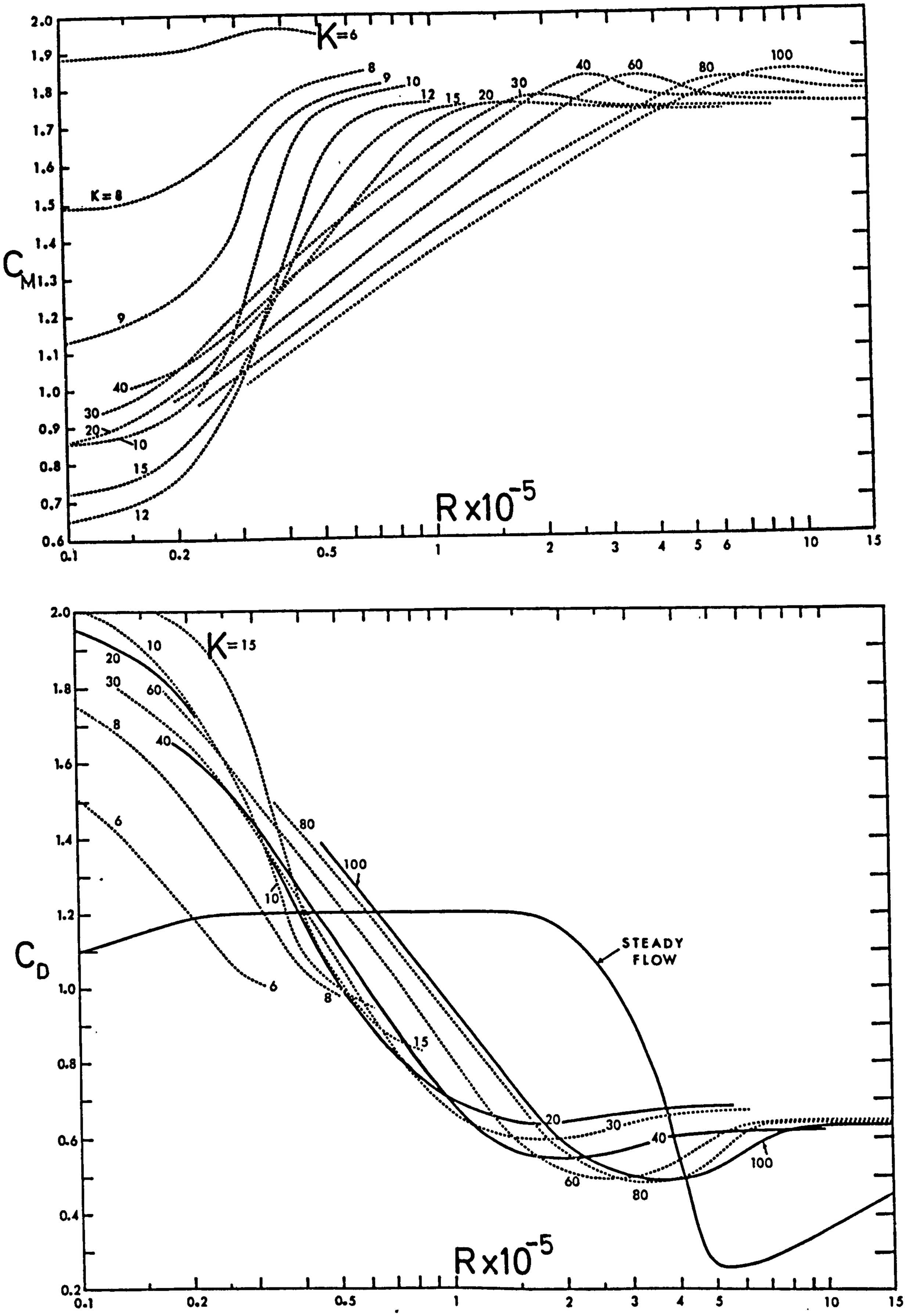

Fig. 12. C_D and C_M for smooth cylinders in oscillatory flow. From Sarpkaya (1976b).

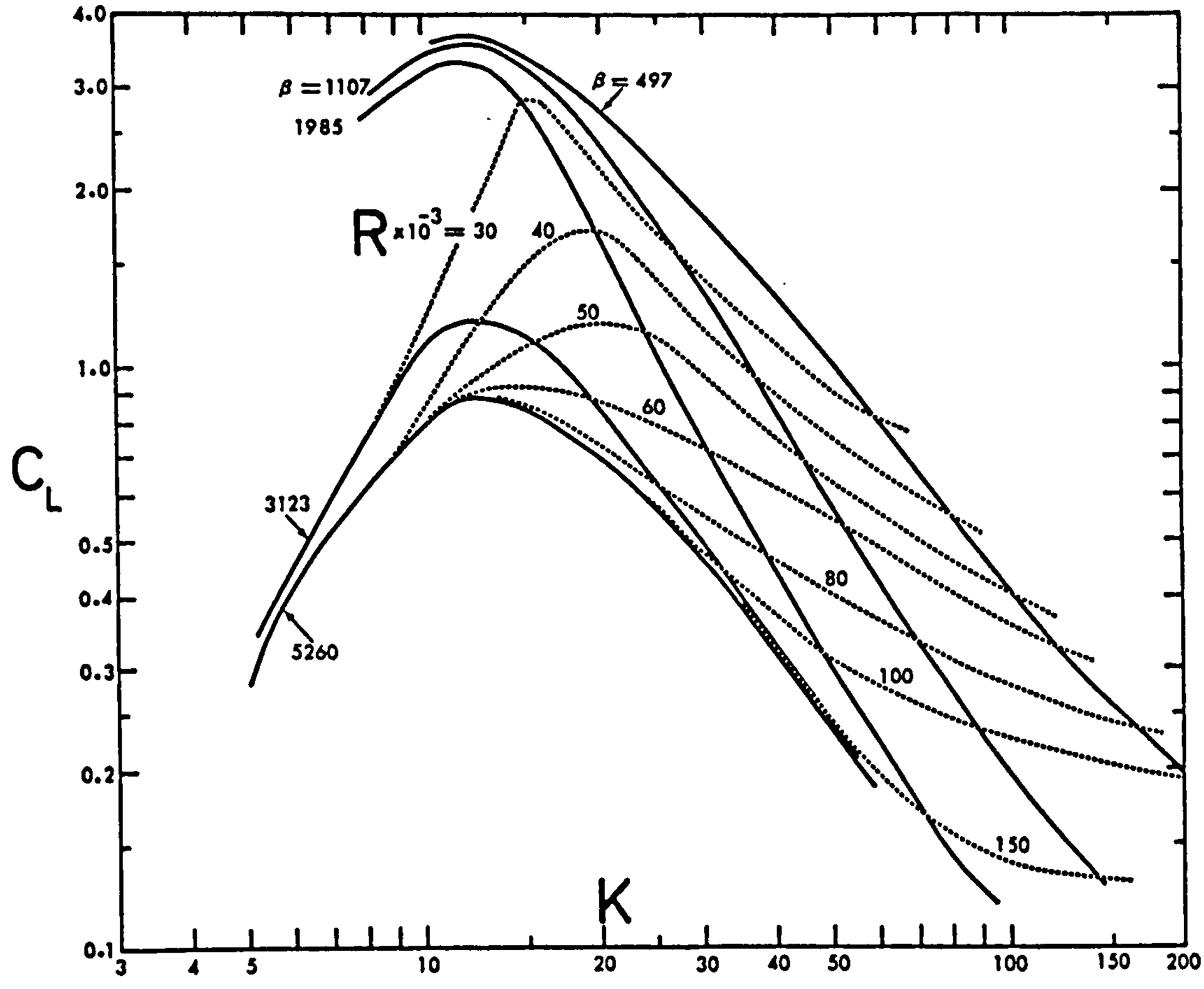

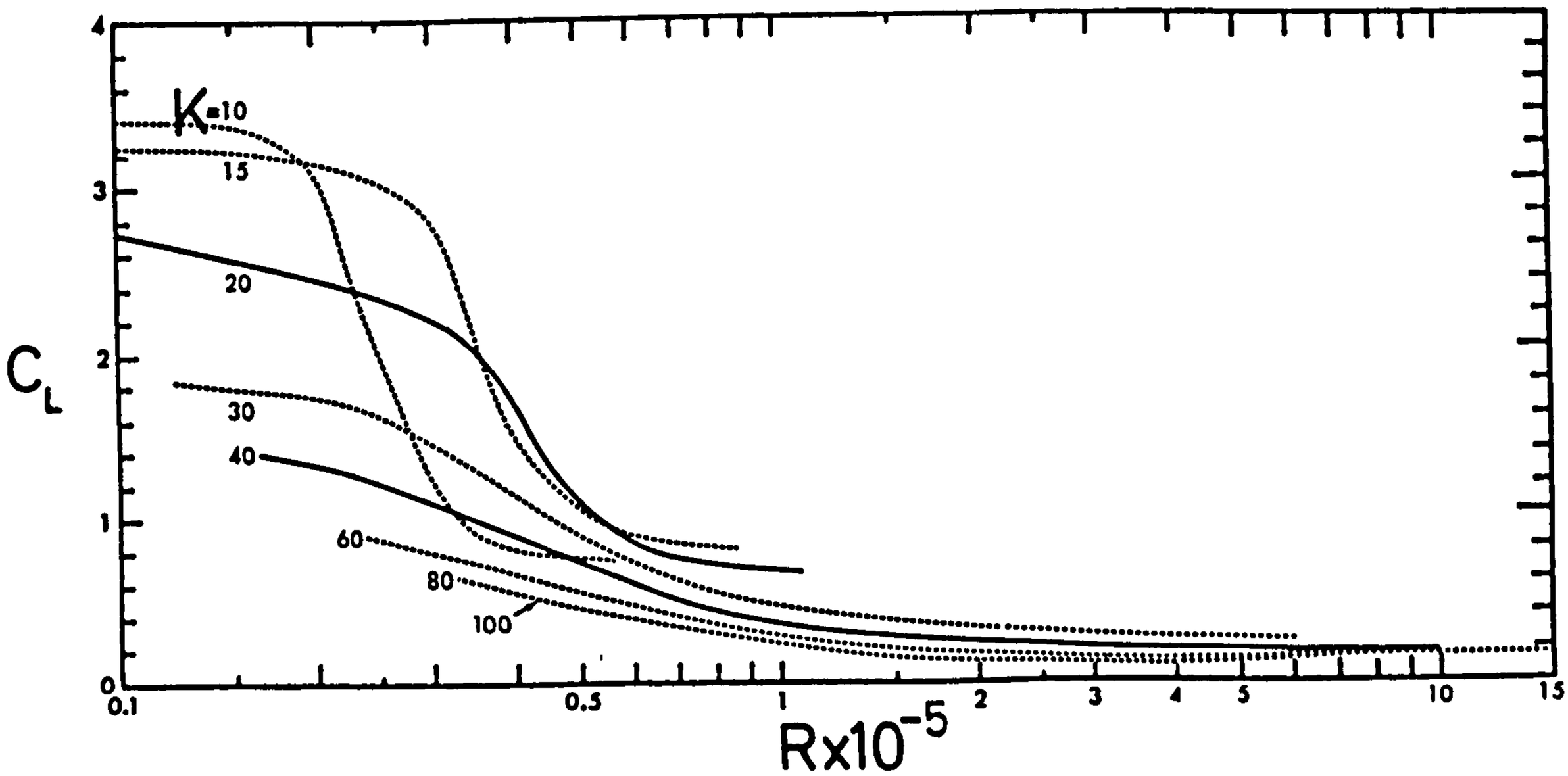

Fig. 13. C_L for smooth cylinders in oscillatory flow. From Sarpkaya (1976b).

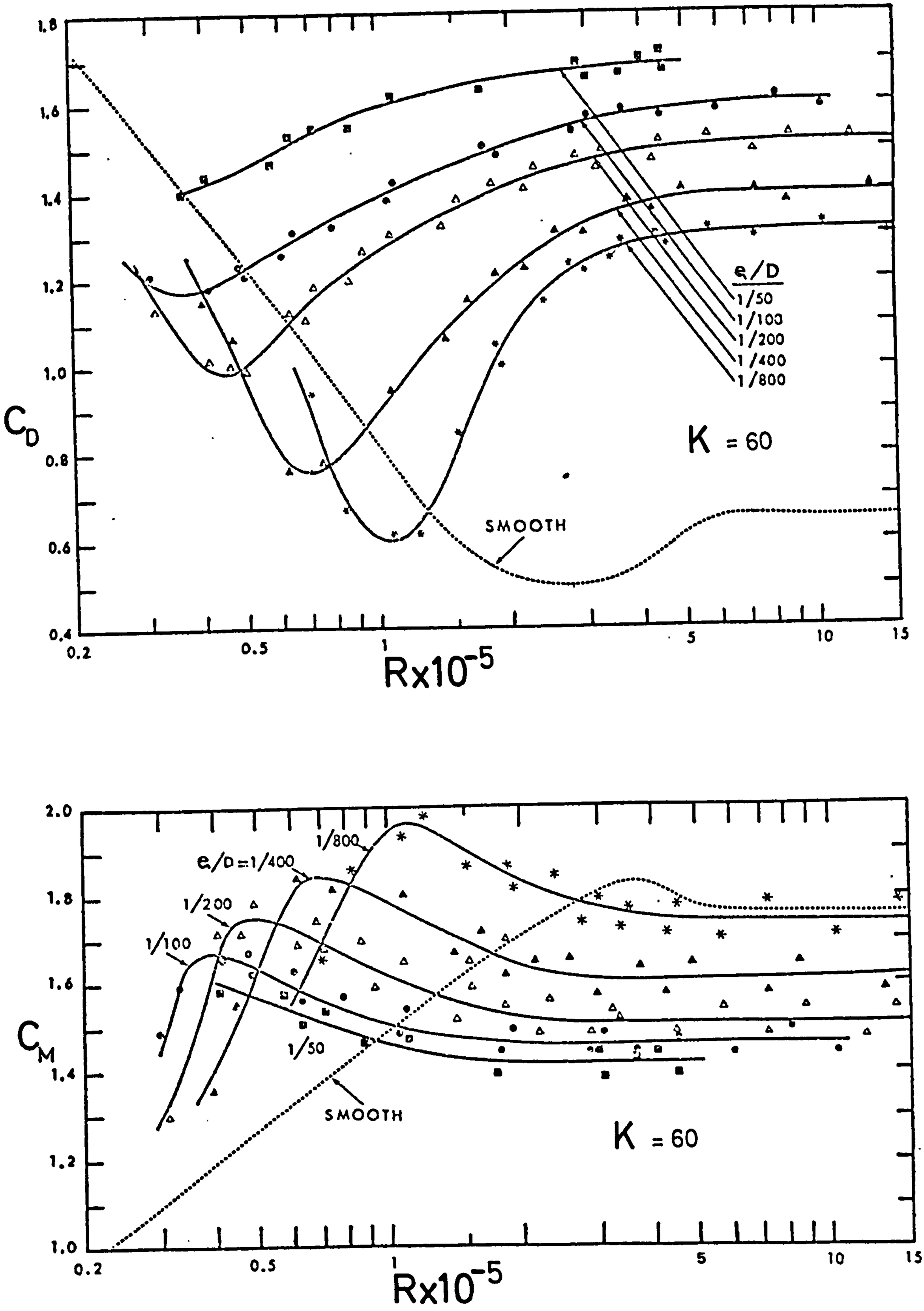

Fig. 14. C_D and C_M coefficients of cylinders versus Reynolds number for various roughnesses. From Sarpkaya (1976b).

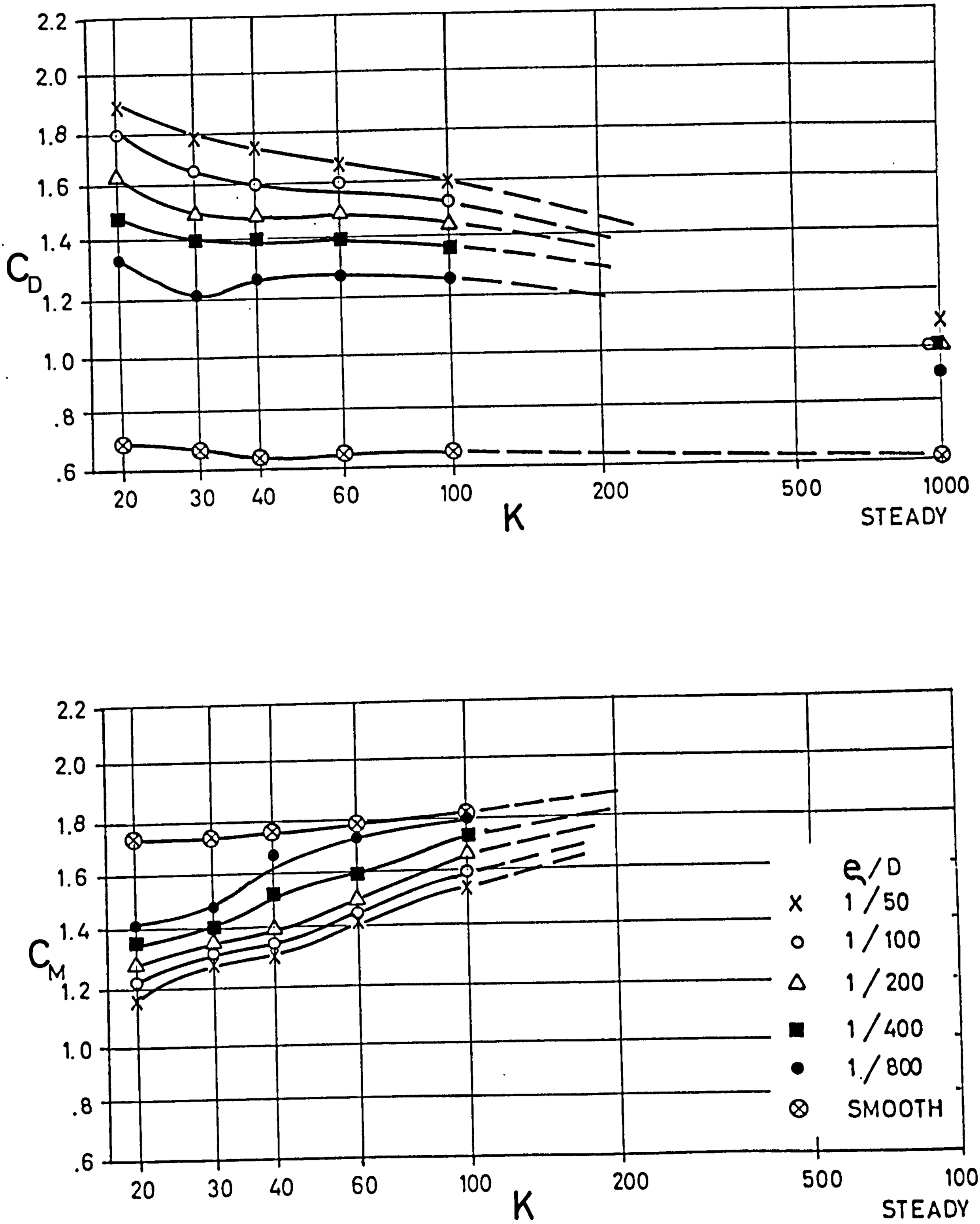

Fig. 15. Transcritical C_D and C_M values in oscillatory flow for various roughnesses.

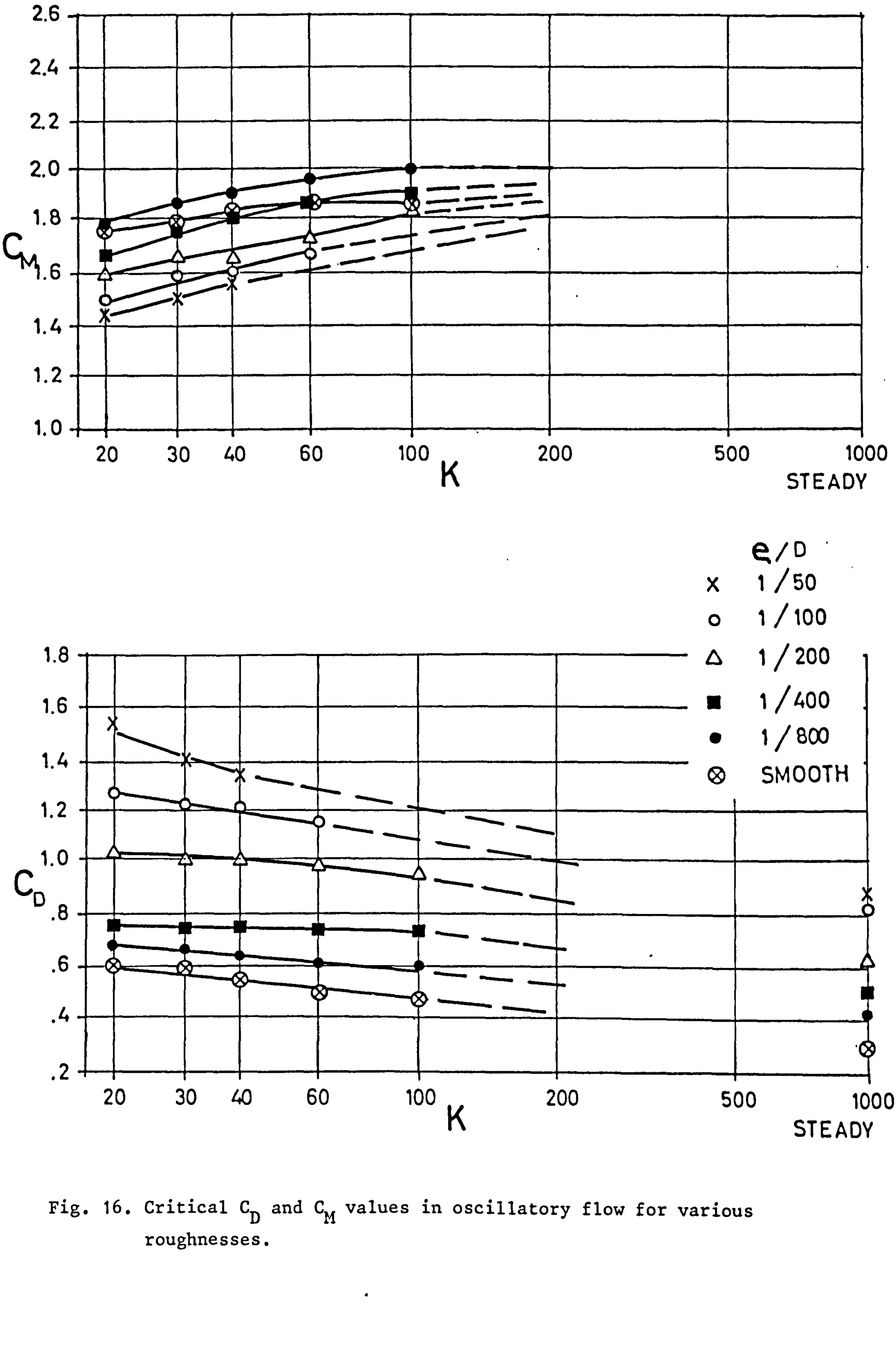

Fig. 16. Critical C_D and C_M values in oscillatory flow for various roughnesses.

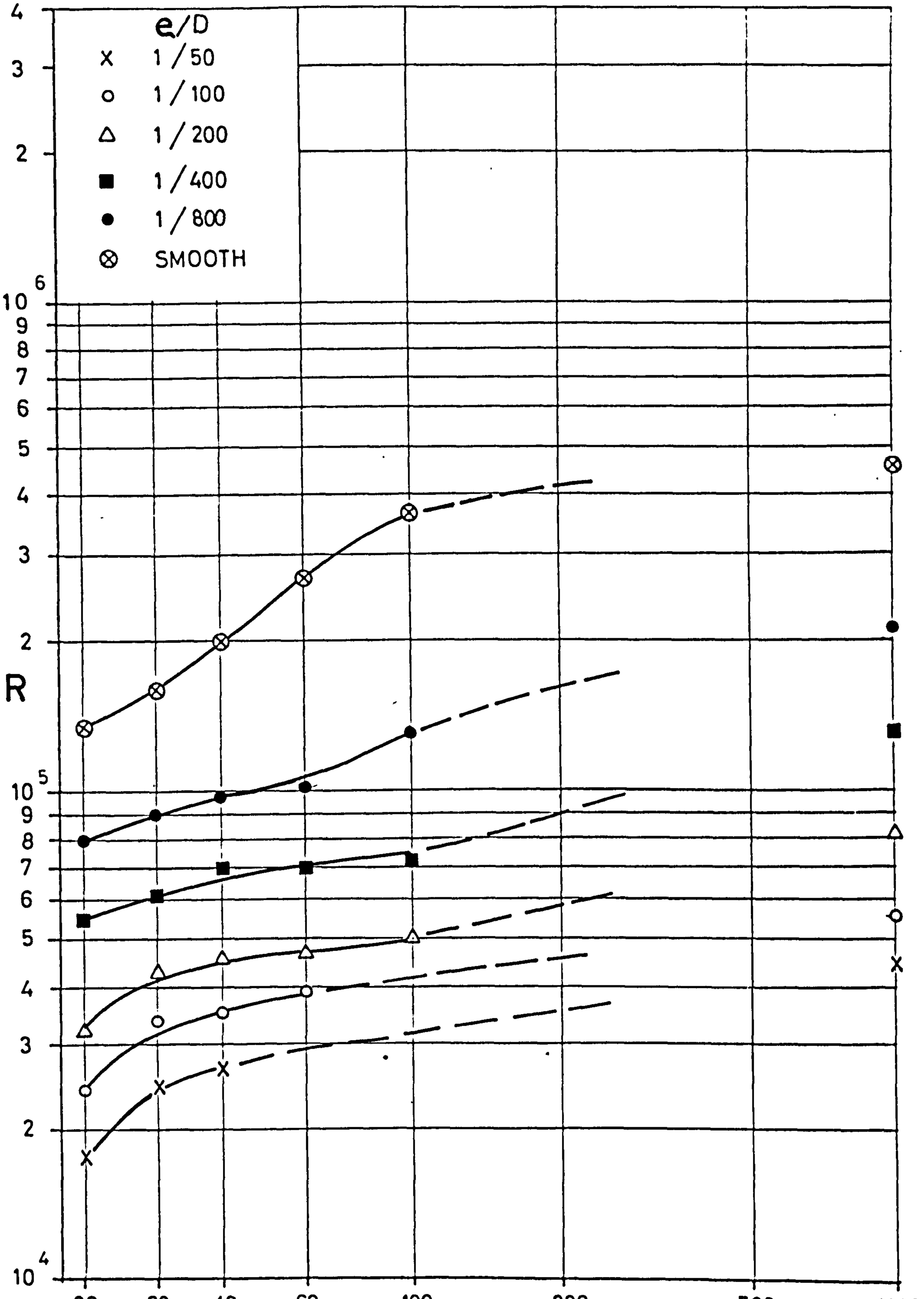

Fig. 17. The value of R and $\dot{K}$ at which C_{DCRIT} occurs for various roughnesses.

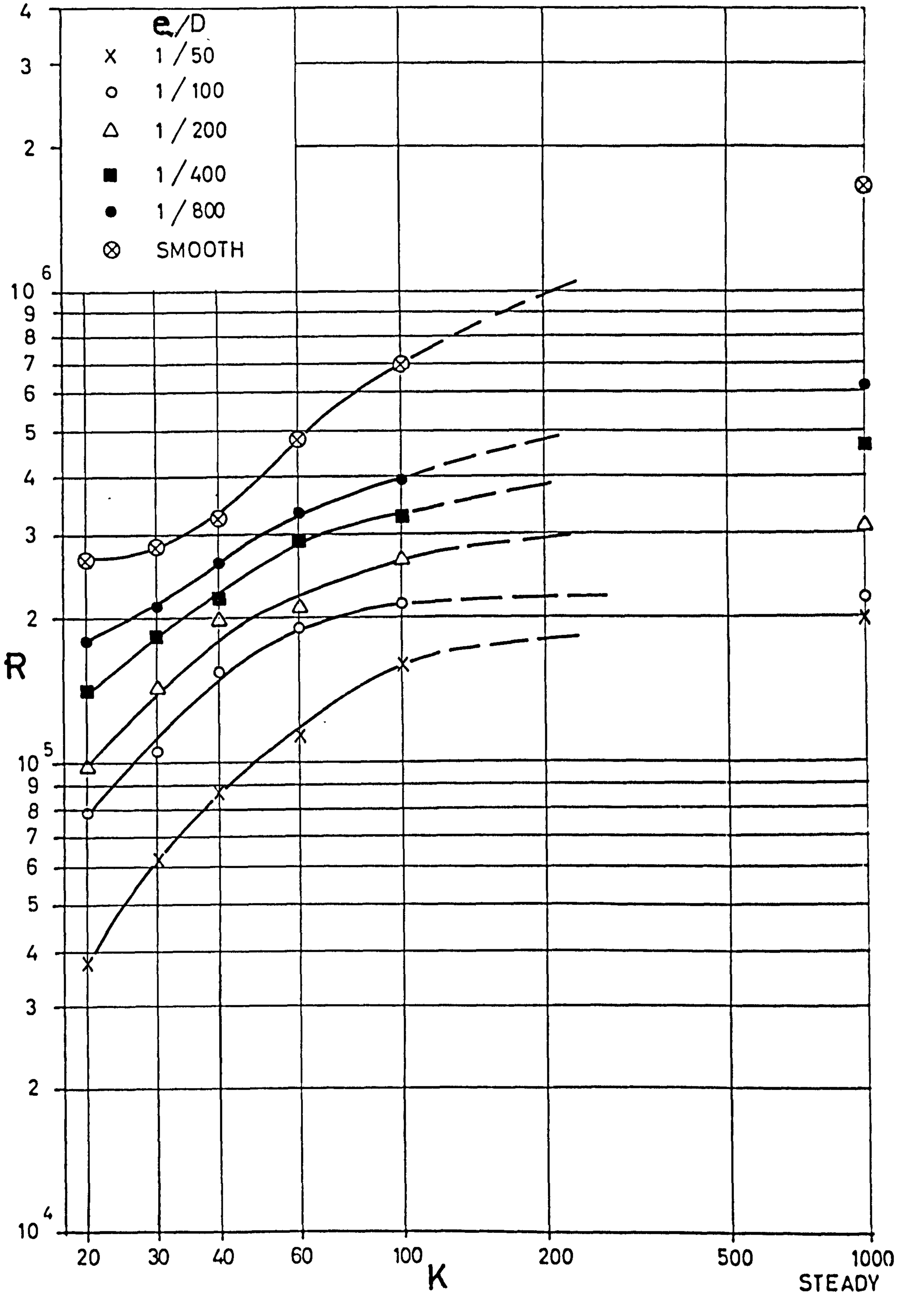

Fig. 18. The value of R and K at which C_D is 95% of its transcritical value for various roughnesses.

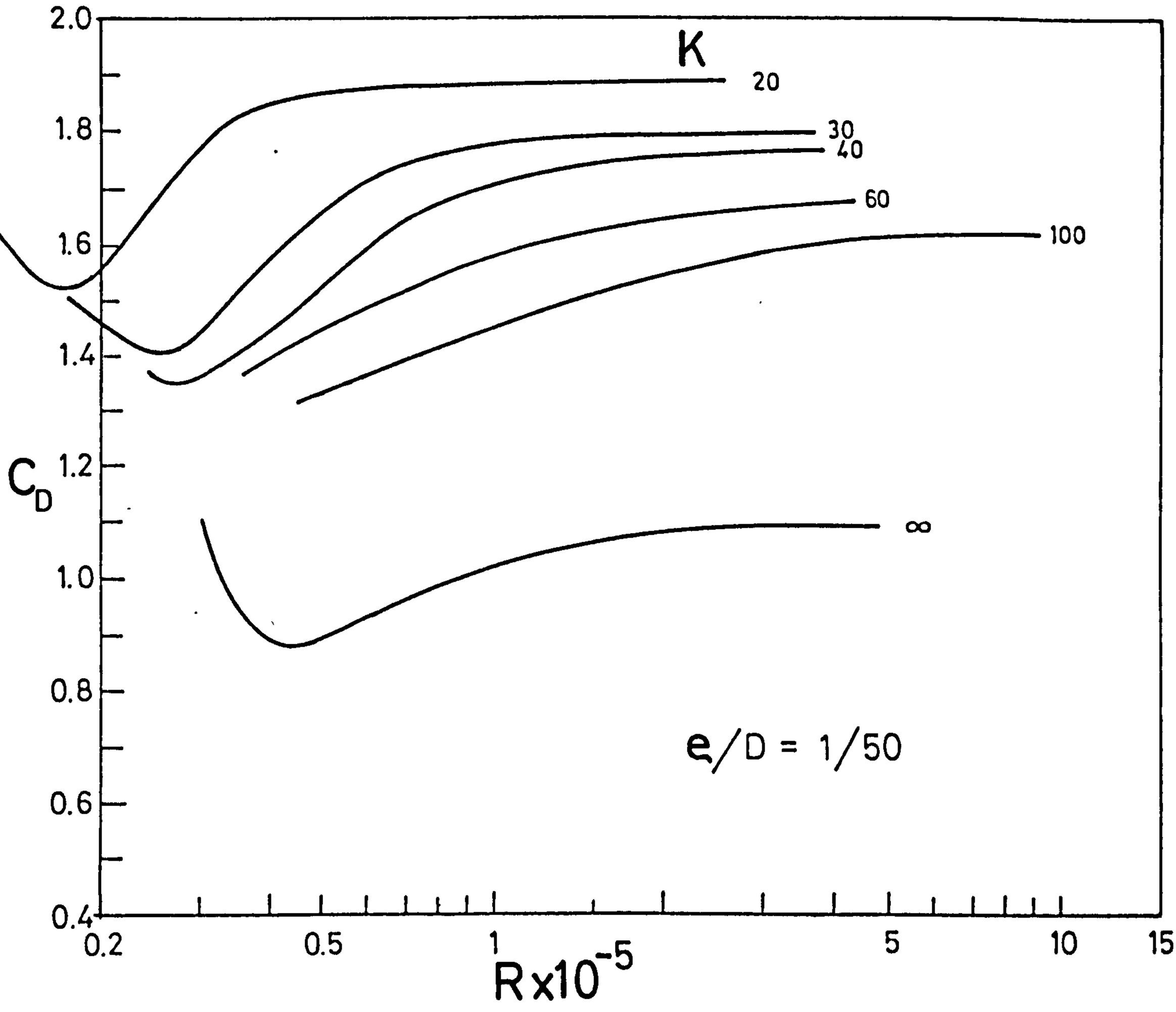

Fig. 19. Curves of C_D versus R for a rough cylinder with e/D = 1/50, at various K.

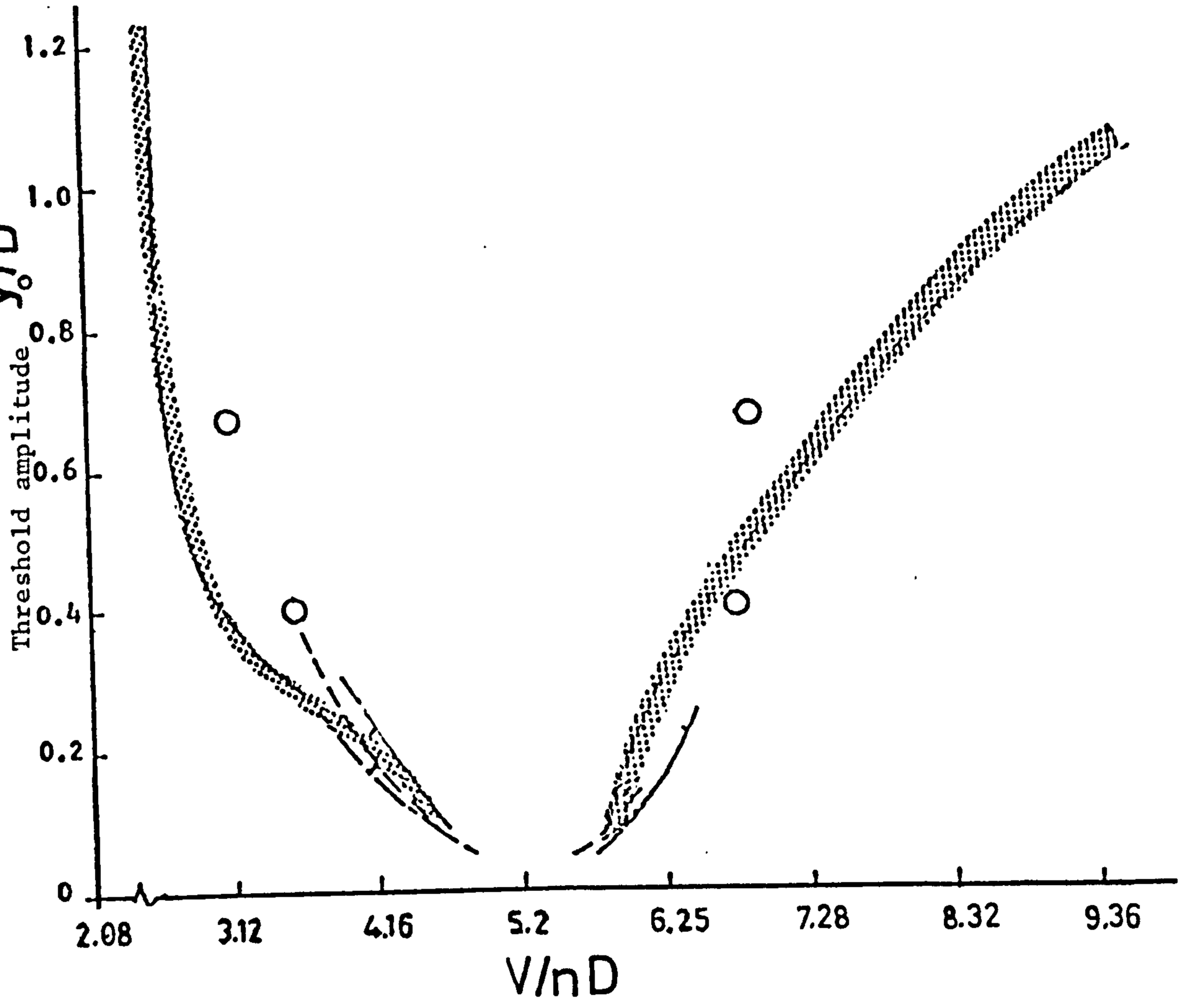

a) Cross-flow oscillations. From Mercier (1973).

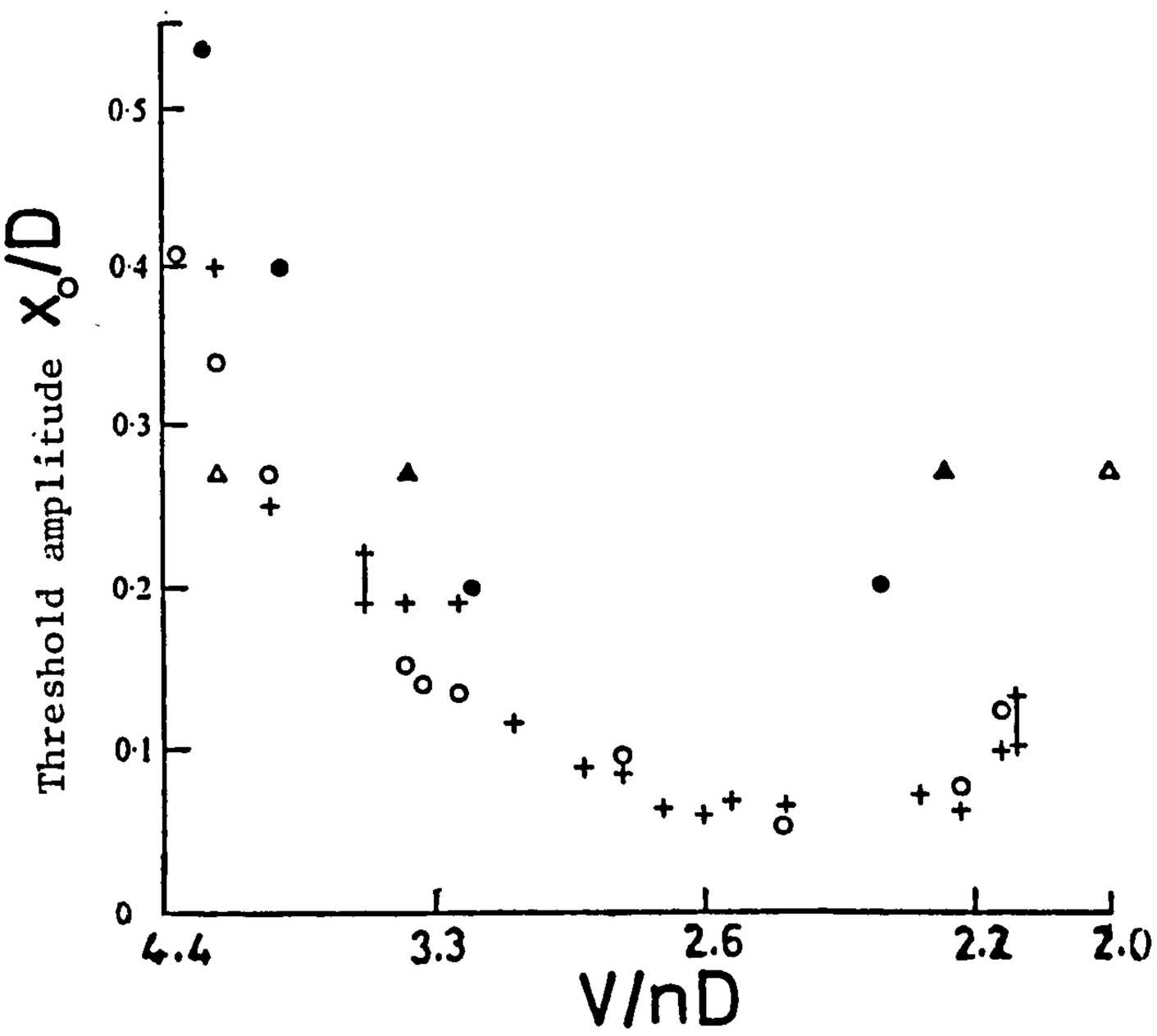

b) In-line oscillations. From Griffin and Ramberg (1976).

Fig. 20. Threshold amplitude for lock-on of the wake to the oscillatory frequency in a) the cross-flow direction, and b) the in-line direction.

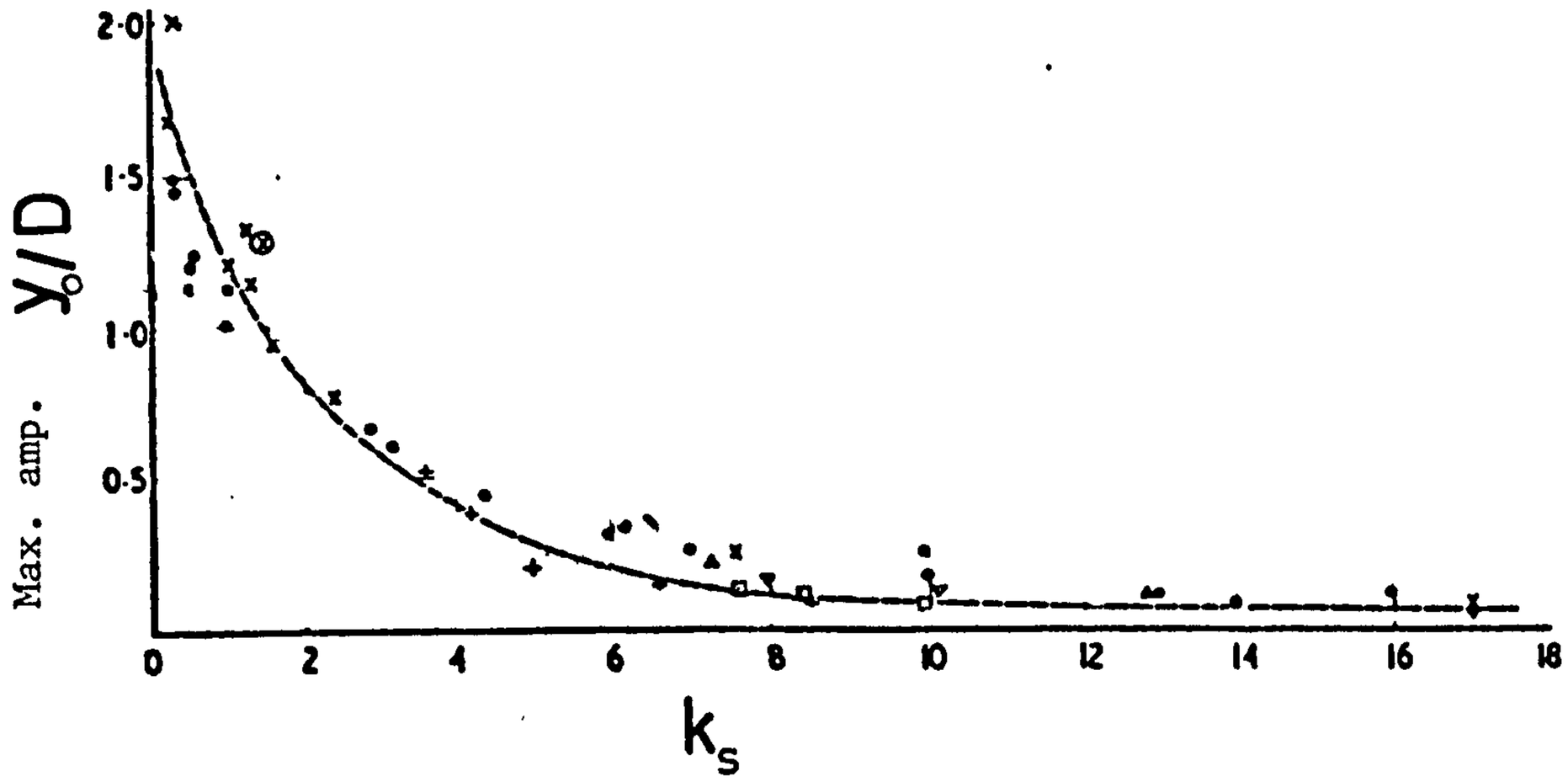

a) Cross-flow oscillations.

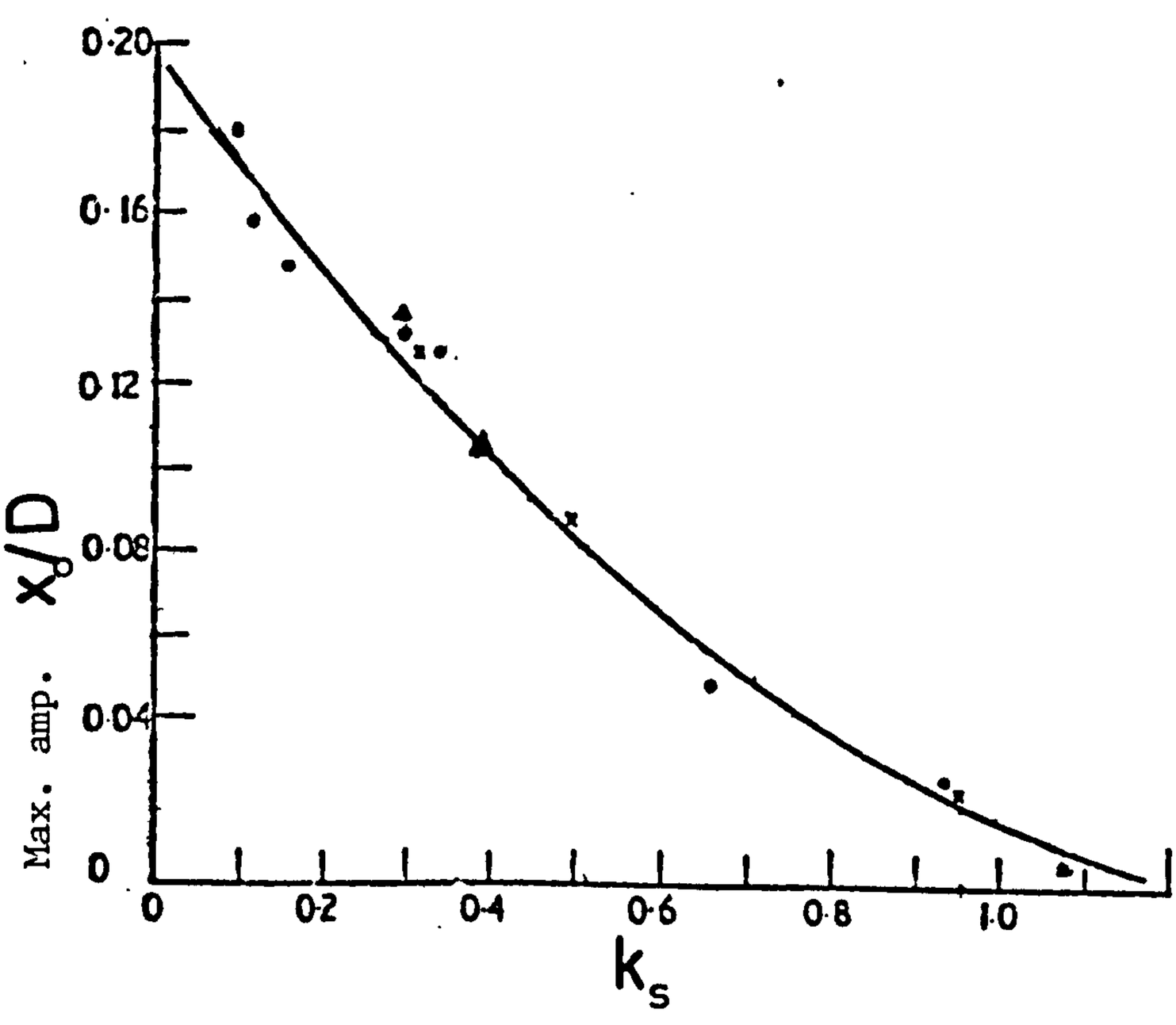

b) In-line oscillations.

Fig. 21. Maximum amplitude of hydroelastic vibration in a) the cross-flow direction, and b) the in-line direction. From King (1975).

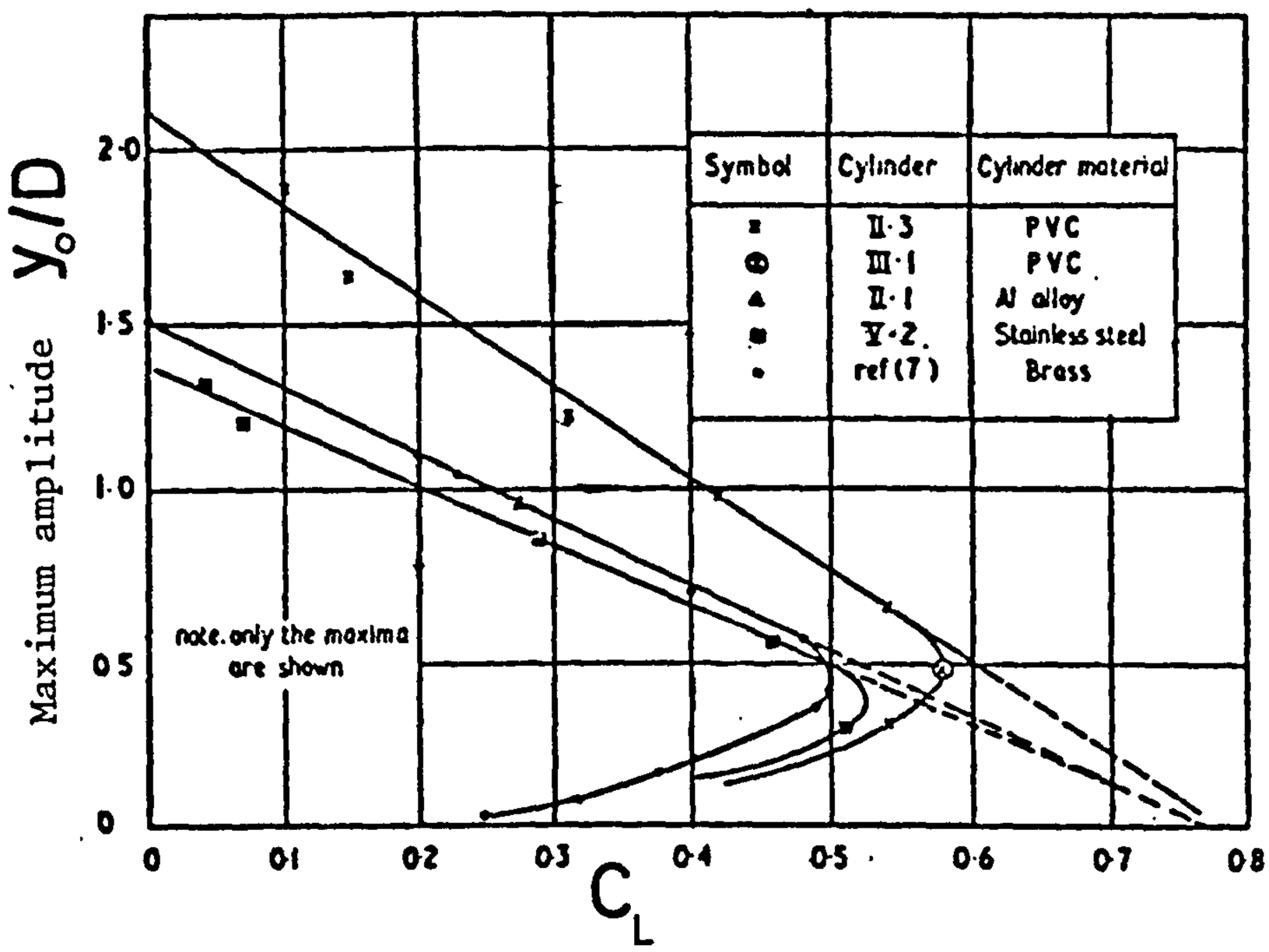

a) Cross-flow instability.

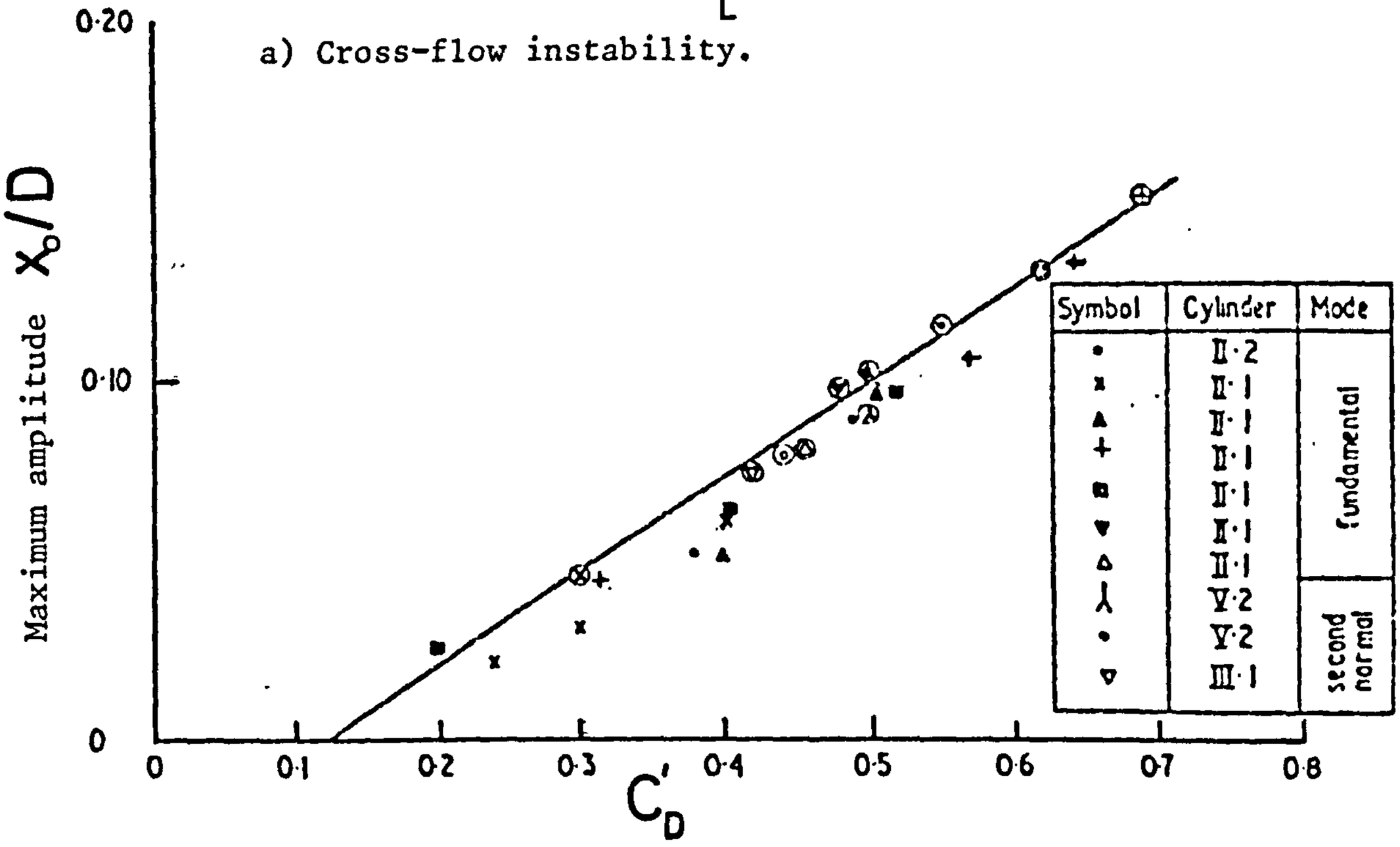

b) First in-line instability.

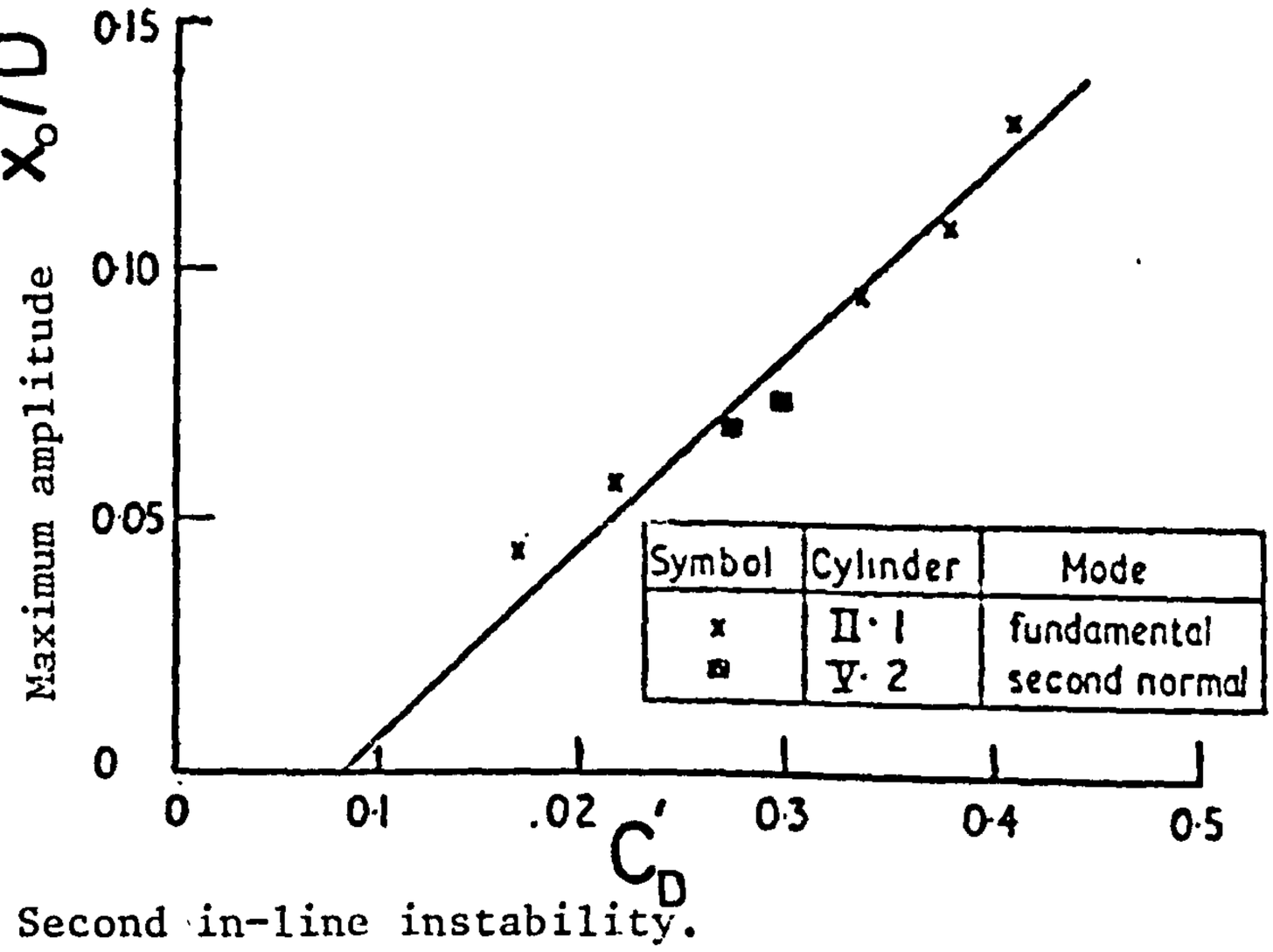

c) Second in-line instability.

Fig. 22. Unsteady lift and drag coefficients, C_L and C_D' calculated from

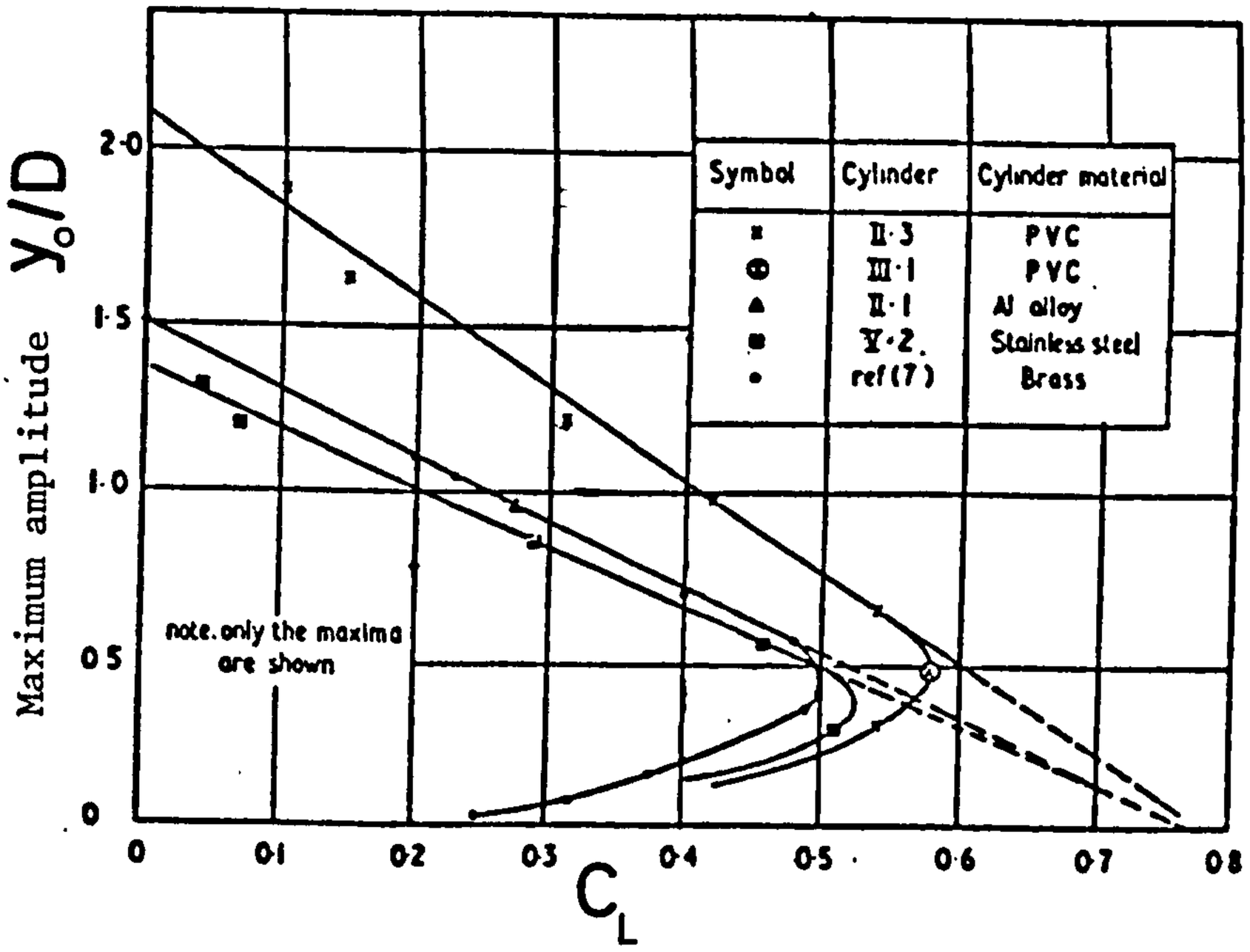

a) Cross-flow instability.

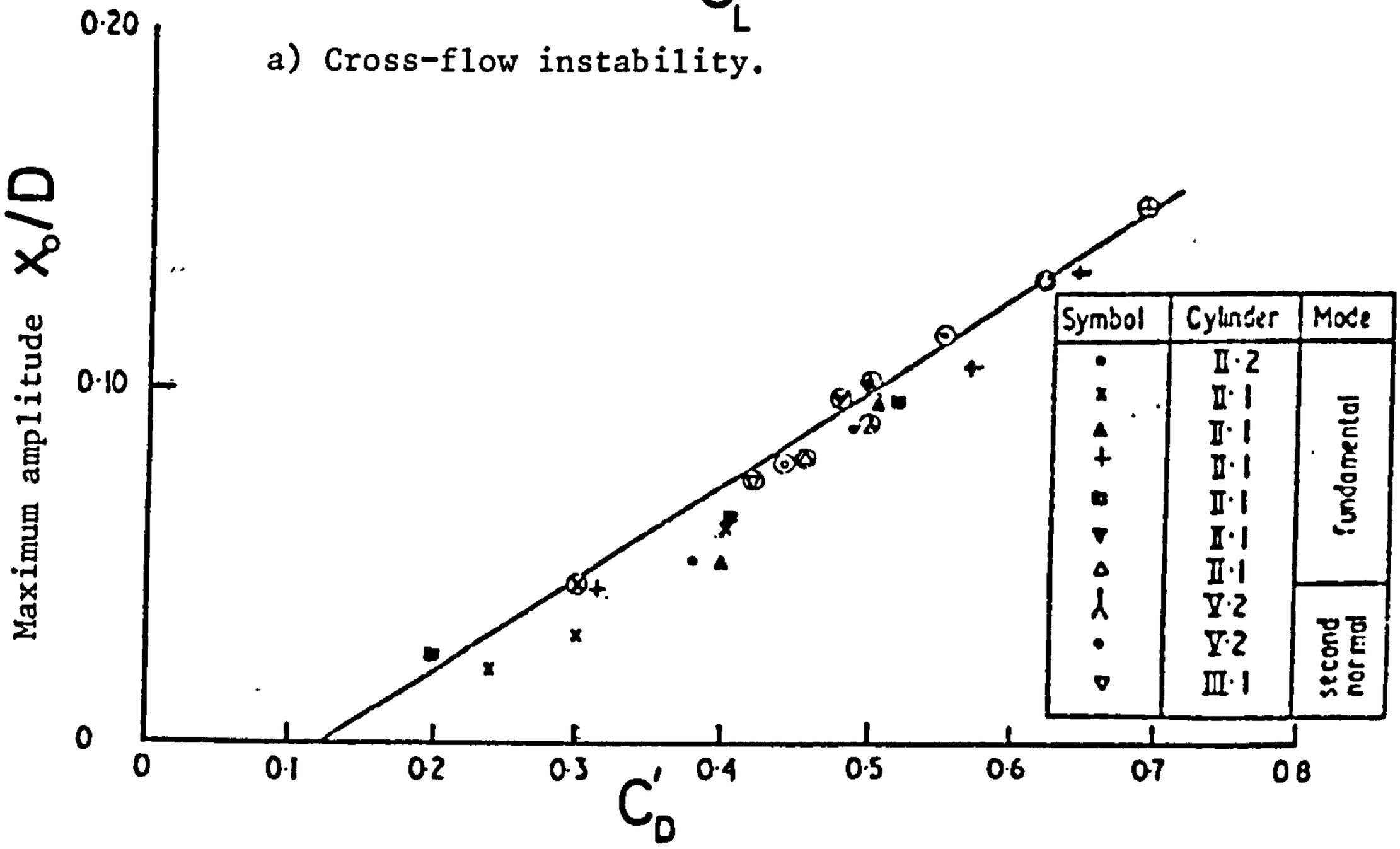

b) First in-line instability.

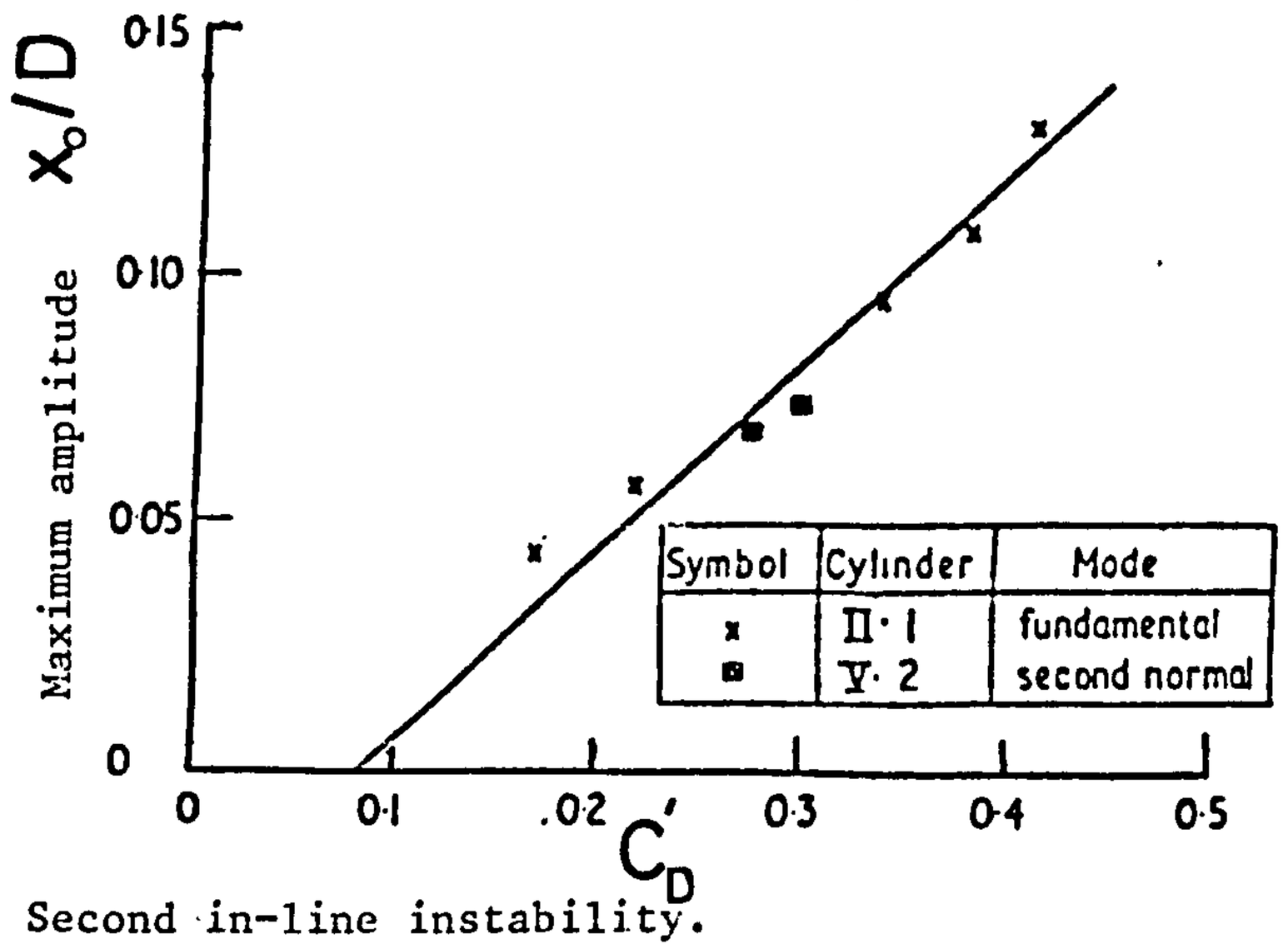

c) Second in-line instability.

Fig. 22. Unsteady lift and drag coefficients, C_L and C_D' calculated from max. response to hydroelastic vibrations. From King (1975).

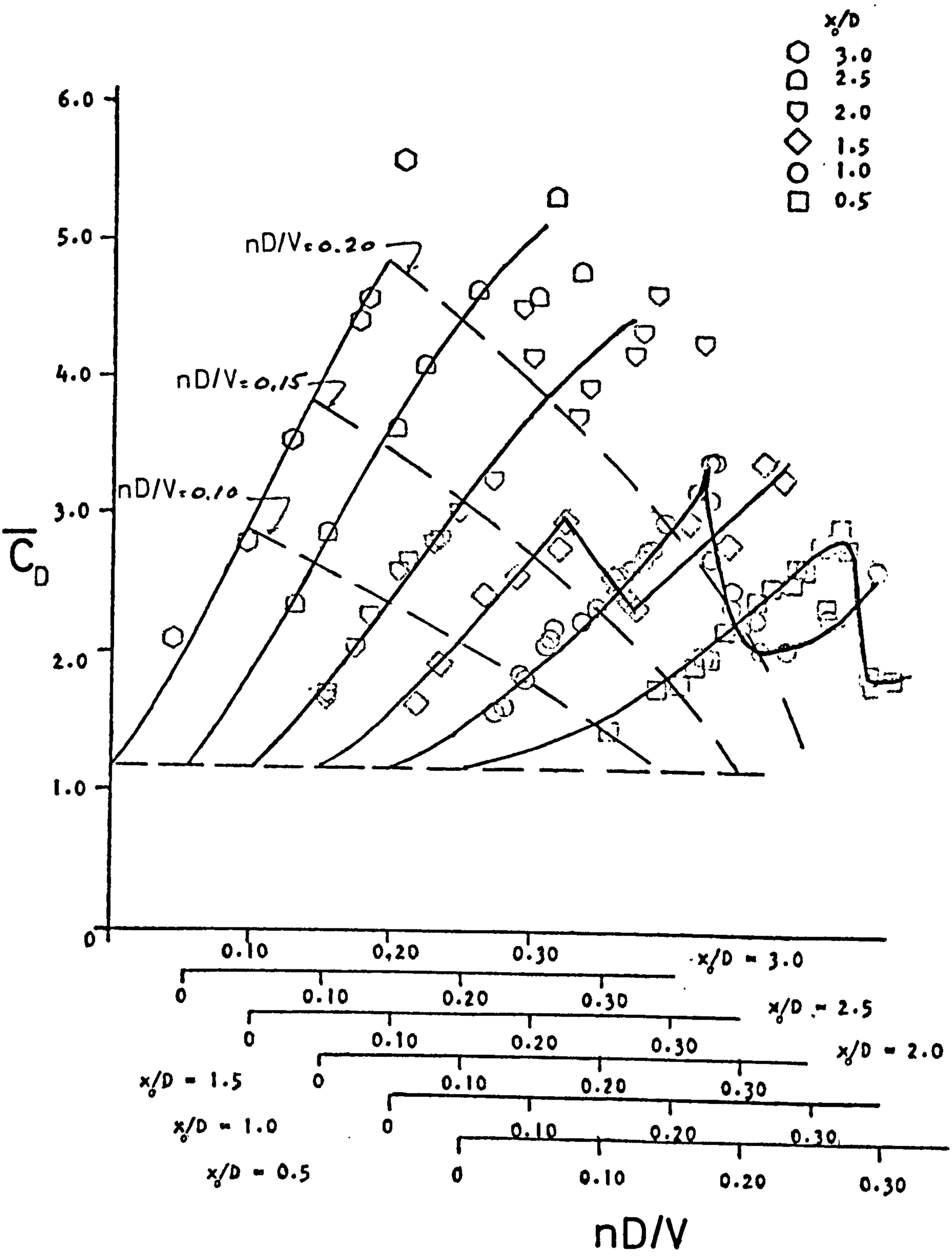

Fig. 23. The steady component of drag coefficient, $\bar{C}_D$ for cylinders oscillating in steady currents. From Mercier (1973).

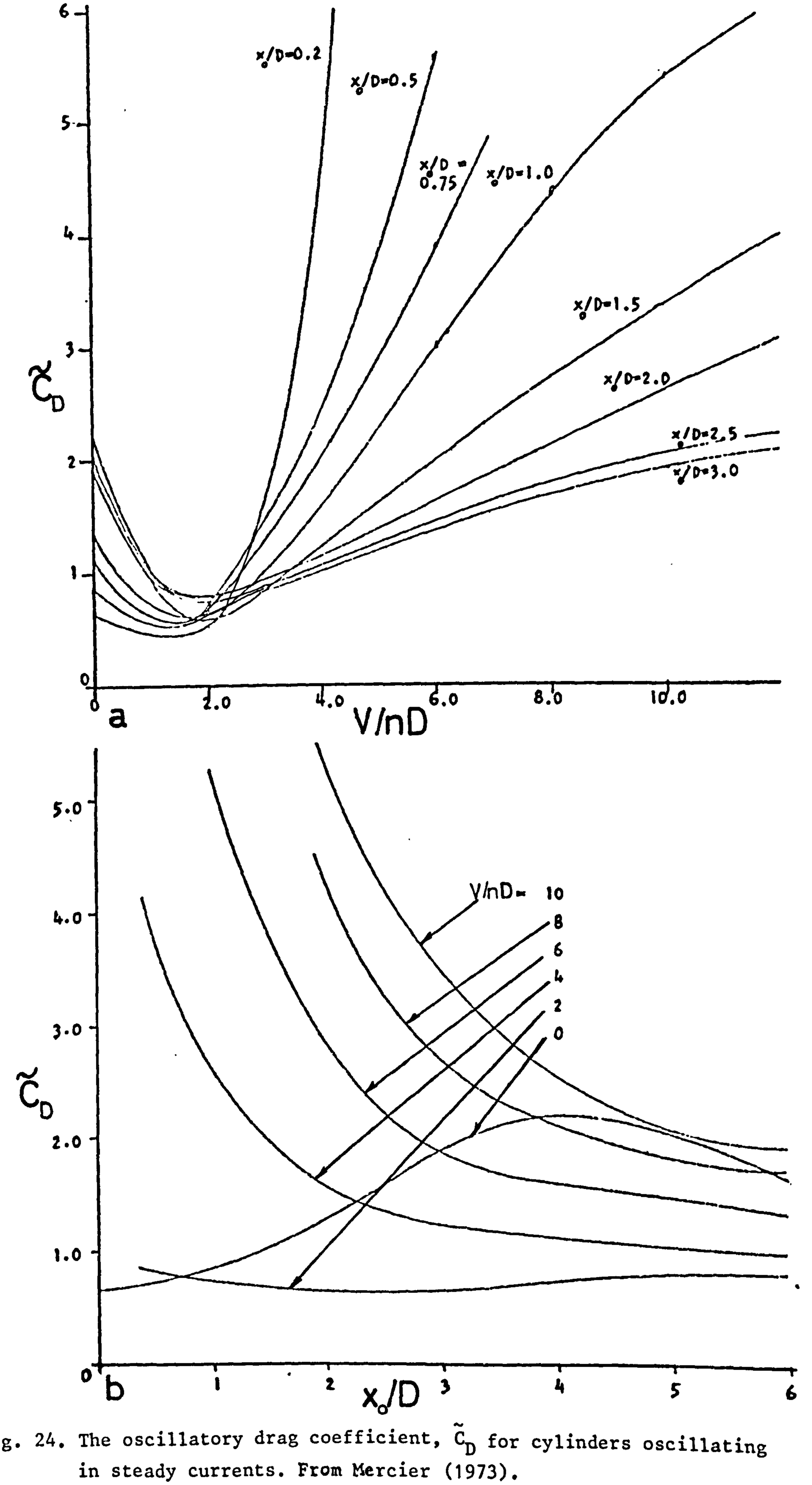

Fig. 24. The oscillatory drag coefficient, $\tilde{C}_D$ for cylinders oscillating in steady currents. From Mercier (1973).

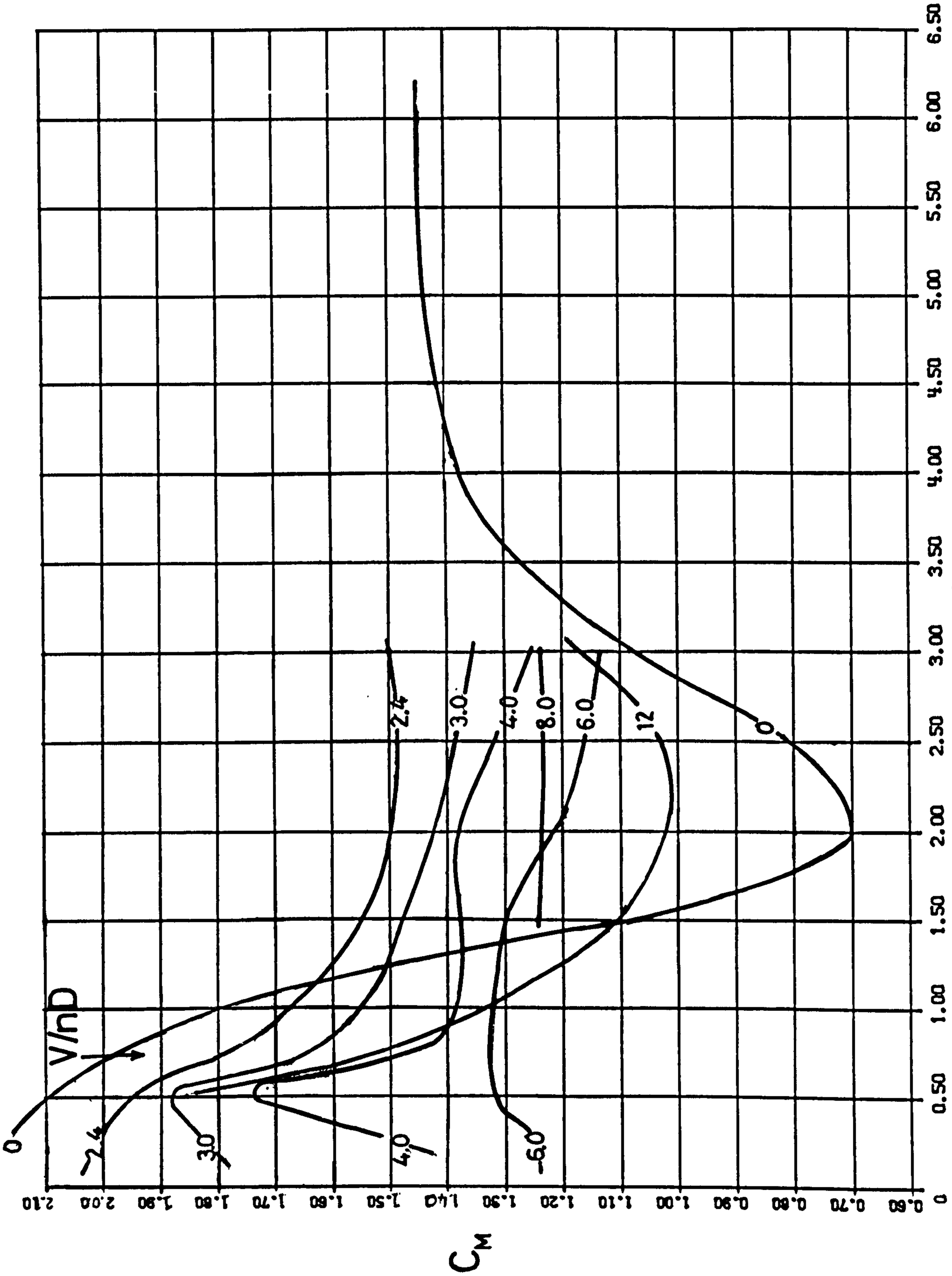

Fig. 25. The inertia coefficient, C_M for cylinders oscillating in steady currents. From data of Mercier (1973).

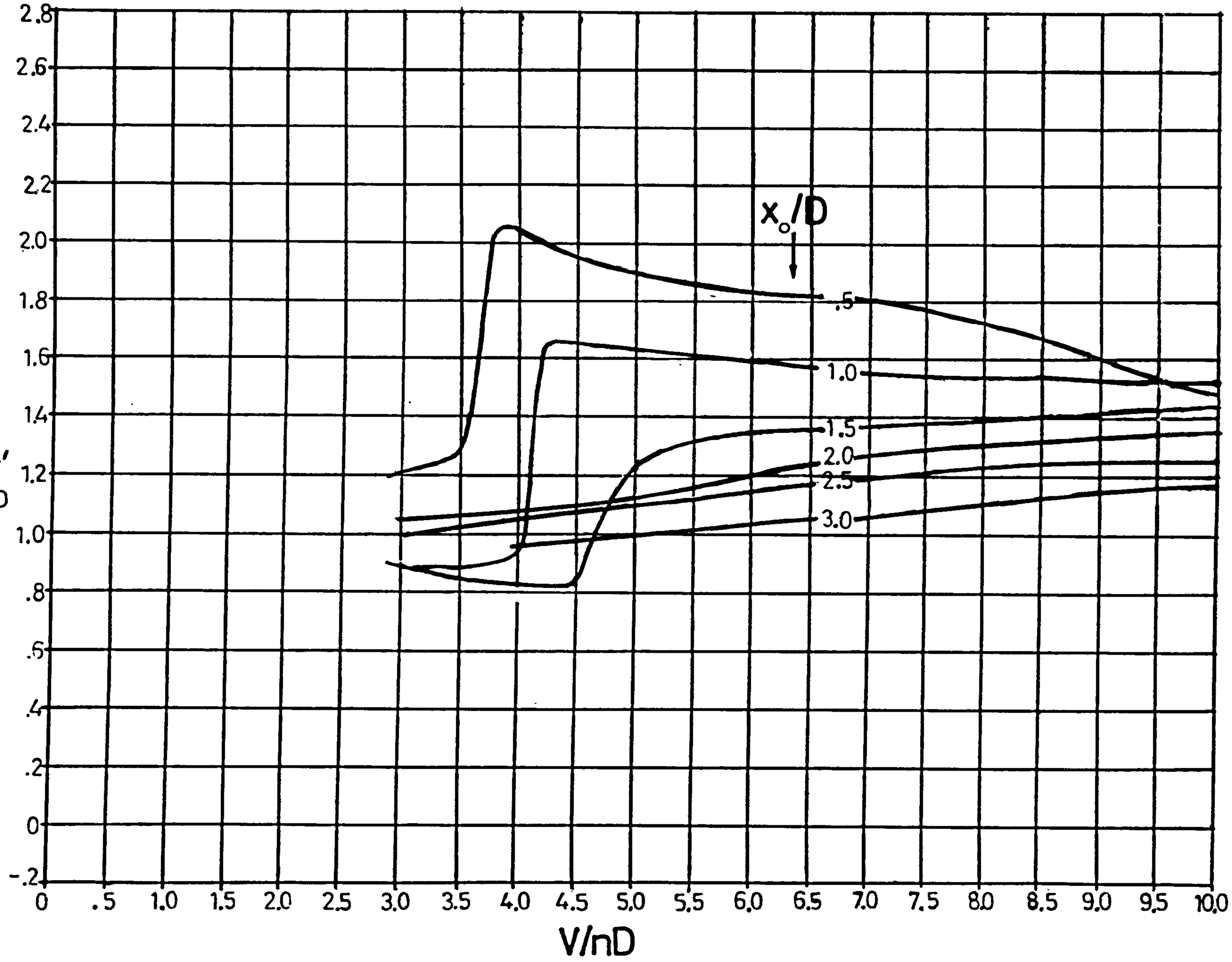

Fig. 26. The steady component of drag coefficient, $\bar{C}_D'$ for cylinders oscillating in steady currents. Data of Mercier (1973). As reanalysed by Matten (1976).

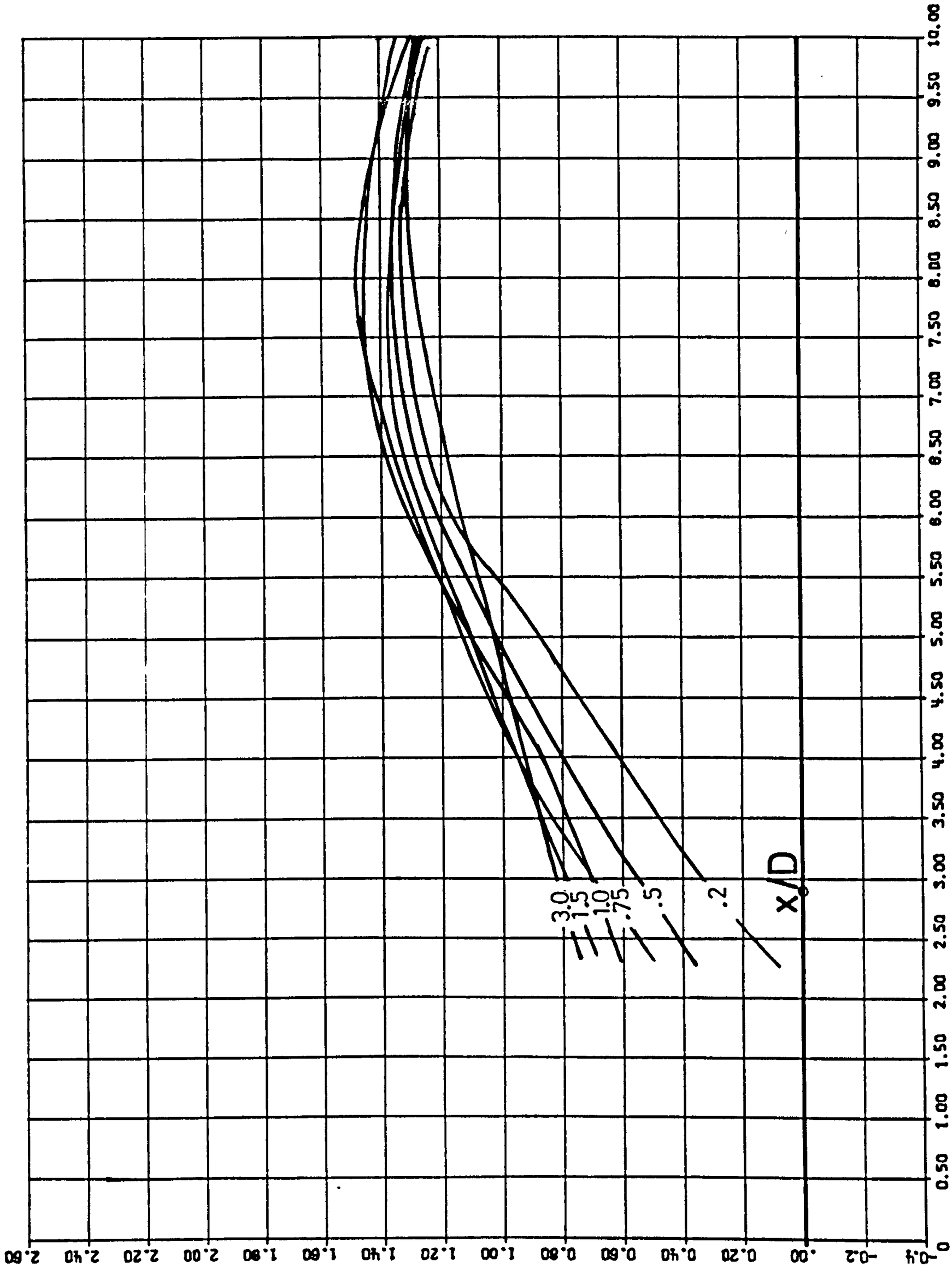

Fig. 27. The oscillatory drag coefficient, $\tilde{C}'_D$ for cylinders oscillating in steady currents. Data of Mercier (1973) as reanalysed by Matten (1976).

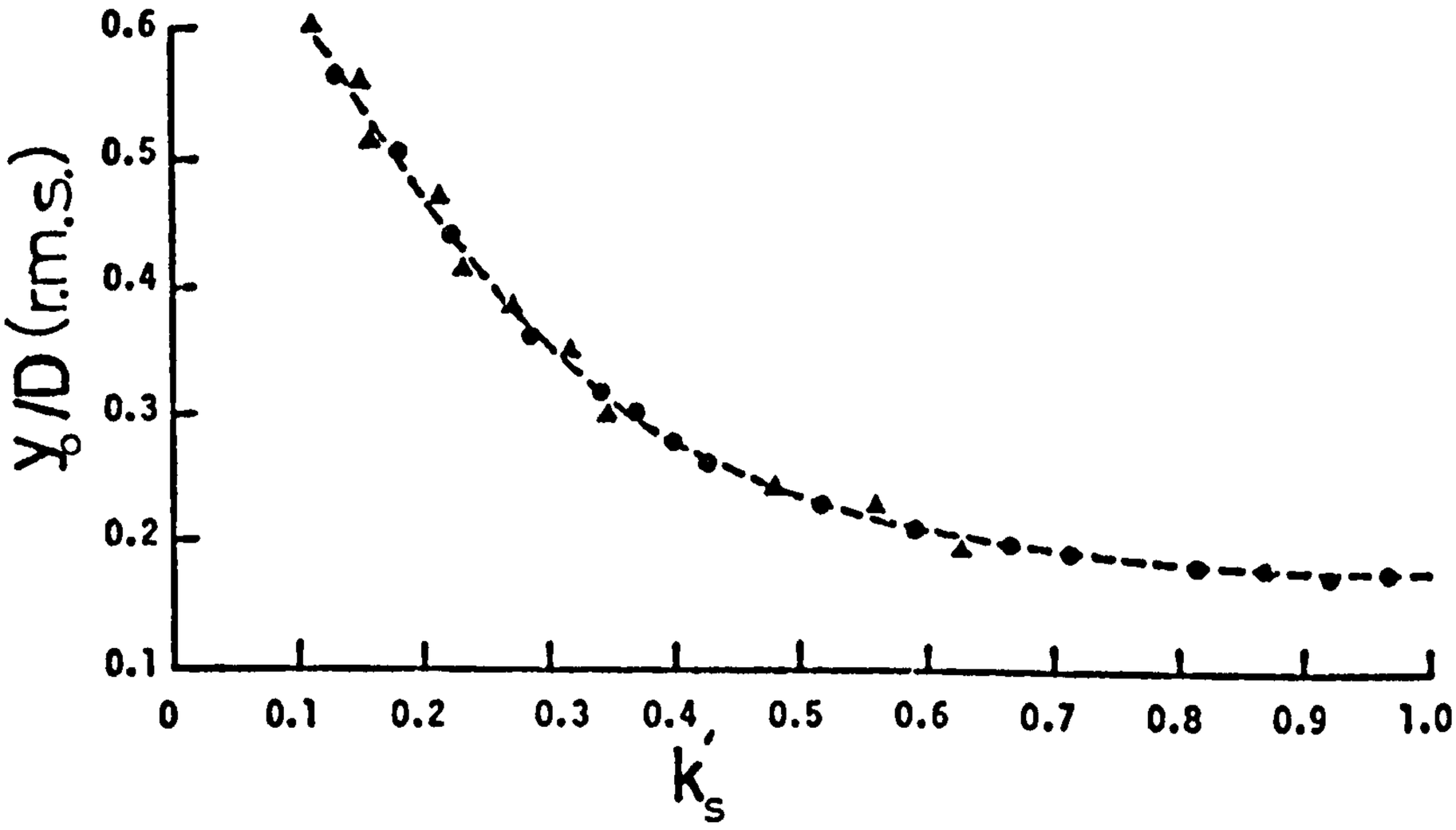

Fig. 28. Maximum amplitude of cross-flow hydroelastic vibrations in oscillatory flows as a function of the modified stability parameter, k_s'. From Sarpkaya (1978).

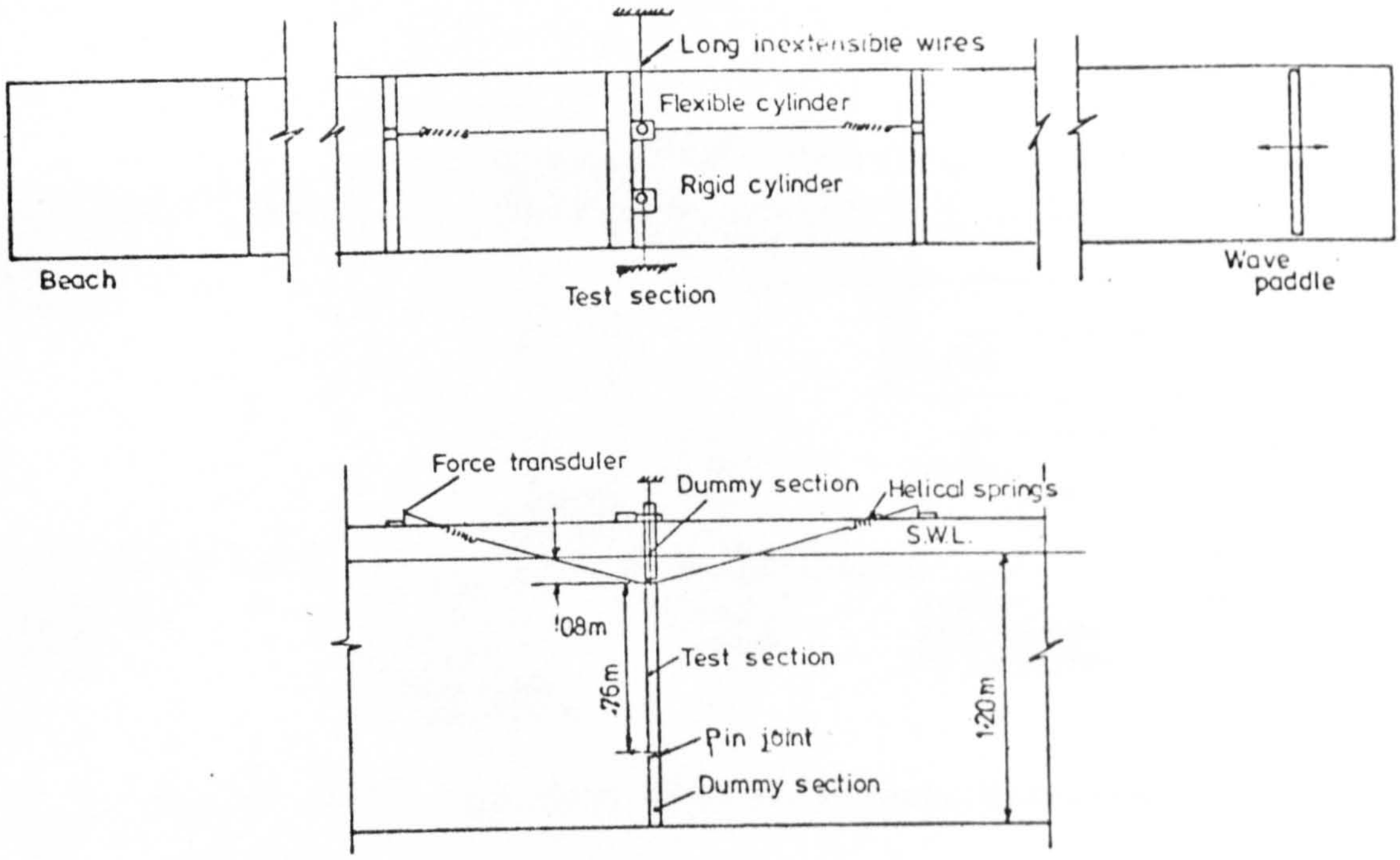

Fig. 29. Sketch of the test set-up for investigating the vibrations of cylinders in waves.

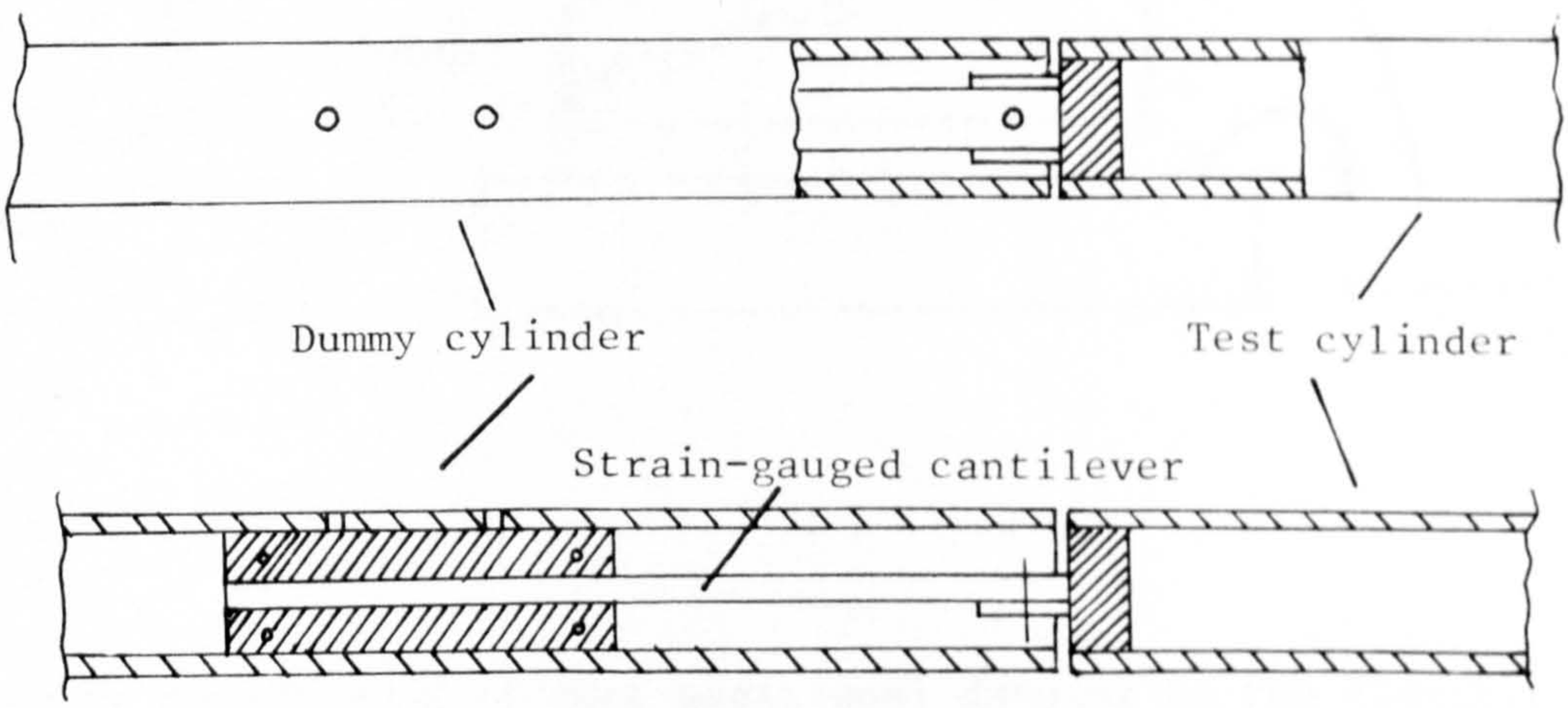

Fig. 30. Sketch of the system used to measure reactions from the rigid cylinder.

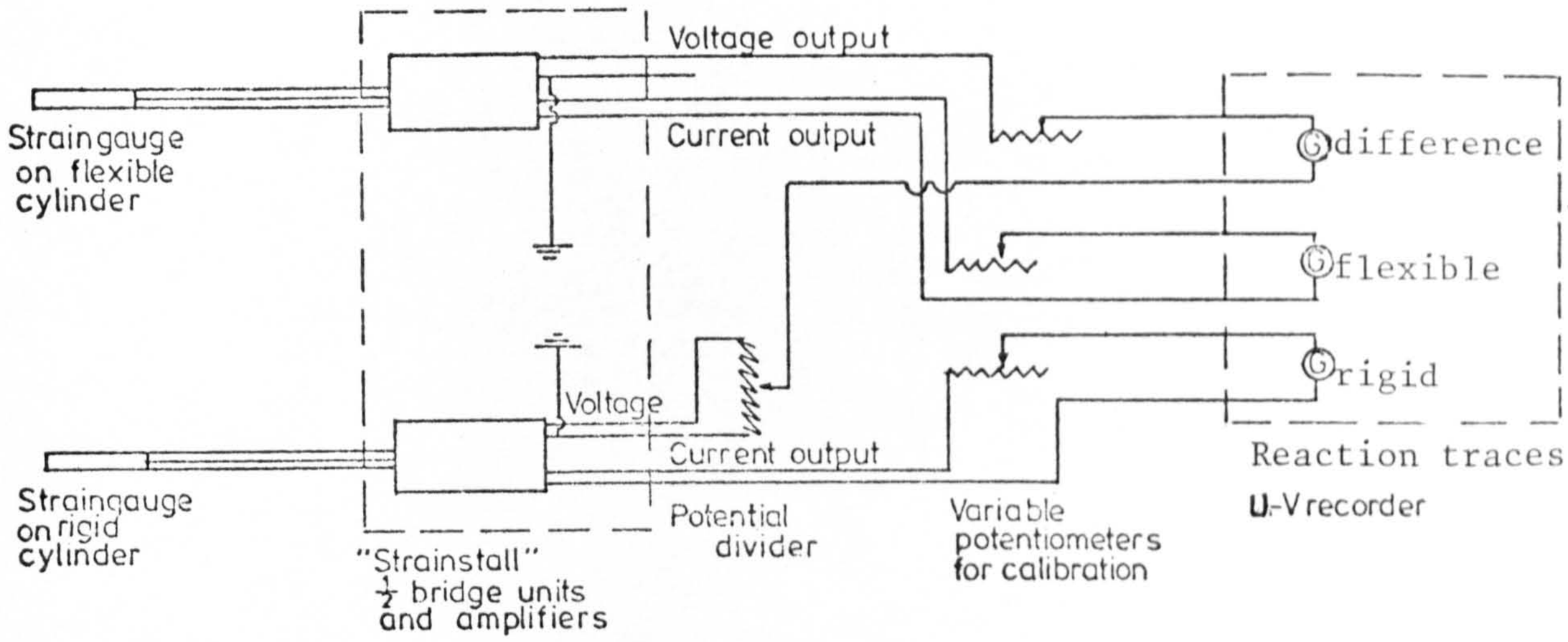

Fig. 31. Sketch of the circuitry used to measure reactions of the cylinders.

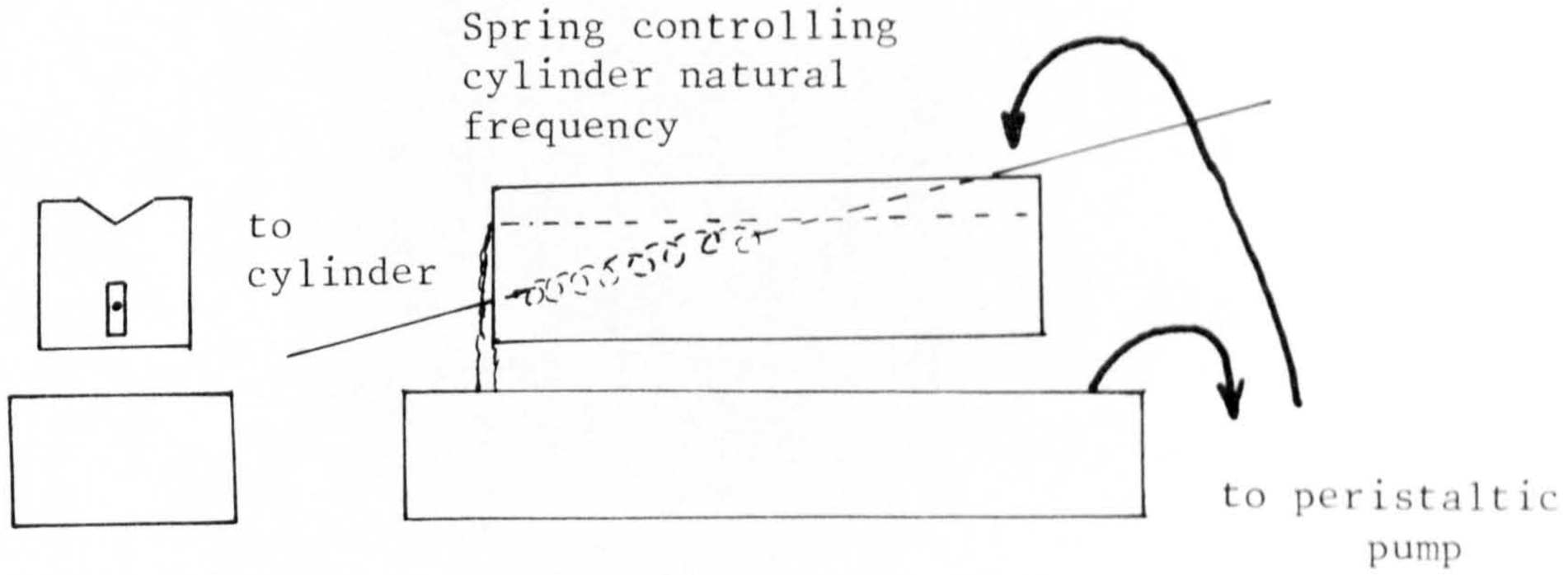

Fig. 32. Method used to give additional damping to the flexible cylinder.

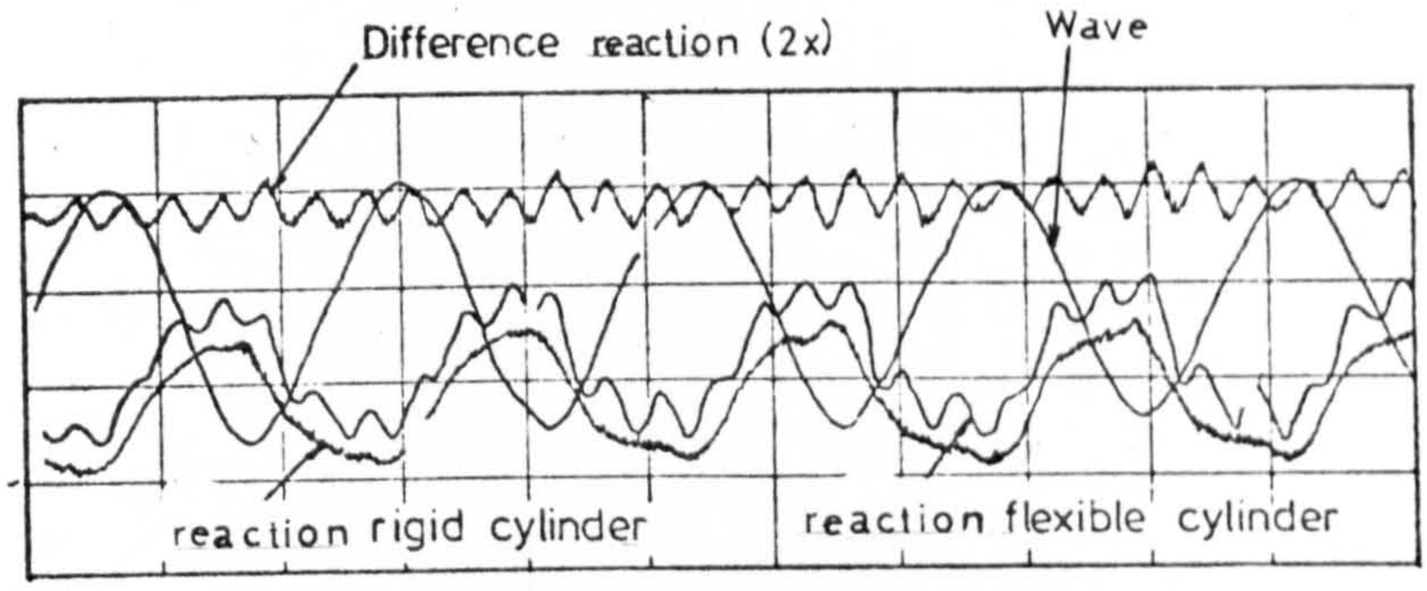

Fig. 33. Example outputs from initial tests in the in-line direction.

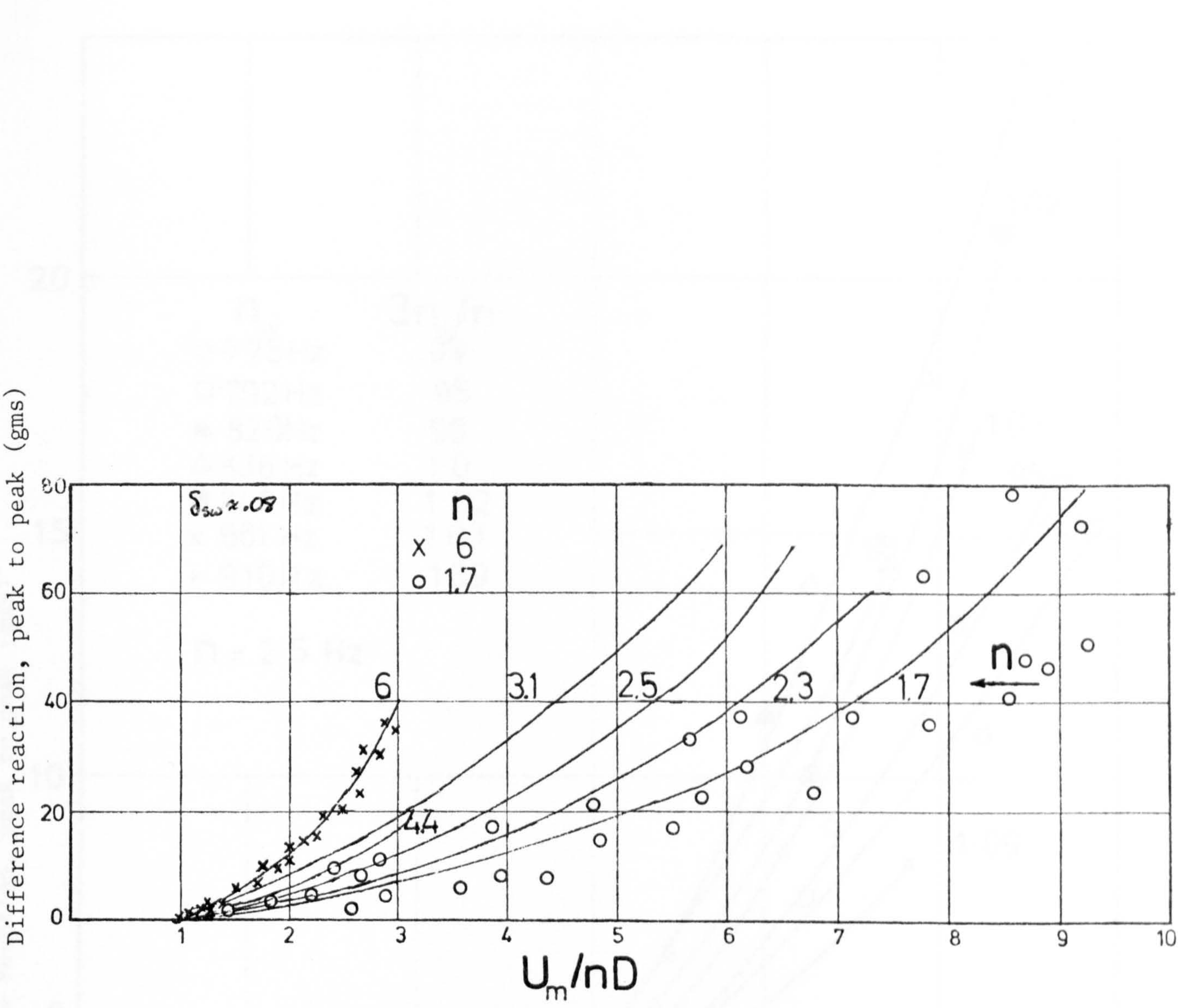

Fig. 34. Results of initial tests in the in-line direction.

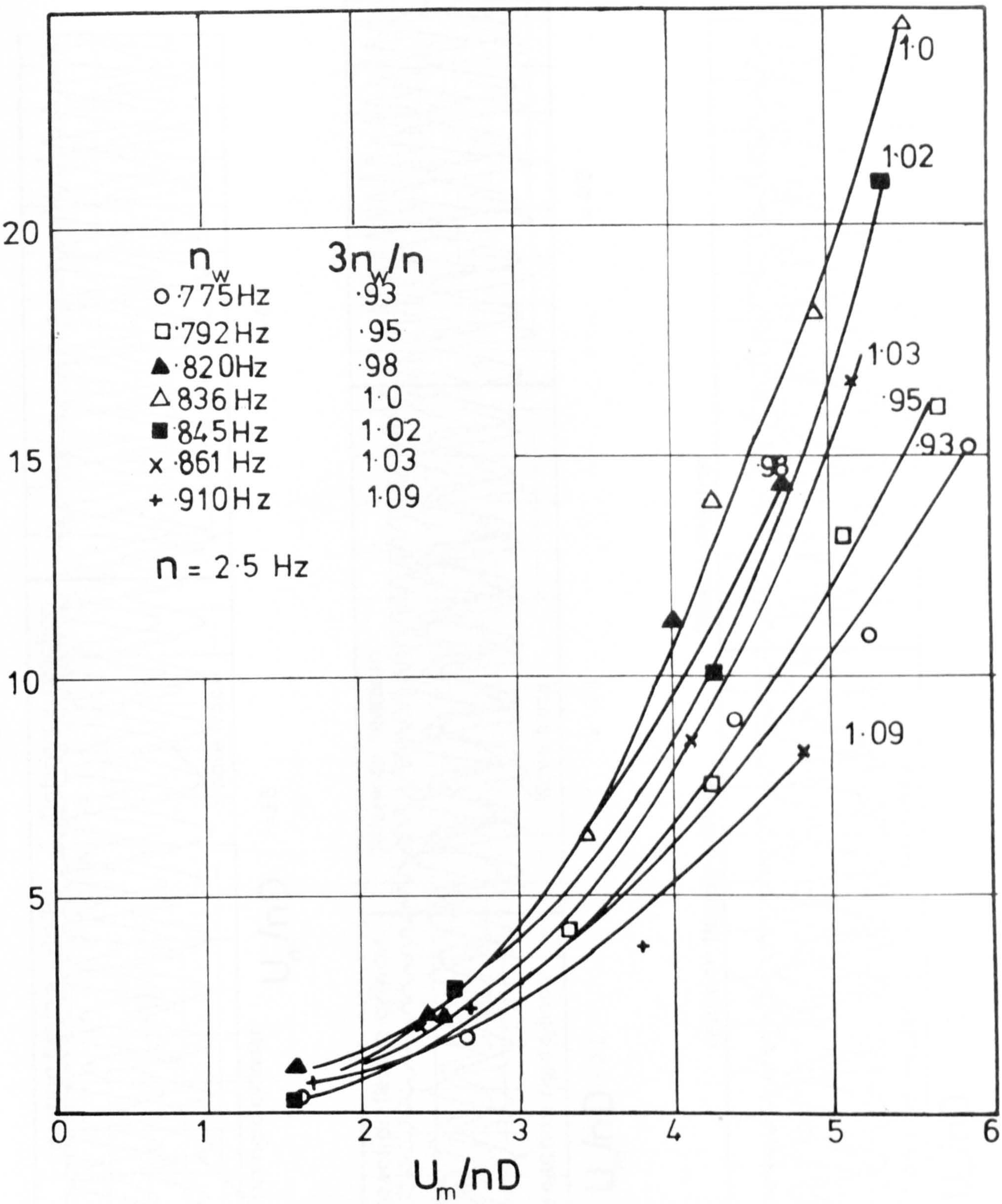

Fig. 35 . Quantitative results illustrating the effect of the frequency parameter on the response.

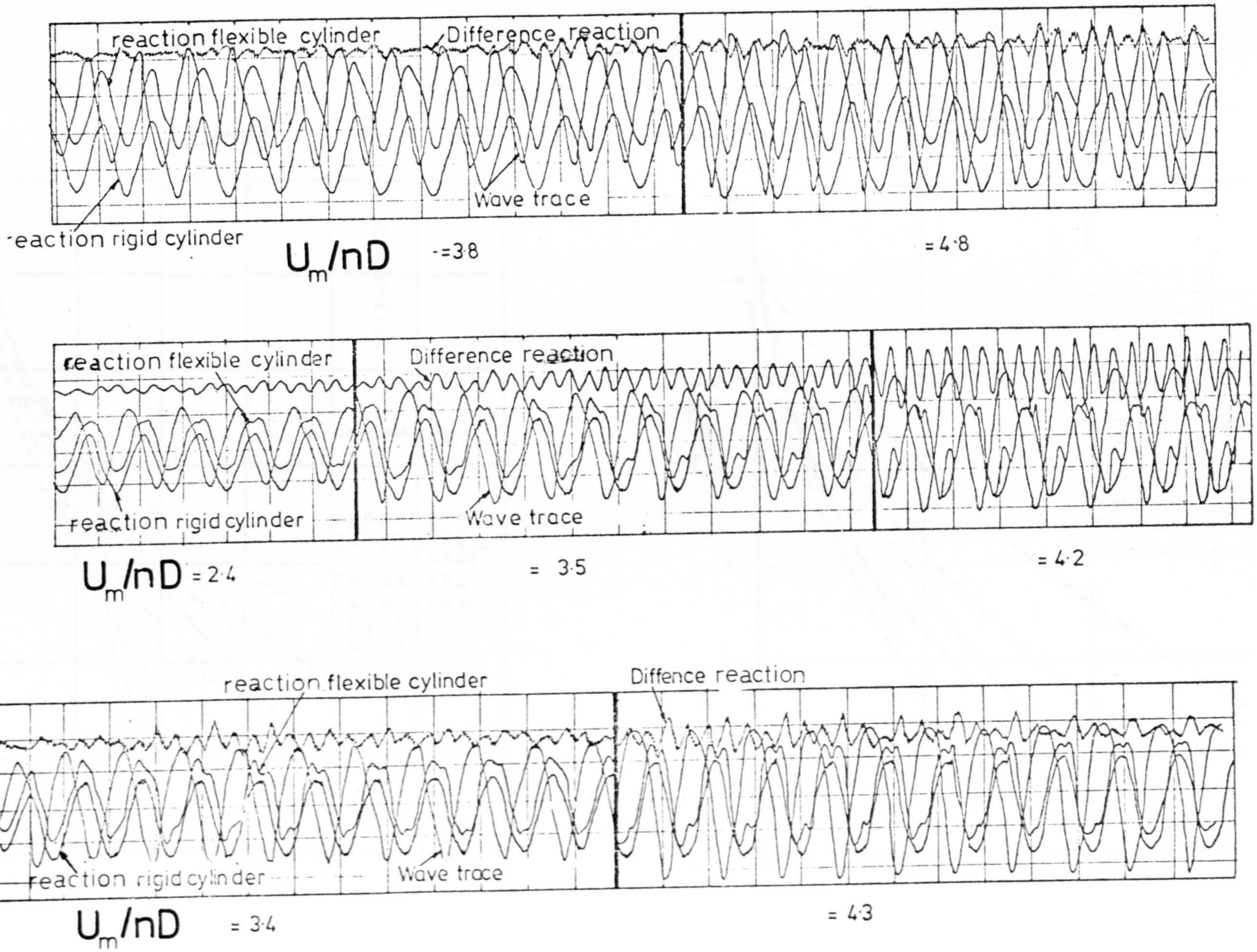

Fig. 36. Traces of the cylinder reactions for various values of $3n_w/n$.

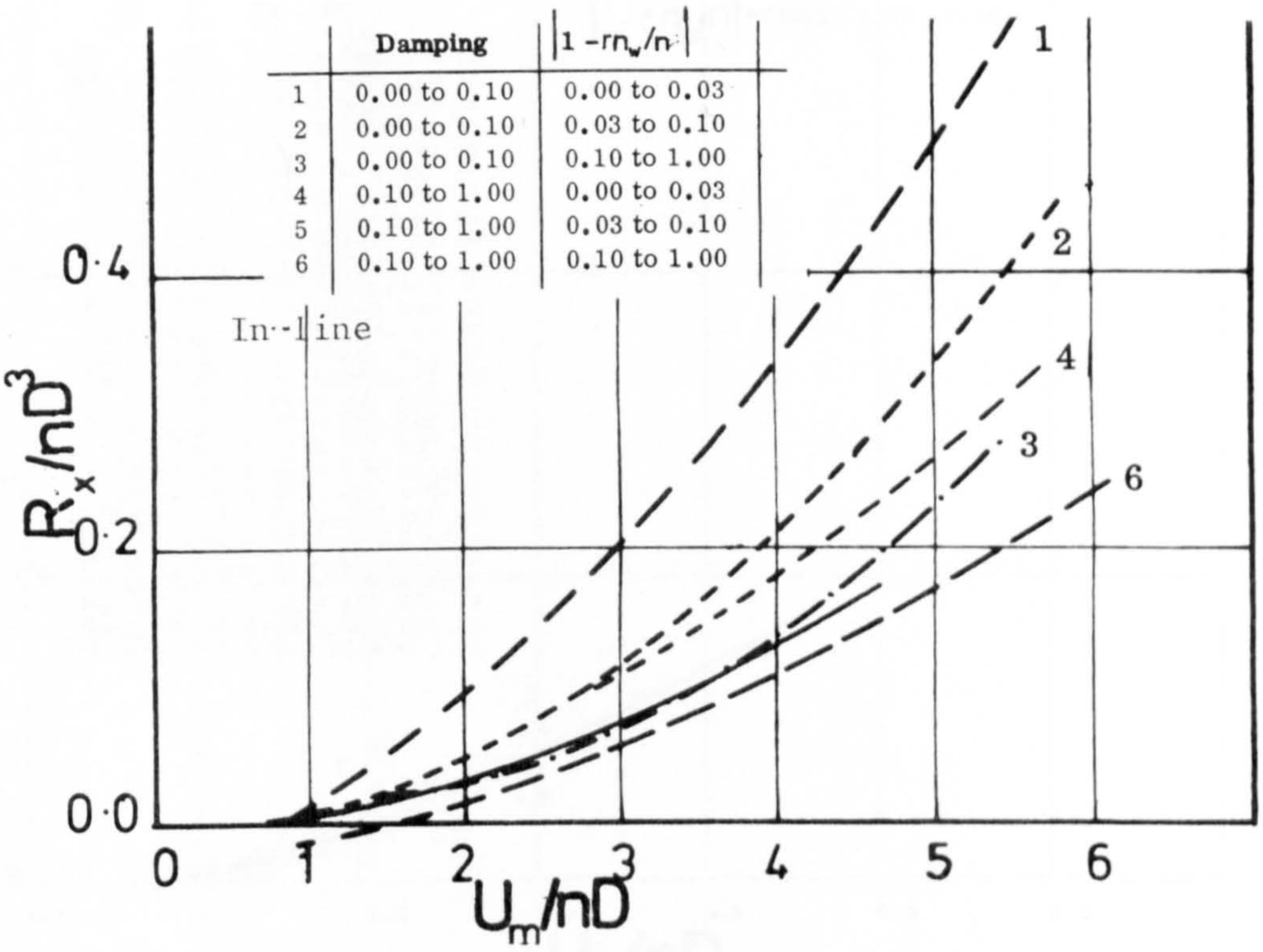

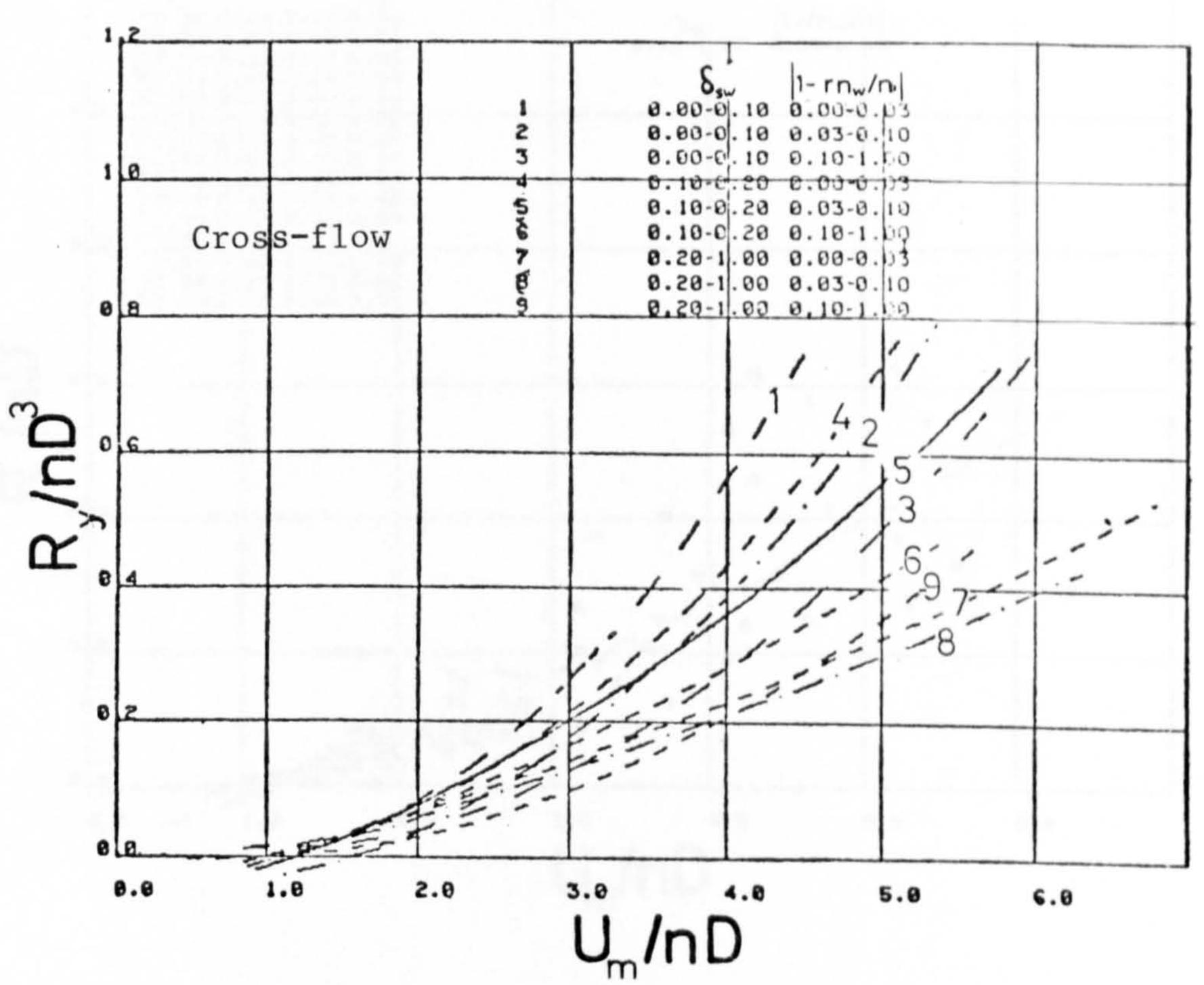

Fig. 37. Averaged results for various values of δ and $|1-rn_w/n|$ for the in-line and cross-flow directions.

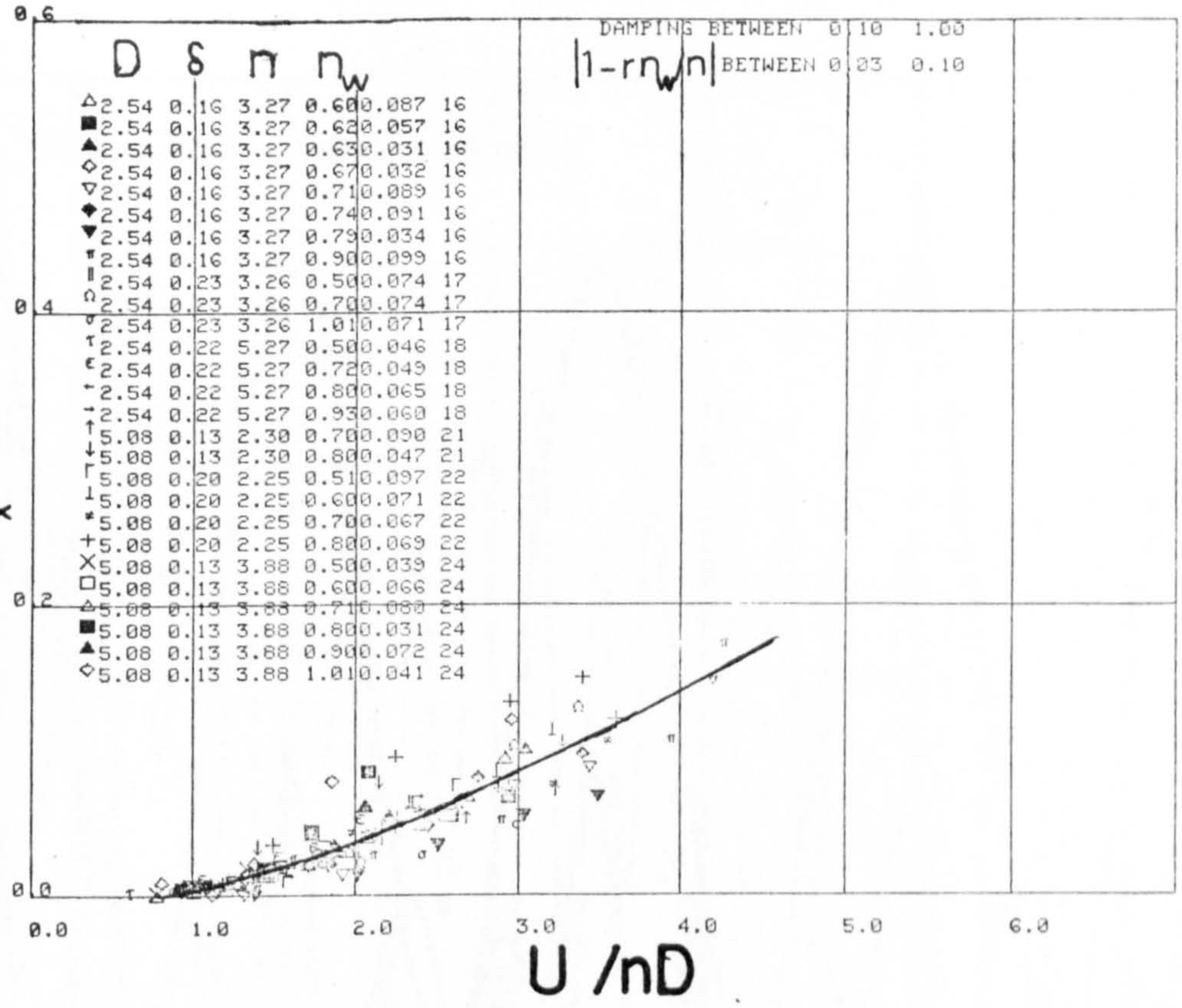

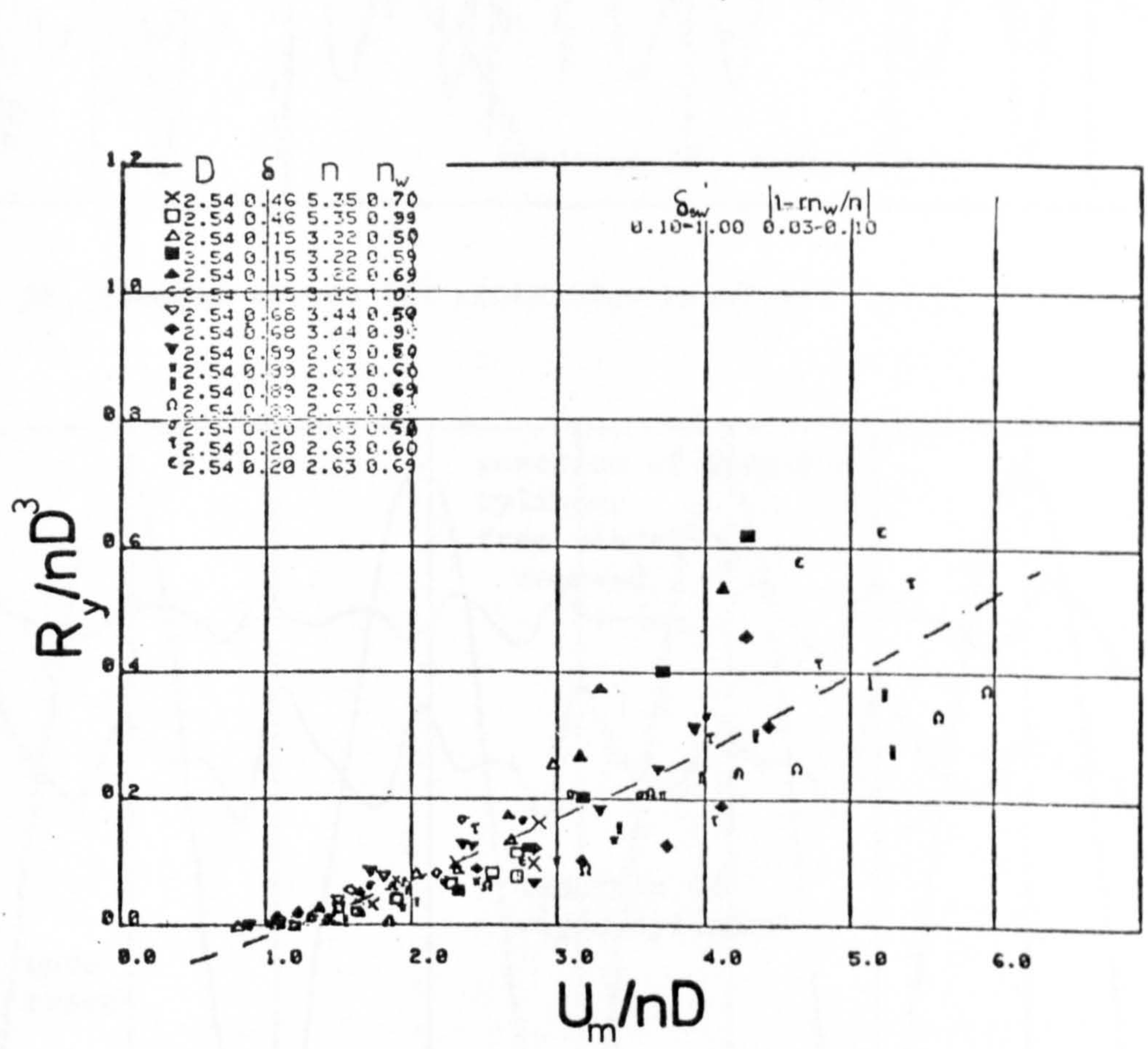

Fig. 38. Example experimental points and averaged curves from Fig. 37 for the in-line and cross-flow directions.

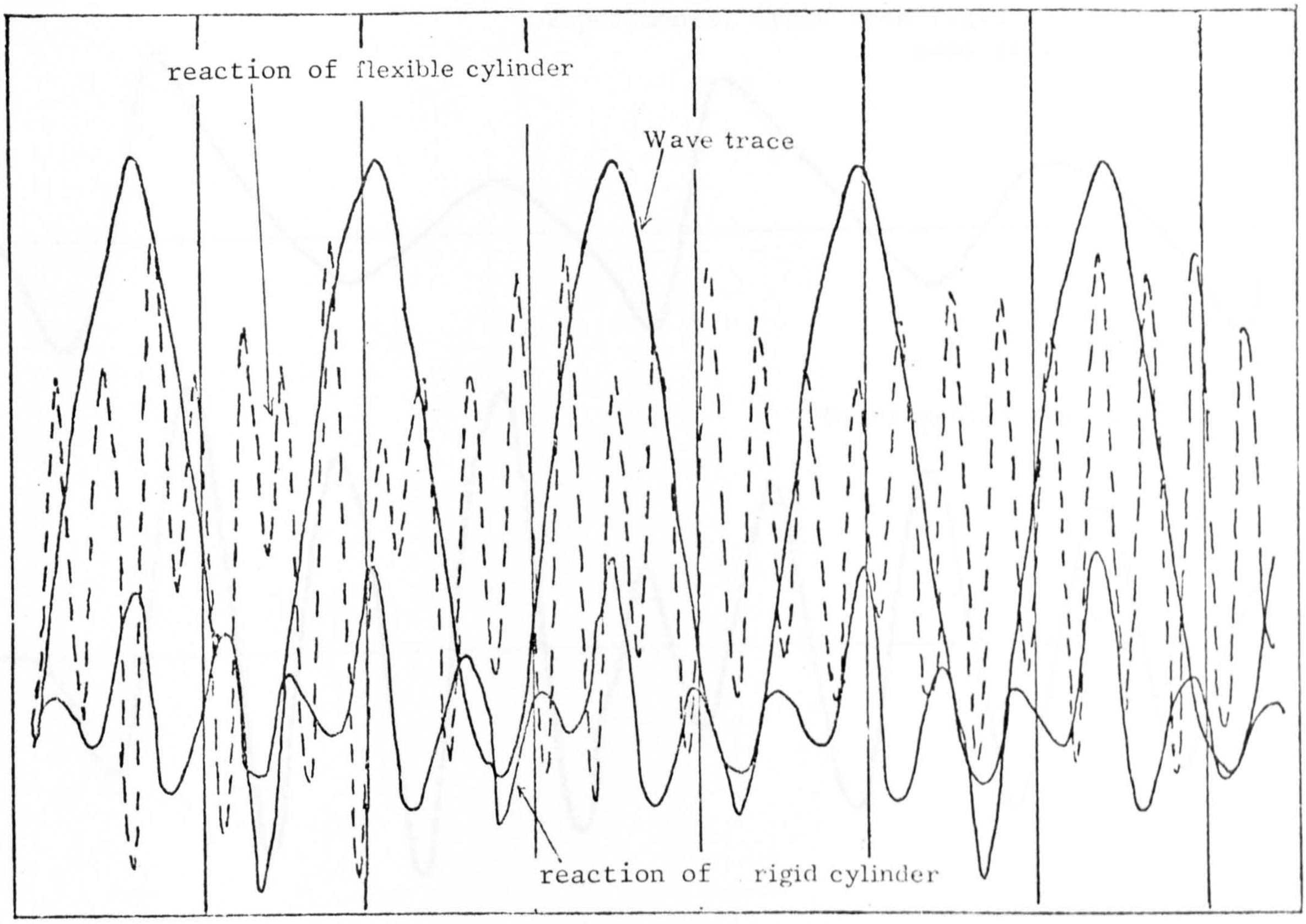

Fig. 39. Example traces for cross-flow results.

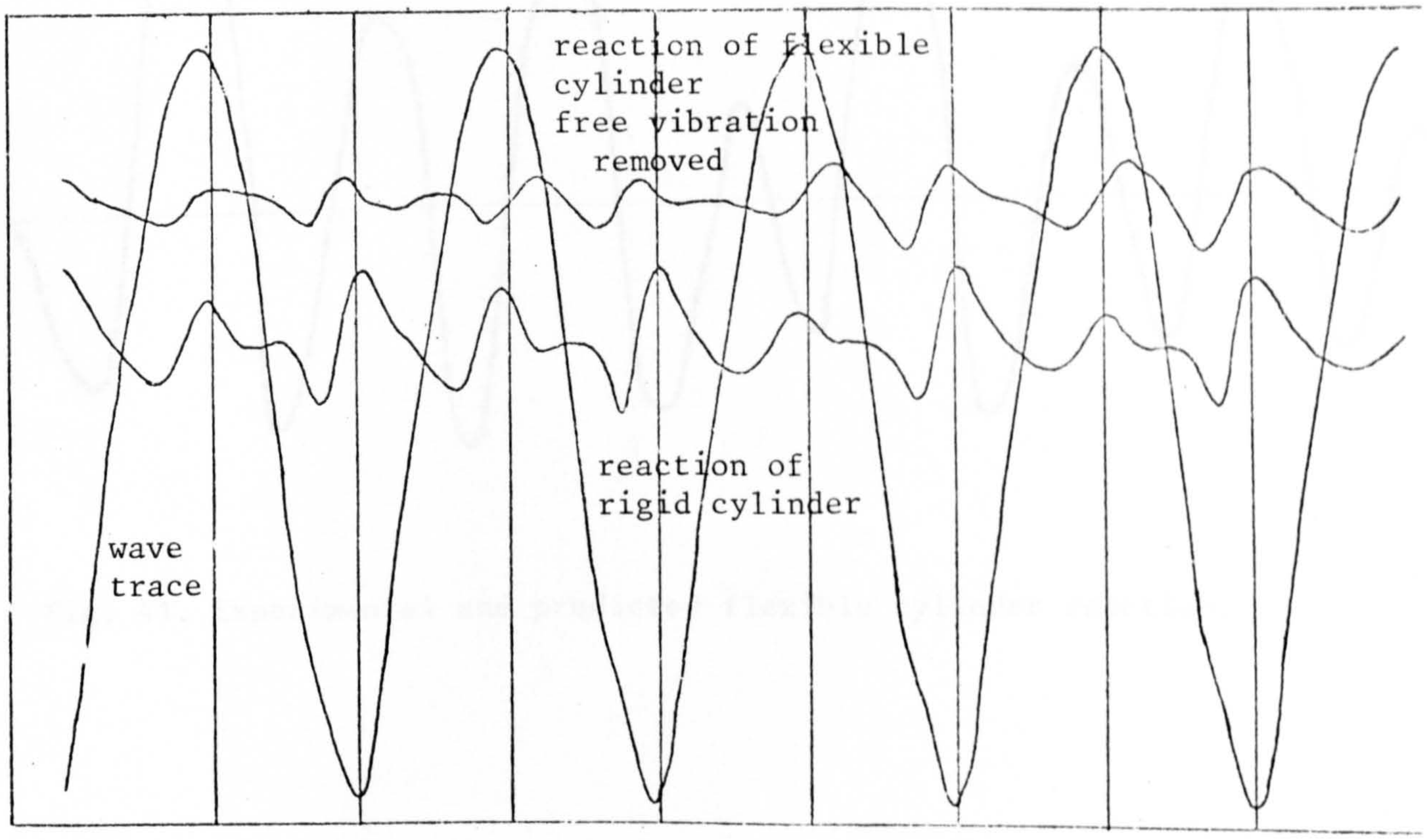

Fig. 40. Trace showing similarity between the reaction of the rigid cylinder and that of the flexible cylinder when free vibration is removed.

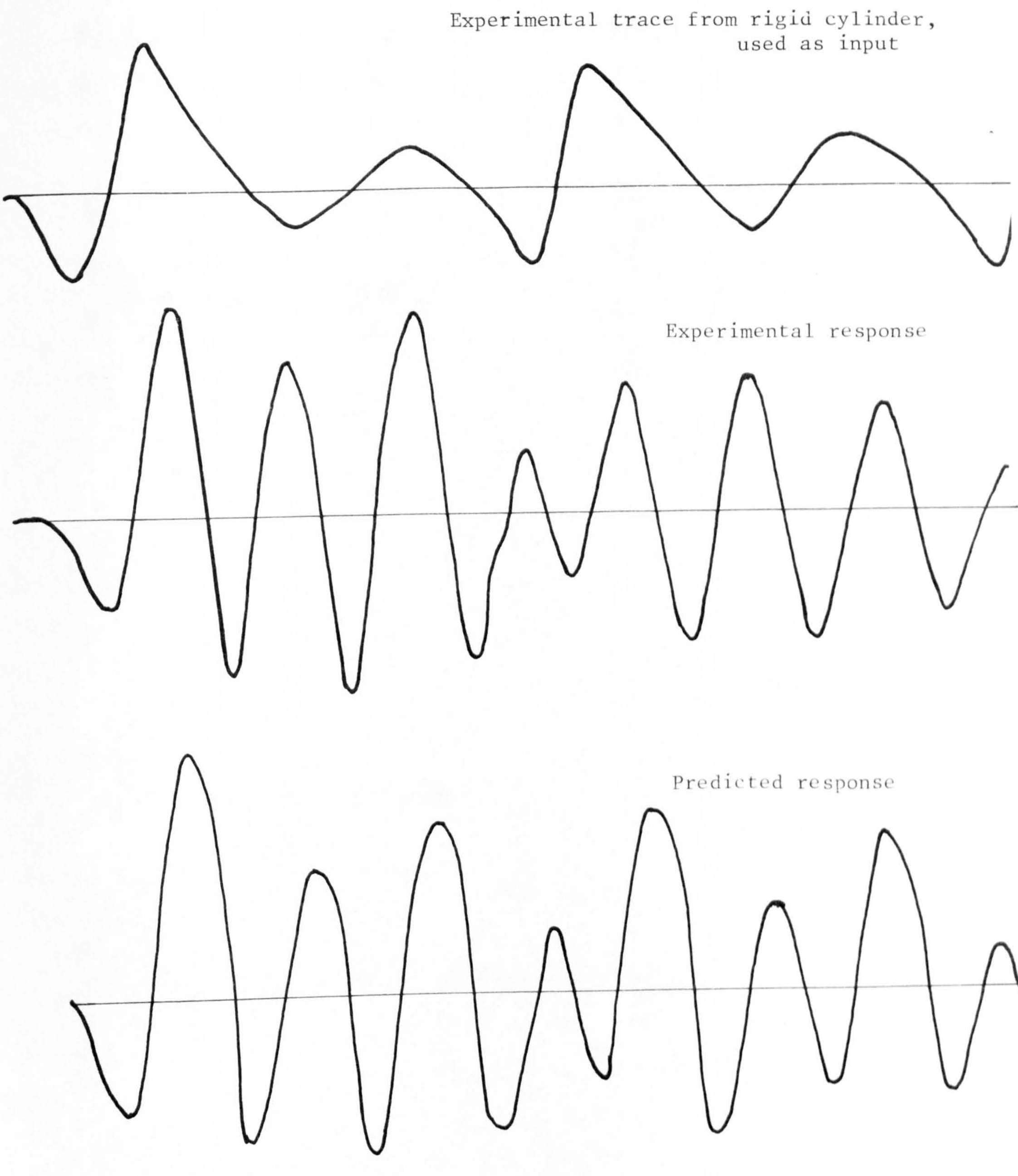

Fig. 41. Experimental and predicted flexible cylinder reaction.

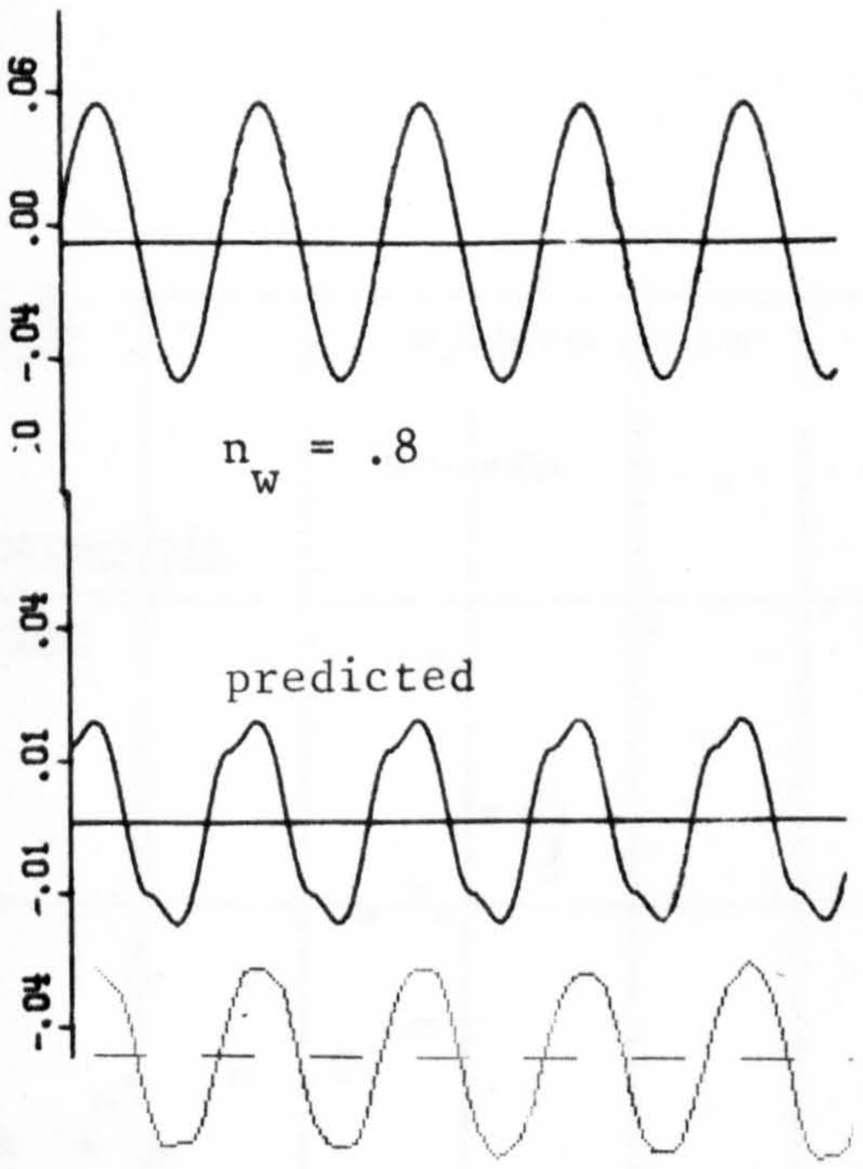

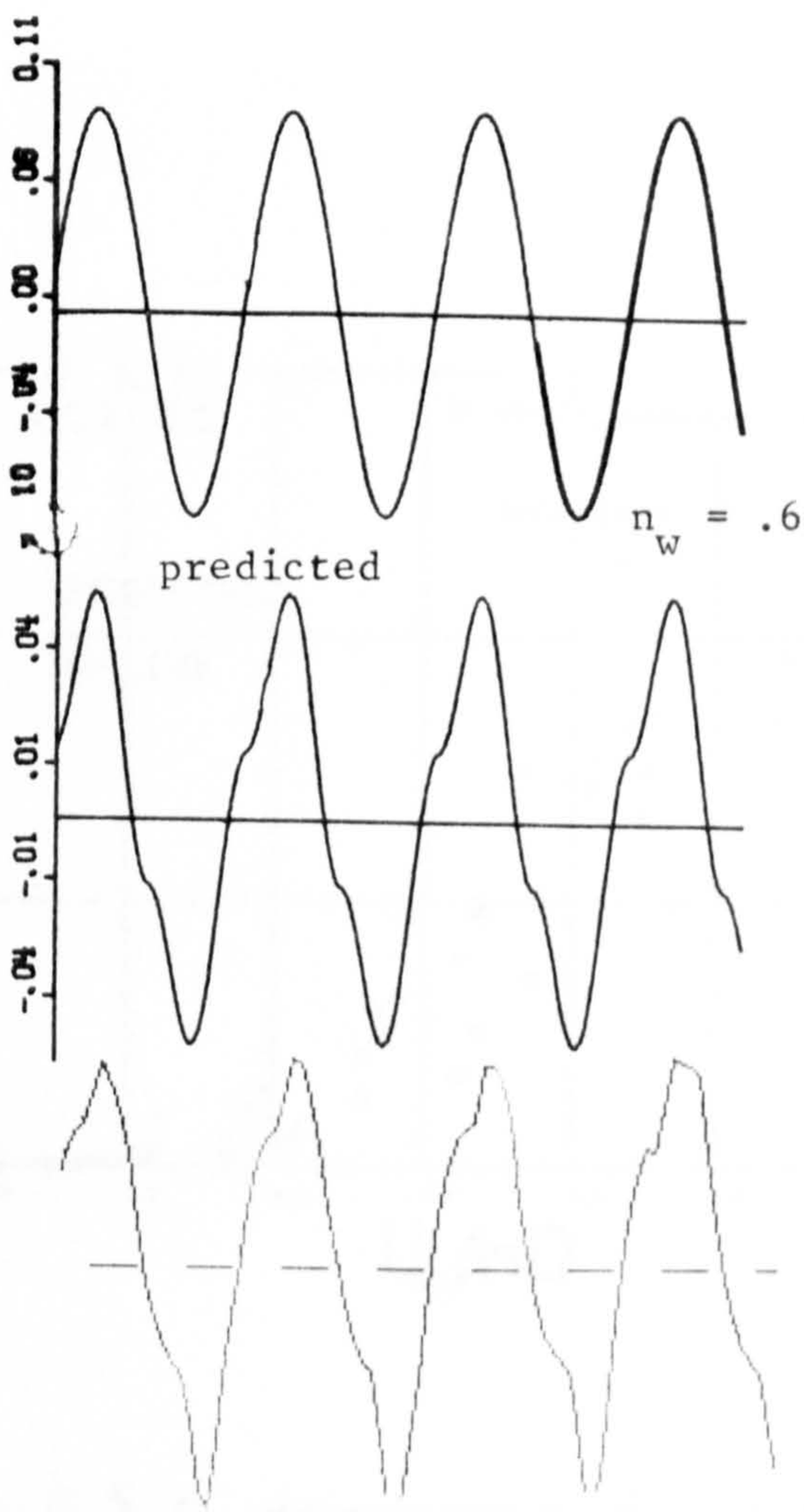

n_w = .6 (wave trace not shown)

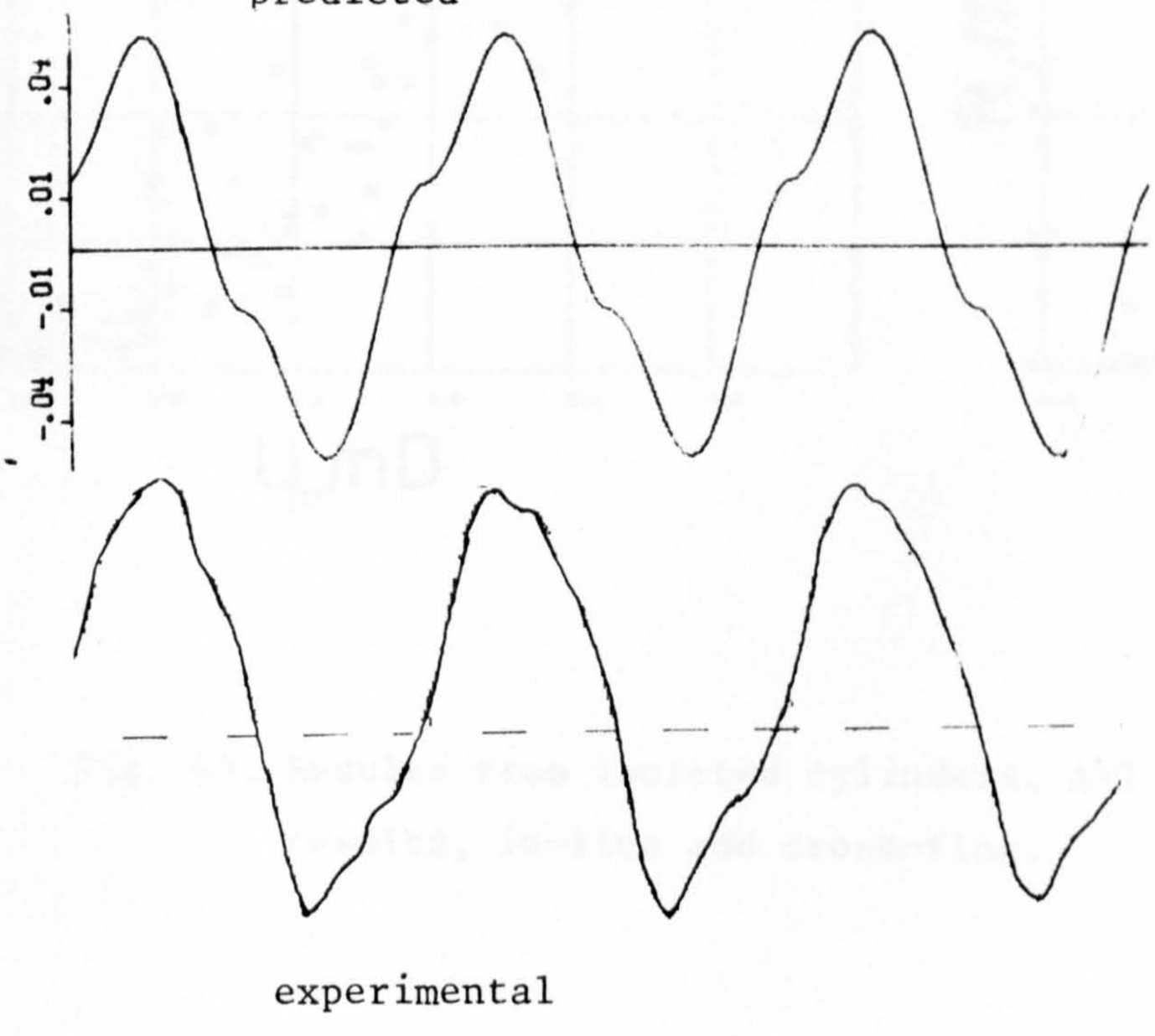

Fig. 42. Experimental curves and curves produced using Morison's formula for the reaction of the rigid cylinder in the in-line direction.

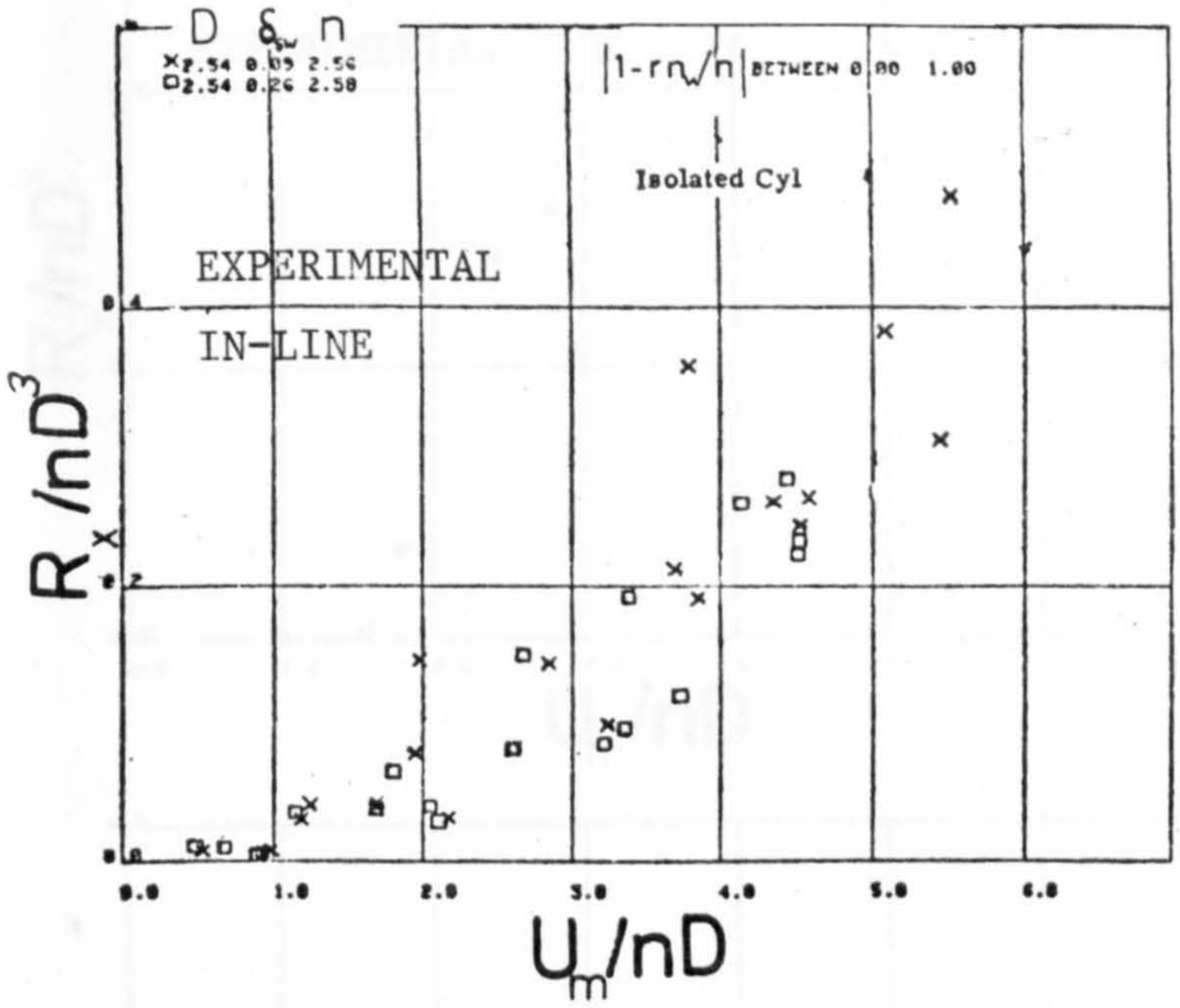

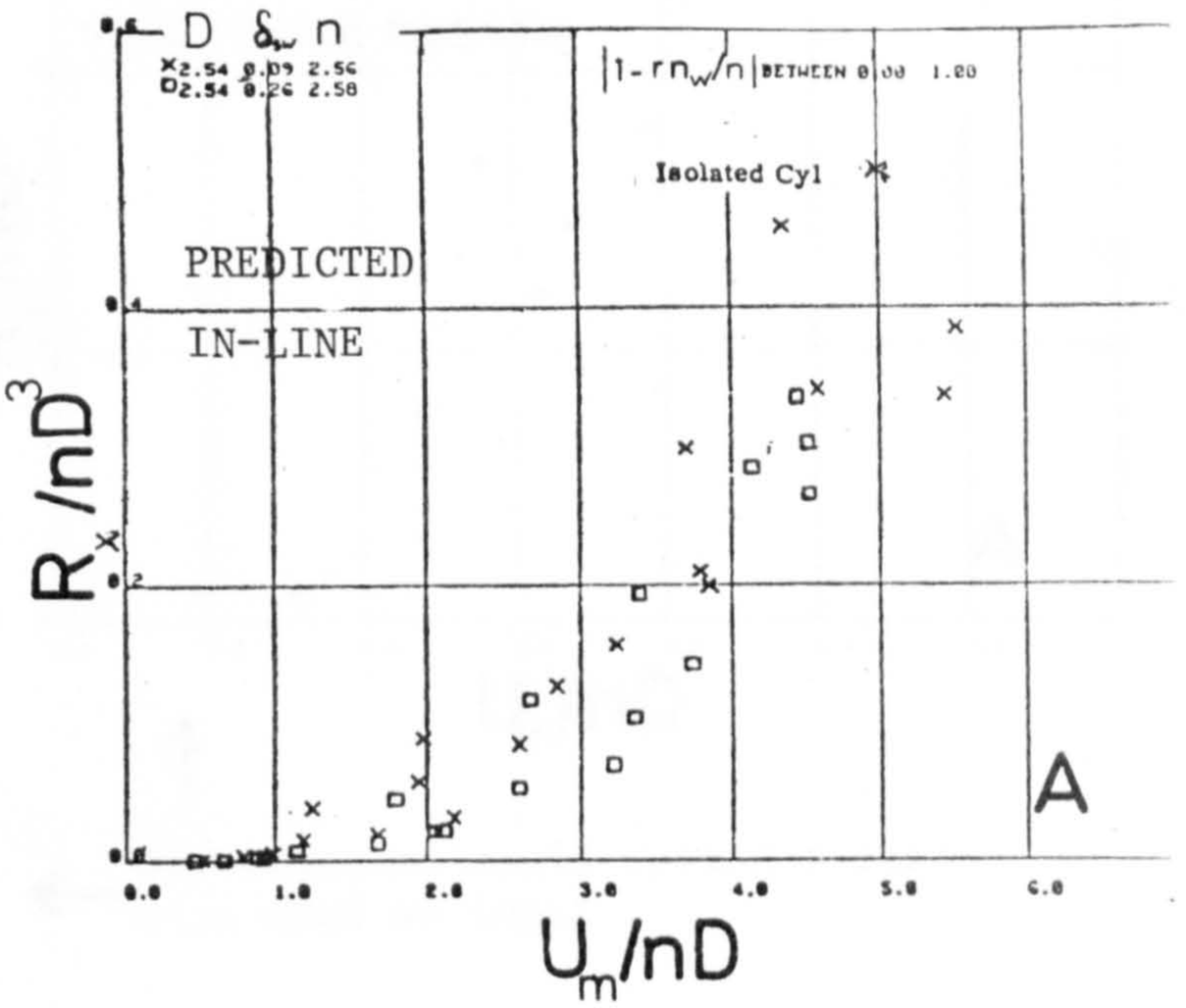

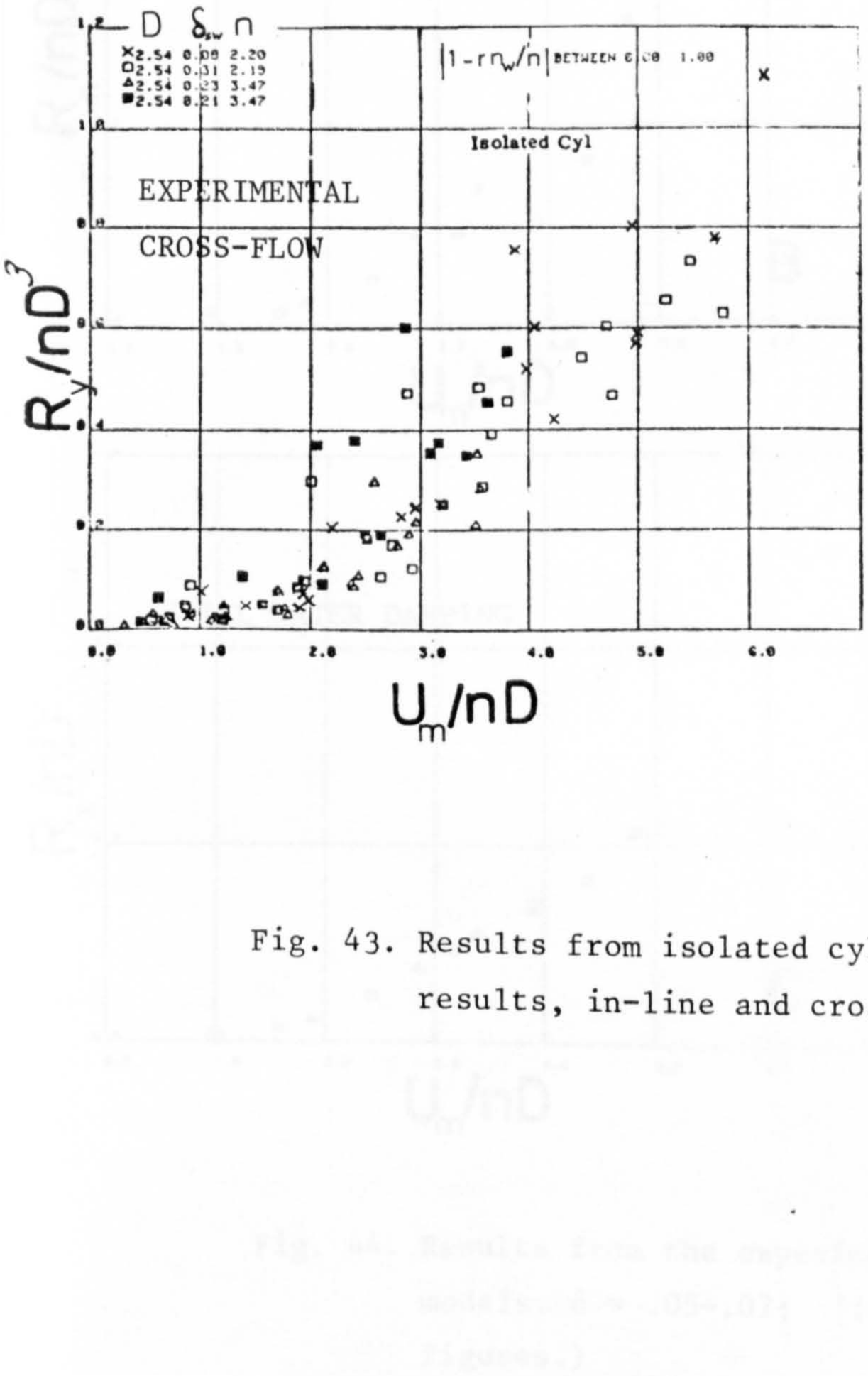

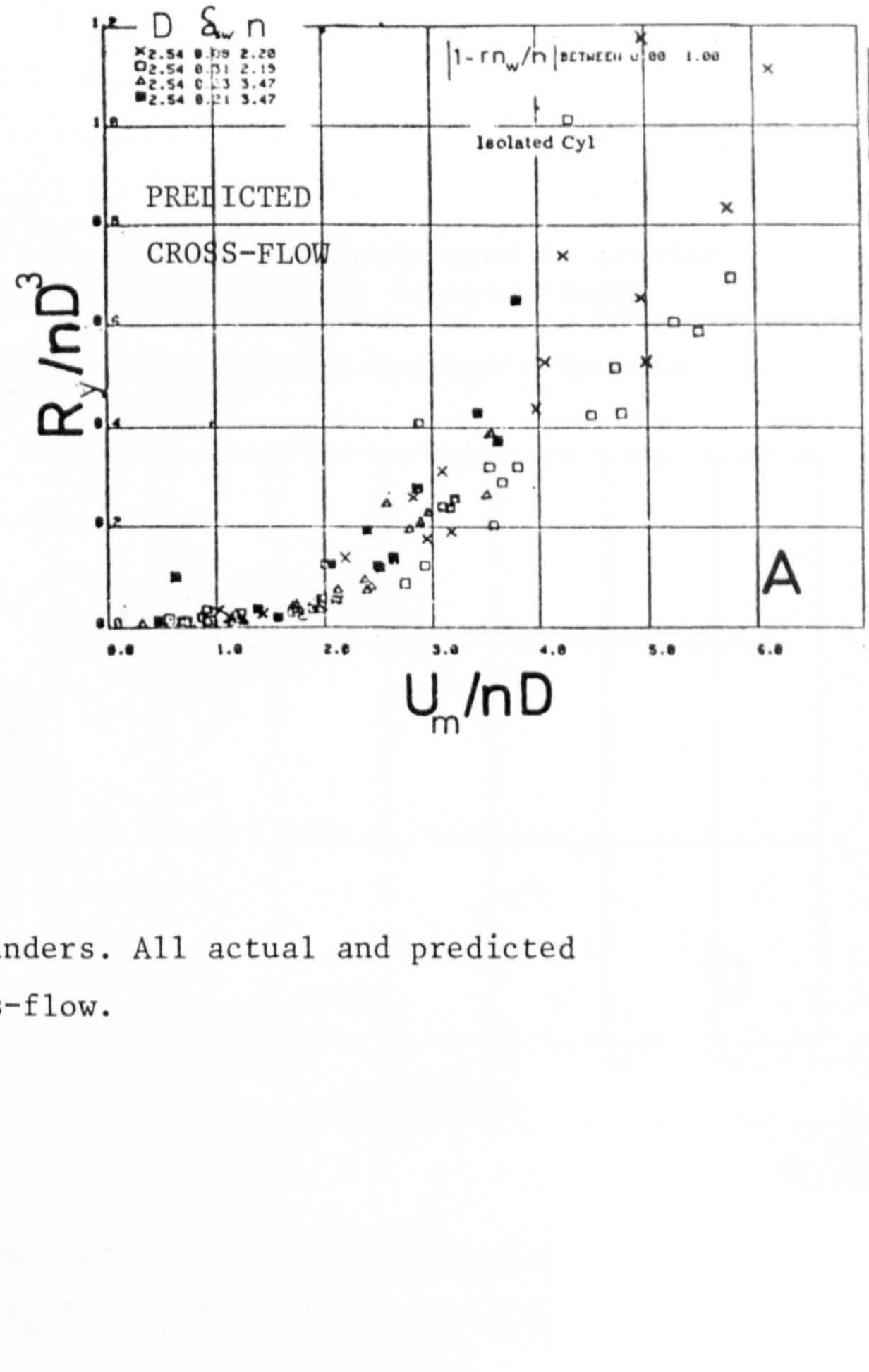

Fig. 43. Results from isolated cylinders. All actual and predicted results, in-line and cross-flow.

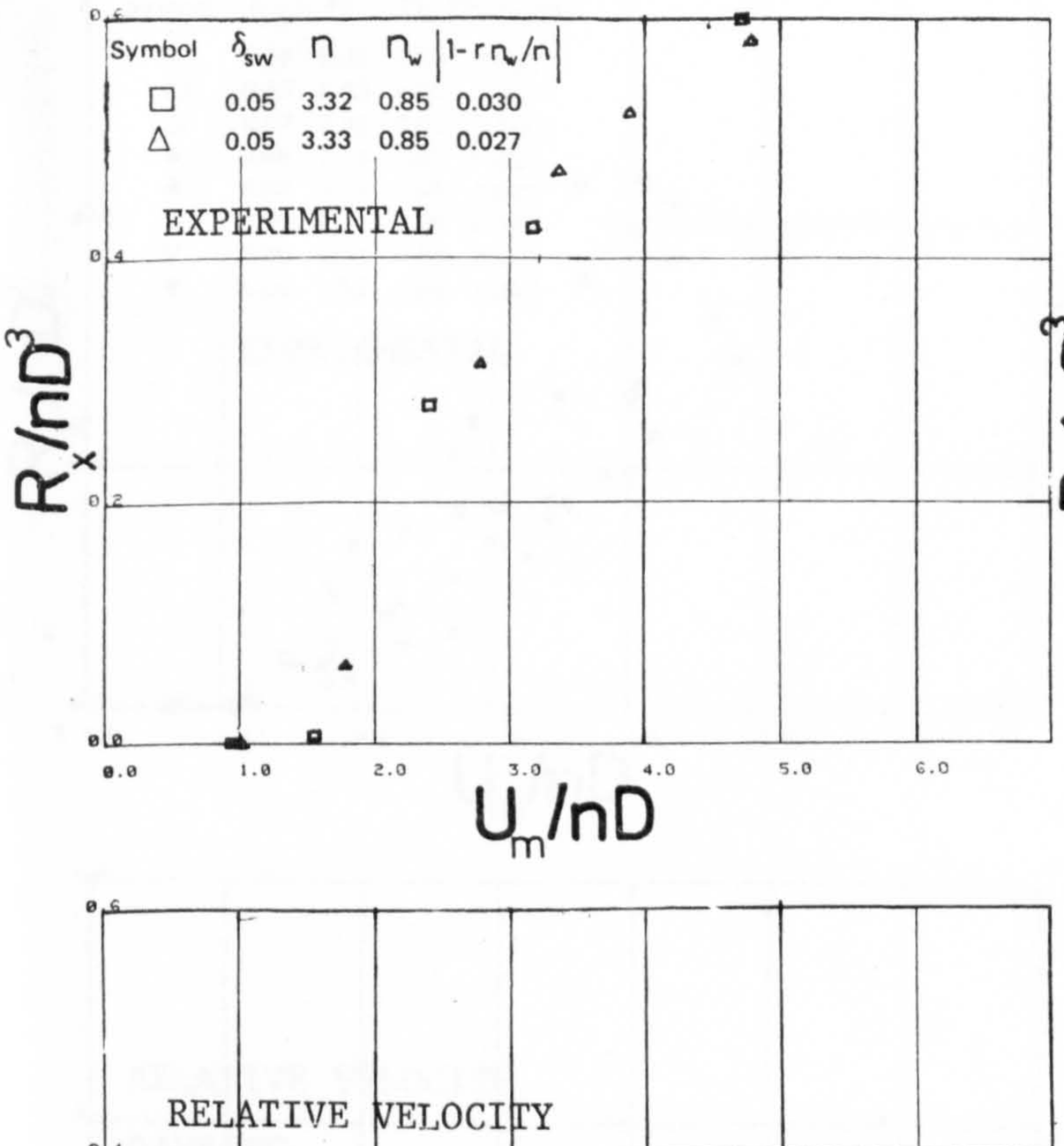

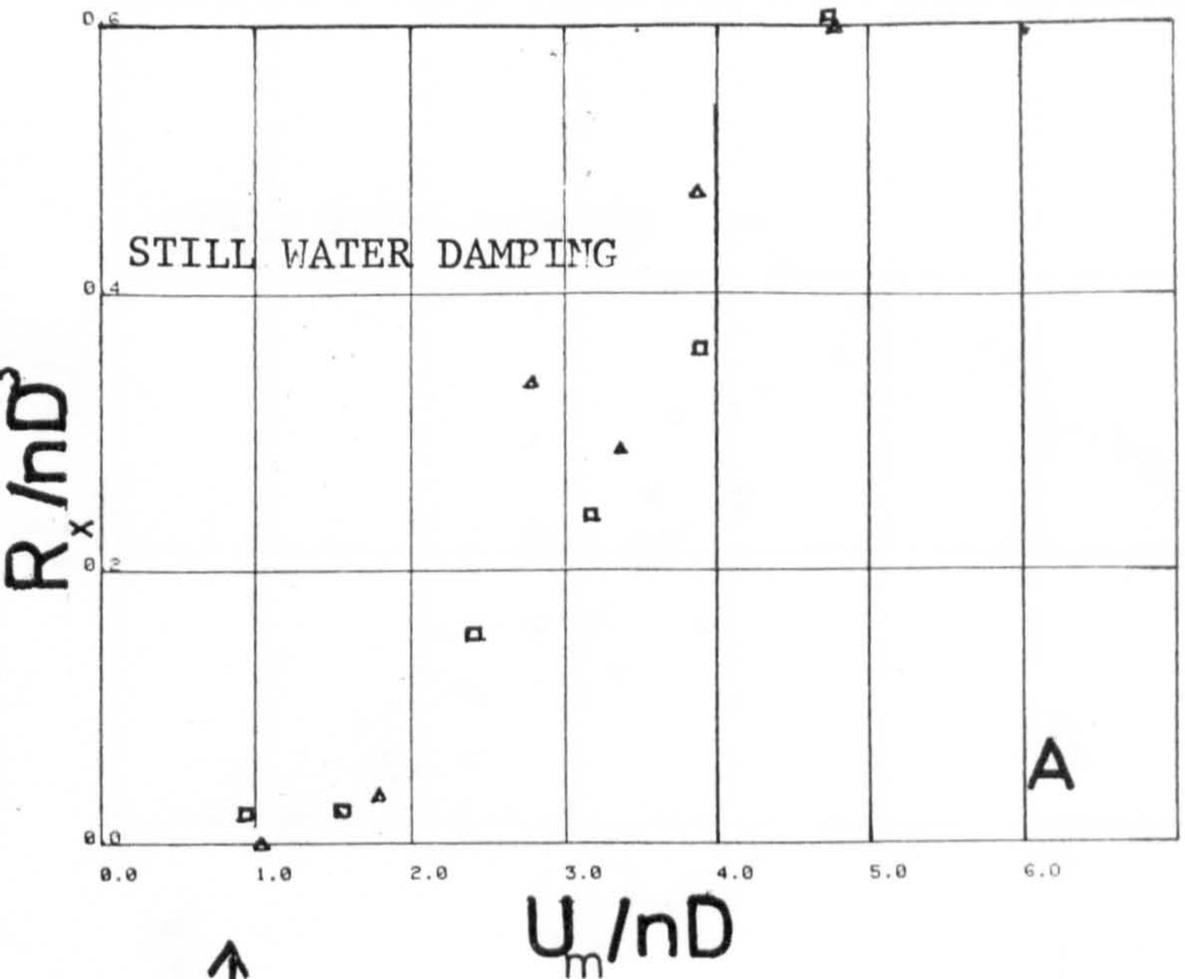

Experimental rigid cylinder reaction used as input

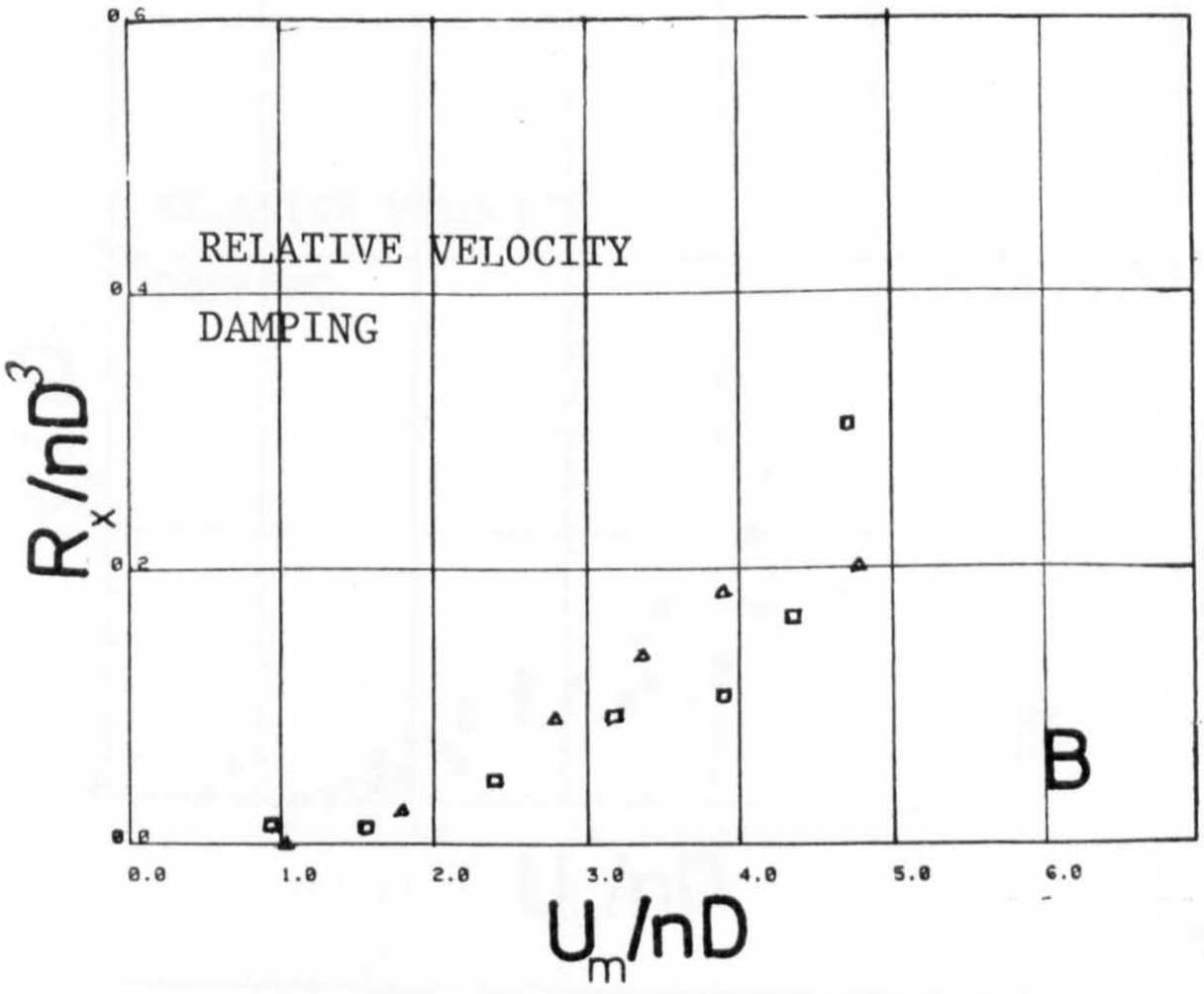

Morison's formula used to predict rigid cylinder reaction input

Full modified Morison's formula used

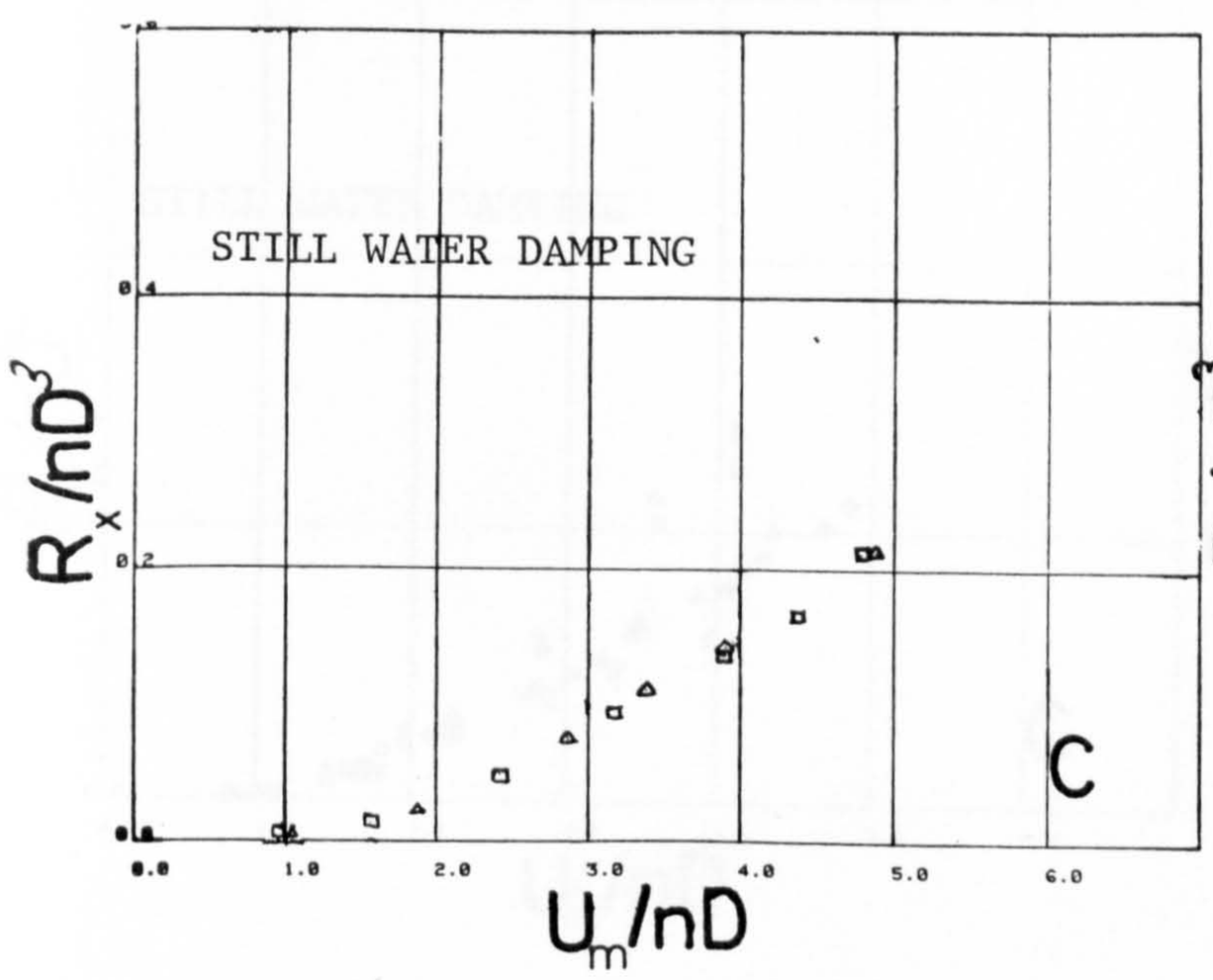

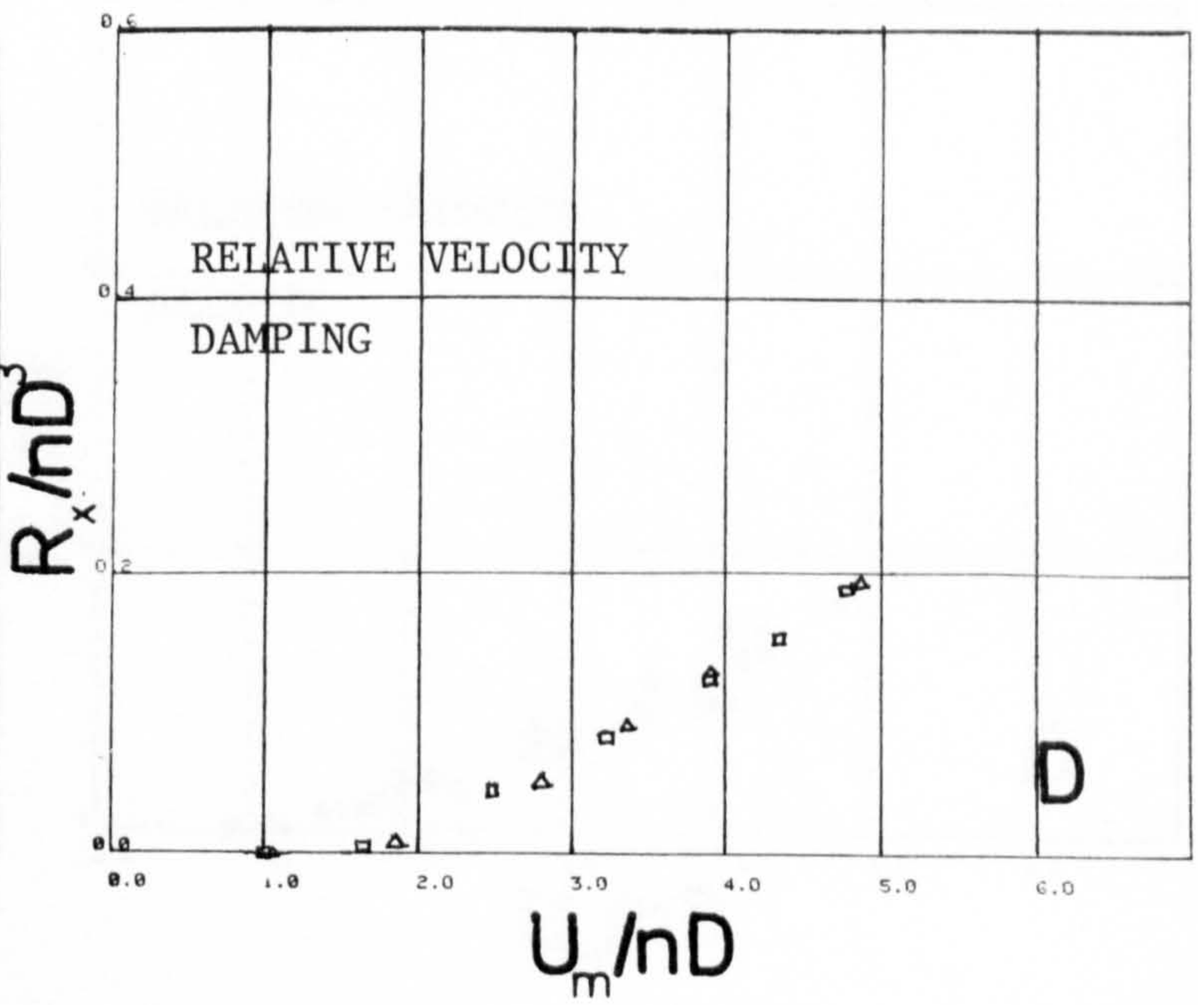

Fig. 44. Results from the experiments and the various mathematical models. δ = .05-.07; $|1-rn_w/n|$ = .03. (Symbols apply to all figures.)

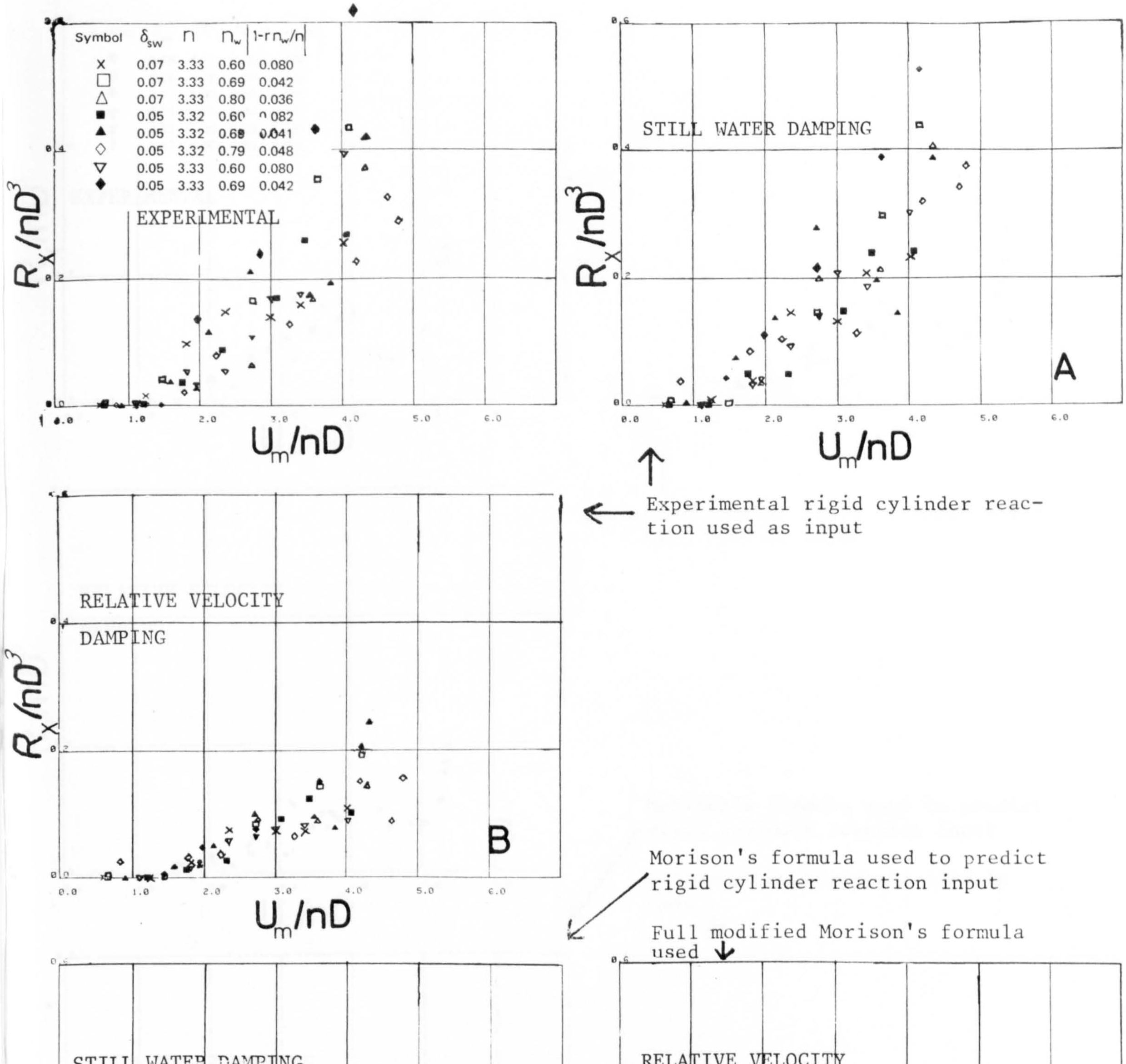

Fig. 45. Results from the experiments and the various mathematical models. δ = .05-.07; $|1-rn_w/n|$ = .03-.1. (Symbols apply to all figures.)

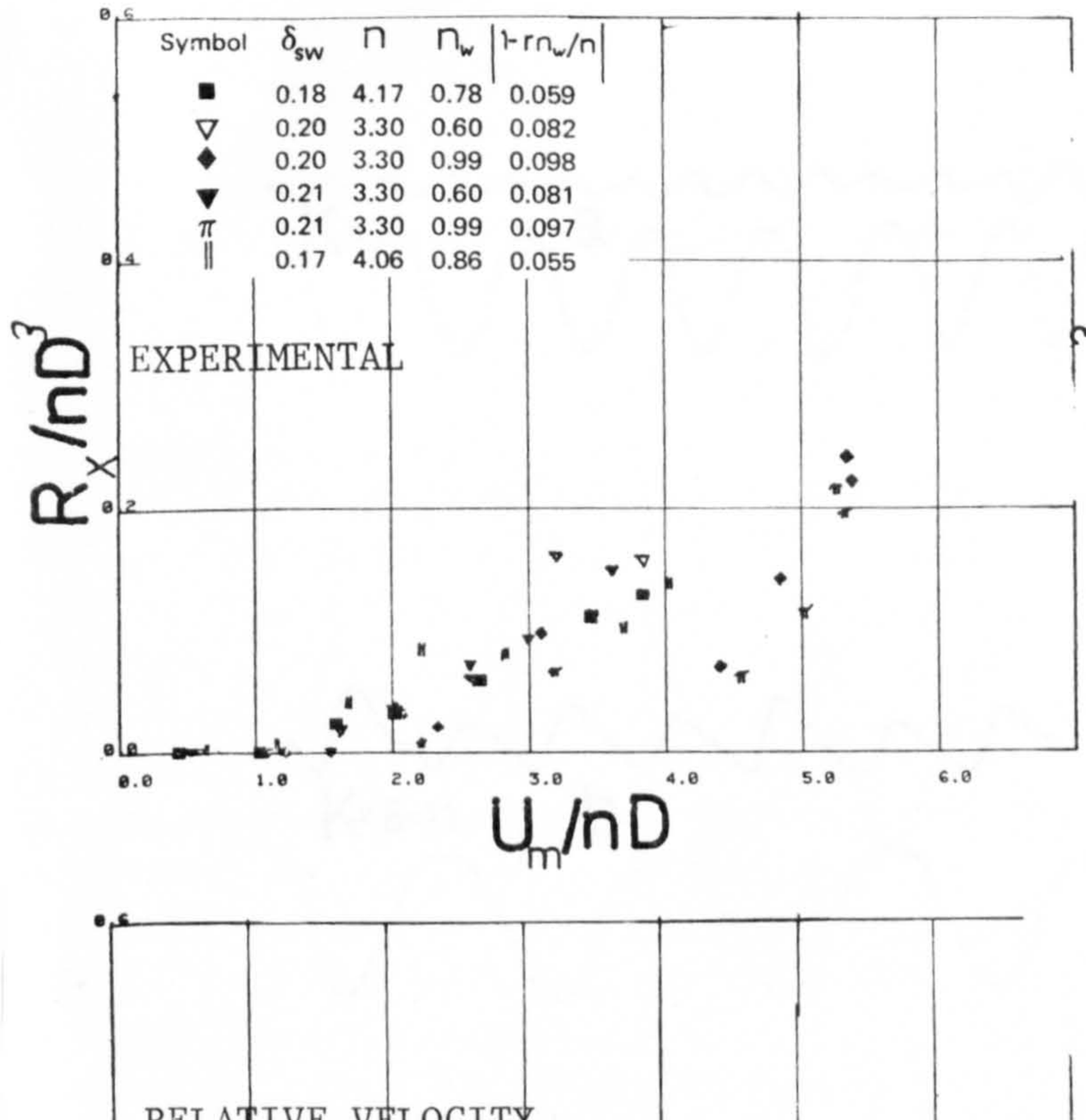

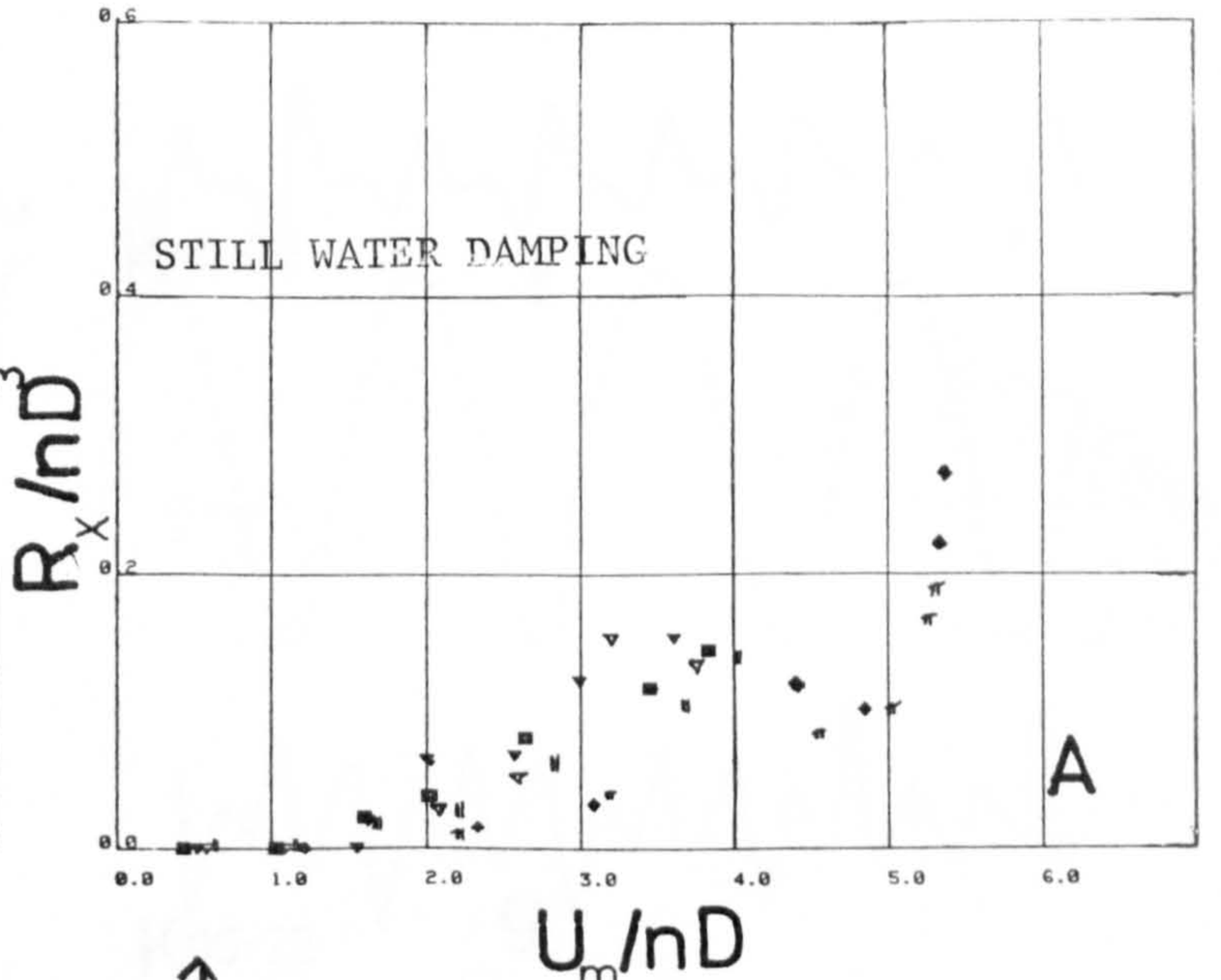

Experimental rigid cylinder reaction used as input

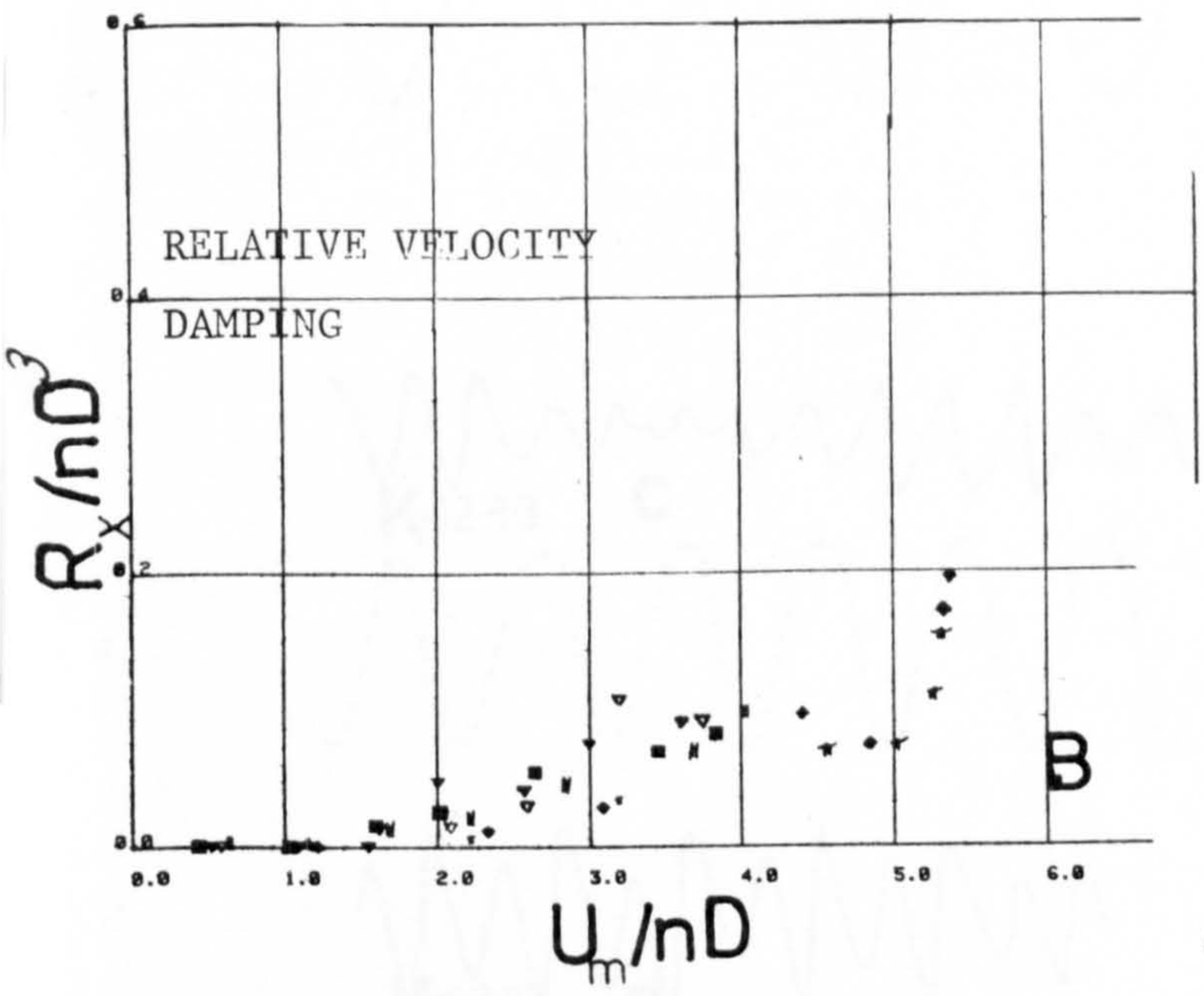

Morison's formula used to predict rigid cylinder reaction input

Full modified Morison's formula used

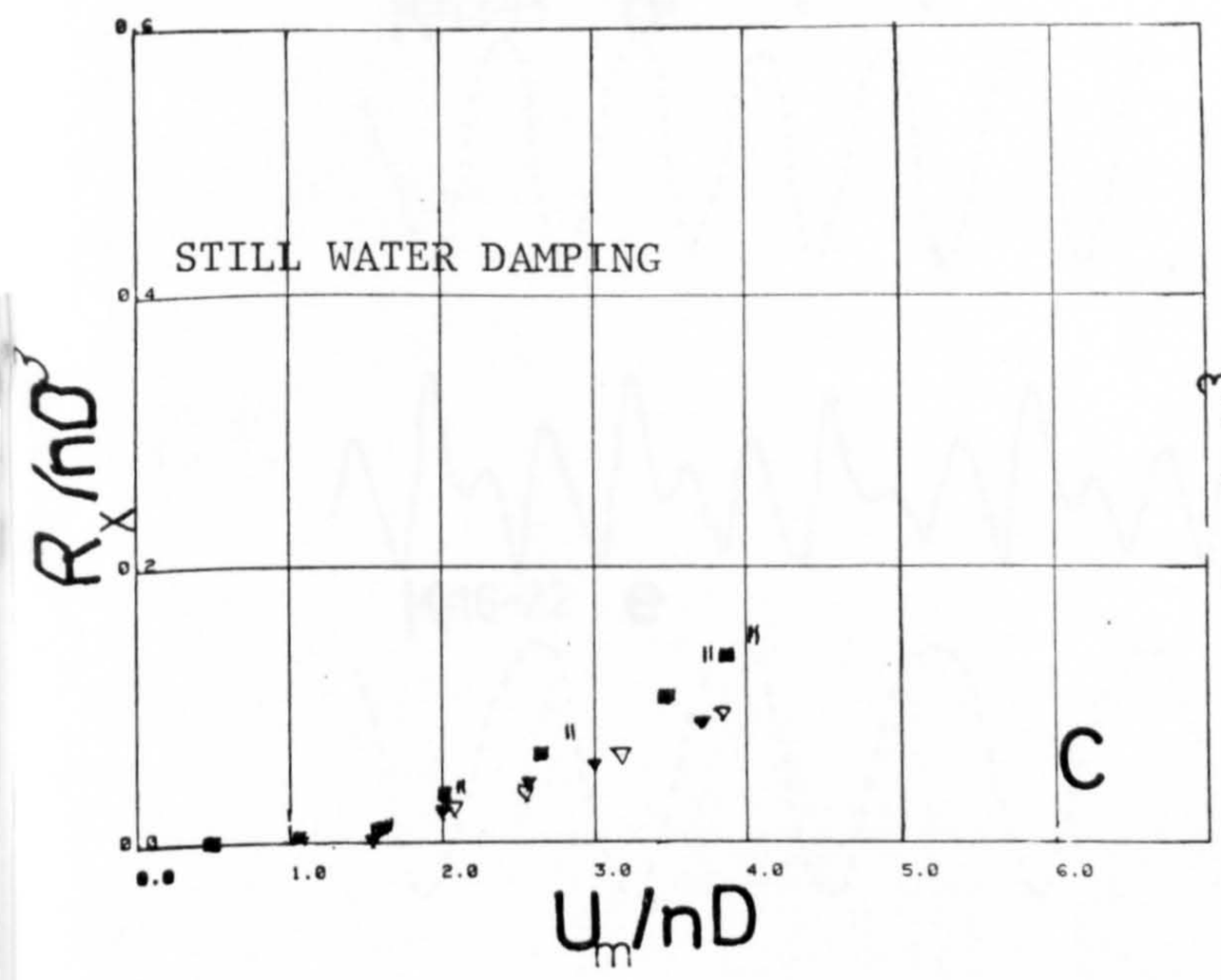

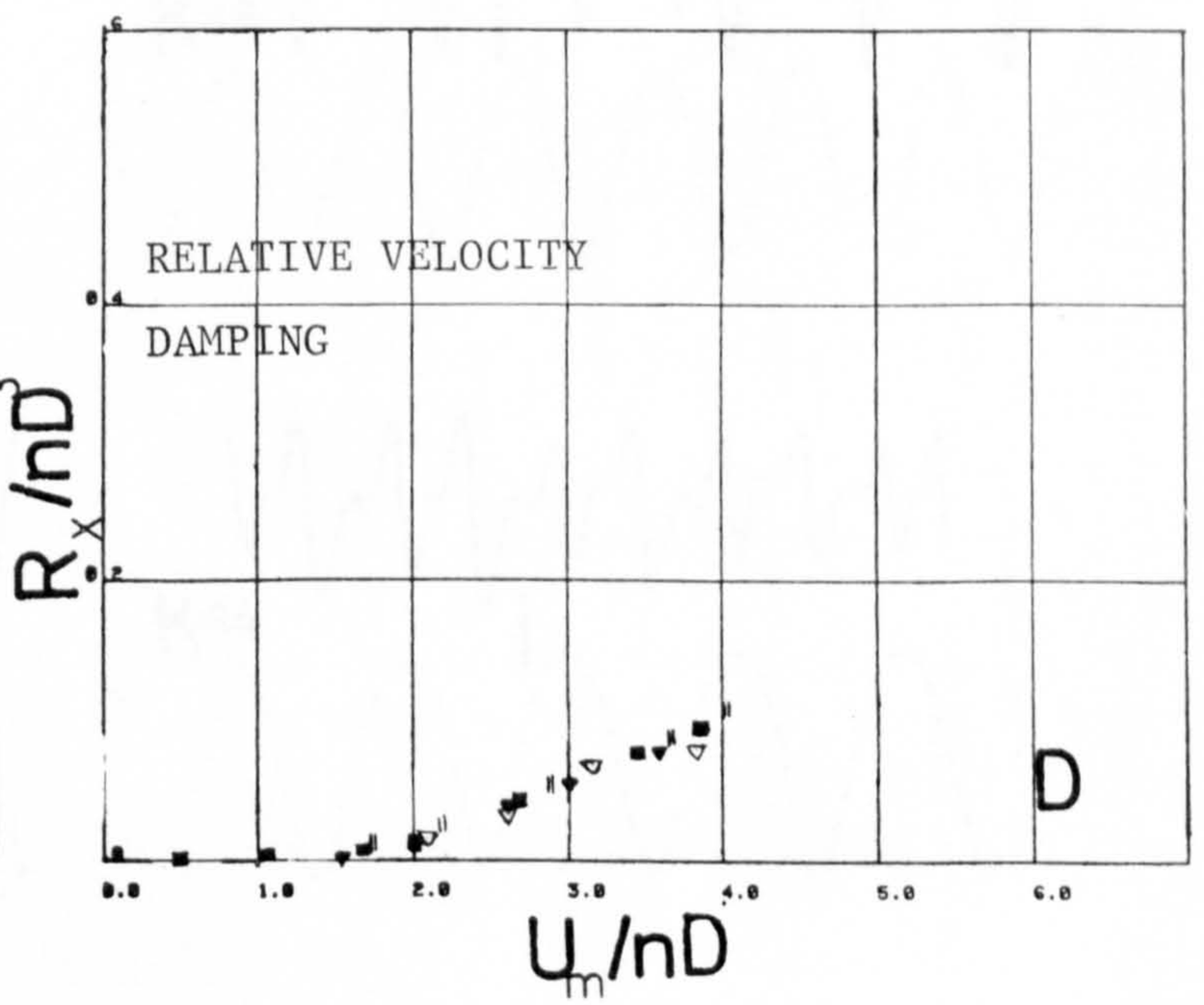

Fig. 46. Results from the experiments and the various mathematical models. δ = .16-.21; $|1-rn_w/n|$ = .1-1.0. (Symbols apply to all figures.)

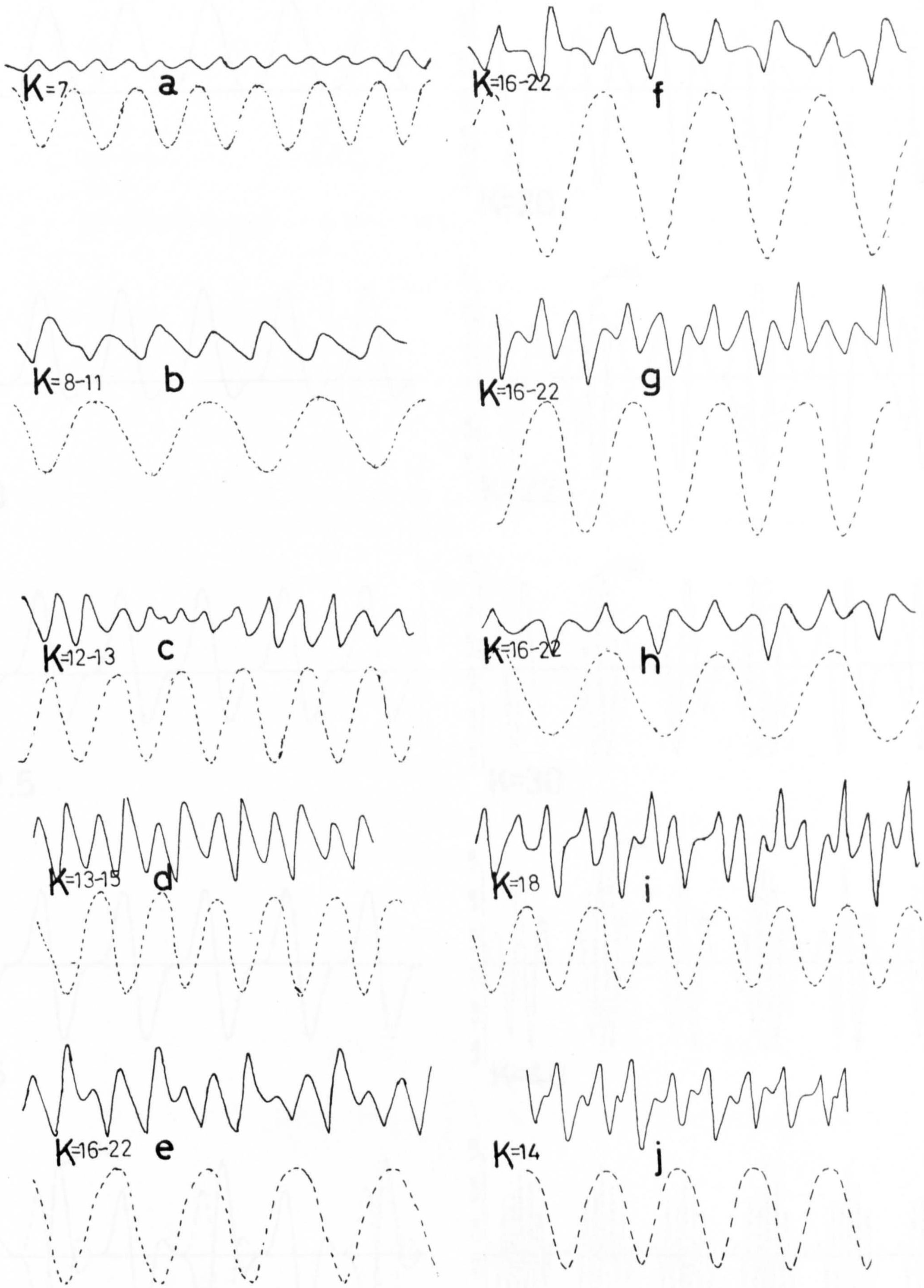

Fig. 47. Traces of the cross-flow reaction on rigid cylinders at various K. Full line - cross-flow reaction. Dashed line - wave trace (drawn upside down).

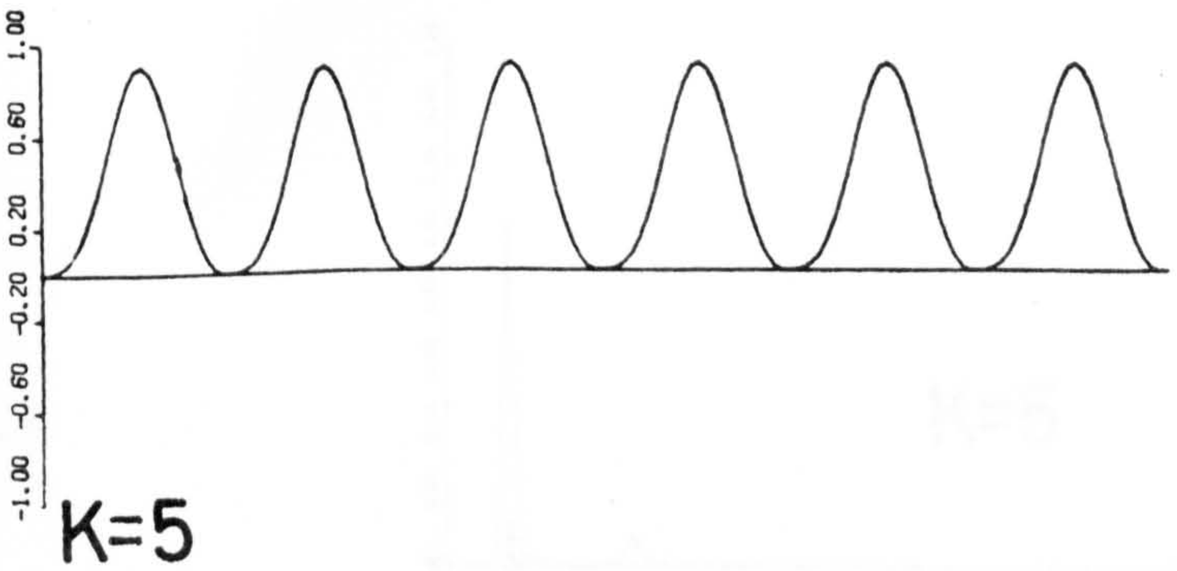

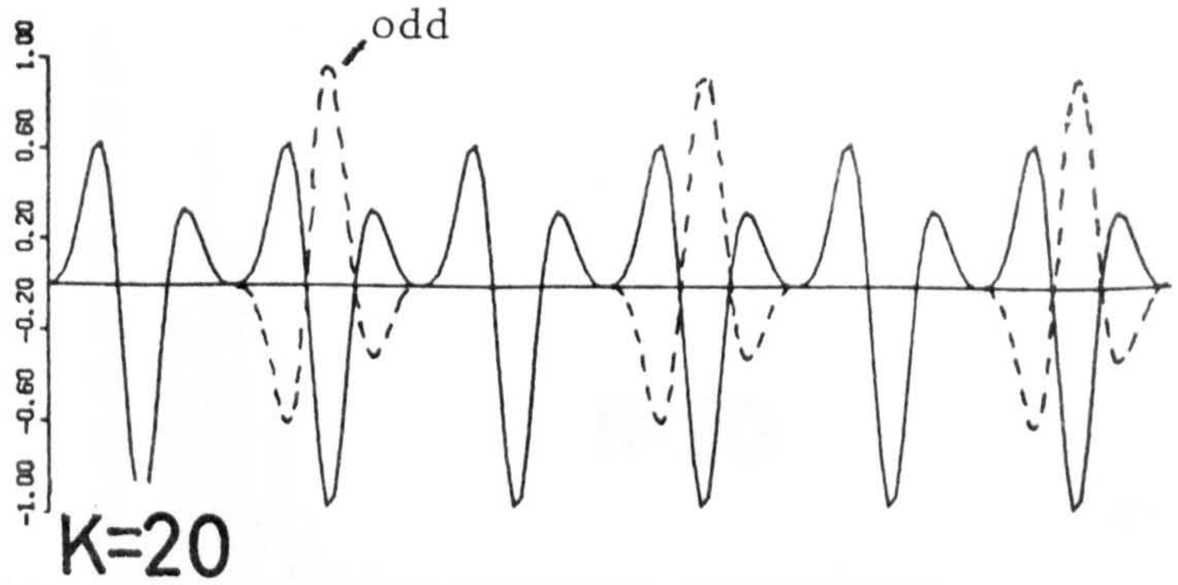

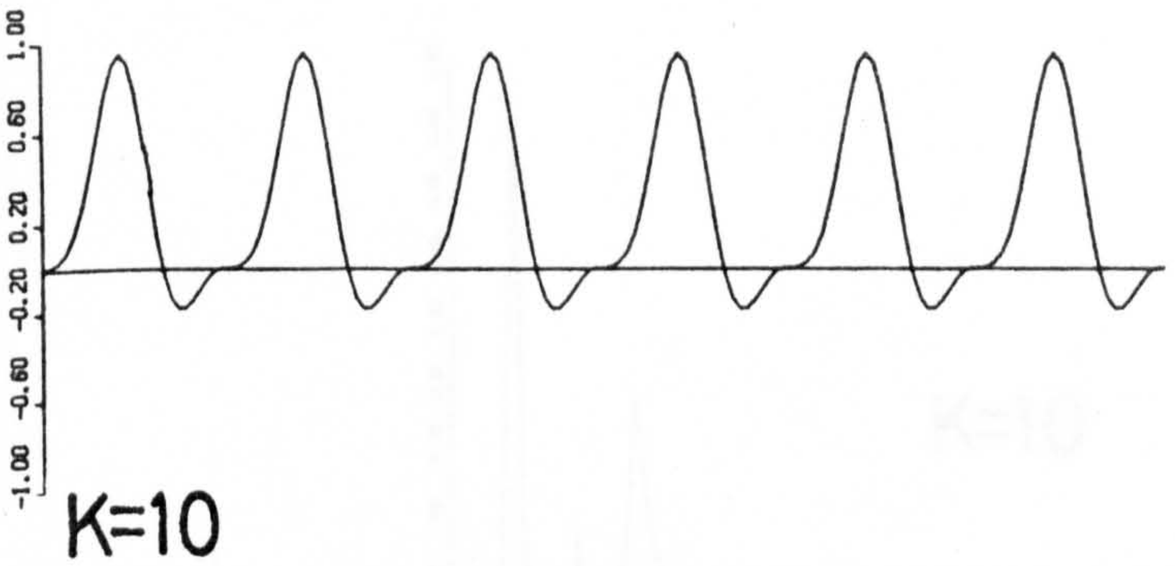

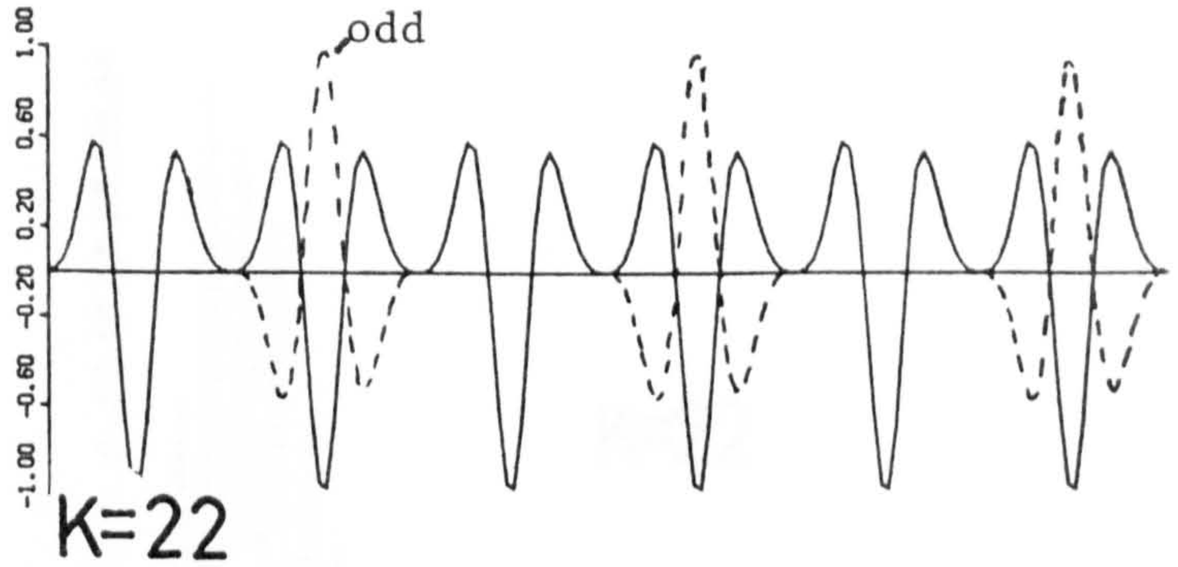

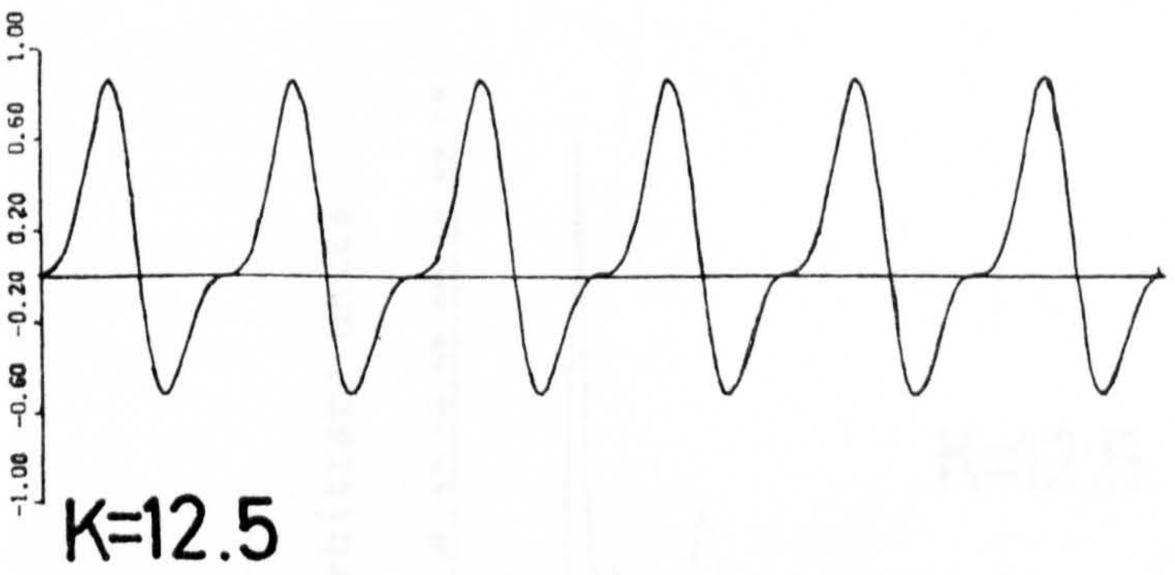

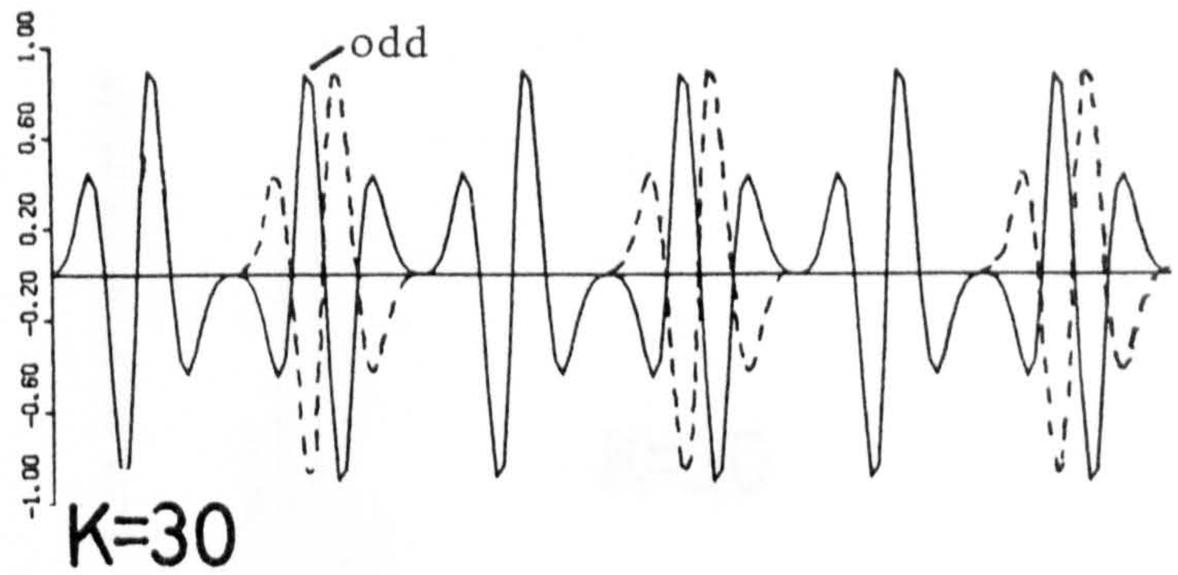

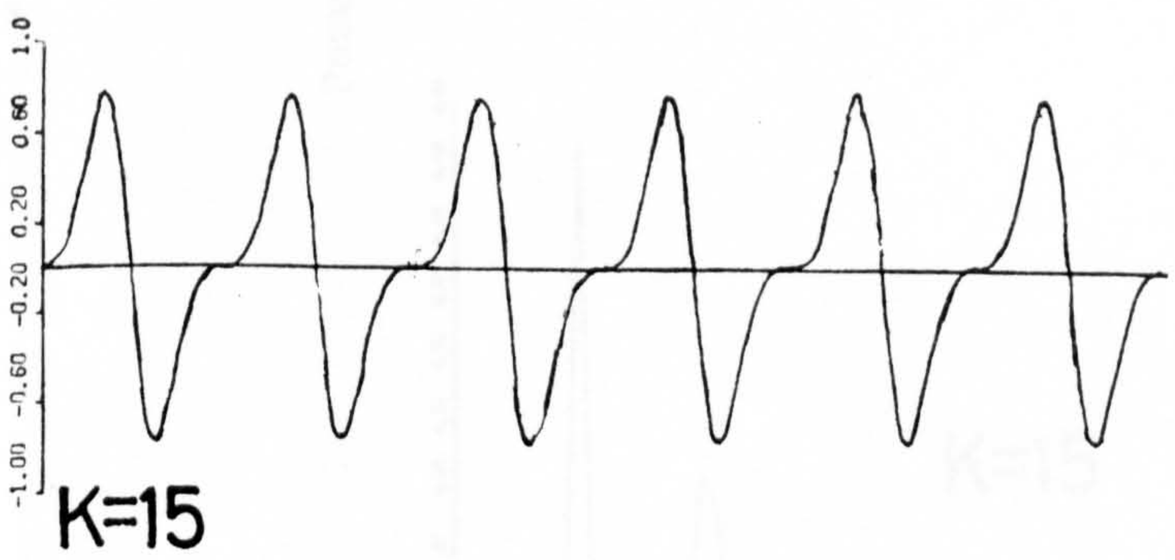

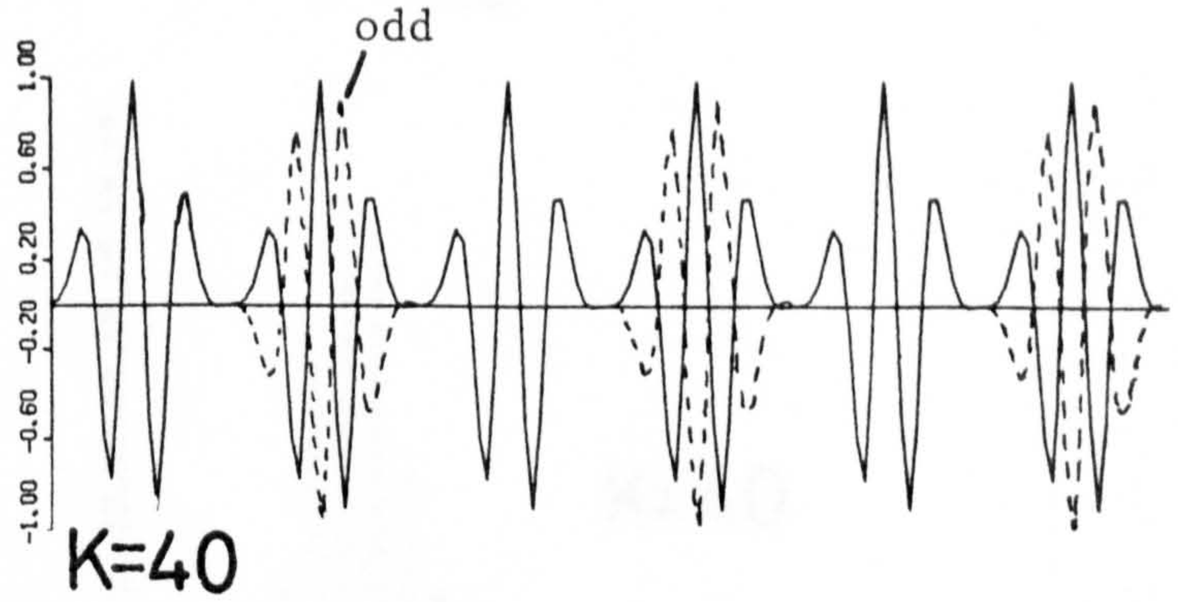

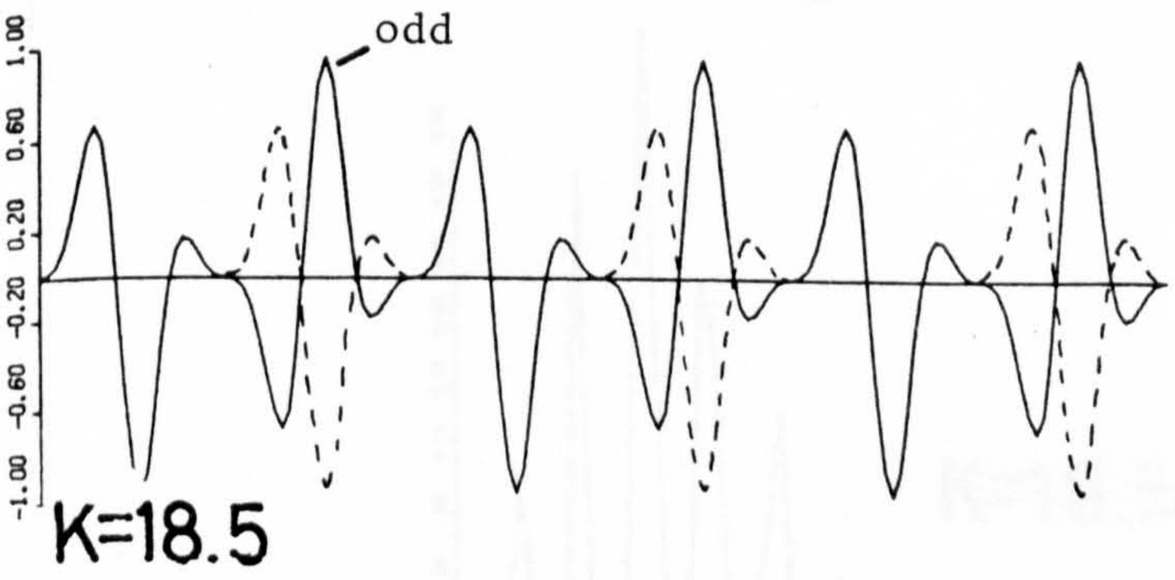

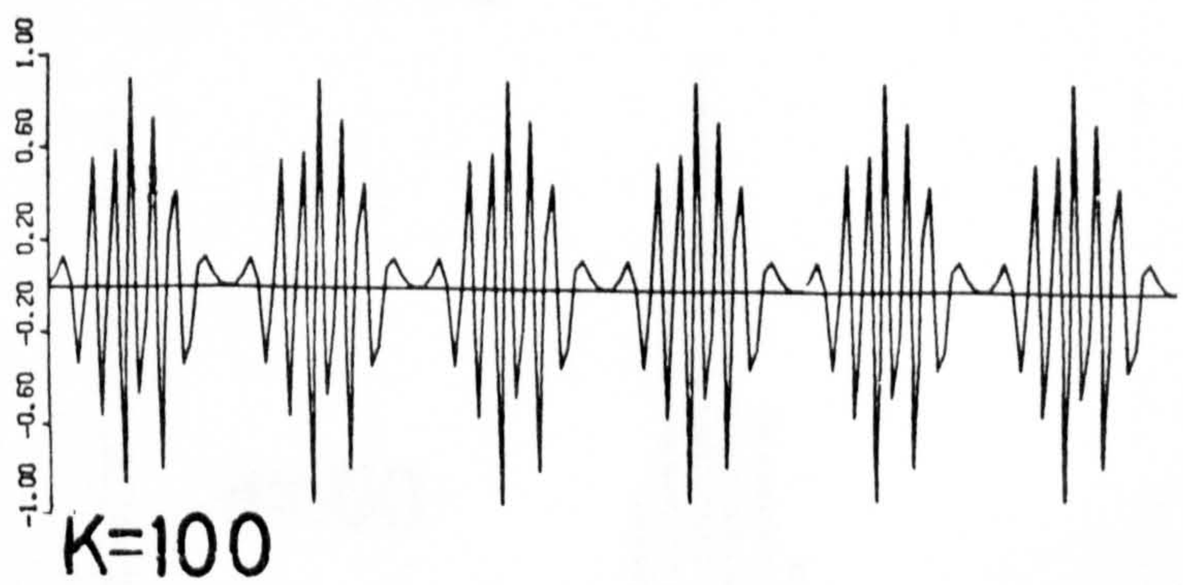

Fig. 48. Traces from the quasi-steady vortex shedding model at various K. For $K \geq 18.5$ both conditions at the beginning of each half cycle are drawn (see text).

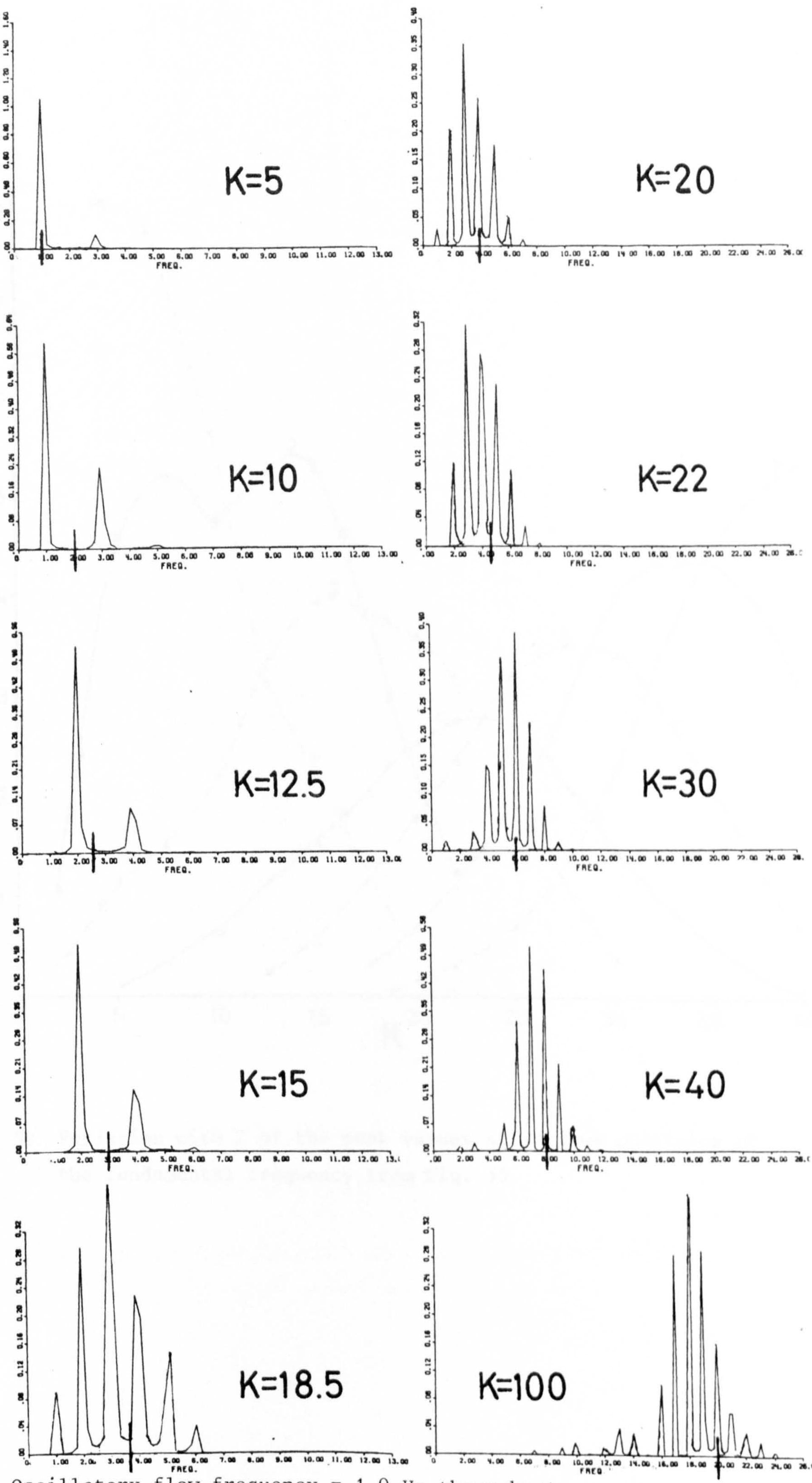

Fig. 49. Spectra obtained from Fig. 48, at various K. Vertical line on axis denotes frequency given by .2U /D.

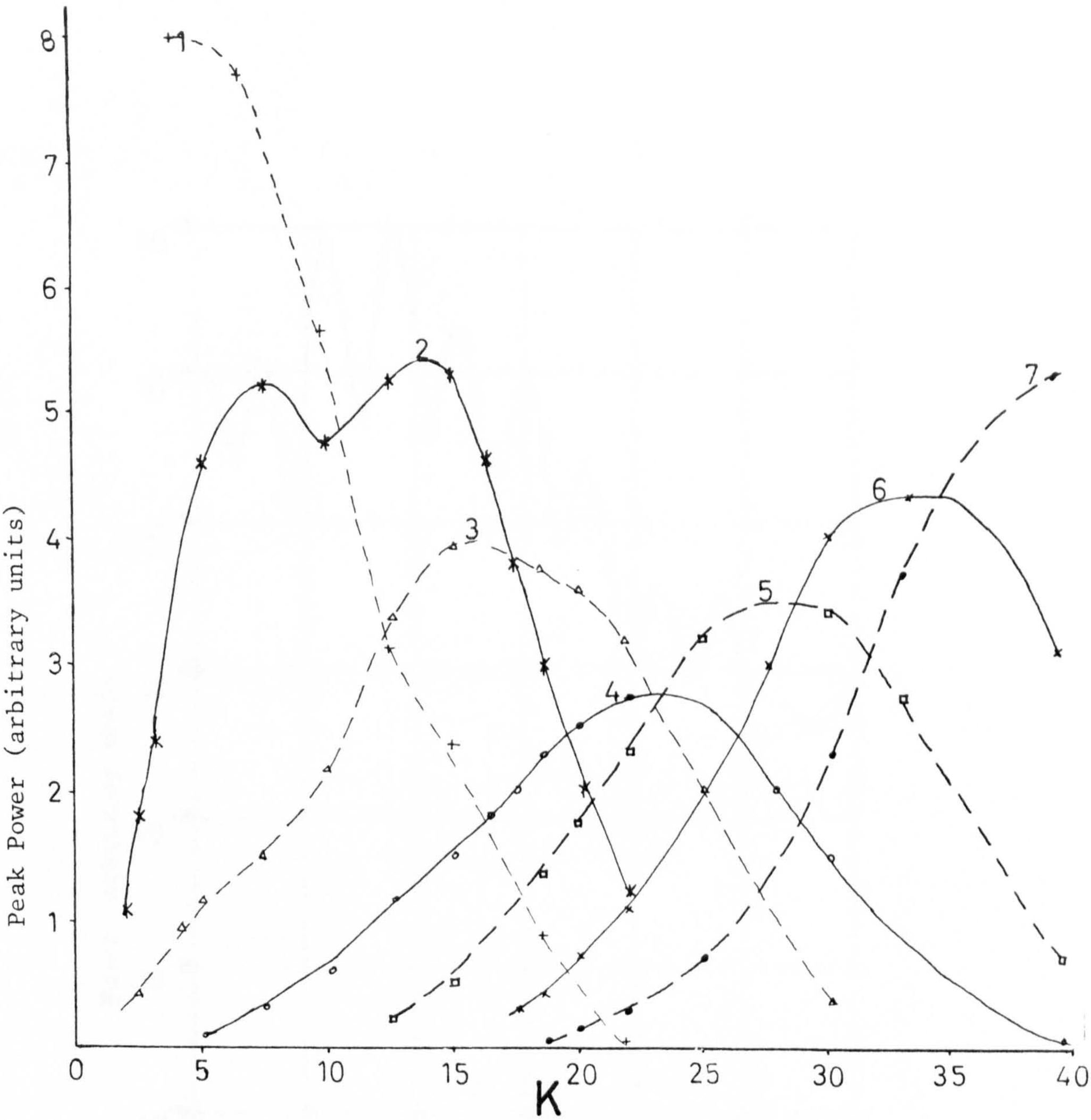

Fig. 50. Variation with K of the peak values at various multiples of the fundamental frequency from Fig. 55.

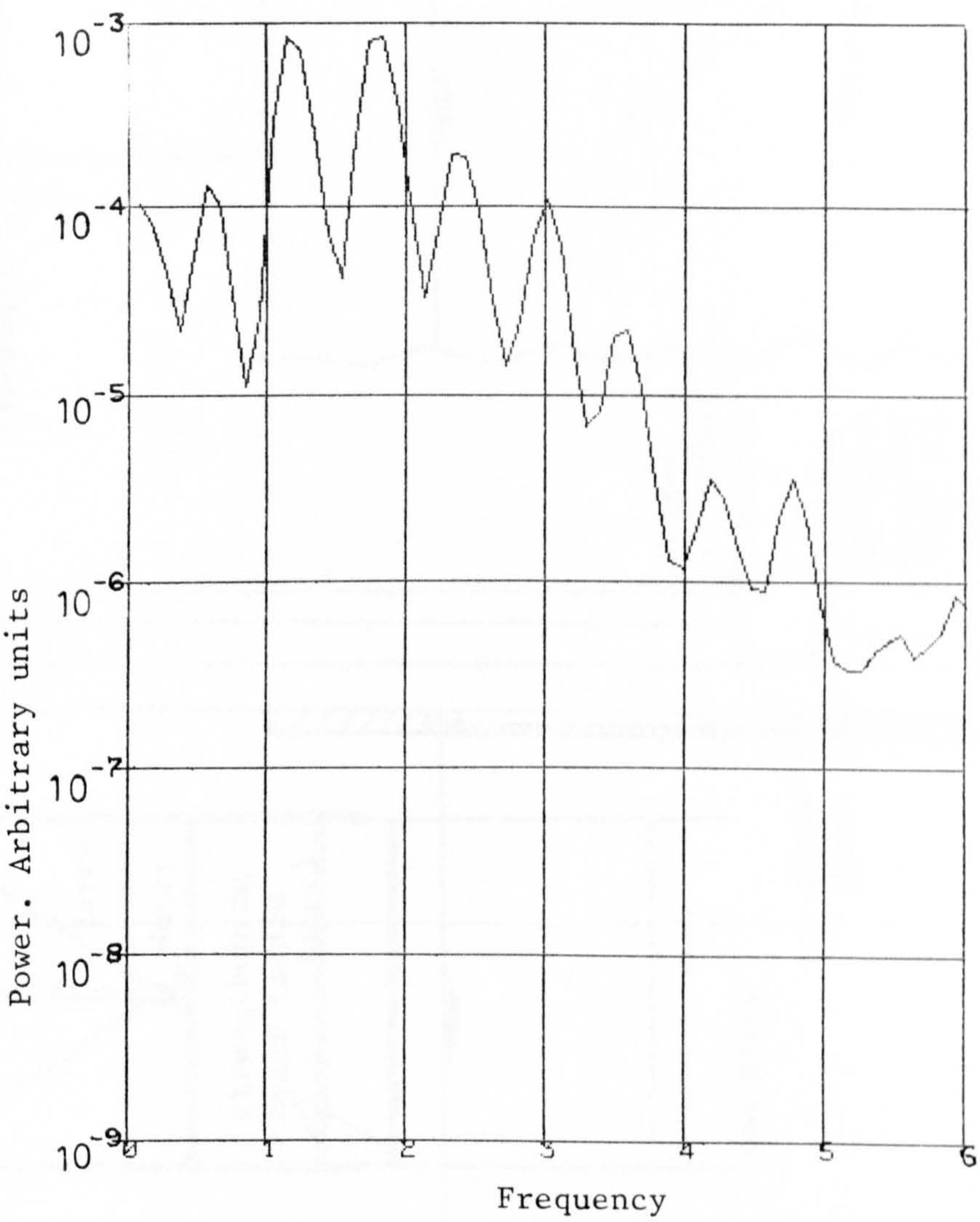

Fig. 51. An example spectrum obtained from analysis of the rigid cylinder cross-flow reaction.

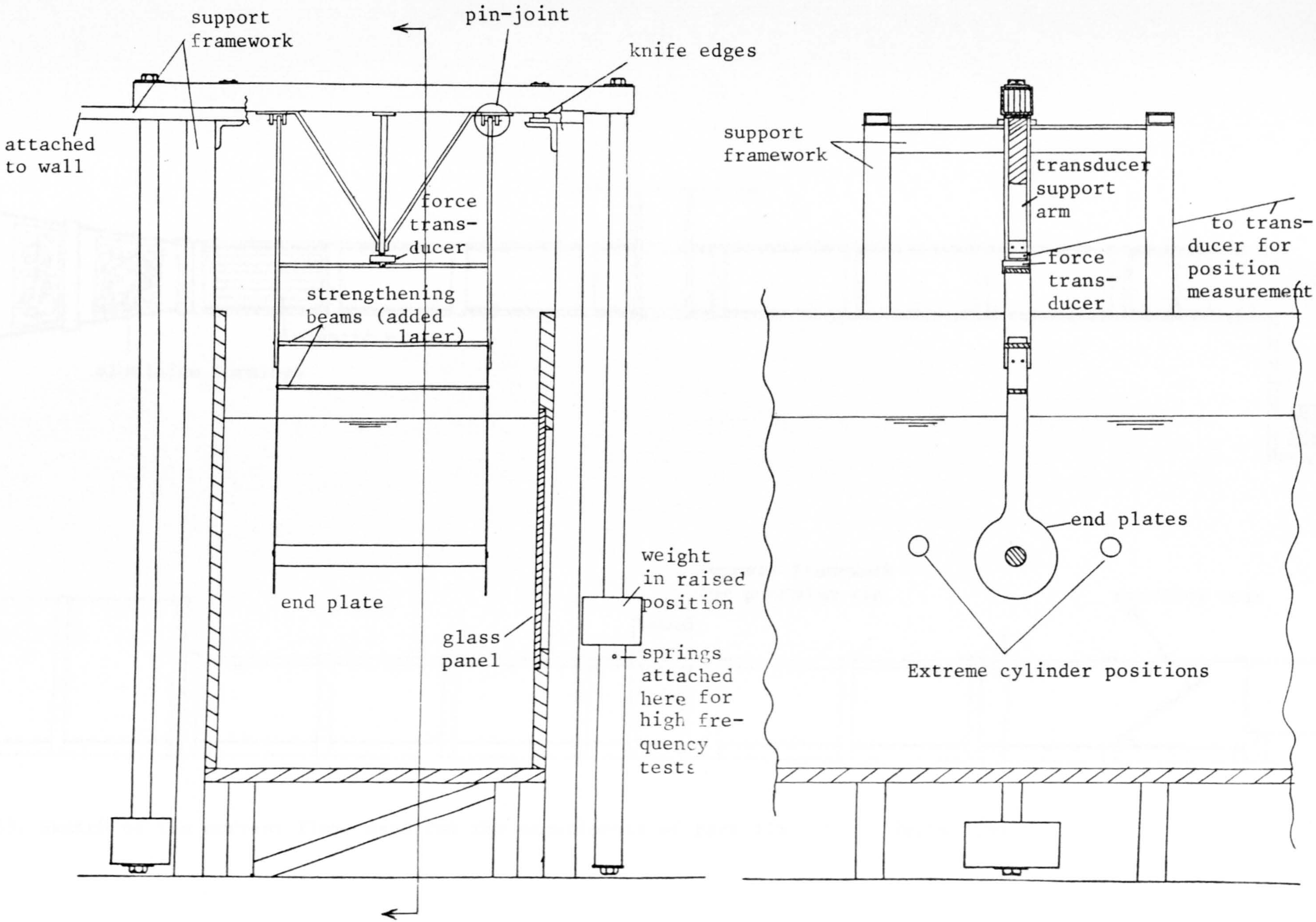

Fig. 52. Detail drawing of the pendulum rig used for the experiments of Part III.

Scale 1:8.6.

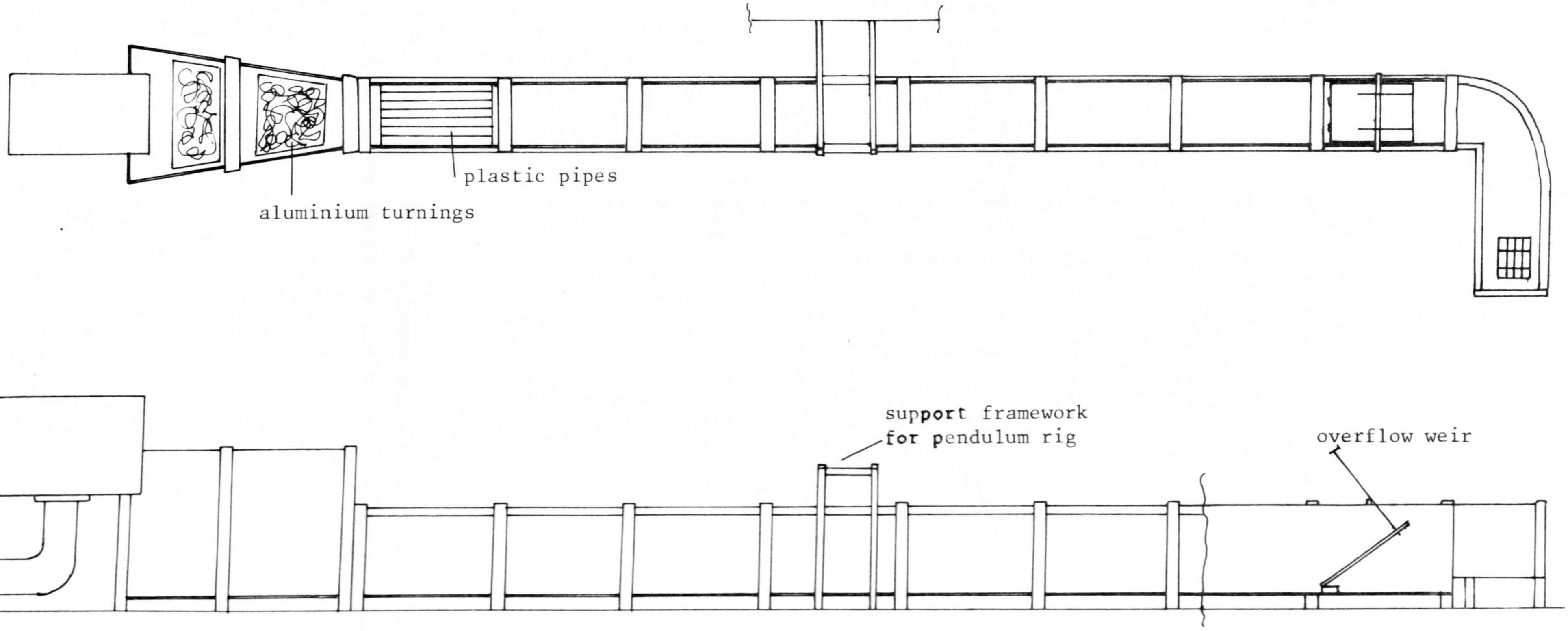

Fig. 53. Sketch of the current flume used for the experiments of Part III. Scale 1:50.

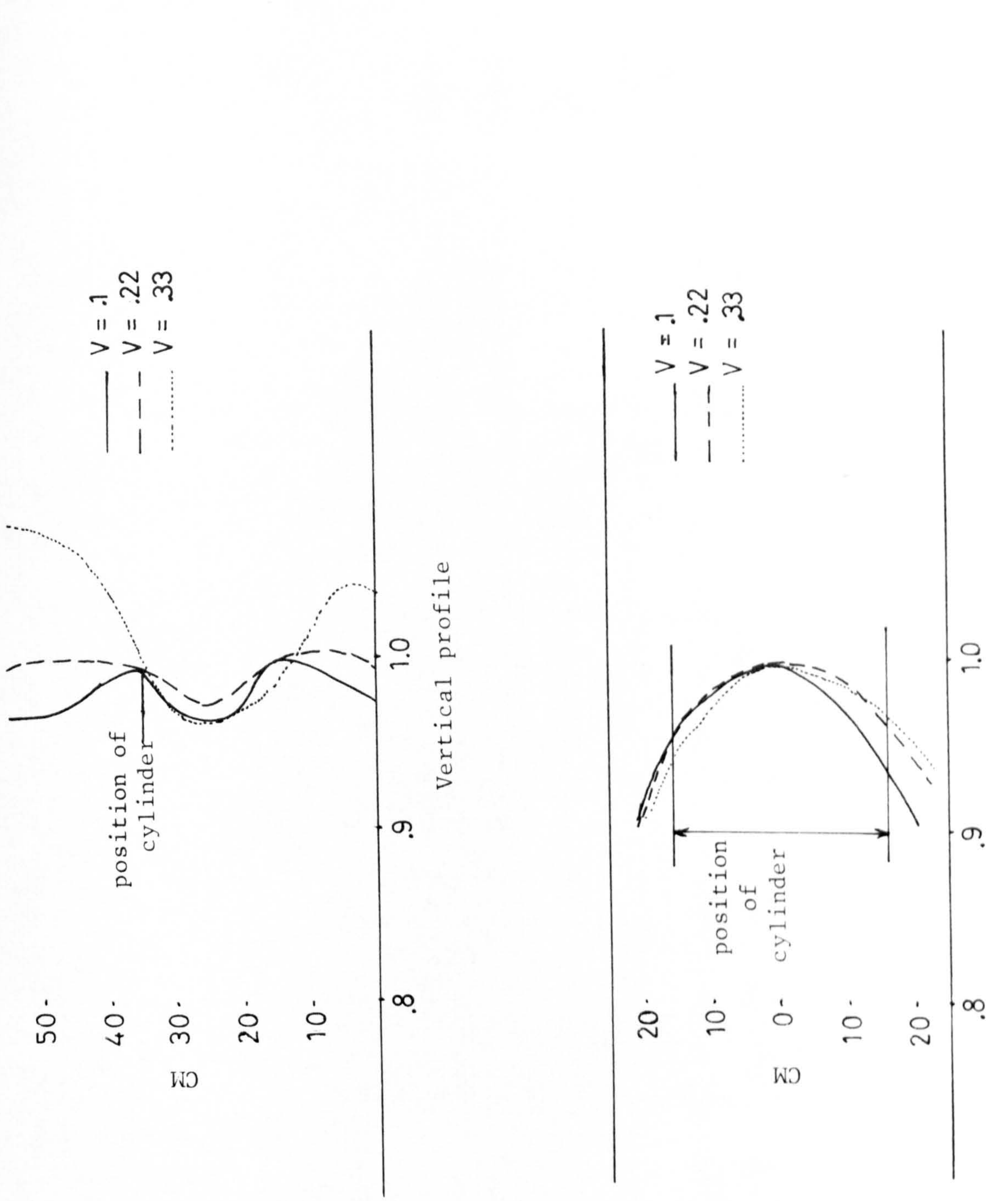

Fig. 54. Flow profiles. Ratio between velocity at various points and that where the centre of the cylinder is during experiments.

Amplifier settings

Digitized data file numbers

Indicates high frequency pendulum

Offset voltage

Test no.

Voltage reading when motion stopped in between test runs

RUN No.	Position 0	Force 1	TAPE 11 rec. speed	Tape footage START	Tape footage STOP	LOS FILE	LOS under-file	CYL DIA.	WTS.	NAT FREQ.	FLOW VEL. HZ	FLOW VEL. m/s	I	Offset VOLTS	COMMENTS	100 range
891	10	50	15/16	1257	1259	D-18: H-D-51	830	.0350	OUT UP	1.397		.288		-9.09		4.62
892	20	50		1259	1261		831							-8.72		4.60
893	50	100		1261	1263		832							-5.59	264	4.62
894	100	200		1263	1265		833							-3.72		I
895	200	500		1265	1267		834							-1.739		4.38
896	200	500		1267	1269		835							-1.739		4.38
897	500	1000	15/16	1269	1271	D-18: H-D-50	836	.0350	OUT UP			.288		-1.239	(CONT.)	
898	500	1000		1271	1273		837							-1.239		4.42
															18.22	

Fig. 55. An example of the manually recorded data for a single test run.

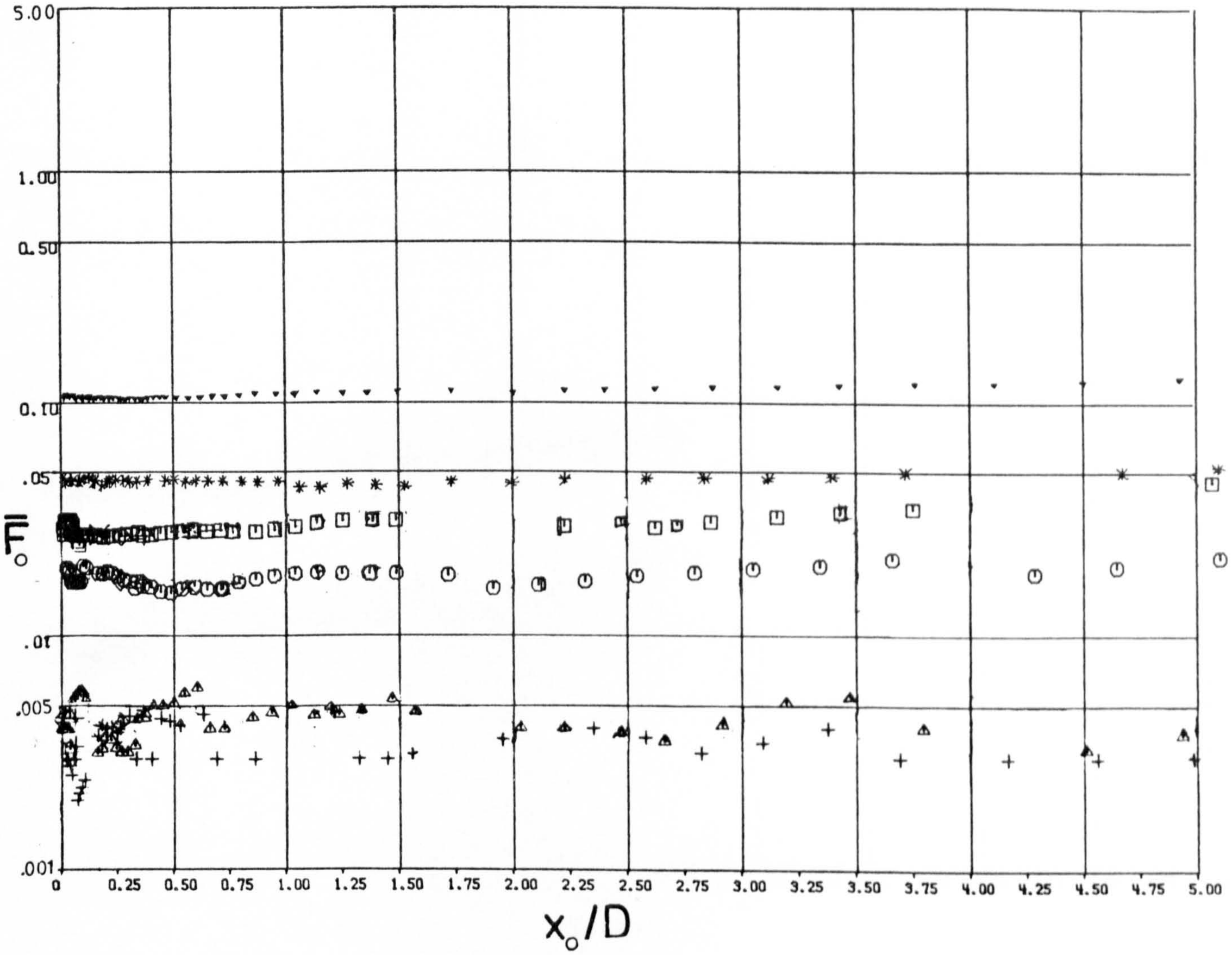

Fig. 56. Steady force measured for the low frequency pendulum with no cylinder attached in various currents.

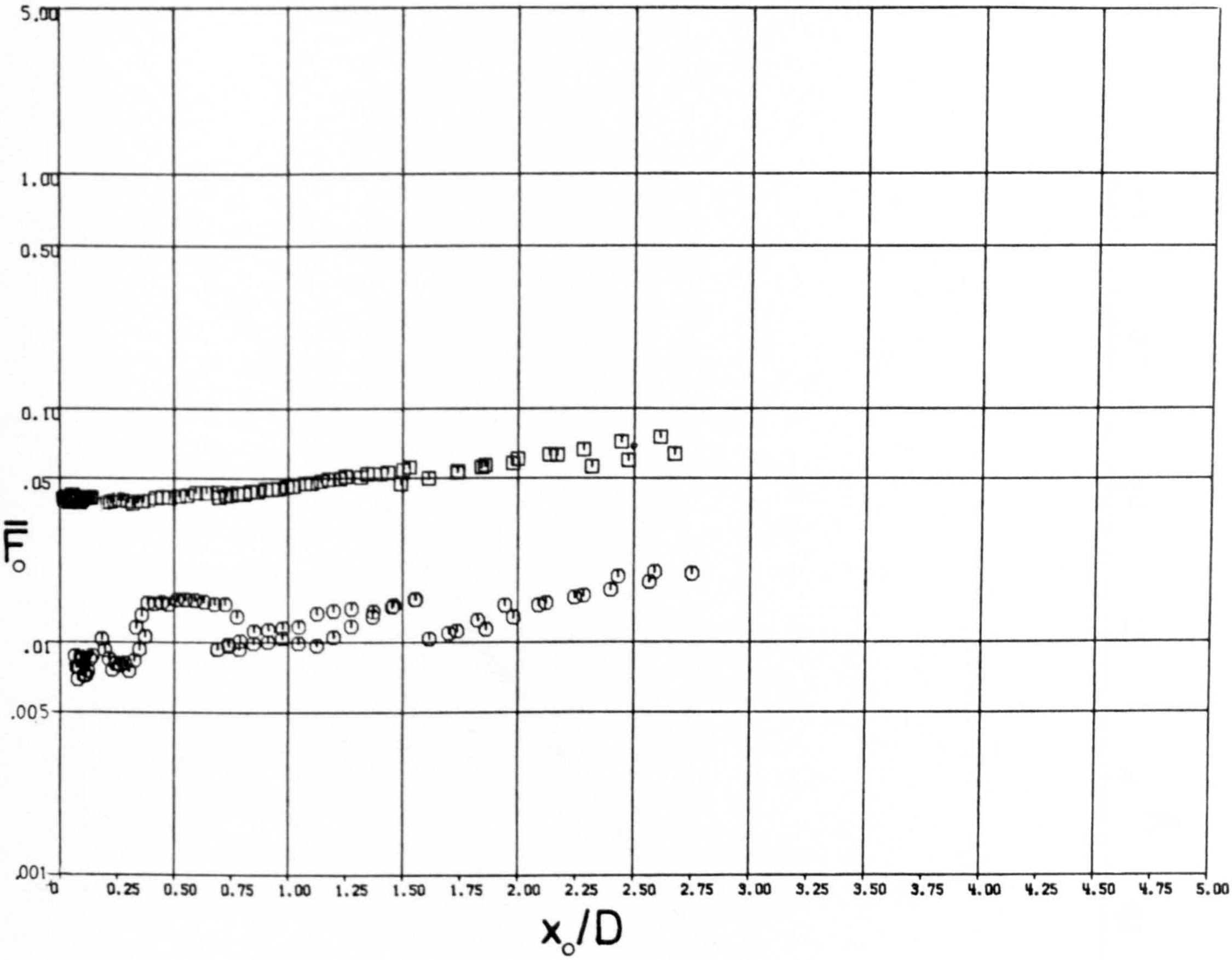

Fig. 57. Steady force measured for the high frequency pendulum with no cylinder attached in various currents.

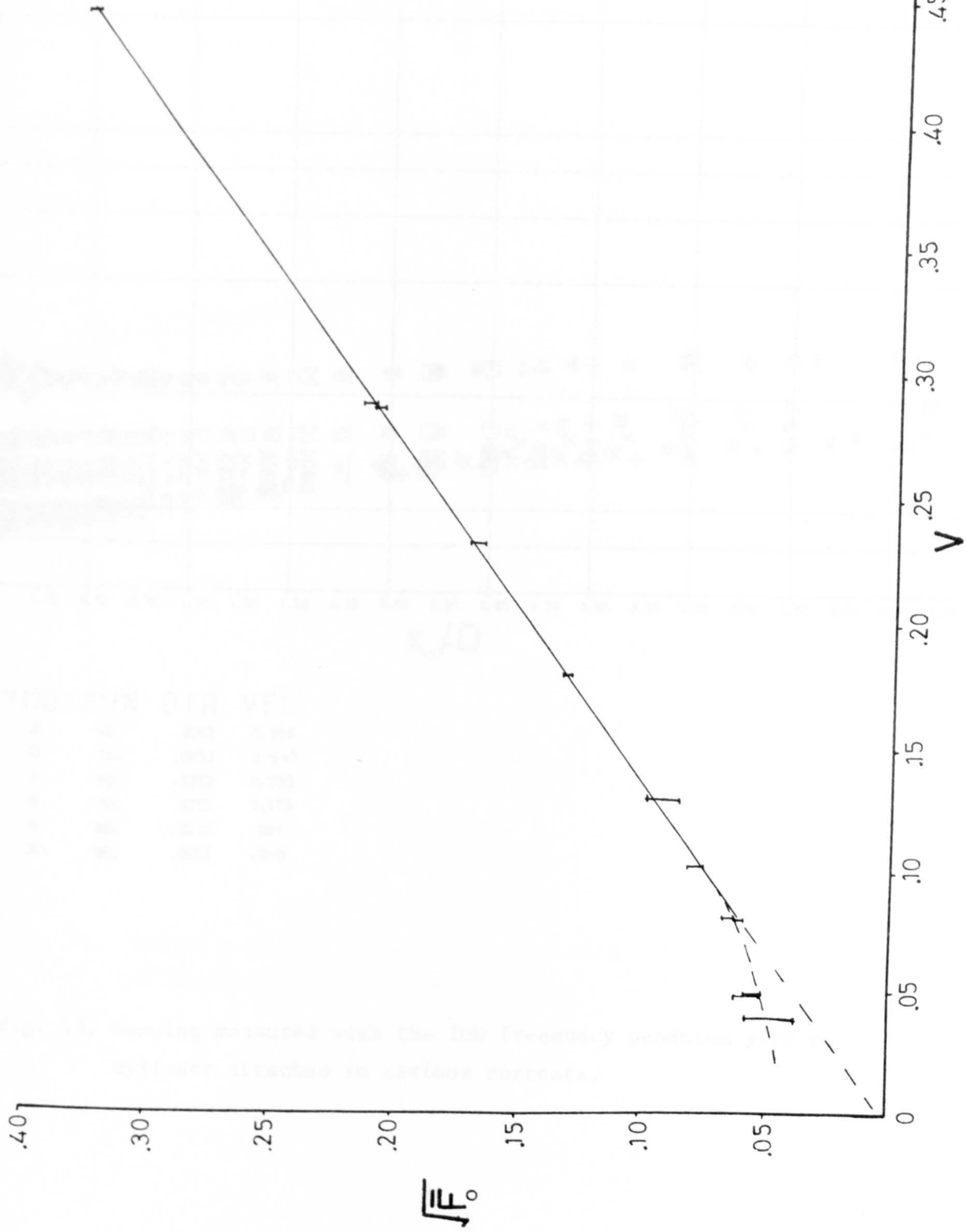

Fig. 58. $\sqrt{F_o}$ versus flow velocity V. (No cylinder attached.)

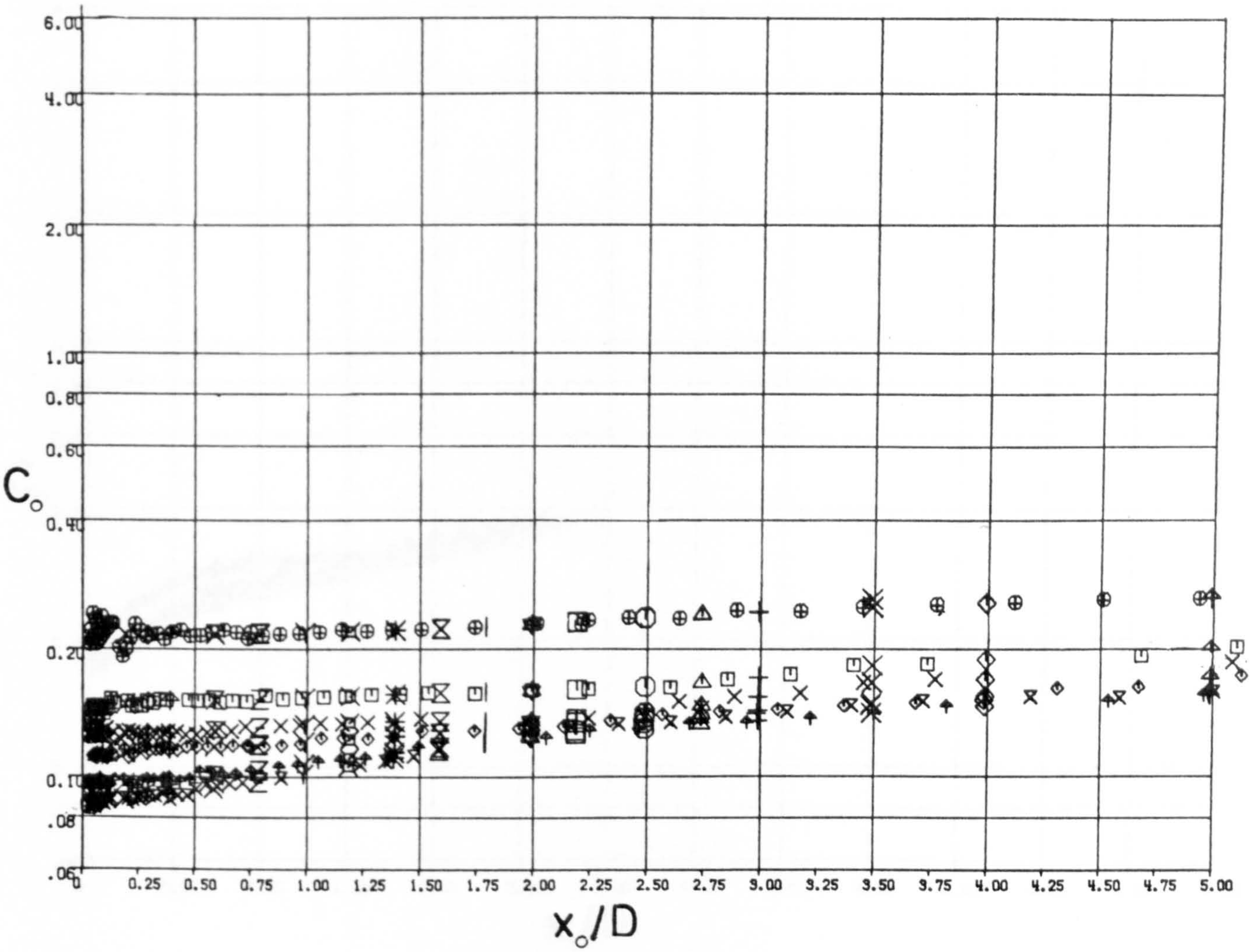

SYMB	RUN	DIA	VEL
□	40.	.0252	0.288
⊕	50.	.0252	0.445
×	60.	.0252	0.233
◇	70.	.0252	0.179
↑	80.	.0252	.081
⧖	90.	.0252	.048

Fig. 59. Damping measured with the low freqeuncy pendulum with no cylinder attached in various currents.

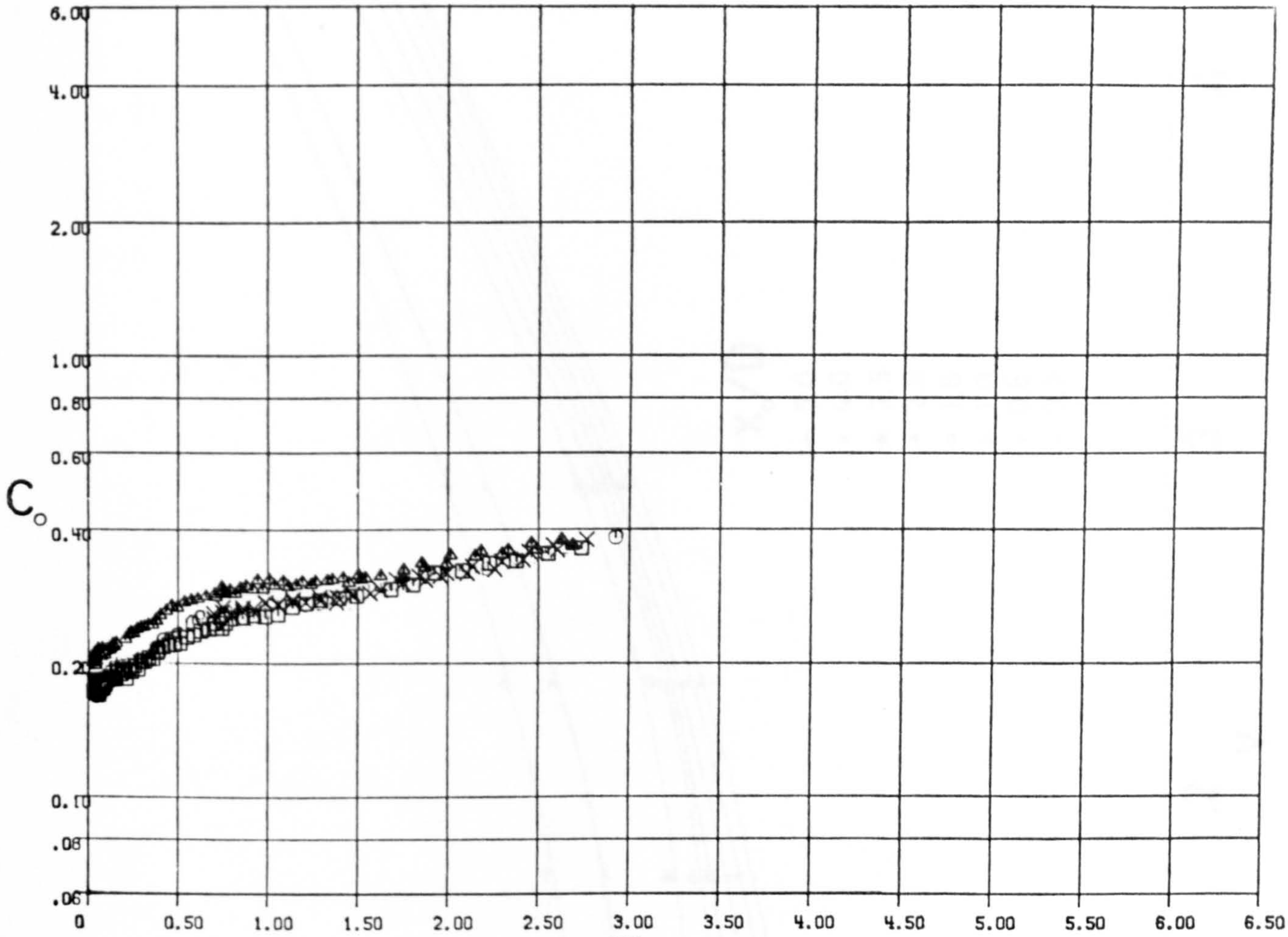

Fig. 60. Damping measured with the high frequency pendulum with no cylinder attached in various currents.

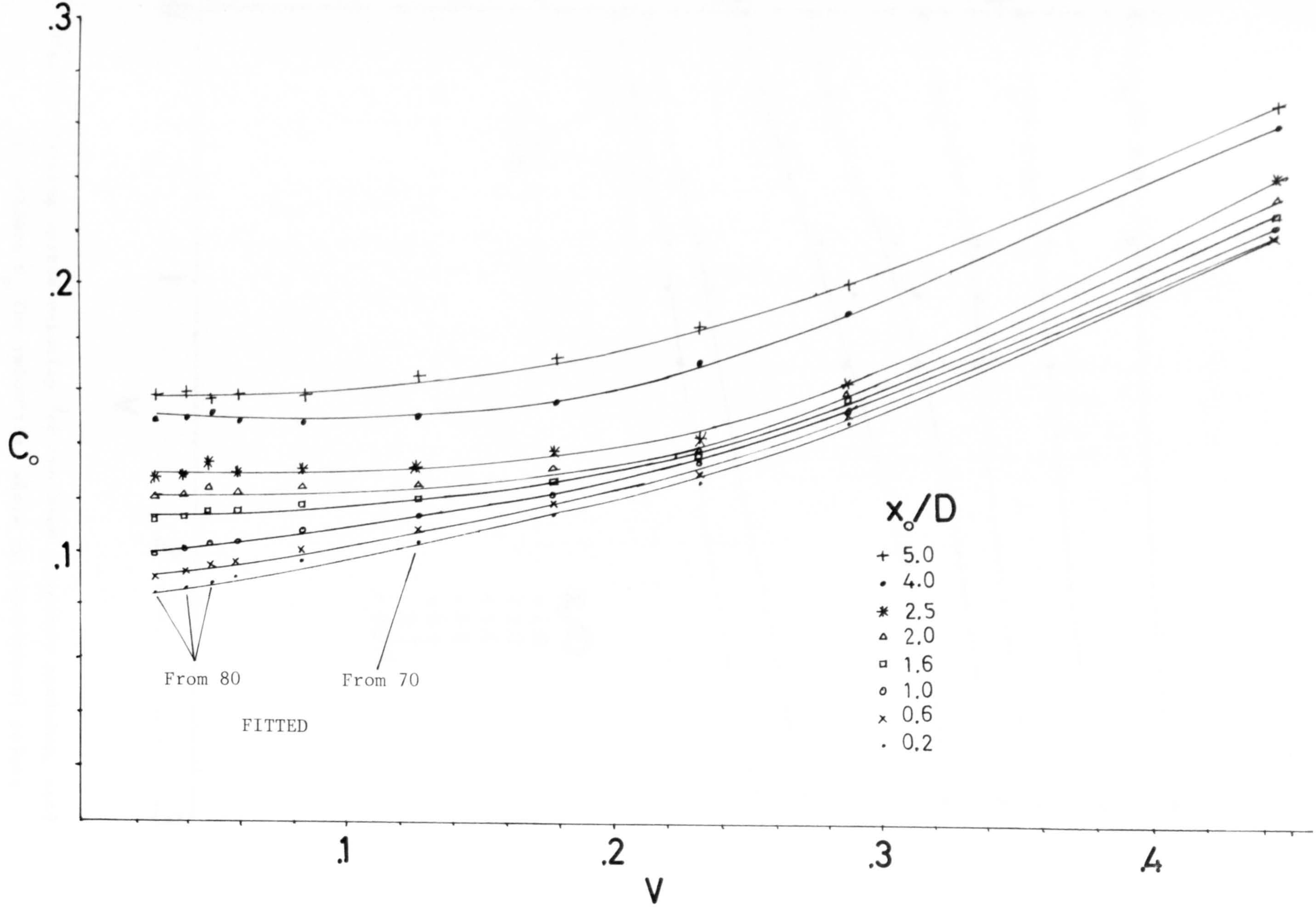

Fig. 61. Damping versus velocity for the low frequency pendulum, used to estimate C_o for velocities where no experimental points exist.

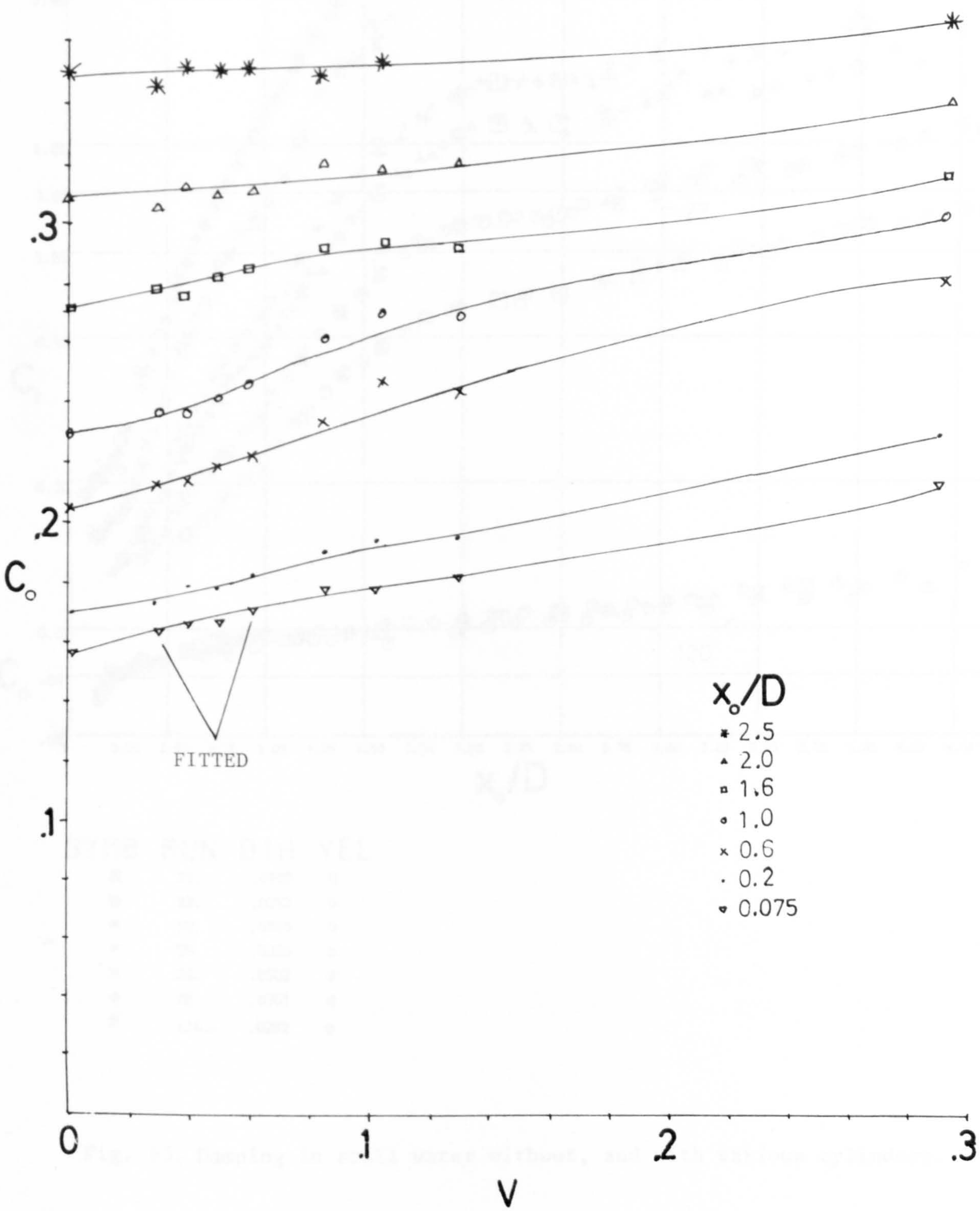

Fig. 62. Damping versus velocity for the high frequency pendulum, used to estimate C_o for velocities where no experimental points exist.

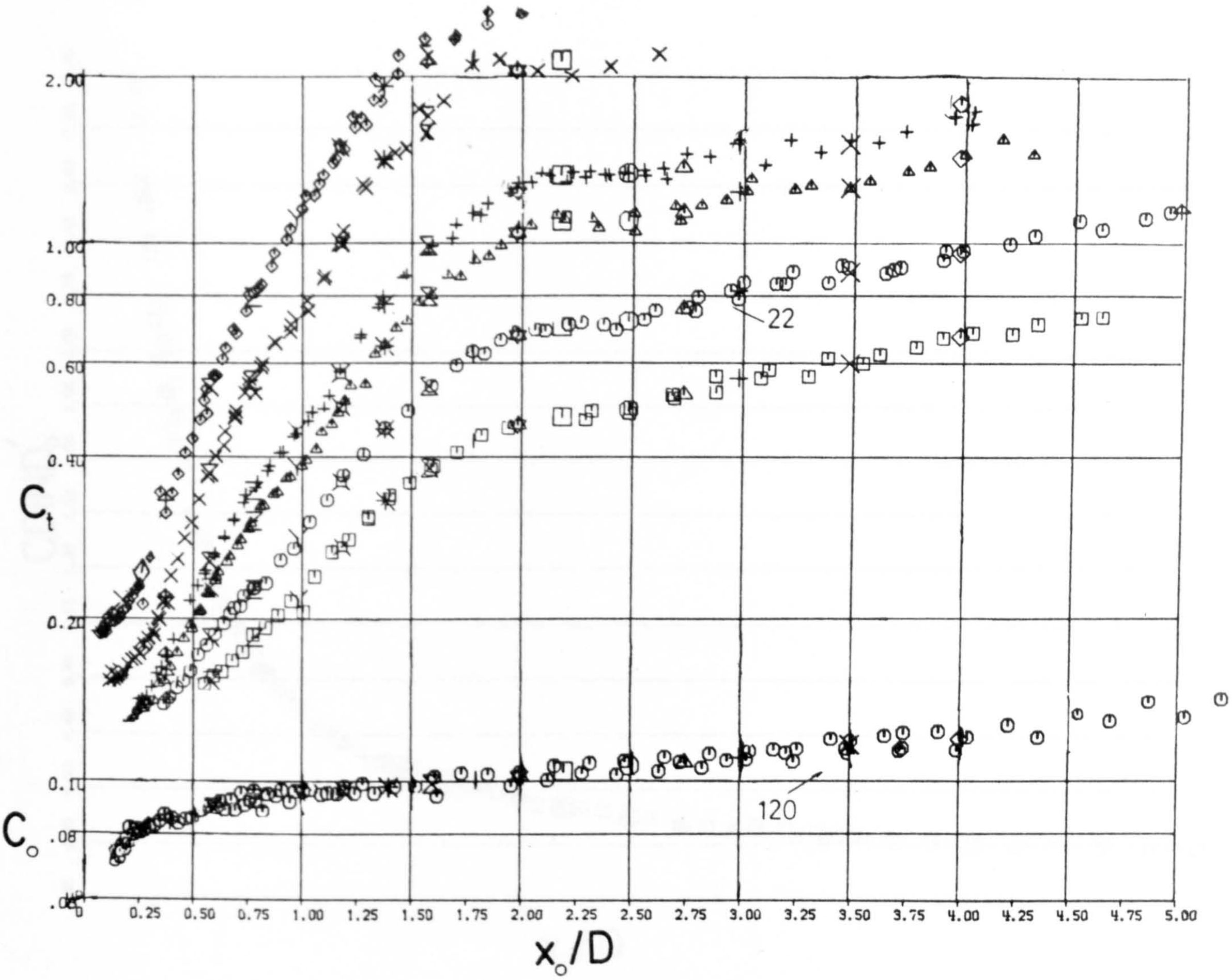

Fig. 63. Damping in still water without, and with various cylinders.

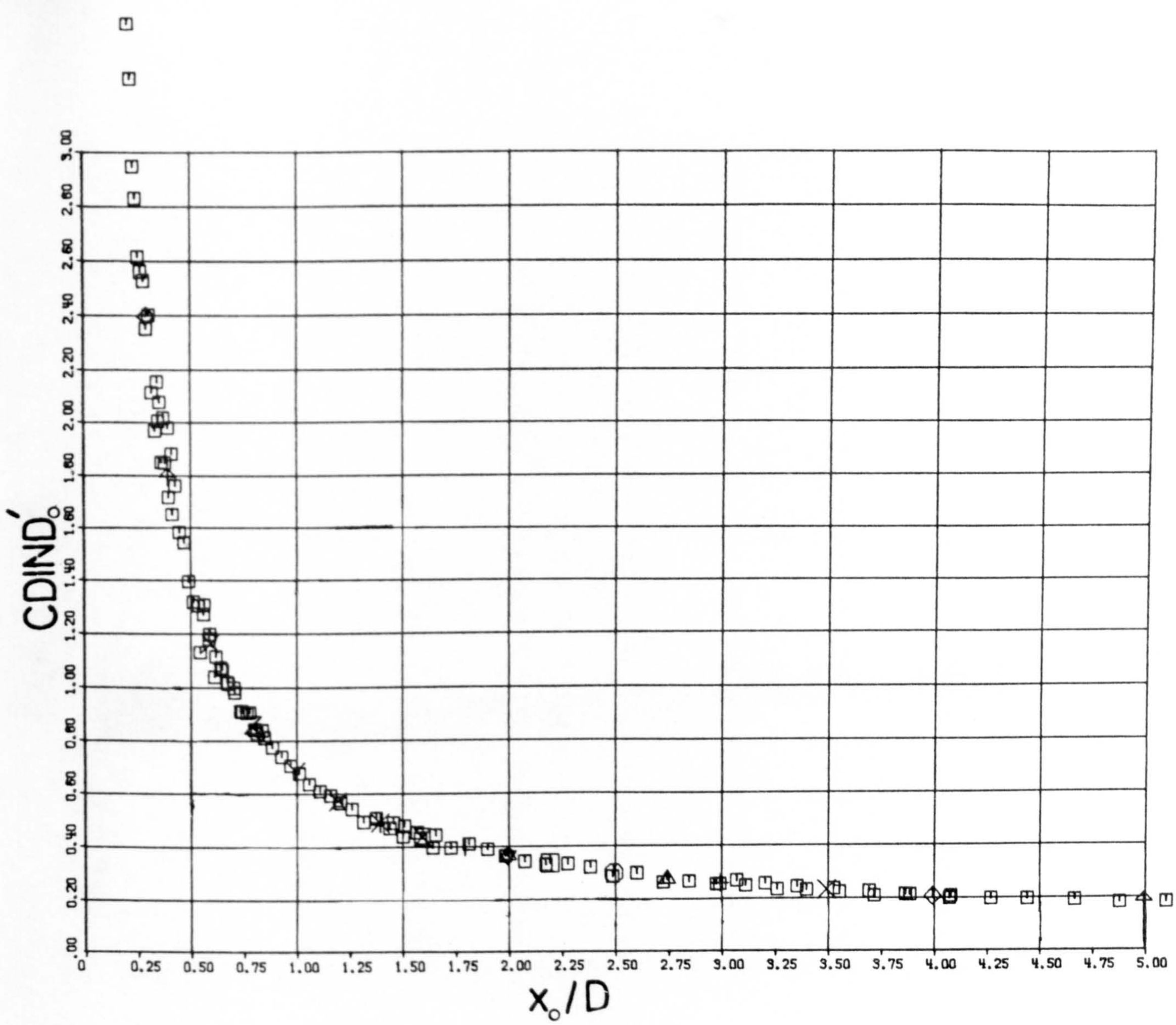

Fig. 64. No cylinder oscillatory drag coefficient, $CDIND'_o$ in still water.

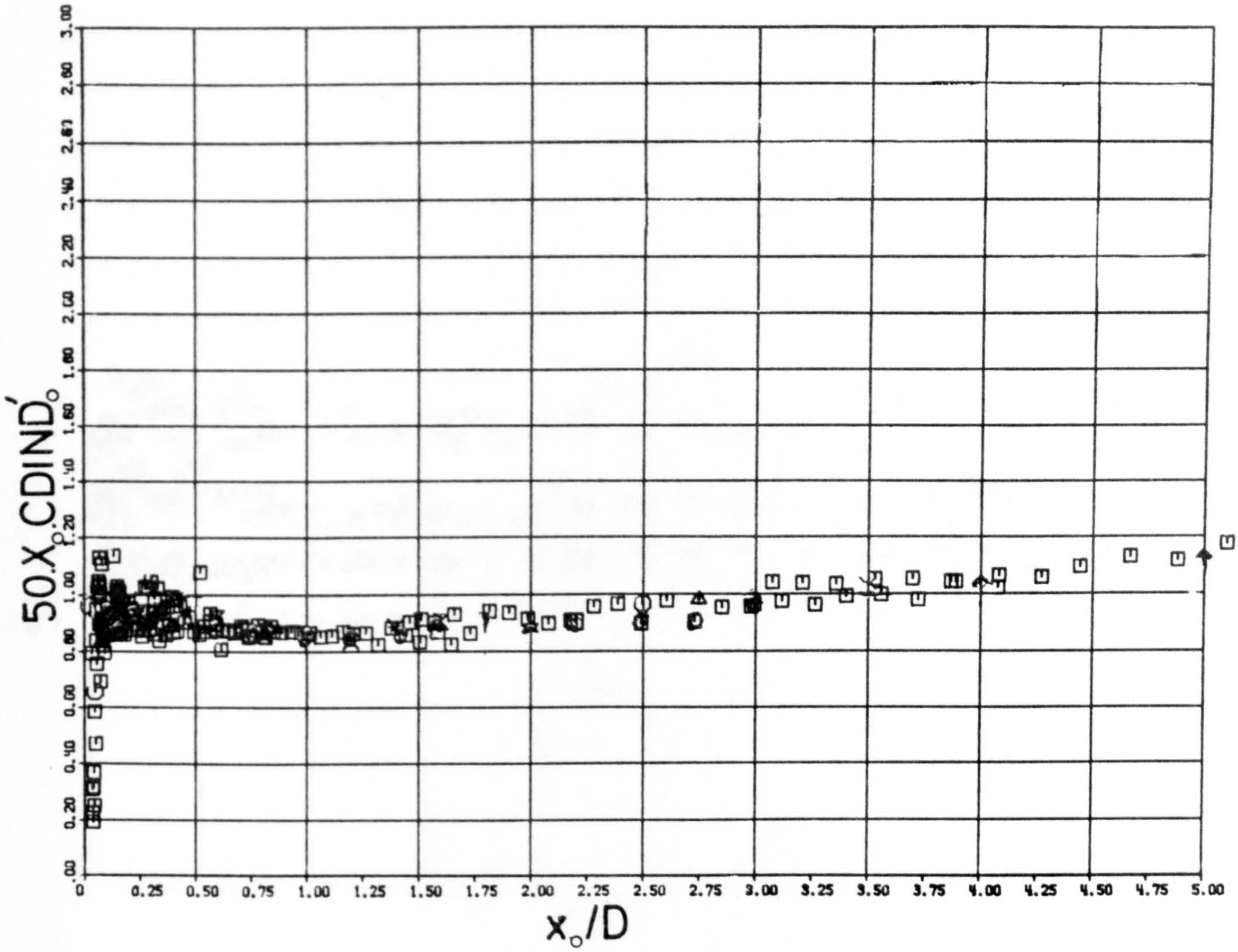

Fig. 65. Data of Fig. 71 replotted as $CDIND_o'$. x_o/D versus x_o/D.

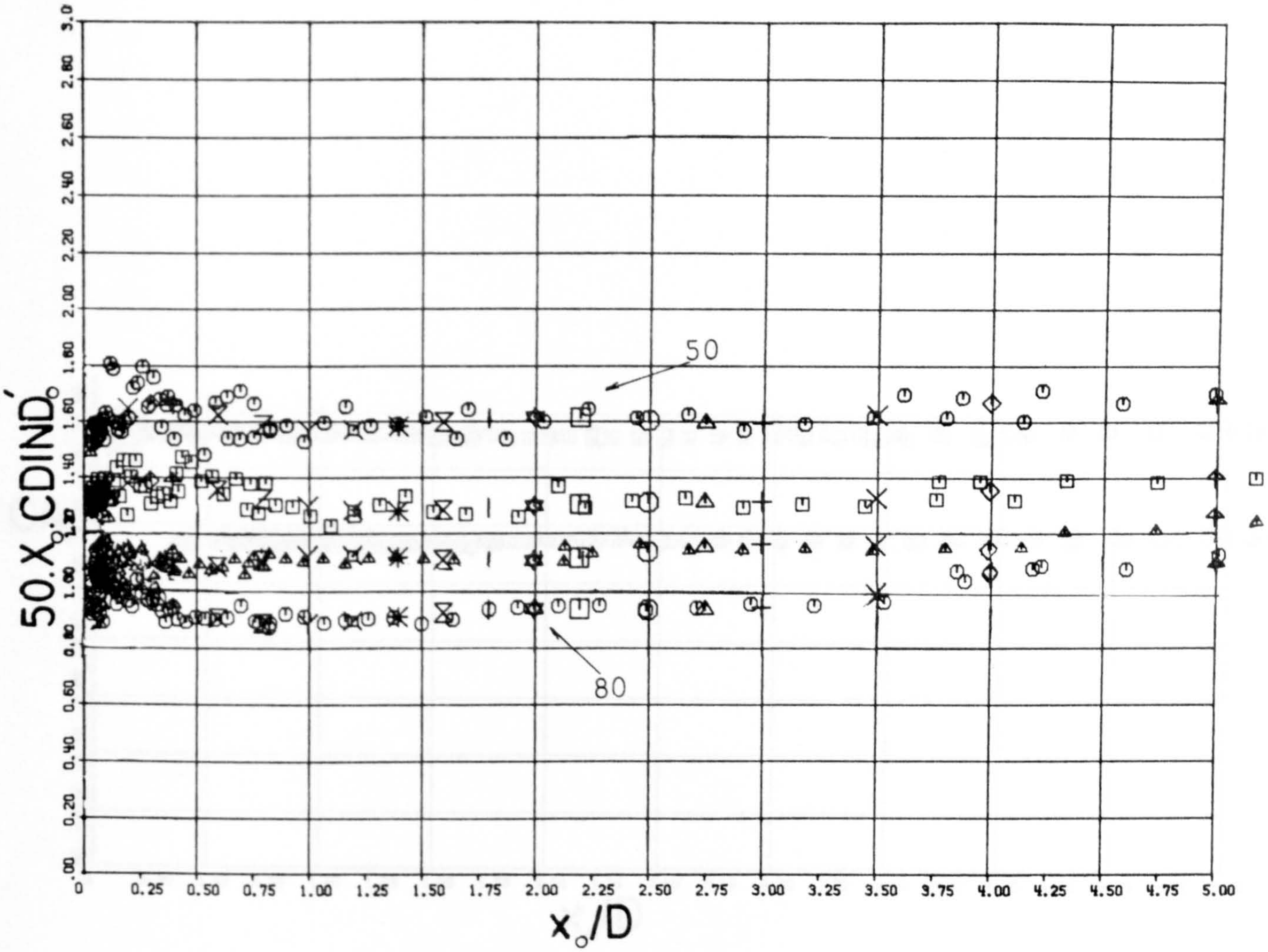

Fig. 66. No cylinder oscillatory drag coefficient, $CDIND'_o$ in various currents.

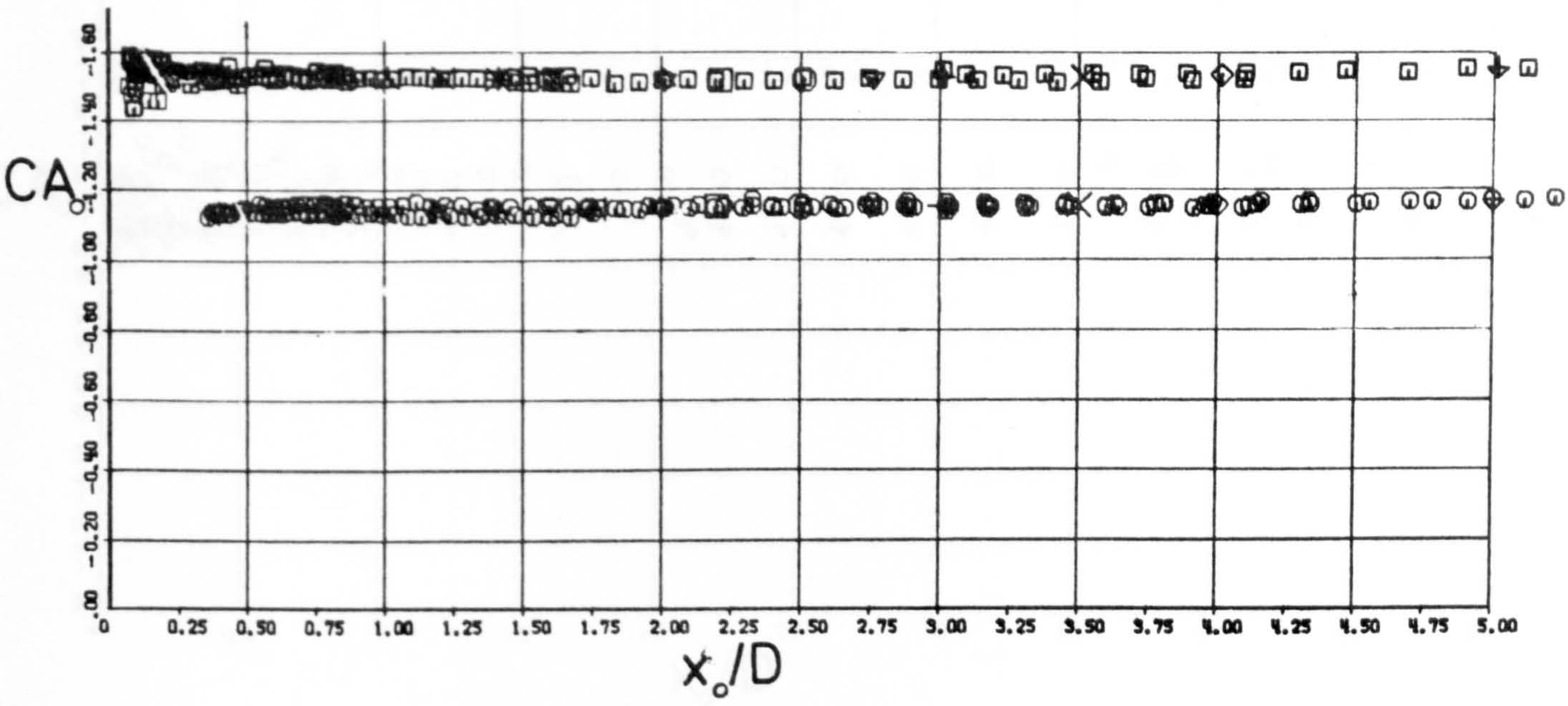

SYMB	RUN	DIA	VEL	
▫	120.	.0252	0	After modifications
●	20.	.0252	0	Before modifications

Fig. 67. Inertia coefficient in still water for the low frequency pendulum with no cylinder attached before and after modifications.

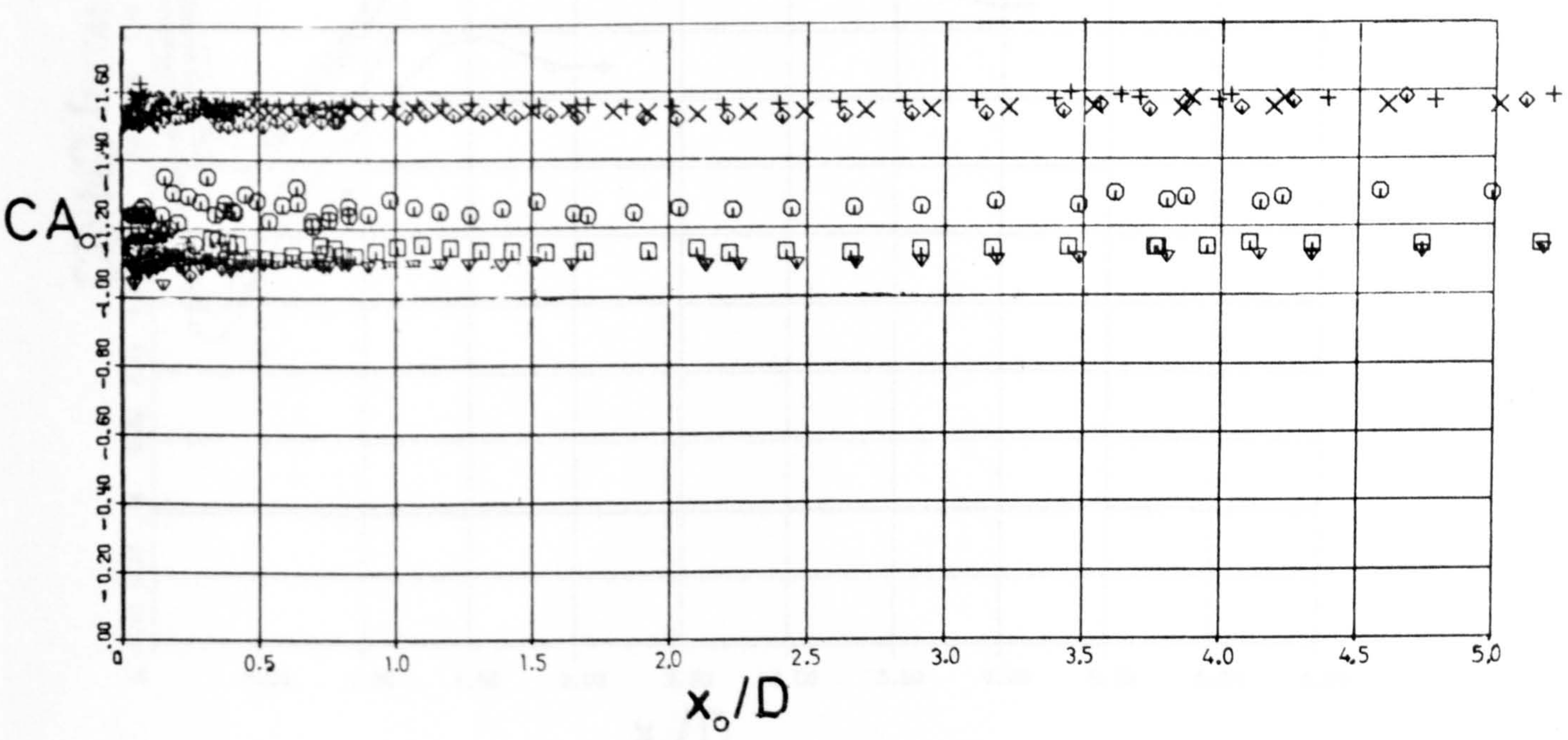

SYMB	RUN	DIA	VEL	
▫	40.	.0252	0.288	Before modifications
○	50.	.0252	0.445	
▽	60.	.0252	0.233	
+	70.	.0252	0.179	After modifications
×	80.	.0252	.081	
◇	90	.0252	.046	

Fig. 68. Inertia coefficient with no cylinder attached in various currents.

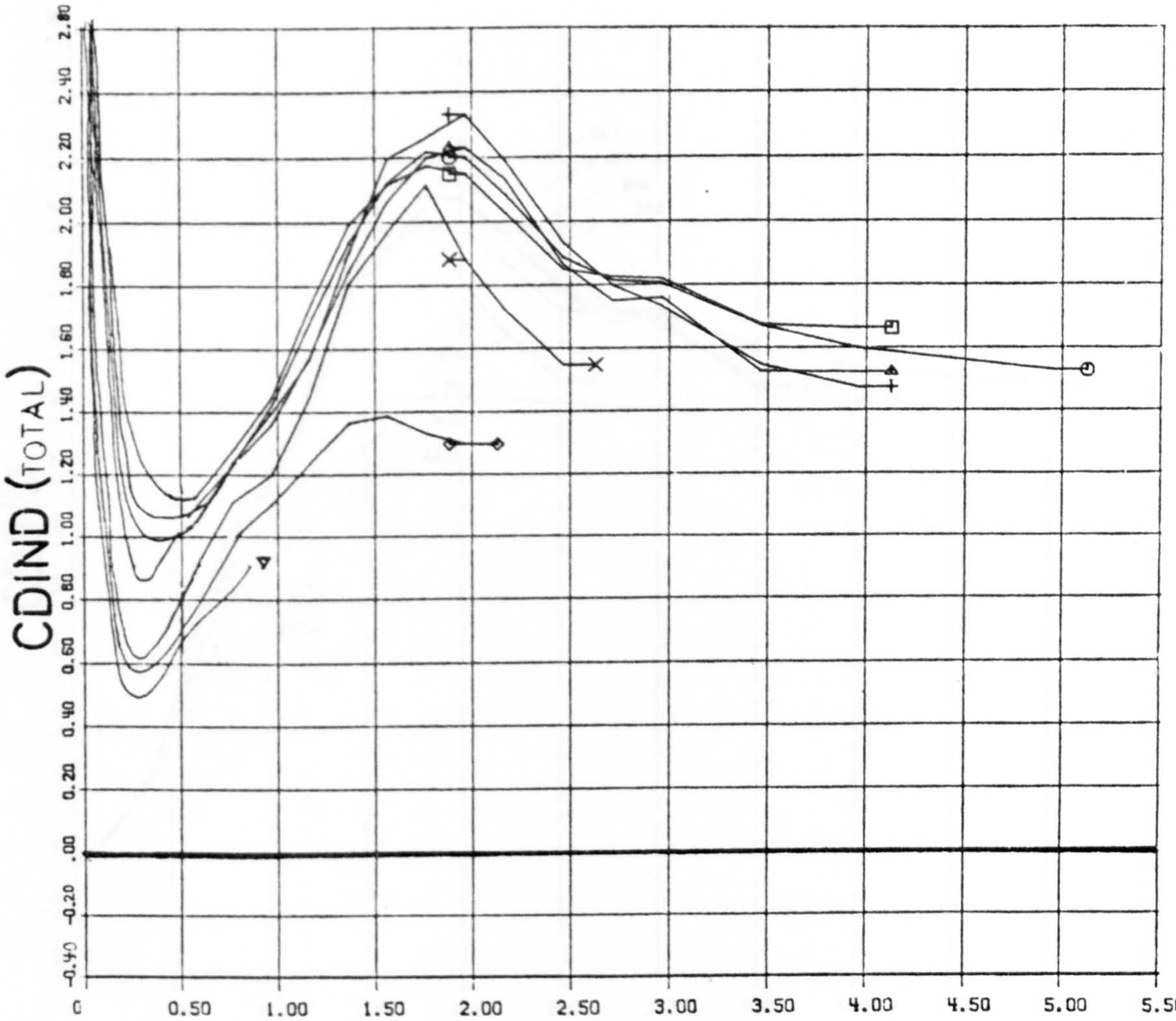

SYMB	RUN	DIA	VEL	V/nD	β
□	21.	.0202	0	0	190
○	22.	.0252	0	0	300
▲	23.	.0320	0	0	490
+	24.	.0350	0	0	580
×	25.	.0502	0	0	1200
◆	26.	.0701	0	0	2340
▽	705.	.0502	0	0	2650

Fig. 69. Still water oscillatory drag coefficient versus x_o/D. Stokes' viscous contribution not removed.

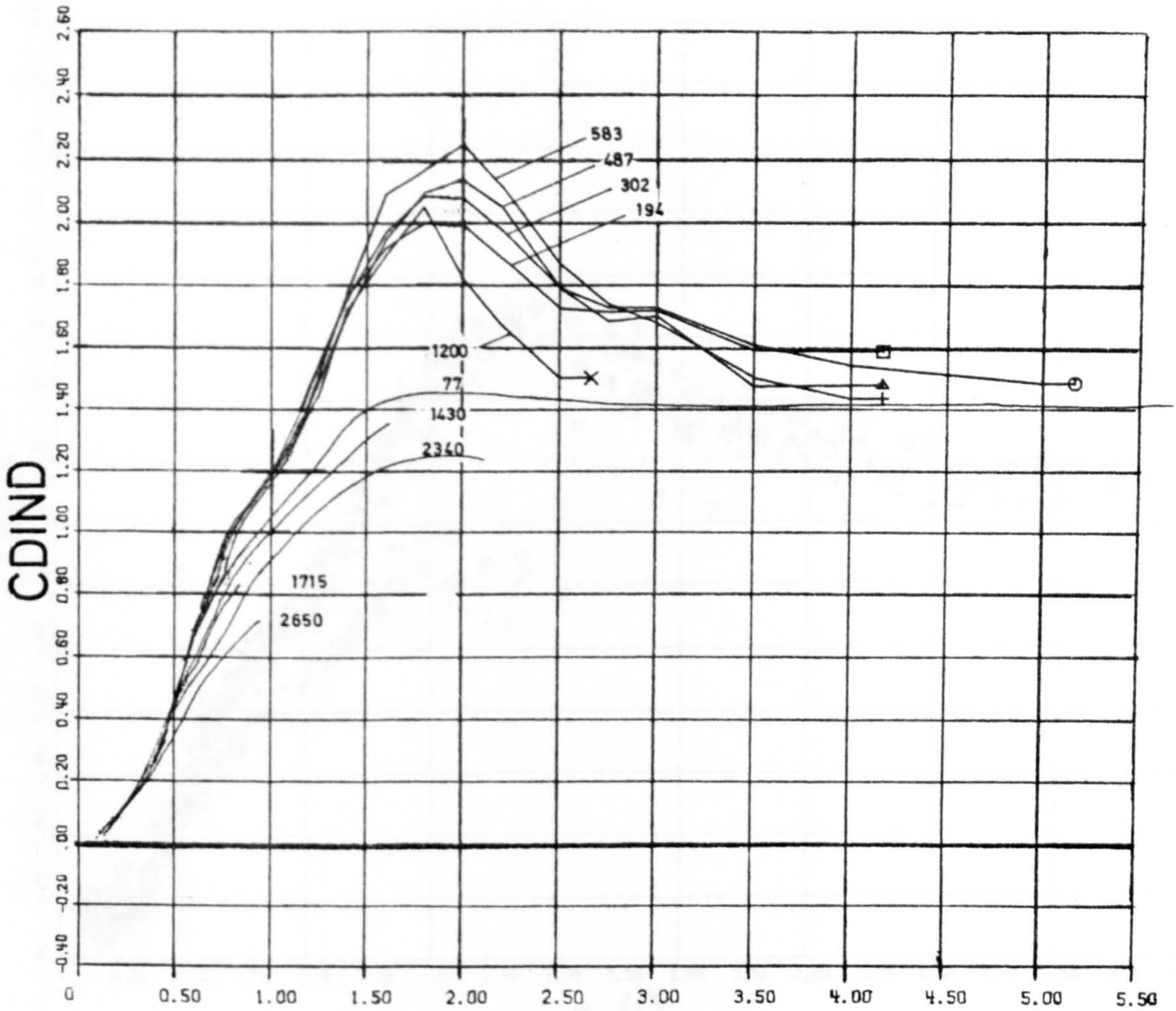

SYMB	RUN	DIA	VEL	V/nD	β
□	21.	.0202	0	0	194
◷	22.	.0252	0	0	302
▲	23.	.0320	0	0	487
+	24.	.0350	0	0	583
×	25.	.0502	0	0	1200
	701.	.0202	0	0	1430
	704.	.0350	0	0	1715
	26.	.0701	0	0	2340
	705.	.0502	0	0	2650

Fig. 70. CDIND versus x_o/D. (Viscous contribution subtracted.)

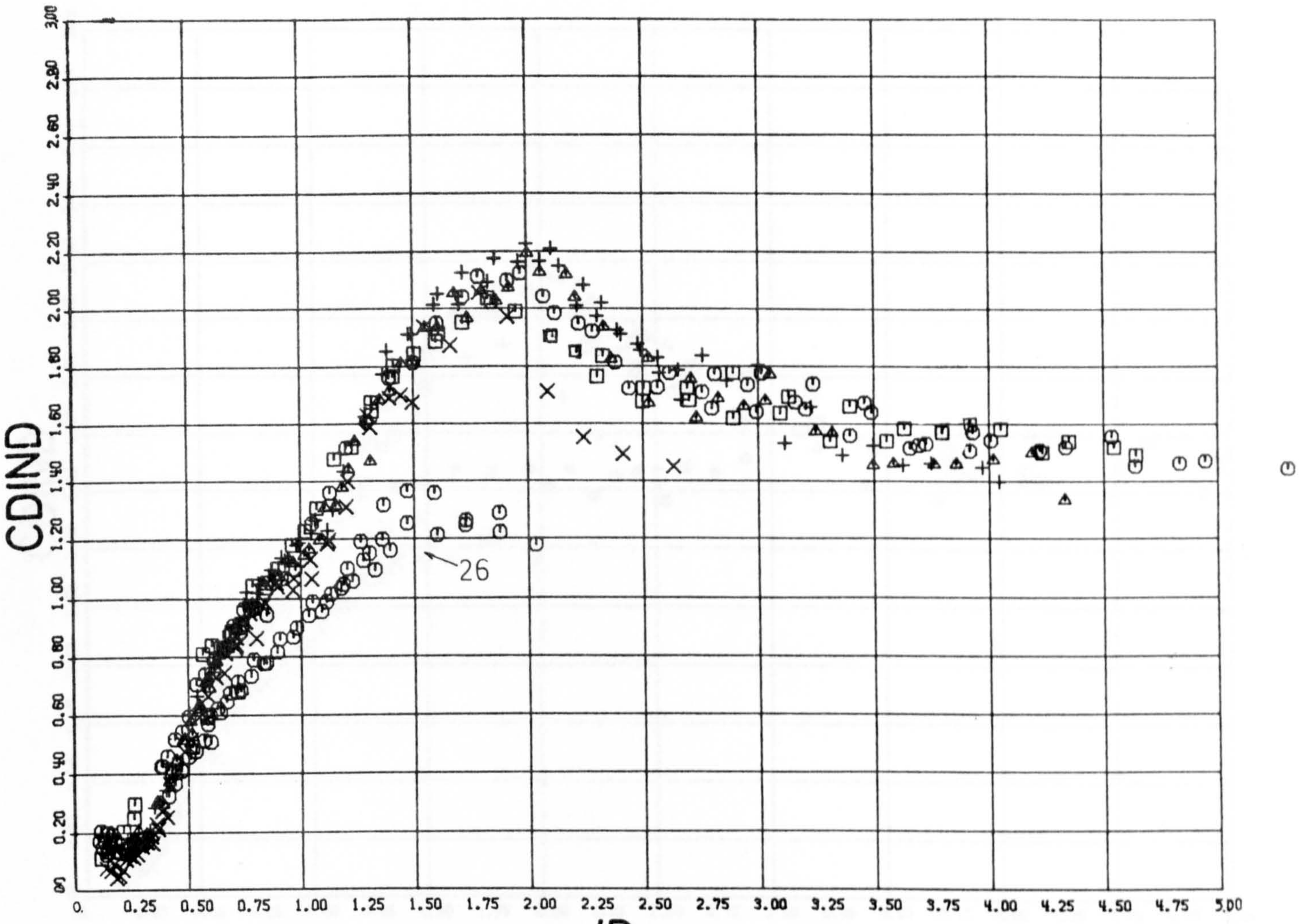

SYMB	RUN	DIA	VEL	β
▣	21.	.0202	0	194
⊙	22.	.0252	0	302
▲	23.	.0320	0	487
+	24.	.0350	0	583
×	25.	.0502	0	1200
⊙	26.	.0701	0	2340

Fig. 71. Some experimental results (actual points) for CDIND versus x_o/D.

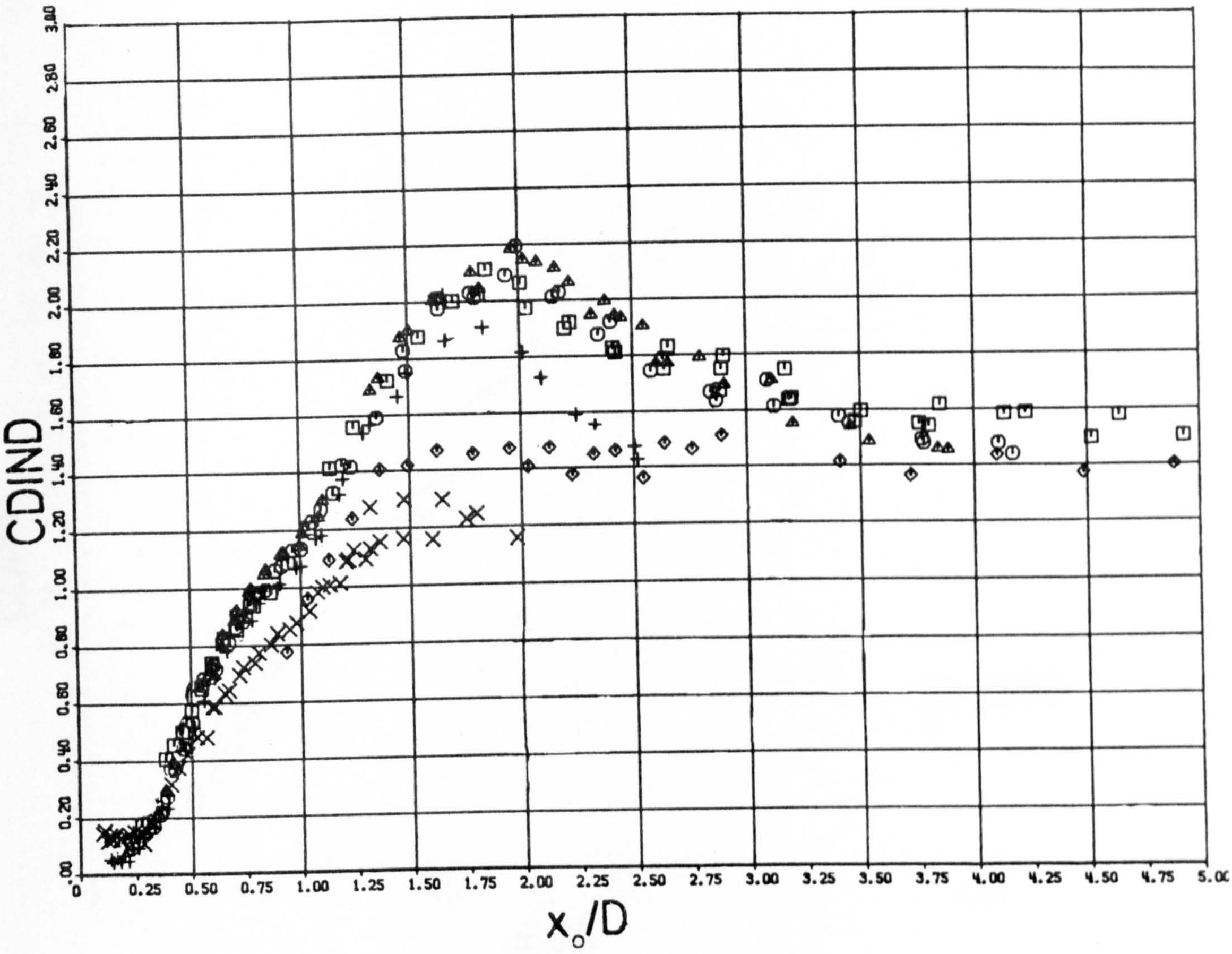

SYMB	RUN	DIA	VEL	β
□	122	.0252	0	300
○	123	.0320	0	490
▲	124	.0350	0	580
+	125	.0502	0	1200
×	126	.0701	0	2340
◆	127	.01275	0	77

Fig. 72. Results similar to those of Fig. 71, but obtained some months later.

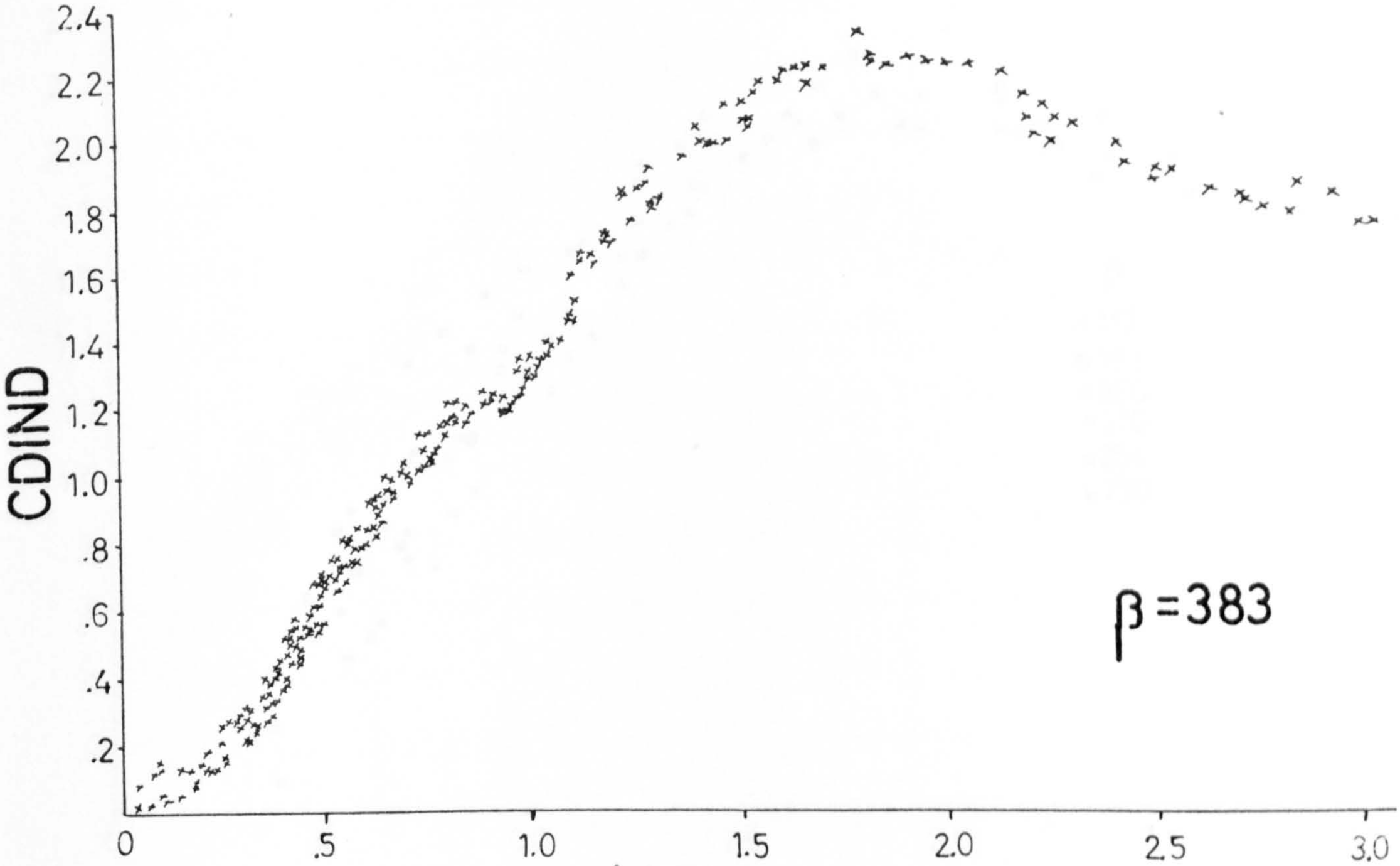

Fig. 73. CDIND versus x_o/D, obtained from a smaller rig and analysed by hand.

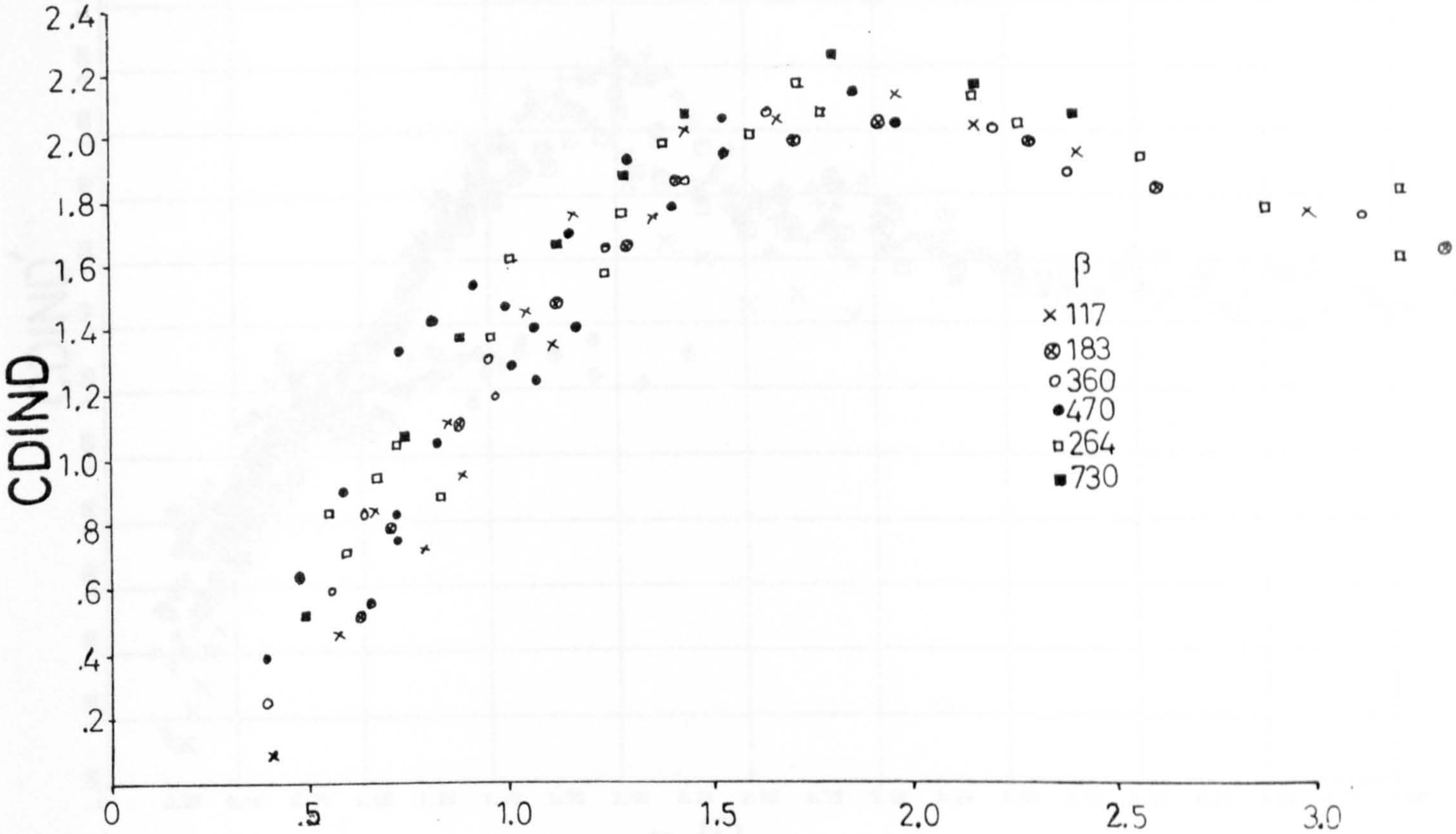

Fig. 74. CDIND versus x_o/D. Results of Sarpkaya and Tuter (1974) replotted, viscous contribution subtracted.

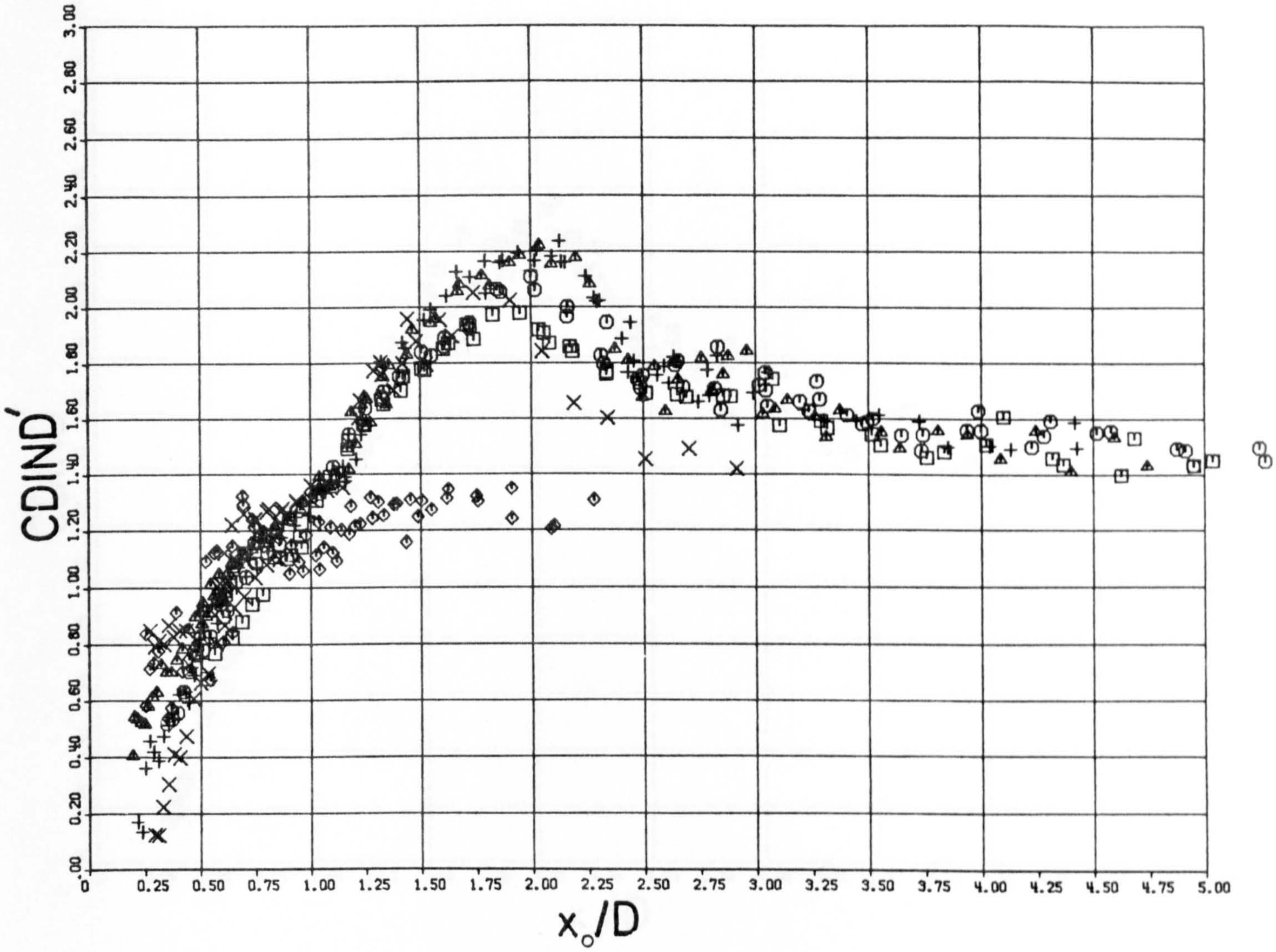

SYMB	RUN	DIA	VEL	β
□	21.	.0202	0	194
○	22.	.0252	0	302
△	23.	.0320	0	487
+	24.	.0350	0	583
×	25.	.0502	0	1200
◇	26.	.0701	0	2340

Fig. 75. The oscillatory drag coefficient in still water derived from Fourier coefficient analysis.

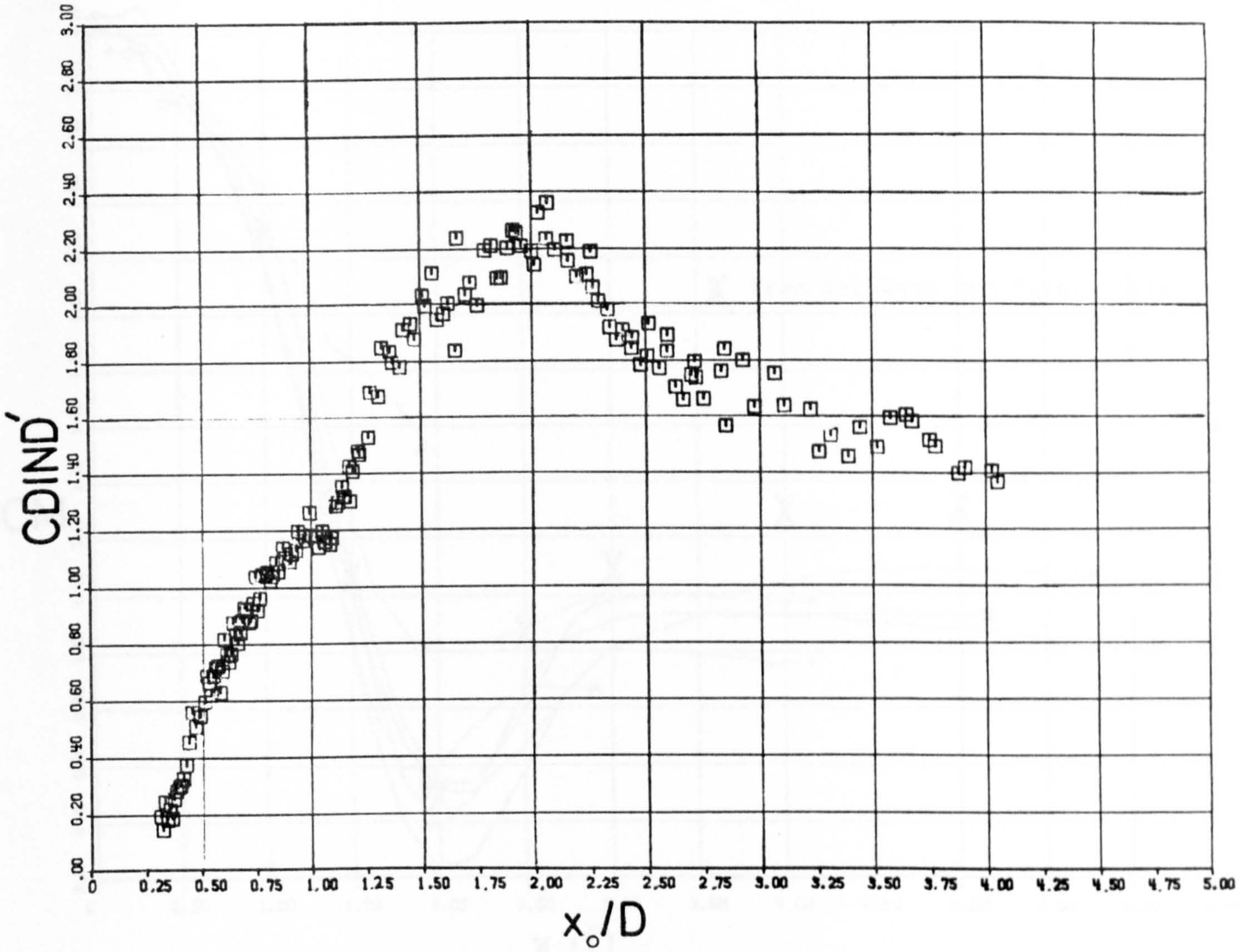

Fig. 76. The oscillatory drag coefficient in still water derived from Fourier coefficient analysis.

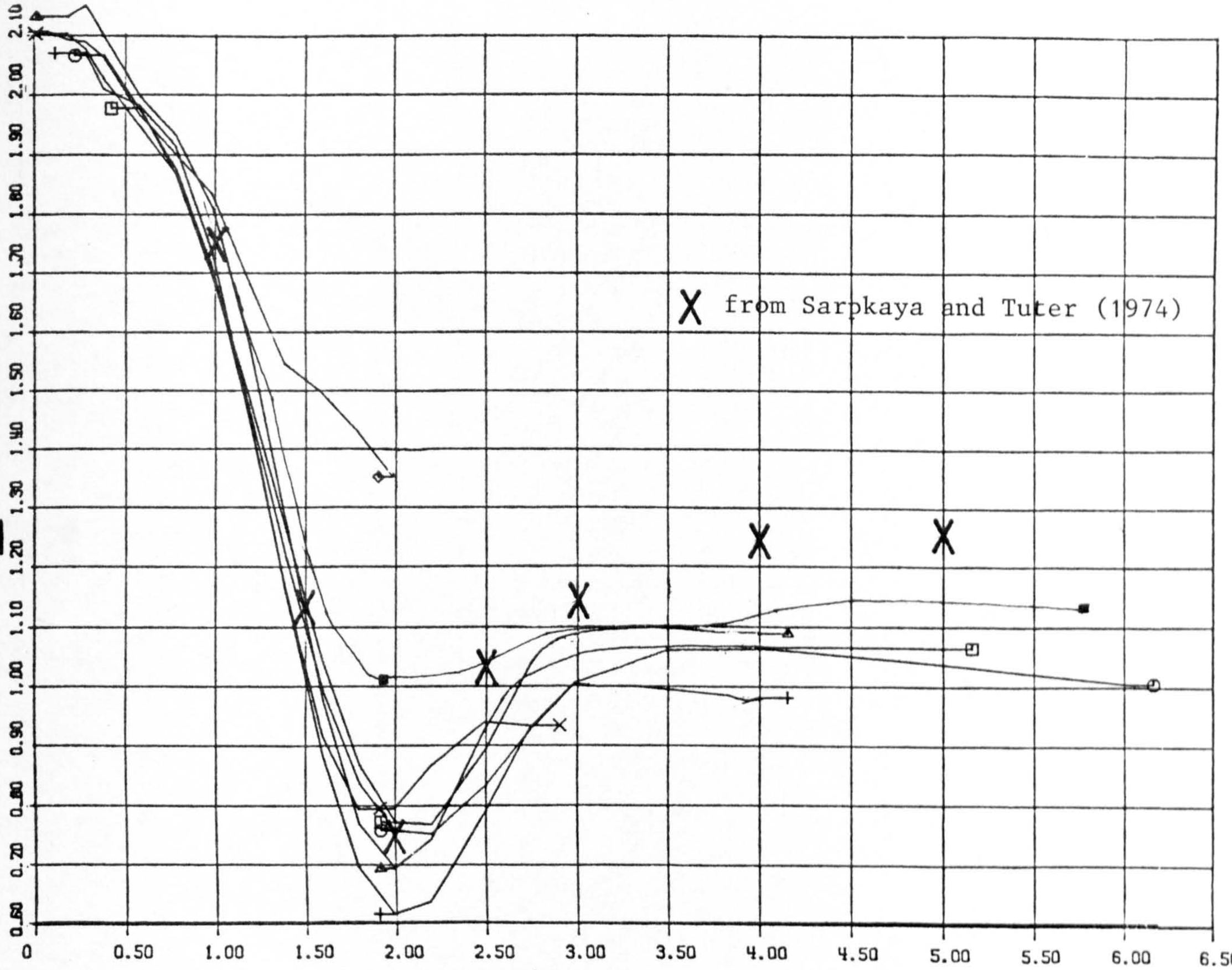

SYMB	RUN	DIA	VEL	V/nD	β
□	21.	.0202	0	0	194
○	22.	.0252	0	0	302
△	23.	.0320	0	0	487
+	24.	.0350	0	0	583
×	25.	.0502	0	0	1200
◇	26.	.0701	0	0	2360
■	127.	.01275	0	0	77

Fig. 77. Inertia coefficient in still water for various β obtained with the low frequency rig.

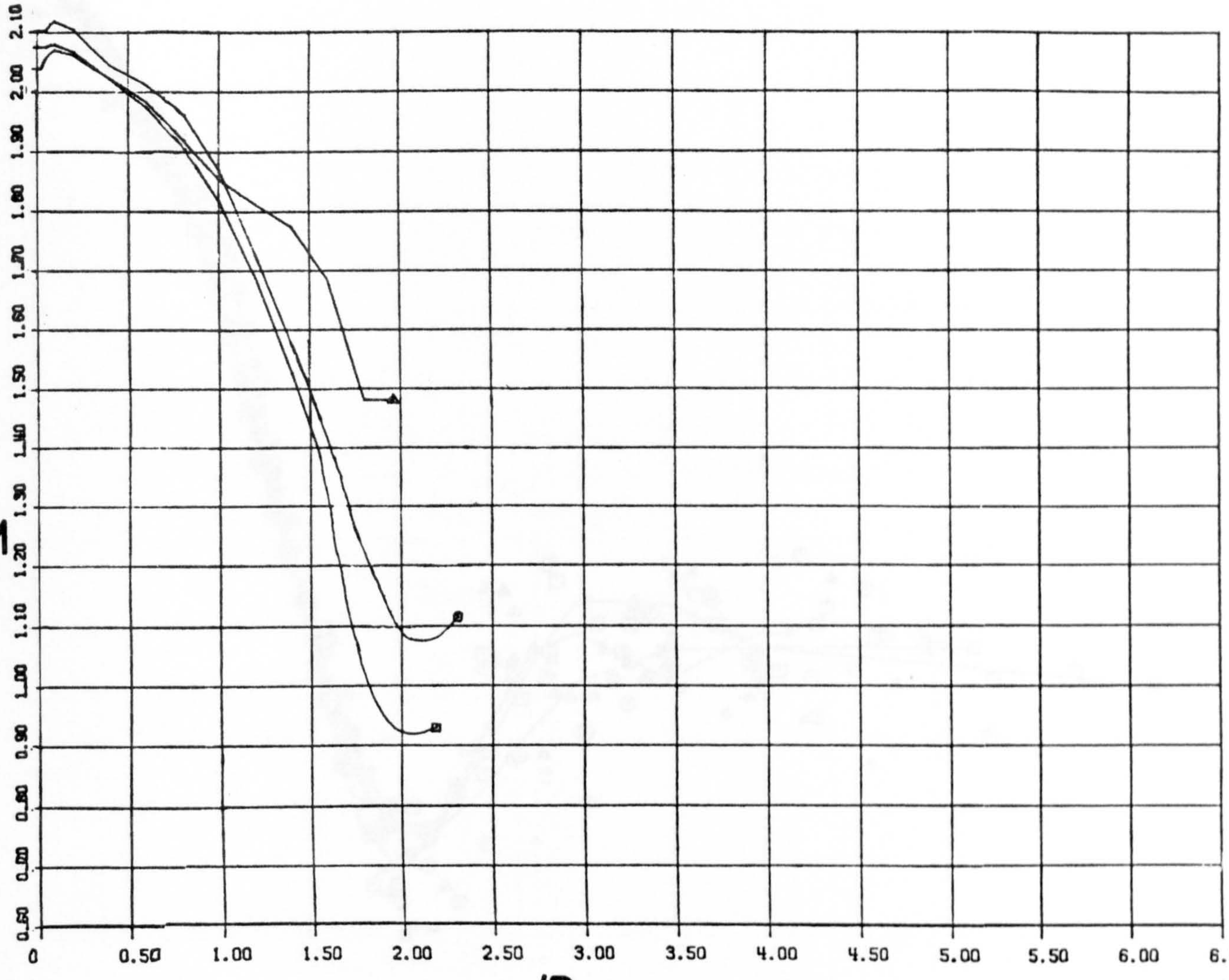

Fig. 78. Inertia coefficient in still water for various β obtained with the high frequency rig.

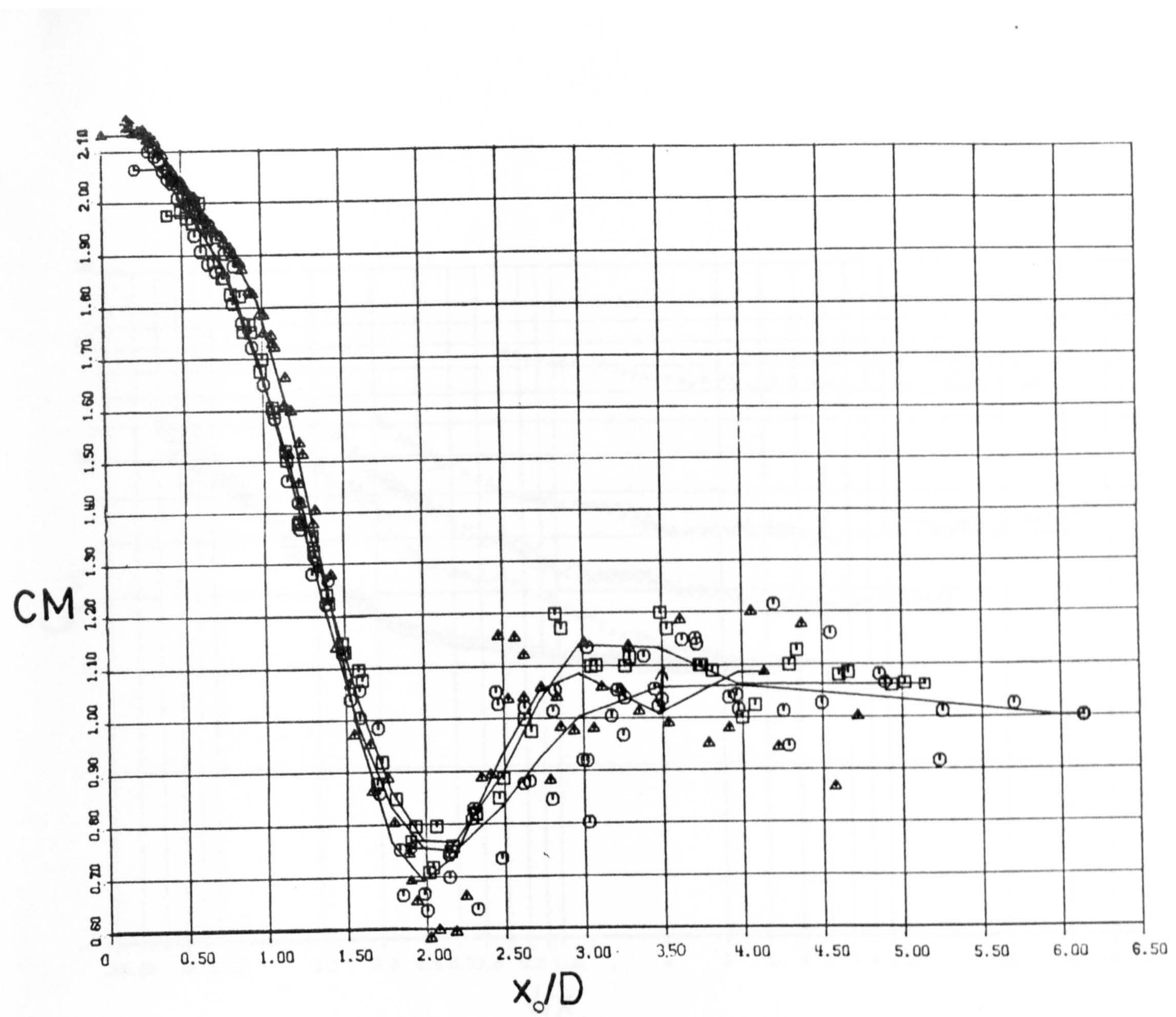

Fig. 79. Example actual points for inertia coefficient in still water.

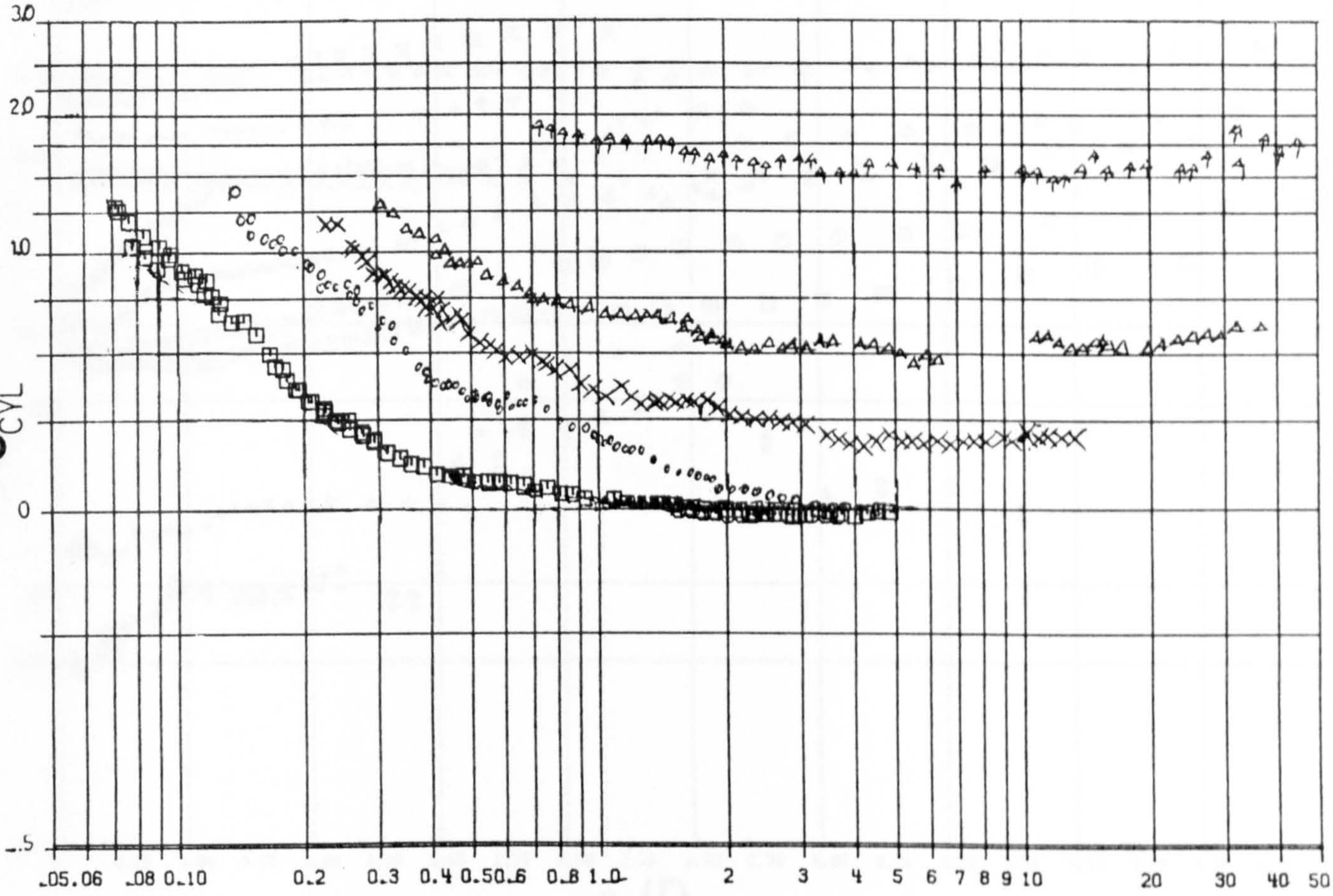

SYMB	RUN	DIA	VEL	V/nD
□	201.	.0202	.039	1.87
○	241.	.0202	.081	2.86
X	251.	.0202	.128	4.52
△	34.	.0350	.128	7.69
†	44.	.0350	.228	17.29

Fig. 80. Damping due to the cylinder in various currents.

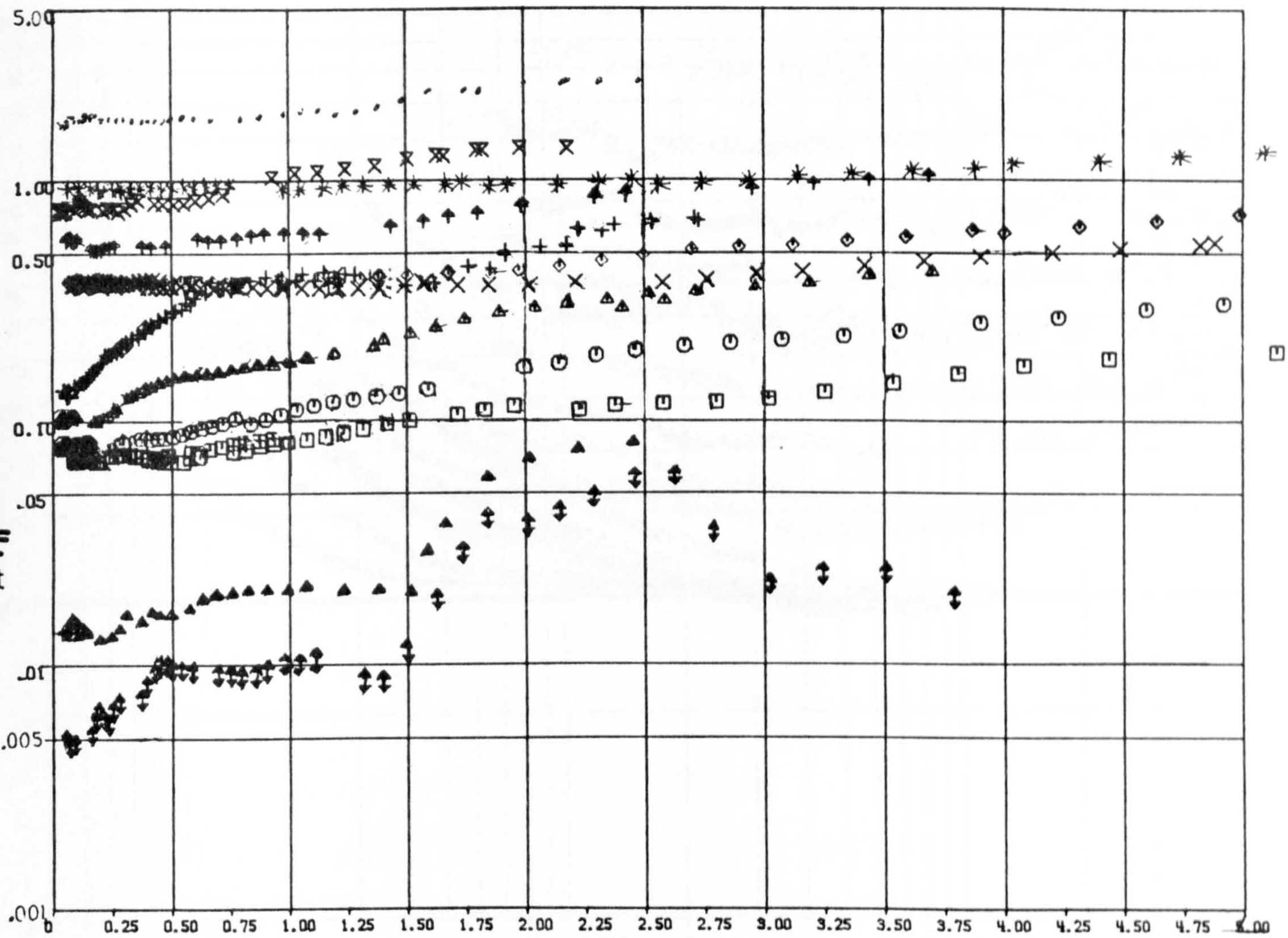

SYMB	RUN	DIA	VEL	V/nD
□	31.	.0202	0.128	13.31
⊙	32.	.0252	0.128	10.67
▲	34.	.0350	0.128	7.69
+	35.	.0502	0.128	5.37
×	41.	.0202	0.288	29.93
◆	42.	.0252	0.288	24.00
✦	44.	.0350	0.288	17.29
⧖	45.	.0502	0.288	12.09

SYMB	RUN	DIA	VEL	V/nD
✱	52.	.0252	0.445	37.10
•	55.	.0502	0.445	18.60
▲	104.	.0350	.039	2.34
↕	134.	.0350	.028	1.68

Fig. 81. Average force on the rig with various cylinders attached in various currents.

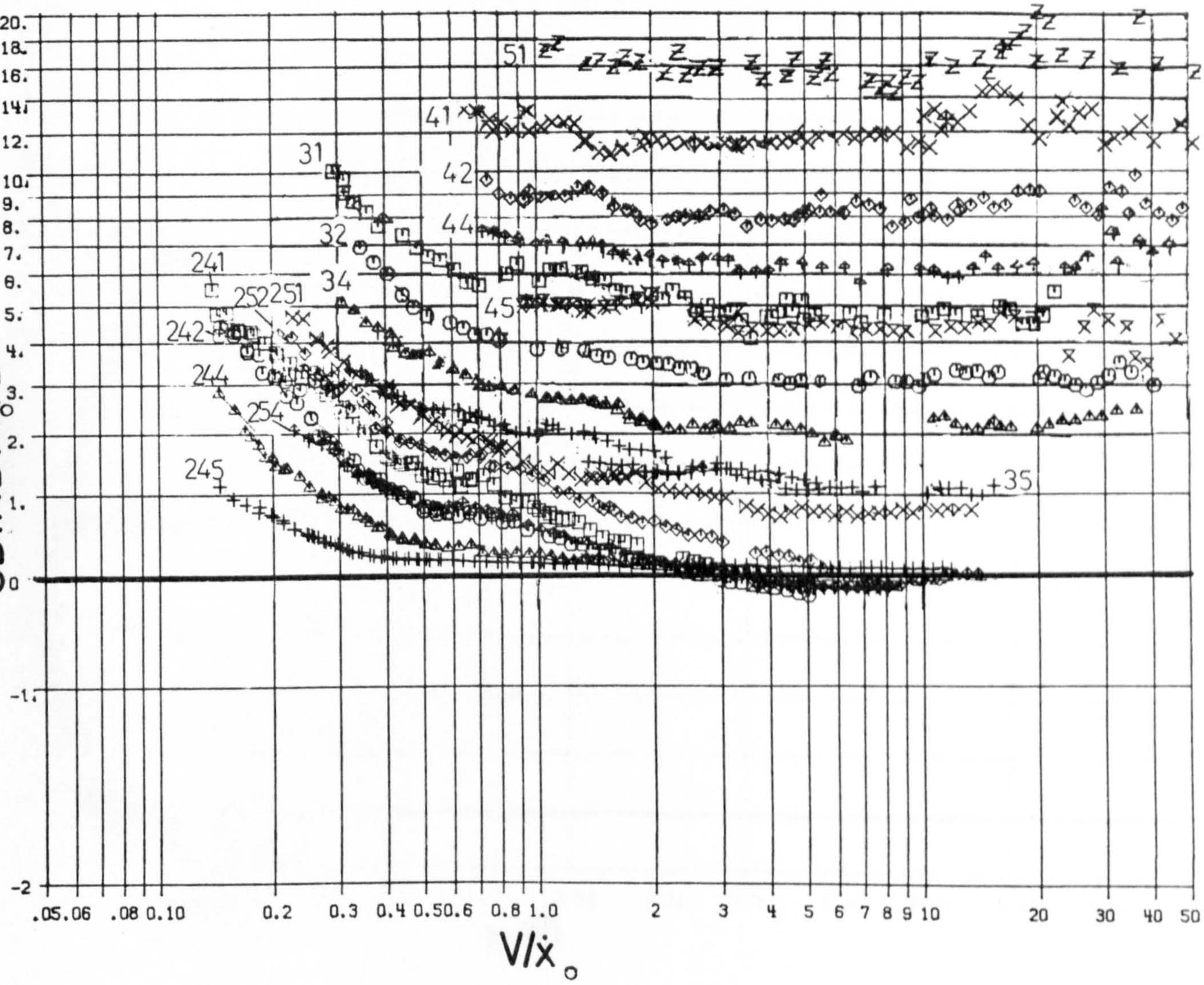

SYMB	RUN	DIA	VEL	V/nD
□	241.	.0202	.081	2.86
○	242.	.0252	.081	2.29
△	244.	.0350	.081	1.66
+	245.	.0502	.081	1.16
×	251.	.0202	0.128	4.52
◇	252.	.0252	0.128	3.63
▽	254.	.0350	0.128	2.62
⊡	31.	.0202	0.128	13.31
●	32.	.0252	0.128	10.67
▲	34.	.0350	0.128	7.69
+	35.	.0502	0.128	5.37
×	41.	.0202	0.288	29.93
◆	42.	.0252	0.288	24.00
▼	44.	.0350	0.288	17.29
⊠	45.	.0502	0.288	12.09
Z	51	.0202	0.445	46.26

Fig. 82. CDIND. x_o/D versus $V/\dot{x}_o$ for various cylinders in various currents, indicating the scatter in the oscillatory drag coefficient.

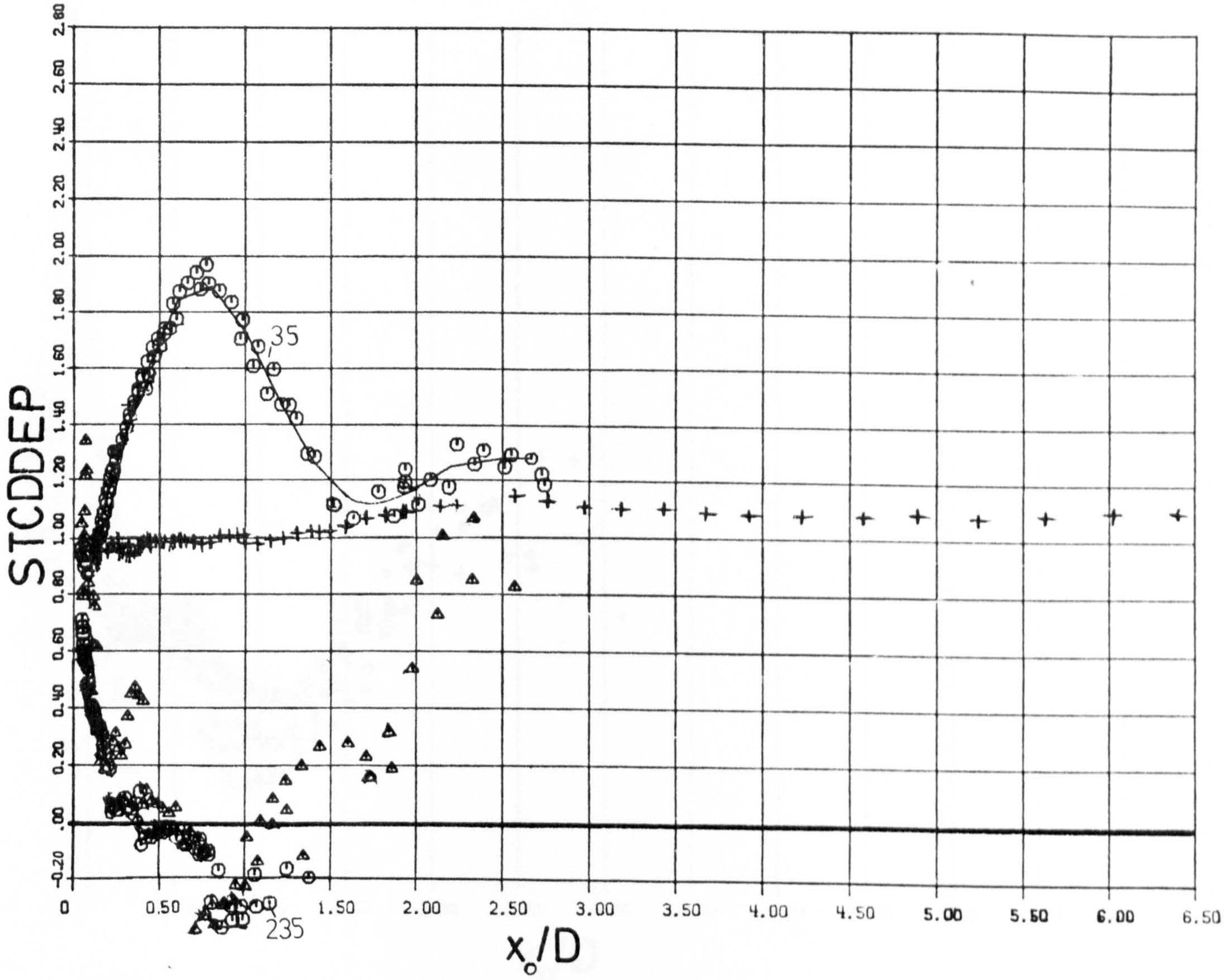

SYMB	RUN	DIA	VEL	V/nD
⊙	35.	.0502	0.128	5.37
+	71.	.0202	0.179	18.60
⊙	235.	.0502	.059	0.84
▲	212.	.0252	.028	0.78

Fig. 83. Example results for STCDDEP versus x_o/D.

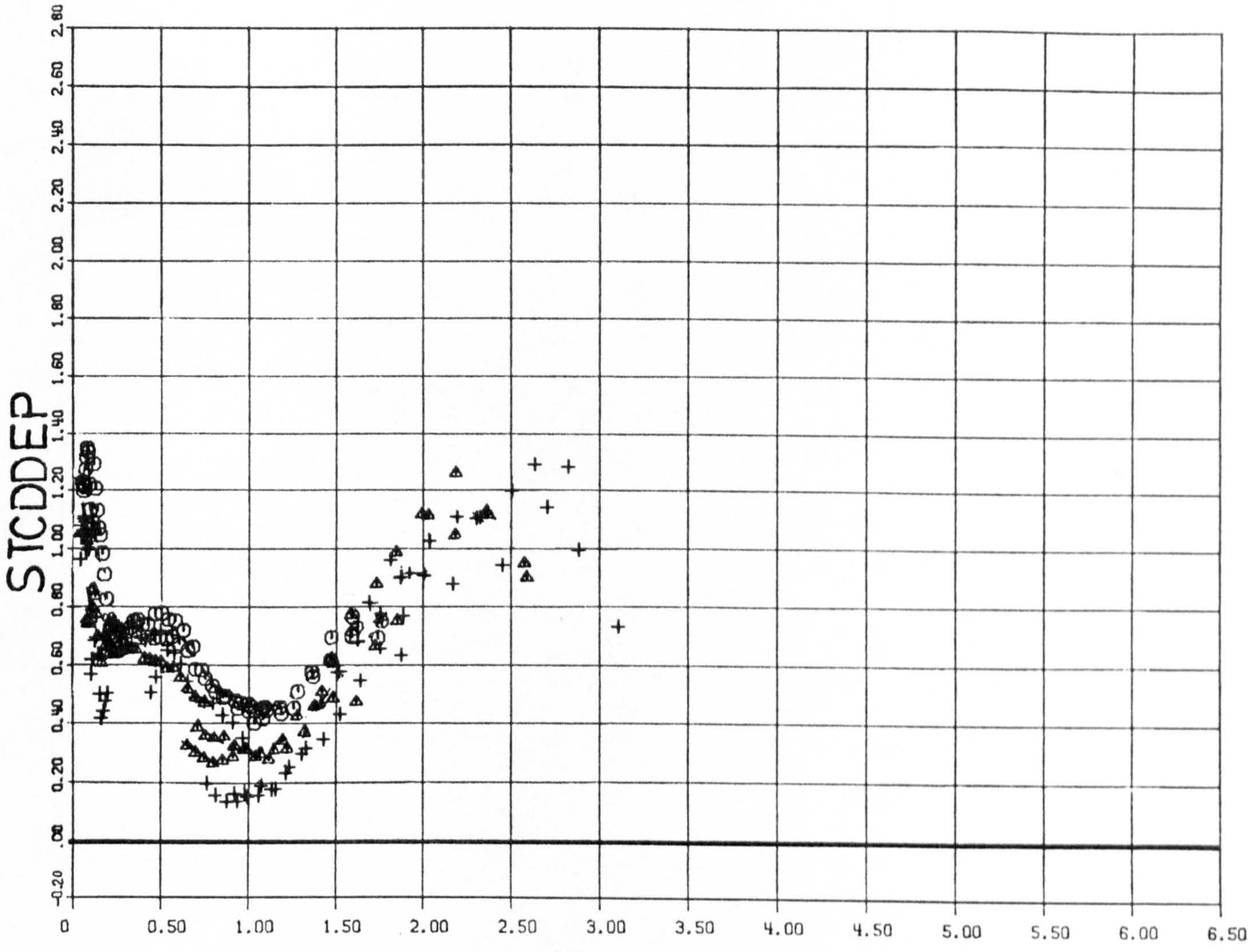

Fig. 84. Example results for STCDDEP versus x_o/D, small range of V/nD.

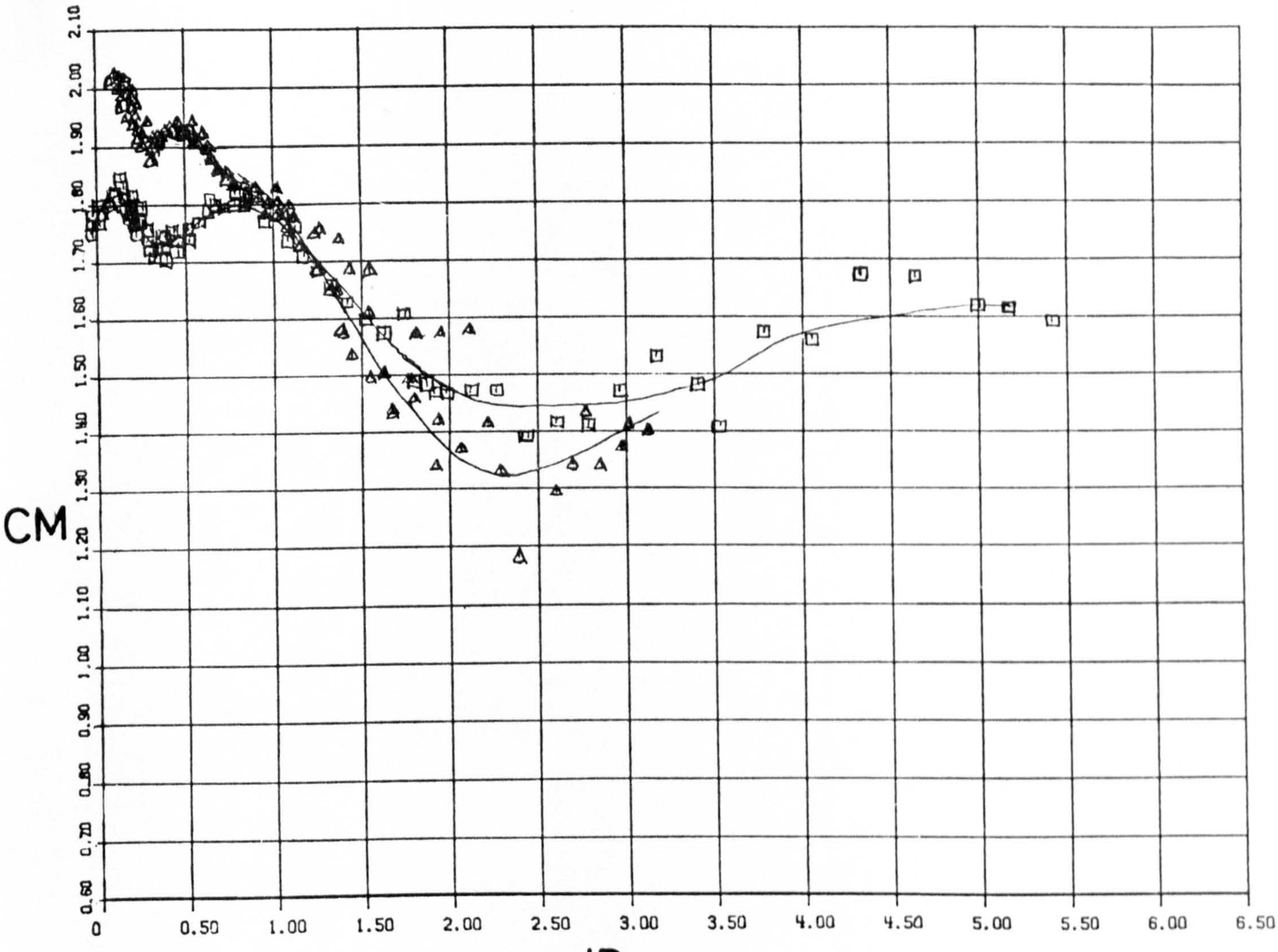

Fig. 85. Example results for CM versus x_o/D, at low V/nD.

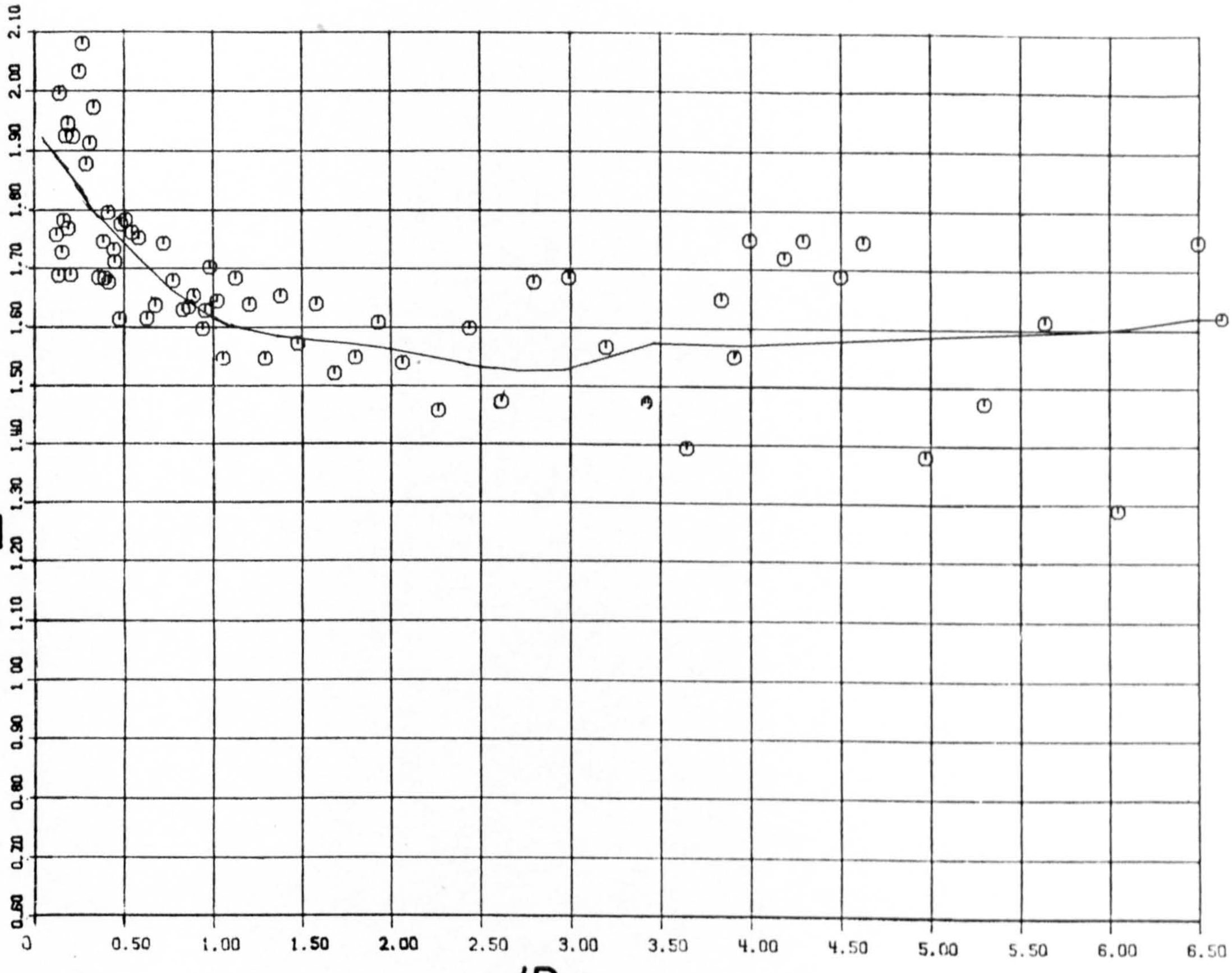

Fig. 86. Example results for CM versus x_o/D, higher V/nD.

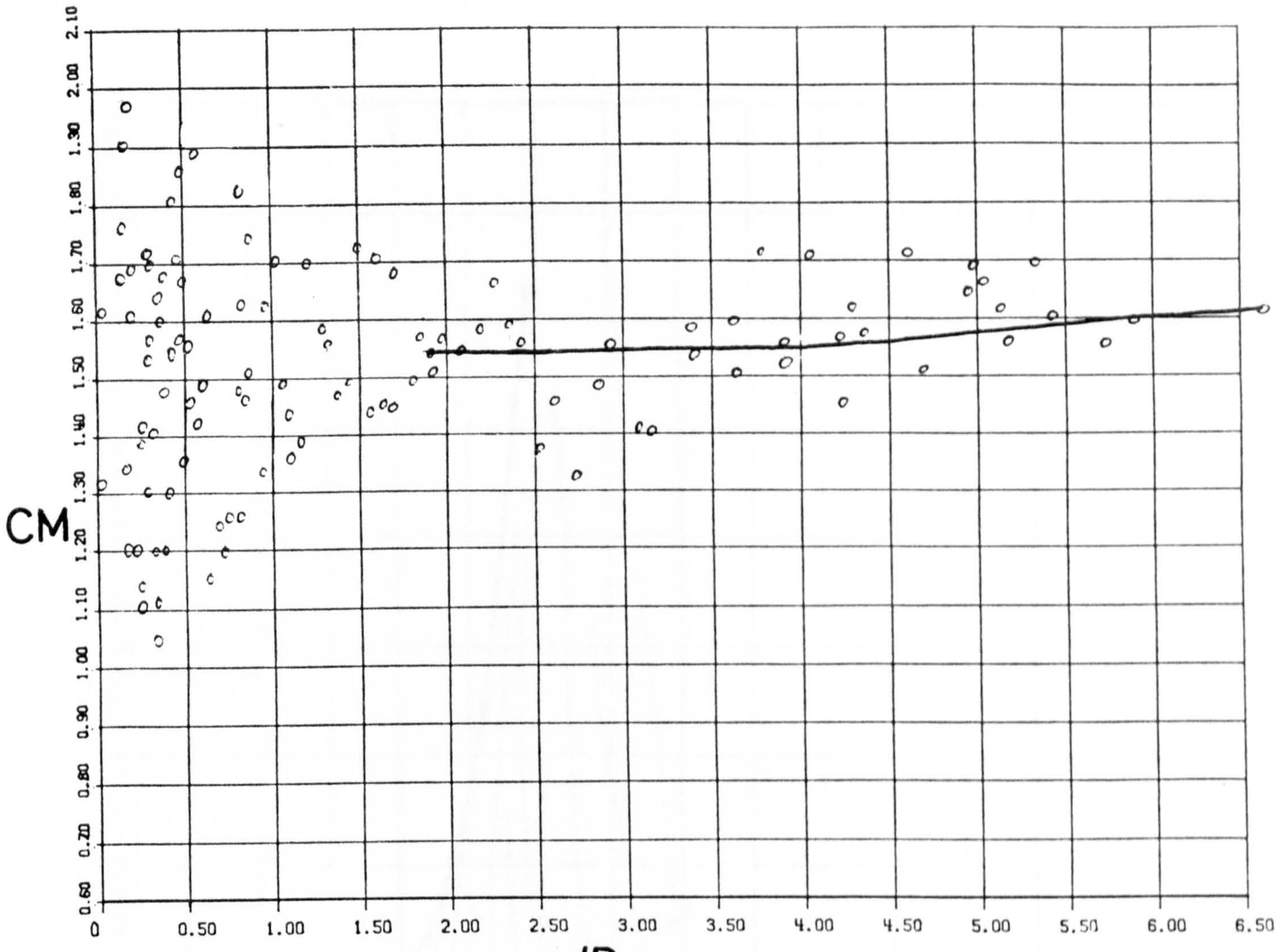

Fig. 87. Example results for CM versus x_o/D, very high V/nD.

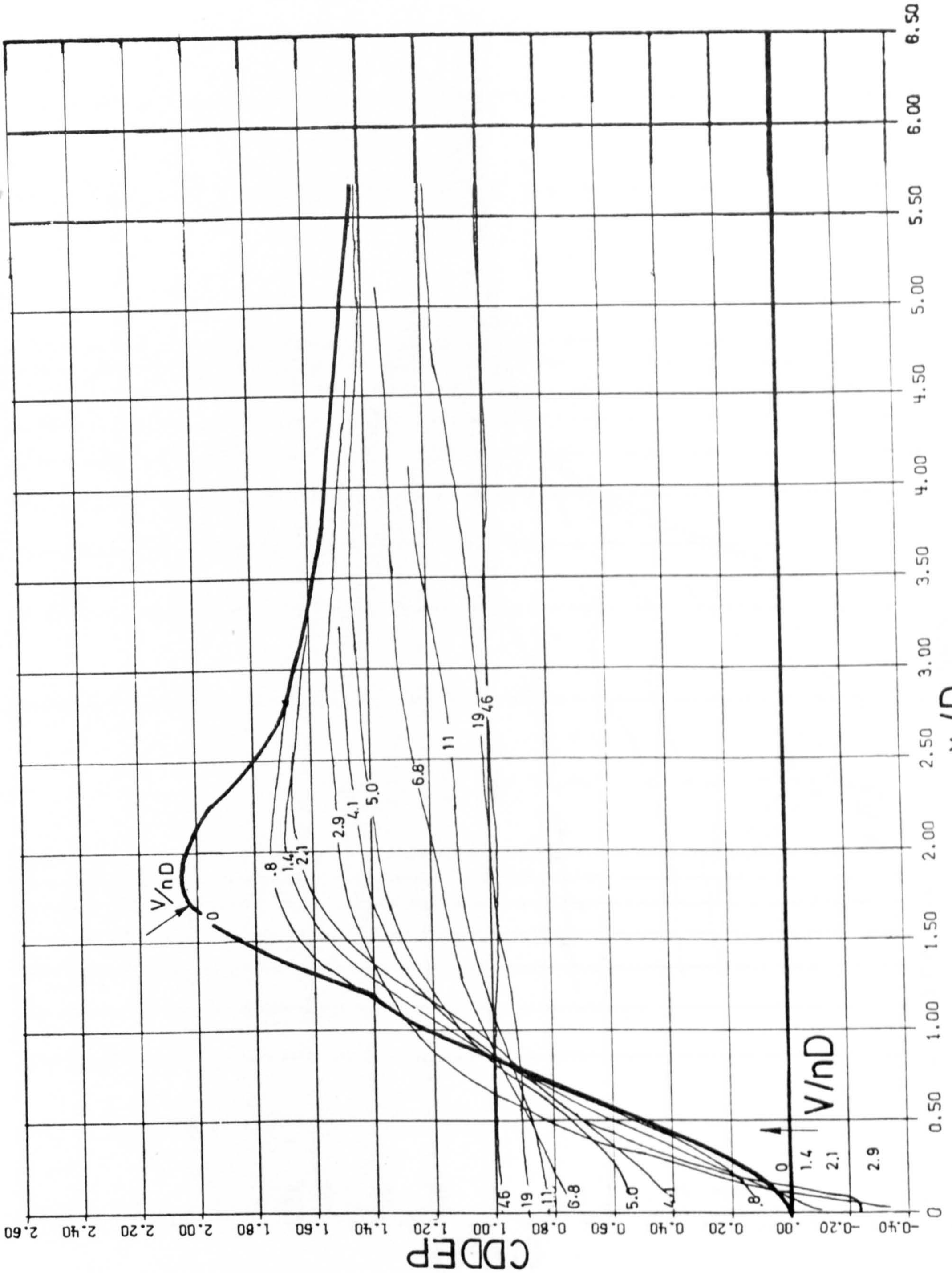

Fig. 88. Oscillatory drag coefficient, CDDEP versus x_o/D for various V/nD.

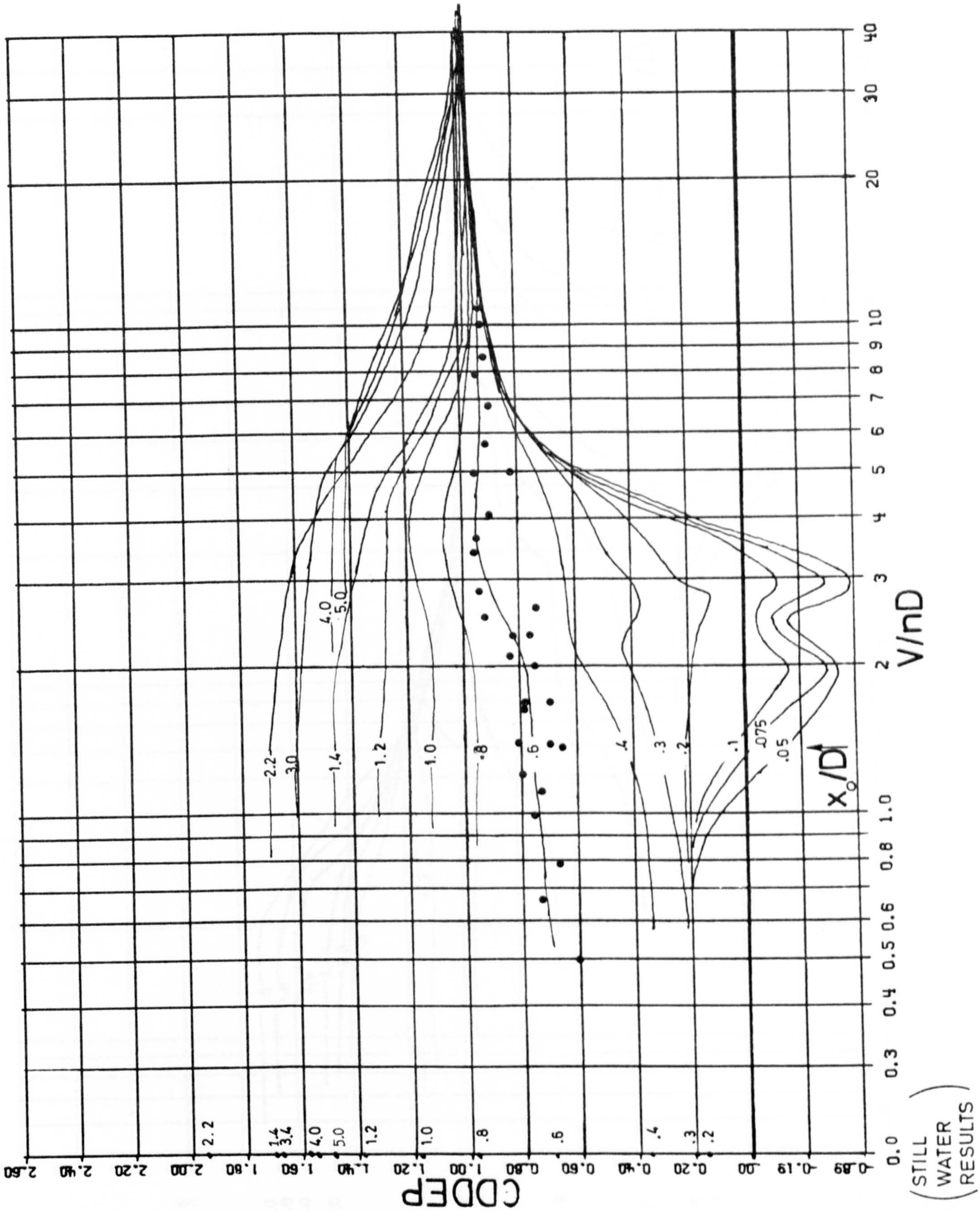

Fig. 89. Oscillatory drag coefficient, CDDEP versus V/nD for various x_o/D.

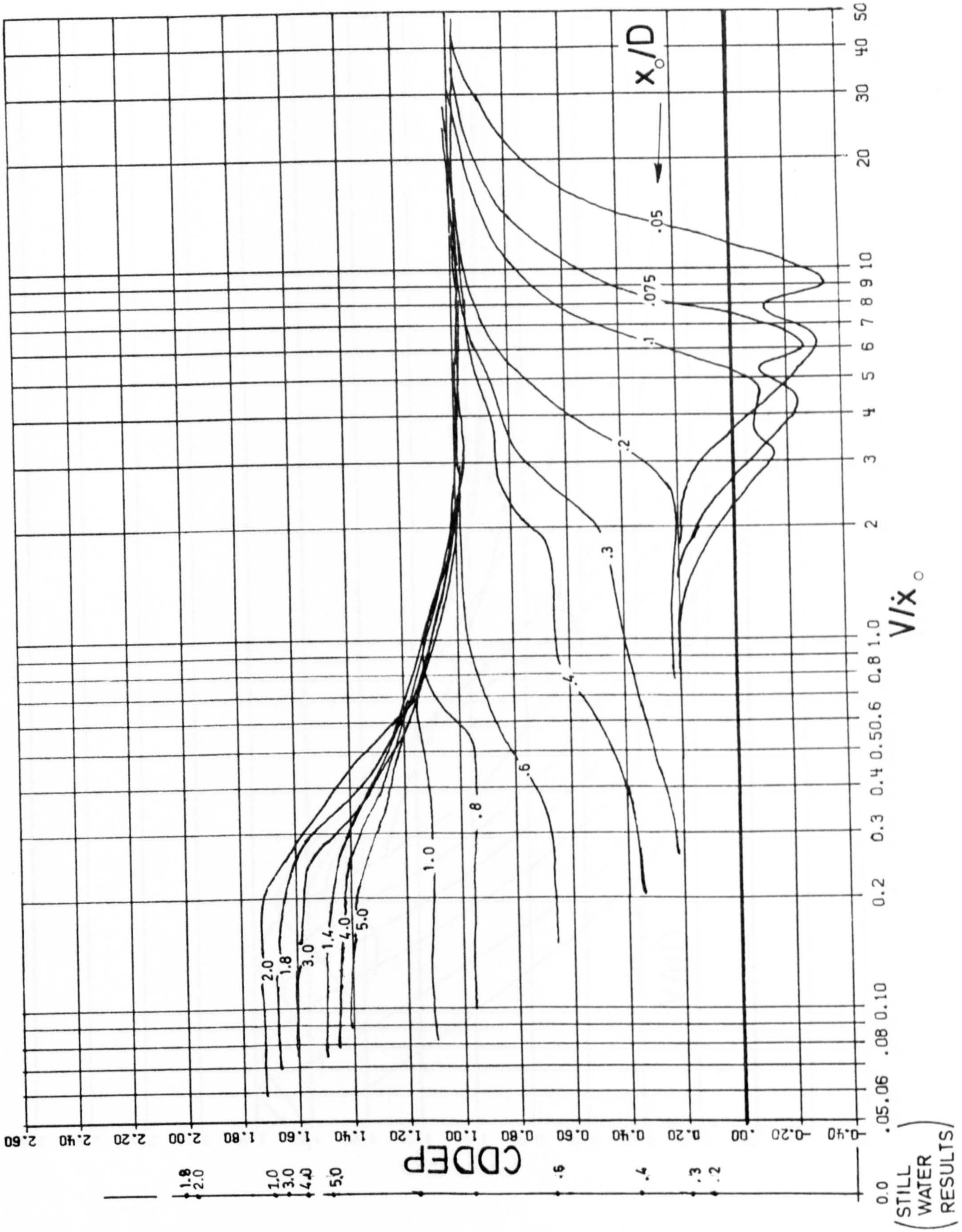

Fig. 90. Oscillatory drag coefficient, CDDEP versus $V/\dot{x}_o$ for various x_o/D.

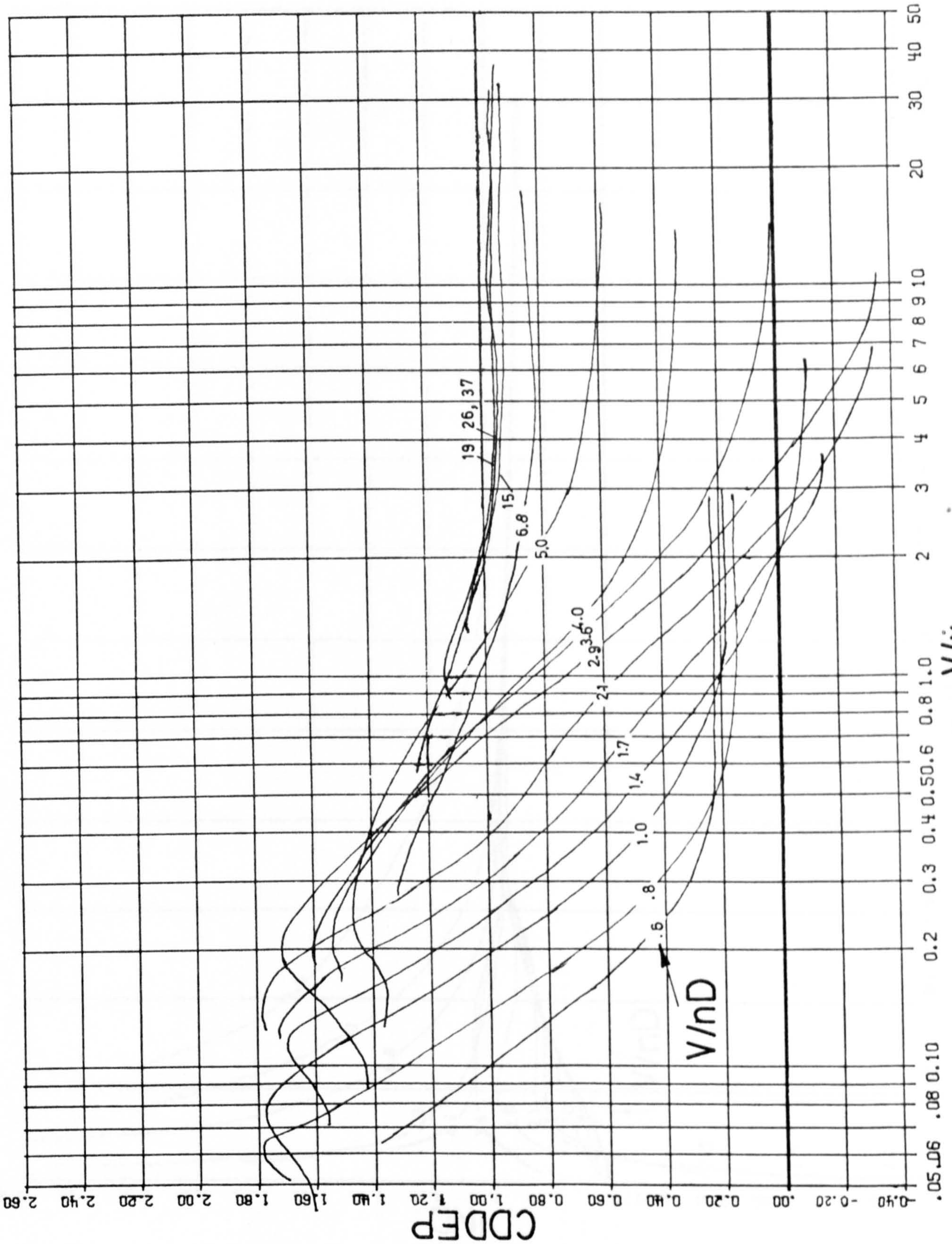

Fig. 91. Oscillatory drag coefficient, CDDEP versus $V/\dot{x}_o$ for various V/nD.

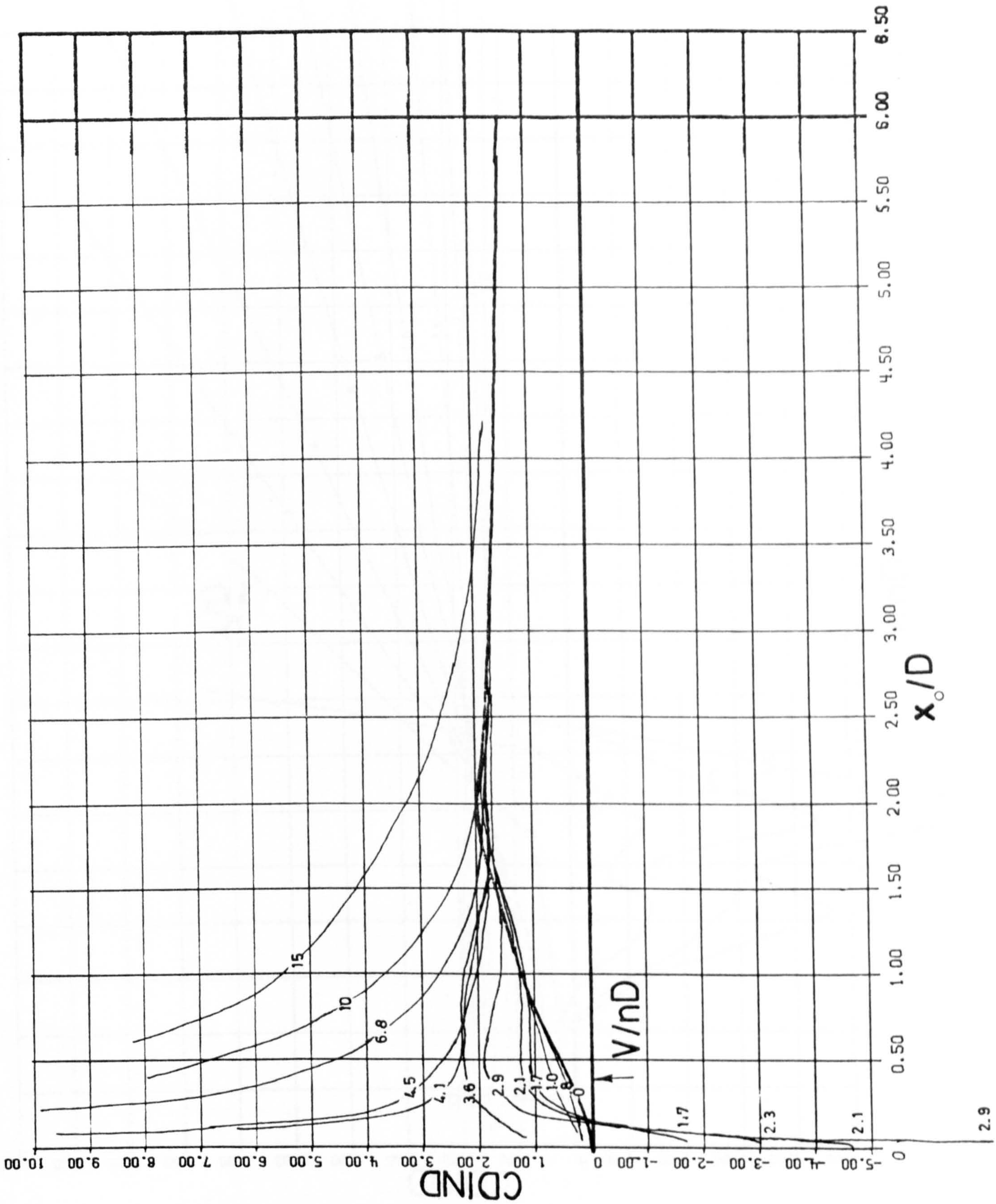

Fig. 92. Oscillatory drag coefficient, CDIND versus x_o/D for various V/nD.

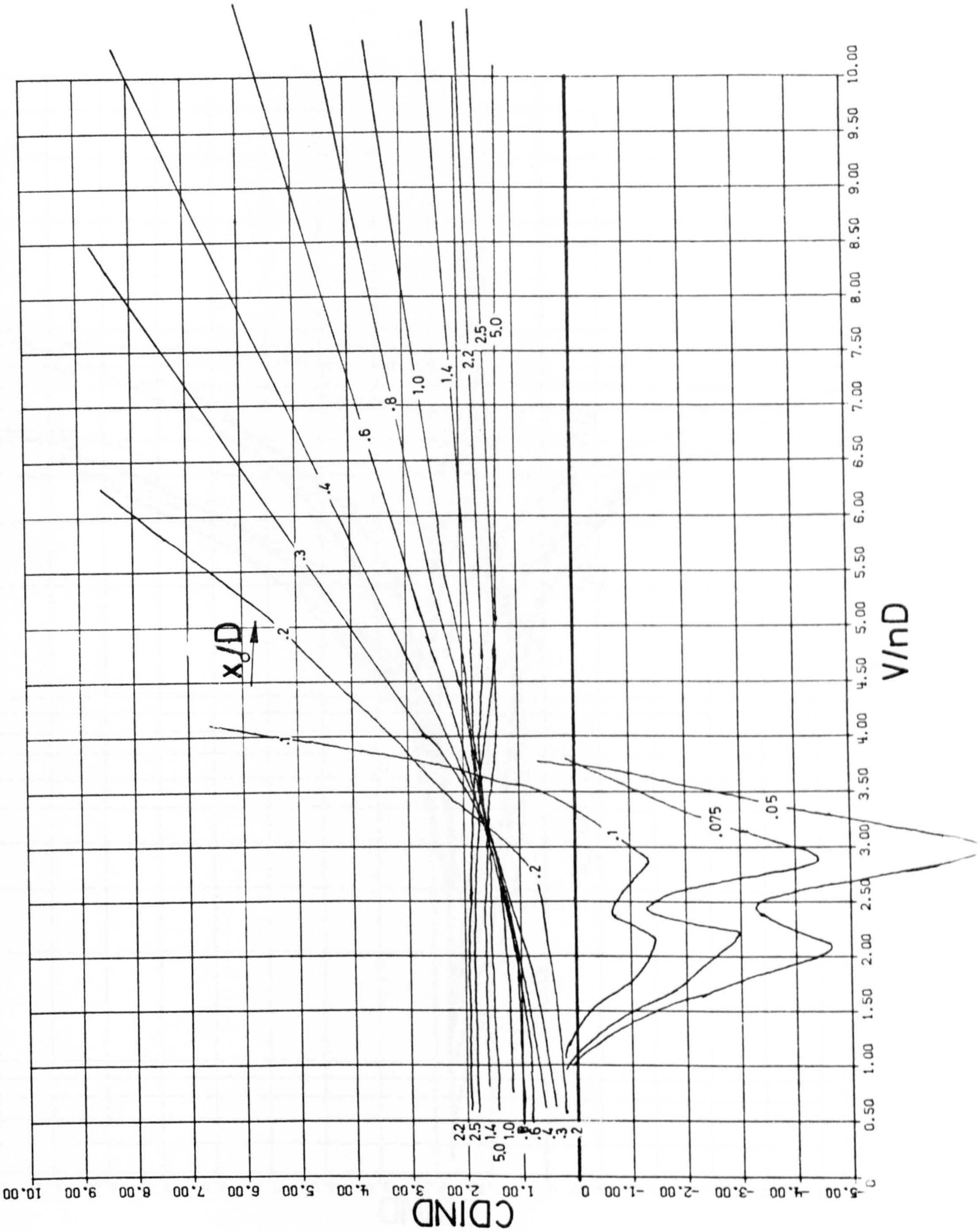

Fig. 93. Oscillatory drag coefficient, CDIND versus V/nD for various x_o/D.

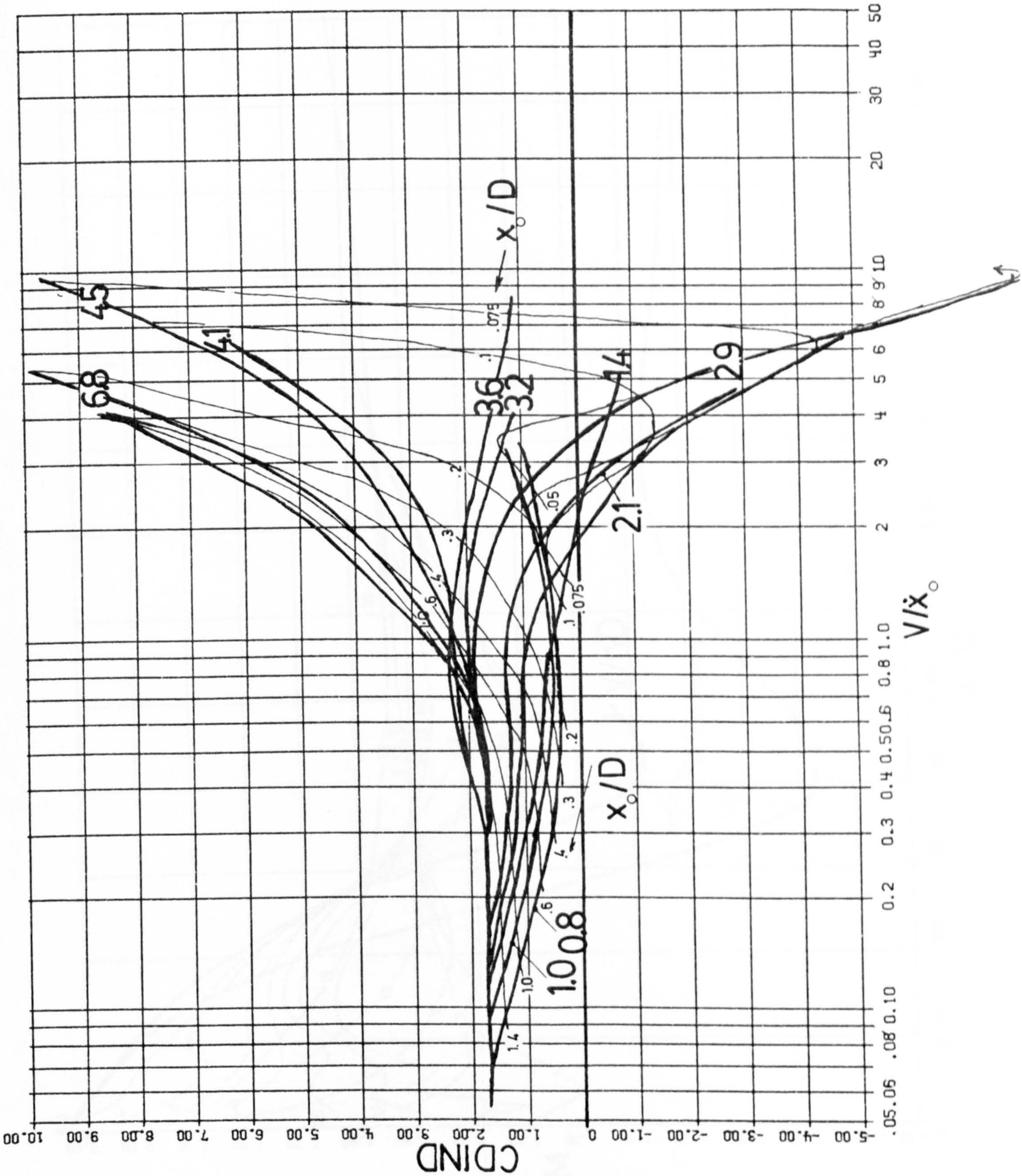

Fig. 94. Oscillatory drag coefficient, CDIND versus $V/\dot{x}_o$ for various x_o/D and V/nD. (Numbers in heavy type denote values of V/nD.)

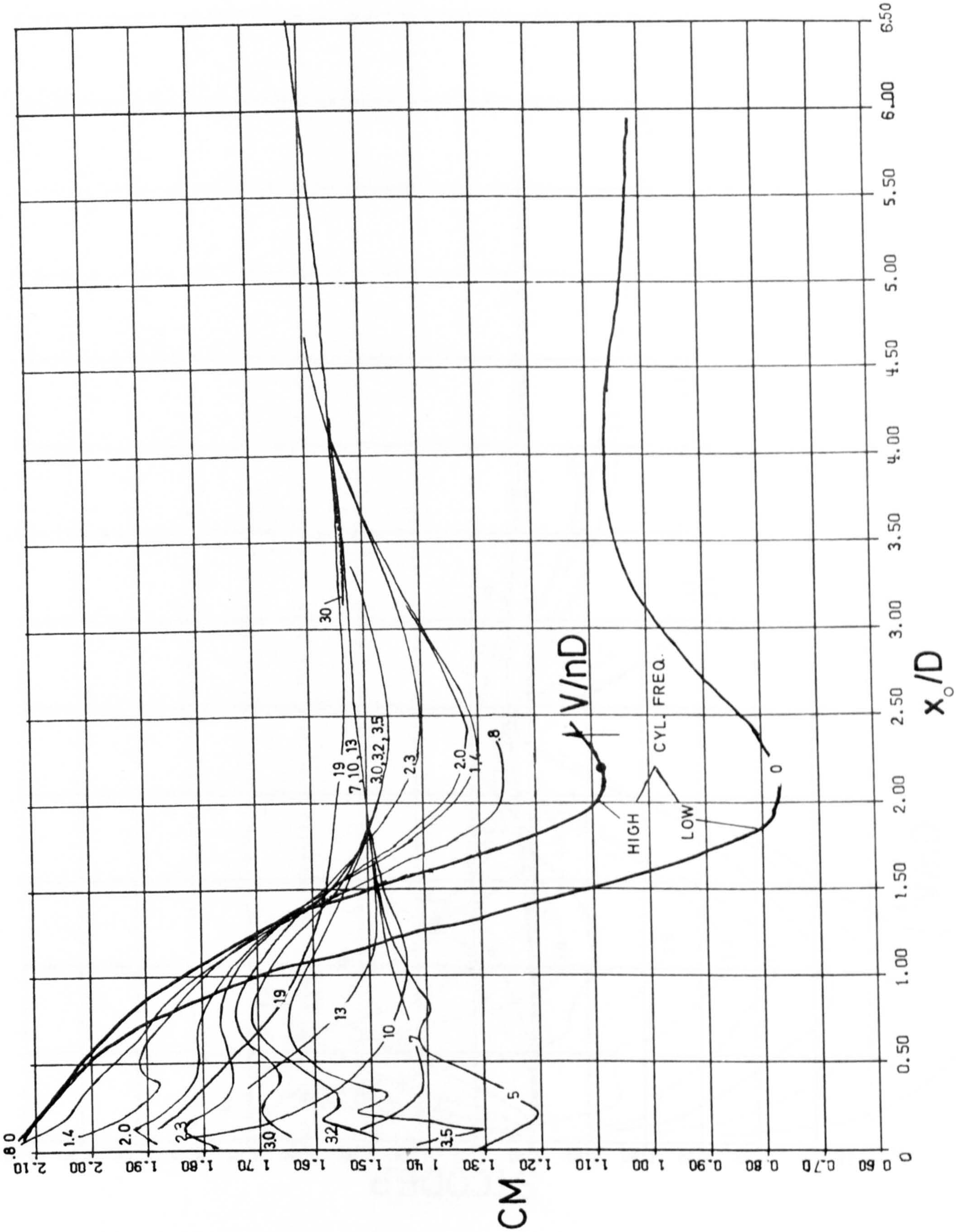

Fig. 95. Inertia coefficient CM versus x_o/D for various V/nD.

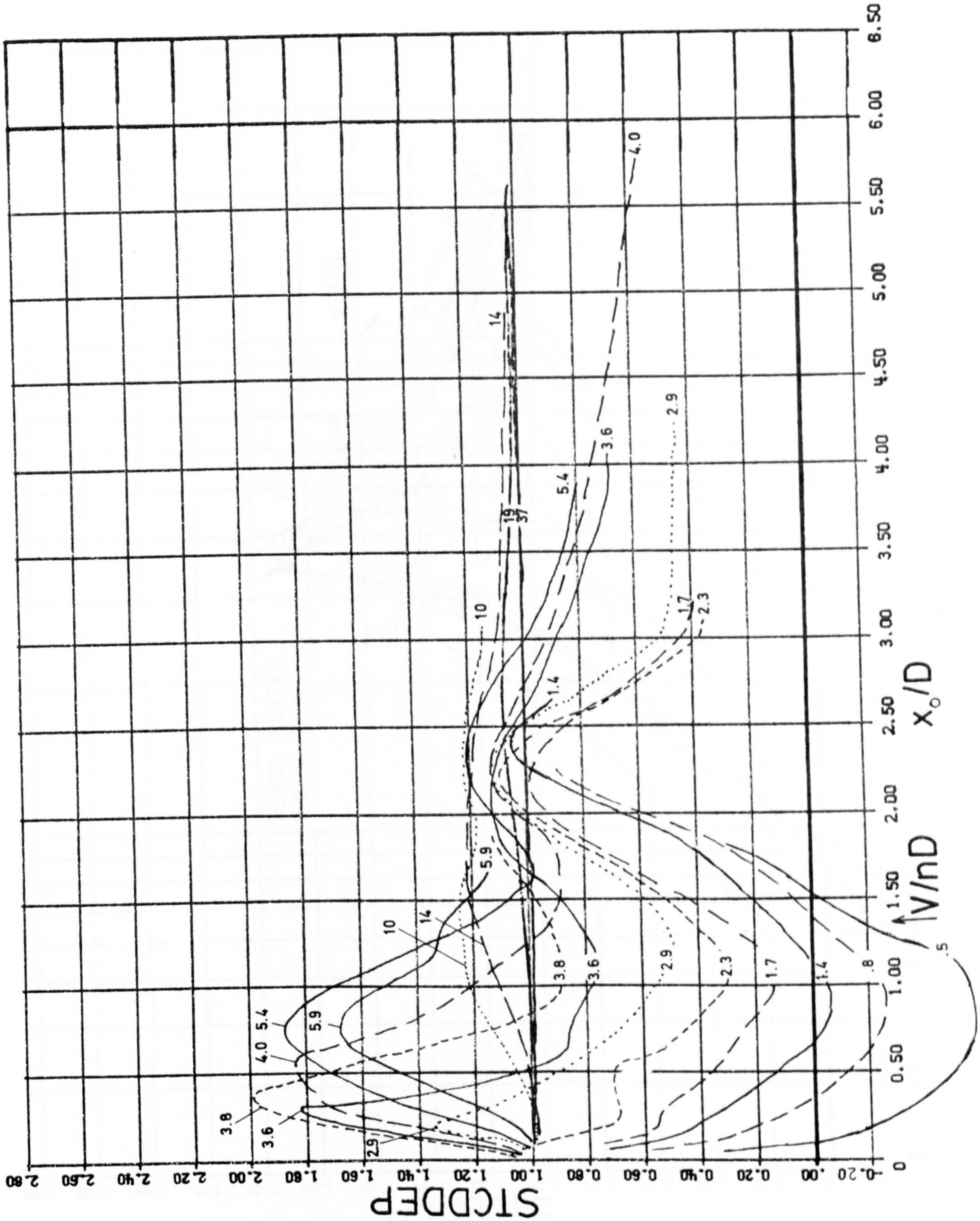

Fig. 96. Steady drag coefficient, STCDDEP versus x_o/D for various V/nD.

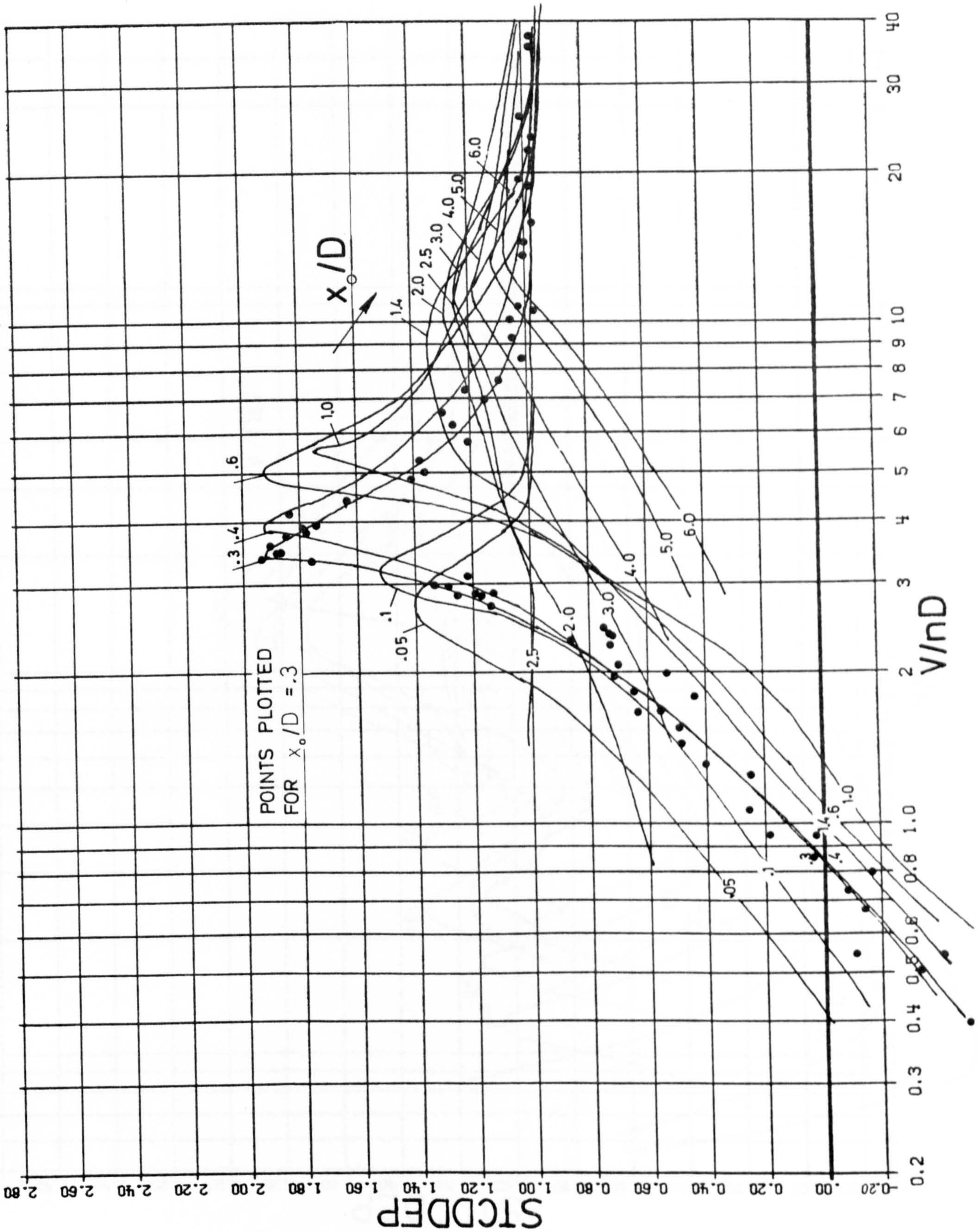

Fig. 97. Steady drag coefficient, STCDDEP versus V/nD for various x_o/D.

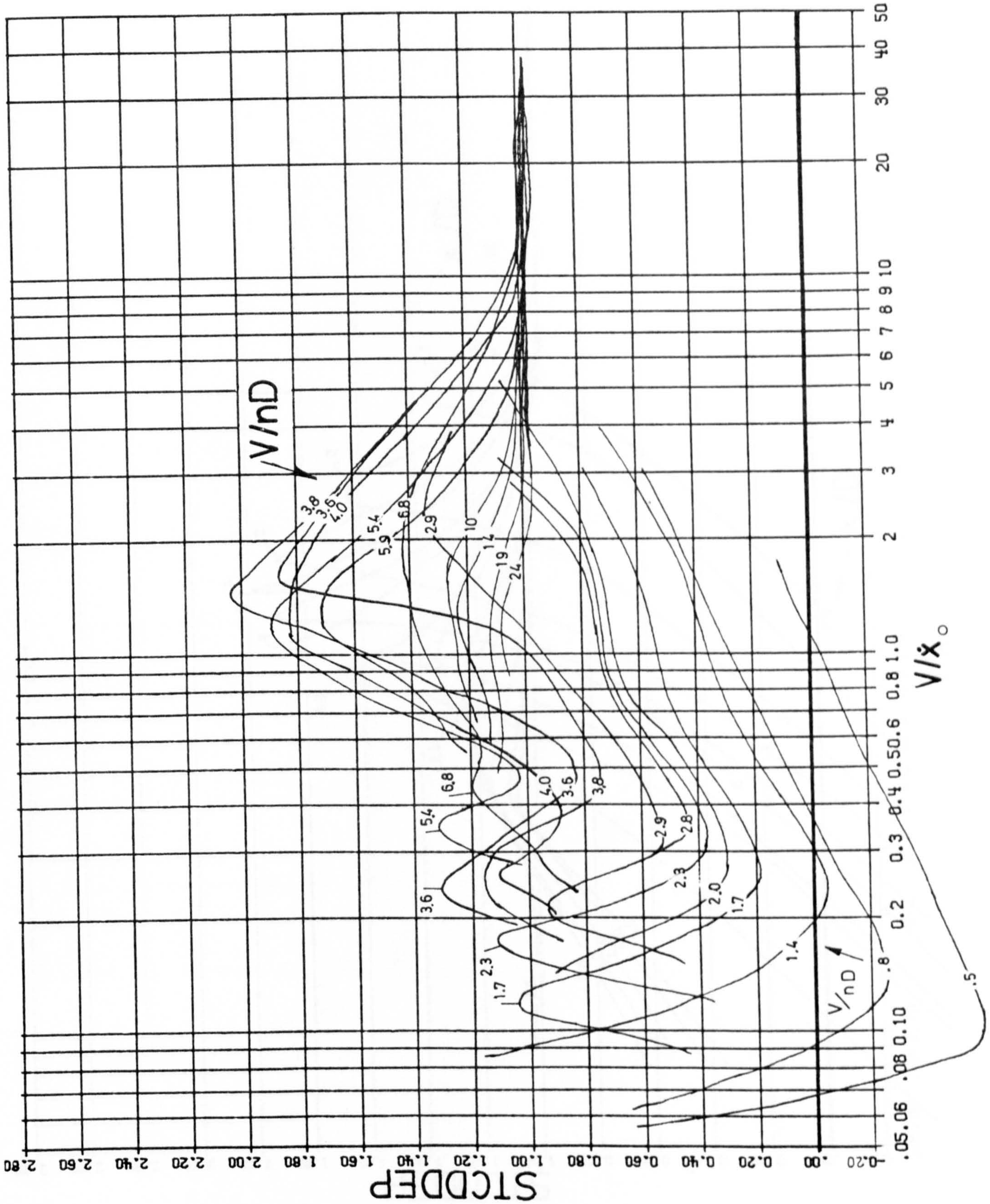

Fig. 98. Steady drag coefficient, STCDDEP versus $V/\dot{x}_o$ for various V/nD.

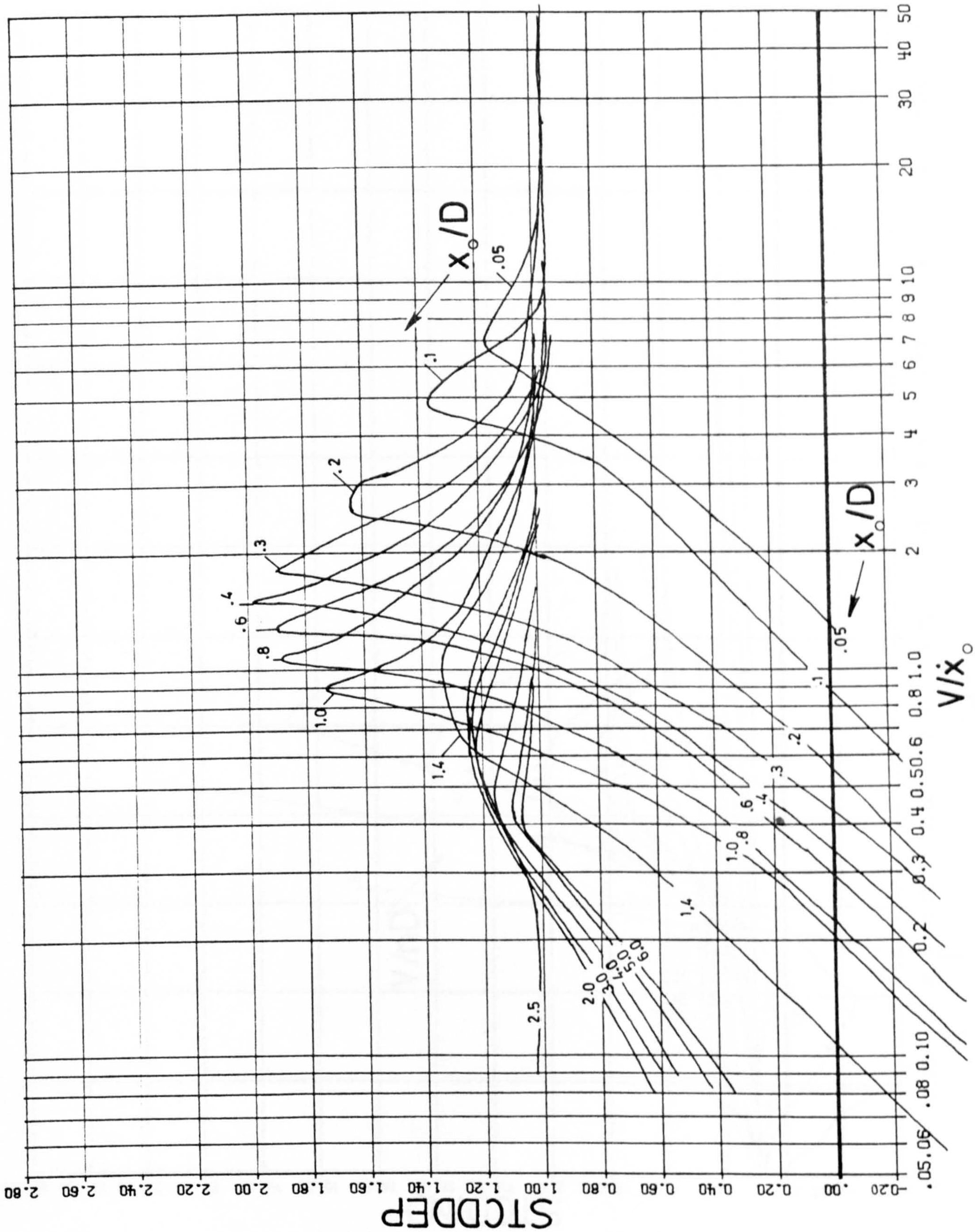

Fig. 99. Steady drag coefficient, STCDDEP versus $V/\dot{x}_o$ for various x_o/D.

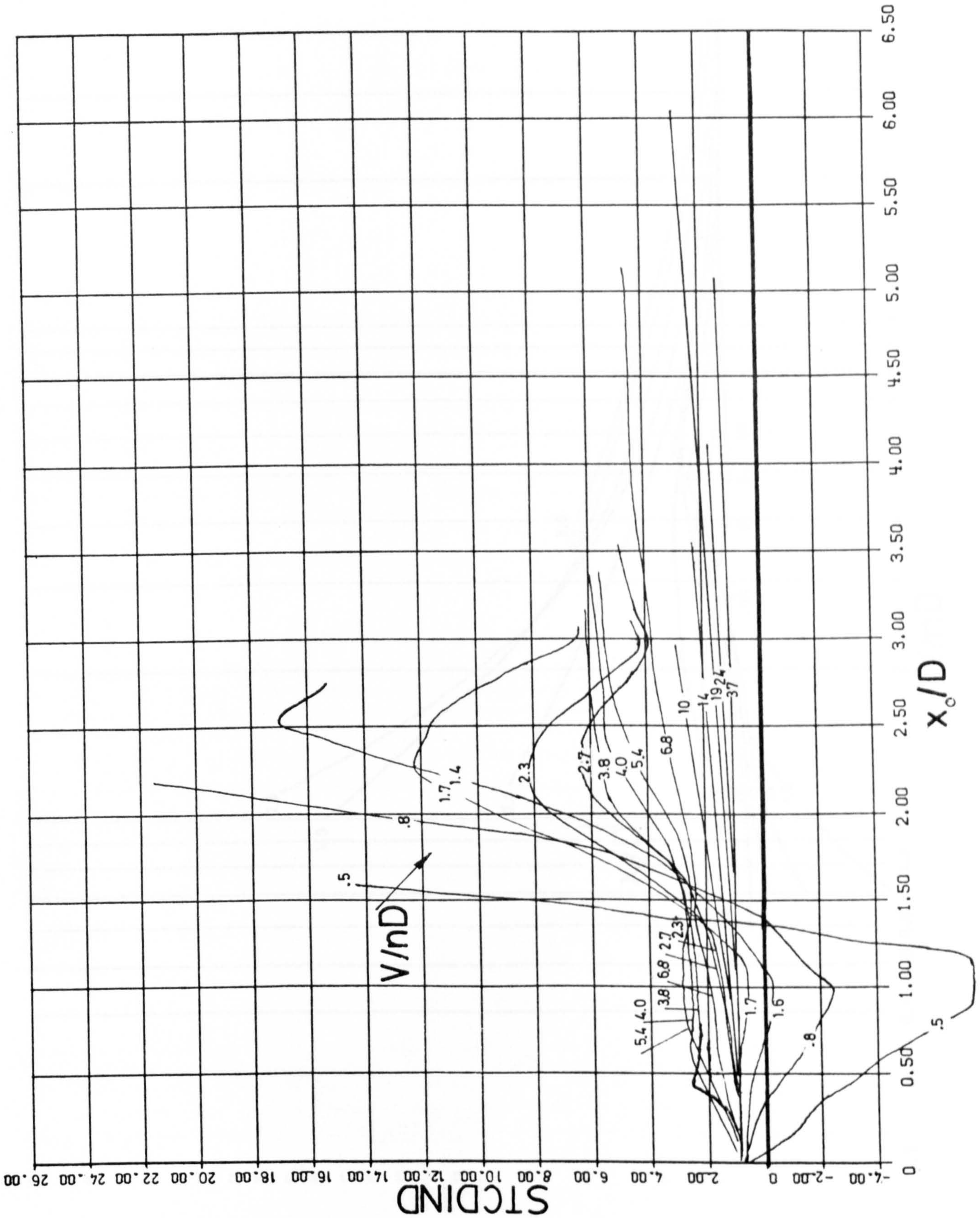

Fig. 100. Steady drag coefficient, STCDIND versus x_o/D for various V/nD.

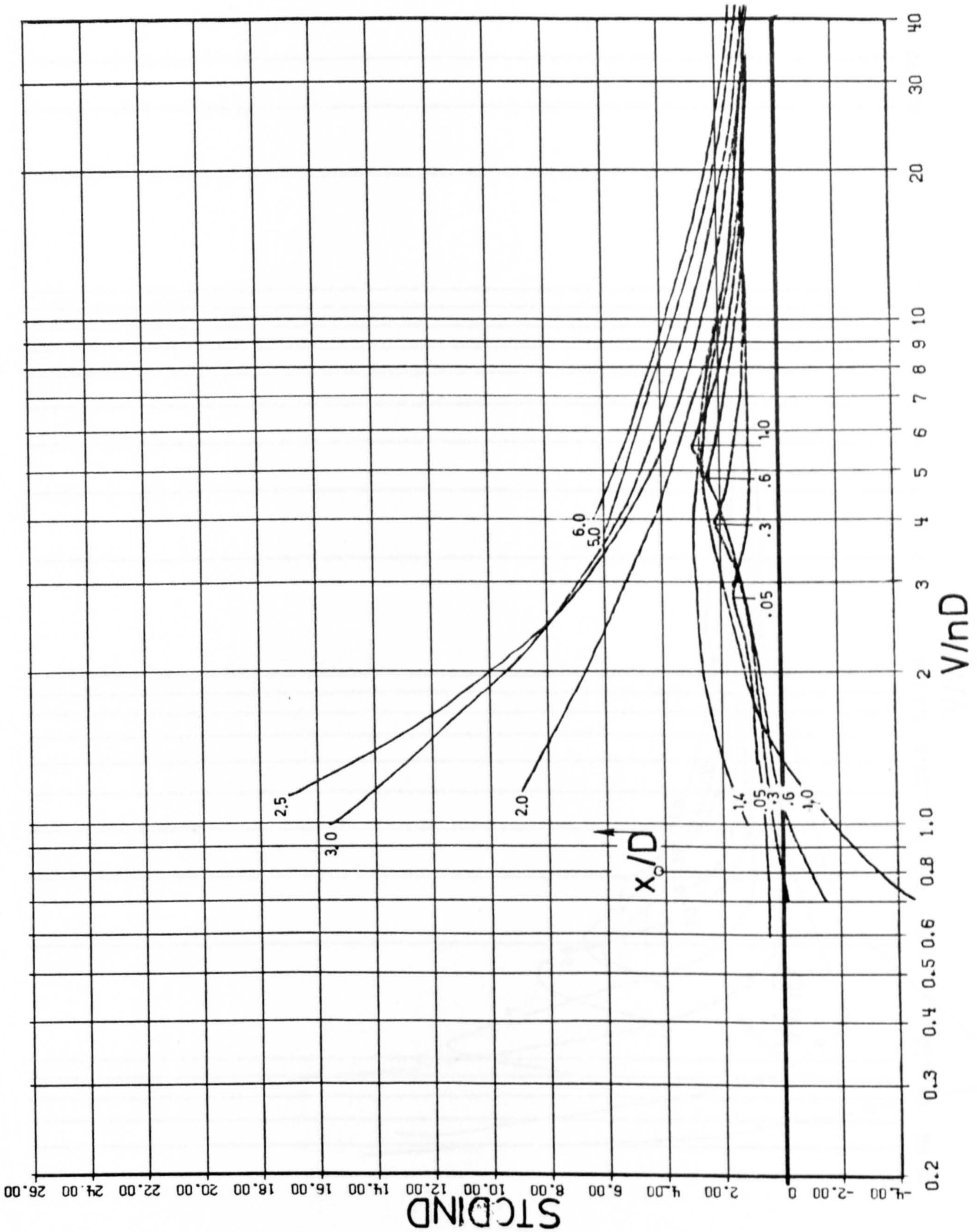

Fig. 101. Steady drag coefficient STCDIND versus V/nD for various x_o/D.

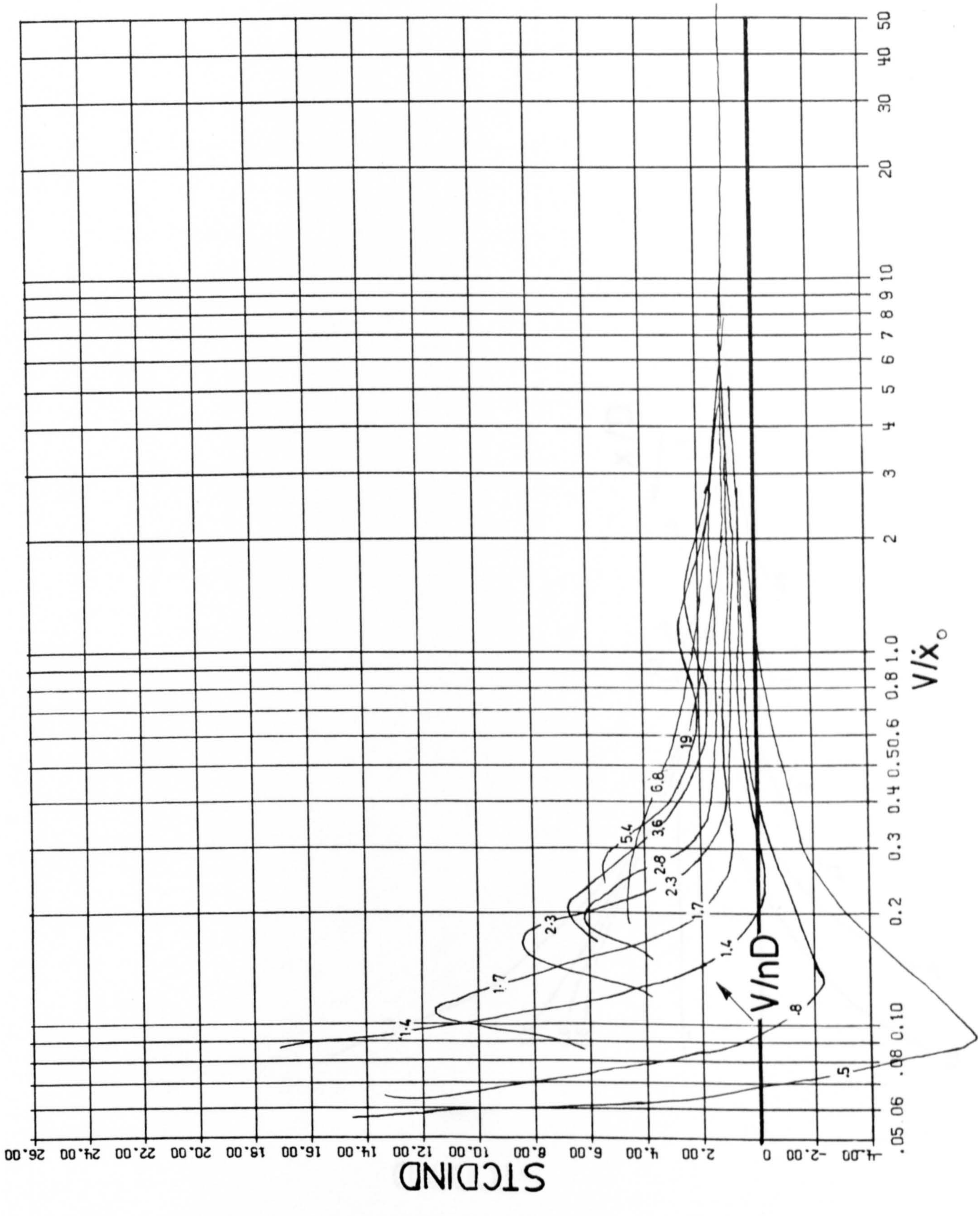

Fig. 102. Steady drag coefficient, STCDIND versus $V/\dot{x}_o$ for various V/nD.

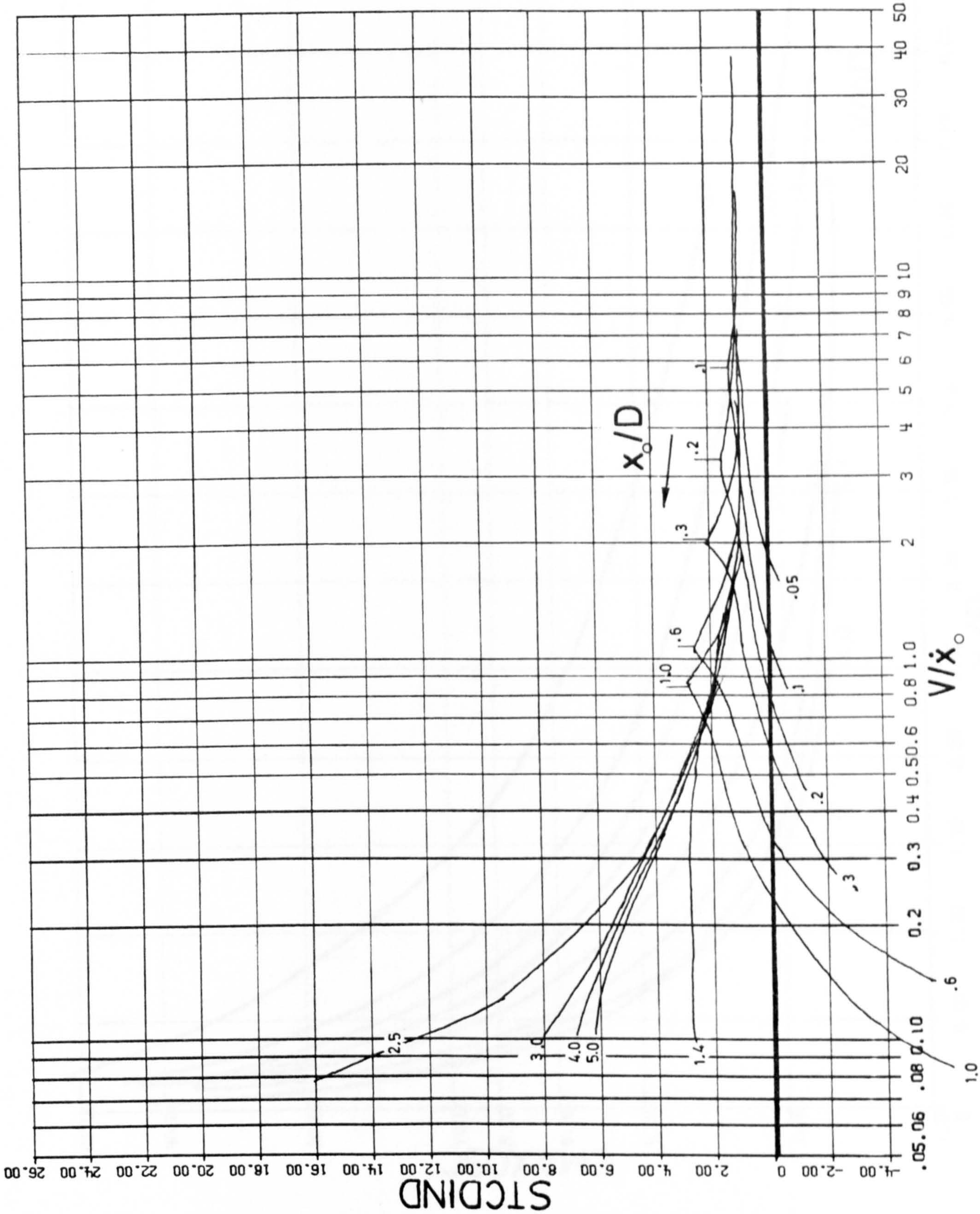

Fig. 103. Steady drag coefficient, STCDIND versus $V/\dot{x}_o$ for various x_o/D.

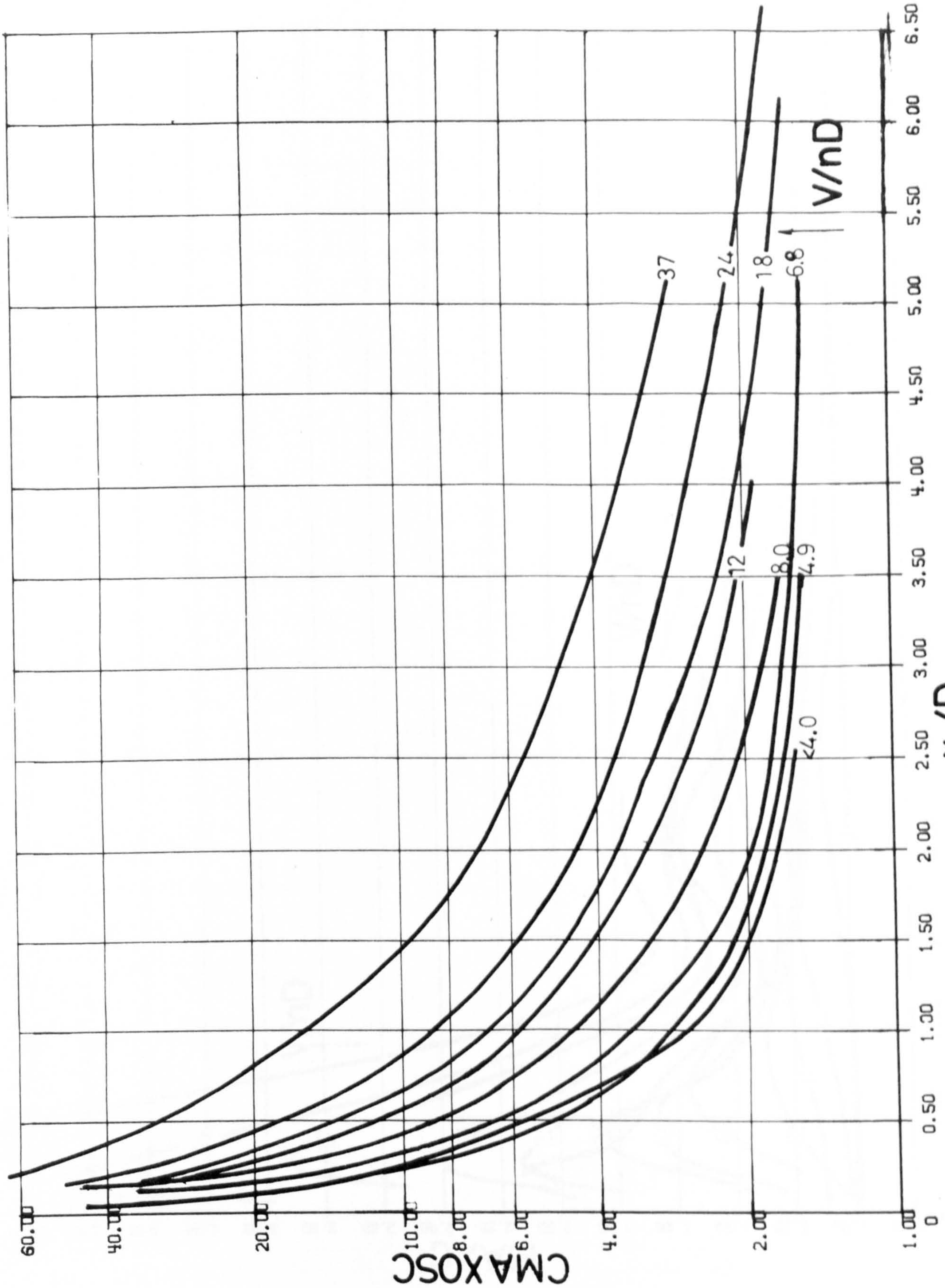

Fig. 104. Maximum oscillatory force coefficient, CMAXOSC versus x_o/D for various V/nD.

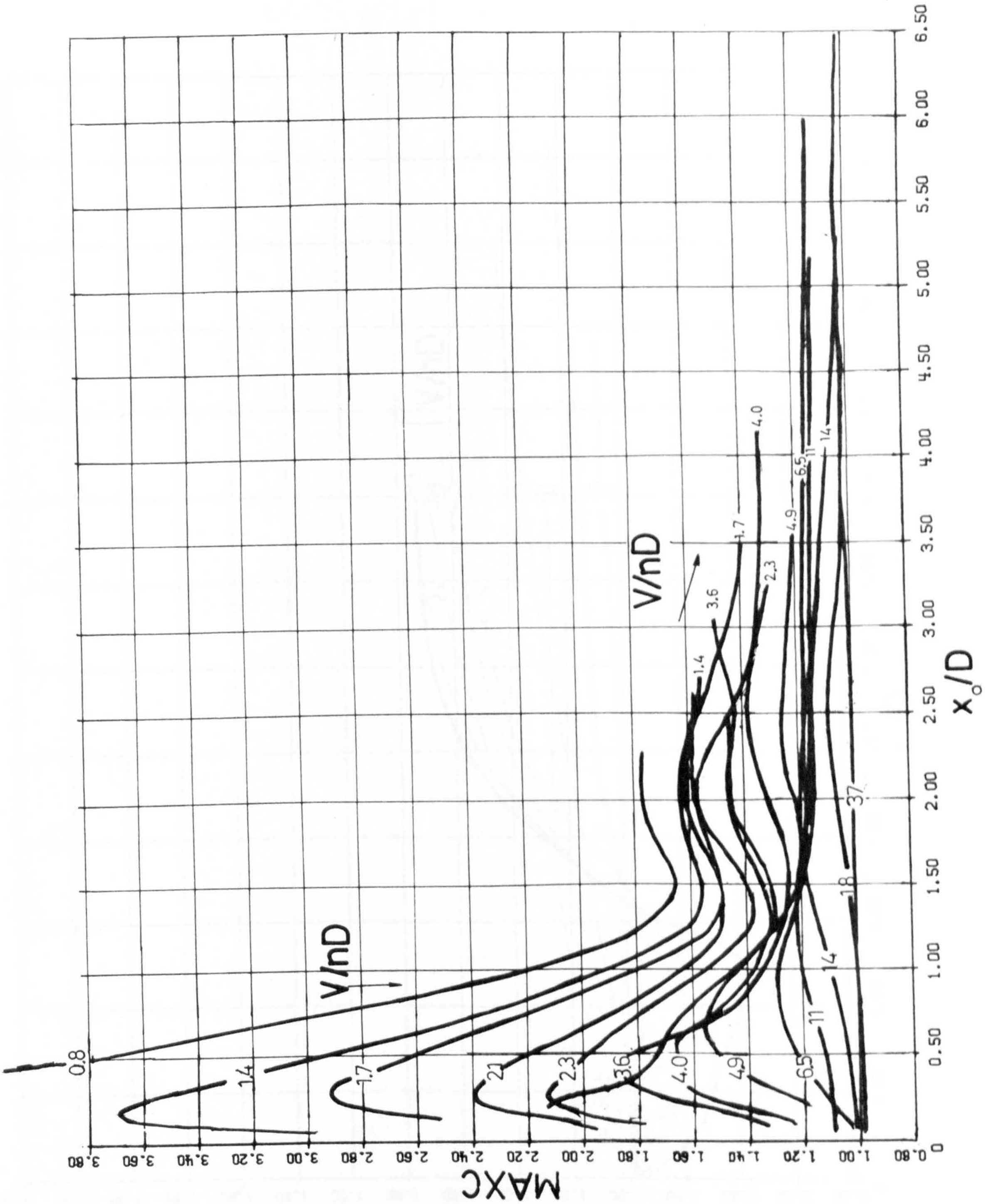

Fig. 105. Total maximum force coefficient (combined steady and oscillatory forces) versus x_o/D for various V/nD.

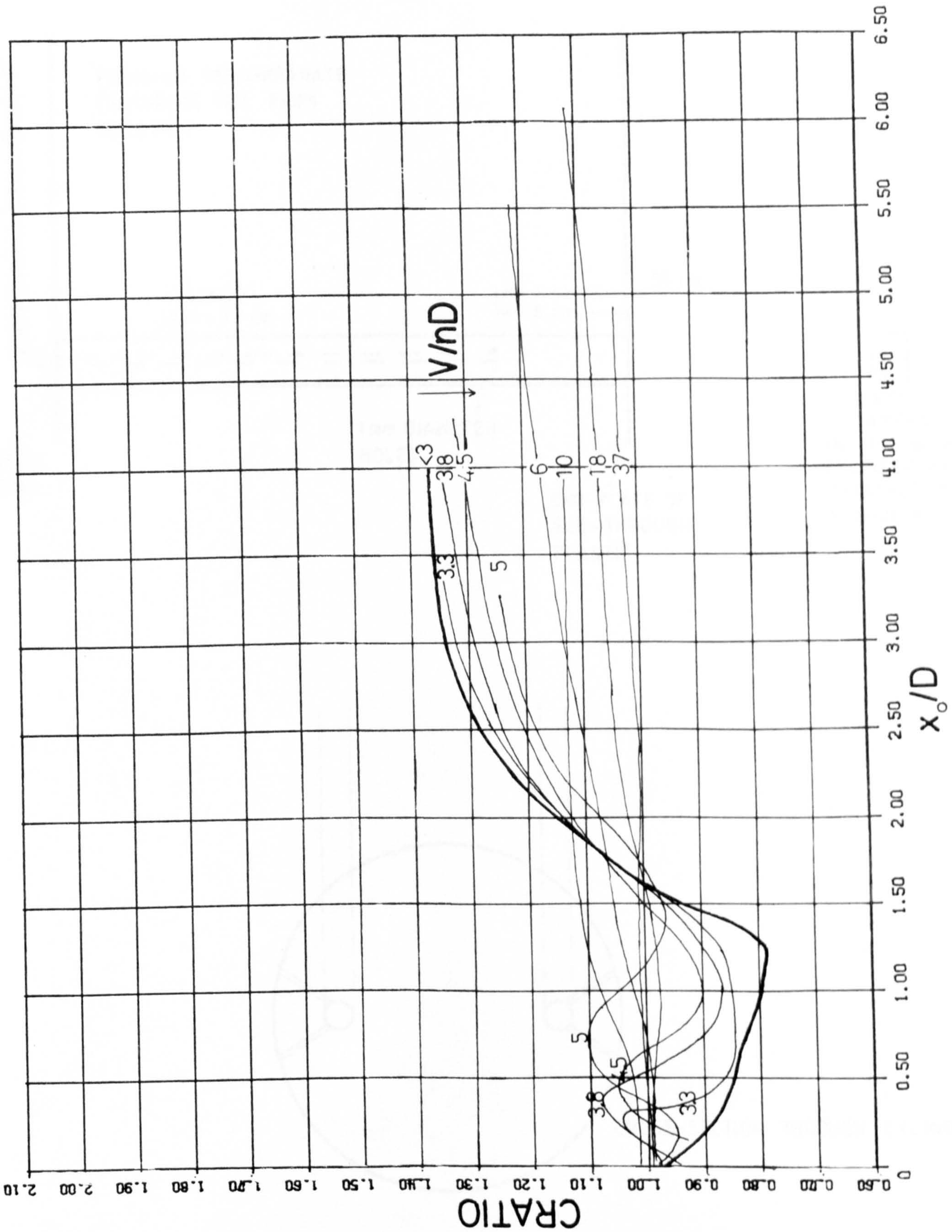

Fig. 106. Ratio between maximum forces and those calculated using equation (23) with CA = 2.0, CDDEP = 1.0 and STCDDEP = 1.0.

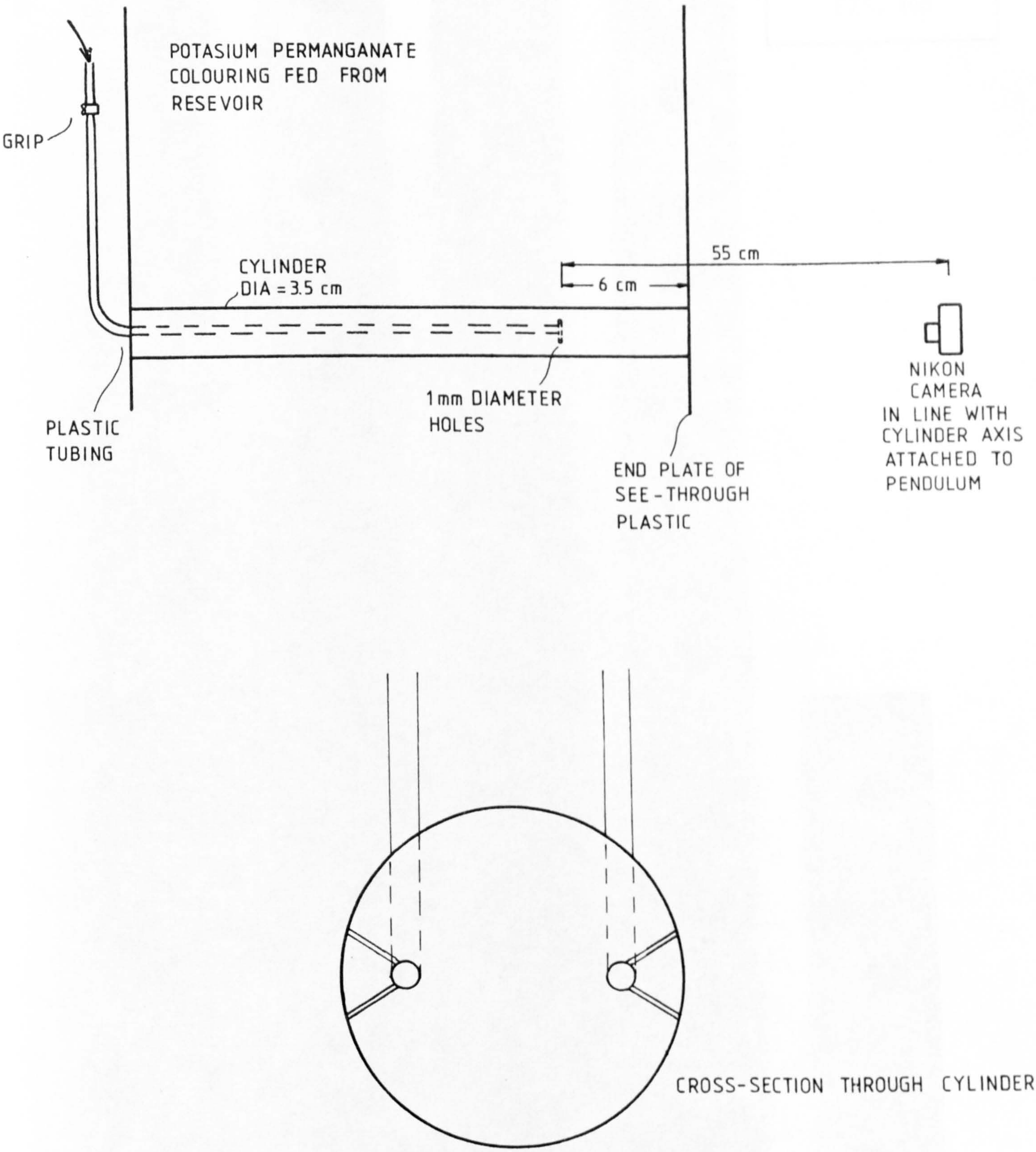

Fig. 107. Sketch of the setup used for the flow visualization experiments.

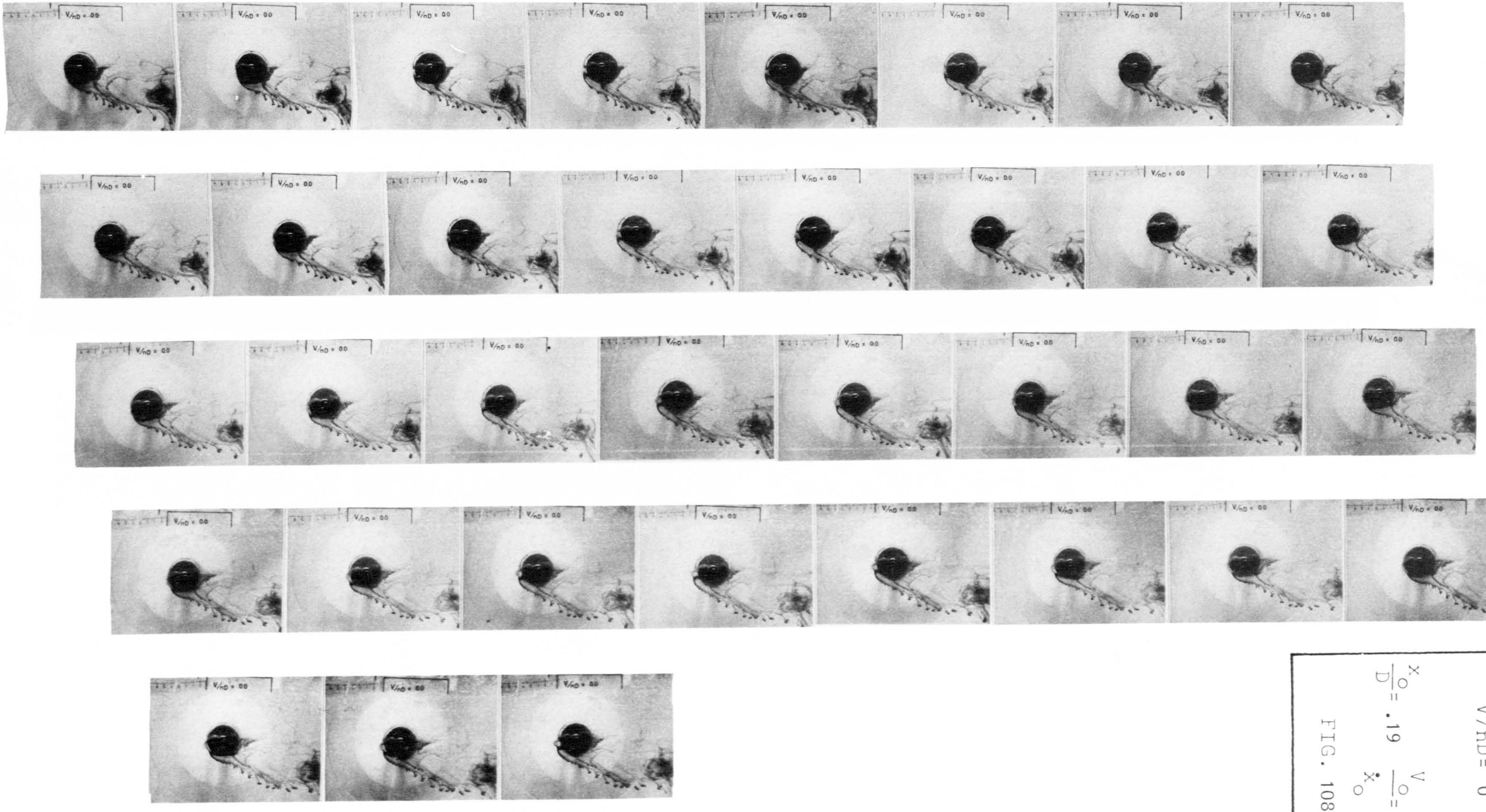

$V/nD = 0$

$\frac{x_o}{D} = .19$ $\frac{V_o}{\dot{x}_o} = 0$

FIG. 108

$V/nD = 0$

$\frac{x_o}{D} = .41$ $\frac{V_o}{\dot{x}_o} = 0$

FIG. 109

$V/nD = 0$

$\frac{x_o}{D} = .66 \quad \frac{V_o}{\dot{x}_o} = 0$

FIG. 110

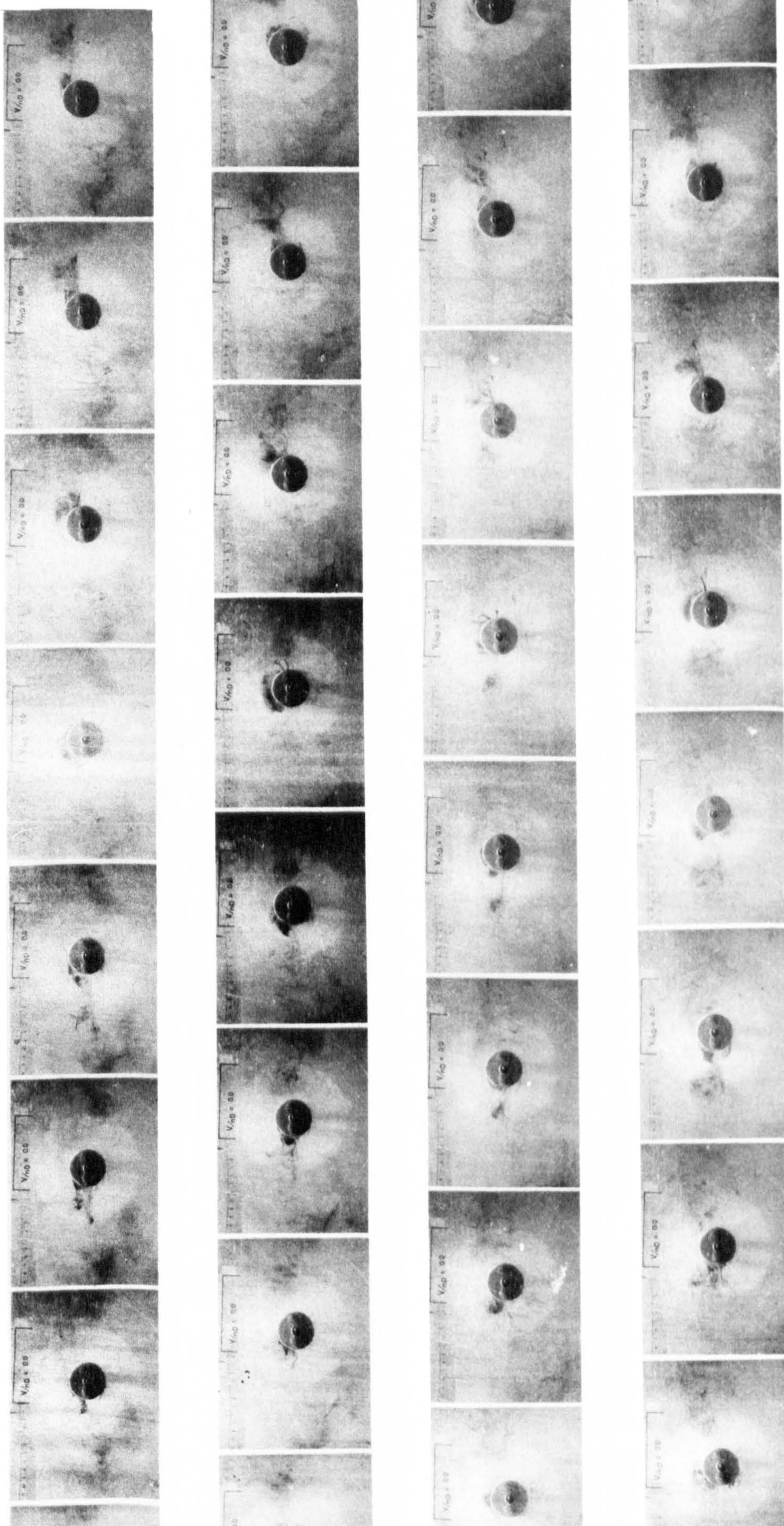

$V/nD = 0$

$\frac{x_o}{D} = .74$ $\frac{V_o}{\dot{x}_o} = 0$

FIG. 111

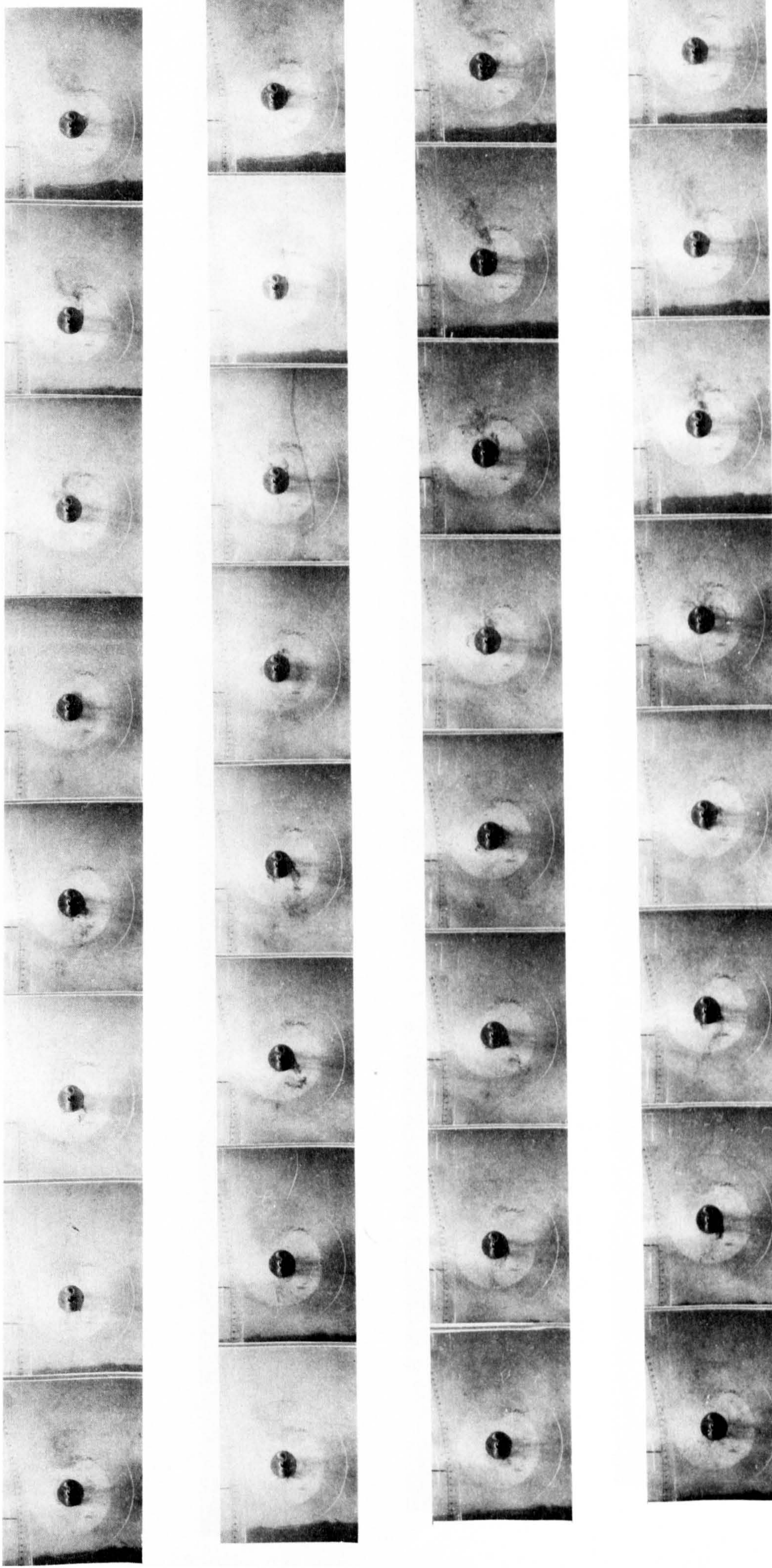

$V/nD = 0$

$\frac{x_o}{D} = 1.13$ $\qquad \frac{V_o}{\dot{x}_o} = 0$

FIG. 112

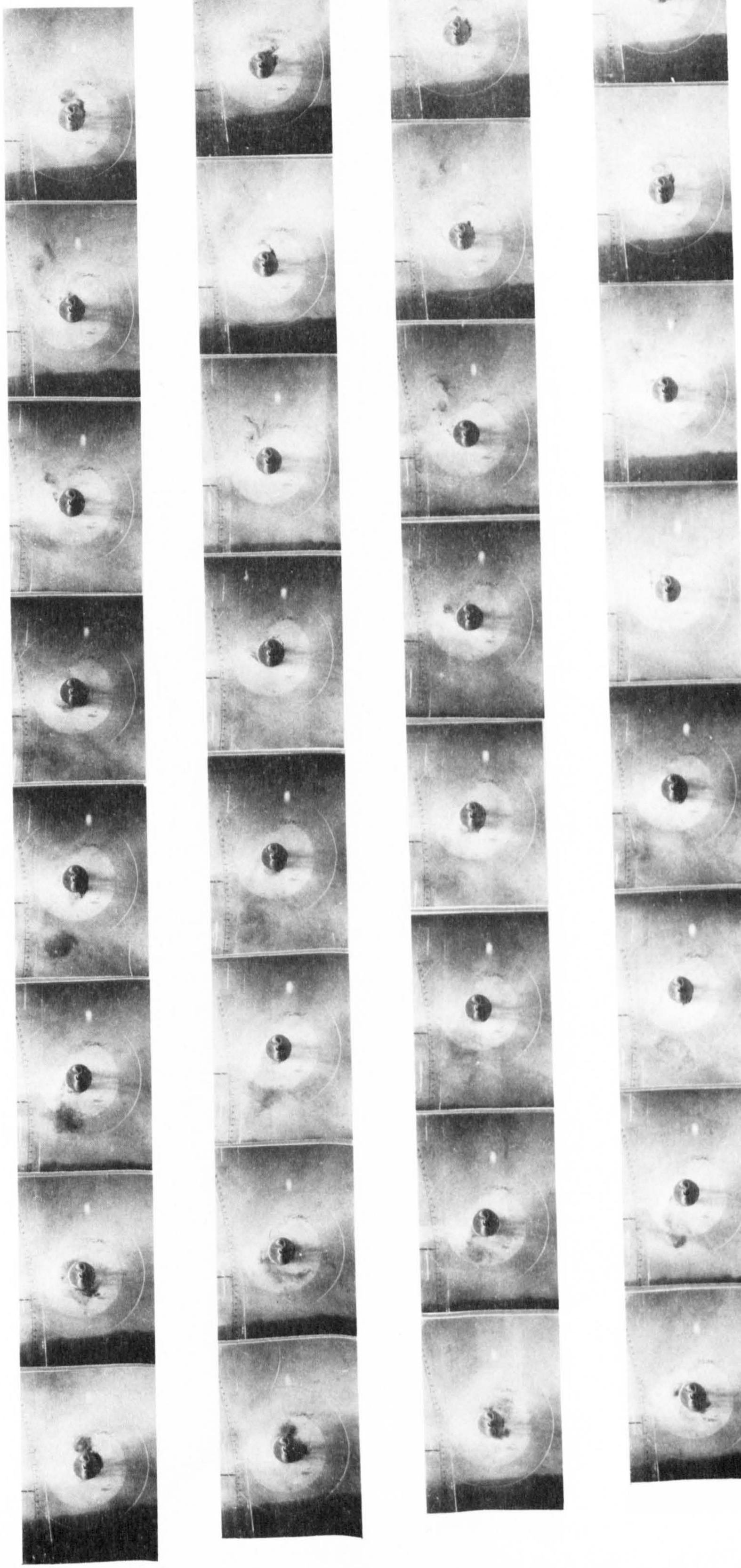

$V/nD = 0$

$\frac{x_o}{D} = 1.79$ $\qquad \frac{V_o}{\dot{x}_o} = 0$

FIG. 113

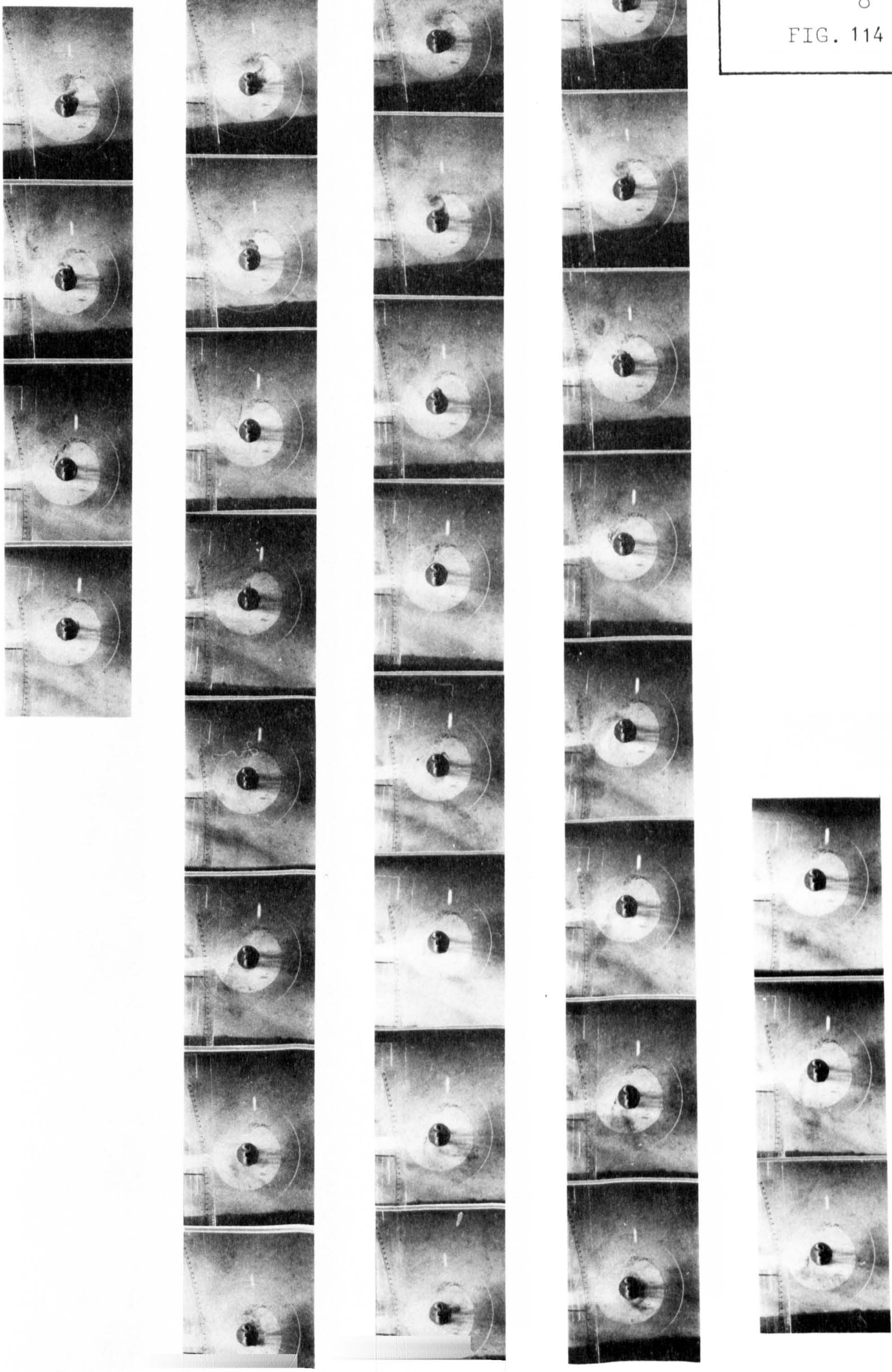

$V/nD = 0$

$\frac{x_o}{D} = 1.96 \quad \frac{V_o}{\dot{x}_o} = 0$

FIG. 114

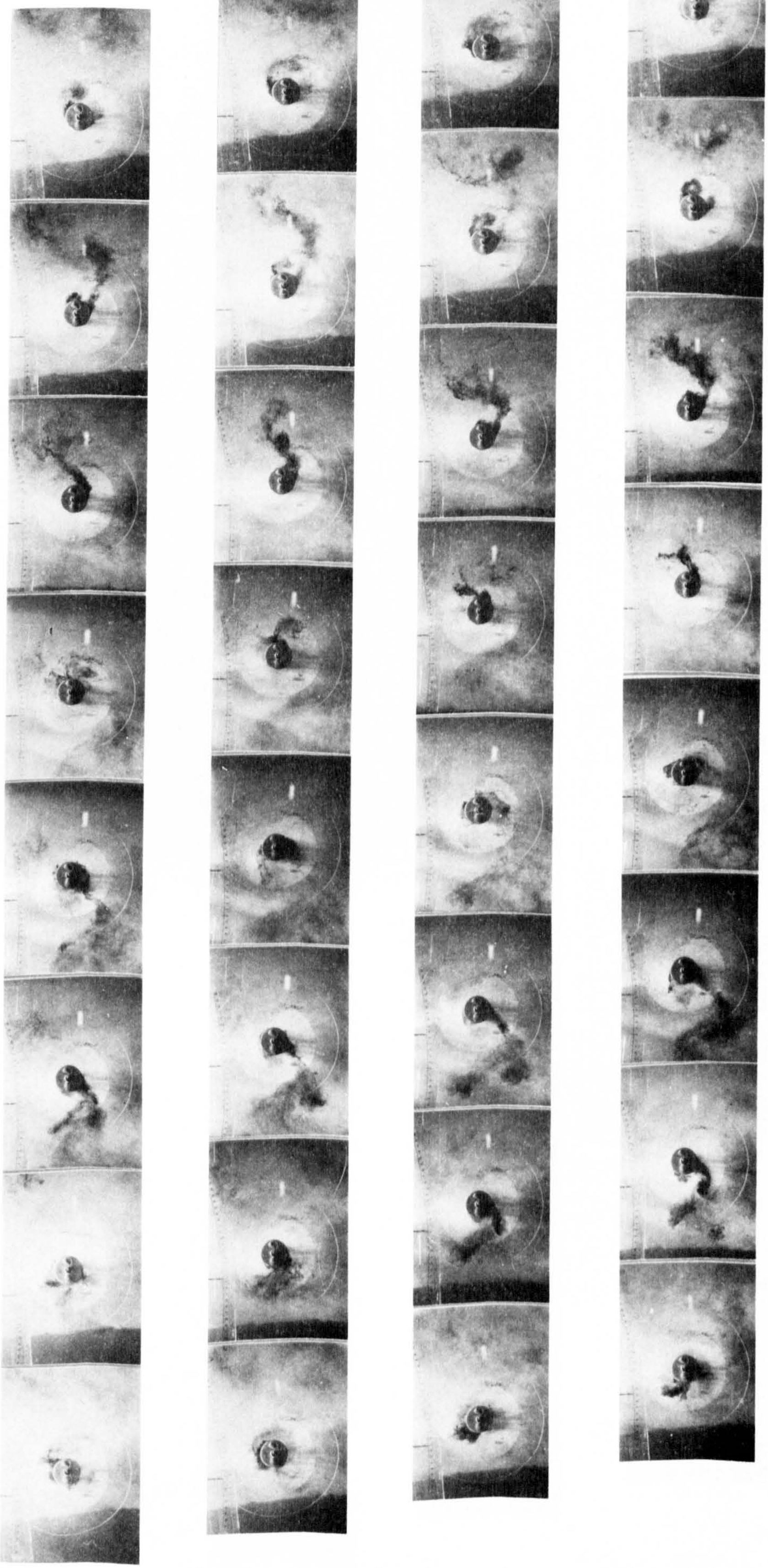

$V/nD = 0$

$\frac{x_o}{D} = 2.11$ $\qquad \frac{V_o}{\dot{x}_o} = 0$

FIG. 115

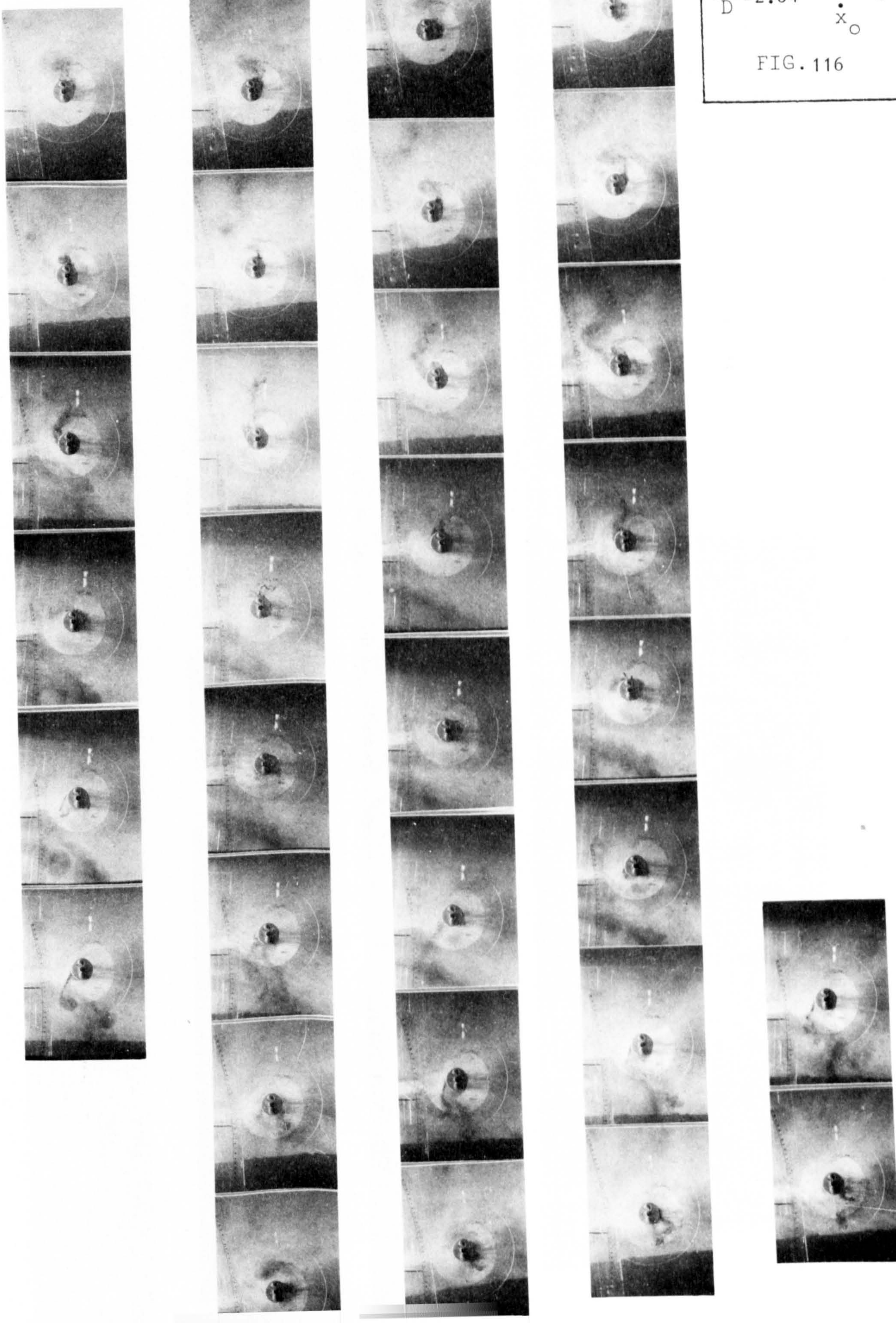

$V/nD = 0$

$\frac{x_o}{D} = 2.64$ $\frac{V_o}{\dot{x}_o} = 0$

FIG. 116

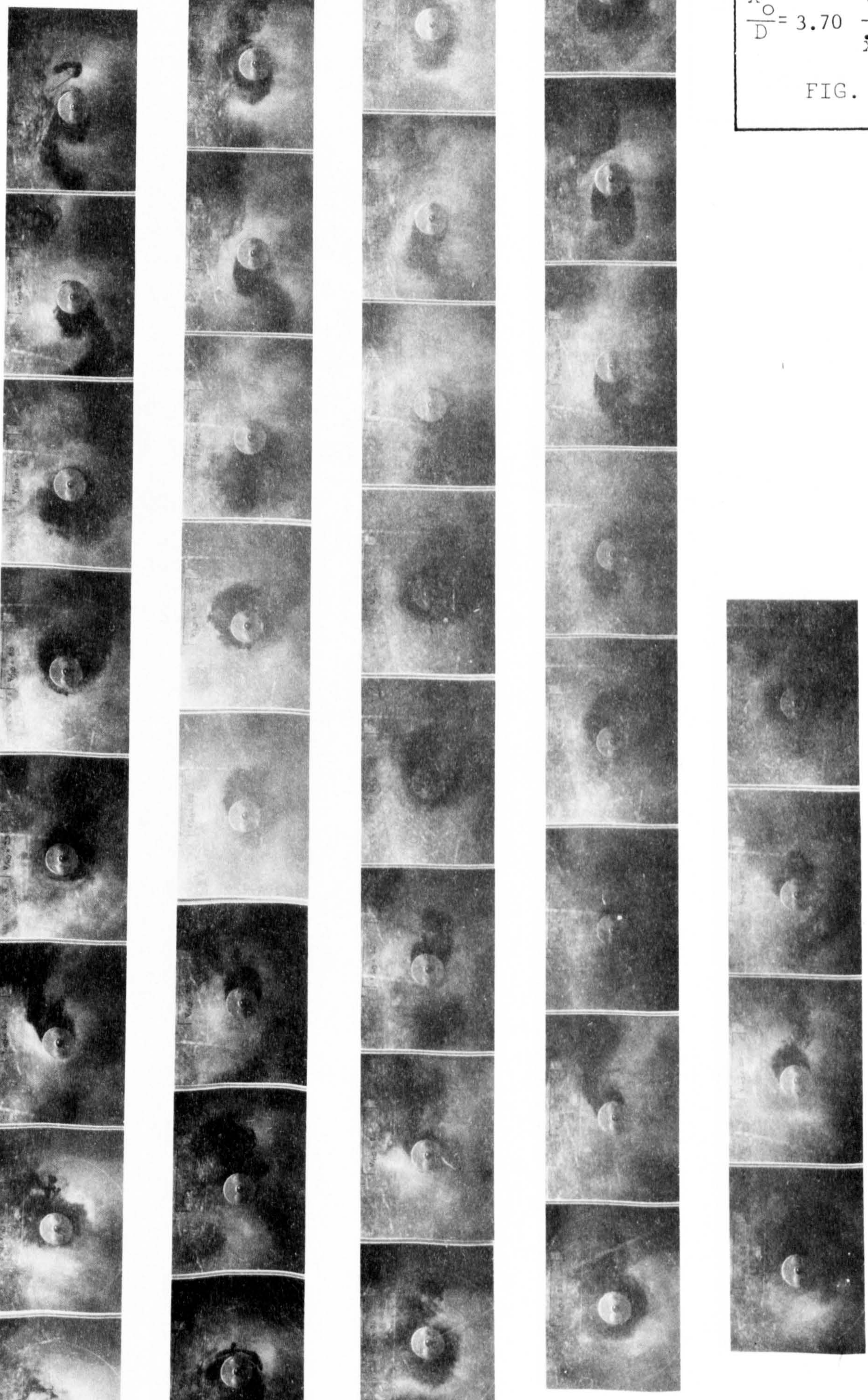

$V/nD = 0$

$\frac{x_o}{D} = 3.70 \quad \frac{V_o}{\dot{x}_o} = 0$

FIG. 117

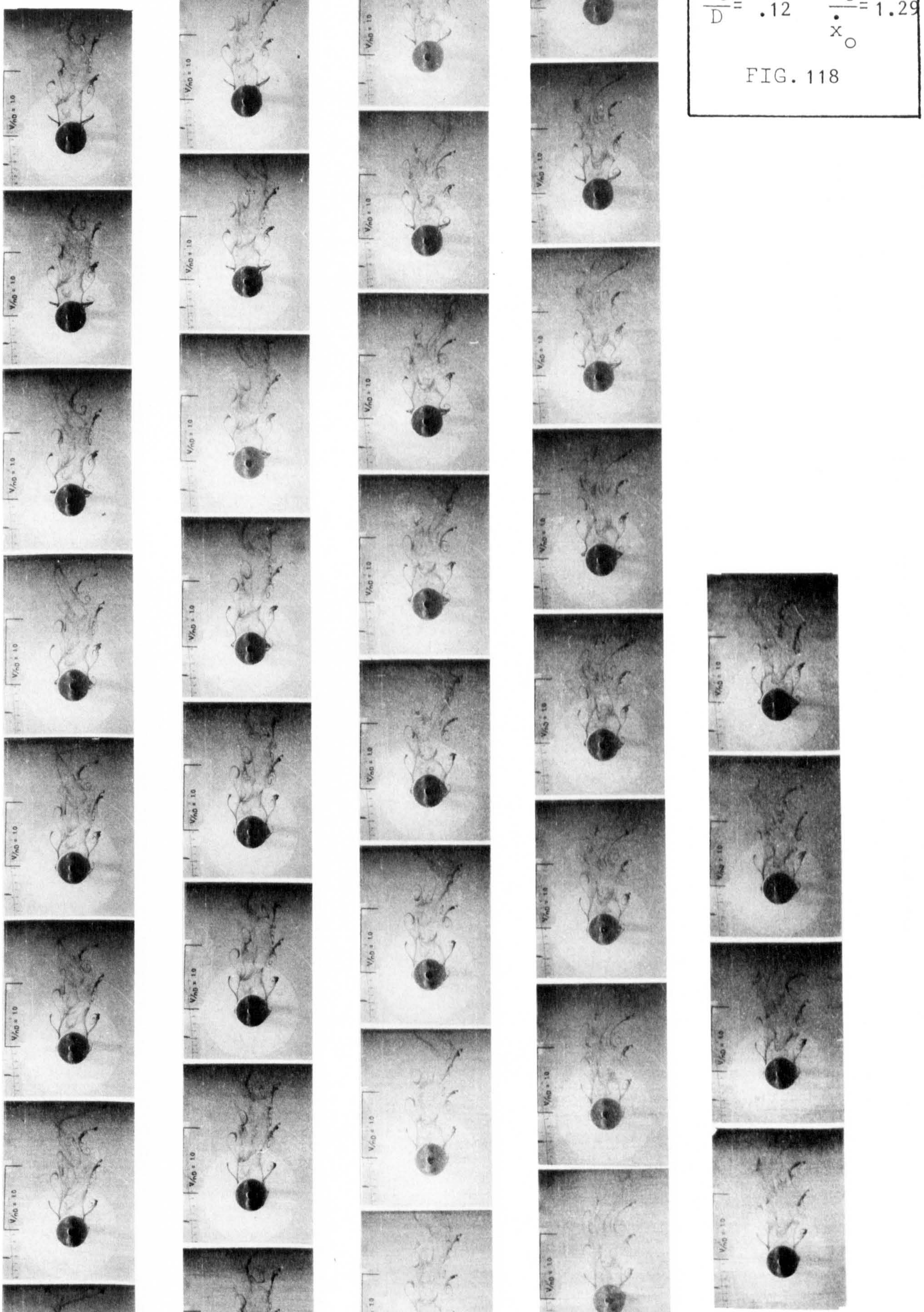

V/nD= 1.0

$\frac{x_o}{D}$= .12 $\frac{V_o}{\dot{x}_o}$= 1.29

FIG. 118

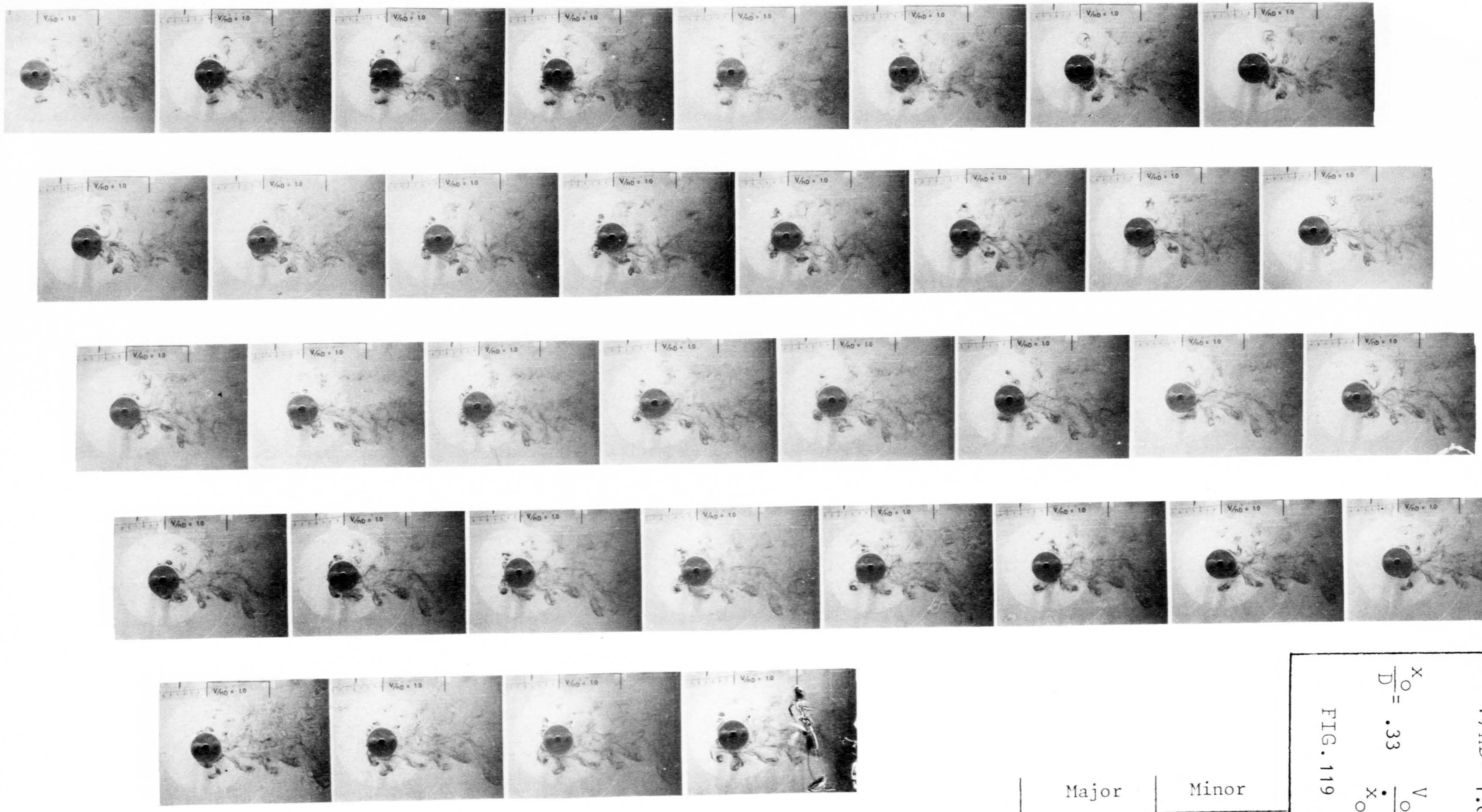

V/nD= 1.0

$\frac{x_o}{D}$ = .33 $\frac{V_o}{\dot{x}_o}$ = .48

FIG. 119

Non-dimensional relative distance travelled in each part cycle

Major	Minor
.62	-.12

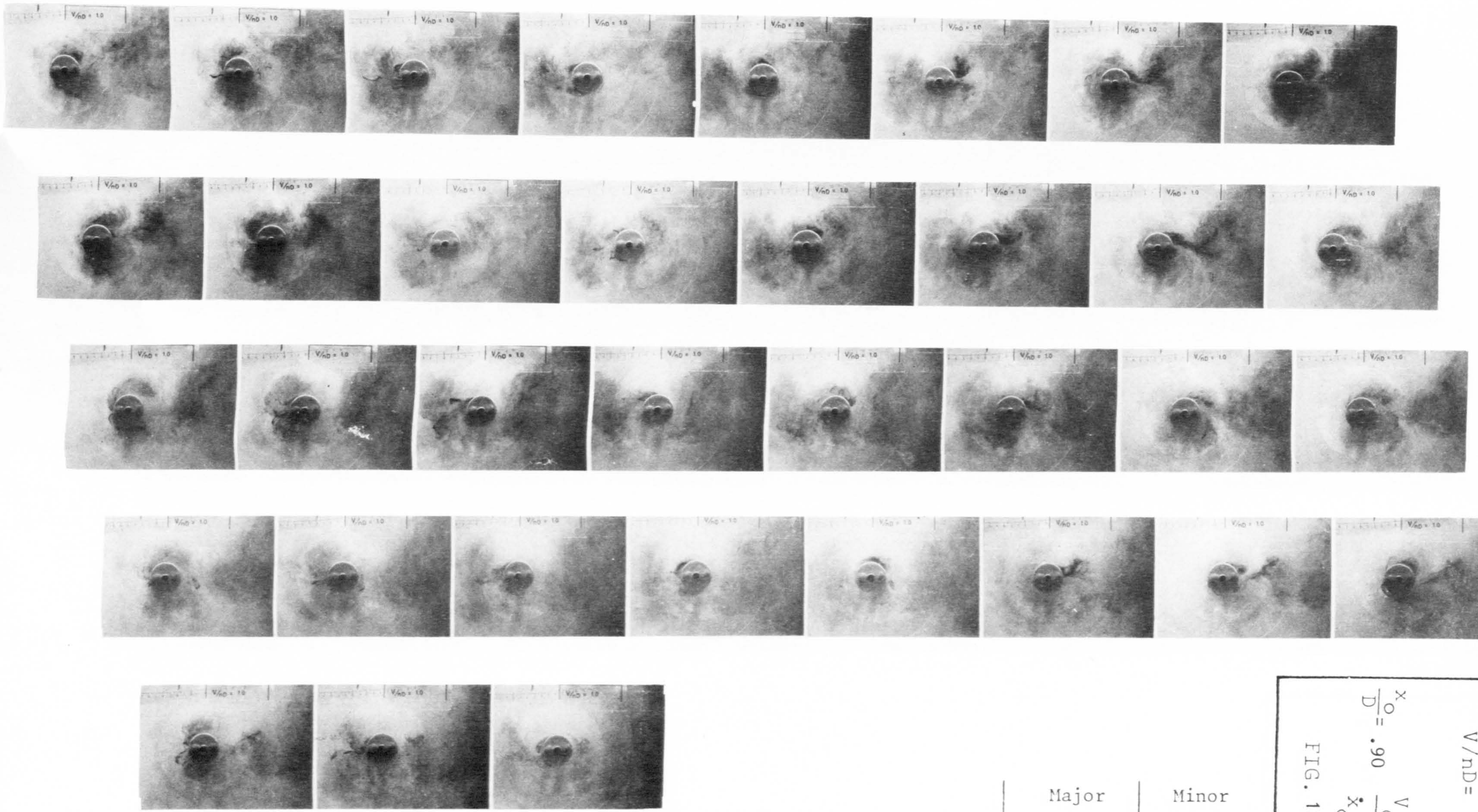

Non-dimensional relative distance travelled in each part cycle

Major	Minor
1.15	-.65

V/nD = 1.0

$\frac{x_o}{D}$ = .90 $\frac{\dot{x}_o}{V_o}$ = .18

FIG. 120

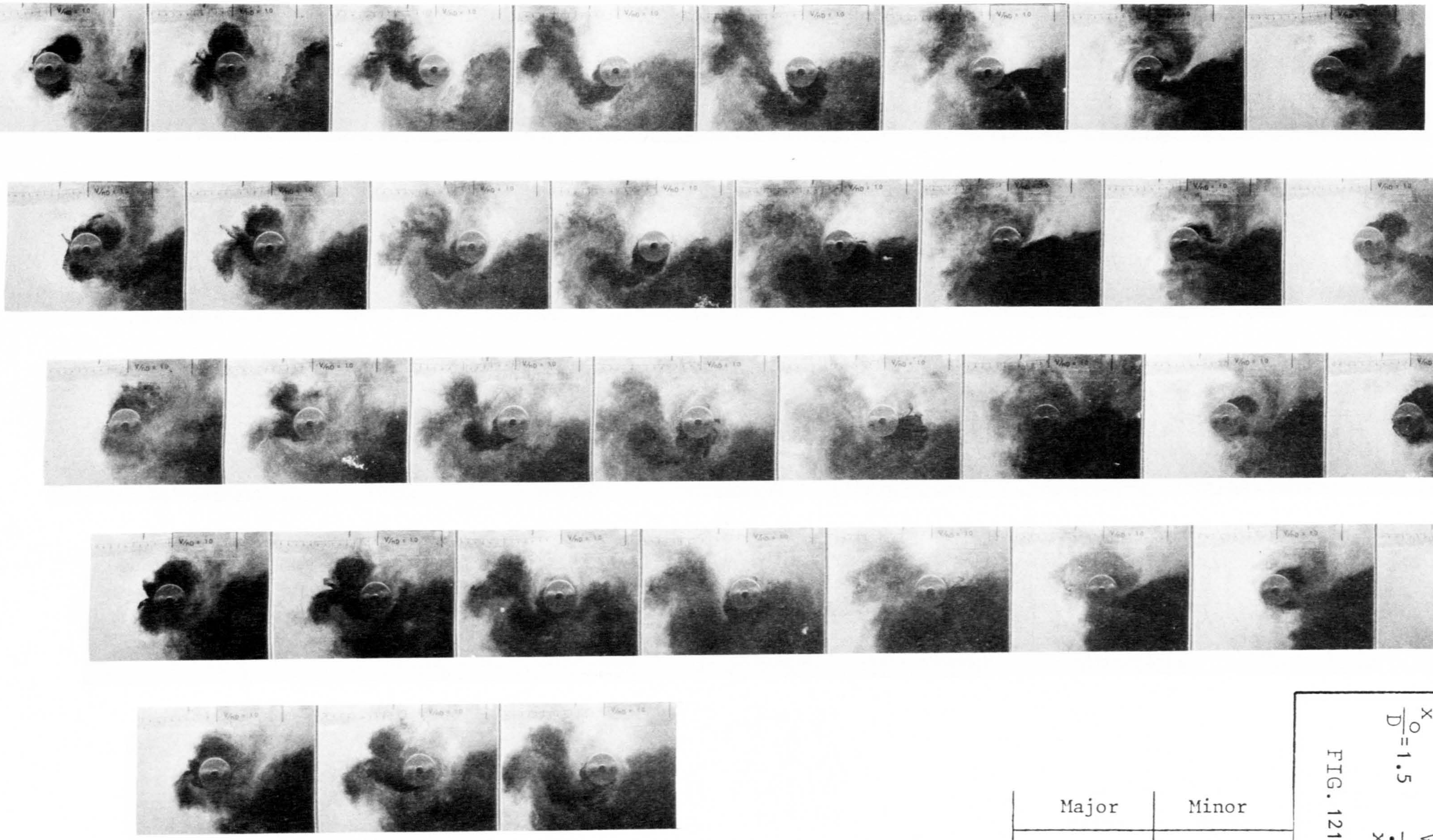

Major	Minor
1.71	-.36

Non-dimensional relative distance travelled in each part cycle

V/nD= 1.0

$\frac{x_o}{D}$=1.5 $\frac{V_o}{\dot{x}_o}$= .11

FIG. 121

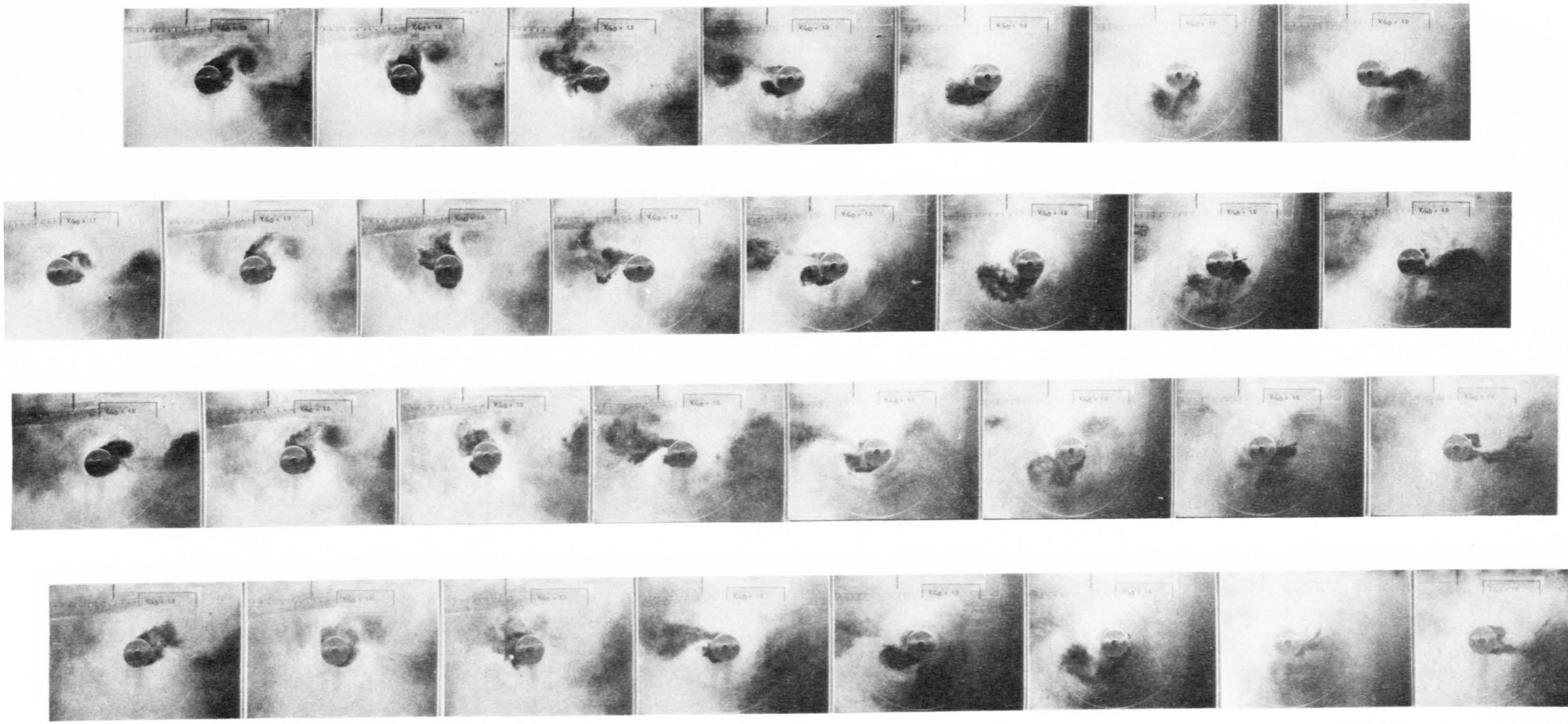

Non-dimensional relative distance travelled in each part cycle

Major	Minor
2.53	-2.02

V/nD= 1.0

$\frac{x_o}{D}$=2.17 $\frac{V_o}{\dot{x}_o}$= .07

FIG. 122

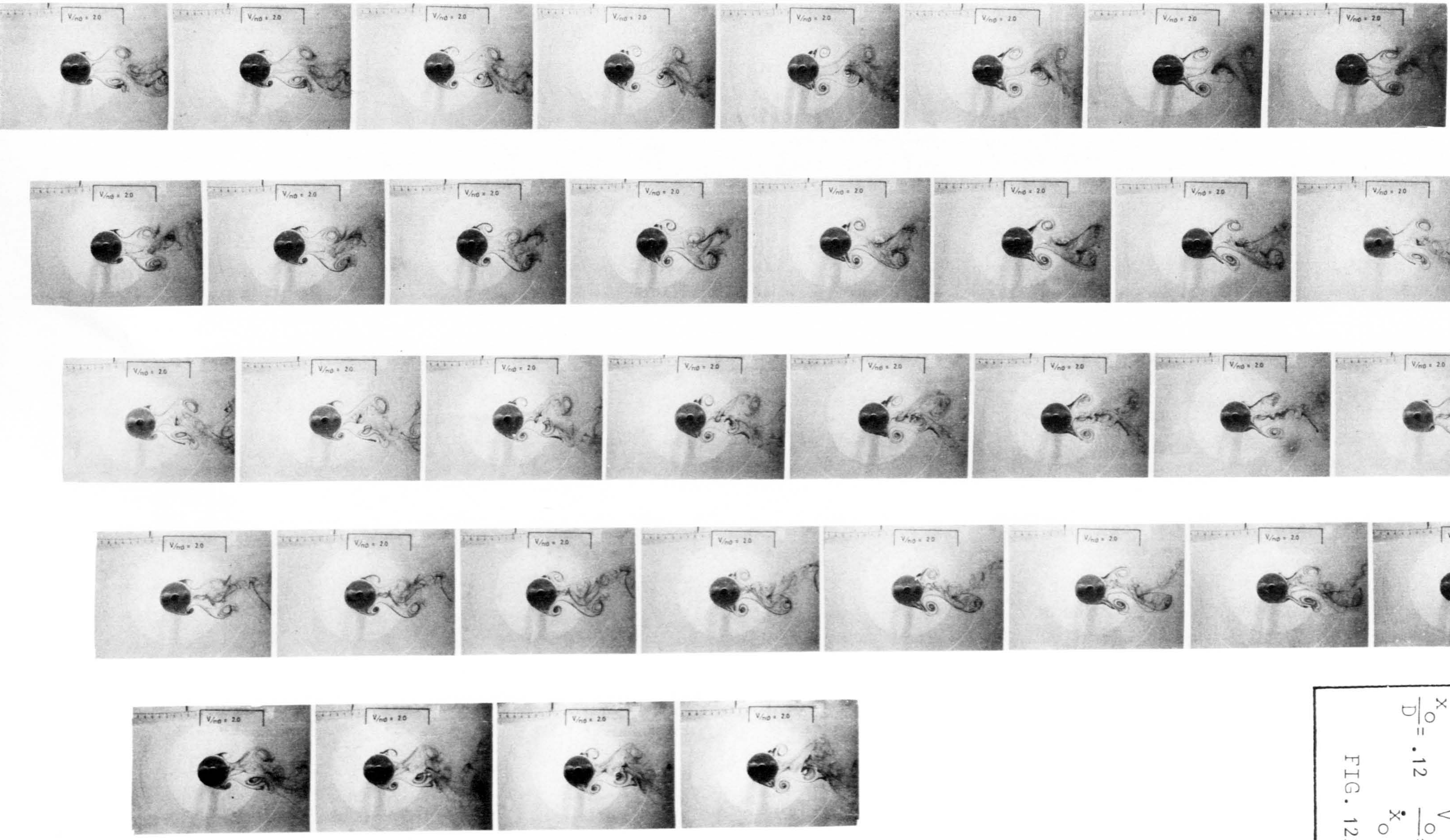

V/nD= 2.0

$\frac{x_o}{D}$ = .12 $\frac{V_o}{\dot{x}_o}$ = 2.65

FIG. 123

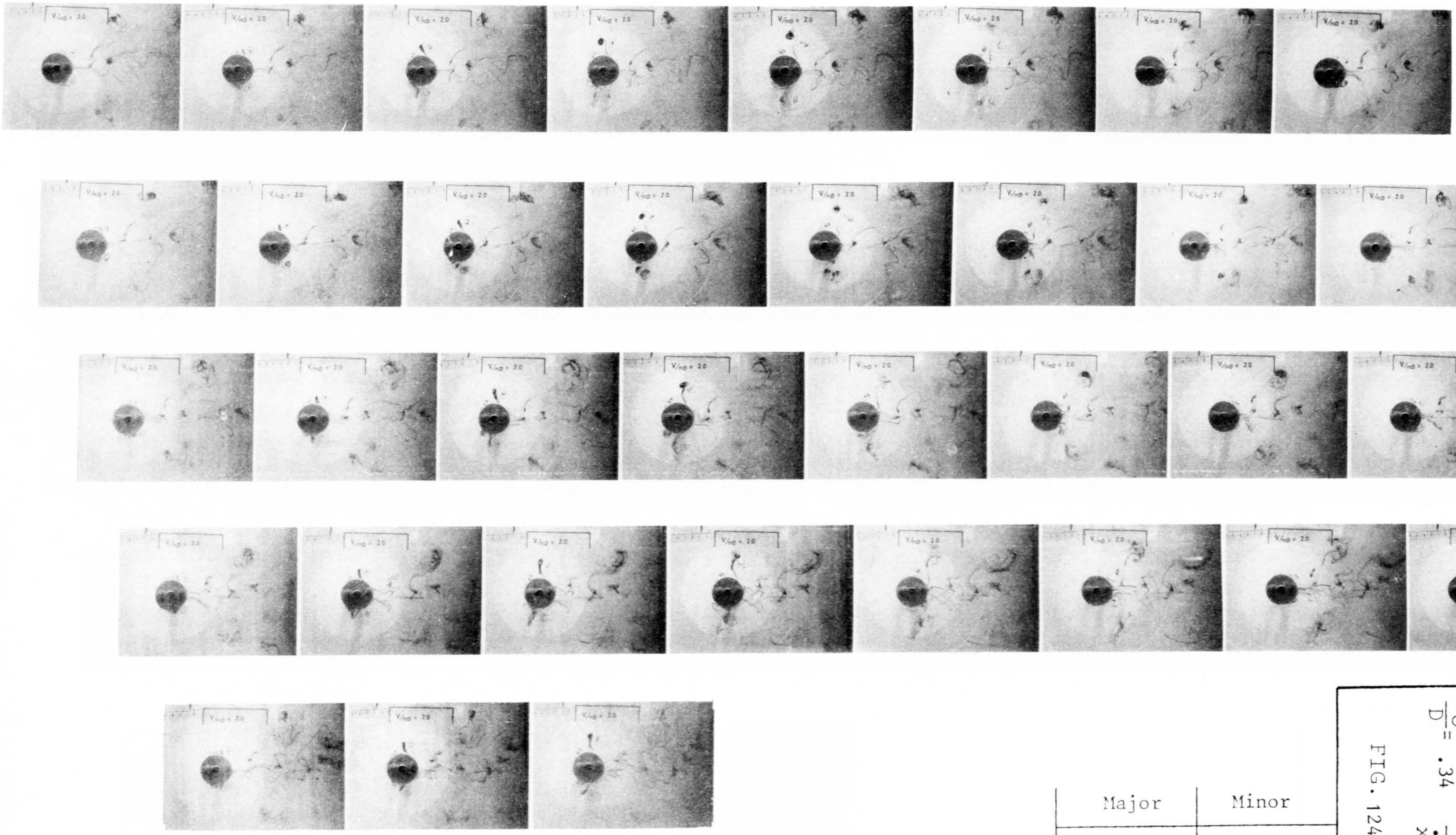

Non-dimensional relative distance travelled in each part cycle

Major	Minor
1.00	-.003

$V/nD = 2.0$

$\frac{x_o}{D} = .34$ $\frac{V_o}{\dot{x}_o} = .94$

FIG. 124

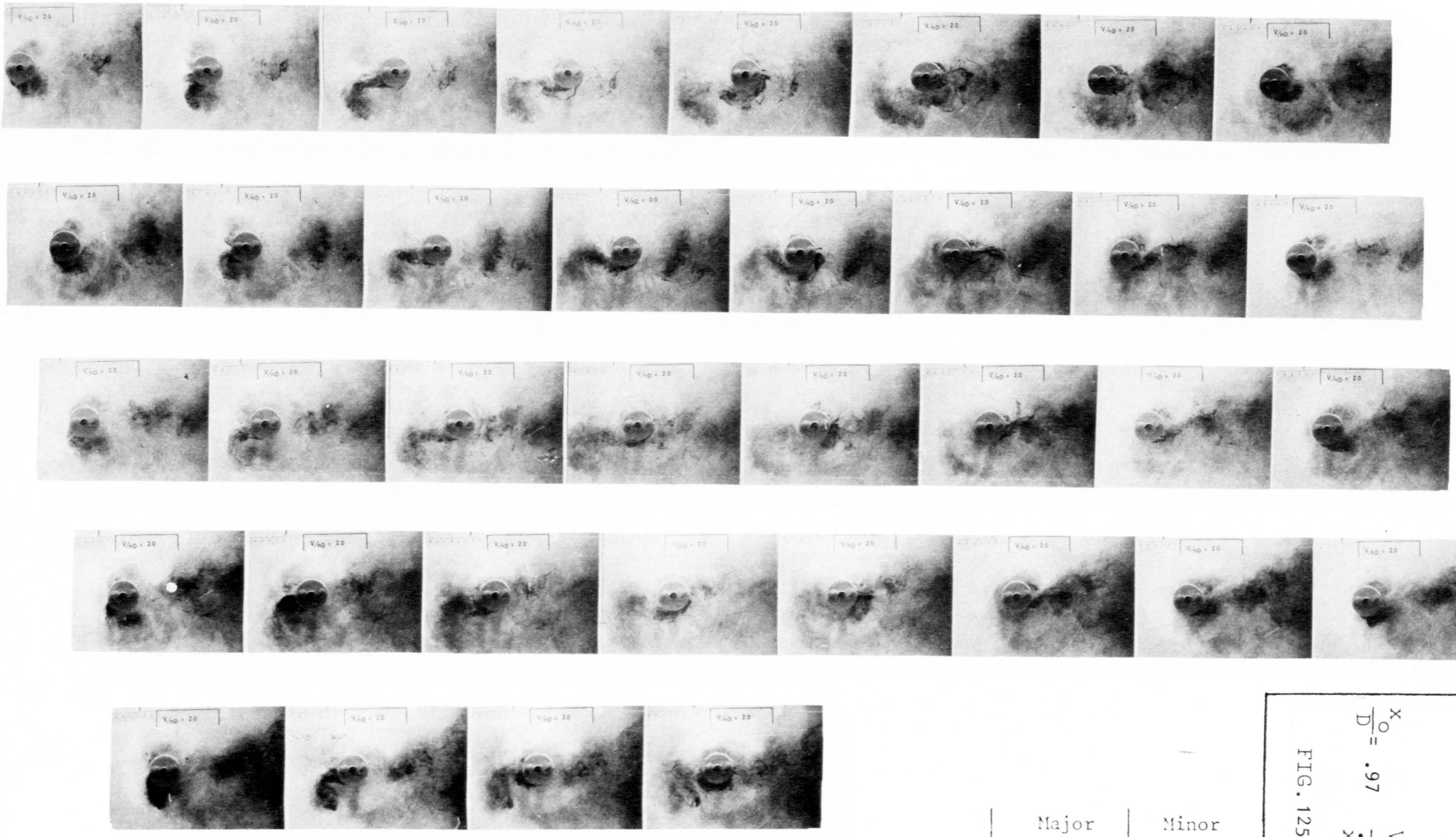

V/nD = 2.0

$\frac{x_o}{D} = .97$ $\frac{V_o}{\dot{x}_o} = .33$

FIG. 125

Non-dimensional relative distance travelled in each part cycle

Major	Minor
1.52	-0.52

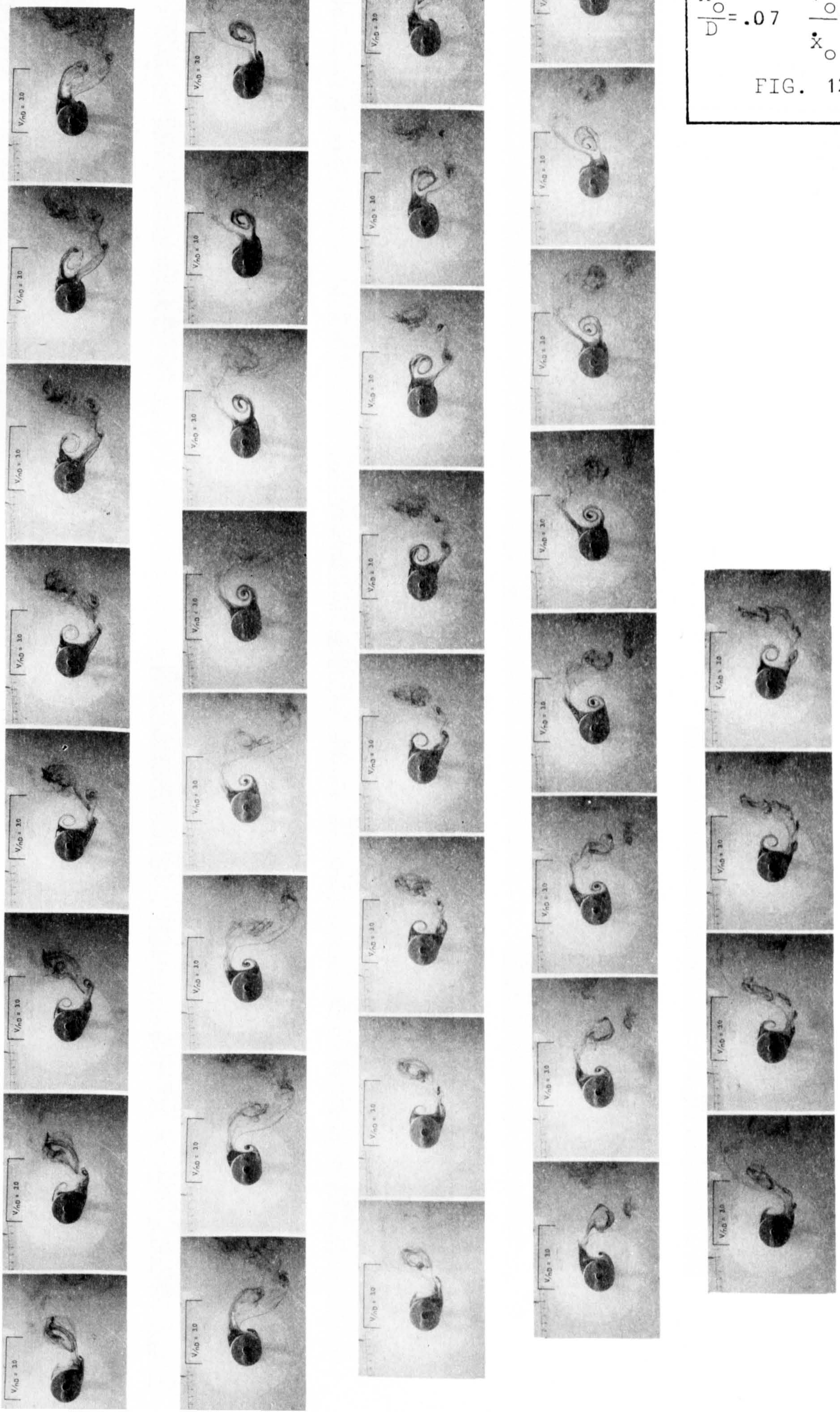

FIG. 126

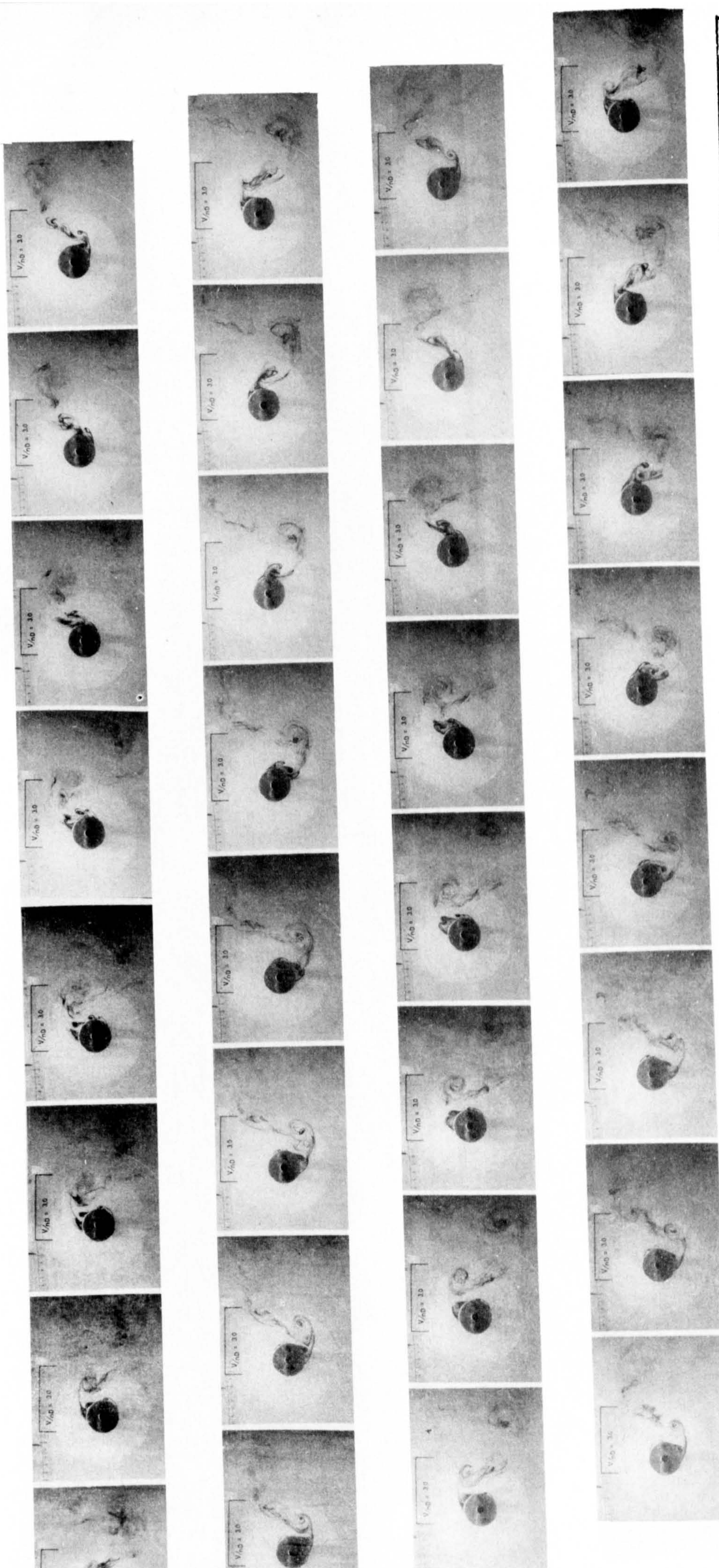

V/nD= 3.0

$\frac{x_o}{D}$ = .19 $\frac{V_o}{\dot{x}_o}$ = 2.46

FIG. 127

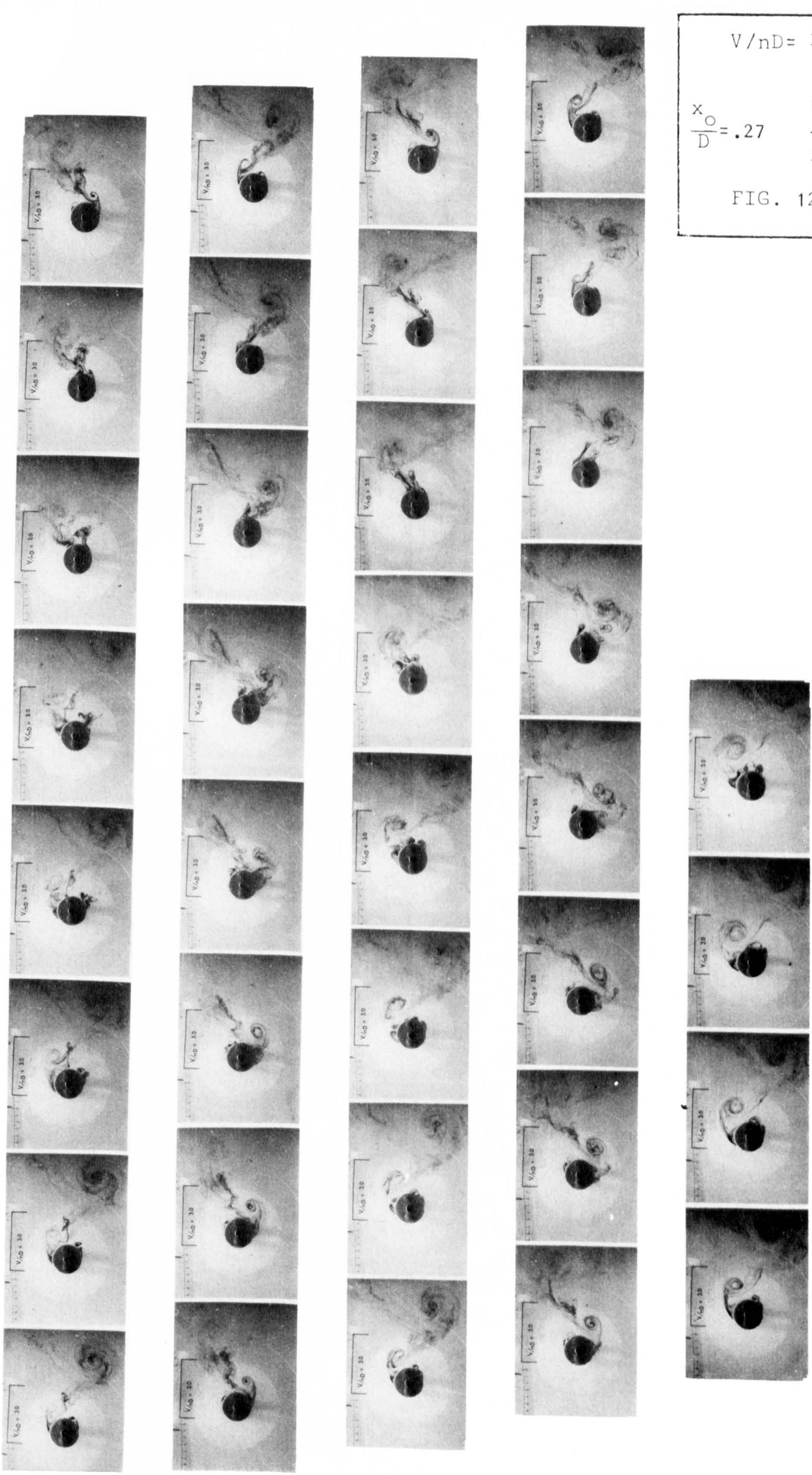

V/nD= 3.0

$\frac{x_o}{D}$ = .27 $\frac{V_o}{\dot{x}_o}$ = 1.77

FIG. 128

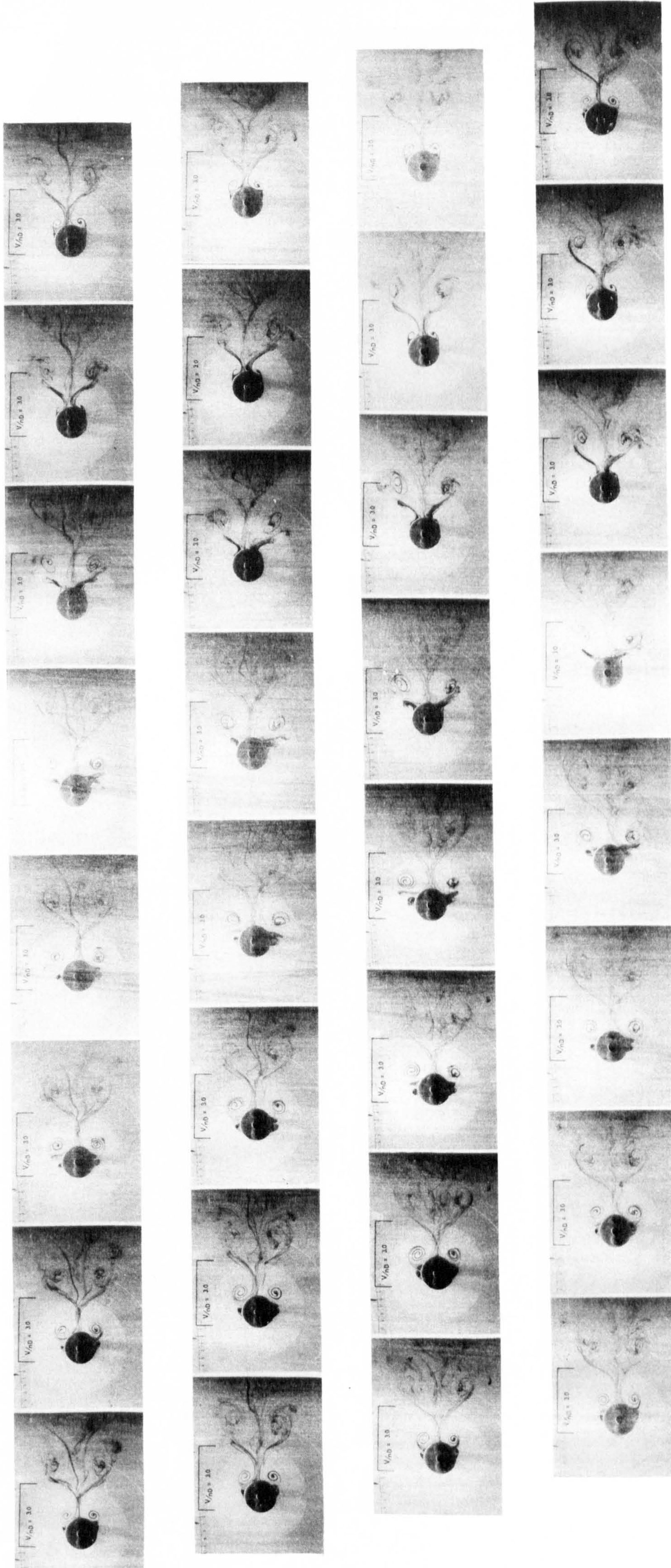

V/nD= 3.0

$\frac{x_o}{D}$= .29 $\frac{V_o}{\dot{x}_o}$=1.65

FIG. 129

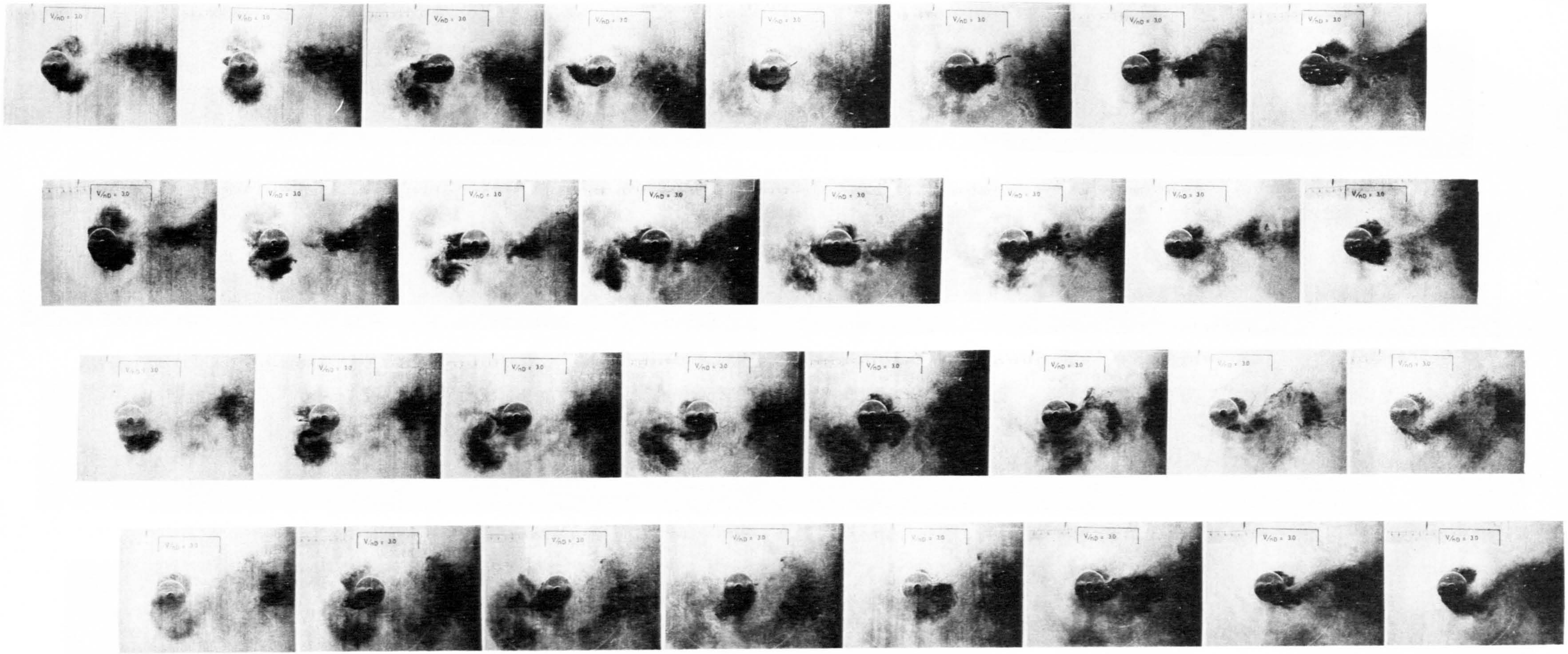

	Major	Minor
Non-dimensional relative distance travelled in each part cycle	2.01	-.51

V/nD= 3.0

$\frac{x_o}{D}$=1.18 $\frac{V_o}{\dot{x}_o}$= .41

FIG. 130

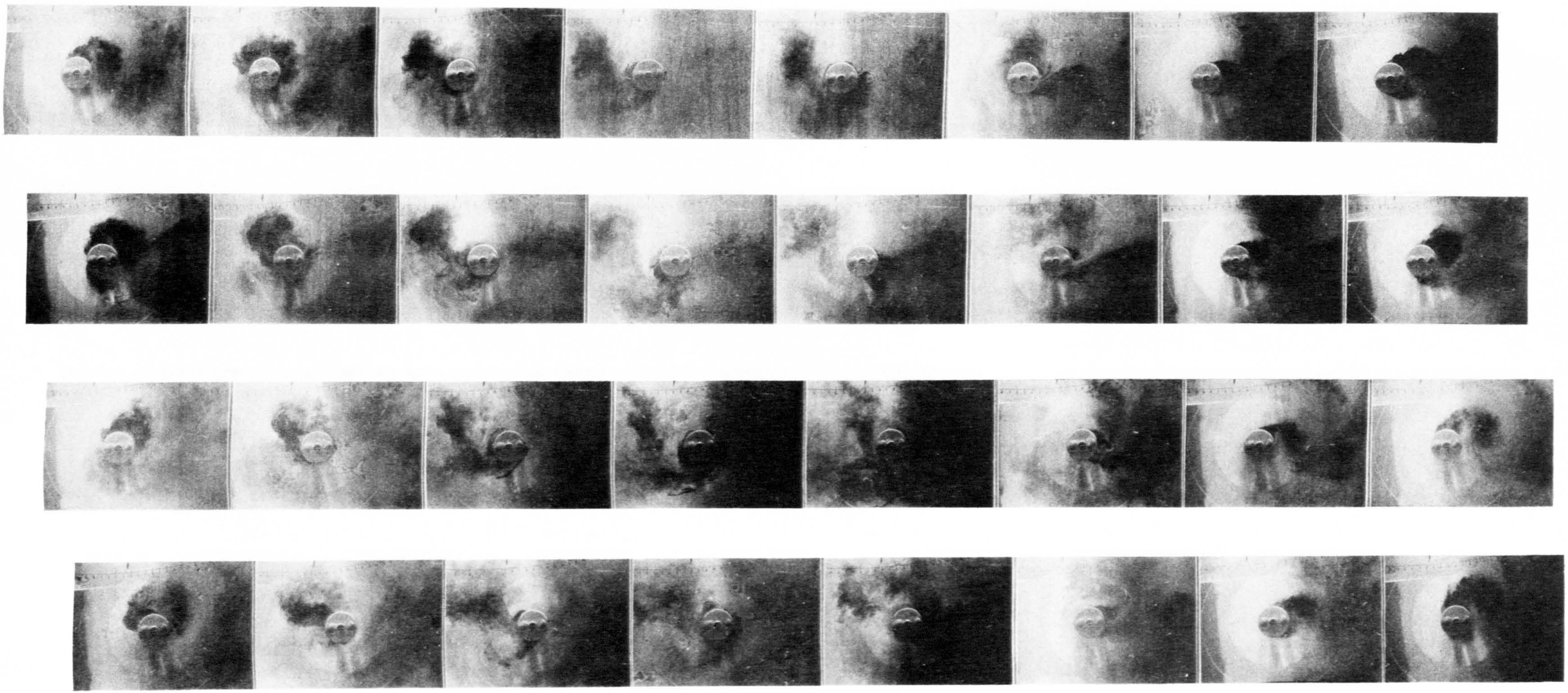

Non-dimensional relative distance travelled in each part cycle

Major	Minor
2.52	-1.02

$\frac{x_o}{D}$=1.71 $\frac{V_o}{\dot{x}_o}$=.28

V/nD= 3.0

FIG. 131

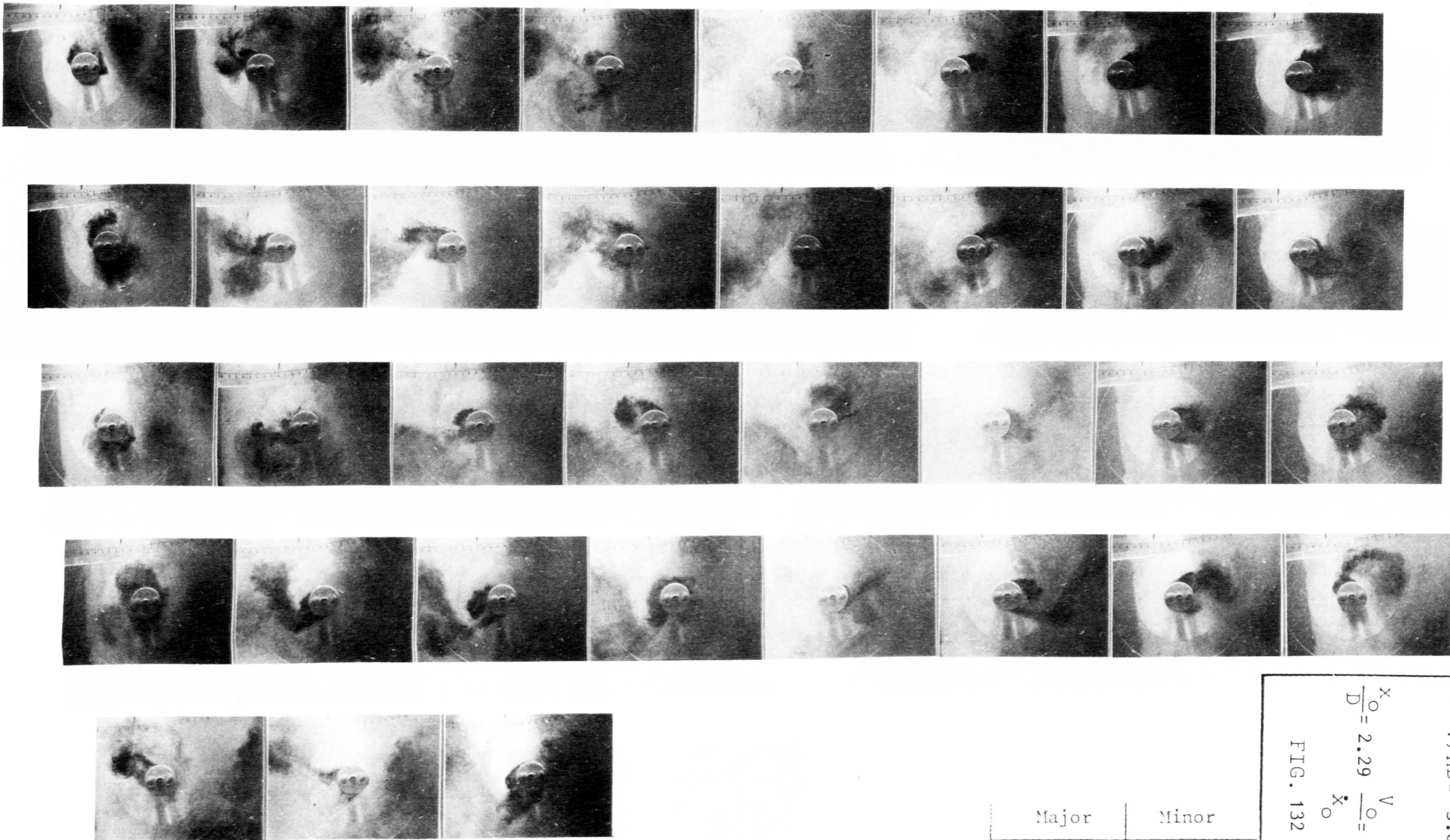

V/nD= 3.0

$\frac{x_o}{D}$= 2.29 $\frac{V_o}{\dot{x}_o}$= .21

FIG. 132

	Major	Minor
Non-dimensional relative distance travelled in each part cycle	3.07	-1.57

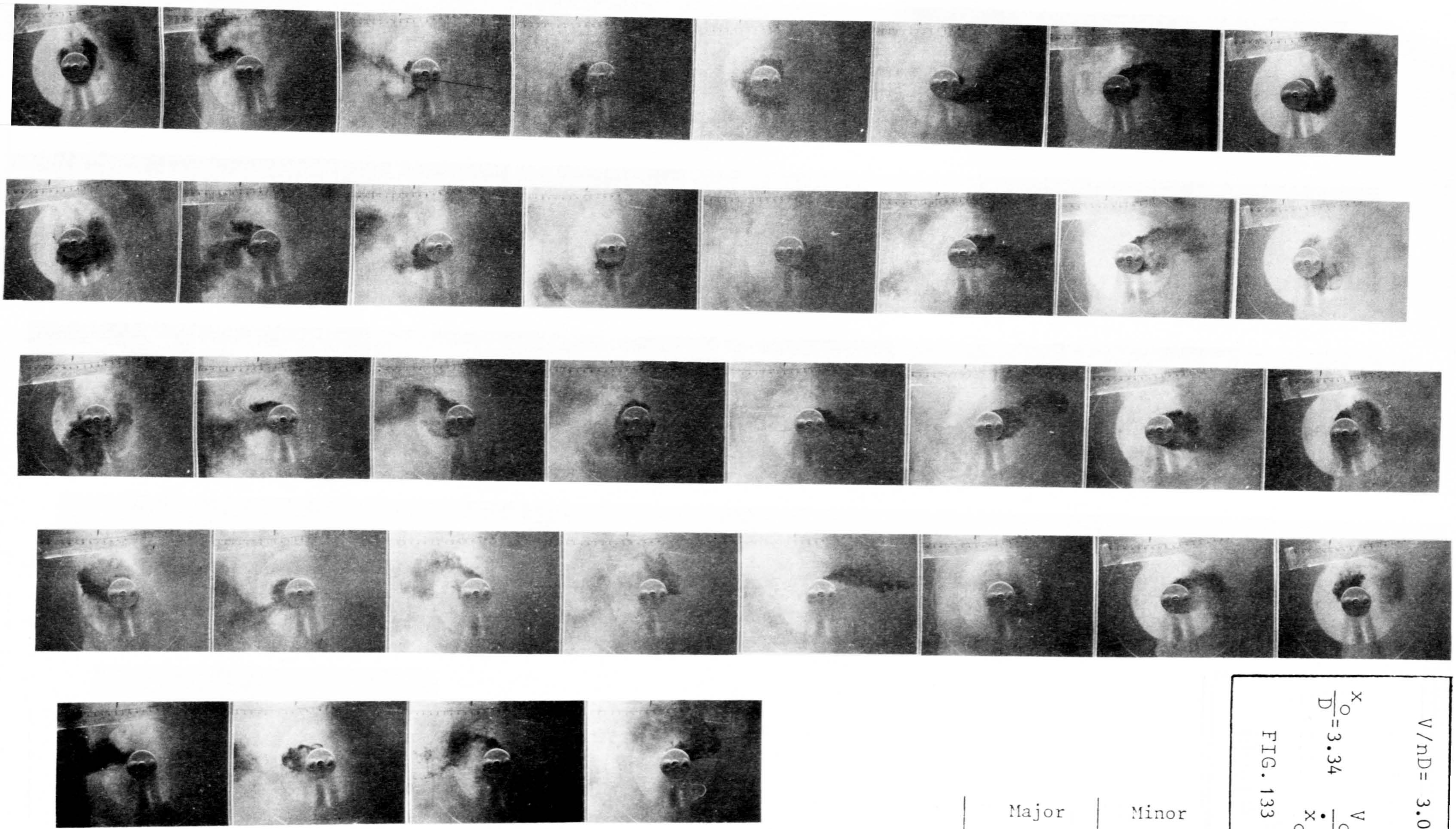

V/nD= 3.0

$\frac{x_o}{D}$= 3.34 $\frac{V_o}{\dot{x}_o}$= .14

FIG. 133

Non-dimensional relative distance travelled in each part cycle

Major	Minor
4.19	-2.69

V/nD= 3.8

$\frac{x_o}{D}$= .09 $\frac{V_o}{\dot{x}_o}$=7.03

FIG. 134

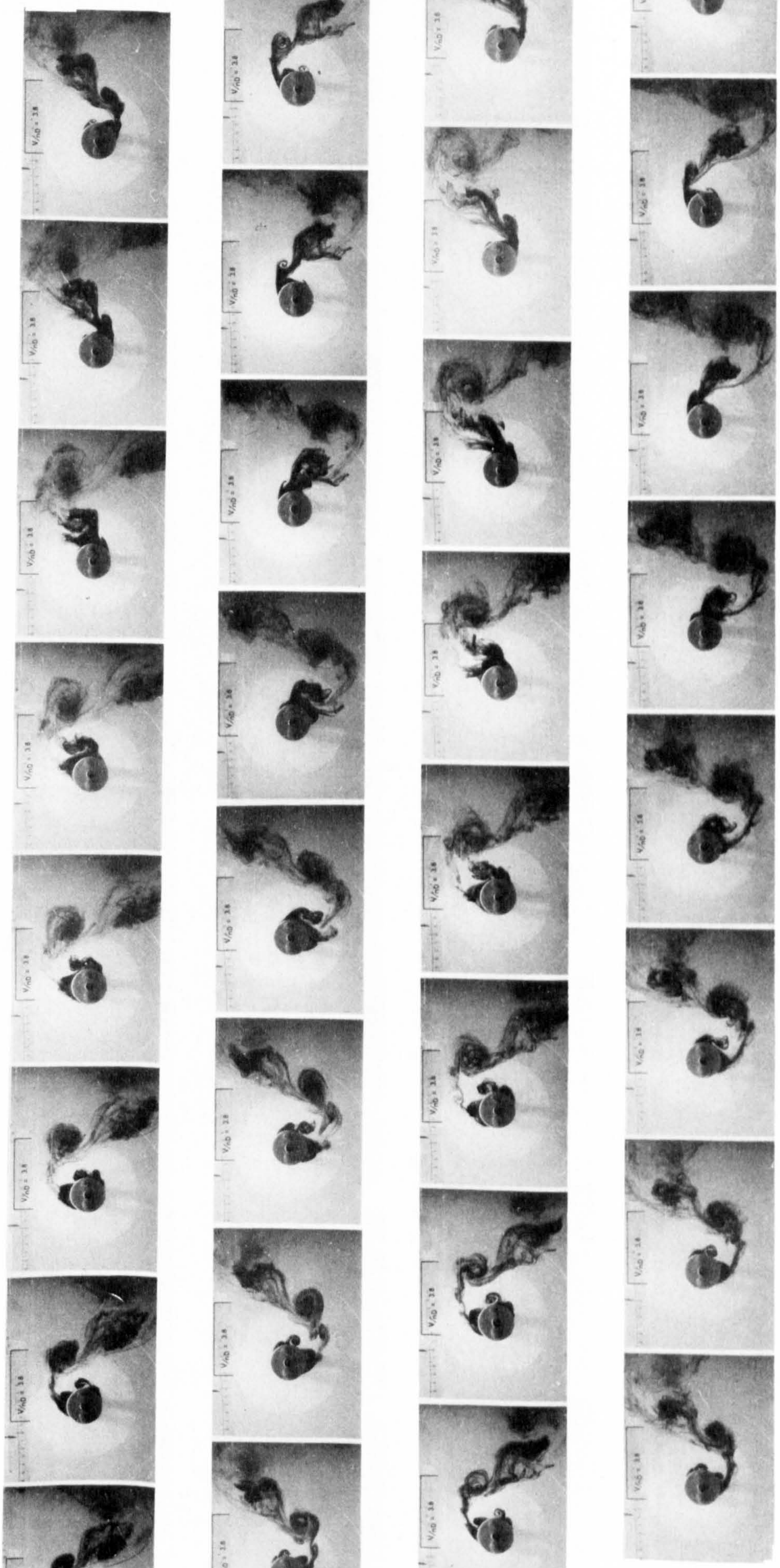

V/nD= 3.8

$\frac{x_o}{D}$= .31 $\frac{V_o}{\dot{x}_o}$= 1.95

FIG. 135

V/nD= 3.8

$\frac{x_o}{D}$= .41 $\frac{V_o}{\dot{x}_o}$=1.68

FIG. 136

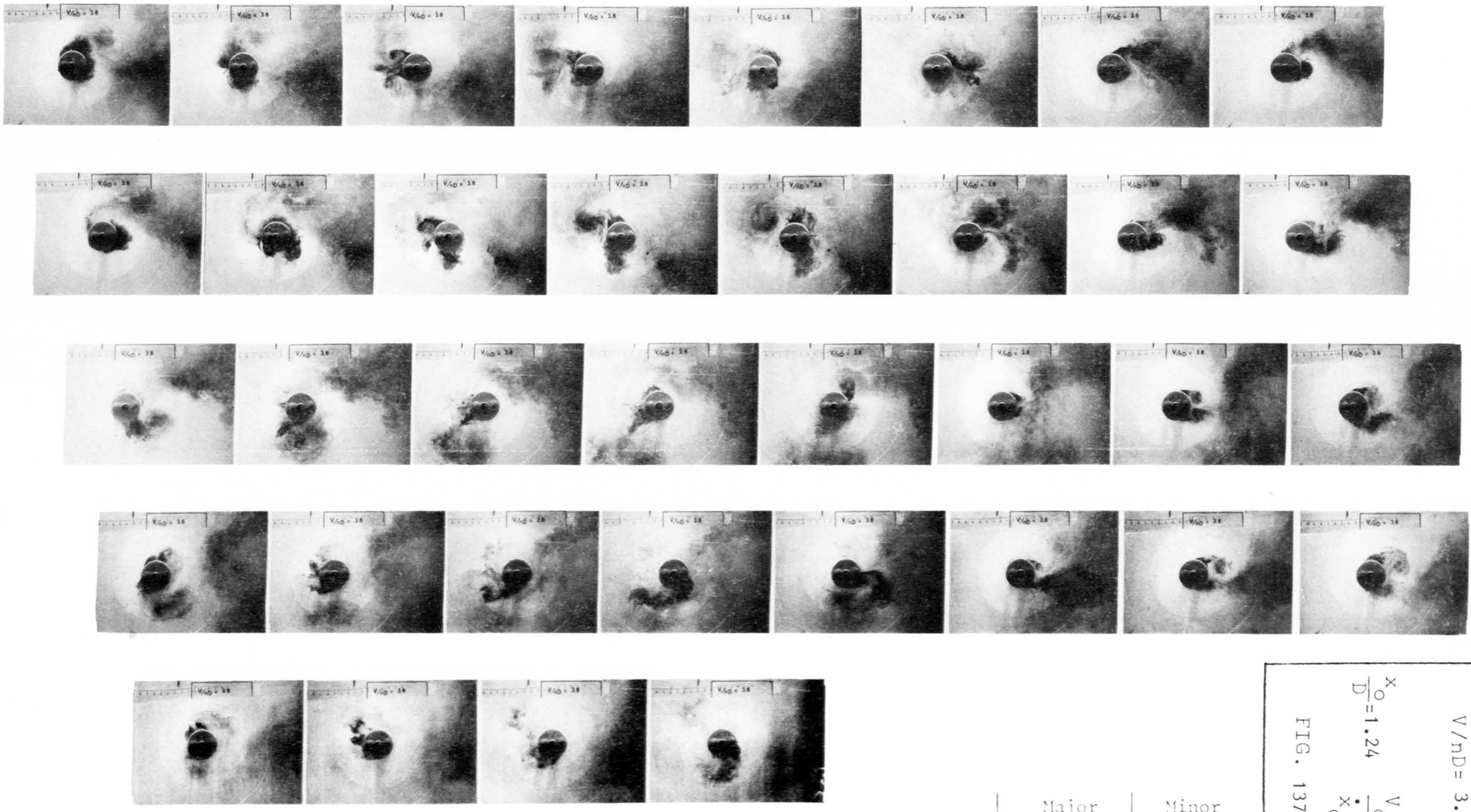

V/nD= 3.8

$\frac{x_o}{D}$=1.24 $\frac{V_o}{\dot{x}_o}$= .49

FIG. 137

	Major	Minor
Non-dimensional relative distance travelled in each part cycle	2.34	-0.44

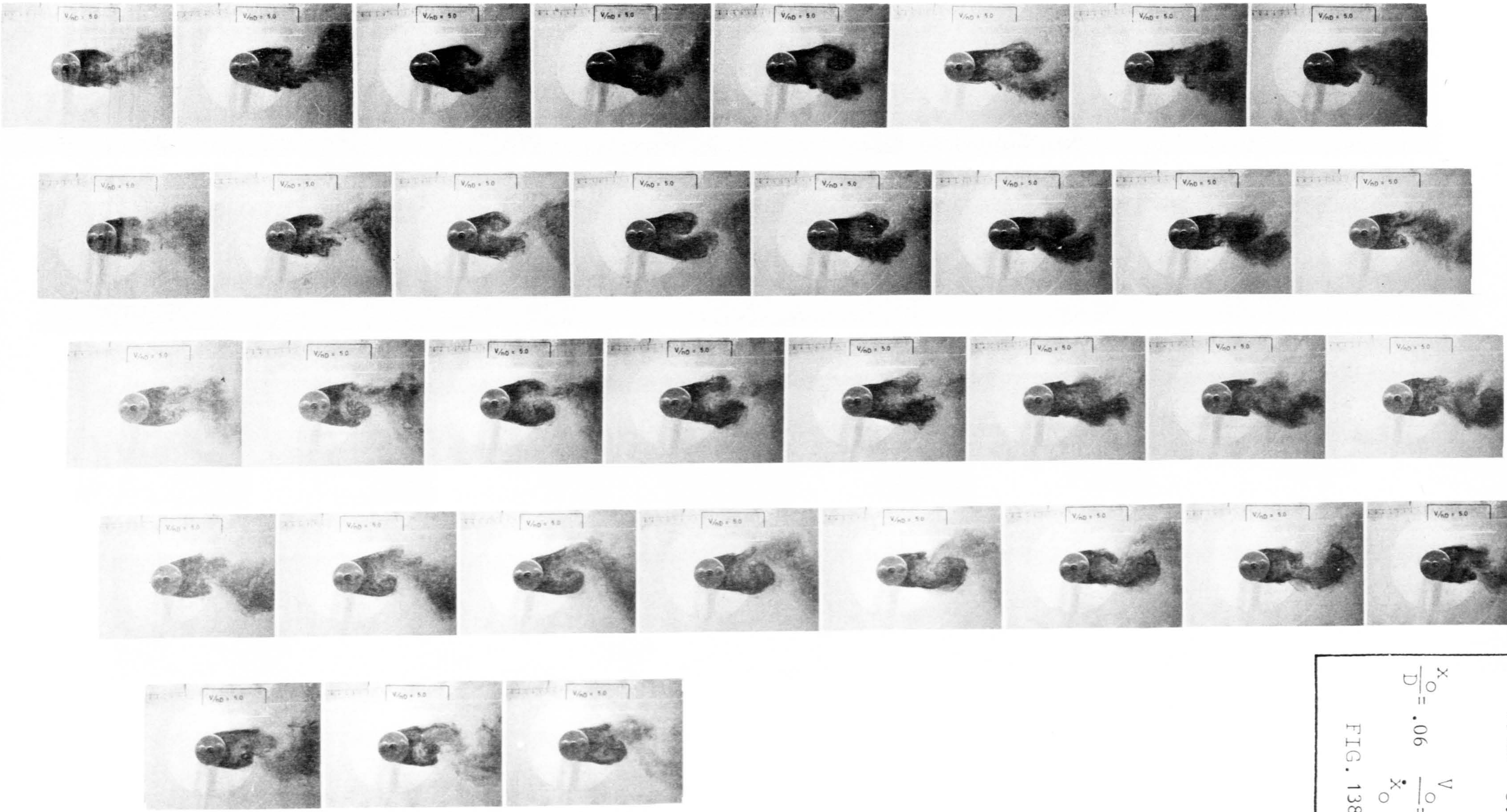

V/nD = 5.0

$\frac{x_o}{D} = .06$ $\frac{V_o}{\dot{x}_o} = 12.6$

FIG. 138

V/nD= 5.0

$\frac{x_o}{D}$= .24 $\frac{V_o}{\dot{x}_o}$=3.32

FIG. 139

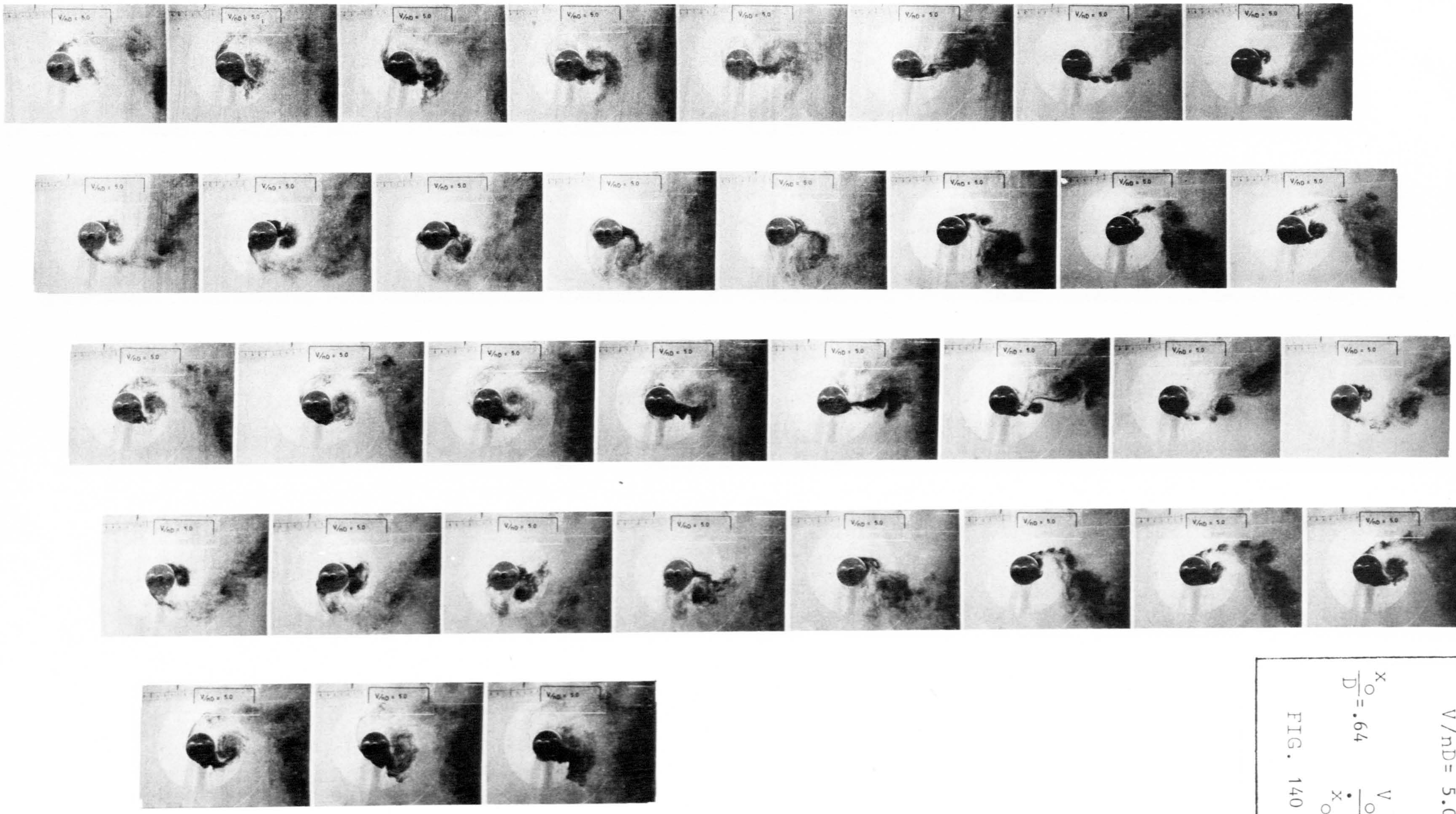

V/nD= 5.0

$\frac{x_o}{D}$ = .64 $\frac{V_o}{\dot{x}_o}$ =1.24

FIG. 140

$\frac{x_o}{D} = 1.69 \quad \frac{V_o}{\dot{x}_o} = .47$

V/nD= 5.0

FIG. 141

	Major	Minor
Non-dimensional relative distance travelled in each part cycle	3.13	-0.63

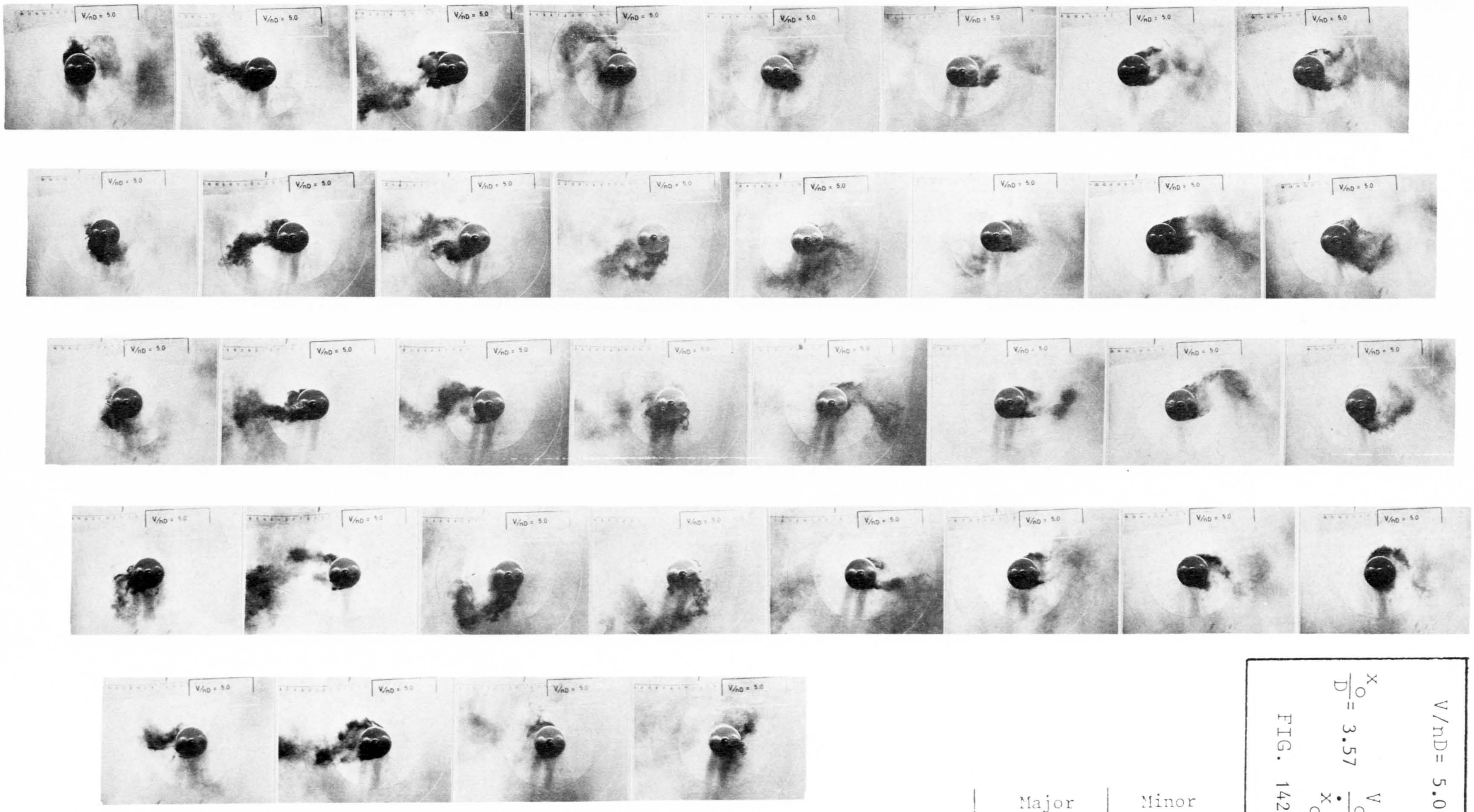

Major	Minor
4.96	-2.46

Non-dimensional relative distance travelled in each part cycle

$V/nD = 5.0$

$\frac{x_o}{D} = 3.57$ $\frac{V_o}{\dot{x}_o} = .22$

FIG. 142

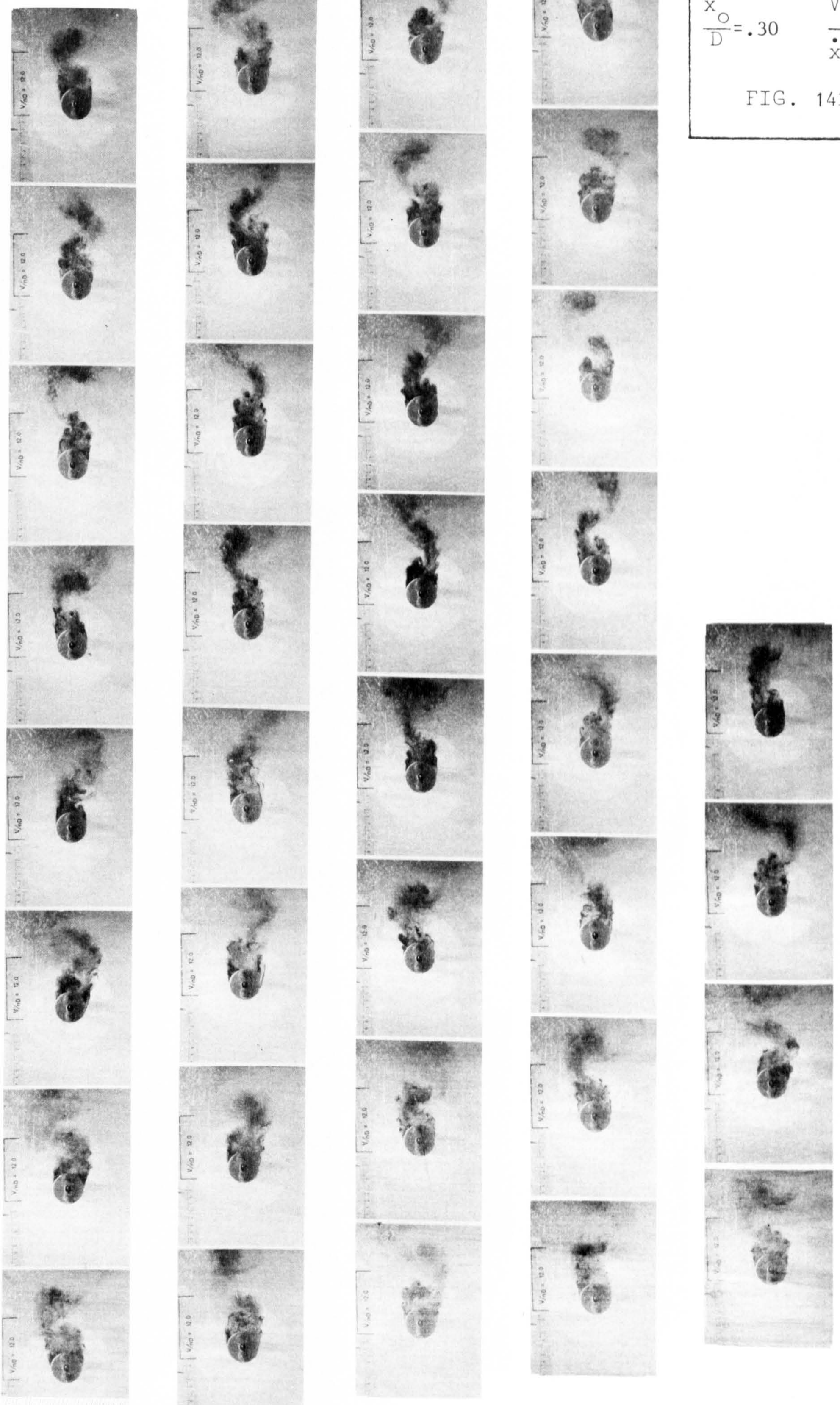

V/nD= 12.0

$\frac{x_o}{D}$=.30 $\frac{V_o}{\dot{x}_o}$=6.37

FIG. 143

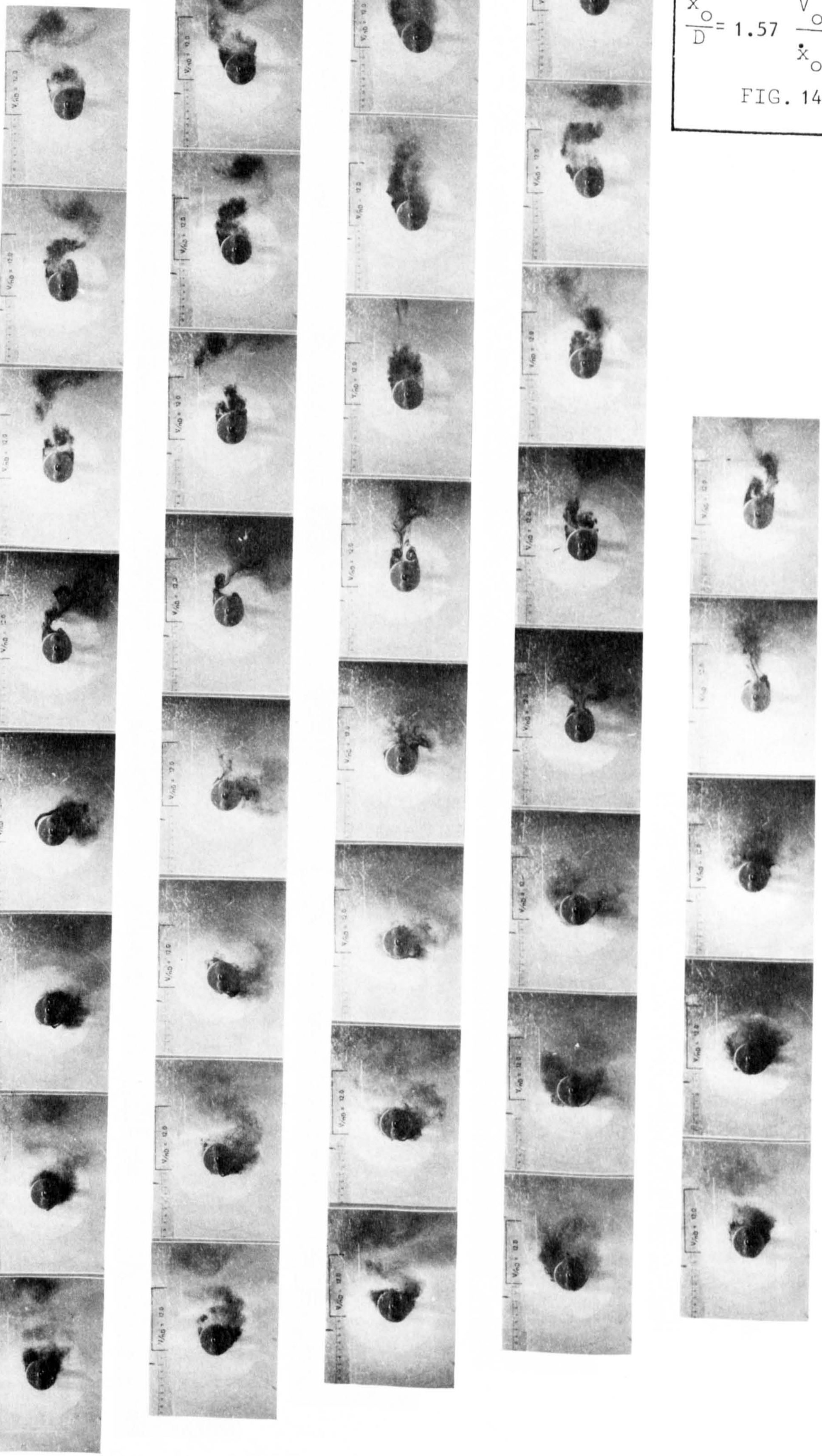

V/nD= 12.0

$\frac{x_o}{D}$= 1.57 $\frac{V_o}{\dot{x}_o}$=1.22

FIG. 144

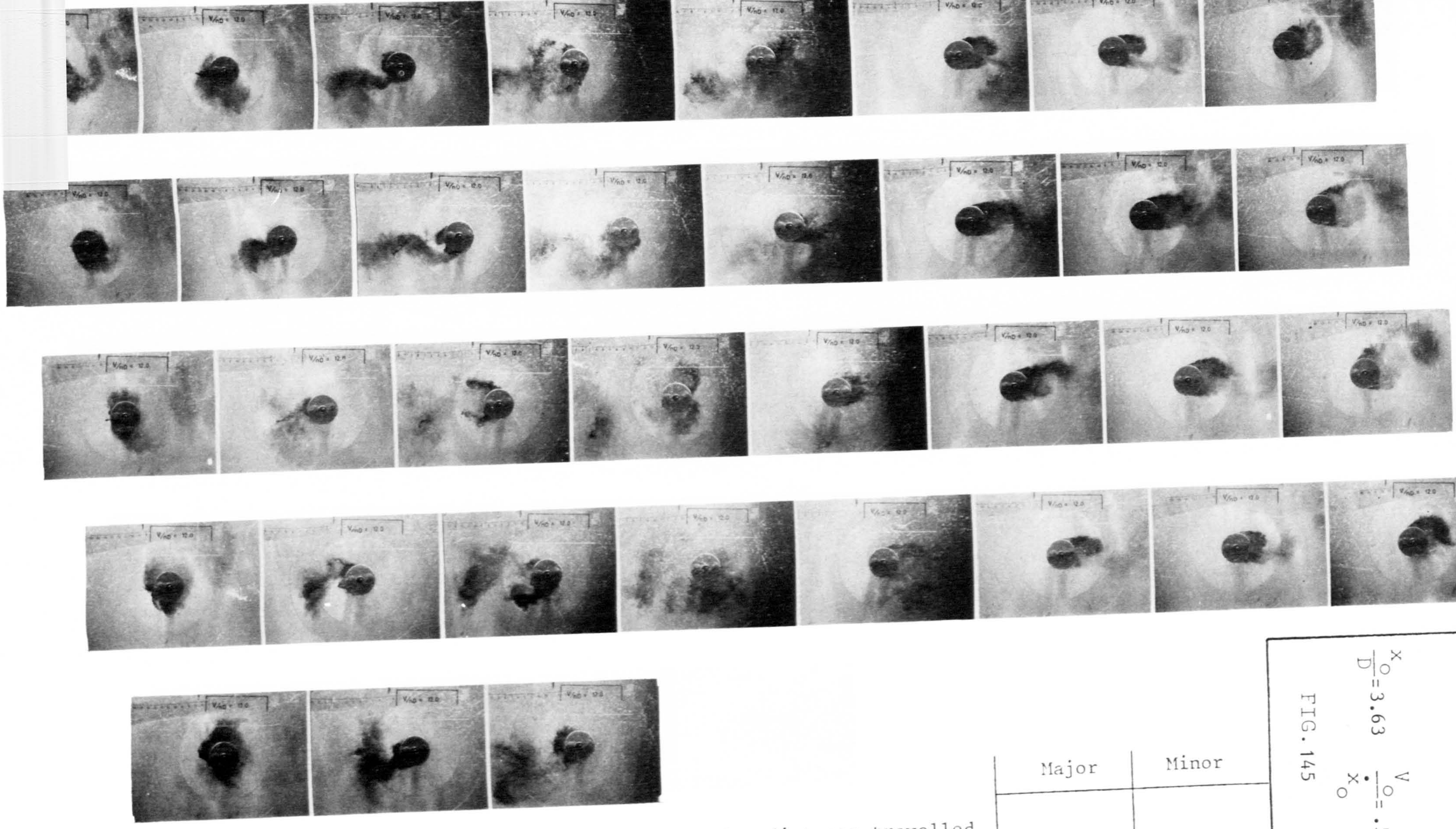

Non-dimensional relative distance travelled in each part cycle

Major	Minor
7.13	-1.14

V/nD= 12.0

$\frac{x_o}{D}$=3.63 $\frac{V_o}{\dot{x}_o}$= .53

FIG. 145

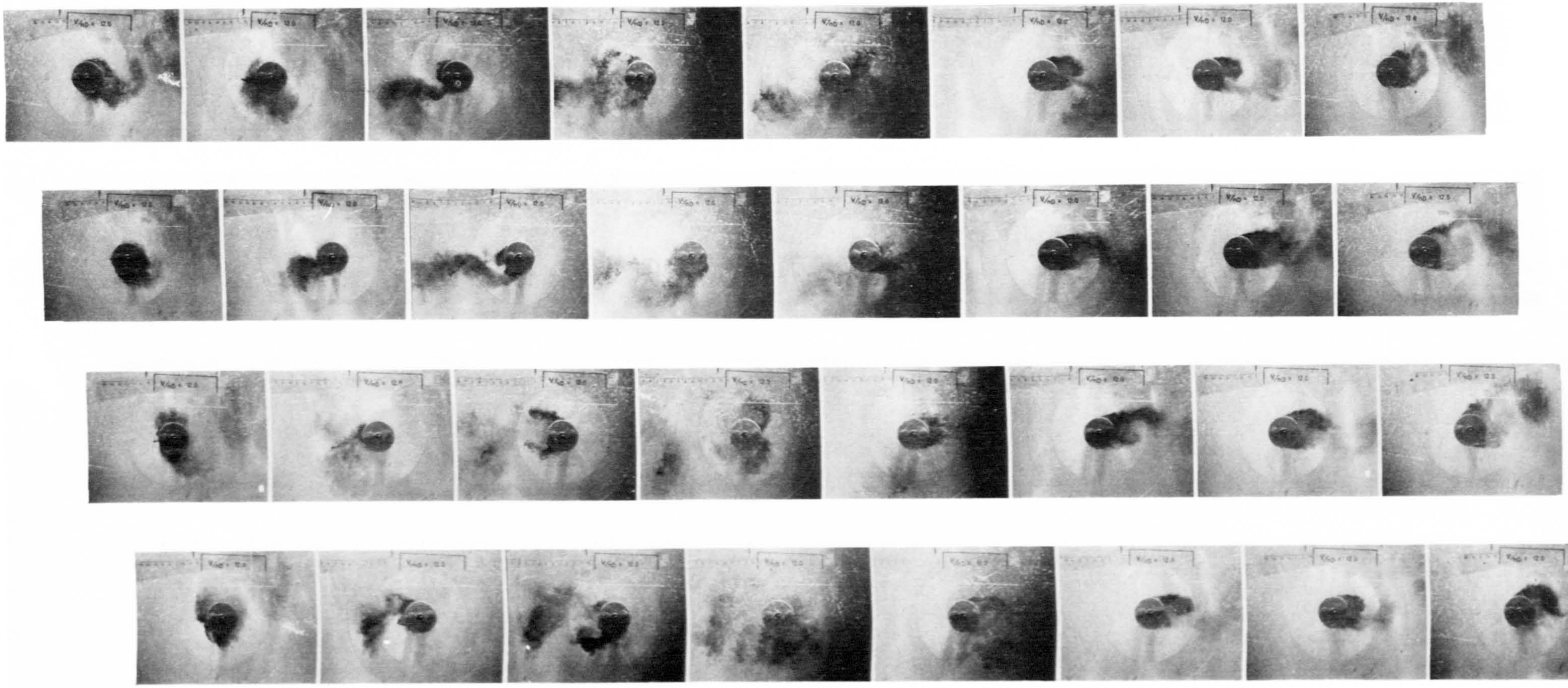

V/nD= 12.0

$\frac{x_o}{D}$=3.63 $\frac{V_o}{\dot{x}_o}$= .53

FIG. 145

Major	Minor
7.13	-1.14

Non-dimensional relative distance travelled in each part cycle

V/nD= 20.0

$\frac{x_o}{D}$= .41 $\frac{V_o}{\dot{x}_o}$=6.95

FIG. 146

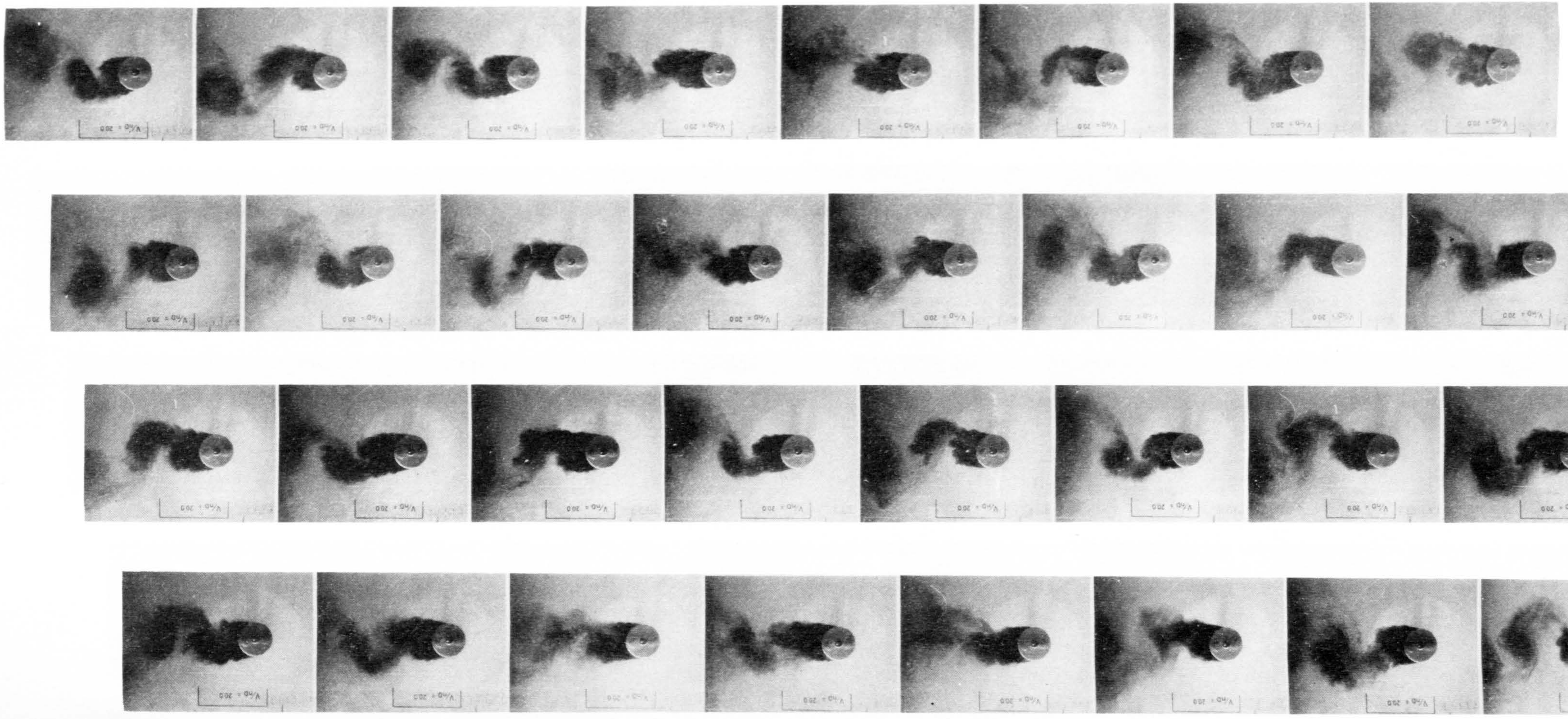

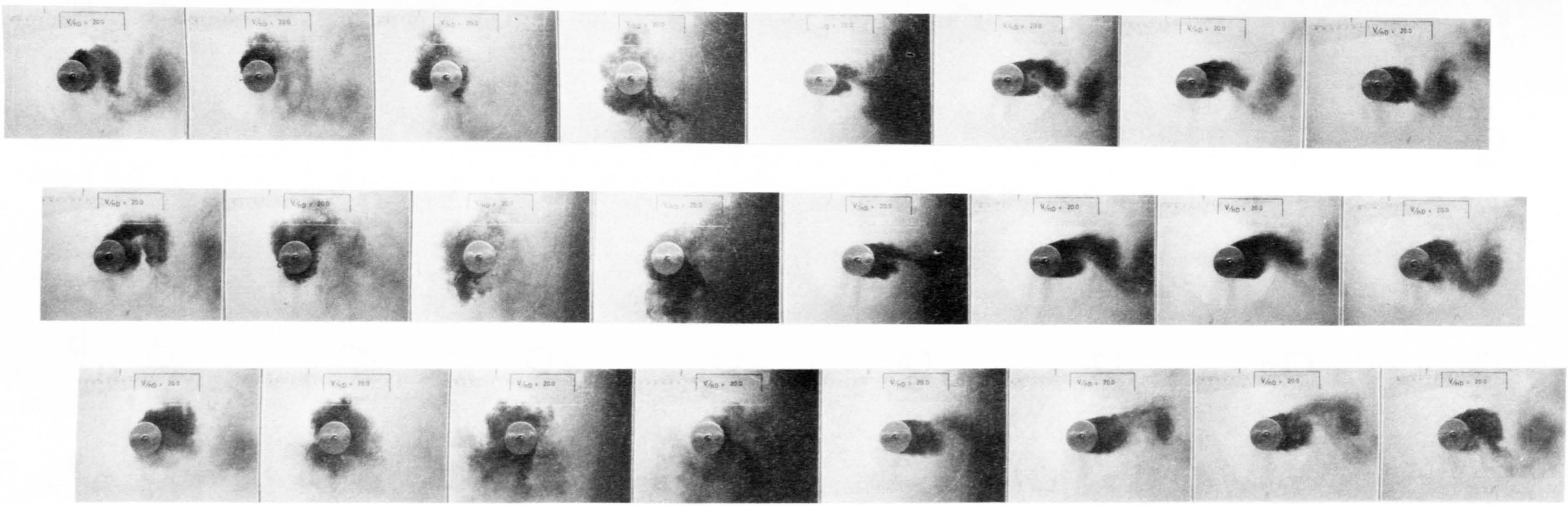

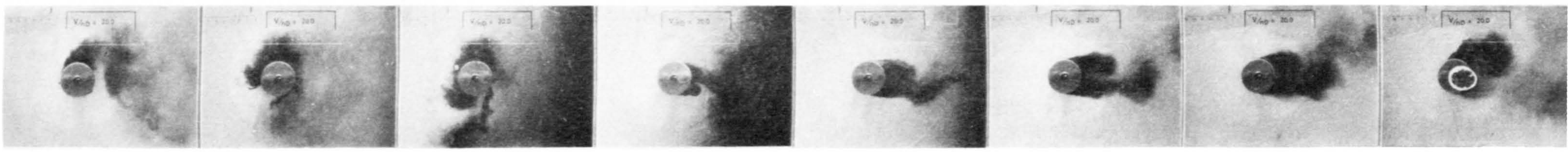

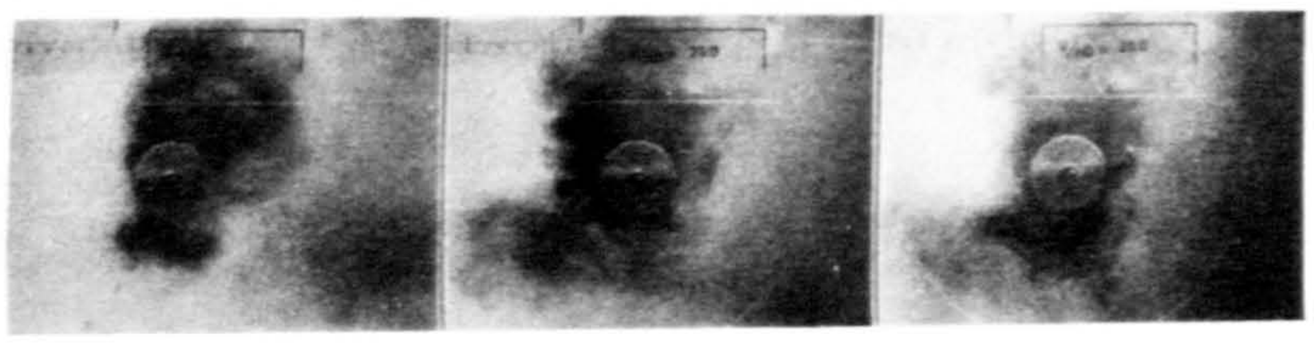

Major	Minor
11.78	-1.78

Non-dimensional relative distance travelled in each part cycle

V/nD = 20.0

$\frac{x_o}{D} = 3.51 \quad \frac{V_o}{\dot{x}_o} = .54$

FIG. 147

PAGE
NUMBERS
CUT OFF
IN
ORIGINAL

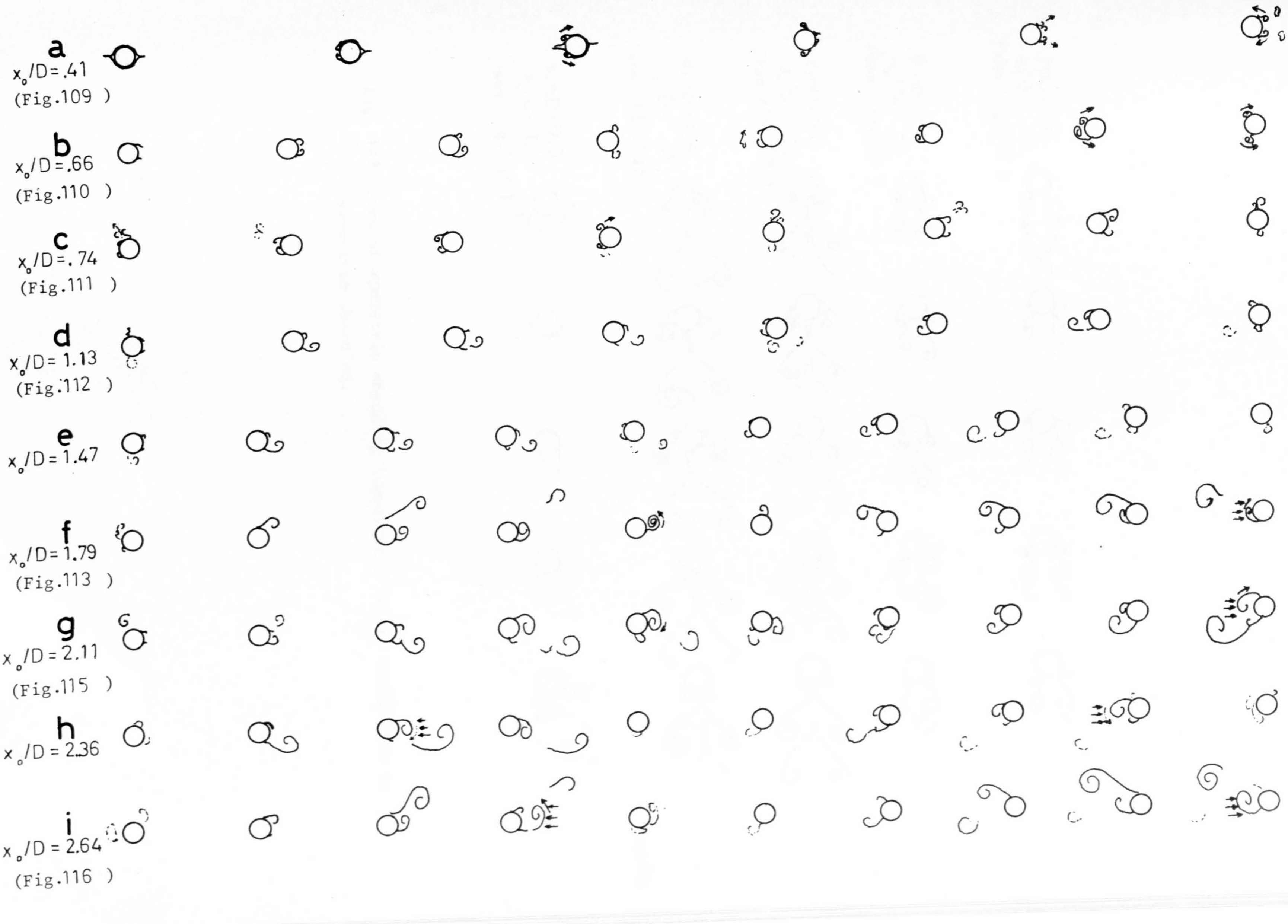

Fig. 148. Sketches of the flow patterns for cylinders oscillating in still water at various x_o/D

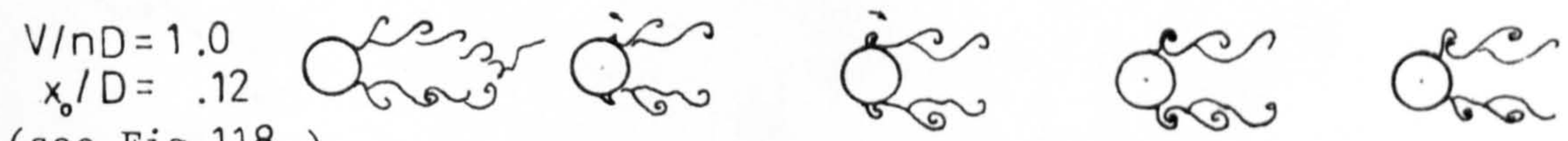

Fig. 149. Form of symmetric shedding immediately before transition to asymmetric shedding.

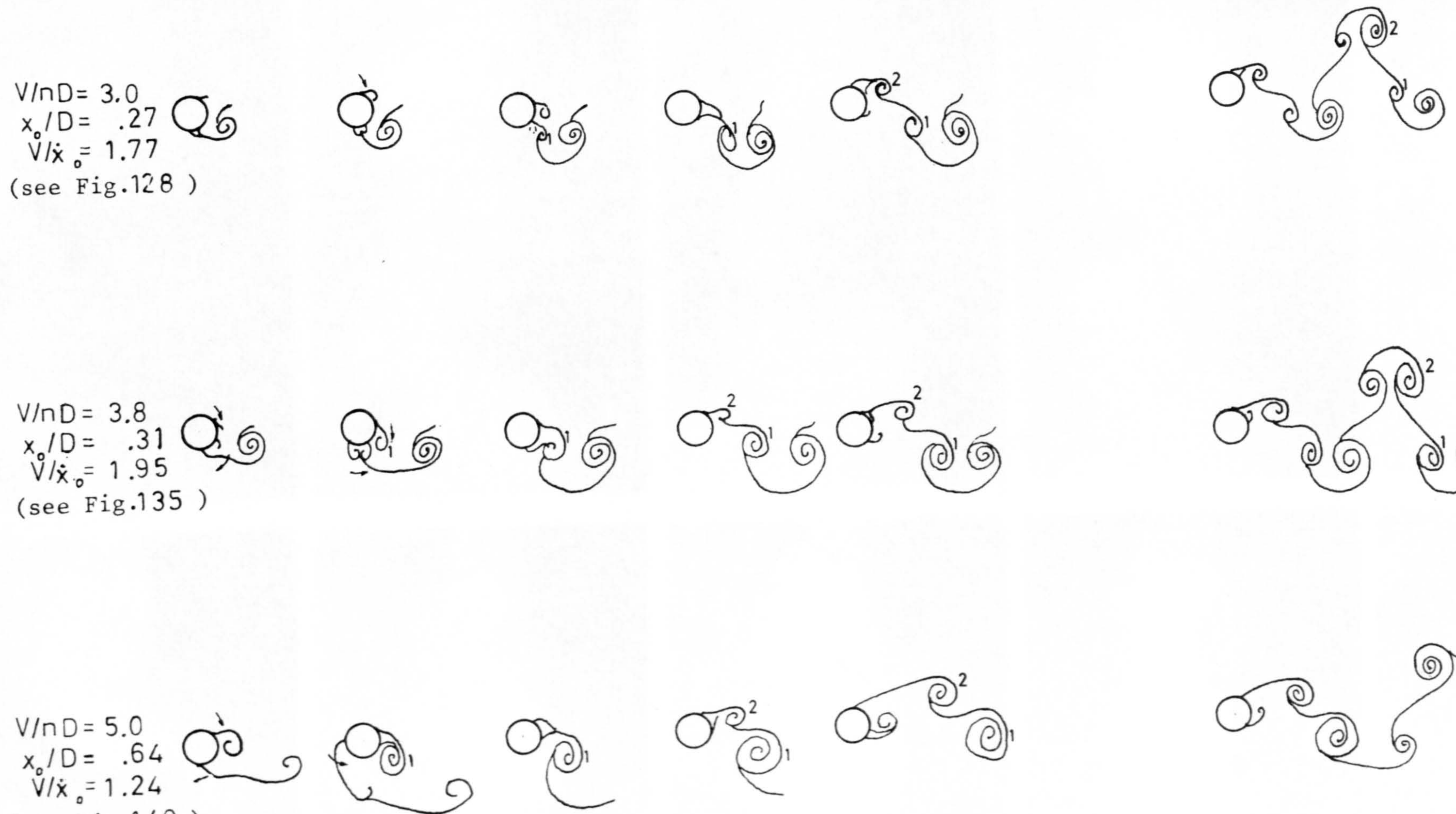

Fig. 150. Form of asymmetric shedding immediately after transition from symmetric shedding at various V/nD.

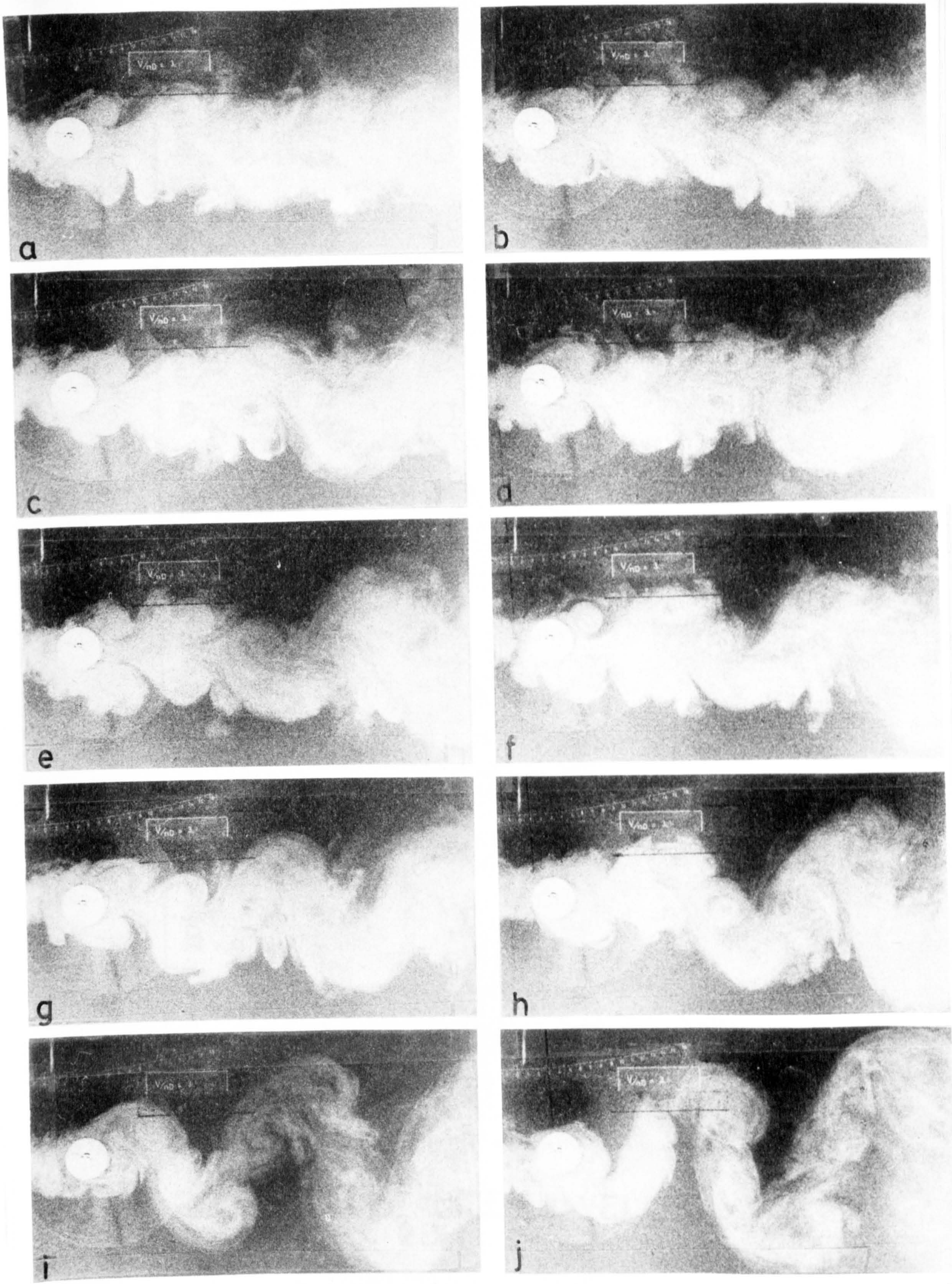

Fig. 151. Flow patterns at the same point at 10 successive cycles showing the change over from symmetric to asymmetric shedding.

Fig. 152. Flow patterns for various values of relative distance travelled, each value obtained with various combinations of V/nD and x_o/D. (A and B denote major and minor part cycles, respectively.)

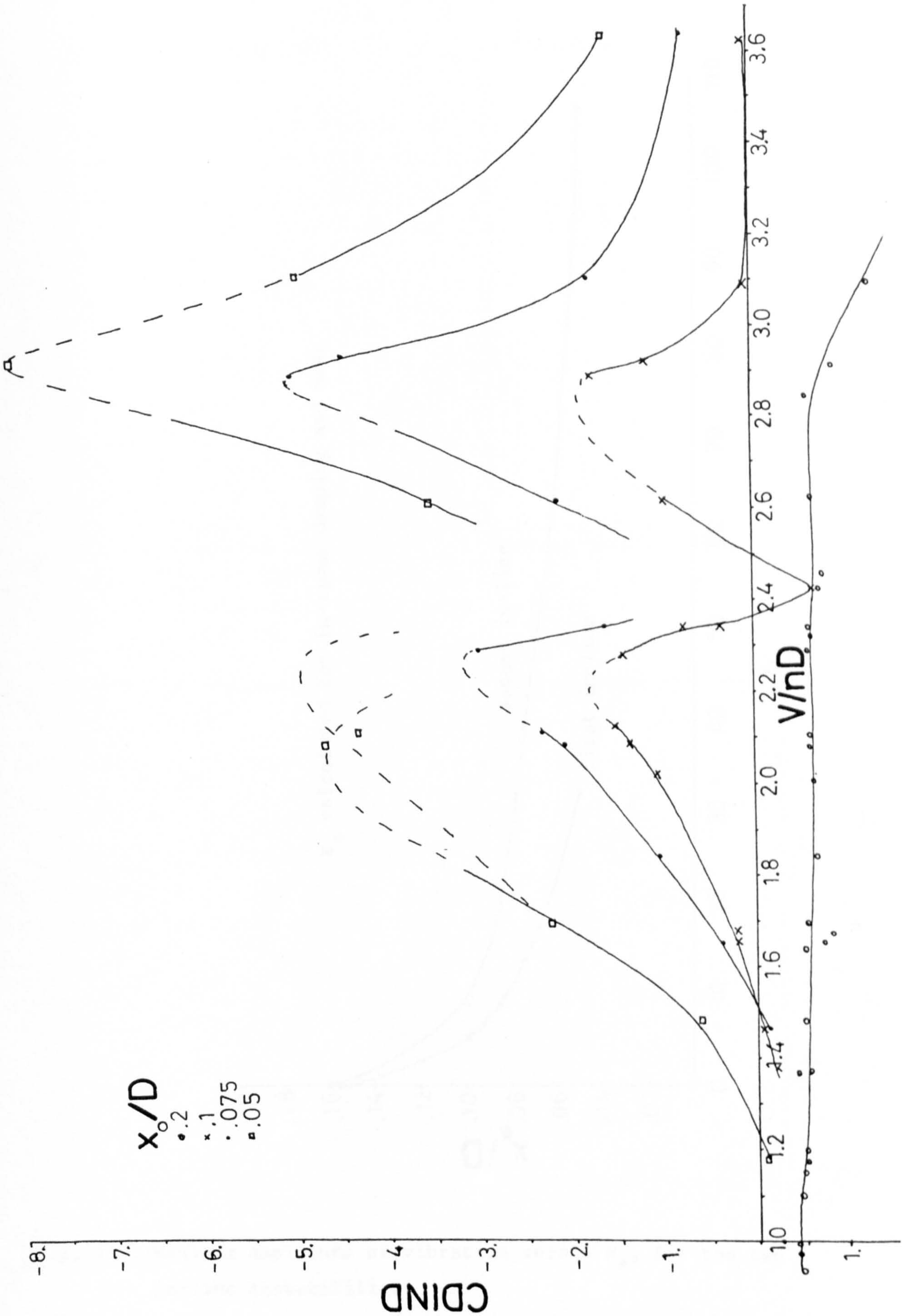

Fig. 153. CDIND versus V/nD in the range where hydroelastic effects occur for various x_o/D.

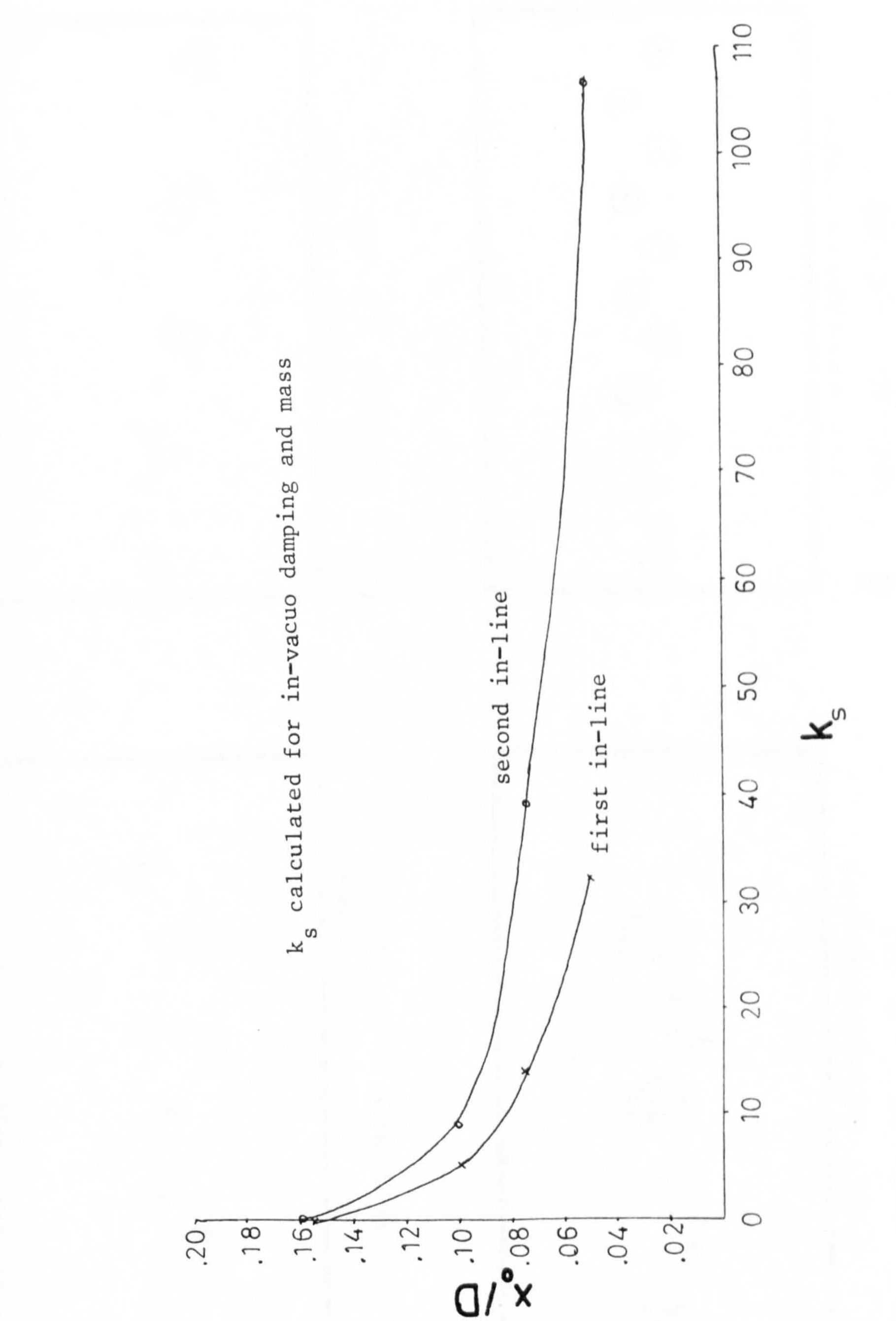

Fig. 154. Maximum amplitude of vibration versus k_s, for the two in-line instabilities.

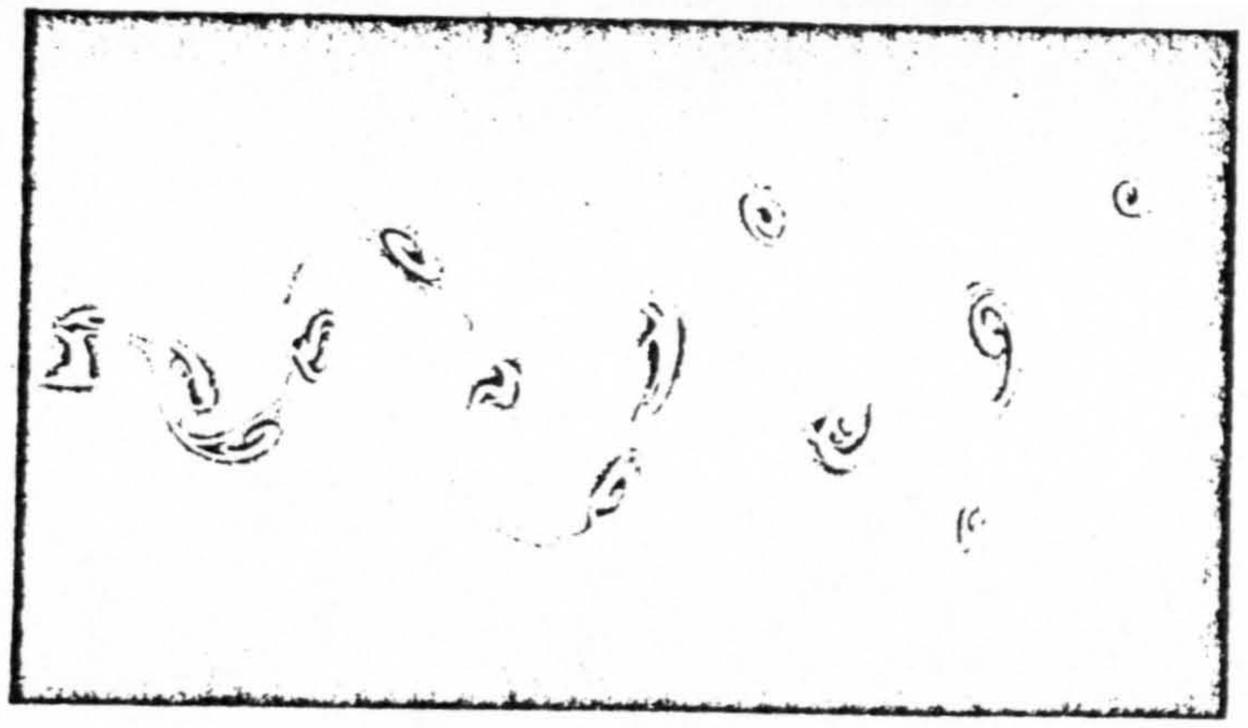

写真 4　1倍の同期領域における渦模様

a　V/nD = 3.82　x_o/D = .267

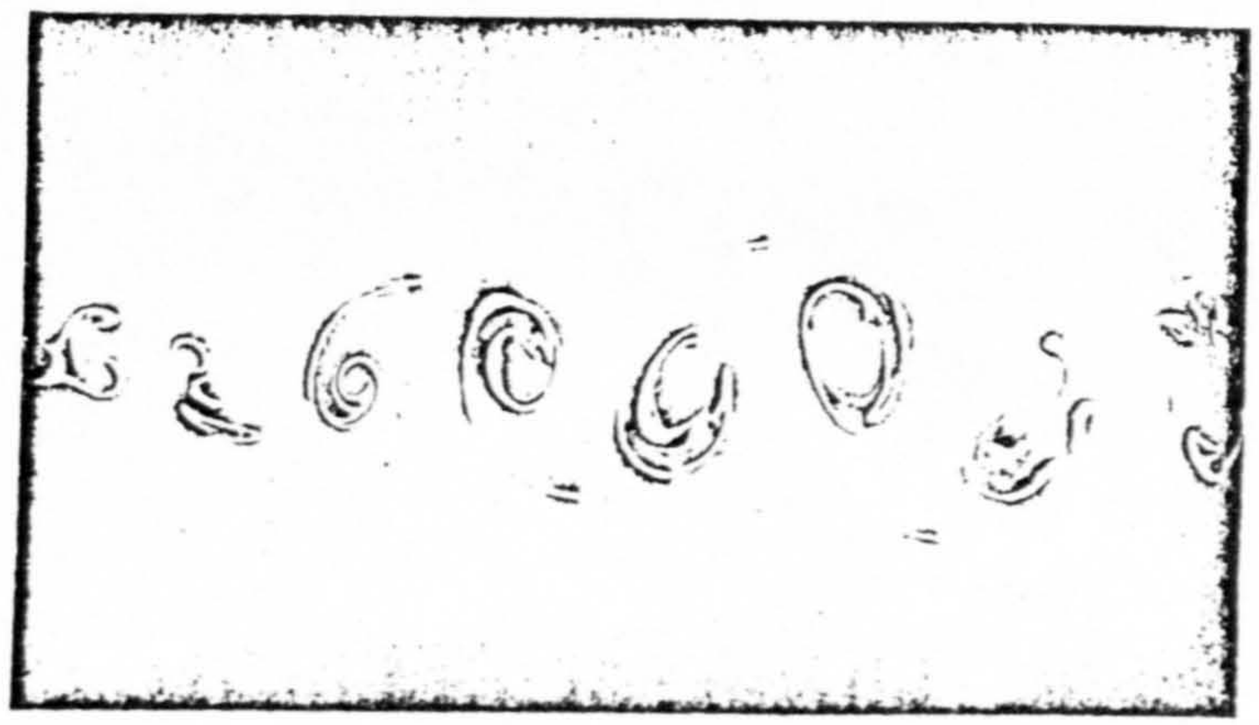

写真 6　½倍の同期領域における渦模様

b　V/nD = 4.90　x_o/D = .267

写真 7　同期領域を越えた S_t での渦模様

c　V/nD = 2.07　x_o/D = .267

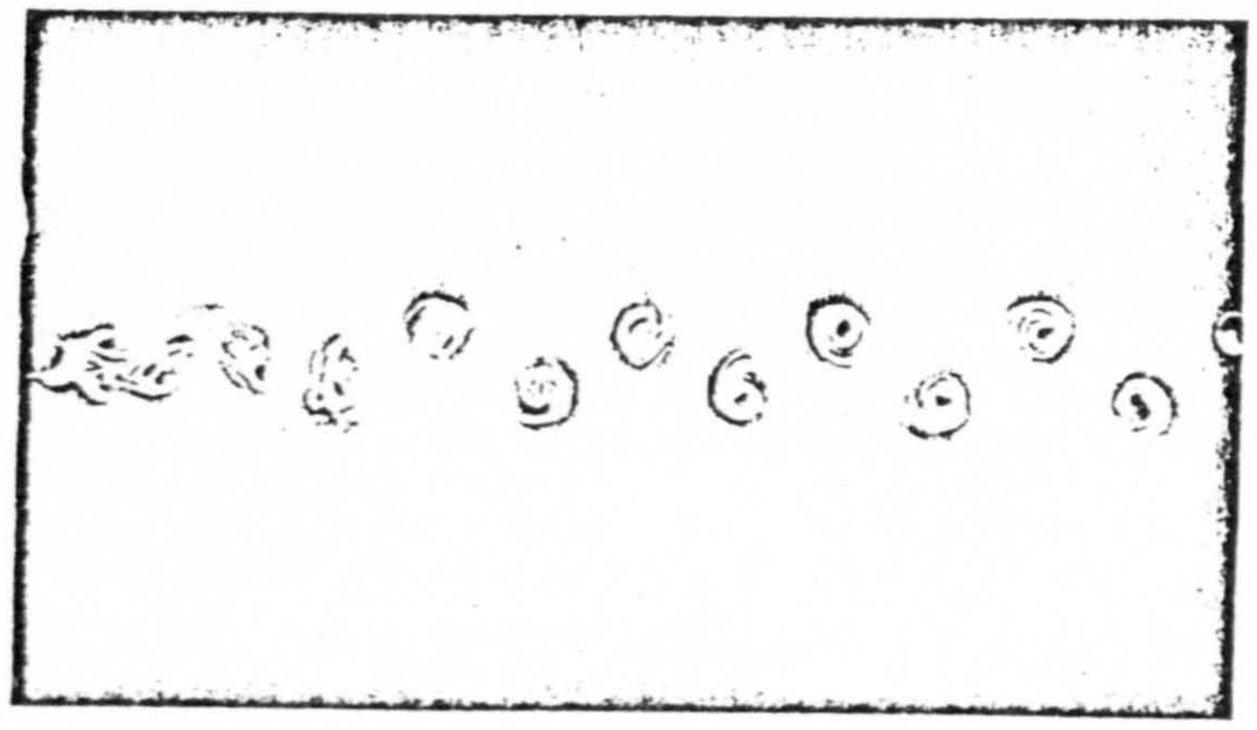

写真 9　同期領域を越えた S_t での渦模様

d　V/nD = 1.60　x_o/D = .178

Fig. 155. Flow patterns at various V/nD and x_o/D, from Tatsuno (1976).